Stellar Laboratories
High-precision Atomic Physics with the Space Telescope Imaging Spectrograph

Dissertation

der Mathematisch-Naturwissenschaftlichen Fakultät
der Eberhard Karls Universität Tübingen
zur Erlangung des Grades eines
Doktors der Naturwissenschaften
(Dr. rer. nat.)

vorgelegt von

Alexander Landstorfer

aus Herrenberg

Tübingen

2021

Gedruckt mit Genehmigung der Mathematisch-Naturwissenschaftlichen Fakultät
der Eberhard Karls Universität Tübingen.

Tag der mündlichen Qualifikation:	20.10.2021
Dekan:	Prof. Dr. Thilo Stehle
1. Berichterstatter:	Prof. Dr. Klaus Werner
2. Berichterstatter:	Prof. Dr. Wilhelm Kley

Zusammenfassung

Fast alle Modelle in der Astrophysik sind abhängig von der Qualität der Daten, die sie verwenden. Hierzu gehören insbesondere Atomdaten, die z.B. in die Berechung der Opazitäten in einer Sternatmosphäre einfließen. Diese Atomdaten werden üblicherweise anhand von Laborspektren bestimmt, wie sie z.B. am National Institute of Standards and Technology der USA gemessen werden. Heiße Sterne, die ihr Flussmaximum im ultravioletten (UV) Spektralbereich haben, liefern ebenso Spektren, deren Linien im Detail studiert werden können. Diese stellaren Spektren werden von UV-Spektrographen im Weltraum, wie z.B. dem Space Telescope Imaging Spectrograph, aufgenommen und haben eine sehr hohe Auflösung und ein sehr hohes Signal-zu-Rausch-Verhältnis, das vergleichbar zu den Laborspektren ist. Dies ermöglicht, die Qualität der vorhandenen Atomdaten mit Sternspektren zu prüfen.

In dieser Arbeit wurden drei heiße Unterzwerge, die in ihren Atmosphären hohe Häufigkeiten der Elemente Ca – Ni aufweisen, als „Sternlaboratorien“ verwendet, indem qualitativ hochwertige UV-Spektren dieser Sterne analysiert und anschließend isolierte Absorptionslinien der eben genannten Elemente untersucht wurden.

Zunächst werden die Entwicklung und die Eigenschaften heißer Unterzwerge gezeigt, dann wird knapp die Theorie zur Entstehung von Sternspektren, mit Schwerpunkt auf dem Profil von Absorptionslinien, vorgestellt. Anschließend wird gezeigt, wie die wissenschaftliche Methode der Spektralanalyse im Allgemeinen durchgeführt wird, wie sie numerisch umgesetzt werden kann und welche wichtige Rolle die Genauigkeit von Atomdaten, die als numerischer Input dienen, für eine erfolgreiche Spektralanalyse spielt. In diesem Zusammenhang werden quantenmechanische Korrekturen, sogenannte „Oszillatorenstärken“, vorgestellt, die zur korrekten Modellierung einzelner Linienstärken erforderlich sind.

Hochaufgelöste Spektren von drei heißen Unterzwergen, nämlich EC 11481–2303, Feige 110 und PG 0909+276, wurden analysiert, und atmosphärische Eigenschaften und Elementhäufigkeiten wurden auf diese Weise bestimmt. In jedem der drei Sterne wurden mehrere tausend einzelne Absorptionslinien von Ca – Ni erfolgreich identifiziert. Anschließend wurden isolierte Absorptionslinien, die als Daten zur Untersuchung der Linienstärken dienen, identifiziert und aufgelistet. Aufgrund der Sternrotation war dies für EC 11481–2303 nicht möglich. In Feige 110 und PG 0909+276 hingegen wurden insgesamt 792 isolierte Absorptionslinien von Ca – Ni gefunden. Zur Identifizierung der isolierten Linien wird einmal eine manuelle Methode vorgestellt, die dann als automatische Prozedur umgesetzt wurde.

Die theoretisch modellierten, isolierten Absorptionslinien wurden dann mit den beobachteten verglichen. Dafür wurde eine automatische Prozedur erstellt, die mit Gaußanpassungen die Linienmitten, -breiten und -stärken bestimmt. Nach der Anbringung gewisser Reduktionskriterien wurden die verbleibenden 457 Absorptionslinien, von denen die meisten Cr – Ni angehören, erfolgreich ausgewertet. Die daraus erhaltenen Ergebnisse konnten zur genaueren Bestimmung der Elementhäufigkeiten verwendet werden. Außerdem wurden

keine systematischen Abweichungen der modellierten und der beobachteten Linienstärken und somit auch der Oszillatorenstärken gefunden. Für Feige 110 beträgt die statistische Unsicherheit der Linienstärken unter den untersuchten Linien 45 % und für PG 0909+276 beträgt sie 72 %.

Schließlich wurden die erhaltenen Ergebnisse verwendet, um starke, isolierte Linien zu finden, deren theoretische Linienstärken besonders gut mit den Beobachtungen übereinstimmen. Die Verwendung dieser Linien als Anhaltspunkte verbessert die Genauigkeit der Häufigkeitsbestimmungen für die Elemente Cr – Ni, insbesondere in Sternen, in deren Spektren nur eine geringe Linienzahl vorliegt.

Summary

Almost all astrophysical models depend on the quality of the used data, including atomic data in particular, which is used, for example, for the calculation of the opacities in a stellar atmosphere. This atomic data is usually determined using laboratory spectra, such as those measured at the National Institute of Standards and Technology in the USA. Hot stars, which exhibit their flux maximum in the ultraviolet (UV) spectral range, also provide spectra whose lines can be studied in detail. These stellar spectra are taken by UV spectrographs in space, such as the Space Telescope Imaging Spectrograph, and have a very high resolution and a very high signal-to-noise ratio, making them comparable to laboratory spectra. This enables the quality of the available atomic data to be verified with stellar spectra.

In this work, three hot subdwarf stars, which exhibit high surface abundances of the elements Ca – Ni, were used as "stellar laboratories" by analysis of high-quality UV spectra and subsequent evaluation of isolated absorption lines of the aforementioned elements.

After the evolution and properties of hot subdwarfs are presented, the basic theory on the formation of stellar spectra, with focus on the absorption-line profile, is introduced. Then, it is shown how the scientific method of spectral analysis is carried out in general, how it can be implemented numerically and which important role the accuracy of atomic data, which serves as numerical input, plays for a successful spectral analysis. In this context, quantum mechanical corrections, so-called "oscillator strengths", which are necessary to correctly model individual absorption-line strengths, are introduced.

High-quality spectra of three hot subdwarf stars, namely EC 11481–2303, Feige 110, and PG 0909+276 were analyzed, and atmospheric properties and element abundances were determined by this means. In each of the three stars several thousands individual absorption lines of Ca – Ni were successfully identified. Afterwards, isolated absorption lines, which serve as data for examining the line strengths, were to be identified and listed. Due to stellar rotation, this was not possible for EC 11481–2303. In Feige 110 and PG 0909+276, however, a total of 792 isolated absorption lines of Ca – Ni was obtained. For isolated absorption-line identification, once, a manual procedure is presented, which was then implemented as an automatic program.

The theoretically modeled, isolated absorption lines were then compared with the observed ones. Therefore, an automatic fitting procedure, which determines line centers, widths, and strengths, was established. After some reduction, the remaining 457 absorption lines, most of which Cr – Ni, were successfully evaluated, whereby a large amount of important statistics was obtained, which could be used for a more precise abundance determination. Besides, no systematic deviations of the modeled and the observed line strengths, and hence the oscillator strengths, were found. For Feige 110, the statistical uncertainty of the line strengths, among the examined lines, is 45 %, while for PG 0909+276 it is 72 %.

At last, the obtained results were used to find strong, isolated absorption lines with good agreement between observations and models. Using these lines as reference points will improve the accuracy of abundance determinations for the elements Cr – Ni, especially in those cases where only a small number of lines is identified in an observation.

Contents

List of Figures

List of Tables

Relevant physical constants

Boltzmann constant	k_{B}	1.38065×10^{-23}	J/K
Electron mass	m_{e}	9.10938×10^{-31}	kg
Elementary charge	e	1.60218×10^{-19}	C
Speed of light in vacuum	c	2.99792×10^{8}	m/s
Parsec[a]	pc	3.08567×10^{16}	m
Planck constant	h	6.62607×10^{-34}	J s
Solar mass[a]	$M_{\odot}$	1.98841×10^{30}	kg
Solar radius[b]	$R_{\odot}$	6.96342×10^{8}	m

References: https://physics.nist.gov/cuu/Constants
[a]Saha 2020, [b]Emilio et al. 2012

1 Introduction

How do we even know anything about the stars? When looking at the night sky, they appear as small dots which are clearly beyond our reach. On a clear night, for example, around 3 000 stars can be seen with the naked eye and differences in brightness, for some possibly also in color (red to blue), can be determined. Of course, even before the telescope was invented, when only the human eye was available as an "instrument", astronomy could be practiced in such a way that the movement of the starry sky could be observed and interpreted. In this way, people could orientate themselves on the high seas, determine the seasons, and even discover some of the planets in our solar system. Finding out more details about the structure of the universe, the various celestial bodies, or even the structure of a star, however, was far beyond the possibilities at that time.

Everything changed thanks to some groundbreaking discoveries and developments from the 17th century on, beginning with the invention of the telescope by Hans Lipperhey in 1608, which was optimized a year later by Galileo Galilei and could then also be used for observing the night sky – modern astronomy was born. In the same year, Johannes Kepler published his *Astronomia Nova* (1609) with the first two Kepler's laws, and in the following years the first moons (Callisto, Io, Europa, Ganymede), the first galaxy[1] (Andromeda) and the first binary systems were discovered. At the end of the 1660s, Sir Isaac Newton developed the reflecting telescope, which is the pioneer of the largest telescopes built today. Besides, the discovery of the law of gravitation led to his famous work *Philosophiae Naturalis Principia Mathematica* (1687), which laid the foundations of both classical mechanics and astrophysics. At the same time, Newton took a closer look at the nature of light. Around 1700 he realized that white sunlight consists of different spectral colors when he bundled the light through a hole and then sent it through a prism. He recorded these and other findings in his lesser-known work *Opticks* (1704), the use of which for astronomy was only to become apparent more than 100 years later.
While, up to 1800, further discoveries, which could be traced back to better observational possibilities thanks to continuously improved telescopes, followed, the question asked at the beginning, *what do we know about the stars*, could still not be answered. Although the construction of large telescopes and the first observatories led to a more detailed exploration of the Milky Way and of celestial objects such as stellar clusters and nebulae, comets and, for example, the discovery of the differential rotation of the Sun, it still was not possible to say anything about the structure and composition of the stars.
Although William Hyde Wollaston found dark lines in the solar spectrum as early as

[1] Strictly speaking, it was spotted by the Persian astronomer Al-Sufi in 964, but it had not been identified as a galaxy.

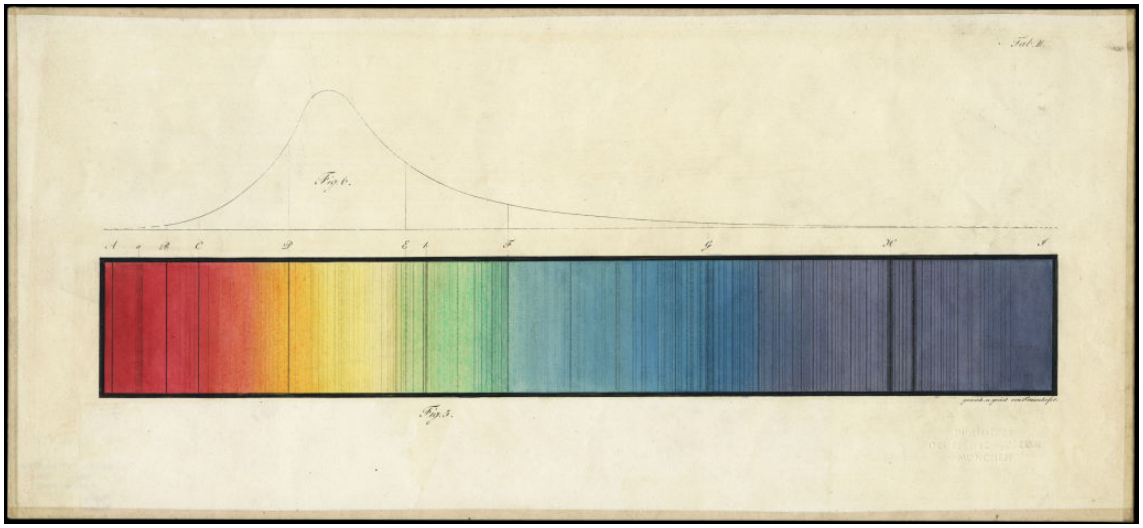

Figure 1: Original print of the solar spectrum by Fraunhofer (1814) from the Deutsches Museum in Munich.
`Reference:`
`https://abenteuer-astronomie.de/was-sind-eigentlich-fraunhoferlinien`

1802, it was Joseph von Fraunhofer who, in 1814, while working on the optimization of lenses, discovered the same lines independently of Wollaston and described them more precisely. Fraunhofer developed the spectroscope in 1814 and made his observations public. That is why the dark lines in the solar spectrum are also called *Fraunhofer lines* (Fig. 1). In 1859, Gustav Robert Kirchhoff and Robert Wilhelm Bunsen established the connection between these absorption lines and atomic processes, whereby hydrogen in the solar spectrum could be identified and thus, for the first time, something could be said about the composition of the Sun – spectral analysis was born (Kirchhoff & Bunsen 1860).

Spectral analysis is one of the great research fields in astrophysics[2]. Thanks to the continuous improvement of instruments (telescopes, spectrographs) and methods, some important discoveries have been made. Spectral analysis was the first to demonstrate the Doppler effect in a stellar spectrum, with which the radial velocity of the star could be determined. At the end of the 1920s, Edwin Hubble applied a similar method to determine the recessional velocity of distant galaxies (Hubble 1936), which indicated an expansion of the universe and ultimately led to today's well-known Big Bang theory. Spectral analysis made it possible to detect magnetic fields on the Sun and some bright stars for the first time, and above all, spectral analysis enabled the determination of stellar surface temperatures and thus the spectral classification of stars (Sect. 2.1).

When having a look at the field of spectral analysis (within astrophysics) today, on the one hand the steady development of telescopes and spectrographs has made observations more and more precise, and on the other hand an optimized method of analysis (of single stars) is available by the use of so-called stellar atmosphere codes (Werner & Dreizler 1999, Hubeny 2010, Sect. 4.2). The basic idea behind these is to calculate a model atmosphere of the star based on a pre-defined set of parameters such as effective temperature, surface gravity, and chemical composition. Using this model atmosphere, a spectrum is simulated,

[2]Spectral analysis covers a larger area of research than just the part within astrophysics, which is, however, not within the scope of this work.

which is compared with the observation. In the last step, the parameters just mentioned are adjusted until the best match is achieved.

Spectral analysis is an important method to verify astronomical theories. The chemical evolution of the Universe is determined by stellar nucleosynthesis. Elements up to iron are produced by nuclear fusion, heavier elements by neutron capture inside hot, evolved stars via the s-process, or in super or kilonovae (neutron star mergers) via the r-process. Ultimately, evolved stars expel a significant part of their matter into the interstellar medium. The formation and evolution of galaxies is determined by the chemical evolution of their components, which results from the processes just mentioned. Even though the modeling of such structures is very complex, spectral analysis provides important boundary conditions for such endeavors.

One difficulty for correctly determining the chemical composition of a star is that atomic data about the respective elements must be available to calculate the model atmosphere. For this purpose, the spectra of the examined elements are conventionally measured in classic laboratories. Energy levels, cross-sections and transition probabilities are then determined with the help of quantum mechanical calculations. So-called model atoms are created from the atomic data obtained in this way. Starting from the relatively simple hydrogen, atomic spectra become rather complex, which is why the lack of completeness and/or precision of atomic data is a limiting factor in the accuracy of spectral analyses today. This thesis is dedicated to this problem, more precisely to the verification of quantum mechanical corrections (i.e., oscillator strengths) for some heavier elements. High-quality spectra of hot, evolved stars are used as "laboratories" for this purpose.

In Sect. 2 the evolution and properties of these stars are explained. In Sect. 3 the formation of stellar spectra, especially absorption lines, is discussed in more detail. Sect. 4 shows how stellar atmosphere codes have been implemented and explains the problem of atomic data. In Sect. 5, the three examined stars and their observations are presented in more detail. Sect. 6 delves into the treatment of the limited resolving power of spectrographs. Sect. 7 presents the spectral analyses of the three program stars and derives the atmospheric parameters and element abundances. Sect. 8 describes two methods with which individual absorption lines are selected for investigation of the line strengths in the stellar spectra. Sect. 9 compares the modeled with the observed line strengths and presents the results. Finally, in Sect. 10, the uncertainty of the aforementioned oscillator strengths, as well as of this work's analysis method, is estimated, and suggestions for improving abundance determinations are given. Independently of the previous, Sect. 11 examines the theoretical line strengths of two more elements.

2 Hot subdwarfs

This chapter first shows how stars with different masses evolve. Then, the evolution and properties of hot subdwarfs are discussed in more detail.

2.1 Stellar evolution

A star forms by the gravitational collapse of a giant molecular cloud which consists largely of hydrogen. If the mass of the resulting body is high enough ($M \gtrsim 0.07\,M_\odot$; Chabrier & Baraffe 1997, 2000), the fusion of hydrogen to helium (also called hydrogen burning) is carried out in the core. All stars which burn hydrogen in the core are called main-sequence stars. Since this phase is the longest in the life of a star (approx. 90%), most of the observed stars belong to the main sequence. The state of equilibrium in which hydrogen burns in the core depends mainly on the stellar mass, so the mass also influences observable properties such as luminosity L and effective temperature $T_{\rm eff}$ (Sect. 3.1). A diagram, which plots the luminosity on the ordinate and the effective temperature on the abscissa, is called Hertzsprung-Russell diagram (HRD, Fig. 2). Now and then, the spectral type of the star is plotted, which is, however, directly related to its effective temperature $T_{\rm eff}$.
As mentioned earlier, all stars that burn hydrogen in the core form the main sequence in the HRD. Different temperatures and luminosities are determined by their mass, which causes heavier main-sequence stars to be hotter and brighter. This also determines the evolution of a star after the first phase of nuclear burning. In the following, the further, typical evolutionary phases of single stars of different masses are explained briefly (cf. Iben 1974, Carroll & Ostlie 1996).

- Very-low-mass stars with an initial mass of $0.07\,M_\odot \lesssim M_{\rm init} \lesssim 0.5\,M_\odot$ only continue to burn hydrogen in a shell after the fusion in the core has expired, since their mass (and thus pressure and temperature) is not sufficient to ignite a nuclear fusion of helium into heavier elements (Laughlin et al. 1997). Ultimately, they give in to gravity and contract into a white dwarf (Fontaine et al. 2001), a stellar corpse with a radius of $\approx 7\,000$ km to 14 000 km, which, due to its high temperature will continue to emit light for billions of years. Since these low-mass stars burn hydrogen in their main-sequence phase so slowly that it lasts for several 100 billion years, none of this type has yet been leaving the main sequence. The universe, with its age of 13.8 billion years, is therefore simply too young.

- When the core-hydrogen supply of low-mass stars with $0.5\,M_\odot \lesssim M_{\rm init} \lesssim 2\,M_\odot$ runs out, the energy production also dries up, which leads to the core becoming

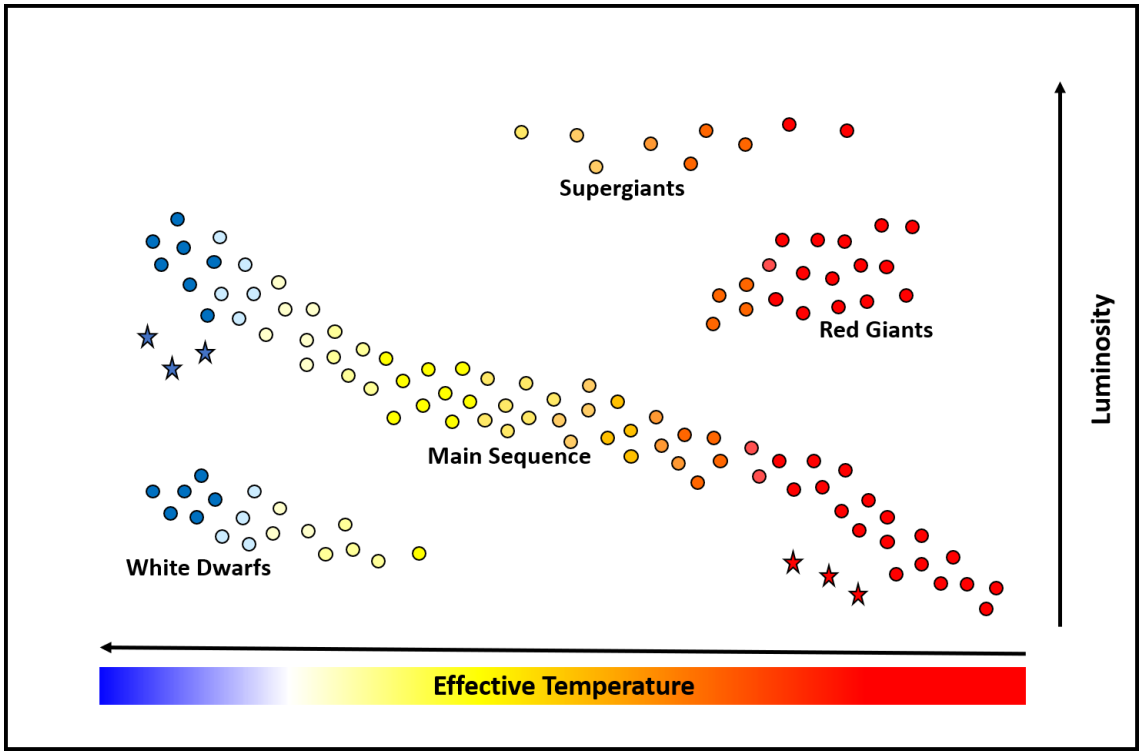

Figure 2: Hertzsprung-Russell diagram. Effective temperature and luminosity are plotted. Main-sequence stars with increasing mass line up from bottom right to top left. Red giants, supergiants, and white dwarfs are indicated. Subdwarfs are to be indicated "under" the corresponding main-sequence stars, cool subdwarfs (red stars) under the cool main-sequence stars, hot subdwarfs (blue stars) under the hot ones.

compressed (as the gas pressure that counteracts gravity becomes weaker). The associated rise in temperature is sufficient to keep hydrogen burning in a shell around the core, which steadily increases the core-helium mass. The envelope is expanded during this process, which leads to a decrease in T_{eff} despite the increasing core temperature, but in turn, due to the larger emitting surface, to an increase in luminosity. When this process reaches its maximum, the star has expanded up to 100 times and the luminosity has increased by about 1 000 times. The star becomes a red giant (Fig. 2). The helium core then reaches such a high density that it is in a degenerate state before fusion is ignited. The degeneracy means that pressure and temperature are no longer dependent on each other. When the helium fusion ignites, this leads to a rapid, further increase in temperature. Since the core is degenerate, however, this increase in temperature is not initially associated with an expansion. As a result, the temperature continues to increase in an unrestrained process until the degeneracy of the core has been lifted. This phenomenon is called "helium flash". After pressure and temperature are dependent on each other again, a huge expansion takes place, which is intercepted by the stellar envelope. Stable helium burning now takes place in the core, and hydrogen burning in a shell around the core. Eventually, the core helium is exhausted, having been converted into carbon and oxygen. Thereby the helium burning is shifted to a shell around the core. The star evolves along the so-called asymptotic giant branch (AGB), whereat both hydrogen- and helium-shell burning are operated. Due to the further increase in luminosity, the

star's outer layers are gradually repelled by a stellar wind. As the stellar surface shifts further inwards, $T_{\rm eff}$ increases. At some point, the star is hot enough to ionize the previously ejected shell, and a planetary nebula is created[3]. As the star has lost a large fraction of its mass through stellar winds, only the carbon-oxygen core (with $M_{\rm core} \lesssim 1.44\,M_\odot$, Chandrasekhar & Milne 1931) remains, surrounded by a thin layer of residual hydrogen and helium. The star becomes a white dwarf with $M \approx 0.6\,M_\odot$.

- Intermediate-mass stars with $2\,M_\odot \lesssim M_{\rm init} \lesssim 8\,M_\odot$ undergo similar evolution as the aforementioned low-mass stars. At the end of their red-giant phase, however, they ignite core-helium fusion without a helium flash, as, to their higher mass, the helium burning ignites before the core reaches a degenerate state. Again, stable helium burning now takes place in the core, and hydrogen burning in a shell around the core, and the further evolution along the AGB is the same as for low-mass stars. For stars with $M_{\rm init} \lesssim 4\,M_\odot$, the carbon-oxygen core will never become large and hot enough to ignite nuclear burning. For stars with $4\,M_\odot \lesssim M_{\rm init} \lesssim 8\,M_\odot$, further nucleosynthesis can lead to core compositions of oxygen, neon, and magnesium. In any case, as the star has lost a large fraction of its mass through stellar winds by then (a residual mass of $M_{\rm core} \lesssim 1.44\,M_\odot$ remains and also a planetary nebula is created), it becomes a white dwarf with $M \approx 0.6\,M_\odot$.

- High-mass stars with $M_{\rm init} \gtrsim 8\,M_\odot$ are able to ignite the fusion of other elements such as carbon, neon, oxygen, and silicon after helium burning in the core (which leads to further expansion and to the star becoming a supergiant, Fig. 2). After iron has formed in the stellar core, no further nuclear fusion can be carried out, since iron has the highest nuclear binding energy of all elements and therefore no more energy can be generated through fusion. The iron core can no longer withstand the gravitation and collapses, due to the larger residual mass of $M_{\rm core} \gtrsim 1.44\,M_\odot$, into a neutron star (Harding 2013) or, at even higher residual masses of about $M_{\rm core} \gtrsim 2.2\,M_\odot$ – $2.9\,M_\odot$ (Kalogera & Baym 1996), into a black hole (Barack et al. 2019), with the rest of the star being repelled in a huge explosion called a supernova.

Only single-star evolution was discussed here. In systems with two or more stars, the evolutionary scenarios can be more complicated and diverse.

[3]Planetary nebula is only a term for the phenomenon just mentioned and has, misleadingly, nothing to do with planets.

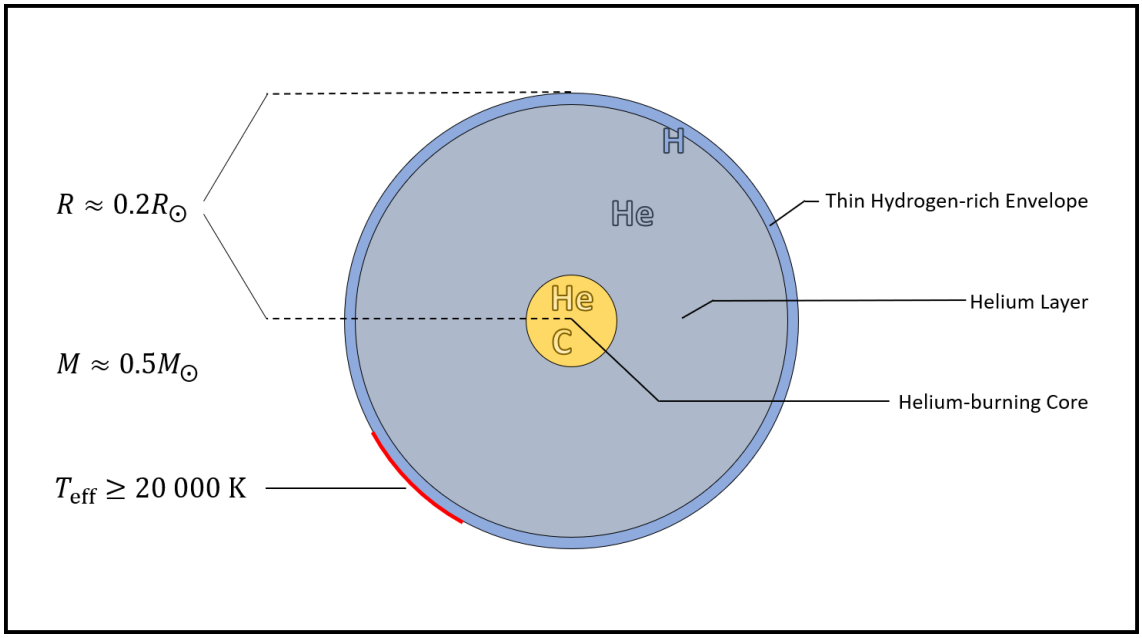

Figure 3: Inner structure of a hot subdwarf (not to scale).

2.2 Formation and properties of hot subdwarfs

Hot subdwarfs of the spectral types O and B (sdO and sdB) are core helium-burning stars with a thin, hydrogen-rich envelope, the mass of which is not sufficient to operate shell burning (Fig. 3). They have a canonical mass of $M \approx 0.5\,M_\odot$, radii of a few tenths of the solar radius, and effective temperatures $T_{\rm eff} \geq 20\,000\,\mathrm{K}$. Due to their smaller size, they are less luminous than main-sequence stars of the same temperature, and are therefore found on the HRD (Fig. 2) between the main sequence and the white dwarfs. The formation mechanism of hot subdwarfs was not mentioned in the previous subsection. This is because the formation and evolution of these stars are not yet fully understood. According to current understanding, several evolutionary mechanisms are possible. A detailed treatise on hot subdwarfs can be found in Heber (2016).

An evolutionary scenario for hot subdwarfs is the so-called "hot-flasher" scenario for red giants. Therefore, a look at the evolution of low-mass stars described in the previous subsection needs to be taken. Castellani & Castellani (1993) have shown that the helium flash can be delayed if the star has previously lost enough mass. If the helium flash occurs when the star is already on the way to becoming a white dwarf, this could generate a convection zone which might engulf almost the entire hydrogen envelope. Depending on the point in time at which the flash occurs, the mixing processes can result in hot subdwarfs with different helium, carbon, and nitrogen abundances (Lanz et al. 2004). Hence, they can be considered as the exposed cores of red giants.

A large fraction of sdB stars was found in close binary systems, which suggests that they also originate from these (Han et al. 2002, 2003). Two preferred scenarios are common-envelope evolution (CE evolution) or Roche-lobe overflow (RLOF). In both cases, an expanding red giant starts transferring material to its companion star.
If the companion star cannot accrete all of the material, a common envelope is created (CE scenario). Due to friction, the two stars approach until enough kinetic energy has

been transferred into the envelope to repel it. What remains is the the red giant core as an sdB star and the companion star, which has barely changed since this development takes place quite rapidly. Since both stars have approached due to the CE evolution, binary systems with short orbital periods (one to ten days) are created in this way.
If the companion star slowly accretes the delivered material, no common envelope is formed (RLOF scenario), but the mass transfer is finally sufficient to expose the core of the giant as an sdB. This creates binary systems with longer orbital periods (10 to 500 days).

A proposed evolutionary mechanism for individual sdO stars is the merging of two helium-rich white dwarfs (Webbink 1984). The formation of individual sdB stars remains an unsolved mystery to this day, whereby the latest research suggests that direct interaction with a companion star is always required (Pelisoli et al. 2020) for the necessary mass loss of the hot subdwarf's progenitor star (i.e., also in the hot-flasher scenario and for sdOs). However, questions remain unanswered, for example, what happened to the companion star just mentioned, whether a CE evolution really leads to an sdB and whether some sdBs (due to their low mass) are even able to operate helium fusion. In any case, further research is required to fully understand how hot subdwarfs are formed.

Hot subdwarfs are also very interesting objects in that their atmospheric composition is rather diverse. Some of them have peculiarities such as very high abundances of heavy elements (Rauch et al. 2010, Naslim et al. 2011, Wild & Jeffery 2017). It is consent that the element abundances in the atmosphere do not reflect those in the interior, but that heavy elements are transported to the surface by diffusion effects. On the one hand, a spectral analysis of hot subdwarfs helps to better understand these processes, on the other hand, these stars (especially those that are enriched in heavy elements) are suitable for investigating individual absorption lines of heavy elements.

3 Stellar spectra

The following section aims to show how energy, that is generated by nuclear fusion in the stellar core and heats the star, is ultimately emitted into space from the outer layers, called stellar atmosphere, in the form of electromagnetic waves (Fig. 7). Several processes are explained which, beginning with the formation of the black-body flux and ending with the observed stellar spectrum through a telescope, play an important role in understanding and evaluating observations (a detailed explanation can be found, e.g., in Unsöld 1968, or Hubeny & Mihalas 2014).

3.1 Black-body flux vs. stellar spectrum

Any energy a main-sequence star emits in the form of electromagnetic waves originates in the stellar core, where hydrogen is fused into helium. At very high pressure (thus also density ρ) and temperature T, the hydrogen nuclei overcome the Coulomb barrier (electromagnetic repulsion of the protons) and ultimately fuse to form a helium nucleus, which, due to the excess binding energy of a helium nucleus compared to four hydrogen nuclei, releases energy. Because the inner stellar layers are opaque, the photons created inside cannot escape. Rather, energy is transported by radiation and convection to the outer stellar layers, from where it is emitted into space. All the light that we can observe from a star thus emerges from these outer layers, called the stellar atmosphere.

When having a look at the spectral energy distribution emitted by the stellar photosphere, it is, as a first approximation, the flux of a black body:

$$W_\lambda(\lambda, T) = \frac{2\pi hc^2}{\lambda^5} \frac{1}{e^{\frac{hc}{\lambda k_\mathrm{B} T}} - 1} \quad ,$$

with h denoting Planck's constant, c the speed of light, λ the wavelength, and k_B the Boltzmann constant.

Observed stellar spectra differ from the black-body flux. On the one hand, effects in the stellar atmosphere itself (Sect. 3.2) lead to a modification of the spectrum, on the other hand, there are further effects until the light reaches the spectrograph (Sect. 3.3). The approximation, however, is still suitable for defining T_eff of the stellar atmosphere. T_eff denotes the temperature that a black body would need to have to radiate with the same total flux per area as the star. This can be determined by spectral analysis; for the Sun it is $T_\mathrm{eff} = 5\,777\,\mathrm{K}$ (Fig. 4).

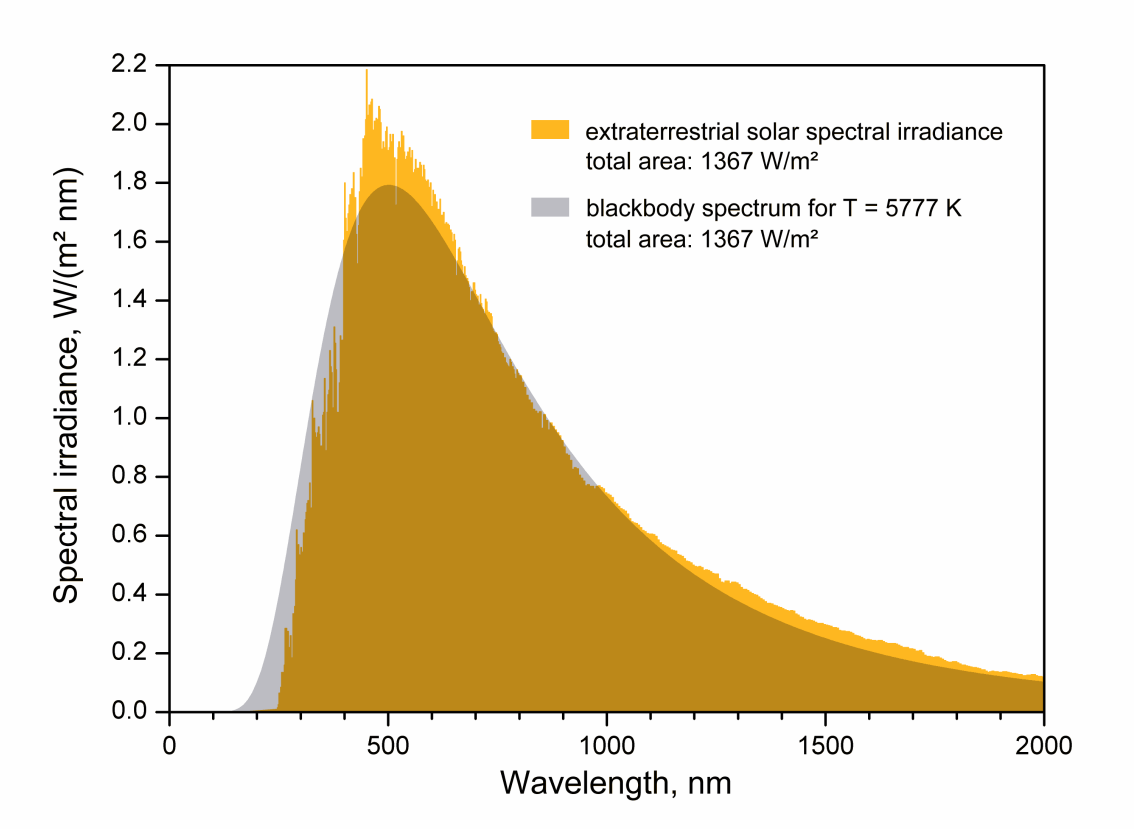

Figure 4: The Sun's observed spectral irradiance (yellow) compared to a black body with $T = 5\,777\,\mathrm{K}$ (grey).
Reference: M. Iqbal: An Introduction to Solar Radiation, Academic Press 1983, Table C1. CC BY-SA 3.0, https://commons.wikimedia.org/w/index.php?curid=758192

3.2 Absorption lines – shape and width

The deviation from the black-body flux to the real stellar spectrum is mainly due to absorption lines and edges caused by elements in the stellar atmosphere. A thorough understanding of the line absorption coefficient is necessary to be able to successfully perform a spectral analysis.
In simplified terms, absorption lines are created by a photon (with energy $E = h\nu$, with the photon's frequency ν) that is absorbed by an electron in the atomic shell, which is thereby raised to a higher energy level. It could be assumed that absorption lines are arbitrarily sharp since an atomic transition has a certain energy that corresponds to a fixed frequency (or wavelength). The following subsections will show that this is not the case (cf. Unsöld 1968).

3.2.1 Natural line shape and width

A classical consideration of the electron as a harmonic, damped oscillator driven by the oscillating electric field provides (with $\omega = 2\pi\nu$ the angular frequency of the photon, ω_0 the resonance frequency of the oscillation and the damping γ) as a profile function of the absorbed photon energy

$$\varphi(\omega) = \frac{\gamma}{(\omega_0 - \omega)^2 + (\gamma/2)^2} \quad . \tag{1}$$

This is a Lorentzian profile (Fig. 5). The line width (usually defined as the "Full Width at Half Maximum", FWHM) results from the damping constant, in this case, $\varphi(\omega = \omega_0 \pm \gamma/2) = 1/2\,\varphi_{\max}$, from which follows $\triangle\omega_{\mathrm{FWHM}} = \gamma$. Classically, $\gamma = \gamma_{\mathrm{cl}}$ can be derived from the theory of radiation damping. Therefore, it is (with $\lambda = c/\nu$)

$$\gamma_{\mathrm{cl}} = \frac{2e^2\omega_0^2}{3m_{\mathrm{e}}c^3} \Rightarrow \triangle\lambda_{\mathrm{FWHM,cl}} = \frac{2\pi c}{\omega_0^2}\,\gamma_{\mathrm{cl}} = \frac{4\pi e^2}{3m_{\mathrm{e}}c^2} \quad ,$$

with m_{e} denoting the electron mass and e the elementary charge. The line width is thus independent of λ_0, namely

$$\triangle\lambda_{\mathrm{FWHM,cl}} = 1.18 \times 10^{-4}\,\text{Å} \quad .$$

A quantum mechanical treatment arises from the uncertainty relation between energy and time ($\triangle E\ \triangle\, t = \hbar/2$) and from the fact that excited states in the atom only have a limited lifetime τ. This leads to a blurring of the level energies and thus also of the absorbed photon's frequency, it follows

$$\triangle\omega_{\mathrm{FWHM,qm}} = \gamma_{\mathrm{qm}} = 1/\tau_l + 1/\tau_u \quad ,$$

with the lifetimes τ_l, τ_u of the transition's lower and upper energy level. As can be seen, the quantum mechanical line width is dependent on the specific transition. Two examples of prominent hydrogen lines are

$$\begin{array}{ll} \mathrm{Ly}\,\alpha \text{ line } (\lambda = 1\,215.7\,\text{Å}): & \gamma_{\mathrm{qm}} = 0.31\,\gamma_{\mathrm{cl}} \\ \mathrm{H}\,\alpha \text{ line } (\lambda = 6\,562.8\,\text{Å}): & \gamma_{\mathrm{qm}} = 1.18\,\gamma_{\mathrm{cl}} \end{array} \quad .$$

3.2.2 Pressure broadening

In the stellar atmosphere, collisions between the particles repeatedly occur. There are several approaches to a correct description, such as impact theory and statistical theory. In case of the former, it is considered how the collisions lead to the oscillation in the absorbing atom being disturbed, which becomes noticeable in a phase shift of the oscillation. A Fourier-analysis of the oscillation's intensity spectrum leads to the profile function

$$\varphi(\omega) = \frac{1/\pi\tau}{(\omega_0 - \omega)^2 + (1/\tau)^2} \quad ,$$

where τ denotes the average time between two collisions. It is $\tau \sim N^{-1}$ (inversely proportional to the collision partner's density). τ can be expressed explicitly via the cross-section in terms of pressure, temperature, molecular weight, and particle density. This results in an approach for the angular frequency perturbance

$$\triangle\,\omega = \frac{2\pi\,C_n}{r^n} \quad , \tag{2}$$

where r is the distance between the interfering particle and the absorbing atom and the constant C_n can be determined experimentally or by quantum mechanical calculations.

Table 1: Parameter n (Eq. 2) of the impact theory and corresponding interaction.

n	Interaction	Collision partners
2	Linear Stark effect	Hydrogen (or hydrogen-like ions with a central coulomb field) and charged particles
3	Resonance broadening	Neutral atoms among each other
4	Quadratic Stark effect	Atoms (or ions) and charged particles
6	Van der Waals interaction	Metals and hydrogen

The exponent n is determined by the type of interaction (Table 1).
In the statistical theory of pressure effects, in contrast to the impact theory, the temporal course of the disturbance is ignored and, instead, the question is asked: "What is the probability of a frequency disturbance occurring in a certain range?". Especially for the linear Stark effect, Holtsmark's theory of statistical fields (Holtsmark 1919) provides a good approximation. Otherwise, it can be said that the calculation of the micro-field around the absorber is very time-consuming.

Both impact theory and statistical theory can be considered as borderline cases (for small and large distances to the absorber) of a correct description of pressure broadening. This, however, is only possible through complex quantum mechanical calculations.

3.2.3 Thermal Doppler broadening

The Doppler effect generally describes the compression or expansion of a signal by changing the distance between the source and observer during the signal's transmission. A well-known example is a change in the siren's frequency when an ambulance passes by. Similar to sound waves, the effect also occurs with electromagnetic waves. For calculation, only the radial velocity component v_{rad} between source and observer is relevant (the signal velocity is c). The following holds (non-relativistic)

$$c = \lambda\nu \Rightarrow \lambda = cT \quad ,$$

with period T. If the source and the observer move away from one another with a radial velocity v_{rad}, the wavelength increases by

$$\triangle\lambda = v_{\mathrm{rad}}T = \lambda \cdot \frac{v_{\mathrm{rad}}}{c} \tag{3}$$

or decreases when the source and the observer move towards each other, with the displacement $\triangle\lambda$. For the wavelength λ' perceived by the observer it is

$$\lambda' = \lambda \pm \triangle\lambda = \lambda\left(1 \pm \frac{v_{\mathrm{rad}}}{c}\right) \quad . \tag{4}$$

Since all particles that absorb photons in the stellar atmosphere move thermally, they perceive a photon's wavelength differently depending on their own velocity. The velocity distribution of the particles in the stellar atmosphere is a Maxwell-Boltzmann distribution. For the fraction $\frac{\mathrm{d}N}{N}$ of particles whose radial velocity lies in the interval $[\xi, \xi + \mathrm{d}\xi]$, the following applies

$$\frac{\mathrm{d}N}{N} = \frac{1}{\sqrt{\pi}} e^{-\left(\frac{\xi}{\xi_0}\right)^2} \frac{\mathrm{d}\xi}{\xi_0}$$

and thus for the mean velocity or the mean squared velocity

$$\overline{v} = \frac{2}{\sqrt{\pi}}\,\xi_0 \quad \text{or} \quad \overline{v^2} = \frac{3}{2}\xi_0^2 \quad .$$

Kinetic gas theory now gives the mean particle energy

$$\overline{E_{\text{kin}}} = \frac{1}{2}m\overline{v^2} = \frac{3}{2}k_{\text{B}}T \quad \Rightarrow \quad \xi_0^2 = \frac{2k_{\text{B}}T}{m} \tag{5}$$

with particle temperature T and mass m. Furthermore, it follows from Eq. 3 that $\frac{\triangle\lambda_{\text{D}}}{\lambda} = \frac{\triangle\omega_{\text{D}}}{\omega} = \frac{\xi_0}{c}$ and thus for the (normalized) line profile

$$\varphi(\omega) = \frac{1}{\sqrt{\pi}\,\triangle\,\omega_{\text{D}}}\,e^{-\left(\frac{\omega_0-\omega}{\triangle\omega_{\text{D}}}\right)^2} \quad , \tag{6}$$

which is a Gaussian profile (Fig. 5). The line's FWHM is

$$\triangle\lambda_{\text{FWHM,D}} = \triangle\lambda_{\text{D}} \cdot 2\sqrt{\ln 2} = \frac{\lambda}{c}\sqrt{\frac{8\,k_{\text{B}}\,T\ln 2}{m}} \quad .$$

In hot stellar atmospheres ($T \approx 50\,000\,\text{K}$) the Doppler broadening for a line in the range of $\lambda = 1\,000\,\text{Å} = 10^{-7}\,\text{m}$ is

for atomic hydrogen ($m = 1.66 \times 10^{-27}\,\text{kg}$): $\triangle\lambda_{\text{FWHM,D}} \approx 0.16\,\text{Å}$
for atomic oxygen ($m = 2.66 \times 10^{-26}\,\text{kg}$): $\triangle\lambda_{\text{FWHM,D}} \approx 0.04\,\text{Å}$

and therefore is significantly wider than the natural line width.

3.2.4 Microturbulence

In addition to the thermal movement of particles, a "turbulence" movement occurs in reality, which is caused by vortices of different sizes and can thus be well averaged over the entire stellar atmosphere. If a turbulence velocity ξ_{t} is introduced, Eq. 5 becomes

$$\xi_0^2 = \frac{2k_{\text{B}}T}{m} + \xi_{\text{t}}^2 \quad . \tag{7}$$

To be able to estimate the turbulence's influence on the line width, it makes sense to compare the summands in Eq. 7:

$m = 2.66 \times 10^{-26}\,\text{kg}$, $T = \ 5\,000\,\text{K}$: equal when $\xi_{\text{t}} \approx \ 2.3\,\text{km/s}$
$m = 1.66 \times 10^{-27}\,\text{kg}$, $T = \ 5\,000\,\text{K}$: equal when $\xi_{\text{t}} \approx \ 9.1\,\text{km/s}$
$m = 2.66 \times 10^{-26}\,\text{kg}$, $T = 50\,000\,\text{K}$: equal when $\xi_{\text{t}} \approx \ 7.2\,\text{km/s}$
$m = 1.66 \times 10^{-27}\,\text{kg}$, $T = 50\,000\,\text{K}$: equal when $\xi_{\text{t}} \approx 28.8\,\text{km/s}$.

3.2.5 Line shape

To finally determine the absorption line profile created in the stellar atmosphere, the above-mentioned effects have to be combined. Mathematically, this is realized by convolution of the Lorentzian and Gaussian functions. Let $\mathcal{L}(\omega,\gamma)$ be a Lorentzian profile and $\mathcal{G}(\omega,\sigma)$ a Gaussian profile (σ^2 is the variance of the Gaussian profile), then

$$\mathcal{V}(\omega,\gamma,\sigma) = (\mathcal{G} * \mathcal{L})(\omega) = \int \mathcal{G}(\tau)\mathcal{L}(\omega-\tau)\,\mathrm{d}\tau \tag{8}$$

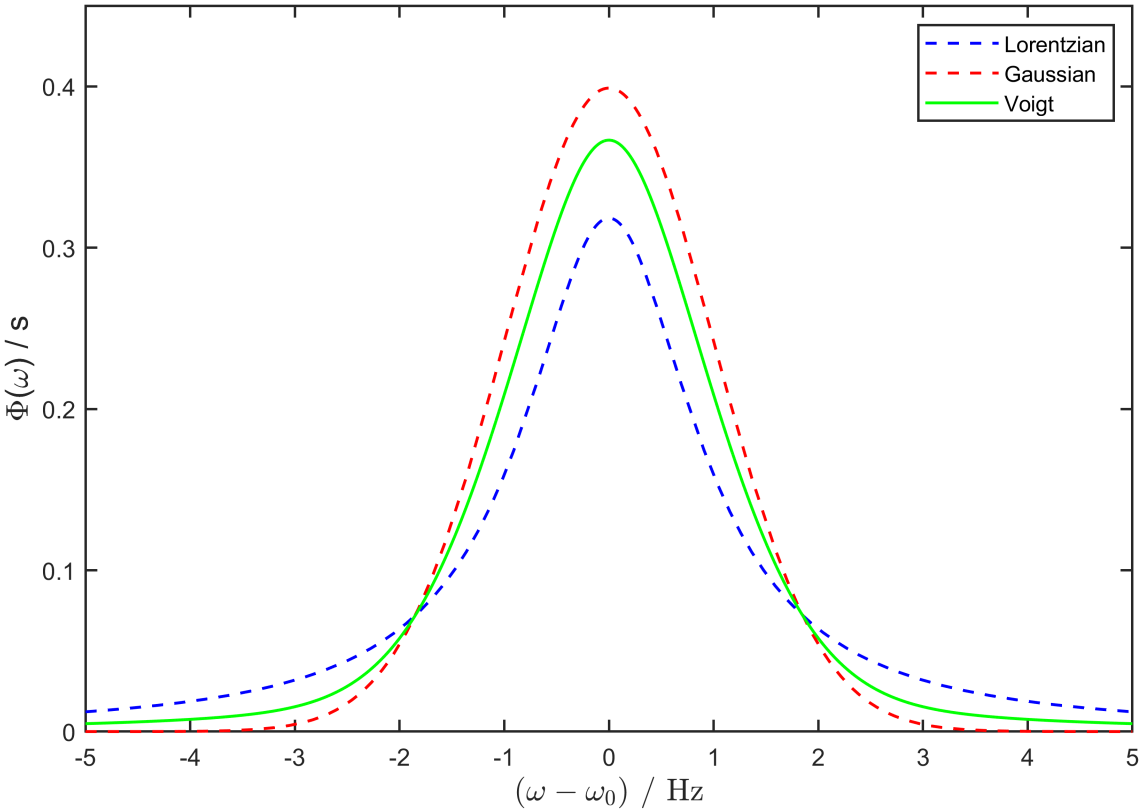

Figure 5: Example of a convolution of a Lorentzian and a Gaussian profile: The Voigt profile.

is the Voigt profile of the absorption line (Fig. 5). The integral in Eq. 8 cannot be evaluated analytically, but must be compiled numerically.
Finally, concerning the line shape, it can be noted that the line center takes on the shape of a Gaussian profile, i.e., is determined by thermal Doppler broadening and microturbulence, whereas the line wings are mainly determined by a Lorentzian profile, i.e., the natural line shape and pressure broadening.

3.2.6 Equivalent width

To describe the strength of an absorption line (or emission line), the equivalent width W_λ of the line is defined by (the radiation flux f is plotted as a function of the wavelength λ)

$$W_\lambda = \int (1 - f_\lambda / f_c)\, \mathrm{d}\lambda \tag{9}$$

where f_λ describes the absorption line flux and f_c the flux continuum. W_λ then indicates the width of a rectangle, which extends from the continuum flux to a flux of zero and has the same area as the original absorption line (Fig. 6; Carroll & Ostlie 1996). The equivalent width is suitable as a measure of the line strength since it is independent of broadening mechanisms and quantitatively indicates the portion of energy that is missing due to an absorption line at the corresponding location in the spectrum.

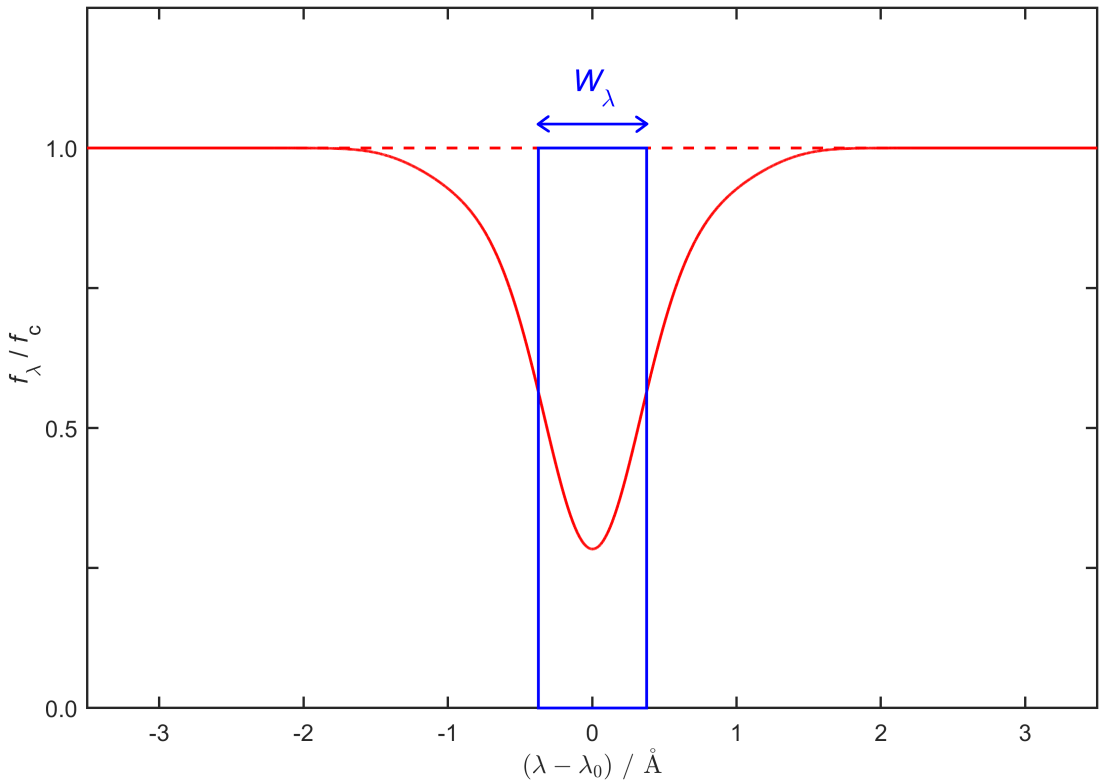

Figure 6: Equivalent width W_λ of an absorption line as the width of the blue rectangle which has the same area as the absorption line.

3.3 Impacts on a stellar spectrum

So far, effects have been considered that originate in the stellar atmosphere itself and therefore directly influence the absorption cross-section. The resulting spectrum is called emergent stellar spectrum and the corresponding flux is called astrophysical flux. Apart from these, however, other effects have an impact on the observed stellar spectrum (Fig. 7).

Rotational broadening

Stellar rotation leads to a broadening of spectral lines. Light coming from the one side of the star moving towards the observer is blue-shifted due to the Doppler effect, while light from the other side is red-shifted. When having a look at the stellar "disk" with the axis of rotation $\vec{\omega}$ as the perpendicular bisector of the sides and $\xi \in [0,R]$ the distance from the center to the edge (R is the stellar radius), the same applies as for thermal Doppler broadening

$$\triangle\lambda = \frac{\lambda}{c} \cdot \xi \cdot \omega \cdot \sin i \tag{10}$$

where the maximum displacement is obtained, when $\xi = R$. $v_{\mathrm{rot}} = \omega \cdot R \cdot \sin i$ then is, for the observer, the effective stellar rotational velocity at the equator with the angular velocity ω and the angle i between the axis of rotation and the line of sight (only v_{rot} can be determined by spectral analysis).
Since the entire surface of single stars is observed at once due to the limited resolving power of a telescope, parts of positive and negative Doppler shift contribute equally to the spectrum. The brightness distribution on the stellar "disk" is decisive for individual

spectral line broadening. Set $x = \frac{\xi}{R}$ ($x \in [-1,1]$ denotes the position on the stellar disk from $-R$ to R). The following then holds for the normalized intensity distribution $A(x)$ of a line

$$A(x) = \frac{\frac{2}{\pi}\sqrt{1-x^2} + \frac{\beta}{2}(1-x^2)}{1 + \frac{2}{3}\beta}$$

with limb darkening $\beta \in [0,\infty]$. For the sake of solvability, usually, no limb darkening is assumed, meaning $\beta = 0$, and thus $A(x)$ is simplified to

$$A(x) = \frac{2}{\pi}\sqrt{1-x^2} \quad , \tag{11}$$

so to a semi-ellipse. The FWHM of the line can be determined using Eqs. 10 and 11. It is

$$\triangle\lambda_{\mathrm{FWHM}} = \sqrt{3} \cdot \triangle\lambda = \sqrt{3} \cdot \lambda \cdot \frac{v_{\mathrm{rot}}}{c} \quad .$$

Examples for a line in the range of $\lambda = 1\,000\,\text{Å}$ are

in case of slow rotation ($v_{\mathrm{rot}} = 2\,\frac{\mathrm{km}}{\mathrm{s}}$): $\triangle\lambda_{\mathrm{FWHM}} \approx 0.01\,\text{Å}$
in case of relatively rapid rotation ($v_{\mathrm{rot}} = 40\,\frac{\mathrm{km}}{\mathrm{s}}$): $\triangle\lambda_{\mathrm{FWHM}} \approx 0.23\,\text{Å}$

and thus rotation, depending on its velocity, can have a significant influence on the line width.

Stellar radial velocity

The radial velocity v_{rad} of the star influences the observed spectrum. According to the Doppler effect, there is a red or blue shift of the entire spectrum. For the observed wavelength λ' follows with Eq. 3

$$\lambda' = \lambda \pm \triangle\lambda = \lambda\left(1 \pm \frac{v_{\mathrm{rad}}}{c}\right) \quad .$$

Interstellar absorption lines

After leaving the star, the photons penetrate the interstellar medium (ISM) that is consisting of gas and dust. A resulting effect is the appearance of additional absorption lines. Since the gas and dust clouds usually move with a different relative velocity v_{rad} than the star, these absorption lines can usually be distinguished from those of the emergent stellar spectrum due to their different wavelength shift.

Extinction

Another effect caused by the ISM is extinction of the spectrum. Due to absorption and scattering on gas or dust particles, a wavelength-dependent weakening of the light occurs. Extinction averagely describes all these processes that take place on the line of sight between observer and star. Since photons of smaller wavelengths are more strongly scattered, this process is also called reddening.
Extinction can be described by the color excess $E_{\mathrm{B-V}}$ (where B−V means the ratio of the calibrated stellar flux in the B band and the calibrated stellar flux in the V band). In the ultraviolet (UV) and optical range, Fitzpatrick's law (1999) is commonly used to calculate the extinction's impact on the spectrum. The value for $E_{\mathrm{B-V}}$ can either be taken from the

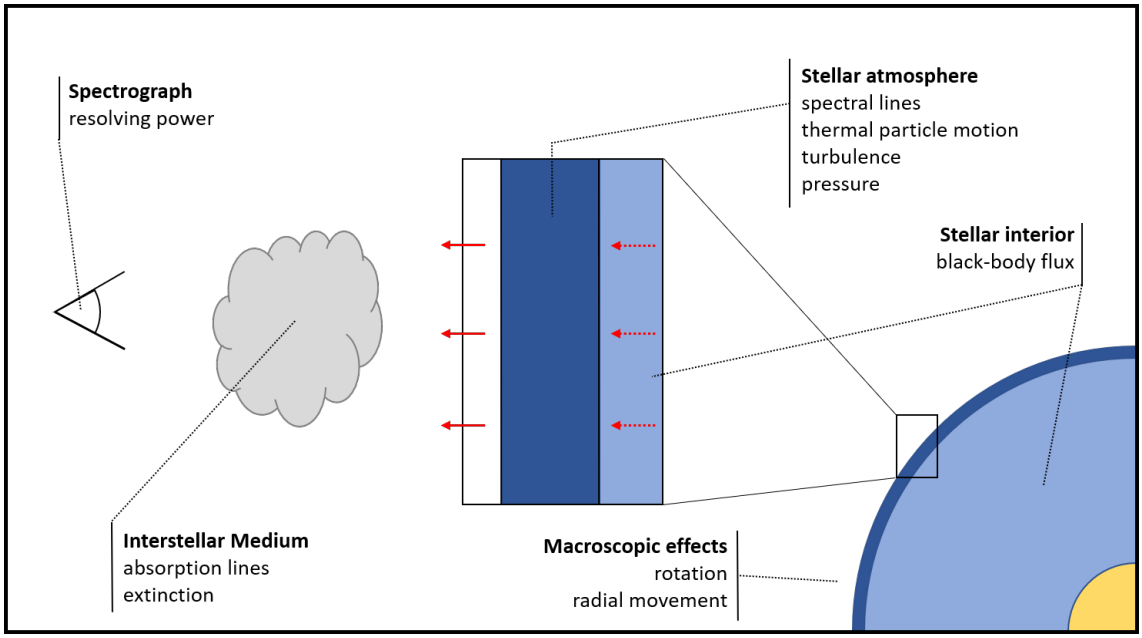

Figure 7: Formation and observation of stellar spectra.

galactic extinction curve (which is, however, inaccurate) or determined by spectral analysis. A uniform description of extinction for the entire electromagnetic spectrum does not currently exist, as there is still no consistent model for the interstellar dust composition. Depending on the spectral range, the effect of extinction can be enormous. Due to absorption edges (mainly hydrogen), e.g., the flux below $\lambda = 911\,\text{Å}$ is strongly absorbed, which has to be considered in spectral analyses (Sect. 7).

Finally, the light has to pass the spectrograph before the spectrum can be investigated. Since in the course of this work some interesting insights into the treatment of resolving power of spectrographs were obtained, Sect. 6 will be dedicated to this topic.

4 Modeling stellar spectra

In the previous section, the formation of stellar spectra was indicated. The basic idea of spectral analysis is to compare the observed spectrum with a theoretical, modeled spectrum. The model must consider all relevant physical effects as precisely as possible and formulate them numerically. This section describes the underlying method, shows which simplifications are made, and, ultimately, how this is implemented at the Institute for Astronomy and Astrophysics Tübingen (IAAT) within the Tübingen model atmosphere package.

Since the stellar atmosphere is an open system, it is not in thermodynamic equilibrium. In moderately hot and/or very compact stars, the mean free path lengths of the photons in the atmosphere are short enough that a local thermodynamic equilibrium (LTE) can be assumed for a small volume element. This generally holds for cool main-sequence stars ($T_{\mathrm{eff}} \leq 25\,000$ K) or old white dwarfs, i.e., spectral type B or later.
In hotter ($T_{\mathrm{eff}} \geq 25\,000$ K) or less compact stars, the mean free path lengths of the photons are large, so that LTE can no longer be assumed ("non-LTE", NLTE). In the simplification of LTE, model atmospheres for these stars would just no longer describe physical reality precisely enough, meaning an analysis with this simplification would not be reliable.
In the case of even hotter, less compact stars, the radiation pressure outweighs the hydrostatic pressure and there is a constant ejection of matter, known as stellar winds. The limit from which stellar winds occur is called the Eddington limit and it also depends on the chemical composition of the atmosphere (Fig. 8). For the stars examined in this work, static model atmospheres are sufficient.

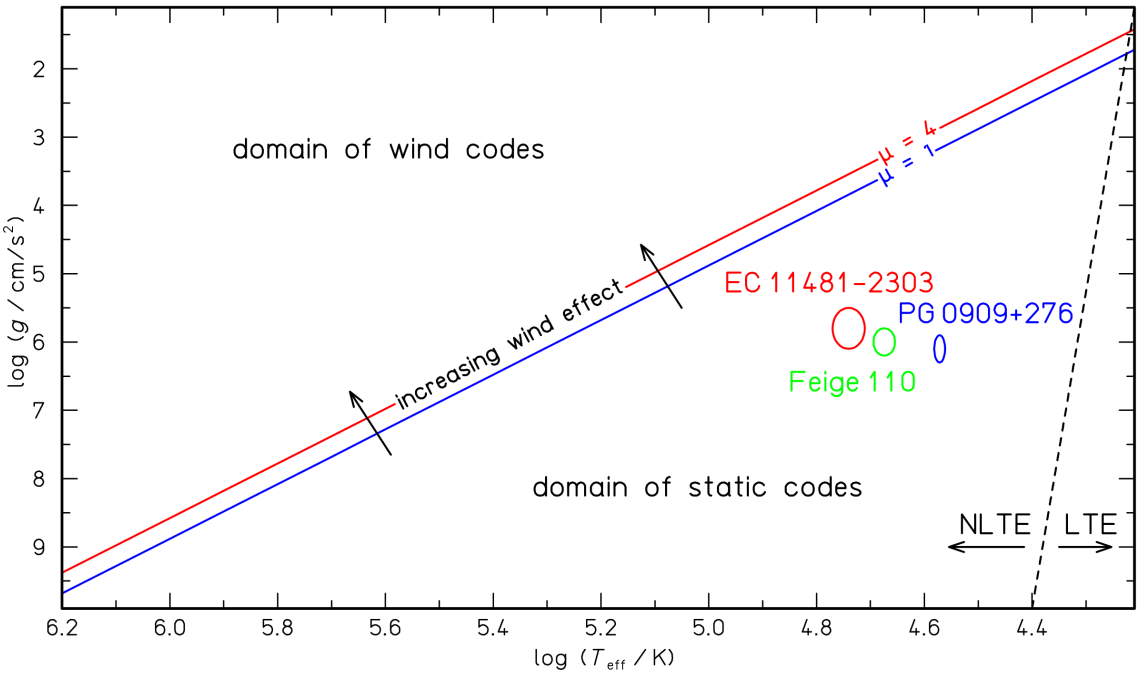

Figure 8: Approximate validity ranges of LTE and NLTE models and the Eddington limits for pure H ($\mu = 1$) and pure He ($\mu = 4$) atmospheres (μ denotes the mean atomic weight). The three stars examined in this work are marked with their error ranges.

4.1 Method

As described in Sect. 3, the stellar spectrum emerges from a thin atmospheric layer. In most stars, this layer can be considered as plane-parallel, since it only corresponds to a tiny fraction ($< 1\,‰$) of the stellar radius. Only in the case of more expanded stars, such as red giants, this simplification no longer applies. For the modeling (Hubeny & Mihalas 2014) of plane-parallel stellar atmospheres, the radiation-transfer equation

$$\mu \frac{\partial I_\nu(\mu)}{\partial \tau_\nu} = I_\nu(\mu) - S_\nu \tag{12}$$

(with the radiation intensity I_ν, the optical depth τ_ν, the angle between the direction of radiation and surface normal $\mu = \cos(\theta)$ and the source function S_ν) has to be solved together with the equations for hydrostatic and radiative equilibrium and the rate equations for atomic occupation numbers. The formal solution of the radiation-transfer equation is

$$J_\nu = \Lambda S_\nu \tag{13}$$

whereby J_ν denotes the angle-averaged intensity,

$$J_\nu = \frac{1}{2} \int_{-1}^{1} I_\nu(\mu)\, \mathrm{d}\mu \quad .$$

The source function is defined as

$$S_\nu = \frac{\eta_\nu}{\kappa_\nu} \quad , \tag{14}$$

with emissivity η_ν and opacity κ_ν. For the radiative equilibrium it is

$$\int_0^\infty \kappa_\nu (J_\nu - S_\nu)\,\mathrm{d}\nu = 0 \quad .$$

For hydrostatic equilibrium, the following equation holds

$$\frac{\mathrm{d}P}{\mathrm{d}r} = g\rho(r)$$

with pressure P, surface gravity g and the density $\rho(r)$ depending on the height r. In addition, particle number and charge conservation must be considered and the occupation numbers of the atomic levels have to be determined.
For LTE models, the source function is represented by $S_\nu \equiv B_\nu(T)$ and the occupation numbers can be determined by the Saha-Boltzmann equation (Saha 1920)

$$\frac{n_\mathrm{e} \cdot N_{i+1}}{N_i} = \frac{2}{\lambda_\mathrm{e}^3}\frac{Z_{i+1}}{Z_i} \cdot \exp\left(-\frac{\epsilon_i}{k_\mathrm{B}T}\right) \quad , \tag{15}$$

with the electron density n_e, the ion density of the i-th ion N_i, the thermal wavelength of the electron $\lambda_\mathrm{e} = \sqrt{\frac{h^2}{2\pi m_\mathrm{e} k_\mathrm{B} T}}$ (m_e is the electron mass), the partition function Z_i of the i-th ion, and the ionization energy ϵ_i. For NLTE models, the occupation numbers of a level i are determined by the rate equations

$$n_i \sum_{i \neq j} P_{ij} - \sum_{i \neq j} n_j P_{ji} = 0 \quad , \tag{16}$$

with the occupation number n_i of level i and the rate coefficients P_{ij} for the transitions between levels i and j. The coefficients have radiative and collisional components, that is $P_{ij} = R_{ij} + C_{ij}$. The radiative components are

$$R_{ij} = 4\pi \int_0^\infty \frac{\sigma_{ij}(\nu)}{h\nu} J_\nu \,\mathrm{d}\nu$$

and

$$R_{ji} = \left(\frac{n_i}{n_j}\right)^\star 4\pi \int_0^\infty \frac{\sigma_{ij}(\nu)}{h\nu} \left(\frac{2h\nu^3}{c^2} + J_\nu\right) e^{-h\nu/k_\mathrm{B}T}\,\mathrm{d}\nu$$

with $(n_i/n_j)^\star$ the Boltzmann LTE occupation ratio (Werner & Dreizler 1999) and the photon absorption cross-section $\sigma_{ij}(\nu)$. Dielectric recombination, where a free electron is captured and thus an excited state of the next lower ion is reached, and autoionization, its inversed process, must also be taken into account for the radiative components. The van Regemorter formula (van Regemorter 1962) is used for the collisional coefficients C_{ij} in the case of bound collisional transitions and the Seaton formula (Seaton 1962) is used for collisional ionization (in a hot plasma it is sufficient to consider collisions with electrons, as these occur much more frequently). The occupation numbers in the NLTE case are dependent on the radiation field, which creates a coupled, highly non-linear system of equations, the solution of which is significantly more complex and time-consuming than the LTE case.

To calculate η_ν and κ_ν, both emission coefficients for spontaneous and induced emission and absorption coefficients for several different processes must be known. In case of absorption lines it applies

$$\kappa_\nu = n_l\,\sigma(\nu)$$

with the occupation number of the lower level n_l and the aforementioned (photon) absorption cross-section $\sigma(\nu)$, which can also be expressed as

$$\sigma(\nu) = \sigma_0 \, \phi(\nu)$$

with the frequency-independent total cross-section σ_0 and the profile function $\phi(\nu)$, which was already dealt with in Sect. 3.2. Analogous to the natural line shape, σ_0 can be derived from consideration of a classical oscillator,

$$\sigma(\nu) = \sigma_0 \, \phi(\nu) = \frac{\pi e^2}{mc} \, \phi(\nu) = 0.0265 \, \phi(\nu) \, \mathrm{cm}^2 \, \mathrm{Hz} \quad .$$

Classically, σ_0 is not dependent on the specific atomic transition. Again, the correct value is provided by a quantum-theoretical consideration as to the specific transition between two energy levels l and u ("lower – upper") then applies

$$\sigma(\nu) = \sigma_{lu} \, \phi(\nu) = f_{lu} \, \frac{\pi e^2}{mc} \, \phi(\nu) \quad ,$$

with the oscillator strength f_{lu}, which provides the connection between the classical oscillator and the quantum-theoretical consideration. The oscillator strength varies from transition to transition and is either calculated or determined in the laboratory. Hence, the absorption coefficient is:

$$\kappa_\nu = n_l \, f_{lu} \, \frac{\pi e^2}{mc} \, \phi(\nu) \quad .$$

4.2 The Tübingen model-atmosphere package

The modeling mentioned above is implemented in stellar atmosphere codes. Among others, noteworthy examples are TLUSTY (Hubeny 2010) and PHOENIX (which is also used to calculate expanding atmospheres, such as novae or stellar winds, Hauschildt & Baron 1999). The Tübingen NLTE Model-Atmosphere Package (TMAP; Werner et al. 2003, Rauch & Deetjen 2003, Werner et al. 2012a) is used by the IAAT to solve the non-linear system of equations just presented for the radiation-transfer equation while fulfilling its constraints. It consists of a compilation of FORTRAN programs, has been developed since the 1980s and has been continuously expanded and improved. TMAP can be used to model plane-parallel, chemically homogeneous, or stratified atmospheres of hot, compact stars, whereby in principle the opacities of all elements (currently, model atoms are available for hydrogen to barium) can be implemented (more on this in the next section). The model atmosphere program is based on the Accelerated Lambda Iteration (ALI, Cannon 1973; Scharmer 1981; Werner & Husfeld 1985) method, where the radiation field is iterated while the rate equations are solved simultaneously. For this purpose, an approximate Λ operator $\Lambda^\star$ is inserted into the formal solution of the radiation-transfer equation, and Eq. 13 becomes (at the n-th iteration)

$$J_\nu^n = \Lambda^\star \, S_\nu^n + (\Lambda - \Lambda^\star) \, S_\nu^{n-1} \tag{17}$$

with the correction term $(\Lambda - \Lambda^\star) \, S_\nu^{n-1}$, which is computed from the previous iteration. The iterations are carried out for typically 90 depth points to appropriately represent the atmospheric structure. If a diagonal operator $\Lambda^\star$ is chosen, the problem is simplified in that the source function S_ν^n becomes local, i.e., is no longer dependent on other depth

points. However, it is better to choose $\Lambda^\star$ tridiagonal, so that adjacent depth points are included, which leads to a significant acceleration of convergence. Either way, the equation for the radiation field can now be solved in an outer iteration cycle, while the secondary conditions are dealt with in an inner cycle, which is is basically a Newton-Raphson method (Hubeny & Lanz 1992). Convergence is achieved when the greatest change in one of the calculation's variables does not exceed a predefined value, i.e., (let x be the variable with the greatest change)

$$| 1 - x^n / x^{n-1} | \leq \varepsilon$$

applies, whereby $\varepsilon \approx 10^{-4}$ is typically chosen. Then it is approximately $S_\nu^n \approx S_\nu^{n-1}$, and Eq. 17 converges to the exact solution Eq. 13.
The ALI method allows stellar atmosphere calculations to be carried out with a certain number of NLTE atomic levels. The absorption and emission coefficients are therefore calculated for a frequency grid. In practice, one ends up with a maximum of a few hundred to a few thousand NLTE levels in order to consider an acceptable number of frequency points while keeping the computing time within certain limits.

Apart from the procedure that has just been described, the program input, in particular the model atoms of the elements the stellar atmosphere consists of, plays a crucial role in realistic modeling.

4.3 The Tübingen model-atom database

"Garbage in, garbage out" appropriately describes the concept that an imprecise or faulty input – no matter how good a computer program may be – also leads to an inaccurate or incorrect result. In the case of TMAP, the accuracy of the atomic data used has a major impact on the model atmosphere and thus on the success of a spectral analysis. For this reason, work continues to this day to improve and expand atomic data, which is accessible in databases such as the Atomic Spectra Database of the National Institute of Standards and Technology[4] (NIST, Kramida et al. 2020), the Opacity Project[5] (OP, Seaton et al. 1994) or Kurucz's line lists[6] (Kurucz 1991, 2011).
The Tübingen Model-Atom Database (TMAD), which is part of the German Astrophysical Virtual Observatory (GAVO), is publicly accessible on the Internet (Müller-Ringat 2013), whereat the data has a format that can be used directly by TMAP but is also compatible with other large databases such as NIST or OP. TMAD contains model atoms from hydrogen to barium (Fig. 10), in several ionization stages (the currently available elements and ions can be found on the TMAD homepage). The ions that are relevant for specific model calculations can thus be loaded from TMAD. The individual model atoms contain data such as level energies, cross-sections, statistical weights, etc., and can become very complex (with increasing atomic number), which is well represented in a Grotrian diagram that shows the atomic levels and transitions (Fig. 9). Finally, it should be mentioned that there are two different sets of model atoms of each element. One for calculating a model atmosphere, and one for calculating a model spectrum. The latter also includes the fine structure splitting of the levels and lines.

[4] `https://www.nist.gov/pml/atomic-spectra-database`
[5] `http://cdsweb.u-strasbg.fr/OP.htx`
[6] `http://kurucz.harvard.edu`

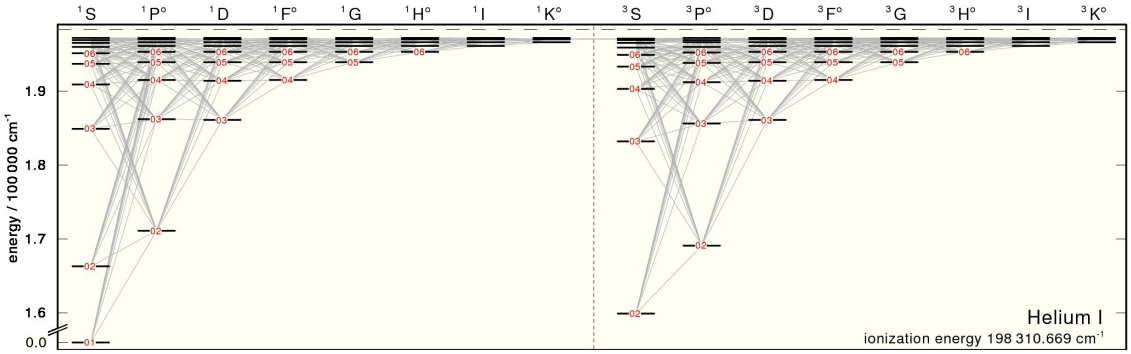

Figure 9: Grotrian diagram of He I with the singlet and triplet electron systems (left and right, respectively). The level energies (horizontal, thick lines) and atomic transitions were taken from NIST, the model atoms from TMAD.
`Reference: http://astro.uni-tuebingen.de/~TMAD`

So far, a total of several thousand NLTE levels are available for calculating model atmospheres. The so-called iron-group elements (calcium – nickel[7], Fig. 10) have to be implemented differently in TMAP, because their respective electron orbits overlap due to partially filled 3d and 4s shells, creating a band structure that leads to an abundance of levels with similar energy and to several hundred million atomic transitions. For taking into account all transitions without exceeding the number of NLTE levels TMAP can operate with, a statistical procedure is required which significantly reduces the number of NLTE levels and transitions. This is presented in the next subsection.

4.4 Implementation of the iron-group elements

The statistical procedure originally developed by Anderson (1985) to reduce the level and transition count of iron-group (IG) elements was implemented in TMAP by Dreizler & Werner (1993). In 1999, the code that produces model atoms for IG elements was rewritten by Deetjen and called Iron Opacity and Interface Code (IrOnIc, Rauch & Deetjen 2003). In the 1990s, first investigations of the influence the IG elements have on a stellar atmosphere showed a line-blanketing effect, where the radiation flux is reduced by additional absorption lines of the IG elements, mainly in the X-ray and UV range. However, since the overall flux is conserved, deeper layers heat up, which leads to a change in the atmospheric structure.
IrOnIc comprises a compilation of FORTRAN programs. The method's principle consists of dividing the energy range between the ground state and the ionization energy of an IG ion into several (typically seven) bands. All real levels l within one band contribute to the energy E_L and to the statistical weight G_L of a generated super level L, which then can be considered as a single NLTE level. It is

$$E_L = \sum_{l \in L} E_l g_l^\star \Big/ \sum_{l \in L} g_l^\star \quad ,$$

$$G_L = e^{E_L / k_\mathrm{B} T^\star} \cdot \sum_{l \in L} g_l^\star \quad ,$$

[7] In this work, the term "iron-group elements" is used for the elements Ca – Ni (in astrophysics it is sometimes used for Cr – Ni) due to their similar treatment in relation to spectral analysis. This term shall not be confused with group eight in the periodic table, wich contains Fe, Ru, Os, and Hs.

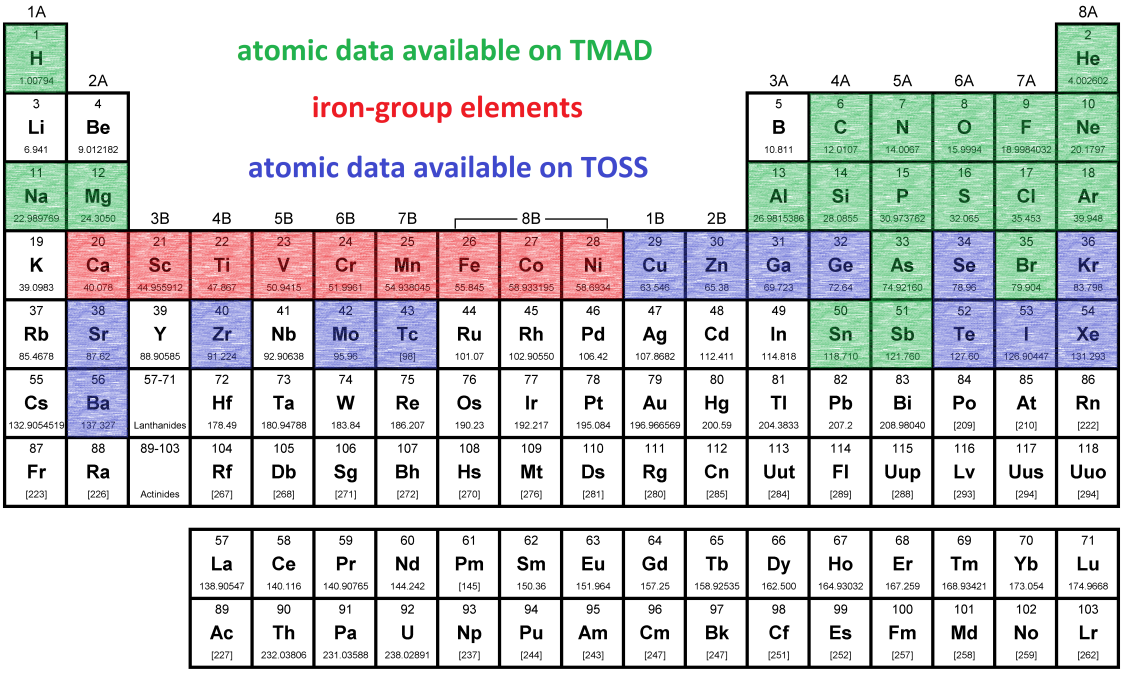

Figure 10: Periodic table of the elements. Elements of which model atoms are available on TMAD (as of May 2021) are colored green, the iron-group elements calcium to nickel are colored red, and elements of which model atoms are available on TOSS (Sect. 4.5) are colored blue.
`Reference: Helmenstine, Todd. (2020, August 25).`
`Basic Printable Periodic Table of the Elements.`
`https://www.thoughtco.com/printable-periodic-table-of-the-elements-608834`

$$g_l^\star = a_s g_l \, e^{E_l/k_\mathrm{B}T^\star} \quad . \tag{18}$$

E_l and g_l are the energy and statistical weight of the real atomic level l, and $T^\star$ is derived from the Saha-Boltzmann equation and is the temperature at which the respective ionization stage is dominant.
a_s is the ratio of the respective element's abundance to that of the most common IG element and is only unequal to one if a generic model atom is created. IrOnIc enables combining several IG elements in a single model atom with a few bands, whereby the respective elements' cross-sections are coadded. This is very useful for examining the influence of several IG elements on the stellar atmosphere with little computing time (e.g., line blanketing) but is not suitable for carrying out high-quality analyses of individual IG elements.
Analogous to Sect. 4.1, cross-sections or coefficients for calculating the radiation field or the occupation numbers must be determined for the IG elements. The photon absorption cross-section for transitions between two bands L and U (Fig. 11) is given by

$$\sigma_{LU}(\nu) = \sigma_0 \sum_{l\in L; u\in U} g_l^\star f_{lu} \, \phi(\nu_{lu} - \nu) / \sum_{l\in L} g_l^\star \quad , \tag{19}$$

where $\sigma_0 = \pi e^2/mc$ denotes the classical oscillator cross-section as above, f_{lu} the oscillator strength of the transition, and $\phi(\nu_{lu} - \nu)$ the line profile derived in Sect. 3.2. The method just mentioned allows all real transitions with their correct wavelength and cross-section to be taken into account when determining the total opacity. Since the $\sigma_{LU}(\nu)$ must be

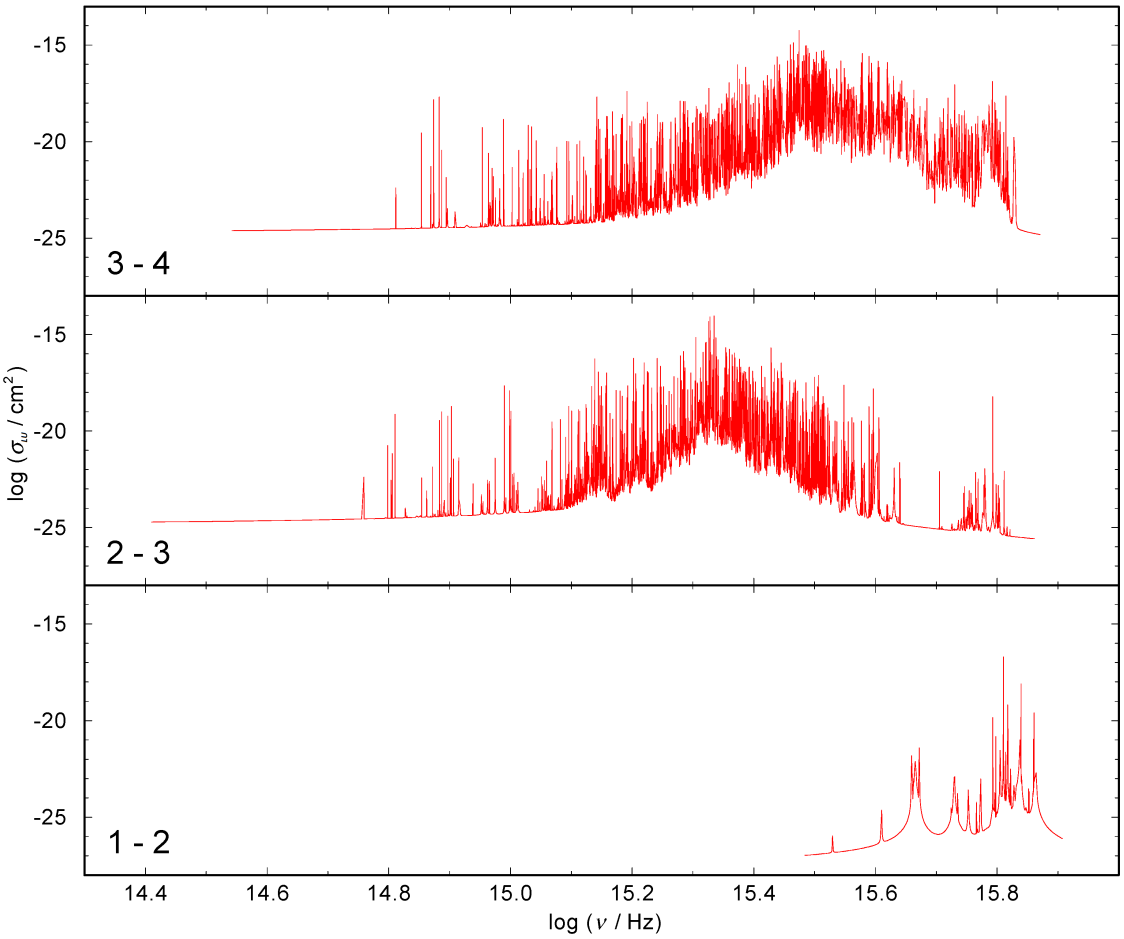

Figure 11: Examples for line-absorption cross sections σ_{LU} of a generic model ion (built from all IG elements, ionization stage V) for three inter-band transitions, shown from *bottom* to *top*: between bands 1 (super level created from 794 individual levels) and 2 (1 726), 2 and 3 (2 762), and 3 and 4 (4 074). The σ_{LU} are coadded from 224, 8 445, and 56 424 individual lines, respectively.

known before the model atmosphere is calculated, the actual temperature and electron density cannot be used. Therefore, $\sigma_{LU}(\nu)$ is determined for $T_{\rm Line} = 3/4\,T_{\rm eff}$ and two different electron densities and then interpolated to the atmospheric values. Intra-band transitions also occur when neglecting parity. For these, the cross-section σ_{LL} is determined analogously. For photoionization, cross-sections that have already been calculated (for example by the OP) can be used and coadded. Otherwise, hydrogen-like cross-sections are used.
The radiative coefficients R_{ij} for the occupation numbers are also computed with σ_{LU}. For the collisional coefficients C_{ij}, the Seaton formula (collisional ionization) and the van Regemorter formula (collisional bound-bound transitions) are used analogously to Sect. 4.1.

Just like TMAD, the IrOnIc service, in this case in a simplified version, is publicly accessible via the Internet with the Tübingen Iron-Group Opacity - IrOnIc WWW Interface (TIRO[8], Müller-Ringat 2013). Inquiries for IG elements are sent to IrOnIc via TIRO and

[8] `http://astro.uni-tuebingen.de/~TIRO`

Table 2: Calculated oscillator strengths of trans-iron elements, verified in observed spectra.

Element	Atomic number	Ionization stages				Reference
		IV	V	VI	VII	
Copper	29	×	×	×	×	Rauch et al. 2020
Zinc	30	×	×			Rauch et al. 2014b
Gallium	31	×	×	×		Rauch et al. 2015
Germanium	32		×	×		Rauch et al. 2012
Selenium	34		×			Rauch et al. 2017b
Krypton	36	×	×	×	×	Rauch et al. 2016b
Strontium	38	×	×	×	×	Rauch et al. 2017b
Zirconium	40	×	×	×	×	Rauch et al. 2017a
Molybdenum	42	×	×	×	×	Rauch et al. 2016a
Tellurium	52			×		Rauch et al. 2017b
Iodine	53			×		Rauch et al. 2017b
Xenon	54	×	×	×	×	Rauch et al. 2017a
Barium	56		×	×	×	Rauch et al. 2014c

after calculation, the URL for downloading the model atoms in TMAP format is sent to the user by email.

4.5 Atomic data sources

As aforementioned, atomic data plays a crucial role in the successful calculation of NLTE model atmospheres. On the one hand, exact data on individual absorption lines is required to compute them in synthetic spectra. On the other hand, cross-sections for entire model atoms are necessary, even outside the investigated spectral range, to precisely determine the occupation numbers and thus the chemical composition of the atmosphere or to take into account effects that influence the rest of the spectrum (e.g., line blanketing for the IG elements). An overview of available data sources and their completeness, but also the current state of research and occurring difficulties shall be presented at this point.

The databases already mentioned, apart from TMAD, are the NIST database, that of the OP and Kurucz's line lists, along with other noteworthy sources such as the Vienna Atomic Line Database (VALD[9]) and the Iron Project (IP[10]), which is an extension and refinement of the OP. Taking these databases into account, almost complete model atoms with relatively well evaluated level energies and cross-sections can be constructed for most elements of atomic number $Z \leq 19$ (Wiese et al. 1996).
For heavier elements, the more complex atomic structure complicates calculations. In many cases, either a reliable evaluation of existing data or laboratory measurements are lacking. As, for example, ten trans-iron elements' ($Z \geq 29$, TIEs) absorption lines were discovered in the white dwarf RE 0503–289 spectrum (Ga, Ge, As, Se, Kr, Mo, Sn, Te, I, and Xe; Werner et al. 2012b) in 2012, only the Kr and Xe abundances could be deter-

[9] `http://vald.astro.uu.se`
[10] `https://www.usm.uni-muenchen.de/people/ip/iron-project.html`

Table 3: Number of LIN and POS lines of IG elements in Kurucz's database.
`Reference: Kurucz 2018`

Element	Ions	LIN lines	POS lines	POS/LIN [%]
Calcium	I – IX	2 692 026	34 396	1.28
Scandium	I – IX	3 591 425	24 776	0.69
Titanium	I – IX	9 265 499	52 960	0.57
Vanadium	I – IX	14 629 831	54 505	0.37
Chromium	I – IX	20 642 560	144 814	0.70
Manganese	I – IX	26 107 668	81 588	0.31
Iron	I – X	61 520 551	314 580	0.51
Cobalt	I – IX	76 559 695	71 064	0.09
Nickel	I – X	114 092 797	119 767	0.11
Σ		329 102 052	898 450	

mined, since oscillator strengths were only available for these elements' ionization stages. From then on, the IAAT, together with international collaborators, continuously calculated oscillator strengths for TIEs, which are publicly available via the Tübingen Oscillator Strengths Service (TOSS[11]). Currently (as of May 2021) data on 14 TIEs is available on TOSS, which contains the ionization stages IV – VII (in spectral analysis, positively charged ions are denoted by Roman numerals, the neutral atom means stage I). The calculation of oscillator strengths allowed determining element abundances in hot stars (Table 2; except for Tc, which has not yet been identified in hot stellar atmospheres). Research is currently being carried out on further element data, e.g., bromine and antimony were discovered in a white dwarf for the first time in 2018 (Werner et al. 2018). A pseudo-relativistic Hartree-Fock method (HFR; Cowan 1981) with core-polarization corrections (CPOL) was used to calculate the oscillator strengths (and transition probabilities) of all the TIEs mentioned above (the HFR+CPOL method can be found in Quinet et al. 1999 and 2002, for example). The quantum-theoretically calculated atomic data could be verified with the help of high-quality spectral analyses (Table 2), in which the models calculated with new data could be compared to the observed stellar spectra and, in addition to determining the element abundances, individual absorption lines could also be identified. The hot stellar atmospheres thus served as laboratories for experimental verification of the calculated atomic data.

In the case of the IG elements calcium – nickel, atomic data is available to a great extent from NIST, the IP, and Kurucz's line lists, the latter containing by far the most data. For example, the Kurucz database contains cross-sections (or gf values) for a total of more than 850 million absorption lines, called LIN lines, of which approx. 330 million belong to the IG elements (ionization stages I – X; Kurucz 2018). Some of the calculated lines' wavelengths could be verified experimentally, hence called POS (positively identified wavelength) lines. The measurements took place either by complex spectral analyses in a laboratory or by analyses of high-quality stellar spectra. For the IG elements, around 900 000 POS lines are available, which is about 0.3 % of the LIN lines (Table 3). Kurucz uses a semi-empirical method (Kurucz 1973) to calculate the weighted oscillator strengths gf.

[11] `http://dc.g-vo.org/TOSS`

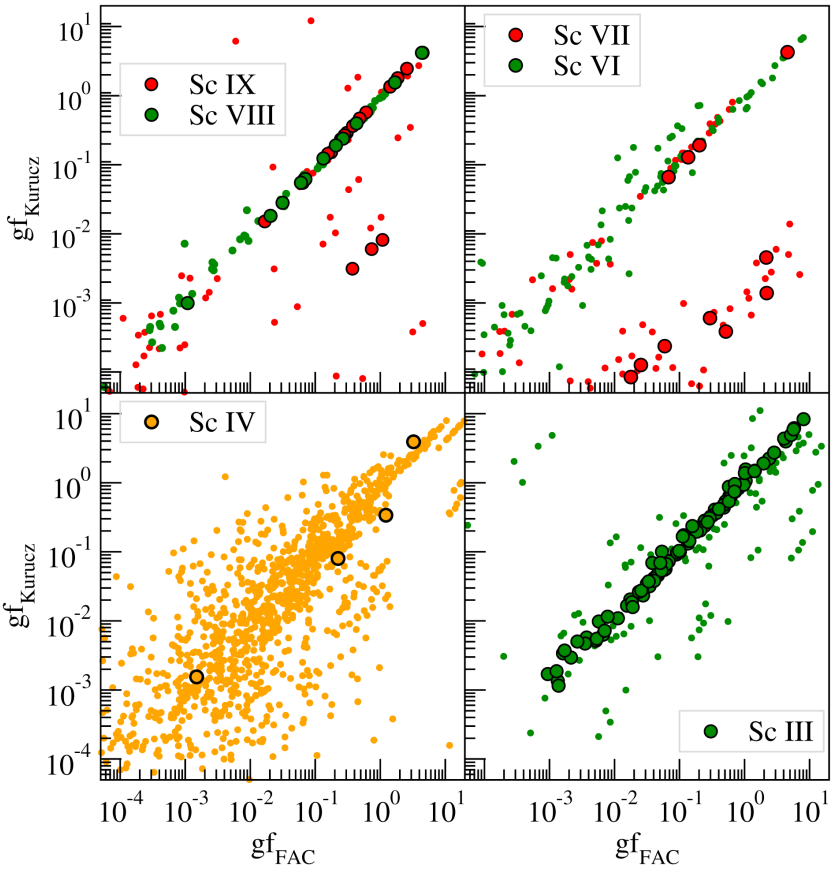

Figure 12: Comparison of the weighted oscillator strengths gf of different scandium ions, calculated by Kurucz and with the flexible Atomic Code (FAC).
`Reference: Massacrier, G. & Artru, M.-C. 2012`

In practice, LIN lines are not suitable for evaluating individual absorption lines in stellar spectra, since the wavelength uncertainties are too large. Nevertheless, they are important to obtain a realistic overall opacity for model atmosphere calculations and must therefore also be taken into account. Only POS lines can be used to evaluate and determine individual lines, i.e., to calculate synthetic spectra. Nevertheless, uncertainties can also arise here. For example, it was shown that depending on the method, large fluctuations can occur in the calculated oscillator strengths. This has already been evaluated for scandium (Massacrier, G. & Artru, M.-C. 2012; Fig. 12) and some large statistical and systematic deviations (about a factor of 1 000 for Sc IV) were found.
A detailed evaluation of the IG elements' oscillator strengths has not yet been carried out, which is partly due to the amount of work involved in this project. To investigate the ionization stages III – VI alone, which would dominate in hot stars with surface temperatures of several tens of thousands of degrees (provided that these stars are rich in IG elements), several thousand absorption lines would have to be investigated individually. However, this would be important to assess the reliability of the POS lines (and also the quality of the LIN lines, as the gf calculation method is the same) in the Kurucz database and to be able to reduce their inaccuracy. In a classic laboratory on Earth, it can be expensive to generate a plasma of the corresponding temperature and density (this can be derived from

Table 4: IG-element ionization energies of stages III – VI.
`Reference: Sansonetti et al. 2013`

	Ionization energy / eV			
Element	III	IV	V	VI
Calcium	50.9	67.3	84.5	108.8
Scandium	24.8	73.5	91.7	110.7
Titanium	27.5	43.3	99.3	119.5
Vanadium	29.3	46.7	65.3	128.1
Chromium	31.0	49.2	69.5	90.6
Manganese	33.7	51.2	72.4	95.6
Iron	30.7	54.8	75.0	99.1
Cobalt	33.5	51.3	79.5	102.0
Nickel	35.2	54.9	76.1	108.0

the Saha-Boltzmann equation, Eq. 15, with the help of the ionization energies, Table 4) for long enough to obtain a sufficient number of spectral lines from the investigated ions.

This work aims to investigate high-resolution spectra of three hot, compact stars that exhibit high abundances of the aforementioned IG elements' ions. For this purpose, a model spectrum is created and analyzed for each of the three stars using the method shown in Sects. 3 and 4. By comparing the observed line strengths with the modeled ones, a method is being developed enabling to evaluate the quality of the corresponding weighted oscillator strengths gf. Then, statistical and systematic uncertainties of the line strengths are checked and strong, isolated absorption lines with good agreement between models and observations are found, which are recommended to be used for the determination of element abundances. Additionally, by investigation of stellar spectra, line-broadening mechanisms and atmospheric properties can be investigated inclusively.

5 Observations

For a successful absorption-line analysis of the investigated ions, these lines must be available in sufficient number and quality. For this, in turn, the following requirements need to be placed on the observed spectra:

- The observed stars must exhibit high abundances of the IG elements to prominently show IG-element absorption lines in their spectra. Weaker lines could then also be examined in this way.
- The observed stars' effective temperatures must be in a range in which the ionization stages III – VI of the IG elements (due to already available atomic data) dominate so that their absorption lines are the best observable.
- The observation must cover the spectral range in which the majority of the absorption lines is expected. Ideally, this is the range where the stars show their maximum flux.
- The quality of the spectrum must be high enough to reduce the uncertainty of the line analysis to a sufficient level.

In the following, the observed stars are introduced, then the spectrograph is presented, and finally, the observations are presented.

Table 5: Effective temperature and surface gravity of our three program stars, determined by spectral analysis.

Star	Type	$T_{\rm eff}$ / K	log (g / cm/s^2)	Distance[d] / pc
EC 11481–2303[a]	sdO	$55\,000 \pm 5\,000$	5.8 ± 0.3	294 ± 4
Feige 110[b]	sdOB	$47\,250 \pm 2\,000$	6.0 ± 0.2	271 ± 4
PG 0909+276[c]	sdB	$37\,290 \pm 640$	6.1 ± 0.2	279 ± 5

References: [a]Ringat & Rauch 2011; [b]Rauch et al. 2014a; [c]Wild & Jeffery 2018; [d]calculated from Gaia EDR3 parallaxes (Gaia Collaboration et al. 2020, https://gea.esac.esa.int/archive)

5.1 Three hot subdwarfs: EC 11481–2303, Feige 110, and PG 0909+276

Hot subdwarfs were already introduced in Sect. 2. They are core helium-burning stars of the spectral types O and B. Some hot subdwarfs exhibit very high atmospheric abundances of heavy elements. This is due to diffusion effects – according to current understanding (Heber 2016) to an interplay of radiative levitation and gravitational settling. In terms of temperature and compactness (expressed by $T_{\rm eff}$ and g), hot subdwarfs are in an ideal range for the enrichment of these heavy elements in the atmosphere.
Since spectral analyses have already been carried out for all three stars, the relevant parameters are already known (Table 5). They all show high IG-element abundances. Besides, the selected stars' effective temperatures have been chosen such they exhibit a flux maximum in the UV range, where the bulk of the examined ions' absorption lines emerges. The different effective temperatures span a range of $\approx 18\,000$ K. This leads to a shift of the dominant ionization stages from star to star, allowing to evaluate all stages III – VI more precisely.

EC 11481–2303 is an sdO-type subdwarf, which was discovered in the *Edinburgh-Cape Blue Object Survey* (Kilkenny et al. 1997) and initially identified as a DA white dwarf. With $m_{\rm V} = 11.76$, it is one of the brighter stars in this catalog. It is located in the constellation Cup and is not visible to the naked eye. Also, a companion star could be identified at a distance of 6.6 arc seconds.
A first spectral analysis was carried out by Stys et al. (2000), performed with LTE models. Optical South African Astronomical Observatory (SAAO[12]) spectra and International Ultraviolet Explorer (IUE; Macchetto 1976) spectra in the UV range were modeled with only hydrogen and helium. With the help of optical spectra, $T_{\rm eff} = 41\,790$ K, $\log g = 5.84$, and the atomic number ratio He/H = 0.014 could be determined. However, the peculiarly flat slope of the UV spectra could not be modeled successfully with these parameters. Nevertheless, by analyzing the interstellar hydrogen Lyman α line at $\lambda = 1\,215$ Å and by determining the extinction, the distance could be determined to about 500 pc, since a nearby star with the same interstellar H I column density $N_{\rm H\,I}$ also exhibits this distance. The absolute magnitude $M_{\rm V} = 3.2$ could thus be determined. Since this is typical for a hot subdwarf, the star has been reclassified as such.
To investigate the cause of the flat UV slope, further research was carried out. Rauch et al.

[12] https://www.saao.ac.za/1-9m-manuals

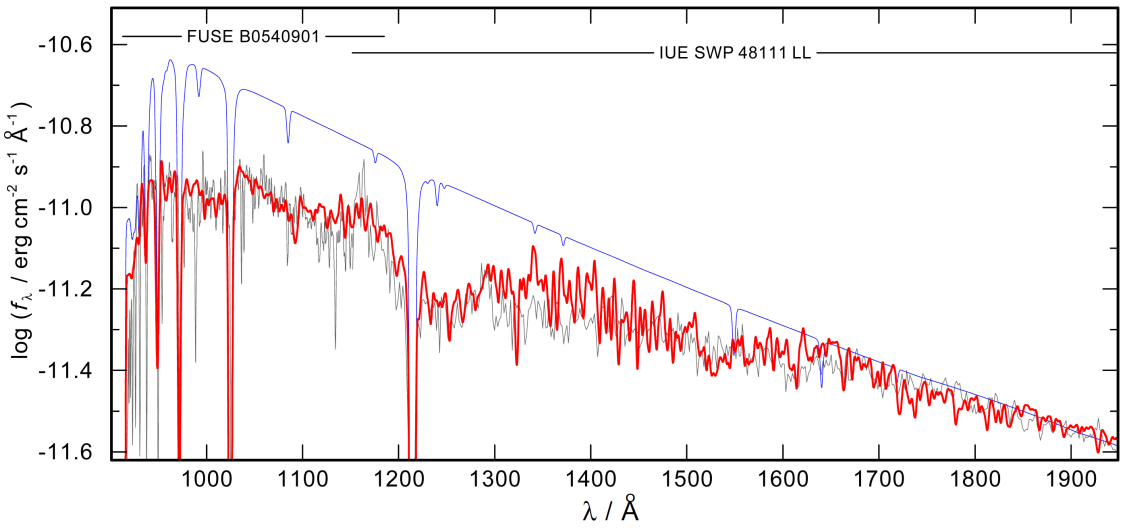

Figure 13: UV spectrum (composed of FUSE and IUE observations) of EC 11481–2303 (gray), compared with a model that contains HHeCNO (blue) and a model that contains H and the IG elements (red, 10 times the solar iron abundance and 1 000 times the solar nickel abundance). The spectra have been convolved with a Gaussian (FWHM = 1 Å) for better representation.
`Reference: Ringat & Rauch 2011`

(2010) used an optical Ultraviolet and Visual Echelle Spectrograph (UVES; Dekker et al. 2000) spectrum of the Very Large Telescope (VLT[13]), the IUE spectra mentioned above, and a Far Ultraviolet Spectroscopic Explorer (FUSE[14]) spectrum in the UV range. The spectra modeled with TMAP (Sect. 4.2) contained H, He, C, N, O, and the IG elements. $T_{\rm eff} = 55\,000$ K, log $g = 5.8$ and the number ratio He/H = 0.0025 were determined. The C, N, and O abundances turned out to be subsolar. In addition, with the help of a generic IG model atom, the flat UV slope could be explained by assuming abundances of at least 10 times solar.
Ringat & Rauch (2011) carried out a more detailed analysis of the IG-element abundances and concluded that the UV slope is best explained by 10 to 100 times the solar iron abundance and 1 000 times the solar nickel abundance (Fig. 13). The other IG elements had little influence on it.

Feige 110 is an sdOB-type subdwarf, which was observed by the 200-inch Hale Telescope of the Palomar Observatory[15], recorded in the *Palomar Sky Survey* in 1956, and catalogued by Feige (1958). With $m_{\rm V} = 11.85$, it is one of the catalog's brighter stars. It is not visible to the naked eye and is located in the constellation Aquarius. Feige 110 is also used as a calibration star, which is why a detailed analysis is interesting.
Based on the Palomar Observatory observations, an early spectral analysis by Greenstein (1971) with use of LTE models resulted in $T_{\rm eff} = 39\,000$ K and log $g = 6.5$, whereat only hydrogen in the model atmosphere was considered. Later, Kudritzki (1976) was able to show that both the consideration of further elements in the model calculation, as well as NLTE effects, have a significant influence on the derived stellar parameters. The

[13]The VLT belongs to the European Southern Observatory, `www.eso.org` .
[14]`http://archive.stsci.edu/fuse`
[15]`https://sites.astro.caltech.edu/palomar/about/telescopes/hale.html`

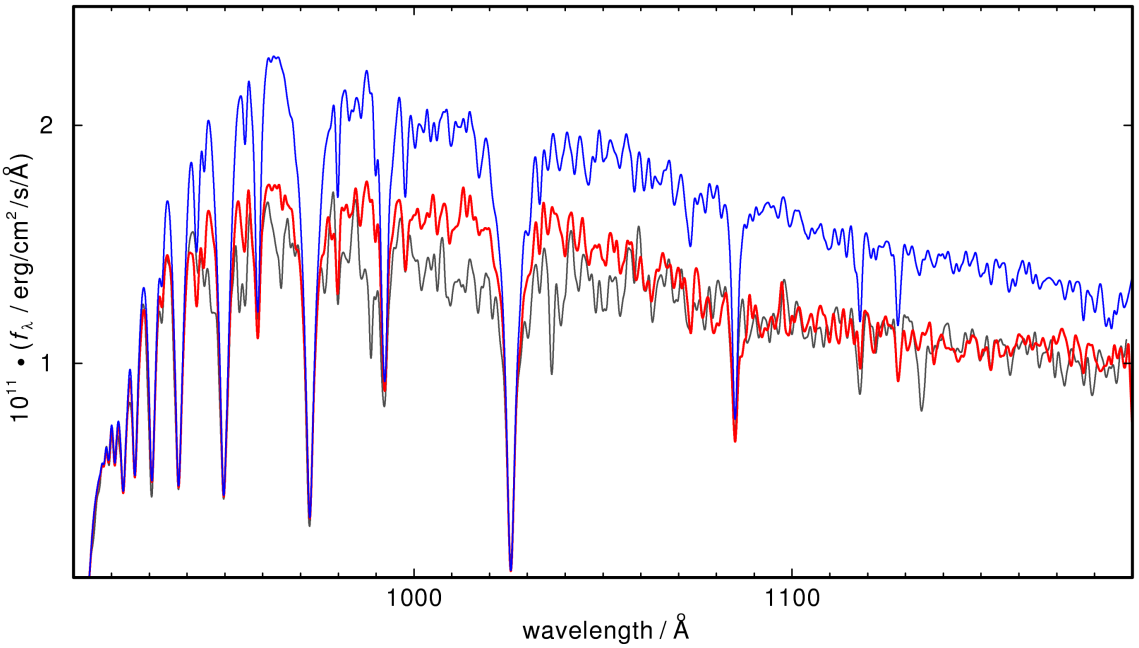

Figure 14: UV spectrum (FUSE) of Feige 110 (gray), compared with a model that contains only IG-element Kurucz's POS lines (blue) and a model that contains IG-element LIN lines (red). The spectra were convolved with a Gaussian (FWHM = 1 Å) for better representation.
`Reference: Rauch et al. 2014a`

deviations between LTE and NLTE turned out to be $\triangle T_{\rm eff} = 4\,000$ K and $\triangle \log g = 0.4$, with a number ratio He/H = 0.1. Further investigations followed, and based on IUE and FUSE spectra in the UV range, interstellar parameters, such as extinction and $N_{\rm H\,I}$, could be determined more precisely. Moreover, Friedman et al. (2002) detected absorption lines of Cr, Fe, and Ni in the FUSE spectrum.
A detailed spectral analysis was performed by Rauch et al. (2014a). In addition to the more precise determination of $T_{\rm eff} = 47\,250$ K, $\log g = 6.0$ and the mass ratio He/H = 0.086, the IG-element abundances could be determined thanks to numerous absorption lines in the FUSE spectrum. Their abundances, except for Ca and Fe, were all found to be at least 30 times solar. It could also be shown that the use of Kurucz's LIN lines, i.e., not only the experimentally determined POS lines (Sect. 4.5), plays a crucial role in the accuracy of the model atmosphere calculation, and thus of the spectral analysis (Fig. 14).

PG 0909+276 is an sdB-type subdwarf. It was discovered in the *Palomar-Green Survey* with $m_{\rm V} \approx 12$, catalogued, and classified as an sdO (Green et al. 1986). PG 0909+276 is located in the constellation Cancer and cannot be seen with the naked eye. The first spectral analysis was performed by Saffer et al. (1994)[16] with an optical spectrum of the 2.3 m-Bok-Telescope at the Kitt Peak National Observatory[17] in Arizona, and $T_{\rm eff} = 35\,400$ K and $\log g = 6.02$ were determined. The star was reclassified as an sdB and further analyses followed.
Based on IUE spectra, Heber & Edelmann (2004) found strongly increased IG-element abundances. However, a detailed analysis was carried out by Wild & Jeffery (2017, 2018)

[16]The star is erroneously called "PG 0909+275" there.
[17]`https://www.as.arizona.edu/bok-23m-telescope`

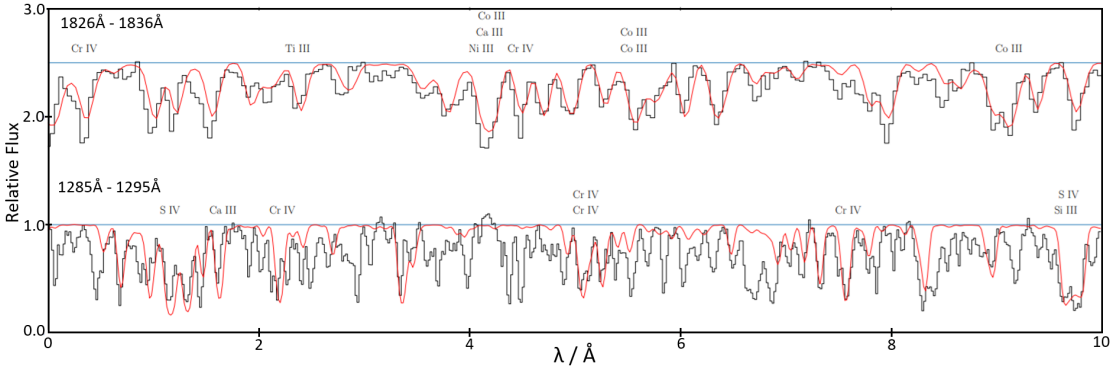

Figure 15: Sections of the normalized PG 0909+276 spectrum (observation in black, LTE model by Wild & Jeffery in red) where some absorption lines of IG elements and TIEs were found. The sections are displayed in the same scaling, with a flux offset of 1.5 units. The horizontal line (blue) denotes the estimated flux continuum.
`Reference: Wild & Jeffery 2017 (Fig.2, modified)`

Table 6: STIS observations (setup: E140M grating, $0\farcs2 \times 0\farcs2$ aperture).

Star	Date	Time / s	ID	S/N at $\lambda = 1\,425$ Å[a]
EC 11481–2303	17.04.2017	2431	OD5601010	≥ 50
Feige 110	03.12.2016	2453	OD5602010	≥ 45
PG 0909+276	28.03.2017	2469	OD5603010	≥ 35

[a]S/N is wavelength dependent (Fig. 47).

some time later. In addition to the IUE spectra, they used high-resolution UV spectra from the Space Telescope Imaging Spectrograph (STIS, Sect. 5.2) and an optical spectrum recorded with the Fiber-Optics Cassegrain Echelle Spectrograph (FOCES; Pfeiffer et al. 1998) of the 2.2 m Telescope of the German-Spanish Astronomical Center at the Calar Alto Observatory[18] in Spain. Thanks to the high-resolution spectra, $T_{\rm eff} = 37\,290$ K, log g = 6.1 and the number ratio He/H = 0.126 could be determined precisely, but it should be mentioned that only LTE model atmospheres were used. The high IG-element abundances could also be confirmed (Fig. 15). Except for Fe they were found to be at least 40 times solar. Furthermore, absorption lines of some TIEs (Cu, Zn, Ga, Ge, Sn, Pb) could be identified.

5.2 The space telescope imaging spectrograph

As shown in Sect. 5.1, spectral observations of all three stars are available, even in the UV range. However, the quality of these observations is not sufficient to analyze the IG-element lines with the desired accuracy. Crucial factors here are the resolving power R of the spectrograph (Sect. 6) and the signal-to-noise ratio (S/N), which indicates the ratio of the mean signal power to the mean noise power. While R is instrument-dependent, S/N can be improved by increasing the observing time. As shown in Fig. 16, STIS has

[18]`https://www.caha.es`

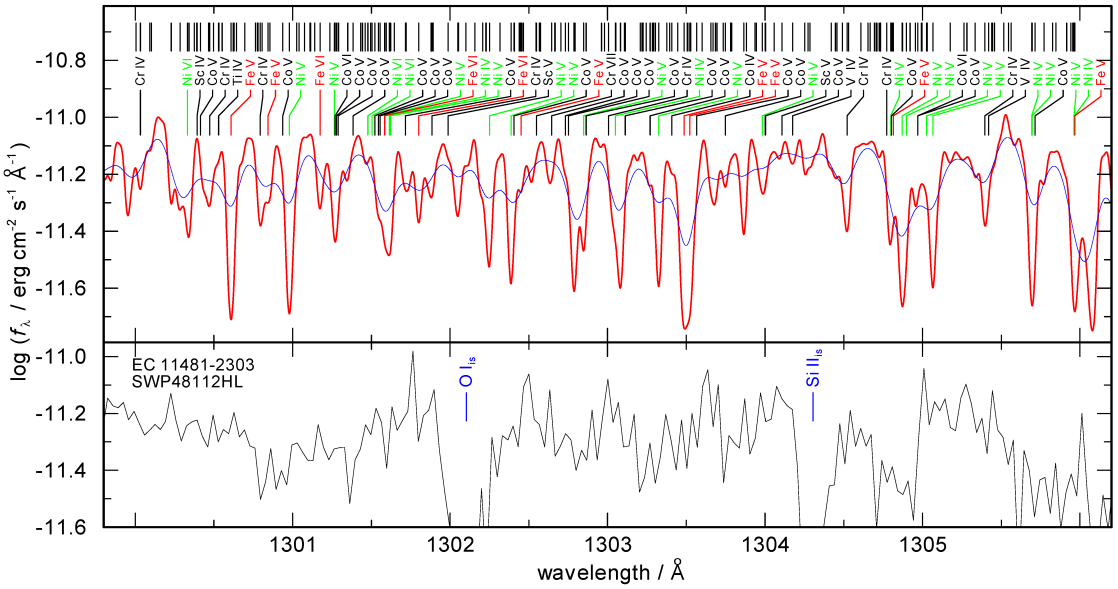

Figure 16: *Top*: Theoretical spectra of EC 11481–2303, calculated with Kurucz's POS lines, and convolved with Gaussian profiles to represent the STIS ($R = 45\,800$, red) and IUE ($R = 10\,000$, blue) resolving powers R. All POS lines are marked above. Also, the corresponding ions are indicated for all lines with $\log(gf) \geq -2$.
Bottom: IUE observation of EC 11481–2303 in the same wavelength range. The index "is" indicates interstellar absorption lines. Poor resolution and S/N prevent an examination of the individual POS lines.

the necessary resolving power for this analysis. It also provides the necessary S/N ≥ 30 whithin a reasonable observing time (Table 6).

STIS (Riley et al. 2019) was installed in the Hubble Space Telescope in 1997 and has been one of its five scientific instruments since. STIS is a versatile imaging spectrograph that enables, among other, spatially resolved spectroscopy for $\lambda = 1\,150$ Å – $10\,300$ Å with medium resolution ($R = 500$ – $17\,000$) and high-resolution ($R = 30\,000$ – $114\,000$) échelle spectroscopy in the UV range. Besides, STIS can record images in the UV range, in the optical range, and using a coronagraph. For the spectral analyses in this work, high-resolution spectra were required. These were taken by the échelle spectrograph with E140M grating, which has an average resolving power of $R = 45\,800$ in the $\lambda = 1\,144$ Å – $1\,709$ Å range (Sect. 6). An échelle spectrograph uses two diffraction gratings perpendicular to each other. The first grating the light passes (after passing a slit) is the échelle grating, which operates in high diffraction orders, which for the most part coincide with one another. This enables a high-resolution spectrum to be captured in a large wavelength range at once. The second, conventional diffraction grating separates the orders. Instead of a continuous spectrum, several spectral bands (in this case 43) are generated that have to be reassembled afterwards.

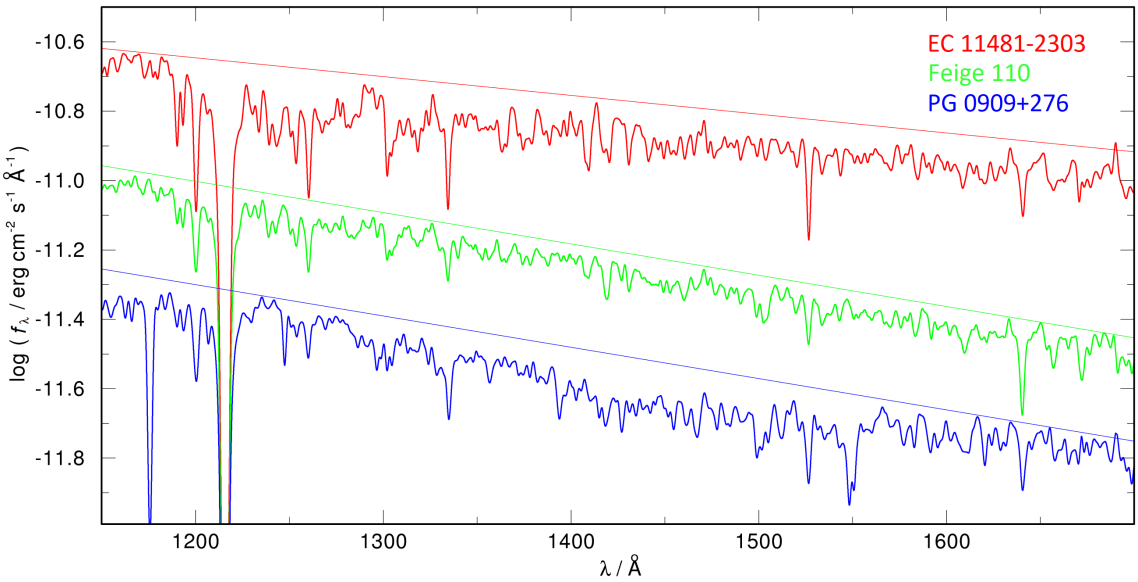

Figure 17: STIS spectra of EC 11481–2303 (×1.04, to prevent too much overlap), Feige 110 and PG 0909+276. For a better representation they were convolved with a Gaussian (FWHM = 2 Å). The straight lines are estimates for the respective continuum.

5.3 The program stars' STIS spectra

In summary, the criteria necessary for this work, which were presented at the beginning of Sect. 5, were met by choosing stars that on the one hand show their flux maximum in the UV range, where the majority of the absorption lines to be investigated is expected, and which, on the other hand, exhibit high IG-element abundances. The spectra were taken with STIS, which is the only instrument that can record spectra in the UV range with the necessary resolution and the necessary S/N.

The observations can be found in the Barbara A. Mikulski Archive for Space Telescopes (MAST)[19]. They are also summarized in Table 6 and are shown in Fig. 17 (after the 43 spectral bands have been correctly reassembled). In each of the spectra, thousands of absorption lines can be seen at first glance (if no convolution is applied), which are largely due to the IG elements. In addition, the line-blanketing effect is shown, as the reduction of the radiation flux occurs, depending on the temperature, more intense at shorter wavelengths in the hotter EC 11481–2303 (corresponding to the dominance of higher IG-element ionization stages) and at longer wavelengths in the cooler PG 0909+276 (dominance of lower ionization stages).

[19] `http://archive.stsci.edu/proposal_search.php?id=14746&mission=hst`

6 Resolving power of a spectrograph

When passing the spectrograph, the entire observed spectrum is broadened due to the limited resolving power R of the apparatus. Theoretically, R is already determined by the instrument components, e.g., in the case of a diffraction grating by the number of illuminated slits, and is therefore known. It is

$$\lambda \,/\, \triangle\lambda = R \quad ,$$

where conventionally $\triangle\lambda \equiv \triangle\lambda_{\mathrm{FWHM}}$ is taken, and some examples for line broadening (near $\lambda = 1\,000\,\text{Å}$) due to the limited resolving power are

STIS	($R \approx 50\,000$, E140M grating):	$\triangle\lambda_{\mathrm{FWHM}} \approx 0.02\,\text{Å}$
FUSE	($R \approx 20\,000$):	$\triangle\lambda_{\mathrm{FWHM}} \approx 0.05\,\text{Å}$.

In practice, even if R is given, the exact spectral Line Spread Function (LSF), which describes the shape of an infinitely sharp absorption (or emission) line on the spectrograph, is highly dependent on the instrument and is therefore by no means trivial to determine. By evaluating hundreds of absorption lines (cf. Sect. 9) in Feige 110 it could be shown that the convolution with a corresponding Gaussian curve on average approximates the line widths too small (Fig. 18), and therefore $\triangle\lambda = \triangle\lambda_{\mathrm{FWHM}}$ is not applicable.
Robertson (2013) has shown that a correction factor β has to be attached to the LSF (which can, depending on the instrument, take the profile of a Gaussian, Lorentzian, sinc^2, or even of a semi-ellipse; Table 7) in order to achieve a consistent treatment of different spectrographs' limited resolving powers.
Having a look at the STIS LSF, it takes more likely the shape of a Lorentzian profile (Fig. 19). Hence, if it is wanted to convolve the spectrum with a Gaussian profile (which is simpler to implement numerically) for treatment of R, the correction factor

$$\beta = \beta_{\mathrm{L}}/\beta_{\mathrm{G}} = 1.424$$

has to be applied, and therefore is, in the case of STIS

$$\triangle\lambda_{\mathrm{FWHM,G}} = \beta\,\triangle\lambda_{\mathrm{FWHM}} = 1.424\,\triangle\lambda_{\mathrm{FWHM}} \quad .$$

The necessity of β is shown with Fig. 19, where the Gaussian approximation of the LSF without correction overestimates the line center clearly while underestimating the line

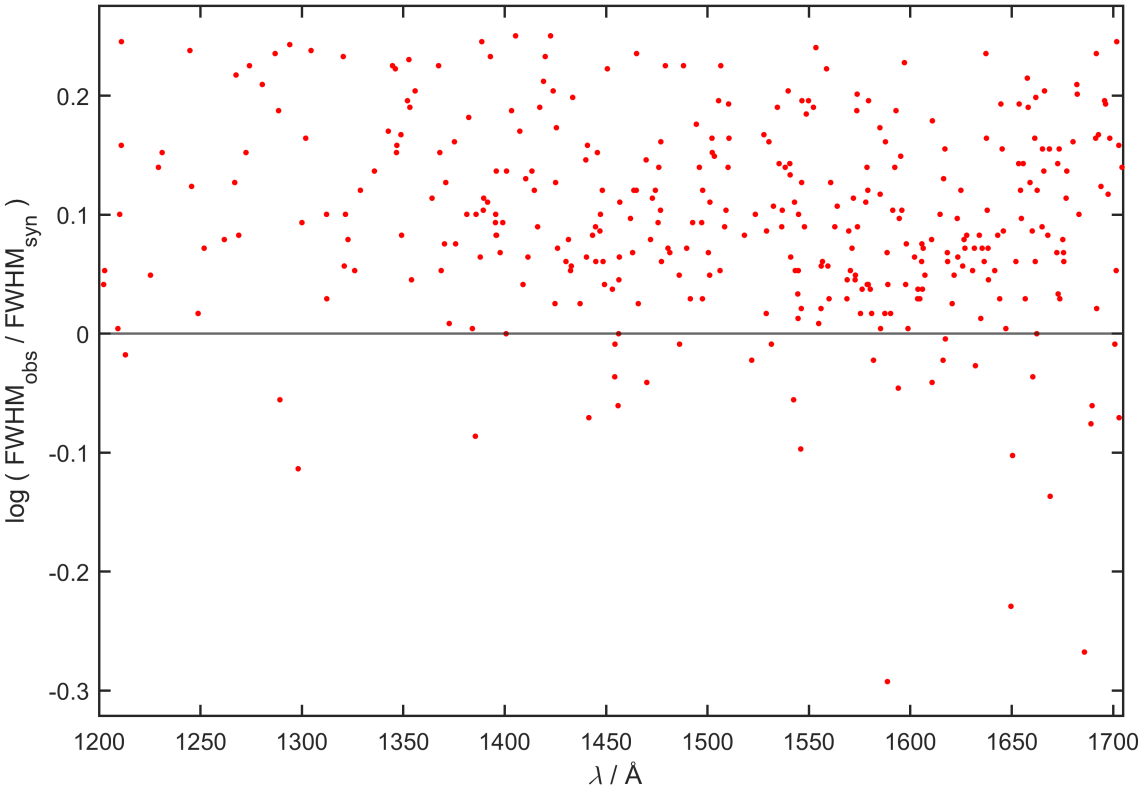

Figure 18: Plot of the ratio of observed and modeled line widths of evaluated lines in Feige 110 against the wavelength λ, with a mean systematic deviation of 25 % (expressed as a non-logarithmic value).

Table 7: Correction factor β for treatment of different LSF shapes.
`Reference: Robertson 2013 (Table 2)`

LSF shape	β
sinc^2	1.129
Gaussian	1.127
Lorentzian	1.605
Semi-ellipse	0.943

wings. Fig. 18, which shows that the adding of β significantly reduces the mean systematic deviation of the evaluated lines' widths from 25 % to 11 % (a mean > 0 is expected, as absorption lines in the observation can be blended by lines which where not considered in the model, Sect. 8), confirms the statement. With correction, the line widths are on average well approximated, while the line wings are still underestimated a little, and even the Lorentzian profile can only approximate the LSF to a certain extent. For the final analysis carried out in this work, convolution with a corrected Gaussian profile ($\beta = 1.424$ as stated) was used for treatment of R.

The exact handling of the line widths plays a negligible role for the evaluation of line strengths by measuring the equivalent widths (Sect. 3.2.6), as these are independent of $\triangle\lambda_{\text{FWHM}}$. However, correct adaptation of the line shape is important for determining atmospheric parameters. In this case, as shown, even with the correction factor, the line

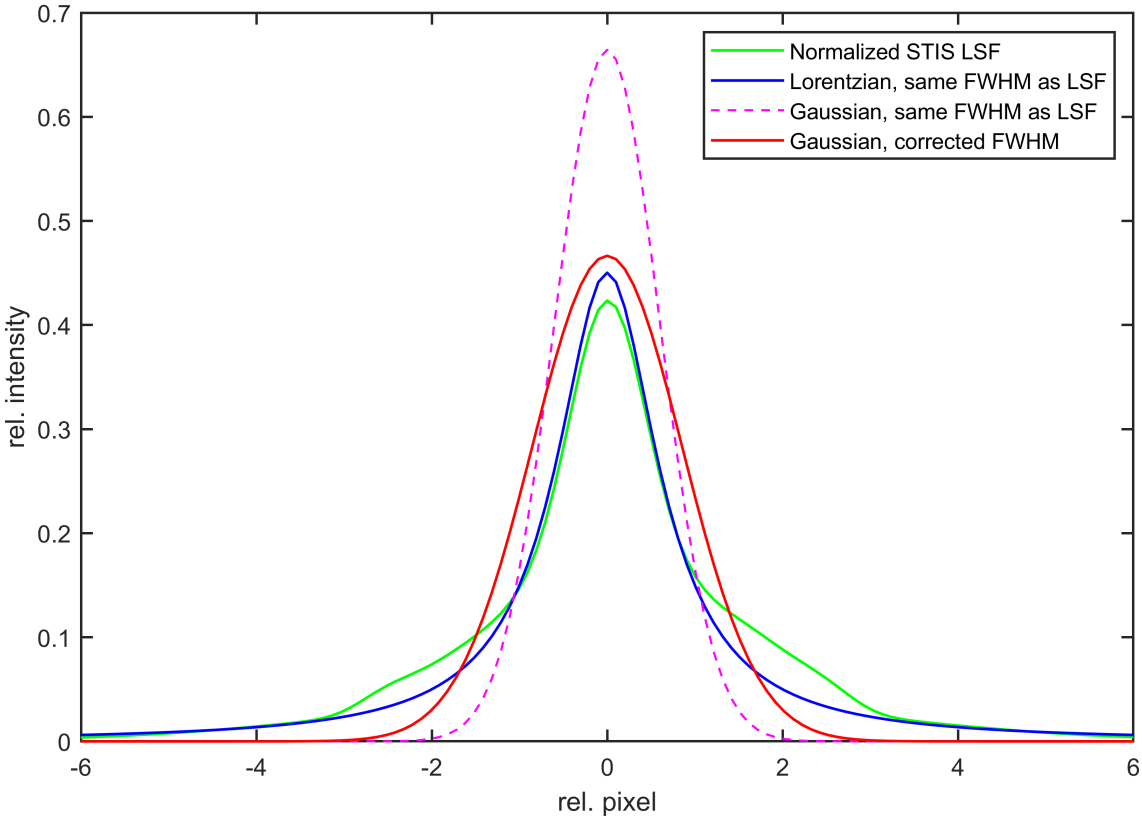

Figure 19: Normalized STIS LSF (E140M grating, $\lambda = 1\,200\,\text{Å}$) compared with a Gaussian and a Lorentzian profile.
`References: https://www.stsci.edu/files/live/sites/www/files/home/hst/instrumentation/stis/performance/spectral-resolution/_documents/LSF/LSF_E140M_1200.txt; Robertson 2013 (Eq. 2 and Table 2)`

wings are underestimated by the LSF adaption in the model and therefore on average smaller than in reality. This in turn might lead, as the line wings are mainly affected by pressure broadening (Sect. 3.2.2), to a slight overestimation of the star's compactness, or in other words, of the surface gravity g (as an increase of g has to compensate the LSF adaption). A detailed investigation of the consequences on g lies, however, not in the scope of this work.

7 Analysis

To examine individual IG-element absorption lines, a detailed spectral analysis of the program stars is necessary. As already shown, the observations meet all the requirements for such an analysis. In the following, the model atmospheres calculated with TMAP are described, the model spectra are shown and all relevant analysis parameters (partly described in Sect. 3), as well as the IG-element abundances, are determined. The basic procedure is as follows:

- First, an NLTE atmosphere model, which considers opacities of all elements with previously determined abundances, up to (yet excluded) the IG elements, is calculated for each of the three stars with TMAP using the parameters and abundances given in Sect. 5. From these models, synthetic spectra are calculated and compared with STIS observations.
- Additionally to the above-mentioned "basic model", individual atmosphere models and synthetic spectra are calculated for each of the IG elements. An absorption line comparison provides the respective IG-element abundance.
- After all abundances and relevant parameters have been precisely determined, an NLTE atmosphere model, which includes all identified elements, is calculated. Due to the line-blanketing effect, some parameters or abundances may have to be readjusted. A "final" atmosphere model is calculated then, using the newly determined parameters.

Then, the IG-element absorption lines can be examined. However, before the procedure just mentioned is presented for each of the stars in detail, an important physical effect, namely interstellar extinction (Sect. 3.3), needs to be taken up again at this point, as it has a great impact on the program stars' observed spectra.

The above-mentioned NLTE atmosphere model is used to calculate the emergent stellar spectrum, which can differ greatly from the observation (Sect. 3.3). Taking EC 11481–2303 as an example ($T_{\rm eff} = 55\,000\,\mathrm{K}$), the flux maximum of the emergent stellar spectrum is obtained at $\lambda \approx 530\,\text{Å}$ (Fig. 20). Due to extinction (more specifically due to the Lyman edge) the flux becomes strongly depressed at wavelengths below $\lambda = 911\,\text{Å}$, and, although this effect can be modeled numerically, the astrophysical flux maximum cannot be observed in practice. For the accuracy of a spectral analysis, however, the consideration of the element opacities in the maximum flux range plays the most important role. With regard to the IG elements, in particular absorption lines in the range around $\lambda \approx 530\,\text{Å}$ must be taken into account, as these have the greatest impact on the flux. Therefore,

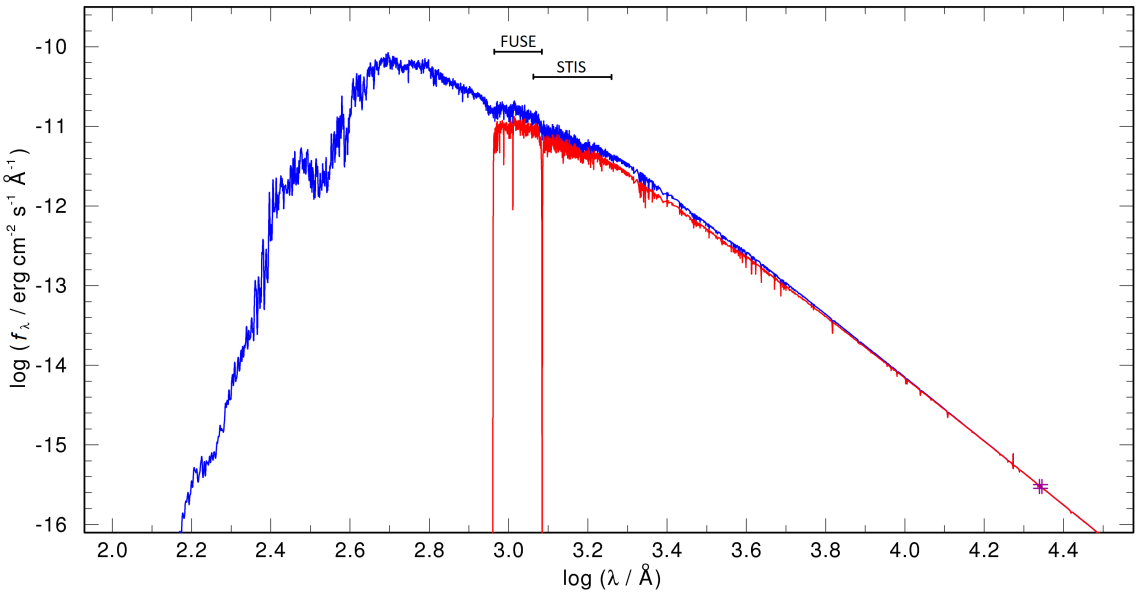

Figure 20: Model spectrum of EC 11481–2303 without (blue) and with interstellar extinction and $N_{\mathrm{H\,I}}$ absorption (red), both normalized to the by 2MASS observed absolute brightness at $\lambda = 22\,000$ Å (purple rhombus at bottom right, cf. Fig. 23). FUSE and STIS ranges are indicated.

the LIN lines (Sect. 4.5) are used. LIN lines may exhibit wavelength uncertainties and are therefore not suitable for an individual line analysis, but on average they correctly represent the total element opacity (not only, but most importantly, in the maximum flux range). In the best case, all LIN lines are used for model-atmosphere calculations. Due to limited computation power and time, however, in practice there is a limit to the resolution with which the LIN lines can be put under calculation, and to obtain the best results, this resolution is set highest (numerically spoken, i.e., the number of frequency points in the grid, Sect. 4.2) at the maximum flux range.

At longer wavelengths, the extinction's impact weakens (Fig. 20). As the effect becomes negligibly small in the infrared (IR; in this case 0.007 % at $\lambda = 22\,000$ Å), IR normalization to observed fluxes is typically used for $E_{\mathrm{B-V}}$ determination (Sect. 7.1, Fig. 23). After calibration, the spectral shapes of the synthetic spectrum and the STIS observation match. The latter can therefore be used to evaluate individual POS lines as well as to carry out the spectral analysis (determination of atmospheric parameters and element abundances).

7.1 EC 11481−2303

First, with the abundances and parameters determined by Rauch et al. (2010) and Ringat & Rauch (2011), an NLTE atmosphere model containing H, He, C, N, and O was calculated using the PRO2 program, which is part of TMAP. TMAD (Sect. 4.3) was used as the atomic-data source. A synthetic spectrum in the range of $\lambda = 1\,144$ – $1\,709$ Å was created with the LINE1_PROF program. For determination of $\log g$ and He/H, optical spectra suit better than UV spectra. On the one hand, a large number of H- and He-absorption lines, which are subject to the linear Stark effect, can be found in the optical range, and on the other hand, due to the observability through ground-based telescopes in the optical range, a long observing time and thus a high S/N can be achieved without any problems. Since both $\log g$ and $T_{\rm eff}$ as well as He/H have already been precisely determined with optical spectra, other element abundances and parameters could be examined in this analysis. This is also confirmed by the first comparison of model and observation, where only parameters such as interstellar H I-absorption, $v_{\rm rad}$, $v_{\rm rot}$, etc., had to be adjusted to obtain good agreement. Then, a model, which contains HHeCNO + IG element, was calculated for each of the IG elements (that is, model atmosphere and synthetic spectrum) in order to determine its abundance. Kurucz's lists (Sect. 4.5) were used as the IG-element atomic data source. With the abundances then known, a model containing the elements HHeCNOCaScTiVCrMnFeCoNi was calculated. With this model, all abundances and parameters could be precisely determined, and individual absorption lines could be examined. Since adding further opacities leads to a continuum shift, the synthetic spectrum had to be normalized after each element being inserted into the model. To prevent calibration inaccuracies, normalization was always carried out in a way that the flux at the red edge of the STIS spectrum, i.e., at $\lambda = 1\,709$ Å, coincides.

Analysis parameters

$T_{\rm eff} = 55\,000 \pm 5\,000$ K and $\log g = 5.8 \pm 0.3$ were determined by Rauch et al. (2010, Fig. 21) and could be confirmed by this work. The interstellar H I column density $N_{\rm H\,I} = 3.5 \times 10^{20}\,{\rm cm}^{-2}$ and the associated radial velocity $v_{\rm rad,H\,I} = -7$ km/s could be determined by fitting the Ly α line (Fig. 22). The stellar radial velocity $v_{\rm rad} = 87$ km/s was obtained by examining further absorption lines, such as N V $\lambda\lambda$ 1 238.82, 1 242.80 Å. $E_{\rm B-V} = 0.035^{+0.005}_{-0.010}$ was determined by flux comparison (Fig. 23) of a PRO2 atmosphere model with UV spectra and absolute brightness in the IR[20] (taken from the Two Micron All Sky Survey, 2MASS; Skrutskie et al. 2006). A relatively high rotational velocity $v_{\rm rot} = 40$ km/s was also determined, which could restrain the investigation of individual absorption lines (cf. Sect. 8). Finally, some interstellar absorption lines of C, N, O, Si, S, Al, and Fe were found, which could easily be distinguished from atmospheric lines due to the lack of rotational broadening (Fig. 24).

[20] For the STIS observation, better consistency was achieved with $E_{\rm B-V} = 0.055$, which slightly reduced $N_{\rm H\,I}$ by about 15 % but did not have any significant impact on other atmospheric parameters.

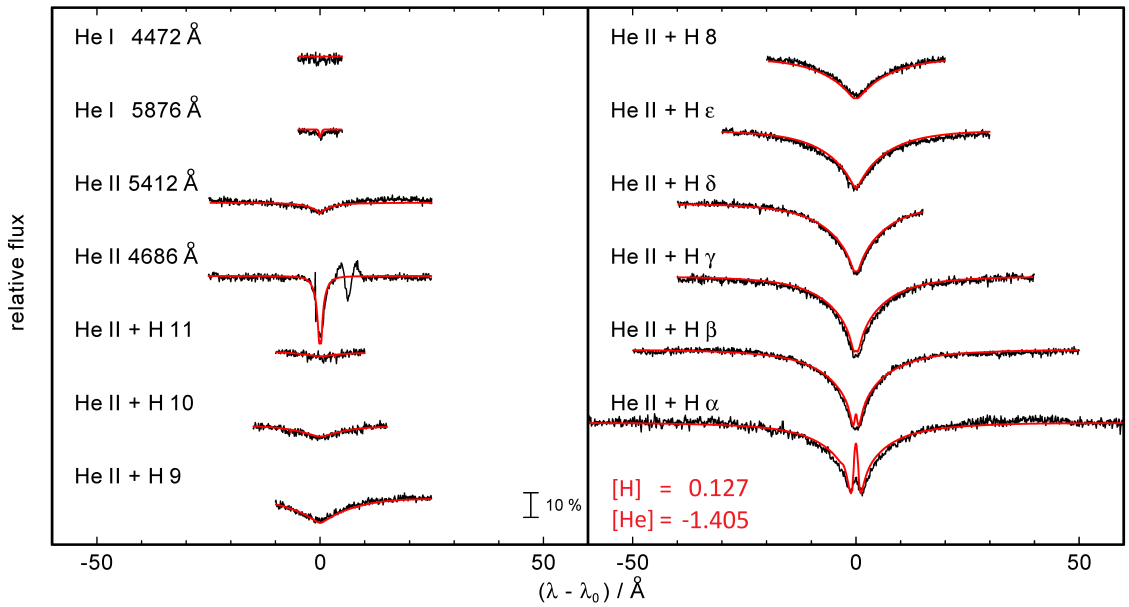

Figure 21: Comparison of hydrogen and helium lines of an optical VLT spectrum (black) and a model spectrum, which contains HHeCNO and a generic IG model atom (red), calculated by Rauch et al. (2010) for the determination of $T_{\rm eff}$, $\log g$, and He/H. [X] denotes log (mass fraction / solar mass fraction) of element X.
`Reference: Rauch et al. 2010 (modified)`

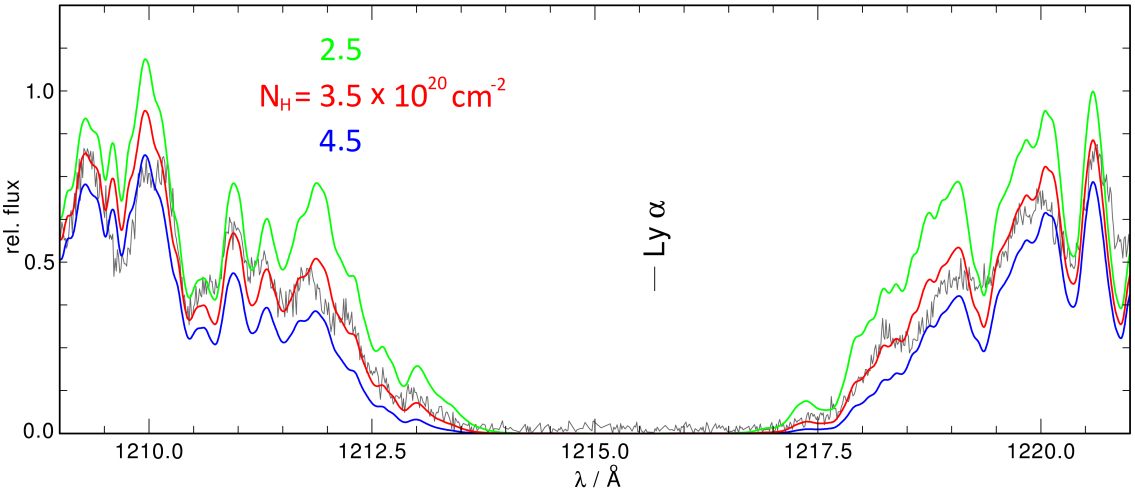

Figure 22: Determination of the interstellar H I column density towards EC 11481–2303 by a Ly α-line fit (observation in gray, models colored).

Abundances

Before the abundance determination is presented it shall be noted that in the case of C, O, and V, no absorption lines could be unambiguously identified (primarily due to stellar rotation), and therefore upper abundance limits were derived. In the case of Ca, Sc, and Ti, the identified absorption lines were strongly blended, hence also upper abundance limits were derived.

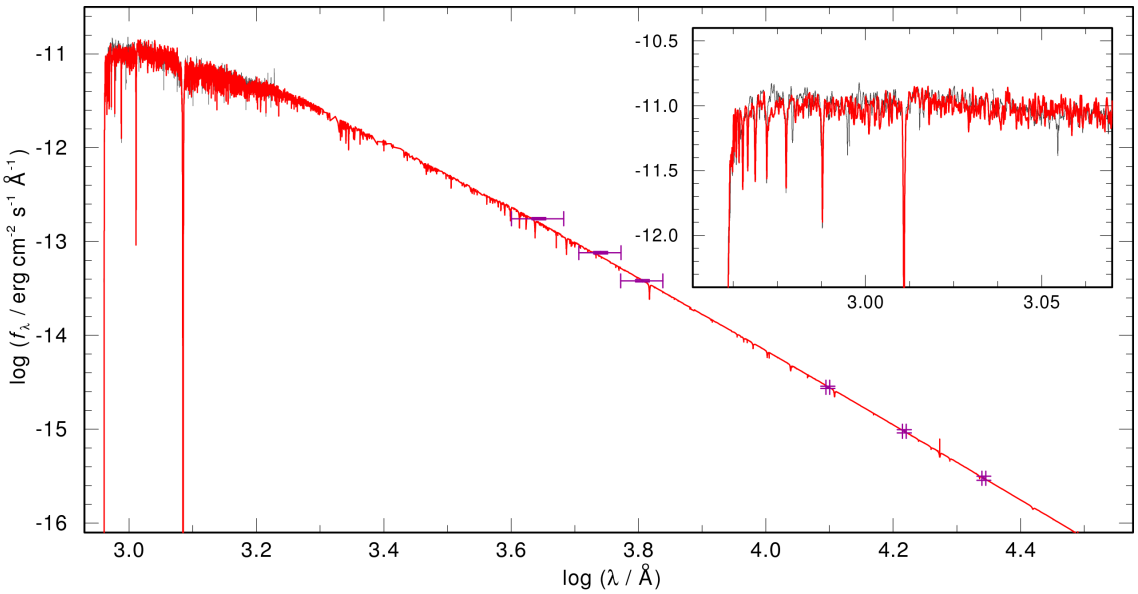

Figure 23: Determination of E_{B-V} for EC 11841–2303 by normalizing the model flux (red) to the absolute brightness measured by 2MASS at $\lambda = 22\,000$ Å (purple rhombus at bottom right) and subsequent Lyman-edge fit (top right section) at $\lambda = 911$ Å using FUSE spectra (gray).

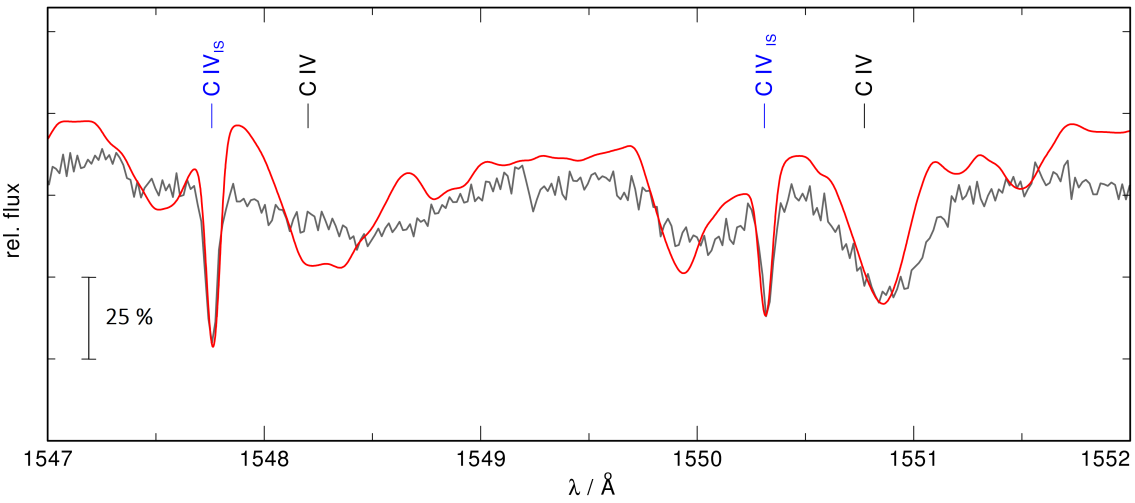

Figure 24: Interstellar C IV lines (blue label with index "IS") in the EC 11481–2303 spectrum (model in red, observation in gray), next to the strongly rotationally broadened atmospheric C IV lines (black label). Further IG-element absorption lines are not labeled.

The hydrogen and helium abundance was initially determined by Rauch et al. (2010, Fig. 21) and could be confirmed by this work's analysis. The atomic number ratio He/H = 0.0025 was obtained. Considering the light metals, only C, N, and O were investigated, since no other element's lines could be identified. For C, C IV λ 1 548.20 Å (Fig. 24) gives an upper limit of [C] < -5.45 ([X] denotes log (mass fraction / solar mass fraction) of element X). The N abundance could be determined using some lines, such as N V $\lambda\lambda$ 1 238.82, 1 242.80 Å, to [N] $= -0.23$. For O, based on the relatively weak O IV λ 1 343.51 Å, an upper limit of [O] < -3.77 was found.

Table 8: EC 11481–2303 photospheric abundances obtained in this work.

Element	Line count[a]	Mass fraction	[X]
H	1	8.73×10^{-1}	0.07
He	1	8.67×10^{-3}	−1.46
C	1	$< 8.37 \times 10^{-9}$	< -5.45
N	6	4.07×10^{-4}	−0.23
O	3	$< 9.75 \times 10^{-7}$	< -3.77
Ca	1	$< 2.79 \times 10^{-2}$	< 2.66
Sc	3	$< 7.83 \times 10^{-4}$	< 4.22
Ti	3	$< 6.25 \times 10^{-4}$	< 2.32
V	1	$< 8.87 \times 10^{-5}$	< 2.49
Cr	> 20	4.91×10^{-3}	2.49
Mn	> 20	6.70×10^{-3}	2.80
Fe	> 50	4.52×10^{-2}	1.57
Co	> 50	6.32×10^{-3}	3.24
Ni	> 50	2.55×10^{-2}	2.57

[a]Applied to the STIS observation spectral range. Only well-identified lines (i.e., no strong line blends) were counted. For Cr, Mn, Fe, Co, and Ni, lower limits for the line counts are given, as many of their lines blend due to stellar rotation.

Using Ca III λ 1 545.30 Å, [Ca] < 2.66 was found. With Sc IV $\lambda\lambda$ 1 482.04, 1 574.92 Å, [Sc] < 4.22 was found, with Ti V λ 1 268.49 Å and Ti IV λ 1 467.34 Å, [Ti] < 2.32 was obtained, and using V IV λ 1 395.00 Å, [V] < 2.49 was obtained. Since many absorption lines were identified for Cr, Mn, Fe, Co, and Ni, their abundances could be determined to [Cr] = 2.49, [Mn] = 2.80, [Fe] = 1.57, [Co] = 3.24 and [Ni] = 2.57. The abundances can be found in Table 8.

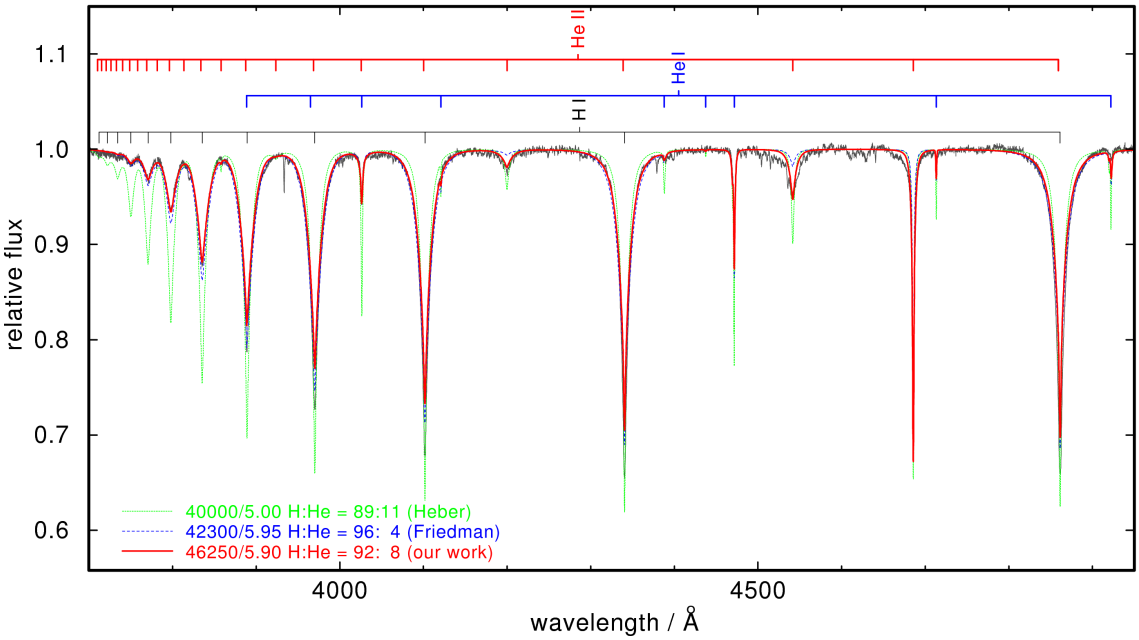

Figure 25: Comparison of hydrogen and helium lines of an optical X-Shooter spectrum (black) with different models containing H+He (H:He is, in this case, given as a mass ratio).

`Reference: Rauch et al. 2014a`

7.2 Feige 110

The procedure is analogous to Sect. 7.1. First, a model, which contains H, He, C, N, O, Si, and S, with the abundances and parameters from Rauch et al. (2014a), was calculated. Comparison of model and observation confirmed the previously determined values for $T_{\rm eff}$, $\log g$, and He/H. Again the interstellar H I absorption, $v_{\rm rad}$, $v_{\rm rot}$, etc., were adjusted. For each of the IG elements, a model containing HHeCNOSiS + IG element was calculated, using TMAD and Kurucz's lists for atomic data. After abundance determination, again a model containing the elements HHeCNOSiSCaScTiVCrMnFeCoNi was calculated, with the corresponding normalization shown in Sect. 7.1.

Analysis parameters

$T_{\rm eff} = 47\,250 \pm 2\,000$ K and $\log g = 6.0 \pm 0.2$ were taken from Rauch et al. (2014a, Fig. 25, where it was concluded that the inclusion of IG elements changes the parameters of their best fit to the aforementioned values). By fitting the Ly α line, $N_{\rm H\,I} = 2.0 \times 10^{20}\,{\rm cm}^{-2}$ and $v_{\rm rad,H\,I} = -7$ km/s were determined. Furthermore, the stellar radial and rotational velocity $v_{\rm rad} = 13.5$ km/s and $v_{\rm rot} \approx 0$ were found, and the extinction $E_{\rm B-V} = 0.020 \pm 0.005$. Finally, interstellar absorption lines of C, N, O, Si, S, Al, and Fe were identified.

Abundances

Some IG-element abundances could be adjusted more precisely by the detailed analysis shown in Sects. 8 and 9. The values presented here are the final values found in this work, i.e., after all adjustments. Additionally, it shall be noted that in the case of C, O, and Sc, no absorption lines could be unambiguously identified, and therefore upper abundance

Table 9: Like Table 8, for Feige 110.

Element	Line count[a]	Mass fraction	[X]
H	1	8.99×10^{-1}	0.09
He	1	7.83×10^{-2}	−0.50
C	1	$< 5.49 \times 10^{-10}$	< -6.63
N	4	1.02×10^{-4}	−0.83
O	1	$< 1.46 \times 10^{-6}$	< -3.59
Si	2	$< 5.12 \times 10^{-8}$	< -4.11
S	4	1.69×10^{-4}	−0.26
Ca	2	1.28×10^{-3}	1.32
Sc	1	$< 2.05 \times 10^{-5}$	< 2.64
Ti	2	8.74×10^{-4}	2.47
V	2	1.42×10^{-4}	2.69
Cr	28	5.45×10^{-3}	2.54
Mn	22	5.76×10^{-3}	2.74
Fe	166	5.44×10^{-3}	0.65
Co	74	1.41×10^{-3}	2.58
Ni	98	2.26×10^{-3}	1.52

[a]Applied to the STIS observation spectral range. Only well-identified lines (i.e., no strong line blends) were counted. In the case of Cr, Mn, Fe, Co, and Ni, the line count refers to the isolated lines used in Sect. 9.2.

limits were derived. In the case of Si, the identified absorption lines were strongly blended, hence also an upper abundance limit was derived.

The hydrogen and helium abundances found by Rauch et al. (2014a) could be adopted, thus the number ratio is He/H = 0.022. Considering the light metals, C, N, O, Si, and S were examined. For C, based on C IV λ 1 548.20 Å, an upper limit of [C] < -6.63 was derived. The N abundance could be determined to [N] = −0.83 using N V $\lambda\lambda$ 1 238.82, 1 242.80 Å. For O, based on the relatively weak O IV λ 1 343.51 Å, an upper limit of [O] < -3.59 was derived. Using Si IV λ 1 393.76 Å, an upper limit of [Si] < -4.11 was found. The S abundance could be derived from several lines, such as S V $\lambda\lambda$ 1 268.49, 1 501.76 Å, to [S] = −0.26.

With Ca III $\lambda\lambda$ 1 463.34, 1 545.30 Å, [Ca] = 1.32 was found. Using Sc III λ 1 603.06 Å, an upper limit of [Sc] < 2.64 was determined, with Ti IV $\lambda\lambda$ 1 451.74, 1 467.34 Å, [Ti] = 2.47 was found, and using V IV λ 1 680.20 Å and V V λ 1 157.58 Å, [V] = 2.69 could be derived. Since many absorption lines were identified for each of the other IG elements, their abundances could be determined to [Cr] = 2.54, [Mn] = 2.74, [Fe] = 0.65, [Co] = 2.58, and [Ni] = 1.52 with the procedure described in Sect. 9.2. The abundances can be found in Table 9.

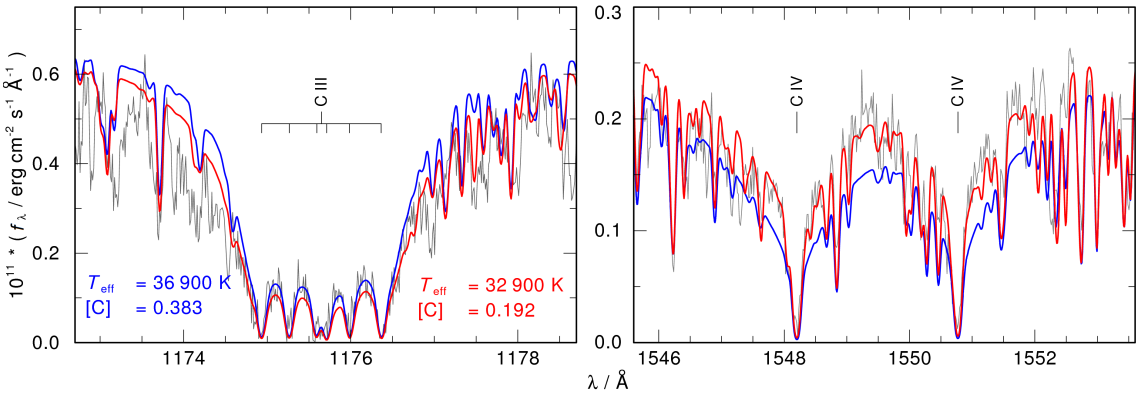

Figure 26: Comparison of some C III (left) and C IV (right) lines in PG 0909+276 (a model with parameters and abundances of Wild & Jeffery (2018) in blue, TMAP model in red, STIS spectrum in gray).

7.3 PG 0909+276

A model containing H, He, C, N, Si, S, and Ar, with the abundances and parameters found by Wild & Jeffery (2018), was calculated. Comparison of model and observation showed an inconsistency of some C III and C IV lines (Fig. 26), therefore the basic parameters $T_{\rm eff}$, $\log g$, and He/H were checked again. For the STIS spectrum, the best fit was accomplished for $T_{\rm eff} = 32\,900$ K, which is 4 000 K less than the value determined by Wild & Jeffery. In addition, the C abundance was reduced to [C] = 0.192. To verify the new values, the models were compared with an optical FOCES spectrum (Fig. 27). However, no consistency could be accomplished by fitting the H and He lines (even changes in the He/H ratio did not result in an optimal agreement) and the best-fit values of the STIS spectrum were selected for further analysis. Analogous to Sect. 7.1, the interstellar H I absorption, $v_{\rm rad}$, $v_{\rm rot}$, etc., were adjusted. For each of the IG elements, a model containing HHeCNSiSAr + IG element was calculated, with the atomic data taken from TMAD and Kurucz's lists. After abundance determination, again a model was calculated that contains all elements HHeCNSiSArCaScTiVCrMnFeCoNi, with the corresponding normalization shown in Sect. 7.1.

Analysis parameters

As just shown, $T_{\rm eff} = 32\,900$ K was chosen to get the best match in the STIS spectral range. $\log g = 6.1 \pm 0.2$ was taken from Wild & Jeffery (2018). By fitting the Ly α line, $N_{\rm H\,I} = 1.1 \times 10^{20}$ cm^{-2} and $v_{\rm rad,H\,I} = 5$ km/s were obtained. Furthermore, the stellar radial and rotational velocity were determined to $v_{\rm rad} = 18.0$ km/s and $v_{\rm rot} \approx 2$ km/s, and the extinction to $E_{\rm B-V} = 0.040^{+0.010}_{-0.015}$. Additionally, interstellar absorption lines of C, N, O, Si, S, Al, and Fe were found.

Abundances

As for Feige 110, some IG-element abundances could be adjusted more precisely by the detailed analysis shown in Sects. 8 and 9. The values presented here are the final values found in this work, i.e., after all adjustments.

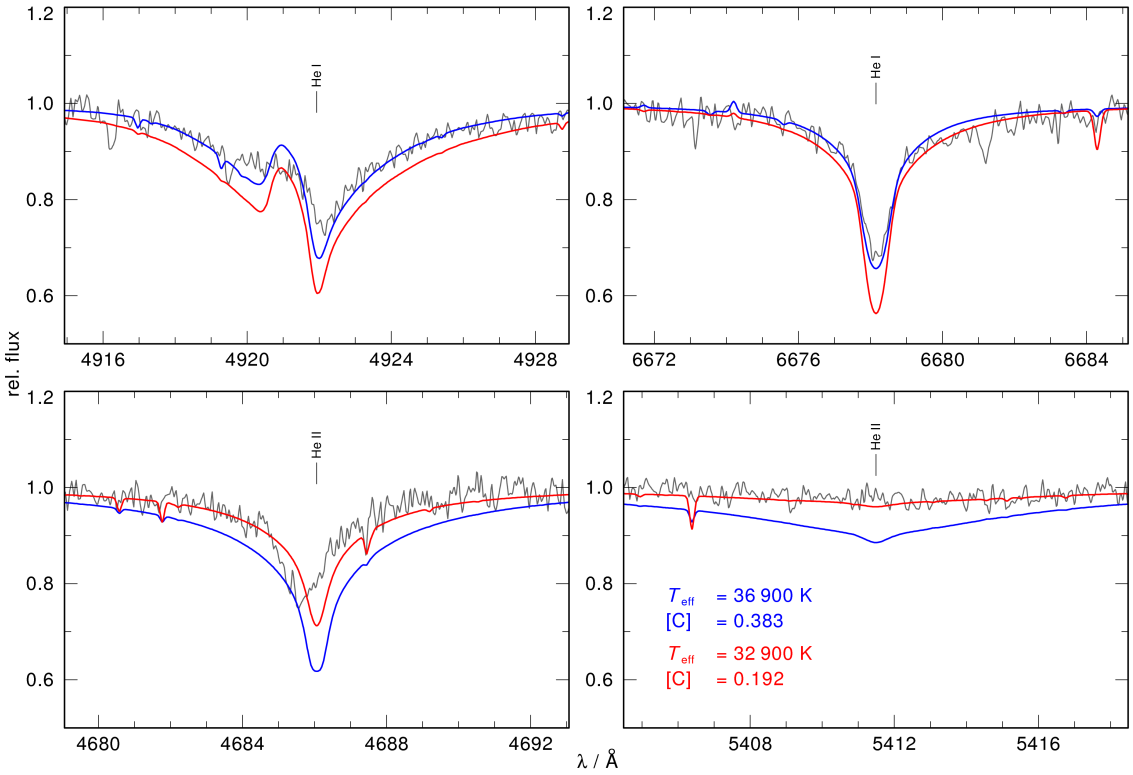

Figure 27: Comparison of selected He I and He II lines in the optical spectral range (a model with parameters and abundances found by Wild & Jeffery (2018) in blue, TMAP model in red, FOCES spectrum in gray).

The hydrogen and helium abundance from Wild & Jeffery (2018) provided the best fit of the spectra, both in the optical and in the UV range, despite slight inconsistencies, and was therefore adopted as such. Thus, the element number ratio is He/H = 0.219. Considering the light metals, absorption lines of C, N, Si, S, and Ar were found. As already shown, the C abundance was determined to [C] = 0.19 based on some C III and C IV lines (Fig. 26). Based on N III λλ 1 183.03, 1 184.55 Å an abundance of [N] = −0.43 was found. The Si abundance was determined to [Si] = −2.68 using Si III λ 1 298.96 Å and Si IV λλ 1 393.76, 1 403.77 Å, the S abundance based on some S III lines, for example S III λλ 1 194.46, 1 200.97 Å, and S IV λλ 1 623.59, 1 623.95 Å to [S] = 1.22, and the Ar abundance was determined using some Ar III lines, for example Ar III λλ 1 669.67, 1 675.48 Å, to [Ar] = 1.13.

With Ca III λλ 1 463.34, 1 496.88 Å, [Ca] = 2.00 was found. Using Sc III λλ 1 603.06, 1 610.19 Å, [Sc] = 4.24 was determined, and with several lines, such as Ti IV λλ 1 451.74, 1 467.34 Å, [Ti] = 2.88 was found. Based on some V lines, such as V III λ 1 694.78 Å and V IV λ 1 226.52 Å, [V] = 3.53 could be derived, and with several lines, such as Mn IV λλ 1 653.83, 1 664.73 Å, [Mn] = 1.98 was found. Since many absorption lines were identified for each of the other IG elements, their abundances could be determined to [Cr] = 2.51, [Fe] = 0.03, [Co] = 3.21, and [Ni] = 2.48 with the procedure described in Sect. 9.3. The abundances can be found in Table 10.

Table 10: Like Table 8, for PG 0909+276.

Element	Line count[a]	Mass fraction	[X]
H	1	5.06×10^{-1}	−0.16
He	2	4.40×10^{-1}	0.25
C	12	3.69×10^{-3}	0.19
N	6	2.58×10^{-4}	−0.43
Si	8	1.38×10^{-6}	−2.68
S	19	5.09×10^{-3}	1.22
Ar	8	9.80×10^{-4}	1.13
Ca	4	6.08×10^{-3}	2.00
Sc	2	8.27×10^{-4}	4.24
Ti	16	2.25×10^{-3}	2.88
V	28	9.72×10^{-4}	3.53
Cr	10	5.10×10^{-3}	2.51
Mn	21	1.01×10^{-3}	1.98
Fe	9	1.29×10^{-3}	0.03
Co	24	5.89×10^{-3}	3.21
Ni	20	2.04×10^{-2}	2.48

[a]Applied to the STIS observation spectral range. Only well-identified lines (i.e., no strong line blends) were counted. In the case of Cr, Fe, Co, and Ni, the line count refers to the isolated lines used in Sect. 9.3.

Table 11: Parameters of the three program stars.

	EC 11481–2303	Feige 110	PG 0909+276
Parallax[a] / mas	3.40 ± 0.05	3.69 ± 0.05	3.58 ± 0.06
D / pc	294 ± 4	271 ± 4	279 ± 5
H_ν / erg/cm^2/s/Hz	9.40×10^{-4}	6.88×10^{-4}	4.97×10^{-4}
m_v[b]	11.778 ± 0.1	11.496 ± 0.1	12.091 ± 0.1
$\log(g$ / cm/s$^2)$	5.8 ± 0.3	6.0 ± 0.2	6.1 ± 0.2
$E_\mathrm{B-V}$	$0.035^{+0.005}_{-0.010}$	0.020 ± 0.005	$0.040^{+0.010}_{-0.015}$
R / km	$72\,300 \pm 5\,500$	$86\,800 \pm 6\,000$	$82\,300 \pm 6\,500$
R / $R_\odot$	0.104 ± 0.008	0.125 ± 0.009	0.118 ± 0.009
M / $M_\odot$	$0.248^{+0.246}_{-0.124}$	$0.567^{+0.332}_{-0.209}$	$0.636^{+0.373}_{-0.234}$

References:
[a]Gaia Collaboration et al. 2020, https://gea.esac.esa.int/archive;
[b]NOMAD catalogue, Zacharias et al. 2004

7.4 Gaia EDR3 and spectroscopic distance

The Early Data Release 3 (EDR3) of the Gaia space probe (Gaia Collaboration et al. 2020; https://gea.esac.esa.int/archive), published in December 2020, provided some interesting parameters of the three subdwarfs. The stellar distances D (Table 11) could be determined trigonometrically from the EDR3 parallax (given in milli arc seconds, "mas"). Besides, the parameters obtained from the spectral analysis and the formula to determine the spectroscopic distance (Heber et al. 1984[21]) could be used to determine additional stellar parameters. It is

$$D = 1.9 \times 10^{10}\, R \sqrt{H_\nu \cdot 10^{0.4 \cdot m_{\mathrm{v}0}}}$$

or

$$D = 7.11 \times 10^{4} \sqrt{M \cdot H_\nu \cdot 10^{0.4 \cdot m_{\mathrm{v}0} - \log g}}\ \mathrm{pc}$$

with the stellar mass M in $M_\odot$, the Eddington flux H_ν, a corrected apparent magnitude $m_{\mathrm{v}0} = m_\mathrm{v} - 3.2\, E_\mathrm{B-V}$ and the stellar radius R. Both equations are connected by a relation for the surface gravity g. H_ν was taken from the TMAP atmosphere model ($H_\nu = F_\nu/4$) at $\lambda = 5\,454$ Å. With the stellar distances D known from Gaia EDR3, the radii and the masses (Table 11) could be determined in this way (the mass determination is uncertain due to an exponential dependence on $\log g$). Distance, radius, and mass are no relevant parameters in the scope of this work, but they provide an important framework for the consistency of the various analyses and observations.

[21] http://astro.uni-tuebingen.de/~rauch/SpectroscopicDistanceDetermination.gif

8 Line identification

The work aims to evaluate isolated IG-element absorption lines. Since thousands of absorption lines show in each of the three spectra, it is not surprising that many of them overlap. This chapter shows how the isolated IG-element absorption lines were found in the respective stellar spectra. Therefore, two methods are presented, a manual and an automatic.

LINE1_PROF allows to change the element abundances in the synthetic spectra. To investigate one of the IG elements (or even just a certain ionization stage), the abundances of all others can be set to approximately zero, whereby absorption lines of a certain element or ion can be easily identified (as this leads to a change in the total flux, the individual spectra must be normalized). The basic procedure was to identify all absorption lines of the individual IG elements in the respective spectra and to find all isolated lines by comparing them with the spectrum that contains all IG elements.

8.1 EC 11481–2303

As shown in Fig. 24, the rotational broadening in EC 11481–2303 hampers the identification of isolated lines. To investigate this effect more closely, two synthetic spectra were created with LINE1_PROF, each containing only HHeCNO + Fe, one considering and one not considering stellar rotation. A comparison with the STIS observation showed that even if only iron as an IG element is taken into account, almost no isolated lines can be found (Fig. 28). After adding other IG elements it became clear that EC 11481–2303 is not suitable for investigating isolated absorption lines due to the relatively high rotational velocity of $v_{\mathrm{rot}} = 40\,\mathrm{km/s}$. For this reason, an identification and listing of the absorption lines of the individual IG elements shall also be dispensed with at this point. In addition, it should be noted that, since no isolated lines could be found, this criterion for determining the element abundances had to be relaxed accordingly in Sect. 7.1 and therefore, even line blends were used which, however, were not suitable for a detailed investigation.

8.2 Feige 110 – manual method

Since Feige 110 showed no recognizable rotation and no further problems that would hinder the identification of isolated IG-element absorption lines, it was carried out successfully. First, a manual method (by hand) was applied, which was then automated as a code, and therefore could be cross-checked for correctness immediately.

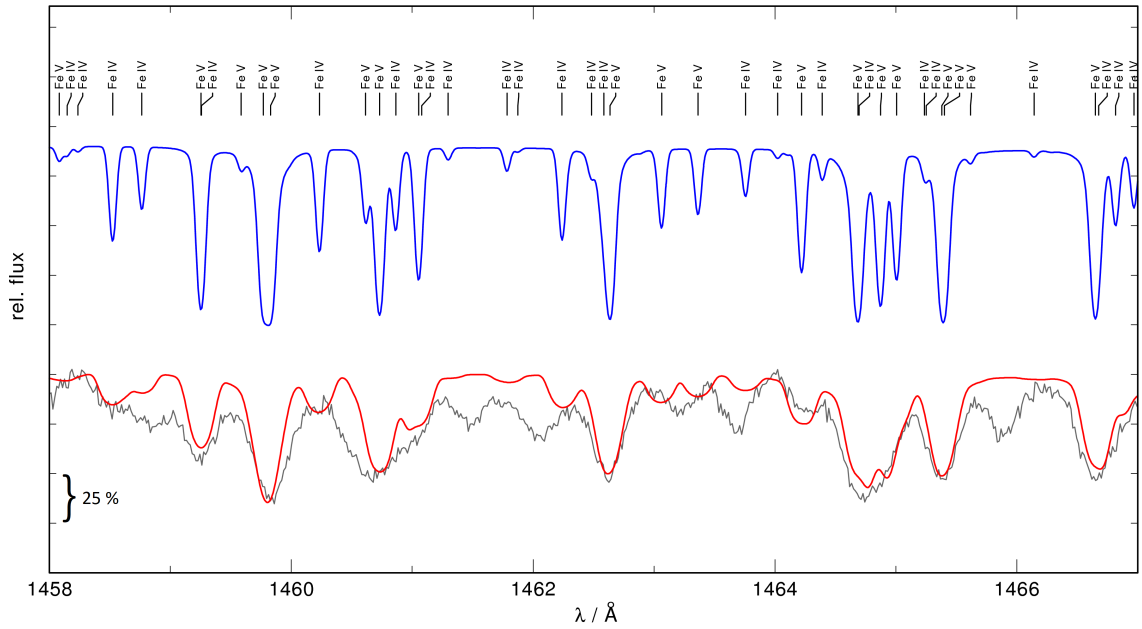

Figure 28: Section of synthetic EC 11481–2303 spectra generated with LINE1_PROF, which contain only HHeCNO + Fe, one with rotational broadening (red) and one without (blue, with offset), and STIS observation (gray). Individual Fe lines are labeled at the top.

Table 12: Segment of the IG-element line list of Feige 110. Ion, weighted oscillator strength $\log(gf)_{\mathrm{Kurucz}}$, and transition energies E_{low} and E_{up} are denoted.

Ion	λ / Å	$\log(gf)_{\mathrm{Kurucz}}$	E_{low} / cm^{-1}	E_{up} / cm^{-1}
Ni IV	1453.438	−1.481	156294.00	225096.40
Ni III	1453.478	0.894	203018.10	134217.60
Ni IV	1453.495	0.190	153533.60	222333.30
Cr IV	1453.514	−1.963	233708.50	164909.70
Fe IV	1453.606	−1.609	183164.49	251958.94
Co IV	1453.611	−0.509	152264.20	221058.40
Fe V	1453.617	0.423	221305.20	290099.10
Mn V	1453.630	−0.395	193781.60	262574.90
Ni IV	1453.643	−1.321	140140.90	208933.60
Ni IV	1453.662	−0.399	144815.10	213606.90
Cr IV	1453.759	−1.018	256306.20	187519.00
Ni V	1453.763	−0.963	247281.80	316068.80
Fe IV	1453.967	−0.707	190406.45	259183.82

A set of synthetic spectra was created with LINE1_PROF. One that contains all the elements HHeCNOSiSCaScTiVCrMnFeCoNi found in Sect. 7, nine others that each contain HHeCNOSiS + IG element (by setting the other IG-element abundances to ≈ 0), and 20 more, which contain single ionization stages, HHeCNOSiS + IG ion (stages III – VI) for Cr – Ni (For Ca – V this was not necessary due to the lower line count). For each of the IG ions, the corresponding atomic transitions of all clearly visible lines (Table 12,

the complete list of manually identified lines contains 5 394 transitions and is a subset of the automatically identified lines which will be shown in the next subsection) with an equivalent width of $W \gtrsim 2\,\mathrm{m\AA}$, the associated weighted oscillator strength $\log(gf)$ (with the statistical weight g and the oscillator strength f of the transition, see Eqs. 18 and 19) and transition energies were taken from Kurucz's line lists[22]. This detailed list with all ions was necessary in order to be able to rule out that an apparently individual IG-element line is an overlap of several transitions of the same element (e.g., different ions). Then, the synthetic spectra in the STIS spectral range $\lambda = 1\,144\,\text{Å} - 1\,709\,\text{Å}$ were compared piece by piece in order to find all isolated lines, i.e., without overlaps (Fig. 29). The result was 456 isolated lines (Table 28 in the appendix).

Even though the just shown method gives a good result with regard to the isolated line identification, it has some weak points. Apart from the considerable amount of time required, the selection criteria, e.g., for which lines are "clearly visible" or the allowed overlap, are not clearly defined, since everything was previously only selected by eye. Nevertheless, the developed method and the corresponding lists were necessary to now be able to implement the same steps as an automatic method.

[22] POS list from `http://kurucz.harvard.edu/atoms.html` .

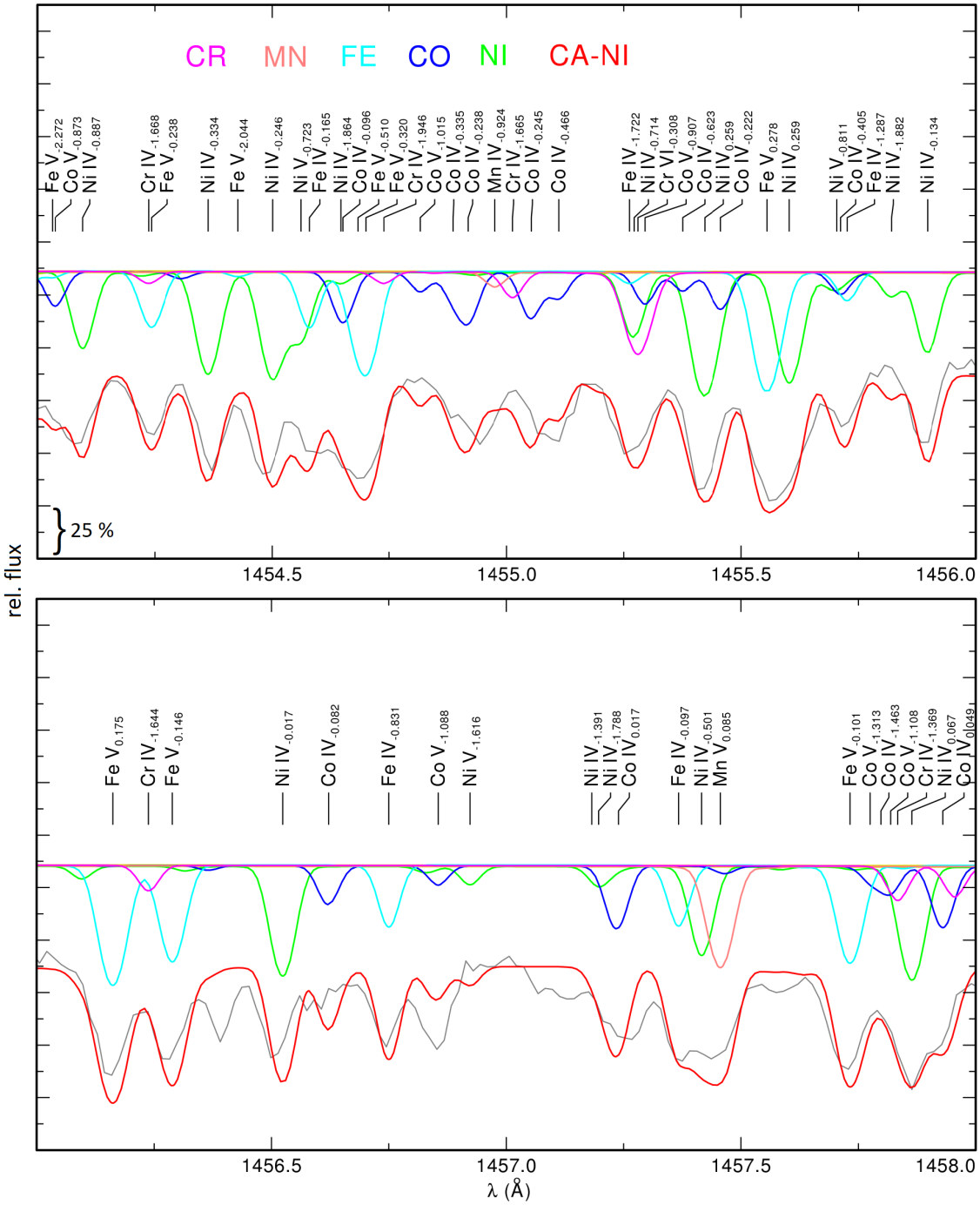

Figure 29: Section of the Feige 110 spectrum (STIS observation in gray, synthetic spectra colored accordingly, with offset) for isolated absorption line identification. Individual IG-ion lines are labeled, with $\log(gf)$ in the index. In the shown section, only two isolated lines (Ni IV λ 1 454.36 Å and Fe IV λ 1 456.75 Å) and two lines with little coverage (Ni IV λ 1 456.52 Å and Co IV λ 1 456.63 Å) could be found.

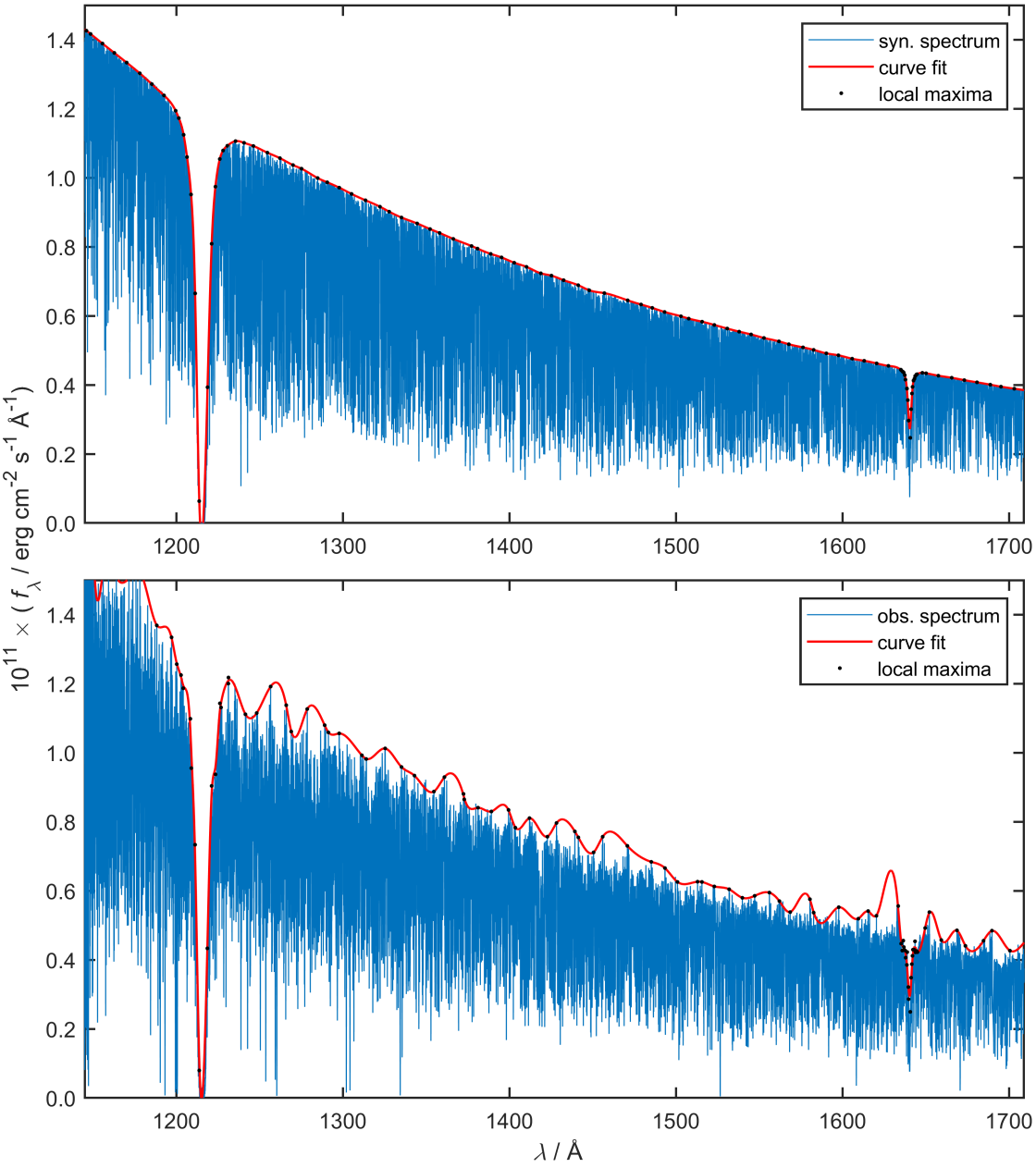

Figure 30: *Top*: Continuum-flux determination of the synthetic spectrum (HHeCNO-CaScTiVCrMnFeCoNi) based on the sectional determination of local maxima and subsequent fitting with cubic splines. *Bottom*: Same method which is unsuccessfully applied on the observed spectrum.

8.3 Feige 110 – automatic method

The automatic method aims to carry out the same steps as the manual method, with clearly defined criteria. In the following, the individual criteria are presented as well as routines that implement them. Finally, it is shown how the method was used to create a list of isolated lines. All routines were written as MATLAB scripts (version 9.7.0, MATLAB 2019) and can be found in the appendix (Sect. A.2).

8.3.1 Continuum-flux determination

To find out which absorption lines are relevant for the evaluation after all, their equivalent widths must be determined. Although several routines for this, e.g., for IRAF[23] or Astropy[24] already exist, these are not fully automatic. Usually, the local continuum has to be determined manually for each absorption line, or at least the wavelength interval has to be selected, which turns out to be time-consuming when evaluating more than 5 000 lines. The first MATLAB script calculates the continuum flux for each point in the spectrum so that the continuum is available as a wavelength-dependent function for the entire spectrum.

For this purpose, the synthetic spectrum created with LINE1_PROF and containing the investigated IG ion was imported into the script. The idea for determining the continuum is to look for local flux maxima in small intervals and to fitting these maxima with a smooth function that represents the continuum. The intervals for determining the local flux maxima were selected in sections between 1 and 5 Å (only smaller than 5 Å in ranges where broad absorption lines, for example of H or He, are found, to also correctly consider the IG-element lines, see, e.g., Fig. 22). The maxima were then fitted with cubic splines, whereby a function that indicates the respective local continuum in the entire wavelength range (Fig. 30) was created.
For further processing, the flux of the synthetic spectrum was subtracted from the continuum flux just created. Small fluctuations ($< 1/100\, f_\lambda$) were set equal to zero, so that the obtained, reduced flux f_{red}, is only unequal to (greater than) zero at points where absorption lines are present.

Strictly repeating the same procedure for the observed spectrum was crowned with little success. Noise of different intensity, sections that are significantly weaker than the synthetic spectrum (due to absorption lines of elements that were not taken into account in the synthetic spectra), or inaccuracies in the reassembling of the échelle orders made it impossible to use a smooth curve as a fit for the obtained continuum (Fig. 30). Therefore, a χ^2 method was applied to determine the factor by which the continuum obtained for the synthetic spectrum has to be multiplied in order to obtain the smallest squared deviation from the observed spectrum. For this purpose, the local maxima in the spectrum were determined again, this time section by section in smaller (due to the more intense noise) intervals between 1 and 2.5 Å. Subsequently, all local maxima were excluded from these maxima (this was necessary to compensate inaccuracies in the reassembling of the échelle orders, i.e., it is expected that the function of the maxima is monotonically decreasing with increasing wavelength), and then, the just mentioned correction factor for the continuum was determined by χ^2 minimization to 1.06 (Fig. 31). This procedure allowed the synthetic spectrum to be normalized more precisely, which also led to a slight change in the examined elements' abundances.

[23] Image Reduction and Analysis Facility, `http://iraf.noao.edu`
[24] `https://www.astropy.org`

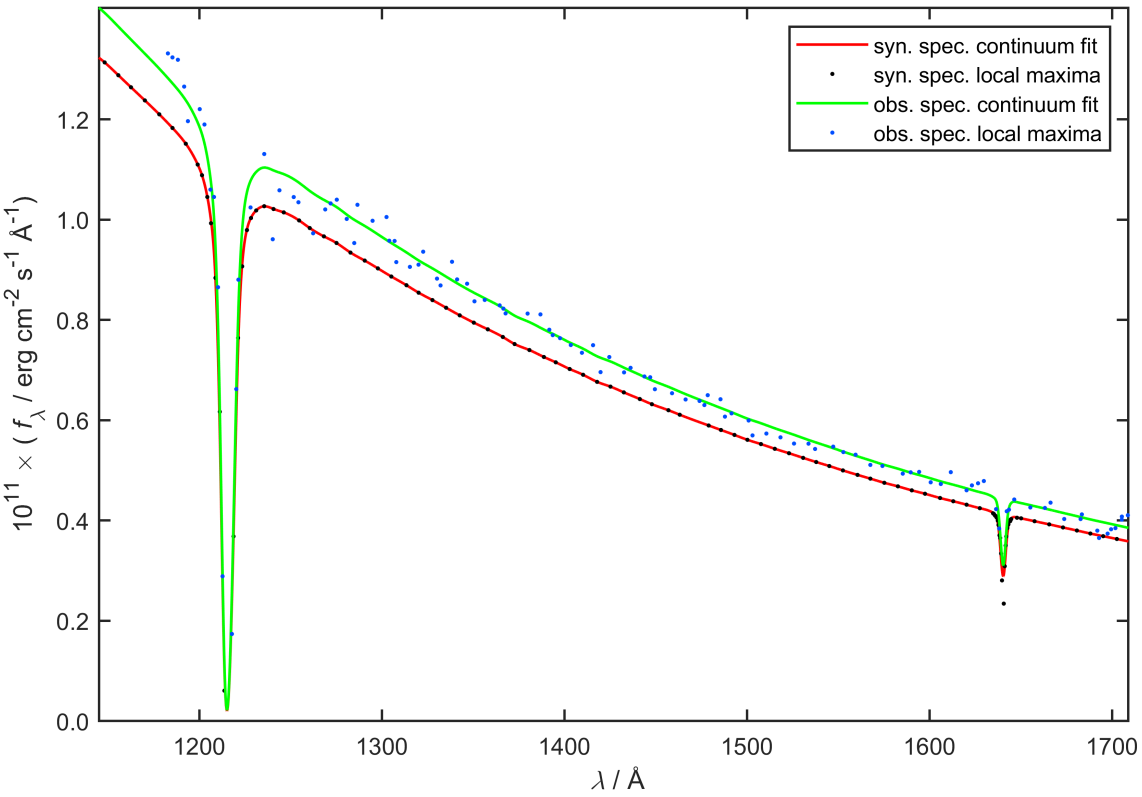

Figure 31: Local maxima and continuum of the synthetic spectrum (HHeCNOSiSCaSc-TiVCrMnFeCoNi), which had to be multiplied by 1.06 to obtain the smallest deviation from the obtained local maxima of the observed spectrum.

8.3.2 Determination of line properties

Each local maximum in the reduced flux approximately corresponds to an absorption line center (unless several lines overlap strongly, more on this later), so these were saved in a list. Then, a certain interval around each local maximum was fitted with a Gaussian profile. The actual line shape corresponds to a Voigt profile, the convolution of a Lorentzian and a Gaussian profile (Sect. 3.2.5), with the properties of the Lorentzian profile mainly showing in the line wings, due to pressure broadening or, more precisely, in the case of the IG elements, the quadratic Stark effect. This is significantly weaker (Sect. 3.2.2) in comparison to the linear Stark effect, which, for example, causes very wide wings of the Ly α line, whereby IG-element absorption-line profiles could be approximated very well by a Gaussian profile (Fig. 32). The fitting interval was either chosen to ± 0.1 Å around the respective local maximum, or, in the case that two local maxima were closer, one third of the distance to the next maximum. Thus, it was prevented that two overlapping lines are incorrectly detected as one.

Therefore, the following profile was used for fitting

$$G(\lambda) = A \cdot \exp\left(-\left(\frac{\lambda - \lambda_0}{\sigma}\right)^2\right) \quad ,$$

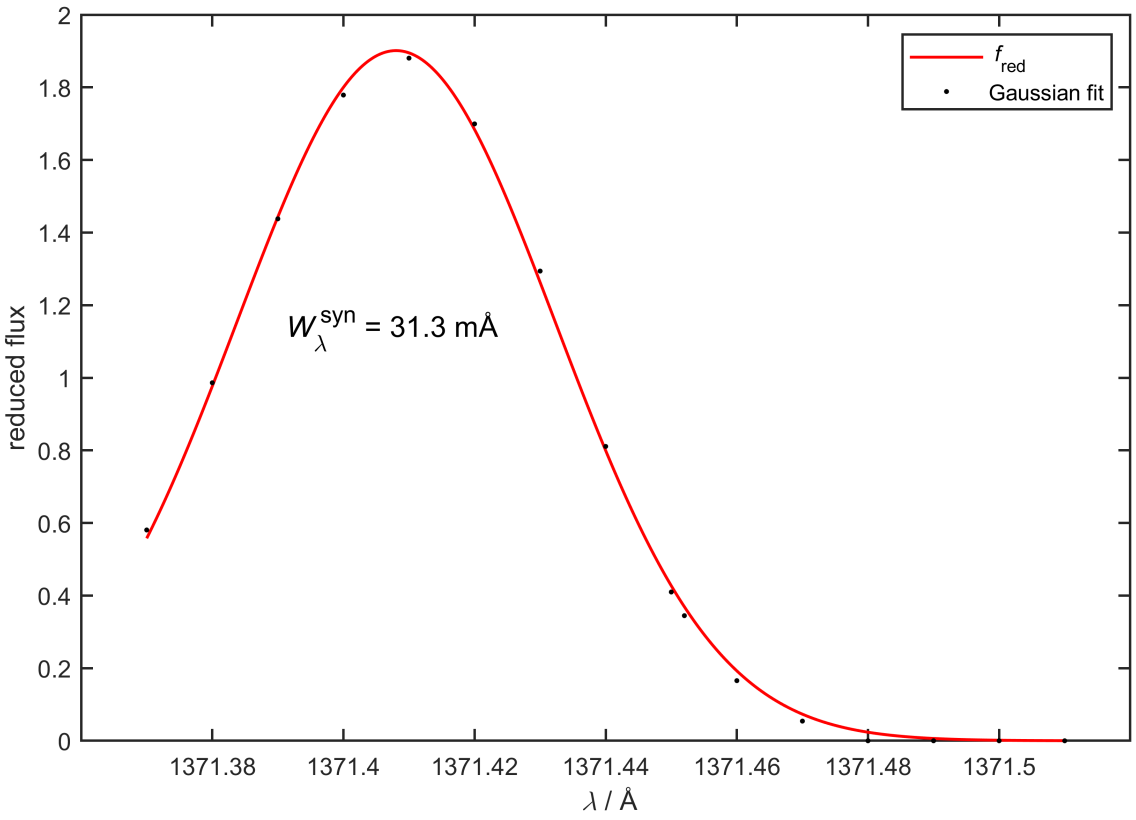

Figure 32: Fitting a Ni IV line in the reduced flux with a Gaussian profile. The fitting interval is 0.1 Å to the right of the local maximum, but only about 0.04 Å to the left, since another absorption line follows. The equivalent width of 31.3 mÅ is given.

from which all relevant line properties could be taken. The line depth A, the line center λ_0, the FWHM $\triangle\lambda_{\mathrm{FWHM}} = 2\sqrt{\ln 2}\,\sigma$ and the equivalent width (Sect. 3.2.6)

$$W_\lambda = 1/f_\mathrm{c} \cdot \int G(\lambda)\,\mathrm{d}\lambda = A\,\sigma\,\sqrt{\pi}/f_\mathrm{c}$$

were obtained and saved in a list. Also, the goodness of each fit was saved. A low goodness of fit is an indication that two absorption lines were too close to each other and could not be successfully fitted with a single Gaussian profile. This was taken into account later.

8.3.3 Determination of the corresponding transitions

First, all lines associated with the elements HHeCNOSiS were deleted from the list of fits that had just been created. For this purpose, a corresponding identification list was read into a script. All lines whose center is closer than 0.03 Å to a line of the just mentioned light metals were removed, leaving only lines of the investigated IG ion under consideration. The corresponding IG ion's list of transitions containing the line center, the transition's associated weighted oscillator strength $\log(gf)$, and transition energies were then read from Kurucz's POS lists. All transitions, which lie in the examined wavelength interval $\lambda = 1\,144$ Å – $1\,709$ Å and feature weighted oscillator strengths of $\log(gf) > -2.5$ (smaller $\log(gf)$ values should not contribute to visible absorption lines), were taken over. Then, all lines with an equivalent width of $W_\lambda < 1.5$ mÅ were removed from the list of fits since these can also be considered not visible. In contrast to the manual method, here,

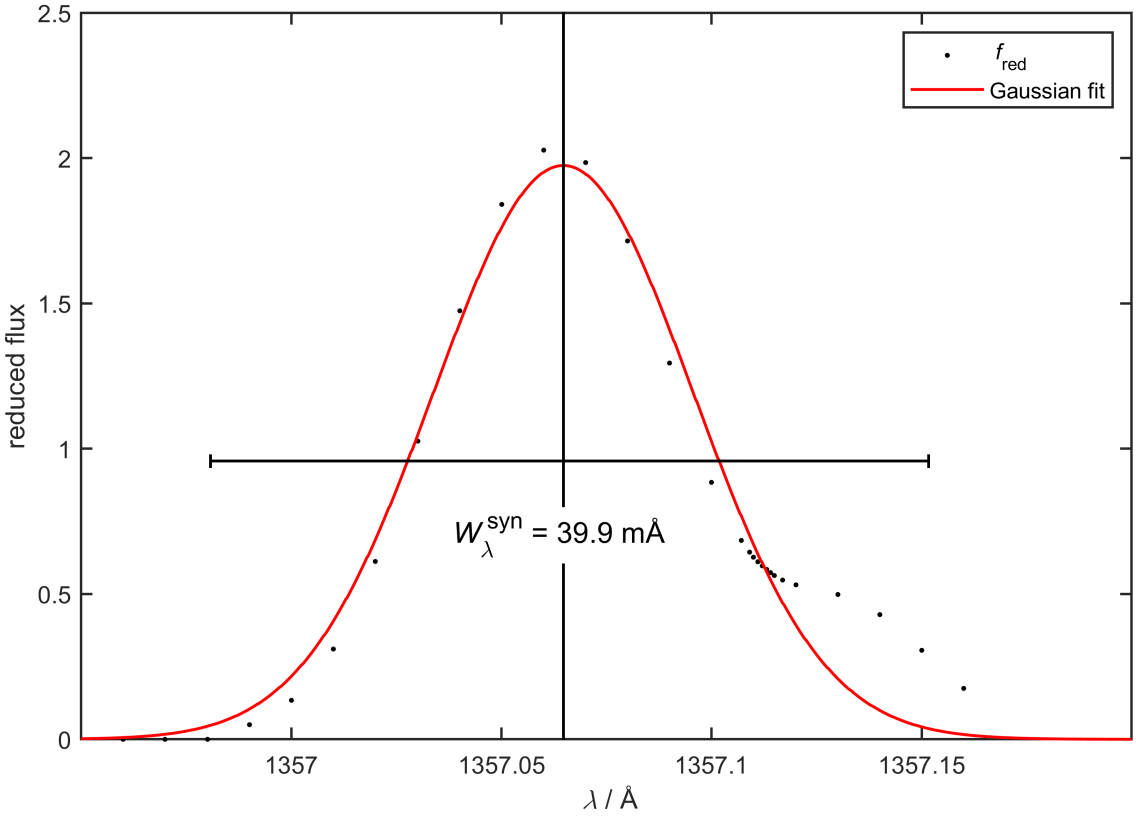

Figure 33: Low-quality fit of a Ni IV line. The line center and the interval from which the transitions from Kurucz's list were still accepted are shown (black).

this criterion is clearly defined by W_λ. After both lists were reduced accordingly, all transitions from Kurucz's POS list that are closer than 0.05 Å to the line center could be adopted for each remaining line in the list of fits. This prevented that multiple transitions, which merge into a seemingly single absorption line, were recognized as just one.

8.3.4 List of transitions corrections

Before the list of transitions of an IG ion could be finalized, the low-quality fits had to be examined. As a rule, several absorption lines overlapped here, so that they no longer had approximately the profile of a Gaussian. Depending on the goodness, all qualified transitions in an interval of $\triangle\lambda = \pm\,(\,0.05 - 0.15)$ Å were taken from the reduced Kurucz's list (Fig. 33), as they could contribute to the overlapping absorption lines.
Finally, for transitions with $\log(gf) > -1$, all significantly weaker transitions close by ($\triangle\lambda < 0.03$ Å and $\triangle\log(gf) > 1.5$) were removed, as these should contribute an insignificant part to the overall line strength.

The routines just presented were carried out analogously for all investigated ionization stages (for elements with few absorption lines several ionization stages could be combined) of the IG elements, and the transitions were saved in corresponding lists. Slightly different from Sect. 8.2, this resulted in a total of 6 068 transitions (to be found at `https://github.com/iaatue/LandstorferPhD`), because some weaker transitions were not taken into account in the manual method. The routine shown below is devoted to creating the list of isolated lines.

Table 13: Statistics of the transitions and isolated lines found with the automatic method in Feige 110.

Element	Ion	Transitions[a]	Isolated lines
Ca	III-VI	17	0
Sc	III-VI	10	0
Ti	III-VI	78	5
V	III-VI	73	5
Cr	III	5	0
	IV	445	44
	V	43	8
	VI	10	0
Mn	III	6	1
	IV	68	9
	V	185	28
	VI	38	1
Fe	III	1	0
	IV	750	149
	V	631	70
	VI	108	6
Co	III	0	0
	IV	680	76
	V	711	53
	VI	162	14
Ni	III	5	0
	IV	771	99
	V	1 106	83
	VI	165	9
Σ		6 068	660

[a]Applied to the STIS observation spectral range. Only lines with an equivalent width of $W_\lambda > 1.5\,\mathrm{m\AA}$ were counted.

8.3.5 Finding isolated lines

First, the list with all transitions from Sect. 8.3.4 and the synthetic spectrum, which contains all found elements HHeCNOSiSCaScTiVCrMnFeCoNi, were read into a script. Analogous to Sects. 8.3.1 and 8.3.2, the continuum flux was determined and Gaussian fits around all local maxima were carried out and saved in a list. All low-quality fits were removed from the list as they cannot belong to an isolated absorption line. In addition, all lines with $W_\lambda < 1.5\,\mathrm{m\AA}$ were removed as well.
An absorption line is considered to be isolated if its area largely results from a single transition in a certain interval around its line center. For each fit, the line area (in the reduced spectra) of the individual IG ions was thus determined in an interval of $\triangle\lambda = \pm 1.82\,\sigma$ (which corresponds to $\approx 99\%$ of the line area) and compared with each other. A line was considered isolated if at least 90% of its area was caused by a single IG ion. The criterion of 90% represents a good compromise in order to obtain a certain number of lines to be evaluated, while not allowing a too large inaccuracy (at least in

Table 14: Like Table 13, for PG 0909+276.

Element	Ion	Transitions	Isolated lines
Ca	II-V	33	0
Sc	II-V	63	1
Ti	II-V	68	1
V	II-V	159	1
Cr	III	690	5
	IV	591	17
	V	39	1
Mn	III	278	4
	IV	104	2
	V	127	1
Fe	III	455	2
	IV	779	10
	V	333	1
Co	III	505	7
	IV	1 280	31
	V	849	6
Ni	II	17	0
	III	1 142	7
	IV	1 006	22
	V	1 010	13
Σ		9 528	132

this step). Finally, it had to be checked whether several transitions of the same ions were so close to one another that they were misinterpreted as a single line. For this purpose, each line in the list of transitions was checked for whether there exists only one qualified transition in the interval $\triangle\lambda = \pm\sigma$ around the line center. If so, the line was added to the list of isolated lines. In this way 660 isolated lines were found (Table 13). These are more than found by the manual method. The extra lines are mostly weaker lines that seem to have been overlooked.

8.4 PG 0909+276

The method used for PG 0909+276 to determine all visible transitions of the IG ions and the isolated absorption lines is analogous to Sect. 8.3. Only some adjustments concerning the continuum-flux determination and the ions of the IG elements to be considered had to be made in the code. A total of 9 528 transitions (to be found at `https://github.com/iaatue/LandstorferPhD`) according to Sects. 8.3.3 and 8.3.4 was determined. At first glance, this sounds like a better result than for Feige 110, but the excess of absorption lines led to more frequent overlaps, which significantly reduced the isolated line count to 132 (Table 14).

9 Evaluation

After the list of clearly visible, isolated IG-element absorption lines for Feige 110 and PG 0909+276 was created from the synthetic spectra, the used theoretical line strengths (from Kurucz's POS lists) had to be compared with the observed ones obtained from the STIS spectra. Therefore, the equivalent width W_λ (Sect. 3.2.6) is a suitable measure. In the following, the used method to determine W_λ for all isolated lines in both the synthetic and the observed spectrum is presented. The results are then summarized for both stars.

9.1 Method

The synthetic spectrum containing all examined elements, the STIS observation, as well as the list of isolated lines created in Sect. 8.3 or Sect. 8.4 were read into a script. Then, according to Sect. 8.3.1, the continuum flux was determined based on the synthetic spectrum and normalized based on the observed spectrum. For each line center from the list of isolated lines, the adjacent local maxima were then searched in the synthetic spectrum. For this interval, the reduced spectrum was created locally, and a Gaussian fit was carried out. Accordingly, the adjacent local maxima around the line center were searched for in the STIS observation. Due to the noise, however, sometimes the maxima were too close to the line center, so that a minimum distance of $1.2\,\sigma$ from the line center was chosen as a further criterion for determining the interval (which includes at least 95% of the line area; σ results from the Gaussian fit in the synthetic spectrum). The reduced spectrum was also created locally for this interval and then a Gaussian fit was carried out.

Where larger deviations of the equivalent widths W_λ^{obs} and $W_\lambda^{\mathrm{Kurucz}}$ (hereinafter W_λ^{syn}) were found, the line properties had to be compared more closely. In some cases, strong deviations were found in the line centers and/or the FWHMs. This could happen when an absorption line in the observation is a blend of lines from other elements that were not taken into account in the model. In that case, it happens to be $W_\lambda^{\mathrm{obs}} > W_\lambda^{\mathrm{syn}}$. Deviations in the line centers could happen due to inaccuracies in the calculations or laboratory measurements in Kurucz's line lists. As a measure for the deviations of W_λ^{obs}, the reduced equivalent width $W_{\lambda,\mathrm{red}}^{\mathrm{obs}}$ is introduced as an empirical variable (Fig. 34):

$$W_{\lambda,\mathrm{red}}^{\mathrm{obs}} = W_\lambda^{\mathrm{obs}} \cdot \frac{\sigma_{\mathrm{obs}}}{\sigma_{\mathrm{syn}}} \cdot \left(1 - \left(\frac{\delta\lambda}{\sigma_{\mathrm{obs}}}\right)^2\right) \quad , \tag{20}$$

with the deviation of the line center $\delta\lambda$ (quadratic dependence on $\delta\lambda$ makes sense since the line center can be roughly approximated as parabolic, and $\sigma_{\mathrm{obs}}/\sigma_{\mathrm{syn}}$ turns out to be a useful factor to compare the relative line widths). $W_{\lambda,\mathrm{red}}^{\mathrm{obs}}$ is a good measure of the

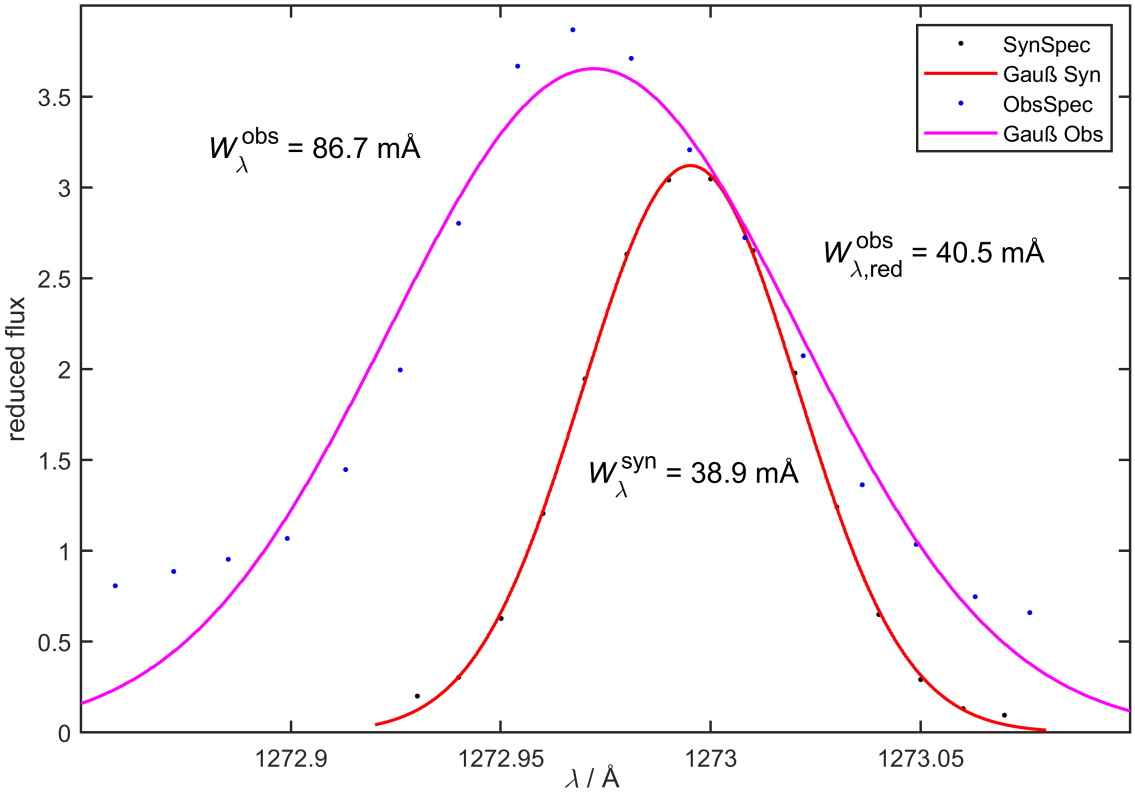

Figure 34: Cr IV line in the synthetic and observed reduced spectrum of Feige 110. The line is clearly covered by a stronger absorption line and will therefore not be evaluated later. The empirically determined reduced equivalent width is indicated.

equivalent width corresponding to the synthetic line-position, even though, as said, it is only empirically determined. The factor $W_{\lambda,\mathrm{red}}^{\mathrm{obs}}/W_\lambda^{\mathrm{obs}}$, which indicates the strength of the necessary correction, was saved for each line and could be used for the subsequent evaluation.

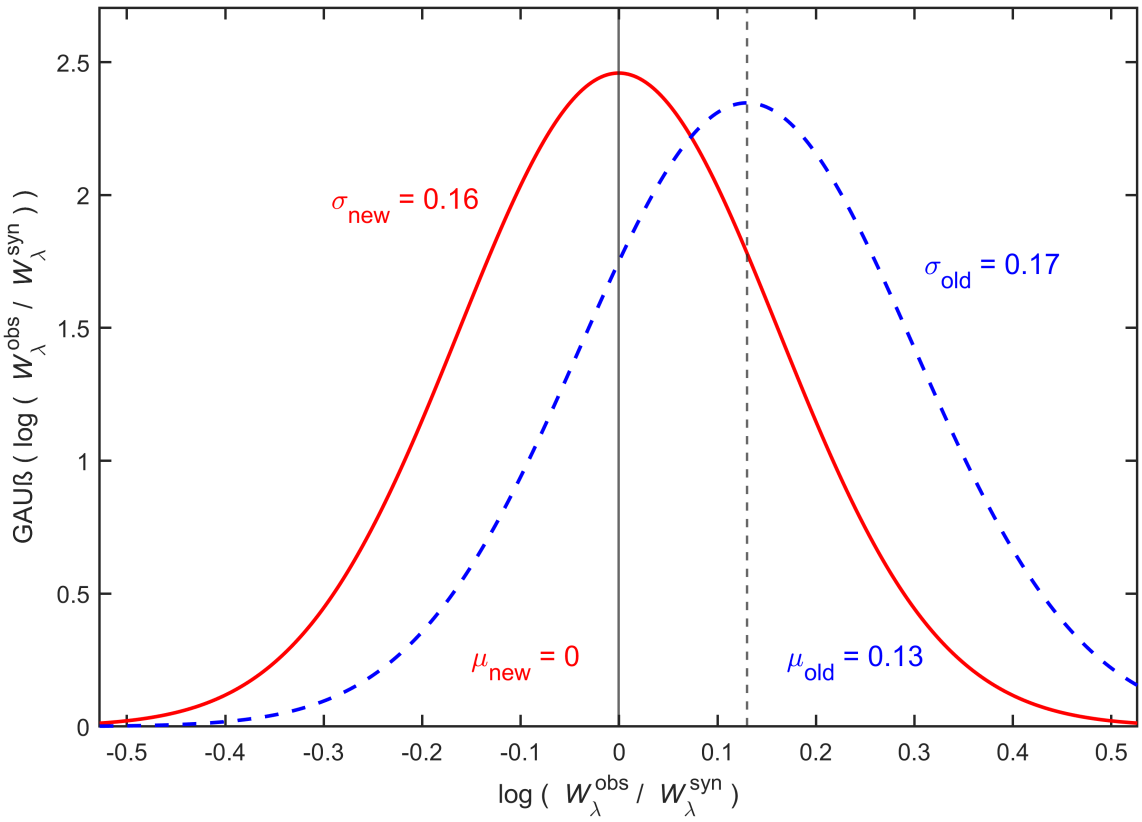

Figure 35: Gaussian fits of $\log(W_\lambda^{\rm obs}/W_\lambda^{\rm syn})$ before (blue, dashed) and after (red) the correct IG-element-abundance adjustments (Table 15), with the mean value μ and standard deviation σ of the fit. $\mu = 0$ corresponds to $W_\lambda^{\rm obs} = W_\lambda^{\rm syn}$.

9.2 Feige 110

From 660 isolated IG-element absorption lines only 599 lines with $\lambda > 1\,200$ Å could be used for the final evaluation, since the noise in the observed spectrum is too high at shorter wavelengths. As an additional criterion, lines with too large corrections of $W_{\lambda,\rm red}^{\rm obs}/W_\lambda^{\rm obs} > 1.8$, $W_{\lambda,\rm red}^{\rm obs}/W_\lambda^{\rm obs} < 0.55$ or $W_\lambda^{\rm obs}/W_\lambda^{\rm syn} > 5$, $W_\lambda^{\rm obs}/W_\lambda^{\rm syn} < 0.2$ were excluded from the evaluation, since in these cases there is usually no more direct relation between the line in the observed and synthetic spectrum (the choice of the above-mentioned reduction criteria was, like the choice for $W_{\lambda,\rm red}^{\rm obs}$ itself, only empirical, see Sect. 9.4). For the 392 remaining lines, the equivalent widths derived from the observation were compared with the synthetic ones (Table 26 in the appendix).

The general equivalent-width distribution could be better represented by Gaussian fitting of the logarithm $\log(W_\lambda^{\rm obs}/W_\lambda^{\rm syn})$ (Fig. 35), since deviations of the quotient are considered uniform in both directions (hence a normal distribution is expected). $\mu > 0$ describes the systematic deviation $W_\lambda^{\rm obs} > W_\lambda^{\rm syn}$, which can be referred to an imprecise abundance determination by hand[25] and can be improved by increasing the abundances. Corresponding adjustments could be made for all IG elements of which enough isolated lines could be

[25]The first evaluation was performed before the corrected broadening for the LSF was applied (Sect. 6), which led to an overestimation of the line center, hence too-low abundances have been determined by hand. This was, as can be seen, corrected by the equivalent-width analysis, which is independent of line broadening.

Table 15: Gaussian-fit statistics of $\log(W_\lambda^{\mathrm{obs}}/W_\lambda^{\mathrm{syn}})$ of the various IG elements (and ions) in Feige 110. The necessary abundance adjustments to obtain $\mu_{\mathrm{new}} = 0$ are given. For Ca – V, too few examined lines were found for a statistically significant statement.

Element	Ion	Line count	μ_{old}	μ_{new}	Abundance	σ
Cr	IV	22	0.09	–0.02		0.19
	V	6	0.17	0.07		0.05
	IV–V	28	0.10	0.0	×3.08	0.17
Mn	IV	5	0.28	0.16		0.21
	V	15	0.06	–0.06		0.09
	III–VI	22	0.12	0.0	×3.44	0.15
Fe	IV	119	0.13	0.02		0.14
	V	48	0.11	–0.04		0.14
	IV–V	166	0.13	0.0	×3.11	0.14
Co	IV	47	0.20	0.01		0.19
	V	26	0.10	–0.02		0.22
	III–VI	74	0.16	0.0	×3.27	0.20
Ni	IV	72	0.12	0.0		0.12
	V	26	0.14	0.01		0.26
	IV–VI	98	0.12	0.0	×4.17	0.17

examined (Table 15), so that the corrected distribution shown in Fig. 35 has $\mu_{\mathrm{new}} = 0$ and therefore does not have any abundance-related systematic deviations (see also Fig. 37). Overall, the spread then amounts to $\sigma = 0.16$ (standard deviation) or, expressed linearly, 45 %.

In addition, individual ionization stages of Cr, Mn, Fe, Co, and Ni were investigated. There, deviations from μ could theoretically be improved by changing T_{eff} (a higher T_{eff} leads to the domination of higher ionization stages and vice versa). Since the tendencies for the different elements, however, do not go in the same direction (for Cr, T_{eff} theoretically has to be increased, but decreased for Mn, Fe, and Co), the deviation is due to other causes, such as inaccuracy due to an insufficient number of lines. This is supported by the fact that in the case of Cr and Mn, which have significantly fewer investigated lines, the variation of μ_{new} of the individual ions is considerably higher than that of Fe, Co, and Ni.

To find further possible systematic uncertainties of the weighted oscillator strengths gf in Kurucz's lists, W_λ^{obs} was plotted against W_λ^{syn} (Fig. 36). A noticeable feature here is that the values for $W_\lambda^{\mathrm{obs}} > W_\lambda^{\mathrm{syn}}$ are more widely spread than for $W_\lambda^{\mathrm{syn}} > W_\lambda^{\mathrm{obs}}$. In principle, this is more likely to be expected than the other way around, since elements that were not taken into account in the model spectrum could also contribute to an absorption line in the observed spectrum. Otherwise, as expected, all values are distributed fairly evenly around the mean $W_\lambda^{\mathrm{obs}} = W_\lambda^{\mathrm{syn}}$ without any further anomalies. So, at least among the examined lines, neither transition-specific strong systematic deviations (as can be found, e.g., in Fig. 12), nor element-specific deviations were found.

Another possible uncertainty is a wavelength dependence. This was also investigated by plotting $\log(W_\lambda^{\mathrm{obs}}/W_\lambda^{\mathrm{syn}})$ against λ (Fig. 38). No noticeable deviations were found here, meaning that a wavelength dependency as a gf-value uncertainty source can be almost

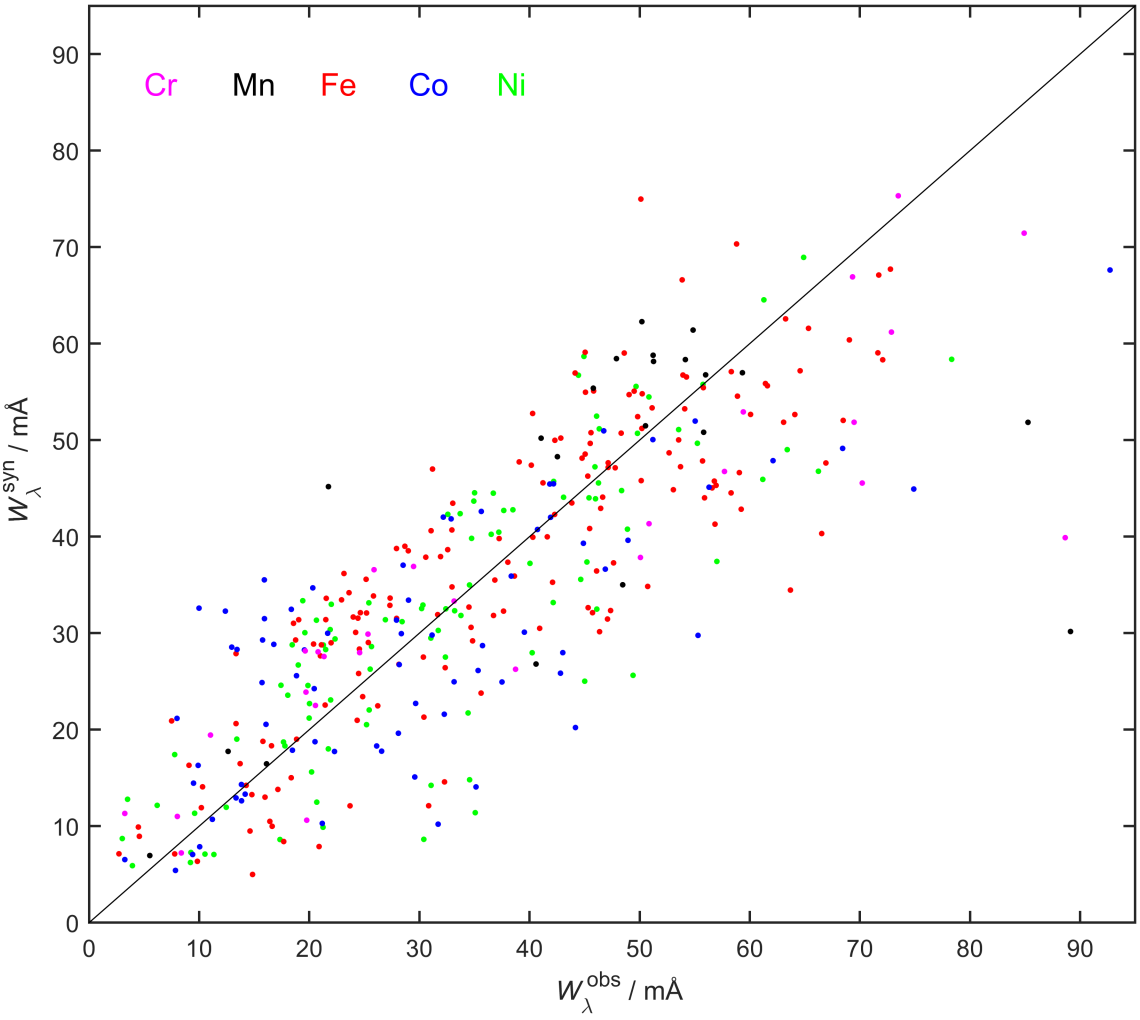

Figure 36: Comparison of the observed equivalent widths with the synthetic ones in Feige 110. As expected, the values scatter around the ideal value of $W_\lambda^{\rm obs} = W_\lambda^{\rm syn}$ (black straight line). The IG elements are color labeled.

excluded. The line widths ($\triangle\lambda_{\rm FWHM}$) of the observation and the model could also be compared to check whether all broadening mechanisms (Sect. 3.2, Sect. 3.3, and Sect. 6) were correctly taken into account. Here, first it was found that the observation has, on average, wider lines than the model (Fig. 18), which has been dealt with in Sect. 6 and therefore has been corrected during the final evaluation. Anyway, deviations of this kind are irrelevant for the line-strength evaluation since the equivalent width of a line is in principle independent of $\triangle\lambda_{\rm FWHM}$. Finally, it was checked whether a slight change of the surface gravity within the error limits $\log g = 6.0 \pm 0.2$ specified in Sect. 7.2 leads to a change in the results. Small but insignificant changes were found when plotting according to Fig. 36 and Fig. 38, which did not lead to deviations in the parameters μ and σ of the Gaussian fit.

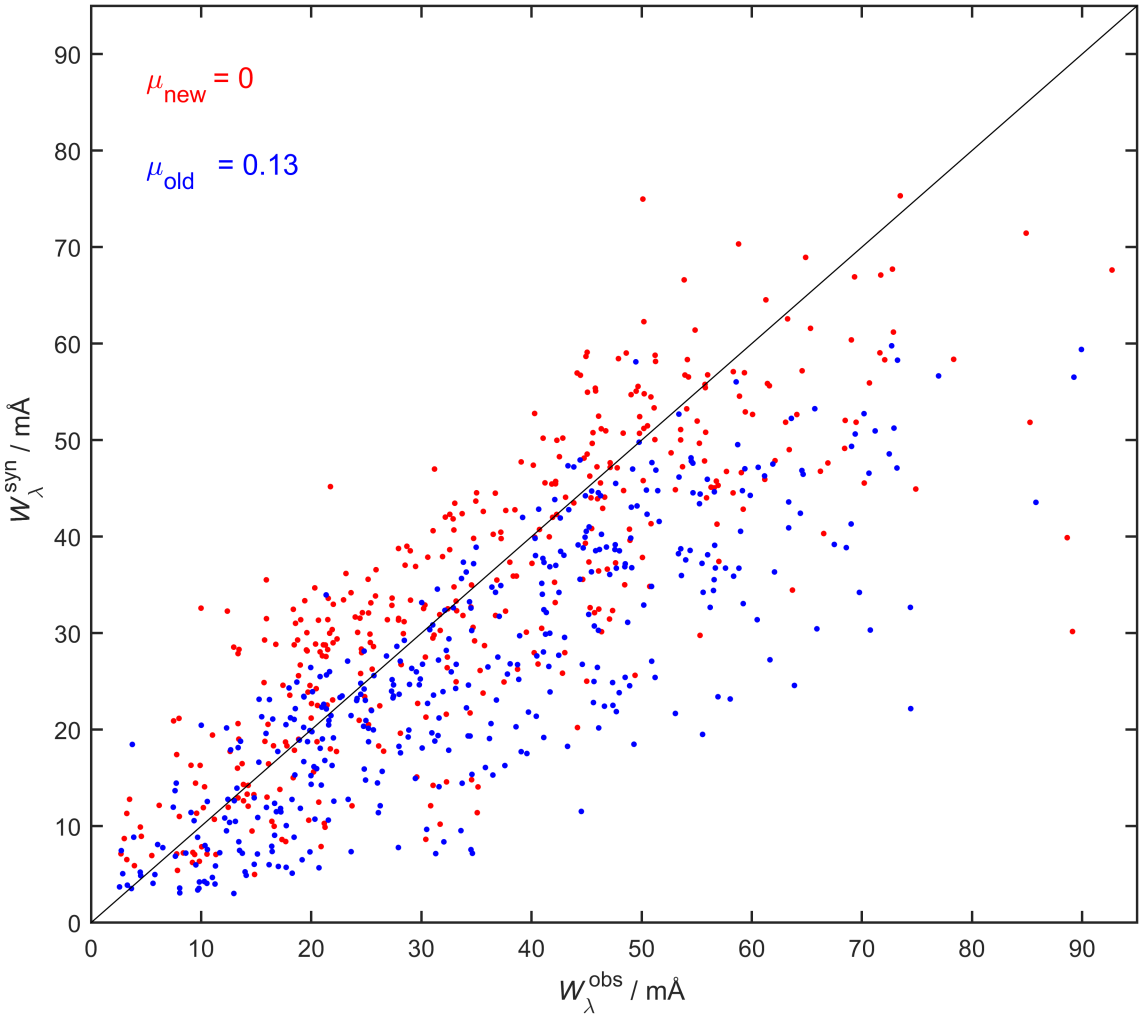

Figure 37: Comparison of the observed equivalent widths with the synthetic ones in Feige 110, before and after the abundance correction.

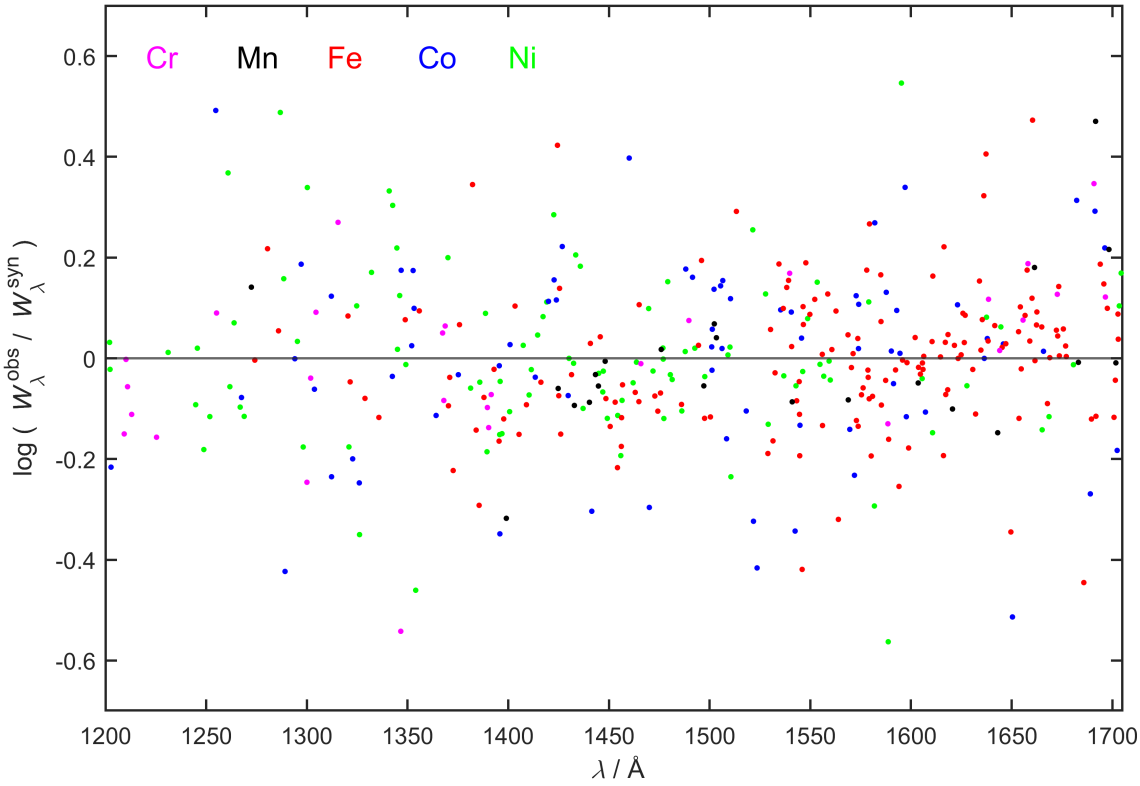

Figure 38: $\log(W_\lambda^{\rm obs}/W_\lambda^{\rm syn})$ in Feige 110, plotted against the wavelength λ. The IG elements are color labeled, and the value for $W_\lambda^{\rm obs} = W_\lambda^{\rm syn}$ is indicated by the black horizontal line at 0.

Table 16: Gaussian-fit statistics of $\log(W_\lambda^{\rm obs}/W_\lambda^{\rm syn})$ of the various IG elements (and ions) in PG 0909+276. The necessary abundance adjustments to obtain $\mu_{\rm new} = 0$ are given. For Ca – V and Mn, too few examined lines were found for a statistically significant statement.

Element	Ion	Line count	$\mu_{\rm old}$	$\mu_{\rm new}$	Abundance	σ
Cr	IV	9	0.08	–0.03		0.13
	III–IV	10	0.12	0.0	×2.59	0.16
Fe	IV	8	0.08	0.01		0.09
	III–IV	9	0.08	0.0	×1.93	0.09
Co	III	5	0.08	0.06		0.16
	IV	17	0.02	–0.02		0.27
	III–V	24	0.04	0.0	×0.98	0.27
Ni	III	6	0.09	–0.10		0.19
	IV	10	0.09	0.01		0.19
	V	4	–0.01	0.12		0.56
	III–V	20	0.08	0.0	×4.70	0.29
Ca – Ni		65	0.06	0.0		0.23

9.3 PG 0909+276

From 132 isolated IG-element absorption lines, only 122 lines with $\lambda > 1\,180\,\text{Å}$ could be used for the final evaluation, since the noise in the observed spectrum is too high at shorter wavelengths. As an additional criterion, lines with too large corrections of $W_{\lambda,\rm red}^{\rm obs}/W_\lambda^{\rm obs} > 1.8$, $W_{\lambda,\rm red}^{\rm obs}/W_\lambda^{\rm obs} < 0.55$ and $W_\lambda^{\rm obs}/W_\lambda^{\rm syn} > 5$, $W_\lambda^{\rm obs}/W_\lambda^{\rm syn} < 0.2$ were again excluded from the evaluation. For the remaining 65 lines, evaluations analogous to Sect. 9.2 were carried out (Table 27 in the appendix).

Investigation and Gaussian fitting of the distribution $\log(W_\lambda^{\rm obs}/W_\lambda^{\rm syn})$ again resulted in $\mu > 0$ or, on average, $W_\lambda^{\rm obs} > W_\lambda^{\rm syn}$. After adjusting the abundances accordingly, $\mu_{\rm new} = 0$ was obtained again (Table 16), whereat it must be noted that the lower line count can lead to less meaningful statistics. Since the tendencies of $\mu_{\rm new}$ point to different directions for the various ionization stages, no statement can be made about a possible change in $T_{\rm eff}$. Here, too, it can be noted that there may not be enough lines of a single ion to obtain a statistically valuable statement. Overall, the spread amounts to $\sigma = 0.23$ or, expressed linearly, 72 %.

Plotting $W_\lambda^{\rm obs}$ against $W_\lambda^{\rm syn}$ (Fig. 39), in contrast to Feige 110, resulted in a stronger general spread, which is not unusual due to the fewer line count. Here, too, no transition-specific or element-specific systematic deviations were found among the examined lines. A possible wavelength dependency was examined again by plotting $\log(W_\lambda^{\rm obs}/W_\lambda^{\rm syn})$ against λ, and no systematic deviations were found here either (Fig. 40). Changes in the surface gravity within the error limits $\log g = 6.1 \pm 0.2$ specified in Sect. 7.3 were also checked, without any noticeable deviations.

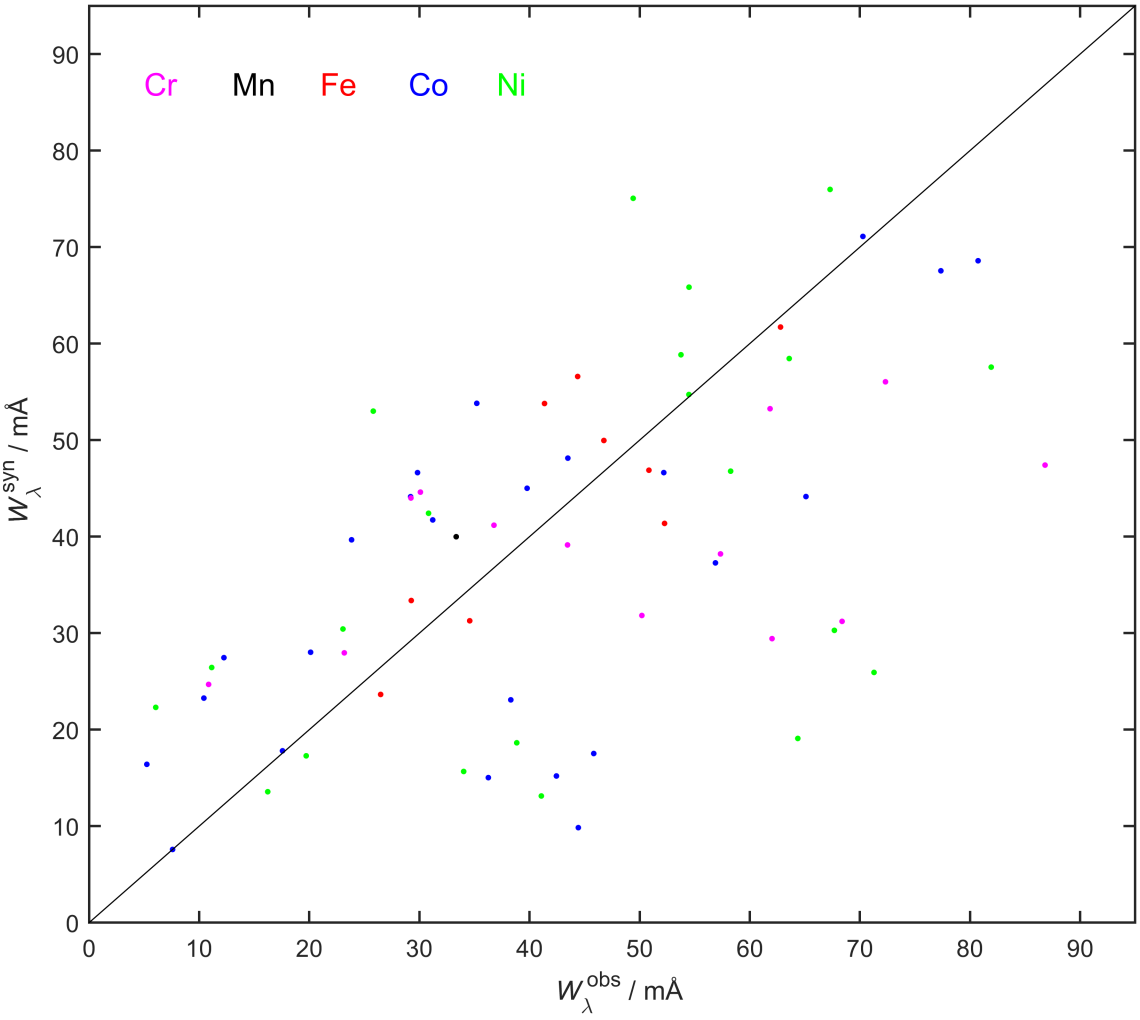

Figure 39: Comparison of the observed equivalent widths with the synthetic ones in PG 0909+276. As expected, the values scatter around the ideal value of $W_\lambda^{\rm obs} = W_\lambda^{\rm syn}$ (black straight line). The IG elements are color labeled.

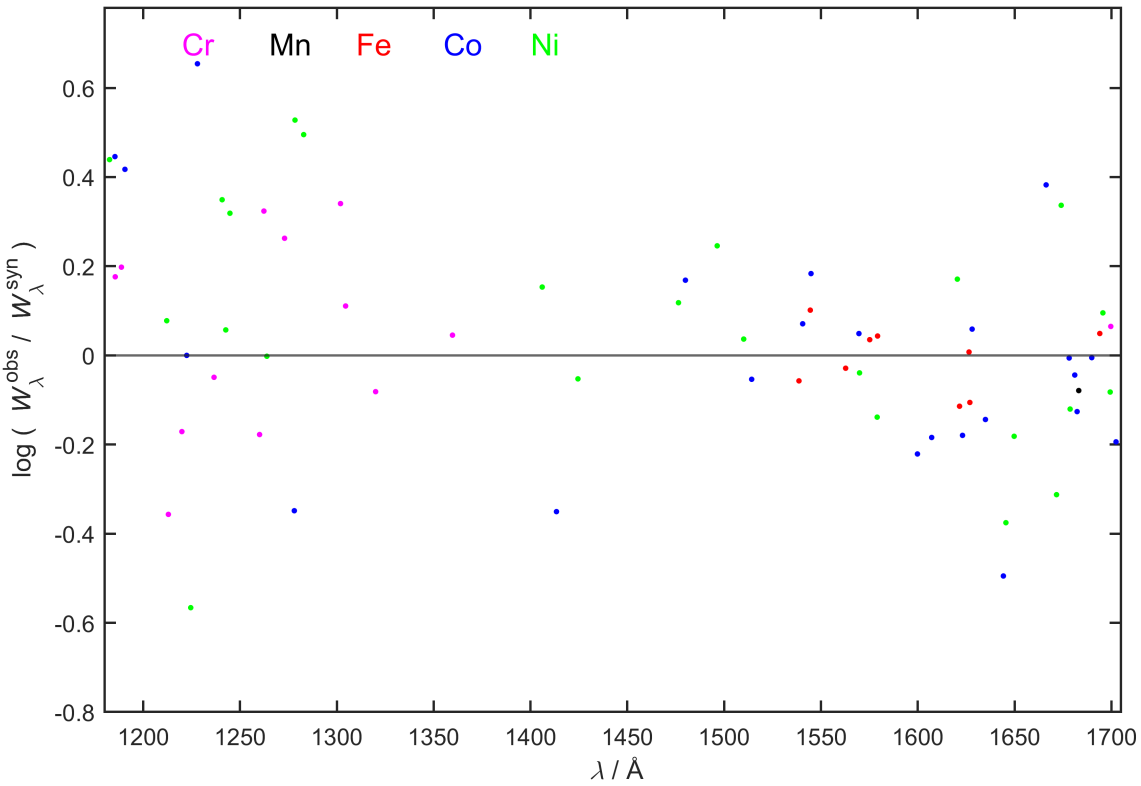

Figure 40: $\log(W_\lambda^{\rm obs}/W_\lambda^{\rm syn})$ in PG 0909+276, plotted against the wavelength λ. The IG elements are color labeled, and the value for $W_\lambda^{\rm obs} = W_\lambda^{\rm syn}$ is indicated by the black constant at 0.

Table 17: Overview of the cumulative IG-element absorption-line reduction in Feige 110, as it was carried out for the evaluation in Sect. 9.2.

Description	(Main-)Reduction	Line count	Reference
visible IG-element lines	$W_\lambda^{\mathrm{syn}} > 1.5\,\mathrm{m\AA}$	6 068	Table 13
isolated lines	min. 90% line area in $\Delta\lambda = \pm 1.82\,\sigma$	660	Sect. 8.3.5
noise in the STIS observation	$\lambda > 1\,200\,\mathrm{\AA}$	599	Sect. 9.2
outliers 1	$W_{\lambda,\mathrm{red}}^{\mathrm{obs}}/W_\lambda^{\mathrm{obs}} < 1.8$ and $W_{\lambda,\mathrm{red}}^{\mathrm{obs}}/W_\lambda^{\mathrm{obs}} > 0.55$	395	Sect. 9.2
outliers 2	$W_\lambda^{\mathrm{obs}}/W_\lambda^{\mathrm{syn}} < 5$ and $W_\lambda^{\mathrm{obs}}/W_\lambda^{\mathrm{syn}} > 0.2$	392	Sect. 9.2

9.4 Reduction criteria

The results obtained in this chapter depend on the criteria for isolated absorption lines and their selection for evaluation (Table 17). In this subsection, some criteria are briefly examined and justified, and it is to be checked whether a change (to a physically meaningful extent) of these criteria leads to different results using the example of Feige 110.

Apart from a few auxiliary conditions, $W_\lambda^{\mathrm{syn}} > 1.5\,\mathrm{m\AA}$ was mainly necessary as a criterion for the selection of visible lines. These lines are literally "visible" since from this limit the relative flux difference can still be perceived with the eye. Since lines with smaller equivalent widths could no longer be evaluated due to the STIS observation's S/N, this turns out to be the lowest physically meaningful limit for the line selection. The criterion for isolated lines, which was determined by the condition that at least 90% of the area of an absorption line must be caused by a single transition, is a sensible compromise so that there are enough lines for evaluation while the permitted inaccuracy in this step is $< 10\%$. Narrowing the criterion to 95% of the area reduces the line count by more than 130 while loosening it to 85% can increase the number of lines by ≈ 80, but also increases the inaccuracy to 15% which is no longer useful.

The fact that all isolated lines with $\lambda < 1\,200\,\mathrm{\AA}$ were excluded from the evaluation is due to excessive noise in the STIS observation. The theoretical S/N (Fig. 47) shows that the noise would have to increase again towards longer wavelengths, but in practice, the shorter wavelengths proved to be much more of a hindrance. From 55 isolated lines with $\lambda < 1\,200\,\mathrm{\AA}$, only 13 could have been evaluated at all (23.6%) since the Gaussian fits in the STIS observation did not succeed for the other lines, or the corrections according to Table 17 would have been too large. In comparison, from 155 isolated lines with $\lambda > 1\,600\,\mathrm{\AA}$ 96 could be evaluated (61.9%), which is proportionally even more than when evaluating all lines (59.2%).

The last two reduction criteria, namely the treatment of larger deviations between the line fits in the synthetic spectrum and the observation, probably have the largest impact on the results. Let it be the comparison of the purely empirical variable $W_{\lambda,\mathrm{red}}^{\mathrm{obs}}$ with W_λ^{obs} or of W_λ^{obs} with W_λ^{syn}. In both cases, it is a matter of checking whether a direct relation

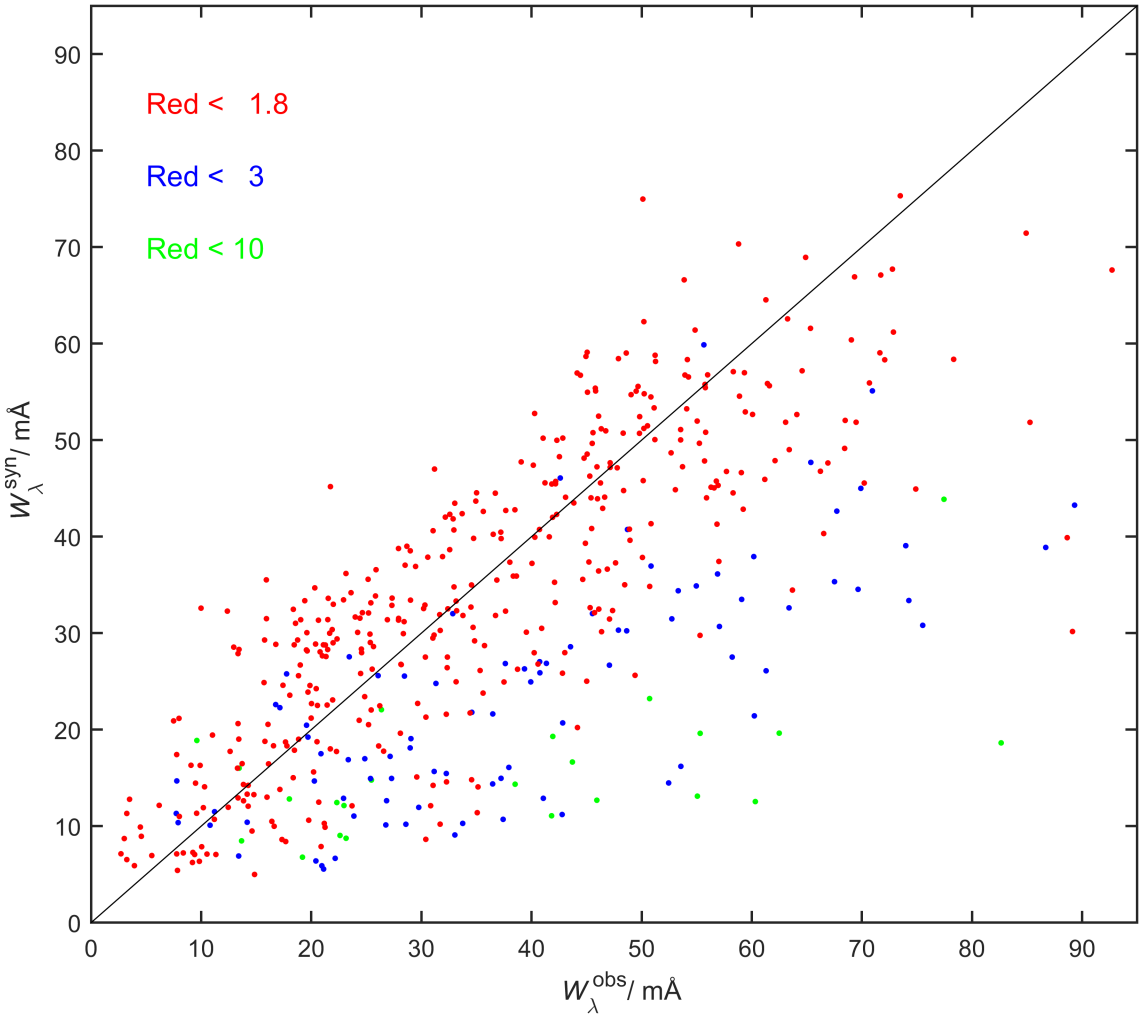

Figure 41: Impact of the correction according to the ratio of $W_{\lambda,\mathrm{red}}^{\mathrm{obs}}$ and W_λ^{obs} (or vice versa). Loosening the reduction leads to an accumulation of outliers with $W_\lambda^{\mathrm{obs}} > W_\lambda^{\mathrm{syn}}$.

between the line in the synthetic spectrum and the observation can still be established. This is no longer the case, for example, if the Gaussian fits differ largely in terms of their width σ or the fitted line center. The allowed factor for the largest permissible deviation could be made dependent on the fact that the distribution of the values in Fig. 36 is fairly symmetrical around the straight line $W_\lambda^{\mathrm{obs}} = W_\lambda^{\mathrm{syn}}$, as it is expected that the inaccuracies of the atomic data are evenly distributed. However, loosening the criteria always led to a broader distribution towards $W_\lambda^{\mathrm{obs}} > W_\lambda^{\mathrm{syn}}$ (Fig. 41). The largest outliers could then be examined by eye and the permitted factor was selected in a way that a relationship between model and observation still could be established for these lines.

10 Improving abundance determinations

The occurrence of strong, isolated absorption lines is crucial for the precise IG-element abundance determination. In the case of stars that are highly enriched in IG elements, as a result of which a large part of their lines overlap, statistical methods such as the χ^2 method are well suited to determine abundances, since here the averaged deviation of the entire modeled spectrum is evaluated. To achieve a reasonable computing time with NLTE models, however, good starting values for these abundances are important, which can only be obtained from clearly visible, isolated lines. In stars that have lower IG-element abundances, these can only be determined using a few lines anyway, which means that their accuracy is also decisive here. In any case, strong, isolated lines serve as prime reference points for the respective element's abundance determination. In the previous section, it was shown that when comparing modeled line strengths with observed ones, statistical deviations arise. In this section, the reliability of Kurucz's oscillator strengths as well as the uncertainty of the analysis presented in this work are discussed. Then, suggestions are given on how to improve IG-element abundance determinations in hot, evolved stars.

10.1 Evaluation with corrected values

The results of the isolated line evaluation in Feige 110 and PG 0909+276 obtained from Sect. 9 could be used to make corrections for the identified isolated lines, so that the models and observations should match exactly. For each isolated line, the ratio $W_\lambda^{\mathrm{obs}}/W_\lambda^{\mathrm{syn}}$ (Tables 26 and 27) was used as a correction factor for the weighted oscillator strength gf of the specific transition, whereby naively a linear relationship to the equivalent width is to be expected (Eq. 19). By simple multiplication the following is obtained

$$gf_{\mathrm{corr}} = gf_{\mathrm{Kurucz}} \cdot W_\lambda^{\mathrm{obs}}/W_\lambda^{\mathrm{syn}}$$

or, as it is more convenient for the handling of atomic data to express logarithmic,

$$\log(gf)_{\mathrm{corr}} = \log(gf)_{\mathrm{Kurucz}} + \log\left(W_\lambda^{\mathrm{obs}}/W_\lambda^{\mathrm{syn}}\right) \quad .$$

The respective transitions in Kurucz's LIN and POS lists were then corrected by substitution of $\log(gf)_{\mathrm{Kurucz}}$ with $\log(gf)_{\mathrm{corr}}$. Afterwards, new atmosphere models and synthetic spectra were calculated for Feige 110 and PG 0909+276 based on the new atomic data. Then, the evaluation shown in Sects. 9.2 and 9.3 was repeated.

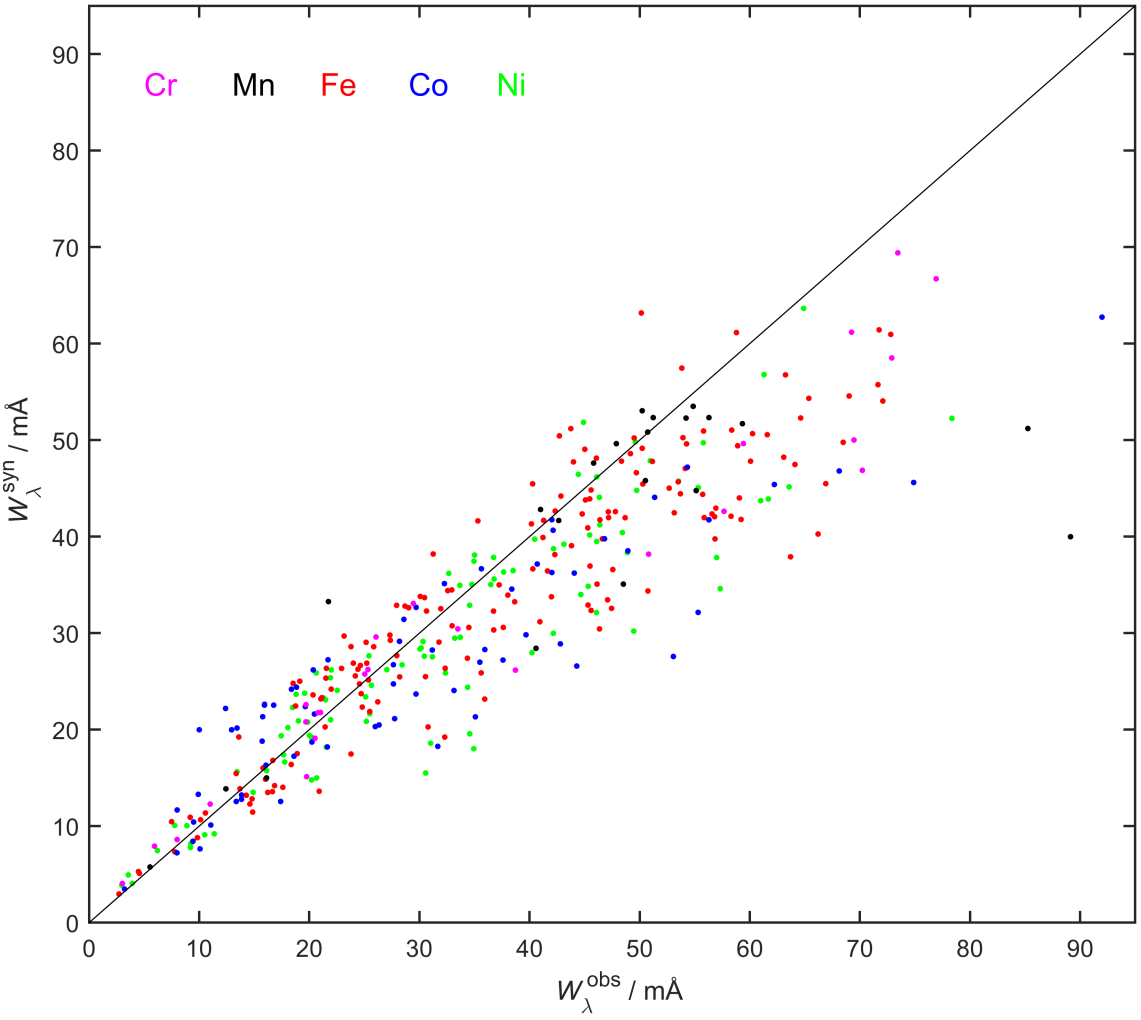

Figure 42: Like Fig. 36, with corrected weighted oscillator strengths.

Analogous to Sect. 9, Gaussian fits have been applied to the distribution $\log(W_\lambda^{\mathrm{obs}}/W_\lambda^{\mathrm{syn}})$ of isolated lines for both stars. In the case of Feige 110, σ reduces from 45 % to 24 % while μ increases slightly by 8 %, and in the case of PG 0909+276, σ reduces from 72 % to 45 % while μ remains unchanged. In both cases, although the statistical uncertainty reduces significantly, an exact match of W_λ^{obs} and W_λ^{syn} cannot be achieved by this method. Additionally, considering Feige 110, the gf correction leads to a distortion of the line strengths in favor of large W_λ^{obs} values (Fig. 42), which is the reason for the increase of μ, hence introduces a systematic uncertainty. As this effect intensifies for stronger lines (i.e., larger W_λ), which are more relevant for abundance determinations, such a correction of gf values is not recommended (the systematic deviation does not occur in PG 0909+276, but the evaluation of Feige 110 is more meaningful due to the higher line count).

10.2 On the analysis uncertainty

To investigate the reliability of the analysis performed in this work, correction factors of mutual lines evaluated in both stars Feige 110 and PG 0909+276 were analyzed (Table 18). In the evaluation performed in Sect. 9, the reference value for the correct line strength was

Table 18: Mutually evaluated lines in Feige 110 and PG 0909+276, with their respective correction factors $W_\lambda^{\mathrm{obs}}/W_\lambda^{\mathrm{syn}}$.

λ / Å	Ion	$\log(gf)_{\mathrm{Kurucz}}$	$\mathrm{corr}_{\mathrm{Fei}}$	$\mathrm{corr}_{\mathrm{PG}}$
1213.00	Cr IV	0.10	0.77	0.78
1263.86	Ni IV	−0.65	1.18	0.96
1304.52	Cr IV	0.57	1.23	1.27
1413.42	Co V	0.55	0.92	0.41
1510.11	Ni IV	−0.57	1.05	1.08
1540.56	Co IV	0.34	1.24	1.17
1544.49	Fe IV	0.48	0.90	1.29
1544.87	Co IV	−0.18	0.74	1.60
1562.75	Fe IV	0.03	1.24	0.93
1569.61	Co IV	−0.14	0.72	1.14
1579.03	Ni IV	−1.21	1.30	0.73
1579.24	Fe IV	−0.82	0.83	1.10
1607.18	Co IV	−0.31	0.78	0.70
1621.57	Fe IV	0.70	1.06	0.77
1623.11	Co IV	−0.97	1.28	0.65
1626.47	Fe IV	0.55	1.08	1.01
1626.90	Fe IV	0.05	1.22	0.81
1682.28	Co IV	−0.54	2.06	0.75
1683.13	Mn IV	0.29	0.98	0.99
1693.99	Fe IV	−0.81	1.54	1.15
1702.38	Co IV	−0.57	0.66	0.64

assumed to be W_λ^{obs}. To investigate the uncertainty of this assumption, the variance of the respective correction factors in Feige 110 and PG 0909+276 which, in the ideal case, should match, was calculated. Therefore, for each line, the mean $\mu_n = (\mathrm{corr}_{\mathrm{Fei}} + \mathrm{corr}_{\mathrm{PG}})\,/\,2$ was taken as a reference value. The variance is then given by (due to symmetry, $\mathrm{corr}_{\mathrm{Fei}}$ or $\mathrm{corr}_{\mathrm{PG}}$ can either be used)

$$\sigma^2 = \sum_{n=1}^{N} \frac{(\mathrm{corr}_{\mathrm{Fei}} - \mu_n)^2}{N}$$

where N denotes the total line count in Table 18 and $n = 1, ..., N$ the respective line's number. A statistical uncertainty of $\sigma = 23\%$ was obtained.

To estimate the overall statistical uncertainty of this work's analysis, all sources of uncertainty have to be taken into account. In Sect. 8.3.5, 10 % uncertainty was allowed when defining a line to be isolated. Other sources of uncertainty could be the determination of the local continuum (Sect. 8.3.1), the reduction performed for the evaluation (Sect. 9.4) or line blends of elements not considered in the model spectrum. The overall statistical uncertainty is obtained by

$$\sigma_{\mathrm{ov}} = \sqrt{\sum \sigma^2} \quad ,$$

and, as not all σ are known explicitly, a lower limit is given by

$$\sigma_{\mathrm{ov}} > \sqrt{0.23^2 + 0.1^2} = 25\,\% \quad .$$

10.3 Results

Kurucz's *gf* values

It was an aim of this work to estimate the gf uncertainty of Kurucz's lines. To get a final result, all 457 evaluated lines (392 from Feige 110, Table 26, and 65 from PG 0909+276, Table 27) were taken into account, with the (weighted) uncertainty of the observed and modeled equivalent widths

$$\sigma_W = \sqrt{\frac{392}{457}\,\sigma^2_{W,\mathrm{Fei}} + \frac{65}{457}\,\sigma^2_{W,\mathrm{PG}}} \quad ,$$

hence, an uncertainty of $\sigma_W = 49\,\%$ was obtained. σ_W, however, is composed of the uncertainty of the input data (i.e., gf values) and the analysis procedure. For the latter, a lower limit was given in the previous subsection by σ_{ov}. The statistical uncertainty of the input data then is

$$\sigma_{\mathrm{Kurucz},\%} < \sqrt{\sigma^2_W - \sigma^2_{\mathrm{ov}}} = 42\,\% \quad ,$$

or, back in the logarithmic regime, it is

$$\sigma_{\mathrm{Kurucz}} < 0.15\,\mathrm{dex} \quad .$$

Therefore, to recall, this work provides an estimate for the statistical uncertainty of Kurucz's data for weighted oscillator strengths $\log{(gf)}_{\mathrm{Kurucz}}$, at least among the evaluated lines, of $\sigma_{\mathrm{Kurucz}} < 0.15\,\mathrm{dex}$, whereat it should be noted that the real uncertainty could be notably lower, about which this work, however, cannot make a statement. Additionally, no systematic uncertainty of Kurucz's gf values was found during the analysis.

Abundance determinations

Although the statistical deviations found in Sect. 9 seem large, ordinarily several lines of each IG element can be evaluated and their mean μ is decisive for the abundance determination. Given the standard deviation σ of a normal distribution of n values, the standard error of the mean is

$$\sigma_\mu \approx \frac{\sigma}{\sqrt{n}} \quad . \tag{21}$$

In Sect. 9, the IG-element abundances have been determined via setting the mean $\mu = 0$. For each element, the uncertainty of μ reduces accordingly to Eq. 21, depending on the line count. As Table 19 shows, in the evaluations performed for Feige 110 and PG 0909+276, the standard errors of the means for the different elements are by a majority $< 15\,\%$. Hence, given enough lines to evaluate, an equivalent-width comparison provides reasonably low statistical uncertainties for abundance determinations.

Before discussing the case when only a few isolated lines are available for an analysis, systematic uncertainties need to be investigated, since these might directly influence μ. Considering the analysis in this work, systematic uncertainties could arise at different points. Most importantly to mention is the normalization of the synthetic spectra to observations. On the one side, the normalization shown in Fig. 20 did not provide the best fit for the STIS range, and the method shown in Sect. 8.3.1 had to be applied. On the other side, elements that are not considered in the model atmosphere calculation might

Table 19: Standard deviation, line count and standard error of the mean for all elements evaluated in Sect. 9.

Star	Element	σ (%)	Line count	σ_μ (%)
Feige 110	Cr	48	28	9.1
	Mn	41	22	8.7
	Fe	38	166	2.9
	Co	58	74	6.7
	Ni	48	98	4.8
PG 0909+276	Cr	45	10	14.2
	Fe	23	9	7.7
	Co	86	24	17.6
	Ni	95	20	21.2

lead to slight overall flux changes, which would also have an impact on the STIS range. Elements that are not considered in the model spectrum, or IG-element LIN lines[26], also lead to falsely identified isolated lines, for which $W_\lambda^{\mathrm{obs}} > W_\lambda^{\mathrm{syn}}$ holds. This would certainly lead to a systematic deviation, as the abundances needed to be raised to compensate this effect, but is partly treated in Sect. 9.4 (i.e., Fig. 41). An exact treatment of systematic uncertainties, e.g., the aforementioned, or other known issues such as Stark broadening (Tremblay & Bergeron 2009) or observational systematics, is far beyond the scope of this work. At this point it shall be emphasized that, for any scientific work, the obtained results are only worth as much as the reliability of the underlying methods. Therefore, although not quantitatively evaluated, systematic uncertainties must be kept in mind when rating this work's results.

In the case of stars exhibiting lower IG-element abundances or for obtaining good starting values for NLTE models in general, reliable absorption lines are needed to provide reference points for the abundance determinations. These happen to be strong, isolated lines, ideally with little to no deviations occurring between observed and modeled line strengths. As has been shown, changing gf values in such a way is not crowned with success, hence another approach is needed.

The most reliable lines are those evaluated in both stars Feige 110 and PG 0909+276 and showing no strong deviations between their respective correction factors (Table 18). Seven lines with deviations $< 10\,\%$ were found (Table 20), that are strongly recommended to be employed for abundance determinations (the respective correction factors have to be applied to the modeled lines' equivalent widths). The uncertainty of each of the lines then is (cf. Sect. 10.2)

$$\sigma_1 \approx \sqrt{(0.25^2 + 0.1^2)}/\sqrt{2} = 19\,\% \quad ,$$

where the factor $1/\sqrt{2}$ comes from the fact that two data points are available per line, respectively.
Among the other evaluated lines, those with $W_\lambda^{\mathrm{obs}} \approx W_\lambda^{\mathrm{syn}}$ could be considered most reliable (although it is clear that even for a randomly spread set of data points, some will

[26]To investigate the effect of IG-element LIN lines in the STIS range, additional models were created. An evaluation analogous to Sect. 9 led to an insignificant change of μ.

Table 20: Most reliable lines in Feige 110 and PG 0909+276, with the average correction factor which has to be applied to $W_\lambda^{\rm syn}$ when comparing with observations.

Ion	λ / Å	$\log(gf)_{\rm Kurucz}$	$({\rm corr_{Fei}} + {\rm corr_{PG}})\,/\,2$
Cr IV	1213.00	0.10	0.78
Cr IV	1304.52	0.57	1.25
Mn IV	1683.13	0.29	0.99
Fe IV	1626.47	0.55	1.05
Co IV	1540.56	0.34	1.21
Co IV	1702.38	−0.57	0.65
Ni IV	1510.11	−0.57	1.07

by chance feature this). We recommend to employ the strongest lines with $W_\lambda^{\rm obs} \geq 40\,{\rm m\AA}$ and with $0.90 \leq W_\lambda^{\rm obs}/W_\lambda^{\rm syn} \leq 1.10$, to obtain an uncertainty of

$$\sigma_2 \approx \sqrt{0.25^2 + 0.1^2} = 27\,\%$$

for each of the 58 remaining lines, which can be found in Table 25 in the appendix. Altogether, 65 IG-element absorption lines are found which are highly recommended to be used as abundance determination reference points.

10.4 Conclusion

With the high-resolution and high S/N STIS spectra, we were able to determine the IG-element abundances of EC 11481–2303, Feige 110, and PG 0909+276. Although, due to stellar rotation, isolated lines could not be analyzed in the case of EC 11481–2303, it was the first time to determine individual IG-element abundances for this star. In the case of Feige 110 and PG 0909+276, 457 isolated IG-element lines, most of which Cr – Ni, have been identified and (automatically) evaluated with the procedures and scripts presented in this work, comparing the theoretically modeled line strengths with the observations.

As a result, we were able to estimate an upper limit for the statistical uncertainty of Kurucz's weighted oscillator strengths $\log(gf)_{\rm Kurucz}$, which is $\sigma_{\rm Kurucz} < 0.15\,{\rm dex}$. Additionally, and more importantly, no systematic deviations have been found between the evaluated lines.
To improve future abundance determinations, it was first tried to establish a correction table for the gf values. This, however, did not lead to an exact match of observations and models, and additionally introduced a systematic distortion. We therefore conclude that this method is not to apply.
Afterwards, it was looked for "reliable" strong, isolated IG-element absorption lines, which could serve as prime reference points for abundance determinations. Hereby, seven lines were found with an estimated statistical uncertainty of $\sigma_1 \approx 19\,\%$, and 58 lines with $\sigma_2 \approx 27\,\%$. Given that several (n) lines of one IG element are available in an observation, the estimated statistical uncertainty of the mean reduces by the factor $1/\sqrt{n}$, hence precise abundance determinations should be possible using these.

That being said, it was the first time to quantitatively analyze (and compare with stellar spectra) weighted oscillator strengths for the IG-element stages III – VI, which are dominant in hot, compact stars. Obtaining the statistical uncertainties is an important step to estimate the reliability of spectral analyses, whenever IG-elements (stages III – VI) are to be identified. To end with a grain of salt, it must not be forgotten that systematic uncertainties (except for the gf values, where none has been found) in the observation or analysis procedure might play a role for abundance determinations, the investigation of which for sure lies in the scope of future research.

11 Cu and Zn line strengths

In Sect. 4.5 some atomic data sources were presented. Kurucz's line lists turned out to be the most extended concerning the IG elements. Furthermore, since 2012, the HFR+CPOL method (Quinet et al. 1999, 2002) was used to calculate oscillator strengths of 14 TIEs (and, except for Tc, their absorption lines have been successfully identified in the spectra of hot, evolved stars), which are available on-demand via TOSS (`http://dc.g-vo.org/TOSS`), containing the ionization stages IV – VII. Besides, oscillator strengths of TIEs are available in Kurucz's line lists (Kurucz 2018, `http://kurucz.harvard.edu/atoms.html`), whereby the most comprehensive data is available for copper (Cu I – X) and zinc (Zn I – IX). Since, as already shown (e.g., in Fig. 12), deviations in the oscillator strengths might occur depending on the calculation method, it is advisable to carry out a quantitative comparison of the two sources. For this purpose, the data for the Cu and Zn ions were obtained from both sources, processed according to the corresponding transitions, and then plotted against each other.

11.1 Atomic data

In the case of the Cu ions, a compilation of atomic data (experimentally determined energy levels, experimentally determined and theoretical ionization energies, etc.) can be found in Sugar & Musgrove (1990), which is also used as the main reference for the NIST database. For Cu VII, there are experimentally determined energy levels to be found in van het Hof et al. (1990). The above-mentioned atomic data of the ions Cu IV – VII were used by Rauch et al. (2020) to calculate oscillator strengths and transition probabilities, which can be obtained via TOSS. The associated transitions' absorption lines could be identified in the spectra of hot, evolved stars, and hence, their energy levels could be verified (Table 21). The HFR+CPOL method was used for oscillator-strength calculation. Also, for Zn IV and Zn V oscillator strengths could already be calculated by Rauch et al. (2014b) using the same method, and absorption lines could be identified in stellar spectra. Atomic data from Sugar & Musgrove (1995), which can also be found in NIST, was used. The oscillator strengths and energy levels used in this chapter were directly obtained from the TOSS website.

Kurucz also uses atomic data from NIST for his line lists, whereby here only the POS lines, i.e., the lines with experimentally determined energy levels, are examined (Table 22). Analogous to the IG elements, a semi-empirical method (Kurucz 1973) is used to calculate the oscillator strengths. These and energy levels used in this chapter were obtained from Kurucz's website, where all available data is on-hand to download.

Table 21: Transitions of Cu and Zn ions available on TOSS, and number of absorption lines identified in stellar spectra.
`References: Rauch et al. 2014b, 2020`

Element	Ion	Transition count	Identified absorption lines
Cu	IV	8 785	1
Cu	V	5 456	52
Cu	VI	3 797	2
Cu	VII	2 253	0
Zn	IV	400	31
Zn	V	1 879	16

Table 22: LIN and POS lines of several TIEs in Kurucz's database.
`Reference: Kurucz 2018`

Element	Ions	LIN lines	POS lines	POS/LIN [%]
Cu	I – IX	102 192 379	60 774	0.060
Zn	I – IX	95 092 537	32 797	0.035
Mo	I – IV	34 705 868	42 311	0.122
Tc	I – V	59 361 284	8 934	0.015
Ru	I – V	90 773 490	13 848	0.015
Rh	I – V	105 934 148	7 828	0.007

11.2 Processing

As just described, atomic data is freely available for download on the TOSS and Kurucz's website. With TOSS, the ions, the wavelength interval of the transitions to be obtained, and the interval of the oscillator strengths can be selected. For the ions Cu IV – VII and Zn IV – V all available transitions were obtained, one list per ion. These were saved as text files and contain the wavelength, $\log(gf)$, electron configuration, and energy levels of all transitions. For Kurucz data, also one list per ion was obtained from the POS lists, with all available transitions being included here by default. The lists were saved as text files and are structured analogously to the lists obtained from TOSS.

Since only transitions that can theoretically be found in stellar spectra and thus serve to determine the abundance of Cu and Zn are to be considered, the lists could be reduced. On the one hand, transitions with $\log(gf) < -2.5$ are usually not visible in the stellar spectrum, meaning that they could be excluded from the evaluation. On the other hand, the wavelength range of interest for the ionization stages considered here is the far UV range, since the corresponding absorption lines are primarily found in the spectra of hot, evolved stars. If the lower limit of the FUSE spectrograph ($\lambda \approx 900\,\text{Å} - 1\,200\,\text{Å}$) and the upper limit of STIS ($\lambda \approx 1\,140\,\text{Å} - 1\,710\,\text{Å}$) is included, a wavelength range that covers both spectrographs, and thus most of the possibly examined lines, is obtained. The lists were therefore reduced to the range $\lambda = 900\,\text{Å} - 1\,710\,\text{Å}$. Finally, to ensure that the same transitions are compared, only those for which the wavelength and the energy levels are almost identical in both lists ($\triangle\lambda, \triangle E < 0.01\,‰$) were taken over. An overview of the reduction can be found in Table 23.

Table 23: Cumulative reduction of the Cu IV – VII and Zn IV – V transitions which are compared in this section.

Reduction	Cu transitions		Zn transitions	
	TOSS	Kurucz	TOSS	Kurucz
none	20 291	22 397	2 279	9 758
$\log(gf) \geq -2.5$	8 802	7 776	1 428	3 970
$\lambda = 900\,\text{Å} - 1\,710\,\text{Å}$	4 099	3 506	987	1 520
$\triangle\lambda, \triangle E < 0.01\,‰$	3 464		965	

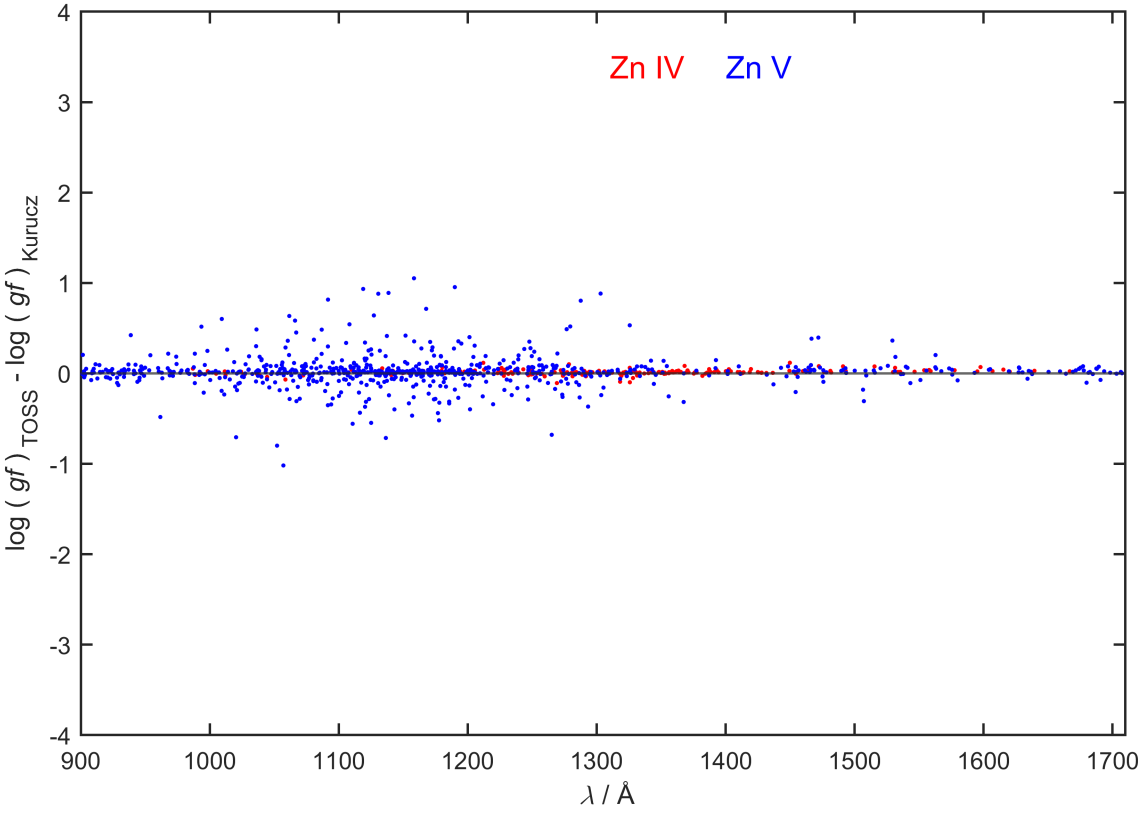

Figure 43: Comparison of the calculated oscillator strengths of Zn IV – V obtained from TOSS and Kurucz, with color labeled ions.

11.3 Evaluation

For the evaluation, the weighted oscillator strengths of the corresponding transitions were subtracted, i.e.,

$$\triangle\log(gf) = \log(gf)_{\text{TOSS}} - \log(gf)_{\text{Kurucz}} \quad ,$$

and then plotted against the wavelength. It should be remembered at this point that subtracting the logarithms is equivalent to dividing the gf values. In the case of the 965 examined transitions of the zinc ions, apart from a slight spread as expected ($\sigma = 0.16$), there was no noticeable systematic deviation of the oscillator strengths (Fig. 43). It should be noted that the mean value of the distribution is above zero ($\mu = 0.02$), which means that the TOSS values are systematically slightly larger than the Kurucz values. In addi-

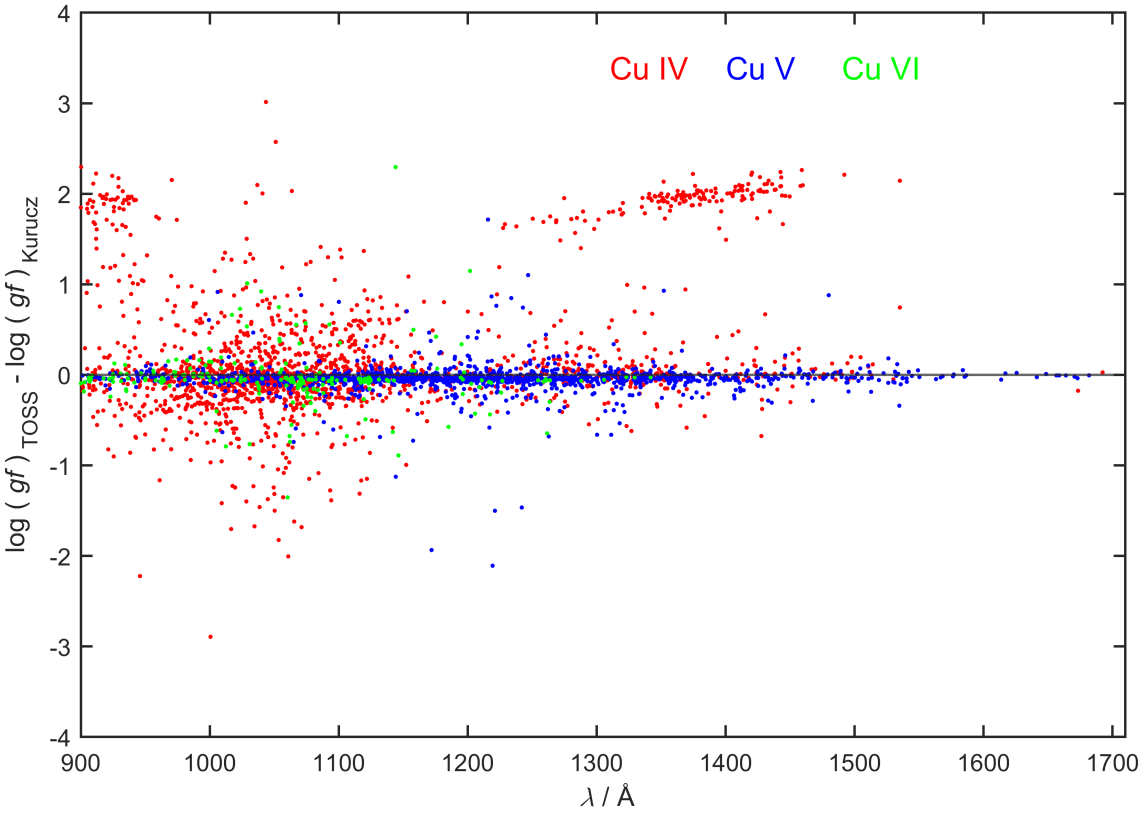

Figure 44: Like Fig. 43, for Cu IV – VI.

tion, the variance of the Zn V ions is significantly larger ($\sigma = 0.16$) than that of the Zn IV ions ($\sigma = 0.01$).

In the case of the 3 464 examined transitions of the copper ions (Cu IV – VI, as there are no common transitions of Cu VII with the applied criteria), especially for Cu IV, significant deviations of the oscillator strengths, which are not due to statistical effects, were found (Fig. 44). First of all, it can be noted that, apart from the strong outliers of Cu IV, the mean value is slightly below zero ($\mu = -0.02, \sigma = 0.24$), i.e., the Kurucz values are slightly larger than the TOSS values. The largest spread is found for the Cu IV ions ($\sigma = 0.30$). Besides, for $\lambda \approx 900\,\text{Å} - 950\,\text{Å}$ and $\lambda \approx 1\,250\,\text{Å} - 1\,450\,\text{Å}$ two accumulations of systematic deviations with $\triangle \log(gf) \approx 2$ show up, meaning that in these areas, the TOSS values are clearly larger than the Kurucz values. Besides, it is interesting to investigate the energy levels of the transitions (Fig. 45), as it can be clearly seen that the oscillator strengths of the transitions with small lower energy levels tend towards the systematic uncertainty shown.

Finally, it was checked whether a plot of $\log(gf)_{\text{TOSS}}$ against $\log(gf)_{\text{Kurucz}}$ provides further information. However, apart from the systematic deviations found for Cu, no other anomalies were found here. It can only be noted that the relative uncertainty increases for smaller $\log(gf)$. This effect was to be expected and can be shown even better when plotted against the wavelength (Fig. 46). It is interesting here that the already mentioned systematic deviations of Cu IV occur independently of $\log(gf)$.

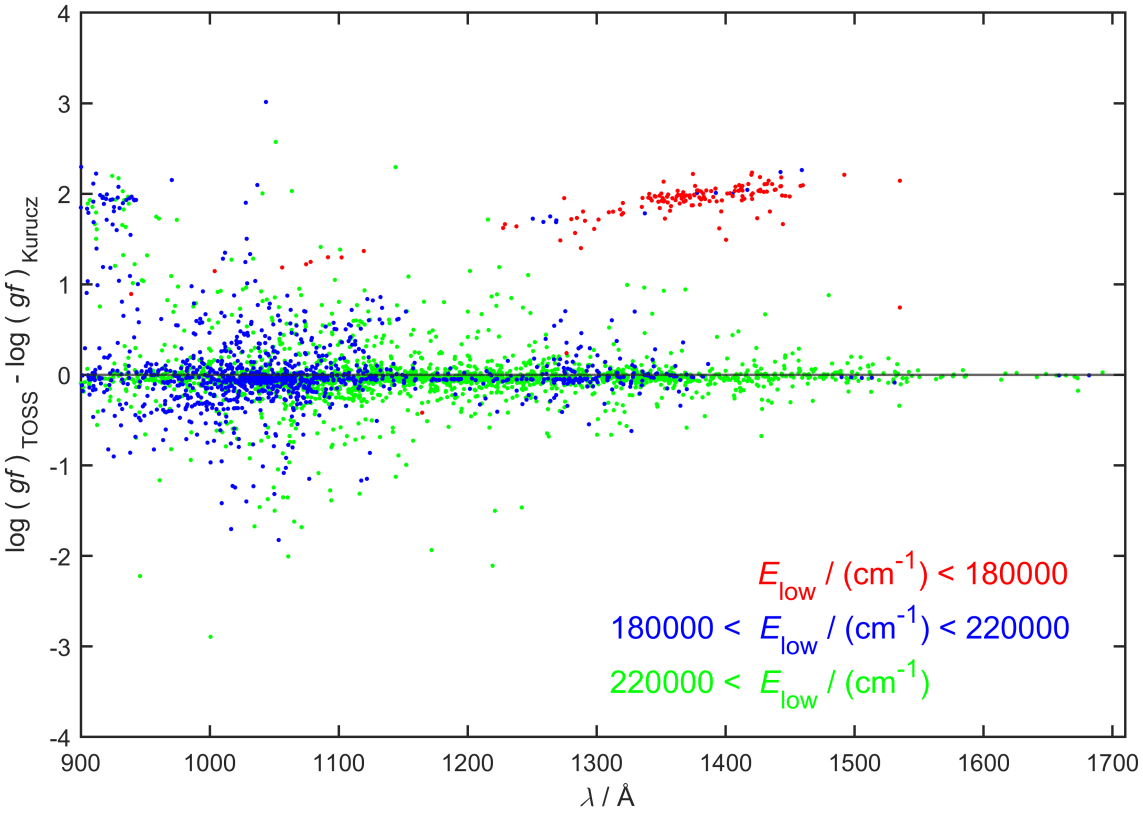

Figure 45: Like Fig. 44, with the transitions' lower energy levels being color labeled.

11.4 Results

The weighted oscillator strengths of the zinc ions from TOSS and Kurucz (with the mentioned criteria, Table 23) largely agree. The statistical deviation decreases significantly for $\lambda > 1\,300$Å, which means that an investigation of absorption lines in the STIS range is probably more reliable than in the FUSE range. Overall, the deviations from TOSS and Kurucz amount to $\triangle\log(gf) = +0.020_{\,\mathrm{sys}} \pm 0.162_{\,\mathrm{stat}}$ (or $+0.006_{\,\mathrm{sys}} \pm 0.050_{\,\mathrm{stat}}$ in the suggested range of $\lambda > 1\,300$Å).

Large statistical and systematic deviations were found between the calculated weighted oscillator strengths of the copper ions, which mainly occur for Cu IV. At first, it shall be assumed that both atomic data sources were equally reliable, before investigating if any of them is favorable in the case of Cu. The aforementioned systematic deviations accumulate in the areas $\lambda \approx 900\,\text{Å} - 950\,\text{Å}$ and $\lambda \approx 1\,250\,\text{Å} - 1\,450\,\text{Å}$ with $\triangle\log(gf) \approx 2$. The second-mentioned accumulation is mainly due to transitions with a low lower energy level $E_{\mathrm{low}} < 180\,000\,\mathrm{cm}^{-1}$ and could be avoided by excluding these transitions without further losing "good" values (Fig. 45). Both accumulations (for the sake of symmetry in the calculation all values with $|\triangle\log(gf)| > 1.5$) cause a systematic deviation of $+0.109_{\,\mathrm{sys}}$. If transitions with $|\triangle\log(gf)| > 1.5$ were excluded in a line analysis, the deviations would decrease to $\triangle\log(gf) = -0.018_{\,\mathrm{sys}} \pm 0.295_{\,\mathrm{stat}}$. Completely excluding Cu IV from the analysis reduces the statistical uncertainty by about 30 %, while reducing the transition count by a little more than half. However, since there is an accumulation of statistical deviations from Cu IV in the FUSE range, it is worthwhile looking at the spectrographs' ranges in a more differentiated manner.

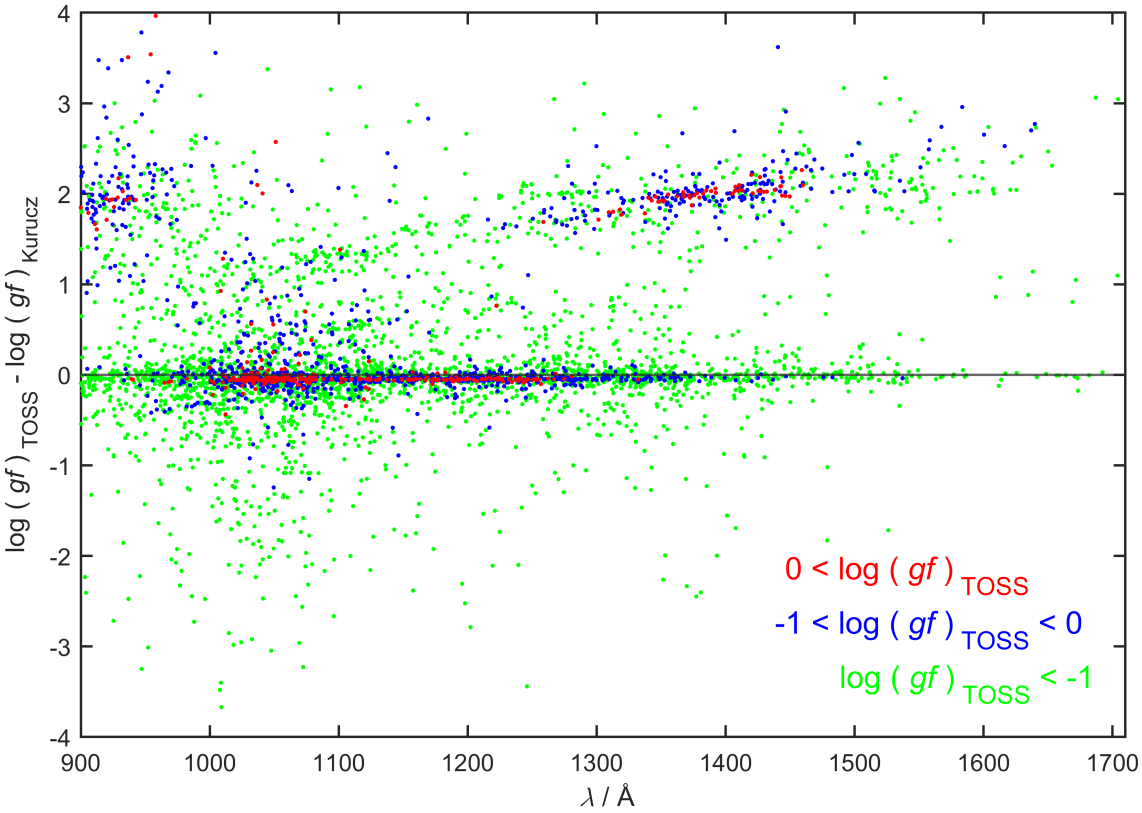

Figure 46: Comparison of the calculated oscillator strengths of Cu IV – VI obtained from TOSS and Kurucz, with different $\log(gf)_{\mathrm{TOSS}}$ ranges color labeled. In contrast to Fig. 44 and Fig. 45, however, $\log(gf) < -2.5$ is also permitted here, provided this was only the case in one of the two lists, because otherwise there would be a distortion in favor of large $\log(gf)_{\mathrm{TOSS}}$ values.

A good result is obtained for an analysis in the STIS range if the transitions with $E_{\mathrm{low}} < 180\,000\,\mathrm{cm}^{-1}$ are excluded and only lines with $\lambda > 1\,180$Å (the noise from STIS usually increases strongly at shorter wavelengths anyway, making this not a major restriction) are considered. Thus for STIS, $\triangle\log(gf) = +0.002_{\,\mathrm{sys}} \pm 0.295_{\,\mathrm{stat}}$ is obtained.
In the FUSE range, the large spread of the Cu IV values, apart from the systematic one, causes a large statistical deviation. Here it makes sense to exclude Cu IV from an analysis, which reduces the line count by a factor of ≈ 3, but also reduces the statistical deviation by a factor of ≈ 2.5, to finally $\triangle\log(gf) = -0.041_{\,\mathrm{sys}} \pm 0.200_{\,\mathrm{stat}}$.

Additionally, with the knowledge gained in this section, there is of course the less physical, but pragmatic possibility of using only those transitions whose deviations do not exceed a certain value, e.g., $|\triangle\log(gf)| < 0.15$ for a line analysis for both the copper and zinc ions. This procedure reduces the uncertainty by definition to the desired value, while still having a reasonable number of transitions available. The criterion just mentioned reduces the number of transitions of zinc ions by 15 % to 822 and that of copper ions by 35 % to 2 250. The remaining transitions can be found in Table 29 and Table 30 in the appendix.

In the presented evaluation there has not yet been made any statement about which atomic data source is favorable in the case of Cu. To especially investigate the deviations

at $\lambda \approx 1\,250\,\text{Å} - 1\,450\,\text{Å}$ with $\triangle \log(gf) \approx 2$, strong Cu IV lines in the spectra of hot, evolved stars can be analyzed. To keep things simple, it is just needed to have a look at the behavior of the strongest transitions with $\log(gf)_{\text{TOSS}} \geq 0.3$. For $\lambda \leq 1\,300\,\text{Å}$, TOSS and Kurucz values largely agree, while for $\lambda \geq 1\,300\,\text{Å}$, all Kurucz values have $\log(gf)_{\text{Kurucz}} \leq -1$ (Fig. 46). Feige 110 proved to be enriched in Cu, hence several lines could be identified in the STIS observation. Without the necessity of calculating an additional atmosphere model, it was checked if strong absorption lines could be identified in the observation for $\lambda \geq 1\,300\,\text{Å}$. If the TOSS values were more precise, no significant change of the line strengths would be expected for strong lines with $\lambda \geq 1\,300\,\text{Å}$, while if the Kurucz values were more precise, strong lines should only be found for $\lambda \leq 1\,300\,\text{Å}$. As Table 24 shows, 15 strong Cu IV lines with $\log(gf)_{\text{TOSS}} \geq 0.3$ were identified in the Feige 110 observation. As the line strengths do not significantly drop for $\lambda \geq 1\,300\,\text{Å}$, gf values from TOSS seem to be more precise in the case of Cu IV. Hence, if an analysis of Cu IV lines at $\lambda \geq 1\,300\,\text{Å}$ is desired, despite the deviation to Kurucz values, it is reasonable to employ gf values from TOSS.

Table 24: Strong Cu IV transitions, some of which identified in the Feige 110 observation. Some lines could not be unambiguously identified due to strong line blends. Uncertainties in the line centers are indicated by the shift $\triangle\lambda$. The equivalent widths were determined analogously to the method described in Sect. 8.3.2. In the case of lower fitting quality, upper limits for the equivalent width are given.

λ / Å	$\log(gf)_{\mathrm{TOSS}}$	$\log(gf)_{\mathrm{Kur.}}$	identified	note	$\triangle\lambda$ / Å	W_λ^{Obs} / mÅ
1192.42	0.50	0.54		heavy noise		
1198.82	0.50	0.55	×	noise	0.06	≤ 47.9
1201.22	0.64	0.68		strong blend		
1214.35	0.33	0.37		Ly α blend		
1222.69	0.40	0.45	×	weak blend	0.01	27.8
1224.32	0.35	0.40	×	weak blend	0.02	25.6
1231.92	0.63	0.68		strong blend		
1246.99	0.32	0.37		strong blend		
1250.32	0.39	0.44		strong blend		
1252.71	0.32	0.37		strong blend		
1266.86	0.53	0.58		strong blend		
1274.74	0.39	0.44	×	blend	0.02	≤ 49.6
1301.41	0.46	−1.26	×	weak blend	0.01	45.7
1309.41	0.51	−1.29	×	weak blend	0.01	41.1
1312.72	0.44	−1.36		strong blend		
1318.12	0.35	−1.48		strong blend		
1340.07	0.35	−1.61	×	weak blend	0.01	54.7
1345.62	0.56	−1.41		strong blend		
1350.40	0.45	−1.47	×	weak blend	0.02	≤ 49.3
1352.57	0.34	−1.58		strong blend		
1362.20	0.43	−1.54		shift	≥ 0.1	
1366.96	0.38	−1.60	×	blend	0	≤ 61.2
1367.52	0.36	−1.62	×	weak blend	0.01	57.8
1377.79	0.37	−1.64		strong blend		
1388.79	0.55	−1.48	×	weak blend	0	46.1
1407.60	0.61	−1.47		strong blend		
1410.53	0.47	−1.63	×	isolated	0.03	47.6
1426.62	0.33	−1.85	×	blend	0.01	≤ 42.5
1429.52	0.37	−1.65		strong blend		
1431.93	0.35	−1.67		strong blend		
1442.40	0.43	−1.65		strong blend		
1443.00	0.43	−1.66		strong blend		
1443.12	0.44	−1.74		strong blend		
1446.30	0.34	−1.64	×	blend	0.01	≤ 72.4
1449.66	0.40	−1.57	×	weak blend	0.02	49.3
1459.85	0.46	−1.63		strong blend		

Acknowledgements

This work is supported by the German Aerospace Center (DLR, grant 50 OR 1704). The TOSS (`http://astro-uni-tuebingen.de/~TOSS`) service, the TIRO tool (`http://astro.uni-tuebingen.de/~TIRO`), and the TMAD tool (`http://astro.uni-tuebingen.de/~TMAD`) used for this thesis were constructed as part of the Tübingen project of the German Astrophysical Virtual Observatory (`http://www.g-vo.org`).

This work is based on observations made with the NASA/ESA *Hubble Space Telescope* obtained from the Space Telescope Science Institute, which is operated by the Association of Universities for Research in Astronomy, Inc., under NASA contract NAS 5–26555. These observations are associated with program 14746.

This work has made use of NASA's Astrophysics Data System (`https://ui.adsabs.harvard.edu`) and the SIMBAD database (`http://simbad.u-strasbg.fr/simbad`), operated at CDS, Strasbourg, France.
This work has made use of data from the European Space Agency (ESA) mission *Gaia* (`https://www.cosmos.esa.int/gaia`), which is processed by the *Gaia* Data Processing and Analysis Consortium (DPAC, `https://www.cosmos.esa.int/web/gaia/dpac/consortium`). Funding for the DPAC has been provided by national institutions, in particular the institutions participating in the *Gaia* Multilateral Agreement.

We thank Robert L. Kurucz and Pascal Quinet for their comments.

List of abbreviations

2MASS	Two Micron All Sky Survey
AGB	Asymptotic Giant Branch
ALI	Accelerated Lambda Iteration
CE	Common envelope
CPOL	Core polarization
DA	Spectral type A White Dwarf (degenerate, A type)
EDR3	(Gaia) early Data Release 3
FOCES	Fiber-Optics Cassegrain Echelle Spectrograph
FUSE	Far-Ultraviolet Spectroscopic Explorer
FWHM	Full Width at Half Maximum
GAVO	German Astrophysical Virtual Observatory
HFR	relativistic Hartree Fock
HRD	Hertzsprung-Russell diagram
IAAT	Institute for Astronomy and Astrophysics Tübingen
IG	Iron group
IP	Iron Project
IR	infrared
IrOnIc	Iron Opacity and Interface Tool
ISM	interstellar medium
IUE	International Ultraviolet Explorer
LIN	Kurucz's line list with identified and calculated lines
LSF	(spectral) line spread function
LTE	local thermodynamic Equilibrium
MAST	Barbara A. Mikulski Archive for Space Telescopes
NIST	National Institute of Standards and Technology
NLTE	non-LTE
NOMAD	Naval Observatory Merged Astrometric Dataset

OP	Opacity Project
POS	Kurucz's line list with identified lines, "positively identified wavelength"
RLOF	Roche-lobe overflow
SAAO	South African Astronomical Observatory
sdB	Spectral type B hot subdwarf (subdwarf, B type)
sdO	Spectral type O hot subdwarf (subdwarf, O type)
STIS	Space Telescope imaging Spectrograph
S/N	signal-to-noise ratio
TIE	trans-iron element
TIRO	Tübingen Iron-group Opacity - IrOnIc WWW Interface
TMAD	Tübingen Model-Atom Database
TMAP	Tübingen NLTE Model-Atmosphere Package
TOSS	Tübingen Oscillator Strengths Service
UV	ultraviolet
UVES	Ultraviolet and Visual Echelle Spectrograph
VALD	Vienna Atomic Line Database
VLT	Very Large Telescope

Bibliography

Anderson, L. S. 1985, ApJ, 298, 848

Barack, L., Cardoso, V., Nissanke, S., et al. 2019, Classical and Quantum Gravity, 36, 143001

Barstow, M. A., Bond, H. E., Holberg, J. B., et al. 2005, MNRAS, 362, 1134

Cannon, C. J. 1973, ApJ, 185, 621

Carroll, B. W. & Ostlie, D. A. 1996, An Introduction to Modern Astrophysics (Cambridge University Press)

Castellani, M. & Castellani, V. 1993, ApJ, 407, 649

Chabrier, G. & Baraffe, I. 1997, VizieR Online Data Catalog, J/A+A/327/1039

Chabrier, G. & Baraffe, I. 2000, ARA&A, 38, 337

Chandrasekhar, S. & Milne, E. A. 1931, Monthly Notices of the Royal Astronomical Society, 91, 456

Cowan, R. D. 1981, The Theory of Atomic Structure and Spectra. (University of California Press, Berkeley)

Dekker, H., D'Odorico, S., Kaufer, A., Delabre, B., & Kotzlowski, H. 2000, in Society of Photo-Optical Instrumentation Engineers (SPIE) Conference Series, Vol. 4008, Proc. SPIE, ed. M. Iye & A. F. Moorwood, 534–545

Dreizler, S. & Werner, K. 1993, Space Science Reviews, 66, 147

Emilio, M., Kuhn, J. R., Bush, R. I., & Scholl, I. F. 2012, ApJ, 750, 135

Feige, J. 1958, ApJ, 128, 267

Fitzpatrick, E. L. 1999, PASP, 111, 63

Fontaine, G., Brassard, P., & Bergeron, P. 2001, PASP, 113, 409

Friedman, S. D., Howk, J. C., Chayer, P., et al. 2002, The Astrophysical Journal Supplement Series, 140, 37

Gaia Collaboration, Brown, A. G. A., Vallenari, A., et al. 2018, A&A, 616, A1

Gaia Collaboration, Brown, A. G. A., Vallenari, A., et al. 2020, arXiv e-prints, arXiv:2012.01533

Green, R. F., Schmidt, M., & Liebert, J. 1986, ApJS, 61, 305

Greenstein, J. L. 1971, in White Dwarfs, ed. W. J. Luyten, Vol. 42, 46

Han, Z., Podsiadlowski, P., Maxted, P. F. L., & Marsh, T. R. 2003, MNRAS, 341, 669

Han, Z., Podsiadlowski, P., Maxted, P. F. L., Marsh, T. R., & Ivanova, N. 2002, MNRAS, 336, 449

Harding, A. K. 2013, Frontiers of Physics, 8, 679

Hauschildt, P. H. & Baron, E. 1999, Journal of Computational and Applied Mathematics, 109, 41

Heber, U. 2016, PASP, 128, 082001

Heber, U. & Edelmann, H. 2004, Ap&SS, 291, 341

Heber, U., Hunger, K., Jonas, G., & Kudritzki, R. P. 1984, Symposium - International Astronomical Union, 105, 223–224

Holtsmark, J. 1919, Annalen der Physik, 363, 577

Hubble, E. P. 1936, Realm of the Nebulae (Oxford University Press, London)

Hubeny, I. 2010, in American Institute of Physics Conference Series, Vol. 1268, Graduate School in Astronomy: XIV Special Courses at the National Observatory of Rio de Janeiro, ed. R. Dupke, J. Alcaniz, R. de La Reza, & S. Daflon, 73–115

Hubeny, I. & Lanz, T. 1992, A&A, 262, 501

Hubeny, I. & Mihalas, D. 2014, Theory of Stellar Atmospheres (Princeton University Press)

Iben, I., J. 1974, ARA&A, 12, 215

Joergens, V. 2005, Reviews in Modern Astronomy, 18, 216

Kalogera, V. & Baym, G. 1996, The Astrophysical Journal, 470, L61–L64

Kepler, J. 1609, Astronomia Nova

Kilkenny, D., O'Donoghue, D., Koen, C., Stobie, R. S., & Chen, A. 1997, MNRAS, 287, 867

Kirchhoff, G. & Bunsen, R. 1860, Annalen der Physik, 186, 161

Kramida, A., Yu. Ralchenko, Reader, J., & and NIST ASD Team. 2020, NIST Atomic Spectra Database (ver. 5.8), [Online]. Available: `https://physics.nist.gov/asd` [2020, November 30]. National Institute of Standards and Technology, Gaithersburg, MD.

Kudritzki, R. P. 1976, A&A, 52, 11

Kurucz, R. L. 1973, SAO Special Report, 351

Kurucz, R. L. 1991, New Opacity Calculations, ed. L. Crivellari, I. Hubeny, & D. G. Hummer (Dordrecht: Springer Netherlands), 441–448

Kurucz, R. L. 2011, Canadian Journal of Physics, 89, 417

Kurucz, R. L. 2018, Astronomical Society of the Pacific Conference Series, Vol. 515, Including All the Lines: Data Releases for Spectra and Opacities through 2017, 47

Lanz, T., Brown, T. M., Sweigart, A. V., Hubeny, I., & Landsman, W. B. 2004, ApJ, 602, 342

Laughlin, G., Bodenheimer, P., & Adams, F. C. 1997, ApJ, 482, 420

Macchetto, F. 1976, Mem. Soc. Astron. Italiana, 47, 431

Massacrier, G. & Artru, M.-C. 2012, A&A, 538, A52

MATLAB. 2019, Version 9.7.0 (R2019b) (Natick, Massachusetts: The MathWorks Inc.)

Müller-Ringat, E. M. 2013, Dissertation, University of Tübingen

Naslim, N., Jeffery, C. S., Behara, N. T., & Hibbert, A. 2011, MNRAS, 412, 363

Newell, E. B. 1973, ApJS, 26, 37

Newton, I. 1687, Philosophiae naturalis principia mathematica (William Dawson & Sons Ltd., London)

Newton, I. 1704, Opticks, or a treatise of the reflections, refractions, inflections and colours of light (William Innys)

Pelisoli, I., Vos, J., Geier, S., Schaffenroth, V., & Baran, A. S. 2020

Pfeiffer, M. J., Frank, C., Baumueller, D., Fuhrmann, K., & Gehren, T. 1998, A&AS, 130, 381

Quinet, P., Palmeri, P., Biémont, E., et al. 2002, Journal of Alloys and Compounds, 344, 255 , proceedings of the Rare Earths‘ 2001 Conference

Quinet, P., Palmeri, P., Biémont, E., et al. 1999, Monthly Notices of the Royal Astronomical Society, 307, 934

Ramírez, I. & Allende Prieto, C. 2011, ApJ, 743, 135

Rauch, T. & Deetjen, J. L. 2003, Astronomical Society of the Pacific Conference Series, Vol. 288, Handling of Atomic Data, ed. I. Hubeny, D. Mihalas, & K. Werner, 103

Rauch, T., Gamrath, S., Quinet, P., et al. 2020, A&A, 637, A4

Rauch, T., Gamrath, S., Quinet, P., et al. 2017a, A&A, 599, A142

Rauch, T., Quinet, P., Hoyer, D., et al. 2016a, A&A, 587, A39

Rauch, T., Quinet, P., Hoyer, D., et al. 2016b, A&A, 590, A128

Rauch, T., Quinet, P., Knörzer, M., et al. 2017b, A&A, 606, A105

Rauch, T., Rudkowski, A., Kampka, D., et al. 2014a, A&A, 566, A3

Rauch, T., Werner, K., Biémont, É., Quinet, P., & Kruk, J. W. 2012, A&A, 546, A55

Rauch, T., Werner, K., & Kruk, J. W. 2010, Ap&SS, 329, 133

Rauch, T., Werner, K., Quinet, P., & Kruk, J. W. 2014b, A&A, 564, A41

Rauch, T., Werner, K., Quinet, P., & Kruk, J. W. 2014c, A&A, 566, A10

Rauch, T., Werner, K., Quinet, P., & Kruk, J. W. 2015, A&A, 577, A6

Riley, A., Biretta, J., Hernandez, S., Ely, J., & Bostroem, K. A. 2019, STIS Instrument Handbook Version [19.0], Baltimore: STScI

Ringat, E. & Rauch, T. 2011, Metal-Abundance Peculiarities in the sdOB Star EC11481-2303: A Progress Report

Robertson, J. G. 2013, Publications of the Astronomical Society of Australia, 30, e048

Saffer, R. A., Bergeron, P., Koester, D., & Liebert, J. 1994, ApJ, 432, 351

Saha, M. 1920, The London, Edinburgh, and Dublin Philosophical Magazine and Journal of Science, 40, 472

Saha, P. 2020, Publications of the Astronomical Society of the Pacific, 132, 021001

Sansonetti, J., Martin, W., & Young, S. 2013, Handbook of Basic Atomic Spectroscopic Data [Version 1.1.3], national Institute of Standards and Technology, Gaithersburg, MD

Scharmer, G. B. 1981, ApJ, 249, 720

Seaton, M. J. 1962, in Atomic and Molecular Processes, ed. D. R. Bates

Seaton, M. J., Yan, Y., Mihalas, D., & Pradhan, A. K. 1994, Monthly Notices of the Royal Astronomical Society, 266, 805

Skrutskie, M. F., Cutri, R. M., Stiening, R., et al. 2006, The Astronomical Journal, 131, 1163

Stys, D., Slevinsky, R., Sion, E. M., et al. 2000, PASP, 112, 354

Sugar, J. & Musgrove, A. 1990, Journal of Physical and Chemical Reference Data, 19, 527

Sugar, J. & Musgrove, A. 1995, Journal of Physical and Chemical Reference Data, 24, 1803

Tremblay, P. E. & Bergeron, P. 2009, ApJ, 696, 1755

Unsöld, A. 1968, Physik der Sternatmosphären, mit besonderer Berucksichtigung der Sonne. (Springer-Verlag)

van het Hof, G. J., Raassen, A. J. J., Uylings, P. H. M., et al. 1990, Physica Scripta, 41, 240

van Leeuwen, F. 2007, A&A, 474, 653

van Regemorter, H. 1962, ApJ, 136, 906

Webbink, R. F. 1984, ApJ, 277, 355

Werner, K., Deetjen, J. L., Dreizler, S., et al. 2002, Model Photospheres with Accelerated Lambda Iteration

Werner, K., Deetjen, J. L., Dreizler, S., et al. 2003, Astronomical Society of the Pacific Conference Series, Vol. 288, Model Photospheres with Accelerated Lambda Iteration, ed. I. Hubeny, D. Mihalas, & K. Werner, 31

Werner, K. & Dreizler, S. 1999, Journal of Computational and Applied Mathematics, 109, 65

Werner, K., Dreizler, S., & Rauch, T. 2012a, TMAP: Tübingen NLTE Model-Atmosphere Package, Astrophysics Source Code Library [record ascl:1212.015]

Werner, K. & Husfeld, D. 1985, A&A, 148, 417

Werner, K., Rauch, T., Knörzer, M., & Kruk, J. W. 2018, A&A, 614, A96

Werner, K., Rauch, T., Kučas, S., & Kruk, J. W. 2015, A&A, 574, A29

Werner, K., Rauch, T., Ringat, E., & Kruk, J. W. 2012b, arXiv e-prints, arXiv:1209.4977

Wiese, W. L., Fuhr, J. R., & Deters, T. M. 1996, Atomic transition probabilities of carbon, nitrogen, and oxygen : a critical data compilation (AIP Press, NY)

Wild, J. F. & Jeffery, C. S. 2017, Open Astronomy, 26, 246

Wild, J. F. & Jeffery, C. S. 2018, MNRAS, 473, 4021

Zacharias, N., Monet, D. G., Levine, S. E., et al. 2004, in American Astronomical Society Meeting Abstracts, Vol. 205, American Astronomical Society Meeting Abstracts, 48.15

A Appendix

All Matlab procedures and line tables presented in the appendix can also be found online, at `https://github.com/iaatue/LandstorferPhD`.

A.1 Figures

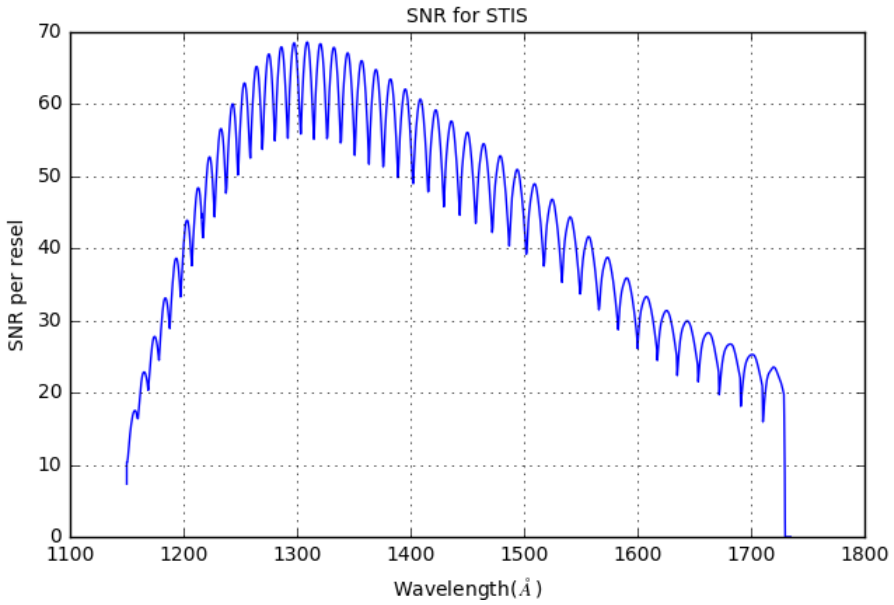

Figure 47: Wavelength-dependent signal-to-noise ratio of STIS for an observation of Feige 110 which corresponds to the observation for this work.
`Reference: http://etc.stsci.edu/etc/input/stis/spectroscopic`

A.2 Matlab procedures

The following Matlab scripts were used for line identification (Sects. 8.3 and 8.4) and evaluation (Sect. 9) and are shown (as an example) as used for Feige 110. For PG 0909+276, an analogous code was used.

The Matlab function **FUNmakeCont** was implemented in several scripts to determine the local continuum of a spectrum. Also, with this function, a reduced spectrum can be generated subsequently by simple subtraction.

```
1  % Input: 'spectrum' of which the local continuum is to be
       determined, 'maxint' the proper interval to find local maxima
        in, 'outlier1' can be used to exclude a maximum from the fit
       , 'wvllow', 'wvlup' and 'int' denote lower and upper
       wavelengths and the interval to find maxima for segments
       which need to be treated seperately
2
3  % Output: 'envelope' including the found maxima, and 'cont'
       which includes the spline-fit of the estimated continuum
4
5  function [envelope, cont] = FUNmakeCont(spectrum,maxint,outlier1
       ,wvllow1,wvlup1,int1,wvllow2,wvlup2,int2,wvllow3,wvlup3,int3,
       wvllow4,wvlup4,int4)
6
7  % set 'int = 0' to exclude a segment from the fit
8
9  % ------------------------- START -- CODE -------------------------
10
11 % general continuum with 'maxint'
12
13 minspecwvl = spectrum(1,1);
14 maxspecwvl = spectrum(length(spectrum),1);
15
16 a = (minspecwvl:maxint:maxspecwvl+maxint/2);
17
18 for i = 1:length(a)
19
20      dist1 = abs(a(i)-maxint/1.9-spectrum(:,1));
21      minDist = min(dist1);
22      idx1 = min(find(dist1 == minDist));
23      dist2 = abs(a(i)+maxint/1.9-spectrum(:,1));
24      minDist = min(dist2);
25      idx2 = max(find(dist2 == minDist));
26
27      for j = 1 : (idx2-idx1+1)
28      b(j) = spectrum(j+idx1-1,2);
29      end
30
31      maxVal = max(b);
32      idMax = max(find(b == maxVal));
```

```
33
34      envelope(i,1) = spectrum(idMax + idx1-1,1);
35      envelope(i,2) = spectrum(idMax + idx1-1,2);
36
37      clear b
38
39  end
40
41  % segments treated seperately with smaller 'int'
42
43  if exist('wvllow1','var')
44
45      for i = 1:length(envelope)
46      if envelope(i,1) > wvllow1 && envelope(i,1) < wvlup1
47
48          envelope(i,1) = 0;
49      end
50      end
51
52  a1 = (wvllow1:int1:wvlup1);
53
54  for i = 1 : length(a1)
55
56      dist1 = abs(a1(i)-int1/2-spectrum(:,1));
57      minDist = min(dist1);
58      idx1 = min(find(dist1 == minDist));
59      dist2 = abs(a1(i)+int1/2-spectrum(:,1));
60      minDist = min(dist2);
61      idx2 = max(find(dist2 == minDist));
62
63      for j = 1 : (idx2-idx1+1)
64      b(j) = spectrum(j+idx1-1,2);
65      end
66
67      maxVal = max(b);
68      idMax = max(find(b == maxVal));
69
70      envelope(i+length(a),1) = spectrum(idMax + idx1-1,1);
71      envelope(i+length(a),2) = spectrum(idMax + idx1-1,2);
72
73      clear b
74
75  end
76  end
77
78  if exist('wvllow2','var')
79
80      for i = 1:length(envelope)
81      if envelope(i,1) > wvllow2 && envelope(i,1) < wvlup2
```

```
82
83          envelope(i,1) = 0;
84      end
85      end
86
87 a2 = (wvllow2:int2:wvlup2);
88
89 for i = 1 : length(a2)
90
91      dist1 = abs(a2(i)-int2/2-spectrum(:,1));
92      minDist = min(dist1);
93      idx1 = min(find(dist1 == minDist));
94      dist2 = abs(a2(i)+int2/2-spectrum(:,1));
95      minDist = min(dist2);
96      idx2 = max(find(dist2 == minDist));
97
98      for j = 1 : (idx2-idx1+1)
99      b(j) = spectrum(j+idx1-1,2);
100     end
101
102     maxVal = max(b);
103     idMax = max(find(b == maxVal));
104
105     envelope(i+length(a)+length(a1),1) = spectrum(idMax + idx1
            -1,1);
106     envelope(i+length(a)+length(a1),2) = spectrum(idMax + idx1
            -1,2);
107
108     clear b
109
110 end
111 end
112
113 if exist('wvllow3','var')
114
115     for i = 1:length(envelope)
116     if envelope(i,1) > wvllow3 && envelope(i,1) < wvlup3
117
118         envelope(i,1) = 0;
119     end
120     end
121
122 a3 = (wvllow3:int3:wvlup3);
123
124 for i = 1 : length(a3)
125
126     dist1 = abs(a3(i)-int3/2-spectrum(:,1));
127     minDist = min(dist1);
128     idx1 = min(find(dist1 == minDist));
```

```
129     dist2 = abs(a3(i)+int3/2-spectrum(:,1));
130     minDist = min(dist2);
131     idx2 = max(find(dist2 == minDist));
132
133     for j = 1 : (idx2-idx1+1)
134     b(j) = spectrum(j+idx1-1,2);
135     end
136
137     maxVal = max(b);
138     idMax = max(find(b == maxVal));
139
140     envelope(i+length(a)+length(a1)+length(a2),1) = spectrum(
            idMax + idx1-1,1);
141     envelope(i+length(a)+length(a1)+length(a2),2) = spectrum(
            idMax + idx1-1,2);
142
143     clear b
144
145 end
146 end
147
148 if exist('wvllow4','var')
149
150     for i = 1:length(envelope)
151     if envelope(i,1) > wvllow4 && envelope(i,1) < wvlup4
152
153         envelope(i,1) = 0;
154     end
155     end
156
157 a4 = (wvllow4:int4:wvlup4);
158
159 for i = 1 : length(a4)
160
161     dist1 = abs(a4(i)-int4/2-spectrum(:,1));
162     minDist = min(dist1);
163     idx1 = min(find(dist1 == minDist));
164     dist2 = abs(a4(i)+int4/2-spectrum(:,1));
165     minDist = min(dist2);
166     idx2 = max(find(dist2 == minDist));
167
168     for j = 1 : (idx2-idx1+1)
169     b(j) = spectrum(j+idx1-1,2);
170     end
171
172     maxVal = max(b);
173     idMax = max(find(b == maxVal));
174
```

```
175       envelope(i+length(a)+length(a1)+length(a2)+length(a3),1) =
              spectrum(idMax + idx1-1,1);
176       envelope(i+length(a)+length(a1)+length(a2)+length(a3),2) =
              spectrum(idMax + idx1-1,2);
177
178       clear b
179
180 end
181 end
182
183 % treating outliers
184
185 if exist('outlier1','var')
186       if outlier1 > 0
187 dist3 = abs(outlier1 - envelope(:,1));
188 minDist = min(dist3);
189 idx3 = find(dist3 == minDist);
190
191 for i = idx3 : length(envelope)-1
192       envelope(i,1) = envelope(i+1,1);
193       envelope(i,2) = envelope(i+1,2);
194 end
195       end
196 end
197
198 % creating Output
199
200 envelope = sortrows(envelope);
201 envelope = envelope(any(envelope(:,1),2),:);
202
203 cont = fit(envelope(:,1), envelope(:,2), 'smoothingspline');
204 end
```

The Matlab script **Feige_make_Contfact** was used to determine the correction factor needed to calibrate the continuum of the synthetic spectrum of Feige 110 based on the observation.

```
% Input: 'obsspec' and 'Feige_synspec', observed and synthetic
    spectra of Feige 110

% Output: 'corrfact' the correction factor for continuum
    calibration

% ------------------------- START -- CODE -------------------------

% reading the input spectra

    A = importdata('obsspec.txt') ;
    obsspec = A.data;
   A = importdata('Feige_synspec');
    synspec = A.data;

% adding a low-pass filter (Savitzky-Golay filter)

    obsspec(:,2) = sgolayfilt(obsspec(:,2),3,11);

[envelope2,~] = FUNmakeCont(obsspec,2.5,0,1144,1180,0);

% S/N correction for the observed spectrum

for n = 1:length(envelope2)

    envelope2(n,2) = envelope2(n,2) - 1/80*envelope2(n,2);

end

% removing local maxima from 'envelope2'

[pks, locs] = findpeaks(envelope2(:,2));

for i = 1:length(locs)

    envelope2(locs(i),:) = 0;

end

envelope2 = envelope2(any(envelope2,2),:);

[pks, locs] = findpeaks(envelope2(:,2));

for i = 1:length(locs)

    envelope2(locs(i),:) = 0;
```

```
45
46 end
47
48 envelope2 = envelope2(any(envelope2,2),:);
49
50 % determining the continuum of 'synspec'
51
52  [envelope, cont ] = FUNmakeCont(synspec
      ,7.5,1467,1200,1230,2.5,1635,1645,0.5);
53
54 % finding 'minfact' to minimize Chi^2 when minfact*syncont =
     obscont applies
55
56 for i = 1:length(envelope2)
57
58     envelope2(i,3) = cont(envelope2(i,1));
59
60 end
61
62 fact = (0.6:0.001:1.5);
63
64 for i = 1:length(fact)
65
66     for j = 1:length(envelope2)
67
68         difenvchi(j) = (abs(fact(i)*envelope2(j,2)-envelope2(j
               ,3)))^2/envelope2(j,3);
69
70     end
71
72     difenv(i) = sqrt(sum(difenvchi));
73
74 end
75
76 mindifenv = min(difenv);
77
78 minfact = fact(min(find(difenv == mindifenv)));
79 corrfact = 1/minfact;
```

The Matlab script **Prepare_Linelists_Feige** was used to find all lines of a chosen ion (e.g., Ni IV) in the synthetic spectrum of Feige 110, and to determine the line properties.

```
% Input: 'Elem','Ion' element and ion, of which all lines are
    looked for, the synthetic spetrum of the corresponding ion '
    FeigeA0_Elem_Ion', and 'idents.txt' a list containing the
    line centers of lighter-element lines to be excluded

% Output: 'linelist' containing the line centers of the
    specified ion's lines, 'equw' containing the associated
    equivalent width, and 'errorsum_final' containing the fit
    quality

% specifying the ion of which the lines are looked for

Elem = 'Ni';
Ion = 'IV';

% ------------------------- START -- CODE -------------------------

% reading the input spectrum and the list of lighter-element
    lines

A = importdata(strcat(Elem,'/','FeigeA0_',Elem, Ion));
synspec = A.data;
idents = importdata('Idents.txt');

% determining the continuum of 'synspec'

 [envelope, cont ] = FUNmakeCont(synspec
    ,7.5,1467,1200,1230,2.5,1635,1645,0.5);

% creating the reduced spectrum

for u = 1 : length(synspec(:,1))

    synspec(u,2) = cont(synspec(u,1))-synspec(u,2);

    if synspec(u,2) < cont(synspec(u,1))/100
        synspec(u,2) = 0;
    end

end

% determination of line properties

% local maxima of the reduced synspec = line centers

[pks, locs] = findpeaks(synspec(:,2));

```

```
40 % determining the fitting interval: either 1) pm 0.1A or 2) up
       to one third the distance to the next maximum
41
42  for k = 1 : length(locs)
43
44 dist = abs(synspec(locs(k),1)-0.1-synspec(:,1));
45 minDist = min(dist);
46 idloc1 = min(find(dist == minDist));
47 dist = abs(synspec(locs(k),1)+0.1-synspec(:,1));
48 minDist = min(dist);
49 idloc2 = min(find(dist == minDist));
50
51 if k > 1
52 testint1 = (synspec(locs(k),1) - synspec(locs(k-1),1));
53 else
54 testint1 = 0.2;
55 end
56
57 if testint1<0.2
58 dist = abs(synspec(locs(k),1)-testint1/3-synspec(:,1));
59 minDist = min(dist);
60 idloc1 = min(find(dist == minDist));
61 end
62
63 if k < length(locs)
64 testint2 = (synspec(locs(k+1),1) - synspec(locs(k),1));
65 else
66 testint2 = 0.2;
67 end
68
69 if testint2<0.2
70 dist = abs(synspec(locs(k),1)+testint2/3-synspec(:,1));
71 minDist = min(dist);
72 idloc2 = min(find(dist == minDist));
73 end
74
75 linelambda = synspec((idloc1 : idloc2),1);
76 linevalue  = synspec((idloc1 : idloc2),2);
77
78 if length(linelambda) > 5
79
80 % Gaussian fit, then determining the line properties
81
82 if k > 5 && k < length(locs)-5
83 options = fitoptions('gauss1', 'Lower', [-10 synspec(locs(k)
       -5,1) 0.0001], 'Upper', [100 synspec(locs(k)+5,1) 1]);
84 end
85 [linefit,gof] = fit(linelambda(:), linevalue(:), 'gauss1');
86
```

```
87 int = linefit.a1*sqrt(pi)*linefit.c1;
88 int = int*1000;
89 int = int/cont(synspec(locs(k),1));
90
91  Equwidth_syn(k) = int;
92  Sigma_syn(k) = linefit.c1;
93  errorsum(k) = gof.sse;
94  coefferr(k) = gof.rsquare;
95
96 else
97
98  Equwidth_syn(k) = 0;
99  Sigma_syn(k) = 0;
100  errorsum(k) = 1;
101  coefferr(k) = 1;
102
103 end
104  end
105
106 % excluding all lines which are closer than 0.03A to a lighter-
      element line center
107
108 b = 1;
109 for m = 1:length(locs)
110
111     a = 0;
112  for n = 1:length(idents)
113  if  abs(synspec(locs(m),1) - idents(n)) < 0.03
114      a = a+1;
115
116  end
117  end
118
119  if a == 0
120
121     linelist(b) = synspec(locs(m));
122     equw(b) = Equwidth_syn(m);
123
124     errorsum_fin(b) = errorsum(m);
125     coefferr_fin(b) = coefferr(m);
126
127      b= b+1;
128
129  end
130 end
```

Based on the created line list, the Matlab script **Make_Linelists_Feige** was used to find the corresponding transitions (in the Kurucz POS list) of a chosen ion (e.g., Ni IV) and subsequently reduce that list.

```
% Input: 'Elem,Ion_Lines.txt' the prepared line list of a chosen
    ion (containing the line properties), 'Elem,Ion.POS' the
    Kurucz POS list of the ion, and 'Elem,Ion_Errors_Final.txt' a
    list containing lines with a goodness < 0.96

% Output: 'G' a matrix containing all identified transitions of
    the specified ion, with the applied reduction criteria

% specifying the ion of which the lines are looked for

Elem = 'Ni';
Ion = 'IV';

% ------------------------- START -- CODE -------------------------

% reading the line list, the Kurucz POS list and the error list

A = importdata(strcat(Elem,'/',Elem,Ion,'_Lines.txt'));
B = importdata(strcat(Elem,'/',Elem,Ion,'.POS'));

if isfile(strcat(Elem,'/',Elem,Ion,'_Errors_final.txt'))
C = importdata(strcat(Elem,'/',Elem,Ion,'_Errors_final.txt'));
end

% reducing the POS list, removing transitions with log(gf)<
    -2.5, and just keeping the interval 1150A < lamda < 1710A

q=1;

for i = 1:length(B(:,1))

    if q < length(B(:,1))+1

    if B(i,1) > 1150 && B(i,1) < 1710
    if B(i,2) > -2.5

    linelist(q) = round(B(i,1),2);
    gflist(q) = B(i,2);
    E_low(q) = B(i,4);
    E_up(q) = B(i,5);

    q = q+1;

    end
    end
    end
```

```
42 end
43
44 % removing lines with equw < 1.5mA
45
46 q=1;
47
48 for i = 1:length(A(:,1))
49
50     if q < length(A(:,1))+1
51
52     if A(i,1) > 1150 && A(i,1) < 1710
53     if A(i,2) > 1.5
54
55     linessyn(q) = A(i,1);
56     equw(q) = A(i,2);
57
58     q = q+1;
59
60     end
61     end
62     end
63 end
64
65 % A transition in the Kurucz POS list is taken when a
     corresponding line exists in the prepared list (line center
     is closer than 0.05A)
66
67 a = 1;
68 for m = 1:length(linelist)
69
70  for n = 1:length(linessyn)
71  if  abs(linelist(m) - linessyn(n)) < 0.05
72      F(a,1) = linelist(m);
73      F(a,2) = gflist(m);
74      F(a,3) = E_low(m);
75      F(a,4) = E_up(m);
76
77      a = a+1;
78
79  end
80  end
81 end
82
83 % for all line centers in the error list, transitions from the
     POS list will be taken in a certain interval (0.05A to 0.15A)
      depending on the goodness-of-fit
84
85  if isfile(strcat(Elem,'/',Elem,Ion,'_Errors_final.txt'))
86
```

```
m = length(F(:,1))+1;

for j = 1:length(C(:,1))

    errcorr = 1/8 * sqrt(C(j,2)) + 1/40;

for k = 1:length(linelist)

    if abs(linelist(k)-C(j,1))< errcorr

    F(m,1) = linelist(k);
    F(m,2) = gflist(k);
    F(m,3) = E_low(k);
    F(m,4) = E_up(k);

    m = m+1;

    end
end
end
 end

% Arranging F to wavelength, deleting double entries

G = sortrows(F);
clear F

for a = 1:length(G(:,1))-1

    if G(a,1) == G(a+1,1) && G(a,2) == G(a+1,2) && G(a,3) == G(a
        +1,3) && G(a,4) == G(a+1,4)

    G(a,:) = 0;

    end
end

F = sortrows(G);
clear G

G = F(any(F,2),:);

% reduction: for lines with log gf > -1, all nearby (< 0.03A)
    weaker transitions (delta log gf > 1.5) are removed

for i = 1:length(G(:,1))

  if G(i,2) > -1.0  && G(i,1) > 0

```

```
134         for j = 1:length(G(:,1))
135 
136         if abs(G(i,1)-G(j,1))<0.03 && (G(i,2)-G(j,2))>1.5
137 
138             G(j,:)=0;
139         end
140 
141         end
142 
143     end
144 
145 end
146 
147 F = sortrows(G);
148 clear G
149 
150 G = F(any(F,2),:);
```

The Matlab script **Prepare_Isolated_Feige** works analogous to the **Prepare_Linelists_Feige** script, except for it is used for the synthetic spectrum which contains all found elements and directly excludes all low-quality (< 0.96) fits.

The Matlab-script **Make_Isolated_Feige** was used to make the list of isolated lines for Feige 110.

```
% Input: 'Isoprep_Lines.txt' a line list of all investigated
    ions, obtained from 'Prepare_Isolated_Feige' (containing the
    line properties), 'FeigeA0_RED_ALL.txt' the reduced synthetic
     spectrum of Feige 110 containing all investigated ions, and
    'FeigeA0_RED_Elem,Ion.txt' reduced spectra for each of the
    investigated ions

% Output: 'ANS' a list of all isolated lines, containing the
    line center and the respective ion

% ------------------------- START -- CODE -------------------------

% reading the prepared line list and the reduced spectrum of all
     ions

A = importdata('Isoprep_Lines.txt');
spec = importdata('FeigeA0_RED_ALL.txt');

% somewhat complicated reading the reduced spectra of the
    different ions and saving in a cell array (LM denotes the
    lighter elements)

E(1) = "Ca";
E(2) = 'Sc';
E(3) = 'Ti';
E(4) = 'V_';
E(5) = 'Cr';
E(6) = 'Mn';
E(7) = 'Fe';
E(8) = 'Co';
E(9) = "Ni";
E(10) = 'LM';

I(1) = "III";
I(2) = 'IV';
I(3) = "V";
I(4) = "VI";
I(5) = 'III-VI';

z = 0;

for x = 1:length(E)

```

```
35      for y = 1:length(I)
36
37          if isfile(strcat(E(x),'/','FeigeA0_RED_',E(x),I(y),'.txt
                ''))
38
39              z = z+1;
40
41      B = importdata(strcat(E(x),'/','FeigeA0_RED_',E(x),I(y),'.
            txt')) ;
42
43      B_cell{1,z} = B(:,1);
44      B_cell{2,z} = B(:,2);
45      B_cell{3,z} = strcat(E(x),I(y));
46
47      clear B
48
49          end
50      end
51 end
52
53 % determining the isolated lines
54
55  for k = 1 : length(A(:,1))
56
57 % determining the line centers and the interval of pm 1.82 sigma
       , so that about 99% of the integrated line flux is considered
58
59 center = A(k,1);
60 sigma = A(k,3);
61 D(k,1) = center;
62 D(k,3) = sigma;
63
64 wlow = center-1.82*sigma;
65 wup  = center+1.82*sigma;
66
67 % determination of the integrated line flux
68
69 dist = abs(wlow-spec(:,1));
70 minDist = min(dist);
71 idloc1 = min(find(dist == minDist));
72 dist = abs(wup-spec(:,1));
73 minDist = min(dist);
74 idloc2 = min(find(dist == minDist));
75
76
77 linelambda = spec((idloc1 : idloc2),1);
78 linevalue  = spec((idloc1 : idloc2),2);
79
80 intflux_lineALL = trapz(linelambda,linevalue);
```

```
81
82  clear linelambda
83  clear linevalue
84
85 for l = 1:length(B_cell(1,:))
86
87     C(:,1) = cell2mat(B_cell(1,l));
88     C(:,2) = cell2mat(B_cell(2,l));
89
90     dist = abs(wlow-C(:,1));
91     minDist = min(dist);
92     idloc1 = min(find(dist == minDist));
93     dist = abs(wup-C(:,1));
94     minDist = min(dist);
95     idloc2 = min(find(dist == minDist));
96
97     linelambda = C((idloc1 : idloc2),1);
98     linevalue  = C((idloc1 : idloc2),2);
99
100    intflux(l) = trapz(linelambda,linevalue);
101
102    intflux_red(l) = intflux(l) / intflux_lineALL;
103
104    clear linelambda
105    clear linevalue
106
107    clear C
108 end
109
110    % test, if only one significant line is in the interval
       (>90% flux)
111
112    if max(intflux_red) < 1.5 && max(intflux) > 0.90*sum(intflux
       )
113
114        [maxval,idmax] = max(intflux_red);
115
116        D(k,2) = idmax;
117
118    else
119        D(k,:) = 0;
120    end
121
122    % if a lighter-element line dominates, remove entry
123
124    if D(k,2) == z
125
126        D(k,:) = 0;
127
```

```
128     end
129 end
130
131 D1 = D(any(D,2),:);
132
133 % if several transitions of the same ion are close, they were
      not removed yet. Here: for each found isolated line it is
      checked wether the integrated flux in the respective ion's
      reduced spectrum is matching the determined line flux
134
135 for n = 1:length(D1(:,1))
136
137     center = D1(n,1);
138     ion = D1(n,2);
139     sigma = D1(n,3);
140
141     % determining the fitting-interval
142
143     wlow = center-2.5*sigma;
144     wup  = center+2.5*sigma;
145
146     F(:,1) = cell2mat(B_cell(1,ion));
147     F(:,2) = cell2mat(B_cell(2,ion));
148
149     dist = abs(wlow-F(:,1));
150     minDist = min(dist);
151     idloc1 = min(find(dist == minDist));
152     dist = abs(wup-F(:,1));
153     minDist = min(dist);
154     idloc2 = min(find(dist == minDist));
155
156     linelambda = F((idloc1 : idloc2),1);
157     linevalue  = F((idloc1 : idloc2),2);
158
159     % calculating the integrated flux
160
161     int1 = trapz(linelambda,linevalue);
162
163     options = fitoptions('gauss1', 'Lower', [-10 linelambda(1)
          0.0001], 'Upper', [100 linelambda(length(linelambda)) 1])
          ;
164     [linefit,gof] = fit(linelambda(:), linevalue(:), 'gauss1',
          options);
165     int2 = linefit.a1*sqrt(pi)*linefit.c1;
166
167     % keeping the line if the deviation is < 0.05
168
169     if 1.05 > int2/int1 > 0.95
170
```

```
171       else
172
173           D1(n,:) = 0;
174
175       end
176
177 end
178
179 D2 = D1(any(D1,2),:);
180
181 % saving in a cell array
182
183 for m = 1:length(D2(:,1))
184
185     ANS{m,1} = D2(m,1);
186     ANS{m,2} = B_cell{3,D2(m,2)};
187     ANS{m,3} = D2(m,3);
188
189 end
```

The Matlab script **Finish_Isolated_Feige** was used to find the respective transitions in a list created from **Make_Linelists_Feige** for each isolated line in Feige 110. The output is to be considered the final list of isolated lines in Feige 110.

```
% Input: 'Isolated_Lines1.txt' the list of isolated lines, and '
    Elem,Ion_FERTIG.txt' for all IG elements, the line lists
    created with 'Make_Linelists'

% Output: 'ANS' corresponding transitions for all isolated lines

% ------------------------- START -- CODE -------------------------

% reading the isolated list

A = readcell('Isolated_Lines1.txt');
B(:,1) = cell2mat(A(:,1));
B(:,2) = cell2mat(A(:,3));

% for each isolated line, reading the corresponding list of
    transitions

z = 1;

for i = 1:length(B)

    center = B(i,1);
    sigma = B(i,2);
    ion = char(A(i,2));
    elem = ion(1:2);

    C = importdata(strcat(elem,'/',ion,'_FERTIG.txt'));

    wl = C(:,1);

    % a transition is considered isolated if only one occurs in
       pm 1 sigma around the line center

    a = 0;

    for j = 1:length(wl)

     if abs(center - wl(j)) < sigma

         a = a+1;
         k = j;

     end
    end

    if a == 1
```

```
43
44          ANS{z,1} = C(k,1);
45          ANS{z,2} = ion;
46          ANS{z,3} = C(k,2);
47          ANS{z,4} = C(k,3);
48          ANS{z,5} = C(k,4);
49
50          z = z+1;
51
52      end
53      clear wl
54 end
```

Finally, the Matlab script **Equ_width_Feige** was used to determine the line properties (especially the equivalent widths) of all isolated lines in the synthetic and observed spectrum.

```
% Input: 'obsspec.txt' the observed spectrum of Feige 110, 'FeigeA0_ALL' the synthetic spectrum of Feige 110 containing all IG elements, and 'Isolated_List1200.txt' a list of all isolated lines (with the corresponding transitions) with lambda > 1200A

% Output: 'ANS' a list of all isolated lines with their line properties taken from the obsspec and the synspec

% ---------------------- START -- CODE ----------------------

% reading the observed and synthetic spectrum, and the list of isolated lines

A = importdata('obsspec.txt');
obsspec = A.data;
A = importdata('FeigeA0_ALL');
synspec = A.data;
A = readcell('Isolated_List1200.txt');
linelist = cell2mat(A(:,1));
gflist = cell2mat(A(:,3));

% determining the continuum of synspec

[envelope, cont ] = FUNmakeCont(synspec,7.5,1467,1200,1230,2.5,1635,1645,0.5);

% Determination of equivalent widths in the synspec

% finding local maxima

[pks, locs] = findpeaks(synspec(:,2));
synspecval = synspec(:,2);

% finding corresponding isolated lines

l = length(linelist);

for k = 1 : l

    clear linefit
    clear linelambda
    clear linevalue

dist = abs(linelist(k)-synspec(:,1));
minDist = min(dist);
```

```
40 idx = min(find(dist == minDist));
41
42 localcont = cont(synspec(idx,1));
43
44 % determining the next local maxima
45
46 dist = abs(linelist(k)-synspec(locs,1));
47 minDist = min(dist);
48 idloc1 = min(find(dist == minDist));
49
50 if linelist(k) > synspec(locs(idloc1))
51     idloc2 = idloc1+1;
52 else
53     idloc2 = idloc1;
54     idloc1 = idloc2-1;
55 end
56
57 % determining the fitting interval
58
59 linelambda = (synspec(locs(idloc1) : locs(idloc2)));
60 linevalue  = (synspecval(locs(idloc1) : locs(idloc2)));
61
62 % local creation of the reduced spectrum
63
64 for n = 1 : length(linevalue)
65     linevalue(n) = localcont - linevalue(n);
66 end
67
68 % fitting a Gaussian, determining line properties
69
70 linefit = fit(linelambda(:), linevalue(:), 'gauss1');
71
72 int = linefit.a1*sqrt(pi)*linefit.c1;
73 int = int*1000;
74 int = int/localcont;
75
76 Equwidth_syn(k) = int;
77 Sigma_syn(k) = linefit.c1;
78 Lambda_syn(k) = linefit.b1;
79
80 end
81
82 clear pks
83 clear locs
84
85 % Determination of equivalent widths in the obsspec
86
87 % finding local maxima
88
```

```
89 [pks, locs] = findpeaks(obsspec(:,2));
90 obsspecval = obsspec(:,2);
91
92 % finding corresponding isolated lines
93
94 for k = 1 : l
95
96     clear linefit
97     clear linelambda
98     clear linevalue
99
100 dist = abs(linelist(k)-obsspec(:,1));
101 minDist = min(dist);
102 idx = min(find(dist == minDist));
103
104 localcont = cont(obsspec(idx,1));
105
106 % determining the fitting interval: 95% of the integrated line
      flux (obtained from synspec) shall be inside, either an
      interval to the next local maxima is taken or at least pm 1.2
       sigma (obtained from the synspec)
107
108 dist = abs(linelist(k)+1.2*Sigma_syn(k)-obsspec(:,1));
109 minDist = min(dist);
110 idobs2 = min(find(dist == minDist));
111
112 dist = abs(linelist(k)-1.2*Sigma_syn(k)-obsspec(:,1));
113 minDist = min(dist);
114 idobs1 = min(find(dist == minDist));
115
116 dist = abs(linelist(k)-obsspec(locs,1));
117 minDist = min(dist);
118 idloc1 = min(find(dist == minDist));
119
120  if linelist(k) > obsspec(locs(idloc1))
121      idloc2 = idloc1+1;
122  else
123      idloc2 = idloc1;
124      idloc1 = idloc2-1;
125  end
126
127 if locs(idloc1) < idobs1
128     idobs1 = locs(idloc1);
129 end
130 if locs(idloc2) > idobs2
131     idobs2 = locs(idloc2);
132 end
133
134  linelambda = (obsspec(idobs1 : idobs2));
```

```
135  linevalue  = (obsspecval(idobs1 : idobs2));
136
137 % local creation of the reduced flux
138
139 for n = 1 : length(linevalue)
140     linevalue(n) = localcont - linevalue(n);
141 end
142
143 % fitting a Gaussian, determining line properties
144
145 options = fitoptions('gauss1', 'Lower', [-10 linelist(k)-1
      0.0001], 'Upper', [100 linelist(k)+1 1]);
146 linefit = fit(linelambda(:), linevalue(:), 'gauss1', options);
147
148 int = linefit.a1*sqrt(pi)*linefit.c1;
149 int = int*1000;
150 int = int/localcont;
151
152 % determining W_obs,red
153
154 if int > 0
155 Sigma_obs(k) = linefit.c1;
156 Lambda_obs(k) = linefit.b1;
157 if Sigma_obs(k)>Sigma_syn(k)
158 Equwidth_obsred(k) = int*Sigma_syn(k)/Sigma_obs(k)*(1-(abs(
      Lambda_syn(k)-Lambda_obs(k))/Sigma_obs(k))^2);
159 else
160 Equwidth_obsred(k) = int*(1-(abs(Lambda_syn(k)-Lambda_obs(k))/
      Sigma_obs(k))^2);
161 end
162 Equwidth_obs(k) = int;
163 else
164 Sigma_obs(k) = 0;
165 Lambda_obs(k) = Lambda_syn(k);
166 Equwidth_obs(k) = 0;
167 Equwidth_obsred(k) = 0;
168 end
169
170 if Equwidth_obsred(k)< 0
171     Equwidth_obsred(k) = 0;
172 end
173
174 Sigma(k) = Sigma_obs(k)/Sigma_syn(k);
175 Del_Lambda(k) = abs(round(1000*(Lambda_syn(k)-Lambda_obs(k))));
176
177 end
178
179 ANS = round([ linelist , Equwidth_syn(:), Equwidth_obs(:),
      Equwidth_obsred(:), Sigma(:), Del_Lambda(:), gflist(:)],2);
```

A.3 Line tables 1

Table 25: Reliable IG-element absorption lines (found in Feige 110 or PG 0909+276), recommended to be employed for abundance determinations.

Ion	λ / Å	$\log(gf)_{\mathrm{Kurucz}}$	W_λ^{Obs} / mÅ	$W_\lambda^{\mathrm{Obs}}/W_\lambda^{\mathrm{Syn}}$
Cr IV	1359.72	−0.66	42.09	1.05
Cr V	1465.86	−0.03	73.52	0.98
Cr V	1644.05	−0.18	69.37	1.04
Mn V	1443.31	0.17	54.19	0.93
Mn V	1448.13	−0.09	56.03	0.99
Mn V	1475.97	−0.24	59.37	1.04
Fe IV	1431.43	−0.24	45.09	0.93
Fe IV	1560.71	−0.48	41.65	1.04
Fe IV	1570.42	0.27	51.16	0.96
Fe IV	1571.24	0.16	58.36	1.02
Fe IV	1578.74	0.14	50.26	0.92
Fe IV	1598.01	0.48	50.24	0.98
Fe IV	1603.73	0.15	54.28	0.96
Fe IV	1604.67	0.08	44.80	0.93
Fe IV	1605.68	−0.25	45.32	0.98
Fe IV	1605.97	0.31	53.96	0.95
Fe IV	1606.34	−0.65	40.34	1.01
Fe IV	1610.47	0.21	58.92	1.08
Fe IV	1614.65	0.04	55.81	1.01
Fe IV	1623.39	0.37	47.17	1.00
Fe IV	1624.91	0.12	54.13	1.02
Fe IV	1630.68	0.06	49.86	0.95
Fe IV	1638.30	0.12	46.51	1.08
Fe IV	1647.09	0.18	71.74	1.07
Fe IV	1659.00	0.12	52.71	1.08
Fe IV	1661.57	0.47	47.17	0.99
Fe IV	1673.68	0.51	63.28	1.01
Fe IV	1676.79	−0.08	46.67	1.06
Fe IV	1677.12	−0.18	43.88	1.01
Fe IV	1701.48	−0.41	41.26	0.91
Fe IV	1707.61	−0.14	47.81	1.02
Fe IV	1708.57	−0.25	42.31	1.00
Fe V	1370.94	−0.47	45.54	0.92
Fe V	1440.79	−0.24	53.58	1.07
Fe V	1654.74	−0.30	48.36	0.95
Co III	1689.85	−0.53	78.47	1.01
Co IV	1594.53	−0.02	51.23	1.02

Table 25 – continued.

Ion	λ / Å	$\log(gf)_{\mathrm{Kurucz}}$	W_λ^{Obs} / mÅ	$W_\lambda^{\mathrm{Obs}}/W_\lambda^{\mathrm{Syn}}$
Co IV	1636.40	0.38	40.75	1.00
Co V	1294.02	0.29	41.95	1.00
Co V	1342.44	0.53	41.89	0.92
Co V	1352.06	0.05	55.08	1.06
Co V	1375.21	−0.06	42.22	0.93
Ni IV	1411.45	0.45	61.31	0.95
Ni IV	1430.19	0.16	55.79	1.00
Ni IV	1432.45	−0.13	43.12	0.98
Ni IV	1444.91	0.34	50.87	0.93
Ni IV	1463.67	0.11	49.84	0.98
Ni IV	1476.82	0.31	53.58	1.05
Ni IV	1487.88	−0.02	45.43	1.03
Ni IV	1492.65	−0.08	46.02	1.05
Ni IV	1509.10	0.14	46.29	1.02
Ni IV	1536.84	−0.27	42.22	0.92
Ni IV	1546.23	0.05	64.92	0.94
Ni IV	1554.80	−0.12	45.97	0.97
Ni IV	1559.92	−0.33	46.35	0.91
Ni IV	1569.92	−0.84	53.71	0.92
Ni V	1202.03	0.12	40.08	1.08
Ni V	1295.30	−0.08	48.40	1.08

Table 26: Line statistics of the evaluated, isolated lines in Feige 110. The weighted oscillator strengths and the energy levels were taken from Kurucz's line lists. W_λ^{Syn} and W_λ^{Obs} are given in mÅ.

λ / Å	Ion	$\log(gf)$	E_{low}/ cm^{-1}	E_{up}/ cm^{-1}	W_λ^{Syn}	W_λ^{Obs}	$W_\lambda^{\mathrm{Obs}}/W_\lambda^{\mathrm{Syn}}$
1202.03	Ni V	0.12	247104.90	330297.60	37.26	40.08	1.08
1202.26	Ni V	−0.44	263735.70	346912.40	23.09	21.96	0.95
1202.75	Co VI	0.50	307627.00	390770.10	16.33	9.94	0.61
1209.29	Cr IV	0.10	263971.00	181277.90	36.64	25.91	0.71
1210.17	Cr IV	0.25	263875.90	181243.10	33.37	33.18	0.99
1210.95	Cr IV	−0.57	241472.80	158892.70	27.99	24.60	0.88
1213.00	Cr IV	0.10	240967.90	158527.70	27.60	21.36	0.77
1225.35	Cr IV	−0.59	241472.80	159863.60	28.17	19.66	0.70
1231.10	Ni V	−0.50	216189.90	297418.10	32.35	33.23	1.03
1244.79	Ni V	−0.66	229408.80	309743.60	24.60	19.92	0.81
1245.62	Ni IV	−0.53	144815.10	225096.40	30.26	31.74	1.05
1248.83	Ni V	−0.25	247281.80	327356.60	31.37	20.68	0.66
1251.81	Ni V	0.48	217048.70	296932.90	58.68	44.98	0.77
1254.76	Co V	−1.15	235961.10	315657.50	10.20	31.74	3.11
1255.15	Cr IV	0.36	257588.60	177916.50	41.38	50.88	1.23
1260.86	Ni V	−1.18	232655.60	311966.50	14.83	34.61	2.33
1261.76	Ni V	0.48	216189.90	295444.30	52.48	46.12	0.88
1263.86	Ni IV	−0.65	145702.20	224824.90	27.50	32.40	1.18
1266.88	Ni V	−0.05	212455.70	291390.00	43.69	34.98	0.80
1267.53	Co V	−0.12	206962.20	285855.70	42.65	35.67	0.84
1268.87	Ni V	0.30	274738.60	353548.70	33.15	25.45	0.77
1272.44	Mn VI	0.07	251403.00	329992.00	34.99	48.51	1.39
1274.15	Fe V	−0.31	390022.60	311538.70	19.04	18.89	0.99
1280.47	Fe V	−0.56	209523.90	287620.20	40.37	66.56	1.65
1285.92	Fe V	−0.89	212818.10	290583.70	30.64	34.73	1.13
1286.81	Ni V	−1.22	243370.50	321081.90	11.41	35.10	3.08
1288.52	Ni V	−0.35	242290.40	319899.10	27.99	40.28	1.44
1289.16	Co V	−0.38	248698.20	326267.90	21.17	8.01	0.38
1294.02	Co V	0.29	249006.80	326285.10	42.04	41.95	1.00
1295.30	Ni V	−0.08	212095.80	289298.00	44.79	48.40	1.08
1297.17	Co V	−0.40	238164.60	315255.40	27.99	43.06	1.54
1298.18	Ni IV	−1.71	145962.50	222993.30	5.90	3.96	0.67
1300.03	Cr IV	−0.72	251017.30	174096.20	19.45	11.06	0.57
1300.23	Ni V	−1.47	212253.40	289163.00	14.25	31.09	2.18
1301.89	Cr IV	−0.89	237798.20	160986.50	22.51	20.60	0.92
1303.75	Co V	−0.11	238390.30	315092.20	33.43	29.05	0.87
1304.52	Cr IV	0.57	250752.70	174096.20	46.81	57.74	1.23
1312.15	Co V	0.16	289449.20	365660.10	25.00	33.19	1.33
1312.26	Co V	0.46	283592.10	359796.70	28.88	16.81	0.58
1315.48	Cr IV	−1.10	247099.10	171081.30	10.63	19.80	1.86
1320.41	Fe V	0.28	216779.10	292513.20	59.10	71.68	1.21
1320.89	Ni V	−0.66	212253.40	287960.00	33.01	22.03	0.67
1321.49	Fe V	−0.05	209523.90	285196.10	50.83	45.62	0.90

Table 26 – continued.

λ / Å	Ion	$\log(gf)$	$E_{\rm low}$/ cm^{-1}	$E_{\rm up}$/ cm^{-1}	$W_\lambda^{\rm Syn}$	$W_\lambda^{\rm Obs}$	$W_\lambda^{\rm Obs}/W_\lambda^{\rm Syn}$
1322.74	Co V	−0.39	242340.30	317941.00	24.88	15.74	0.63
1324.74	Ni V	−0.53	221087.60	296574.00	33.19	42.19	1.27
1326.03	Co V	0.02	244821.20	320234.50	32.49	18.40	0.57
1326.15	Ni IV	−1.20	139886.70	215292.90	17.40	7.80	0.45
1328.85	Fe IV	−1.12	167712.50	242965.62	16.48	13.75	0.83
1332.10	Ni IV	−1.62	147635.90	222705.50	7.10	10.57	1.49
1335.76	Fe V	−0.68	214525.80	289389.70	33.90	25.86	0.76
1340.89	Ni IV	−1.70	140140.90	214718.10	9.88	21.29	2.15
1342.44	Co V	0.53	236158.00	310649.40	45.52	41.89	0.92
1342.61	Ni IV	−1.73	140140.90	214622.80	8.61	17.38	2.02
1344.69	Ni V	−1.23	240959.60	315326.20	12.50	20.72	1.66
1345.00	Ni V	−0.73	279199.50	353548.70	11.97	12.51	1.05
1346.09	Ni IV	−0.35	112151.90	186441.40	45.89	61.22	1.33
1346.63	Cr IV	−1.34	233708.50	159449.20	11.32	3.28	0.29
1346.82	Co IV	−1.51	90554.40	164803.20	17.78	26.60	1.50
1348.84	Fe V	−0.76	234027.40	308165.00	29.25	34.87	1.19
1349.15	Ni IV	−0.86	139619.20	213739.70	26.25	25.55	0.97
1352.06	Co V	0.05	206962.20	280923.50	52.04	55.08	1.06
1352.76	Co V	0.00	276608.80	350532.00	21.61	32.30	1.49
1353.24	Co V	−0.62	249179.70	323076.20	17.74	22.33	1.26
1354.04	Ni V	−1.36	247165.00	321018.30	8.72	3.04	0.35
1355.83	Fe V	−1.86	216652.10	290407.70	13.83	17.20	1.24
1364.17	Co V	0.12	241985.30	315289.80	37.06	28.55	0.77
1367.40	Cr IV	0.22	238561.30	165430.00	52.94	59.46	1.12
1368.01	Cr IV	−0.84	234085.20	160986.50	23.90	19.74	0.83
1368.68	Cr IV	−1.25	251093.10	178030.00	7.23	8.42	1.16
1370.05	Ni IV	−1.12	140140.90	213131.10	21.72	34.46	1.59
1370.30	Fe V	−0.84	217122.50	290099.10	30.12	24.24	0.80
1370.94	Fe V	−0.47	186433.60	259376.10	49.73	45.54	0.92
1372.65	Fe V	−0.99	216538.10	289389.70	31.07	18.59	0.60
1375.21	Co V	−0.06	206476.00	279192.40	45.54	42.22	0.93
1375.79	Fe V	−0.74	216860.40	289545.90	32.33	37.67	1.17
1381.31	Ni IV	−0.34	139886.70	212281.80	39.79	34.78	0.87
1382.27	Fe V	−1.39	233848.90	306193.90	14.62	32.32	2.21
1384.06	Fe V	−0.59	214611.40	286862.70	38.82	27.95	0.72
1385.54	Fe IV	−1.81	155744.87	227919.05	8.95	4.59	0.51
1385.87	Ni V	−0.46	233839.20	305996.30	28.63	25.68	0.90
1387.94	Fe V	0.66	217122.50	289171.90	70.38	58.84	0.84
1388.70	Ni IV	−1.06	140140.90	212150.90	20.50	25.24	1.23
1389.44	Ni V	−0.65	216189.90	288161.60	30.07	19.63	0.65
1389.64	Cr IV	−0.24	255836.90	183875.60	36.96	29.51	0.80
1390.28	Cr IV	−1.03	255803.60	183875.60	11.02	8.06	0.73
1391.55	Cr IV	−0.65	233618.40	161756.30	29.90	25.37	0.85
1392.94	Fe V	−1.46	204975.40	276765.90	22.59	21.48	0.95
1395.44	Fe V	−0.85	214525.80	286187.70	31.45	21.53	0.68
1395.55	Co IV	−0.74	132828.70	204485.30	14.34	13.87	0.97

Table 26 – continued.

λ / Å	Ion	$\log(gf)$	$E_{\rm low}$/ cm^{-1}	$E_{\rm up}$/ cm^{-1}	$W_\lambda^{\rm Syn}$	$W_\lambda^{\rm Obs}$	$W_\lambda^{\rm Obs}/W_\lambda^{\rm Syn}$
1395.73	Ni IV	−0.87	153349.40	224996.50	19.00	13.45	0.71
1395.85	Co V	−0.27	238390.30	310031.10	35.52	15.97	0.45
1395.98	Ni IV	−0.58	110410.60	182044.90	42.74	38.52	0.90
1396.89	Ni IV	−0.66	153349.40	224936.90	24.58	17.47	0.71
1397.75	Fe V	−0.94	214611.40	286154.90	29.04	22.01	0.76
1399.05	Mn V	−0.47	194011.40	265488.40	45.18	21.77	0.48
1400.68	Ni IV	0.55	155308.70	226702.50	56.66	44.47	0.78
1400.89	Co V	−0.94	244485.40	315868.70	13.31	14.23	1.07
1403.37	Fe V	−0.34	209110.10	280367.20	44.09	55.93	1.27
1405.36	Fe V	−0.99	213534.10	284690.30	28.91	20.43	0.71
1407.44	Ni IV	0.29	185967.00	257018.00	31.81	33.81	1.06
1409.03	Fe V	0.08	187157.50	258128.50	66.67	53.89	0.81
1410.36	Ni IV	−1.48	140343.00	211246.80	11.32	9.63	0.85
1411.45	Ni IV	0.45	111195.80	182044.90	64.43	61.31	0.95
1413.42	Co V	0.55	236746.00	307496.40	51.04	46.78	0.92
1414.60	Ni IV	0.31	144815.10	215506.60	49.60	55.28	1.11
1416.22	Fe V	0.19	220621.00	291231.40	54.78	49.08	0.90
1417.28	Ni IV	−0.33	139619.20	210177.00	37.33	45.24	1.21
1419.13	Ni IV	0.16	138446.20	208912.10	48.94	63.45	1.30
1419.98	Co V	0.45	236431.20	306854.60	47.95	62.15	1.30
1422.61	Ni IV	0.19	190932.80	261226.30	25.61	49.44	1.93
1422.77	Co IV	−1.07	136362.90	206648.30	19.66	28.15	1.43
1423.89	Co IV	−0.40	132828.70	203059.00	22.74	29.70	1.31
1424.44	Fe V	−2.10	216652.10	286855.30	7.90	20.93	2.65
1424.79	Mn V	0.02	195302.70	265488.40	58.88	51.26	0.87
1425.09	Fe V	−0.80	204975.40	275146.60	38.71	32.60	0.84
1425.48	Fe IV	−0.27	159342.88	229494.74	41.27	56.87	1.38
1426.05	Fe IV	−0.57	158738.69	228862.61	35.56	25.20	0.71
1426.83	Co V	0.25	235961.10	306046.40	44.98	74.93	1.67
1429.76	Co V	−0.67	236431.20	306372.80	24.24	20.49	0.85
1430.19	Ni IV	0.16	120909.50	190830.30	55.70	55.79	1.00
1431.43	Fe IV	−0.24	154185.85	224045.96	48.52	45.09	0.93
1432.45	Ni IV	−0.13	121807.70	191618.20	44.03	43.12	0.98
1432.84	Mn V	−0.02	200176.90	269968.30	62.37	50.23	0.81
1433.51	Ni V	−1.57	240193.80	309952.50	7.08	11.38	1.61
1435.80	Ni IV	−0.52	122386.10	192033.50	37.41	57.05	1.52
1437.16	Ni IV	−0.05	148358.20	217939.70	42.34	33.72	0.80
1440.31	Mn V	−0.53	195302.70	264732.40	50.25	41.08	0.82
1440.79	Fe V	−0.24	204729.90	274136.10	50.09	53.58	1.07
1441.49	Co IV	−1.27	129195.20	198567.80	6.54	3.27	0.50
1443.31	Mn V	0.17	200670.10	269955.40	58.43	54.19	0.93
1444.78	Mn V	−0.53	176946.30	246161.20	48.28	42.56	0.88
1444.91	Ni IV	0.34	145702.20	214910.50	54.41	50.87	0.93
1445.69	Fe V	−0.43	258434.10	327605.40	27.54	30.40	1.10
1446.94	Ni IV	−0.66	141832.00	210943.60	31.36	26.94	0.86
1447.21	Ni IV	−0.89	146194.30	215292.90	21.18	20.02	0.95

Table 26 – continued.

λ / Å	Ion	$\log(gf)$	$E_{\rm low}$/ cm^{-1}	$E_{\rm up}$/ cm^{-1}	$W_\lambda^{\rm Syn}$	$W_\lambda^{\rm Obs}$	$W_\lambda^{\rm Obs}/W_\lambda^{\rm Syn}$
1448.13	Mn V	−0.09	193781.60	262836.10	56.75	56.03	0.99
1448.49	Fe V	0.16	213534.10	282571.60	55.16	45.85	0.83
1449.19	Ni IV	−0.67	142023.50	211027.60	29.37	22.36	0.76
1450.62	Fe V	−1.62	216538.10	285474.00	14.11	10.34	0.73
1453.09	Fe IV	−0.36	154731.29	223550.14	47.72	39.10	0.82
1454.24	Fe V	−0.24	258769.50	327533.80	31.41	19.07	0.61
1454.36	Ni IV	−0.33	141832.00	210590.60	42.28	32.61	0.77
1455.90	Ni IV	−0.13	171408.00	240094.20	28.76	18.47	0.64
1456.16	Fe V	0.18	186725.50	255399.20	75.04	50.15	0.67
1456.29	Fe V	−0.15	204975.40	273643.10	59.17	45.09	0.76
1456.52	Ni IV	−0.02	146061.50	214718.10	44.45	36.75	0.83
1456.75	Fe IV	−0.83	156224.88	224870.85	31.52	27.96	0.89
1460.07	Co V	−0.87	244821.20	313311.00	14.06	35.19	2.50
1462.01	Ni IV	0.01	145702.20	214101.00	55.50	49.72	0.90
1463.06	Fe V	−1.63	234027.40	302377.10	11.94	10.24	0.86
1463.67	Ni IV	0.11	151574.70	219896.00	50.67	49.84	0.98
1464.87	Fe V	0.07	234027.40	302292.70	55.02	45.12	0.82
1465.01	Fe V	−0.91	216652.10	284911.20	37.33	47.68	1.28
1465.86	Cr V	−0.03	171698.10	239917.50	75.35	73.52	0.98
1469.73	Ni IV	−0.52	146061.50	214101.00	35.54	44.70	1.26
1470.06	Co V	−0.12	243455.20	311479.60	31.51	15.95	0.51
1471.89	Ni IV	−0.38	179792.00	247731.70	18.70	17.70	0.95
1472.80	Fe V	−0.61	214525.80	282423.50	37.99	31.96	0.84
1474.28	Fe V	−0.75	216860.40	284690.30	32.15	25.25	0.79
1475.61	Fe V	−0.19	209523.90	277292.70	50.28	42.88	0.85
1475.97	Mn V	−0.24	178572.50	246324.70	56.99	59.37	1.04
1476.82	Ni IV	0.31	141220.30	208933.60	51.01	53.58	1.05
1476.97	Ni IV	−0.62	145702.20	213408.60	32.49	32.45	1.00
1477.28	Ni IV	−0.74	141220.30	208912.10	28.27	21.52	0.76
1479.21	Ni IV	0.08	171406.00	239009.70	32.46	46.15	1.42
1480.49	Ni IV	−0.49	146194.30	213739.70	32.52	30.23	0.93
1481.41	Ni IV	−0.24	140343.00	207846.20	40.19	36.56	0.91
1486.04	Fe IV	−0.38	160311.64	227604.73	40.67	32.97	0.81
1486.20	Ni IV	0.18	151574.70	218860.60	44.48	35.04	0.79
1487.88	Ni IV	−0.02	152343.70	219553.40	43.98	45.43	1.03
1488.15	Co IV	−0.29	136362.90	203560.60	24.97	37.54	1.50
1489.71	Cr V	−0.17	167491.00	234618.40	71.48	84.96	1.19
1491.51	Co IV	−0.90	154012.20	221058.40	5.43	7.88	1.45
1492.65	Ni IV	−0.08	140140.90	207136.00	43.87	46.02	1.05
1494.47	Fe IV	−1.20	154325.96	221239.21	23.42	24.89	1.06
1495.98	Fe IV	−1.74	154474.85	221320.54	10.50	16.45	1.57
1497.12	Mn V	−0.26	194011.40	260806.20	58.16	51.31	0.88
1497.49	Fe IV	−0.49	154325.96	221104.17	43.43	33.07	0.76
1497.60	Ni IV	−0.25	141832.00	208605.70	40.42	37.24	0.92
1500.41	Fe IV	−0.64	154512.67	221161.02	40.59	31.09	0.77
1501.04	Co IV	0.18	152113.30	218733.80	26.78	28.20	1.05

Table 26 – continued.

λ / Å	Ion	$\log(gf)$	$E_{\rm low}$/ cm^{-1}	$E_{\rm up}$/ cm^{-1}	$W_\lambda^{\rm Syn}$	$W_\lambda^{\rm Obs}$	$W_\lambda^{\rm Obs}/W_\lambda^{\rm Syn}$
1501.18	Co IV	−0.01	150970.90	217585.40	29.99	28.40	0.95
1501.33	Co IV	0.41	152126.20	218733.80	39.36	44.93	1.14
1502.19	Co IV	0.46	90554.40	157123.70	67.64	92.75	1.37
1502.33	Mn V	0.37	178572.50	245135.60	82.08	96.05	1.17
1503.37	Mn V	−0.37	194288.80	260806.20	50.81	55.85	1.10
1505.46	Co IV	0.41	129134.00	195558.90	49.12	68.48	1.39
1506.16	Co V	−0.93	248698.20	315092.20	10.70	11.22	1.05
1506.53	Co IV	−0.62	129228.70	195606.50	18.31	26.16	1.43
1508.42	Co IV	−0.06	160351.40	226646.10	28.33	19.60	0.69
1509.10	Ni IV	0.14	148358.20	214622.80	45.50	46.29	1.02
1510.11	Ni IV	−0.57	146061.50	212281.80	29.46	31.08	1.05
1510.38	Co IV	0.61	188138.40	254347.10	30.24	39.57	1.31
1510.57	Ni IV	−0.73	140140.90	206340.90	33.33	19.45	0.58
1513.30	Fe IV	−1.41	165392.58	231473.32	12.11	23.73	1.96
1518.18	Co IV	−0.02	157513.10	223381.40	41.93	32.93	0.79
1520.16	V IV	0.22	217350.00	151567.30	16.03	13.35	0.83
1521.78	Co IV	−0.10	163870.60	229583.30	28.37	13.47	0.47
1523.57	Co IV	−0.08	163752.90	229388.20	32.34	12.42	0.38
1527.79	Ni IV	0.60	155308.70	220762.60	58.28	78.37	1.34
1528.94	Fe IV	−1.29	154185.85	219590.84	20.63	13.38	0.65
1529.09	Ni IV	−0.63	145192.10	210590.60	28.74	21.32	0.74
1530.26	Fe IV	0.12	159227.90	224576.43	52.61	60.11	1.14
1531.47	Fe IV	−0.90	156049.32	221346.06	33.45	22.96	0.69
1532.49	Fe IV	−0.04	177005.97	242259.25	39.78	37.27	0.94
1534.43	Fe IV	−1.69	162087.81	227258.80	9.51	14.66	1.54
1535.28	Co IV	0.67	158846.70	223981.30	45.31	56.34	1.24
1536.58	Fe IV	−0.30	128191.54	193271.27	45.08	56.61	1.26
1536.84	Ni IV	−0.27	141577.20	206645.70	45.68	42.22	0.92
1538.29	Fe IV	−0.41	128541.85	193549.25	42.87	59.27	1.38
1539.20	Fe IV	−0.29	201212.22	266181.09	21.30	30.47	1.43
1539.75	Cr IV	−0.14	252464.80	187519.00	26.31	38.78	1.47
1540.56	Co IV	0.34	136612.50	201524.10	39.59	48.98	1.24
1540.73	Fe IV	−0.81	155744.87	220649.22	32.68	34.54	1.06
1541.01	Mn V	−0.18	177874.20	242766.90	58.45	47.92	0.82
1542.45	Co V	−0.74	217171.00	282002.80	28.55	12.98	0.45
1542.88	Ni IV	−0.24	141832.00	206645.70	42.67	37.70	0.88
1543.24	Fe V	−0.31	195196.30	259995.20	59.10	48.64	0.82
1544.49	Fe IV	0.48	168526.37	233272.84	55.01	49.53	0.90
1544.63	Fe IV	−0.79	158738.69	223478.96	31.54	24.44	0.77
1544.75	Fe IV	−0.87	159010.39	223745.82	29.29	18.79	0.64
1544.87	Co IV	−0.18	163717.90	228448.10	25.64	18.87	0.74
1545.65	Co IV	−0.67	153265.30	217963.00	12.65	13.89	1.10
1545.95	Fe IV	−1.99	154185.85	218871.21	7.15	2.74	0.38
1546.23	Ni IV	0.05	111195.80	175869.10	68.83	64.92	0.94
1546.40	Fe IV	−0.23	127929.12	192595.28	46.66	59.09	1.27
1546.55	Fe IV	−1.22	158738.69	223398.62	22.47	26.26	1.17

Table 26 – continued.

λ / Å	Ion	$\log(gf)$	$E_{\rm low}$/ cm^{-1}	$E_{\rm up}$/ cm^{-1}	$W_\lambda^{\rm Syn}$	$W_\lambda^{\rm Obs}$	$W_\lambda^{\rm Obs}/W_\lambda^{\rm Syn}$
1547.78	Fe IV	−1.97	156049.32	220658.04	6.36	9.87	1.55
1548.68	Ni IV	−0.36	122386.10	186957.20	40.72	48.93	1.20
1549.78	Fe IV	−1.56	156123.77	220649.22	15.02	18.40	1.23
1552.21	Fe IV	−0.36	156224.88	220649.22	44.49	58.34	1.31
1553.43	Ni IV	−0.52	111195.80	175569.50	46.72	66.27	1.42
1554.80	Ni IV	−0.12	144815.10	209131.90	47.19	45.97	0.97
1555.95	Fe IV	−0.59	138338.83	202608.33	37.36	38.06	1.02
1556.06	Fe IV	−0.57	160311.64	224576.43	38.99	28.71	0.74
1556.67	Ni IV	−0.65	122717.40	186957.20	32.87	30.35	0.92
1558.67	Fe IV	0.05	201212.22	265369.48	30.49	40.97	1.34
1559.33	Ni IV	−0.60	122386.10	186516.10	34.96	34.58	0.99
1559.92	Ni IV	−0.33	111763.30	175869.10	51.11	46.35	0.91
1560.71	Fe IV	−0.48	156123.77	220197.25	39.96	41.65	1.04
1562.75	Fe IV	0.03	138338.83	202328.53	45.78	56.82	1.24
1563.94	Fe V	−0.99	212818.10	276759.20	27.93	13.38	0.48
1568.72	Fe IV	−0.31	138338.83	202085.22	40.86	45.49	1.11
1568.85	Mn V	−0.14	195302.70	259043.80	55.49	45.82	0.83
1569.61	Co IV	−0.14	159482.30	223192.40	30.06	21.70	0.72
1570.42	Fe IV	0.27	167795.92	231473.32	53.29	51.16	0.96
1571.24	Fe IV	0.16	154731.29	218375.12	57.03	58.36	1.02
1571.92	Co IV	0.36	148105.50	211722.00	34.75	20.36	0.59
1572.76	Co IV	−1.08	136611.20	200193.80	7.08	9.45	1.33
1572.90	Fe IV	−0.85	156123.77	219700.53	38.53	29.04	0.75
1573.59	Fe IV	−0.40	154474.85	218023.81	45.78	50.18	1.10
1573.77	Fe IV	−0.96	156049.32	219590.84	28.78	21.14	0.73
1573.92	Co IV	0.15	153524.90	217060.70	29.84	31.18	1.04
1574.04	Co IV	0.16	159851.50	223382.30	36.74	46.92	1.28
1575.41	Fe IV	−0.09	156224.88	219700.53	49.93	42.33	0.85
1576.22	Fe V	−1.21	195933.00	259376.10	29.09	25.39	0.87
1578.02	Fe IV	−1.21	154474.85	217845.29	23.79	35.63	1.50
1578.61	Fe IV	−0.74	155744.87	219091.67	34.77	32.99	0.95
1578.74	Fe IV	0.14	165720.94	229062.58	54.76	50.26	0.92
1579.03	Ni IV	−1.21	146061.50	209391.40	15.60	20.25	1.30
1579.24	Fe IV	−0.82	156012.29	219333.90	32.87	27.34	0.83
1579.38	Fe IV	−0.69	165720.94	229037.02	34.45	63.72	1.85
1580.24	Fe IV	−0.72	158738.69	222020.09	36.16	23.18	0.64
1580.90	Fe IV	−1.37	127766.15	191021.18	18.78	15.82	0.84
1581.83	Ni V	−1.28	229413.00	292631.00	12.18	6.24	0.51
1582.03	Co IV	−0.09	159638.10	222848.10	29.84	55.33	1.85
1584.99	Fe IV	−0.84	127929.12	191021.18	32.35	47.40	1.47
1585.11	Fe IV	−0.32	160311.64	223398.62	44.83	53.09	1.18
1585.30	Fe IV	−0.55	156012.29	219091.67	37.85	30.61	0.81
1587.41	Fe IV	−1.13	171476.39	234472.00	18.34	16.60	0.91
1587.72	Co IV	−0.24	132729.10	195712.40	26.11	35.37	1.35
1588.52	Cr IV	−0.26	249932.50	186980.80	28.10	20.84	0.74
1588.70	Ni V	−1.22	229408.80	292353.40	12.82	3.52	0.27

Table 26 – continued.

λ / Å	Ion	$\log(gf)$	$E_{\rm low}$/ cm^{-1}	$E_{\rm up}$/ cm^{-1}	$W_\lambda^{\rm Syn}$	$W_\lambda^{\rm Obs}$	$W_\lambda^{\rm Obs}/W_\lambda^{\rm Syn}$
1588.90	Fe V	−0.81	219486.90	282423.50	34.24	23.64	0.69
1590.24	Co IV	−0.60	132828.70	195712.40	17.86	18.50	1.04
1591.32	Co IV	−0.02	160351.40	223192.40	31.43	27.97	0.89
1592.33	Fe IV	−0.84	165392.58	228193.67	25.82	24.52	0.95
1592.92	Co IV	−0.21	132828.70	195606.50	28.69	35.76	1.25
1594.05	Fe IV	−1.42	155744.87	218478.36	16.31	9.10	0.56
1594.53	Co IV	−0.02	102773.90	165488.50	50.01	51.23	1.02
1595.25	Ni V	−0.46	306962.90	369649.10	8.64	30.44	3.52
1595.80	Fe IV	0.17	201212.22	263876.91	31.91	31.69	0.99
1597.07	Co IV	−0.41	163752.90	226367.60	20.25	44.21	2.18
1597.68	Co IV	0.49	162889.00	225479.80	42.18	32.21	0.76
1598.01	Fe IV	0.48	183164.49	245742.29	51.16	50.24	0.98
1598.82	Fe V	−0.58	195196.30	257742.30	47.08	31.22	0.66
1602.06	Fe IV	0.20	159227.90	221647.49	55.80	61.46	1.10
1603.58	Mn IV	0.36	137930.10	200290.40	61.48	54.88	0.89
1603.73	Fe IV	0.15	156123.77	218478.36	56.48	54.28	0.96
1604.67	Fe IV	0.08	165600.96	227919.05	48.08	44.80	0.93
1605.55	Ni IV	0.15	179655.00	241939.00	31.16	28.46	0.91
1605.68	Fe IV	−0.25	155744.87	218023.81	46.22	45.32	0.98
1605.97	Fe IV	0.31	165392.58	227660.25	56.68	53.96	0.95
1606.34	Fe IV	−0.65	156224.88	218478.36	39.92	40.34	1.01
1607.18	Co IV	−0.31	163717.90	225938.70	20.59	16.10	0.78
1610.47	Fe IV	0.21	159010.39	221104.17	54.49	58.92	1.08
1610.71	Ni IV	−0.75	145962.50	208046.80	26.67	19.02	0.71
1610.85	Fe IV	−0.76	127929.12	190008.28	34.85	50.77	1.46
1614.65	Fe IV	0.04	159227.90	221161.02	55.37	55.81	1.01
1616.13	Fe IV	−0.68	159227.90	221104.17	33.59	21.56	0.64
1616.39	Fe IV	−1.60	165392.58	227258.80	10.00	16.70	1.67
1617.04	Fe V	−0.94	196838.60	258680.00	35.98	38.67	1.07
1617.26	Fe IV	−0.21	156012.29	217845.29	47.36	40.19	0.85
1618.23	Fe IV	−1.01	156049.32	217845.29	28.35	24.58	0.87
1618.38	Fe V	−1.67	216860.40	278650.70	13.30	14.83	1.12
1620.61	Mn III	0.97	173306.45	111601.45	6.96	5.55	0.80
1621.57	Fe IV	0.70	168526.37	230195.02	61.50	65.37	1.06
1623.11	Co IV	−0.97	137280.90	198890.90	7.87	10.08	1.28
1623.39	Fe IV	0.37	183159.61	244759.25	47.13	47.17	1.00
1624.91	Fe IV	0.12	162087.81	223629.59	53.19	54.13	1.02
1625.79	Fe IV	−0.83	190435.47	251944.03	13.01	16.01	1.23
1626.47	Fe IV	0.55	154325.96	215808.91	67.64	72.81	1.08
1626.90	Fe IV	0.05	128541.85	190008.28	52.68	64.12	1.22
1627.77	Ni IV	−0.92	145702.20	207136.00	22.67	20.05	0.88
1630.68	Fe IV	0.06	162074.42	223398.62	52.38	49.86	0.95
1632.08	Fe IV	0.08	154731.29	216002.72	56.89	44.17	0.78
1634.00	Fe IV	−0.96	154185.85	215385.23	32.11	45.75	1.42
1634.72	Fe IV	−2.02	190811.79	251984.20	35.48	36.89	1.04
1635.40	Fe IV	0.10	190811.79	251958.94	35.25	42.13	1.20

Table 26 – continued.

λ / Å	Ion	$\log(gf)$	$E_{\rm low}$/ cm^{-1}	$E_{\rm up}$/ cm^{-1}	$W_\lambda^{\rm Syn}$	$W_\lambda^{\rm Obs}$	$W_\lambda^{\rm Obs}/W_\lambda^{\rm Syn}$
1636.17	Fe IV	−1.76	159342.88	220461.33	8.42	17.73	2.11
1636.40	Co IV	0.38	137280.90	198390.50	40.70	40.75	1.00
1637.26	Fe IV	−1.67	154731.29	215808.91	12.13	30.89	2.55
1637.51	Ni IV	−0.87	152343.70	213412.10	17.99	21.77	1.21
1637.89	Co IV	−0.71	137336.40	198390.50	18.75	20.56	1.10
1638.30	Fe IV	0.12	189975.01	251014.02	42.91	46.51	1.08
1638.50	Cr V	0.33	168089.50	229120.80	77.97	102.09	1.31
1641.60	Fe IV	−0.17	189975.01	250891.05	20.95	24.37	1.16
1643.06	Mn V	−1.62	184635.60	245497.80	17.76	12.67	0.71
1644.05	Cr V	−0.18	167176.40	228001.80	66.96	69.37	1.04
1644.63	Ni IV	−0.93	146061.50	206865.50	22.02	25.48	1.16
1645.27	Fe IV	−0.75	168526.37	229306.61	26.76	28.18	1.05
1645.85	Co IV	0.14	137325.60	198084.50	35.88	38.37	1.07
1647.09	Fe IV	0.18	128191.54	188904.55	67.13	71.74	1.07
1649.60	Fe V	−1.90	214525.80	275146.60	9.93	4.50	0.45
1650.39	Co IV	0.11	167856.50	228448.10	32.67	10.01	0.31
1653.41	Fe IV	0.31	167712.50	228193.67	57.12	64.61	1.13
1653.64	Fe IV	−1.00	159227.90	219700.53	27.64	21.05	0.76
1654.30	Fe IV	−0.56	161571.59	222020.09	36.42	46.13	1.27
1654.74	Fe V	−0.30	216860.40	277292.70	50.79	48.36	0.95
1655.64	Cr V	−0.50	168089.50	228489.10	61.23	72.90	1.19
1656.65	Fe IV	−0.04	128541.85	188904.55	51.89	63.09	1.22
1657.67	Fe IV	−0.91	160778.60	221104.17	31.46	47.12	1.50
1658.08	Cr IV	0.28	127208.30	187519.00	45.57	70.24	1.54
1659.00	Fe IV	0.12	177005.97	237283.09	48.65	52.71	1.08
1660.10	Fe IV	−0.05	128191.54	188428.78	52.08	68.51	1.32
1660.37	Fe IV	−1.82	168566.43	228793.86	5.00	14.91	2.98
1661.34	Mn IV	−0.47	111506.00	171698.30	26.82	40.62	1.51
1661.57	Fe IV	0.47	190318.34	250502.29	47.61	47.17	0.99
1662.32	Fe IV	−0.15	127929.12	188086.05	47.88	55.73	1.16
1662.52	Fe IV	0.22	160311.64	220461.33	58.25	72.11	1.24
1664.94	Fe IV	−0.83	156049.32	216111.69	31.82	36.77	1.16
1665.14	Ni IV	−0.35	159498.50	219553.40	30.34	21.95	0.72
1665.80	Co IV	−0.80	136519.10	196550.20	12.93	13.39	1.04
1667.76	Fe IV	−0.18	190318.34	250279.06	33.62	27.38	0.81
1668.55	Ni IV	−0.77	152343.70	212275.90	23.55	18.08	0.77
1668.93	Fe V	−1.55	220621.00	280539.70	14.26	14.31	1.00
1672.21	Fe IV	0.24	183164.49	242965.62	47.19	53.74	1.14
1672.66	Cr IV	0.37	127195.70	186980.80	51.88	69.50	1.34
1672.86	Fe IV	0.16	156224.88	216002.72	55.56	61.63	1.11
1673.37	Fe IV	−0.02	190435.47	250195.07	32.62	45.35	1.39
1673.68	Fe IV	0.51	168566.43	228315.03	62.49	63.28	1.01
1675.15	Ti V	−0.07	494035.70	434339.40	12.06	14.31	1.19
1675.66	Fe IV	0.53	168526.37	228204.33	60.31	69.06	1.15
1676.79	Fe IV	−0.08	168566.43	228204.33	44.05	46.67	1.06
1677.12	Fe IV	−0.18	164950.50	224576.43	43.45	43.88	1.01

Table 26 – continued.

λ / Å	Ion	$\log(gf)$	$E_{\rm low}$/ cm^{-1}	$E_{\rm up}$/ cm^{-1}	$W_\lambda^{\rm Syn}$	$W_\lambda^{\rm Obs}$	$W_\lambda^{\rm Obs}/W_\lambda^{\rm Syn}$
1680.20	V V	0.02	148143.35	207660.00	56.02	70.73	1.26
1680.67	Ni IV	−1.02	147635.90	207136.00	18.29	17.83	0.97
1682.28	Co IV	−0.54	152113.30	211556.60	10.30	21.23	2.06
1683.13	Mn IV	0.29	152986.00	212399.30	51.54	50.57	0.98
1685.83	Fe IV	−1.18	160015.88	219333.90	20.91	7.51	0.36
1689.06	Co IV	−0.02	157513.10	216717.80	29.40	15.78	0.54
1689.61	Fe IV	−0.84	159010.39	218195.66	31.66	24.02	0.76
1690.87	Cr IV	0.06	124734.40	183875.60	39.91	88.70	2.22
1691.37	Co IV	−0.56	163870.60	222994.20	15.13	29.62	1.96
1691.68	Mn IV	0.12	131170.10	190282.80	30.19	89.16	2.95
1691.86	Fe IV	−0.75	158738.69	217845.29	32.10	24.67	0.77
1693.99	Fe IV	−0.81	159342.88	218375.12	30.14	46.39	1.54
1695.77	Fe IV	−0.29	154474.85	213445.05	47.58	66.96	1.41
1696.24	Co IV	−0.11	140863.50	199817.30	25.83	42.84	1.66
1696.54	Cr V	−1.51	167176.40	226119.80	37.87	50.12	1.32
1697.50	Fe IV	−0.36	156123.77	215033.81	45.27	56.98	1.26
1698.31	Mn IV	0.44	112882.80	171765.00	51.88	85.29	1.64
1700.82	Fe IV	0.05	164950.50	223745.82	52.71	40.31	0.76
1701.48	Fe IV	−0.41	156049.32	214821.74	45.54	41.26	0.91
1701.75	Mn V	−1.78	203811.80	262574.90	16.46	16.17	0.98
1702.38	Co IV	−0.57	141076.00	199817.30	14.46	9.51	0.66
1702.78	Fe IV	−0.99	158738.69	217466.19	26.41	32.37	1.23
1702.93	Fe V	−2.13	216652.10	275374.30	7.15	7.81	1.09
1703.43	Ni IV	−1.69	147635.90	206340.90	7.27	9.29	1.28
1704.36	Ni V	−1.68	232655.60	291328.50	6.25	9.24	1.48
1707.61	Fe IV	−0.14	162087.81	220649.22	47.08	47.81	1.02
1708.57	Fe IV	−0.25	164950.50	223478.96	42.26	42.31	1.00

Table 27: Like Table 26, for PG 0909+276.

λ/ Å	Ion	$\log(gf)$	$E_{\rm low}$/ cm^{-1}	$E_{\rm up}$/ cm^{-1}	$W_\lambda^{\rm Syn}$	$W_\lambda^{\rm Obs}$	$W_\lambda^{\rm Obs}/W_\lambda^{\rm Syn}$
1185.41	Co V	−0.50	241582.40	325941.40	13.79	41.13	2.98
1185.56	Cr IV	−0.13	257714.40	173366.00	37.90	55.57	1.47
1190.57	Co IV	−1.83	137280.90	221274.10	18.02	44.43	2.47
1212.15	Ni IV	−1.84	141577.20	224075.30	12.37	12.27	0.99
1213.00	Cr IV	0.10	240967.90	158527.70	22.37	17.50	0.78
1219.98	Cr IV	0.56	241832.50	159863.60	43.17	26.92	0.62
1222.47	Co IV	−2.09	136612.50	218414.00	7.81	5.67	0.73
1224.55	Ni V	−0.22	232545.90	314208.80	20.36	4.47	0.22
1228.01	Co IV	−2.48	136519.10	217951.40	9.71	41.19	4.24
1236.58	Cr IV	−0.16	255836.90	174968.60	40.37	35.63	0.88
1242.64	Ni V	−0.55	234125.40	314599.20	15.37	18.28	1.19
1260.10	Cr IV	0.09	266878.00	187519.00	43.69	28.25	0.65
1262.33	Cr III	−1.23	17167.54	96386.31	30.74	60.47	1.97
1263.86	Ni IV	−0.65	145702.20	224824.90	55.13	53.03	0.96
1265.14	Ti IV	−1.19	196804.27	275847.01	26.38	23.39	0.89
1278.04	Co IV	−1.09	154012.20	232257.00	23.09	9.48	0.41
1278.39	Ni V	−0.46	242290.40	320513.80	23.27	78.42	3.37
1282.87	Ni V	−1.12	235736.50	313686.60	11.82	39.52	3.34
1304.52	Cr IV	0.57	250752.70	174096.20	56.19	71.23	1.27
1320.03	Cr IV	−1.03	233117.30	157361.40	27.63	21.90	0.79
1359.72	Cr IV	−0.66	232896.60	159352.00	40.13	42.09	1.05
1406.06	Ni III	−0.17	183035.25	111914.53	59.61	80.50	1.35
1413.42	Co V	0.55	236746.00	307496.40	25.08	10.27	0.41
1424.51	Ni III	0.81	183904.88	113705.12	80.83	66.41	0.82
1476.43	Ni IV	0.22	159818.40	227549.40	81.54	107.59	1.32
1480.01	Co IV	−0.29	160404.30	227971.60	43.05	64.04	1.49
1496.41	Ni IV	−0.78	141220.30	208046.80	56.43	99.91	1.77
1510.11	Ni IV	−0.57	146061.50	212281.80	58.29	62.80	1.08
1514.23	Co IV	−0.13	154012.20	220052.20	44.61	39.57	0.89
1538.64	Fe III	0.57	147326.85	82334.23	35.31	28.84	0.82
1540.56	Co IV	0.34	136612.50	201524.10	68.58	80.45	1.17
1544.49	Fe IV	0.48	168526.37	233272.84	41.35	53.28	1.29
1544.87	Co IV	−0.18	163717.90	228448.10	36.12	57.89	1.60
1562.75	Fe IV	0.03	138338.83	202328.53	50.27	46.52	0.93
1569.61	Co IV	−0.14	159482.30	223192.40	45.61	52.15	1.14
1569.92	Ni IV	−0.84	121807.70	185505.30	58.07	53.71	0.92
1575.19	Fe IV	−0.36	138844.03	202328.53	49.24	63.19	1.28
1579.03	Ni IV	−1.21	146061.50	209391.40	41.87	30.67	0.73
1579.24	Fe IV	−0.82	156012.29	219333.90	31.14	34.28	1.10
1599.83	Co IV	−0.64	140863.50	203370.30	38.92	23.66	0.61
1607.18	Co IV	−0.31	163717.90	225938.70	49.24	34.59	0.70
1621.57	Fe IV	0.70	168526.37	230195.02	53.52	41.20	0.77
1623.11	Co IV	−0.97	137280.90	198890.90	44.42	29.07	0.65
1626.47	Fe IV	0.55	154325.96	215808.91	62.08	62.89	1.01
1626.90	Fe IV	0.05	128541.85	190008.28	55.12	44.50	0.81

Table 27 – continued.

λ/ Å	Ion	$\log(gf)$	$E_{\rm low}$/ cm^{-1}	$E_{\rm up}$/ cm^{-1}	$W_\lambda^{\rm Syn}$	$W_\lambda^{\rm Obs}$	$W_\lambda^{\rm Obs}/W_\lambda^{\rm Syn}$
1628.07	Co IV	0.01	159851.50	221274.10	61.18	77.51	1.27
1634.94	Co IV	−1.11	144764.20	205928.70	26.97	20.42	0.76
1644.21	Co IV	−1.18	154012.20	214831.60	15.47	5.41	0.35
1645.51	Ni III	−1.76	78482.43	139253.70	28.72	11.54	0.40
1649.77	Ni III	−0.49	54657.83	115272.26	79.46	49.58	0.62
1666.28	Co III	−1.06	71875.10	131888.90	18.67	36.27	1.94
1671.66	Ni IV	−1.33	122386.10	182206.80	54.91	25.85	0.47
1674.06	Ni IV	−2.23	159818.40	219553.40	15.41	34.06	2.21
1678.18	Co III	−1.00	105130.60	164718.90	20.97	17.90	0.85
1678.67	Ni IV	−2.09	122717.40	182288.40	29.42	23.34	0.79
1681.07	Co III	−1.25	47003.40	106489.40	52.00	43.71	0.84
1682.28	Co IV	−0.54	152113.30	211556.60	42.11	31.38	0.75
1683.13	Mn IV	0.29	152986.00	212399.30	33.54	33.34	0.99
1689.85	Co III	−0.53	47415.70	106592.60	77.57	78.47	1.01
1693.99	Fe IV	−0.81	159342.88	218375.12	23.04	26.44	1.15
1695.60	Ni III	0.06	97995.81	156972.08	49.87	58.33	1.17
1699.36	Ni III	−0.76	71067.35	129913.10	68.08	54.45	0.80
1699.67	Cr IV	−0.49	118571.50	177406.50	53.73	61.82	1.15
1702.38	Co IV	−0.57	141076.00	199817.30	46.27	29.84	0.64
1705.29	Co III	−0.69	106558.90	165199.80	26.83	38.37	1.43

A.4 Spectra

In the following, the observed and modeled spectra are shown. It is started with Feige 110, followed by PG 0909+276. The EC 11481–2303 spectrum is shown at last, as it could not be evaluated for a line analysis.

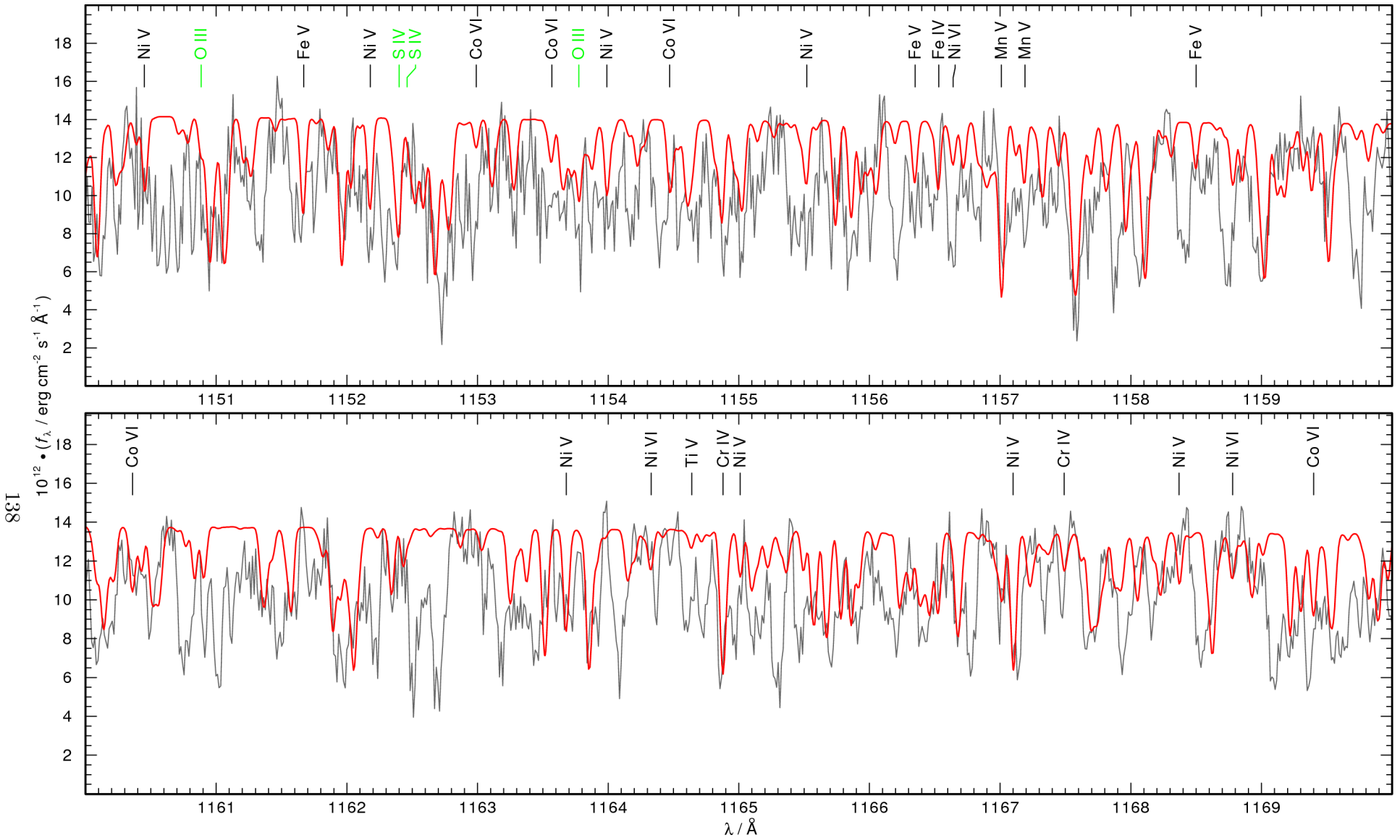

Figure 48: STIS observation (black) of Feige 110 compared with the TMAP model (red). Isolated IG-element absorption lines (black), HHeCNOSiS absorption lines (green) and prominent interstellar absorption lines (blue) are identified.

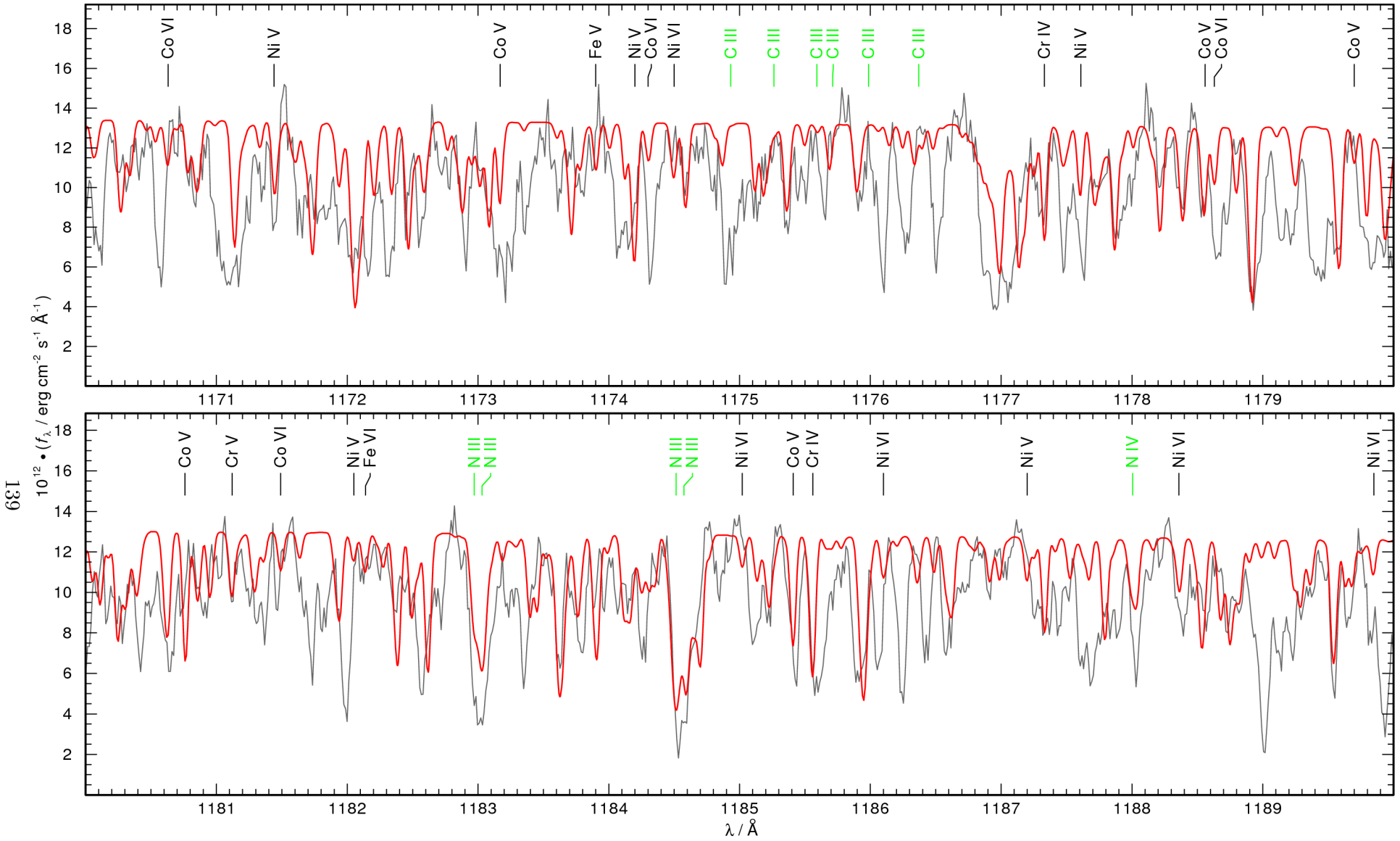

Figure 48: continued.

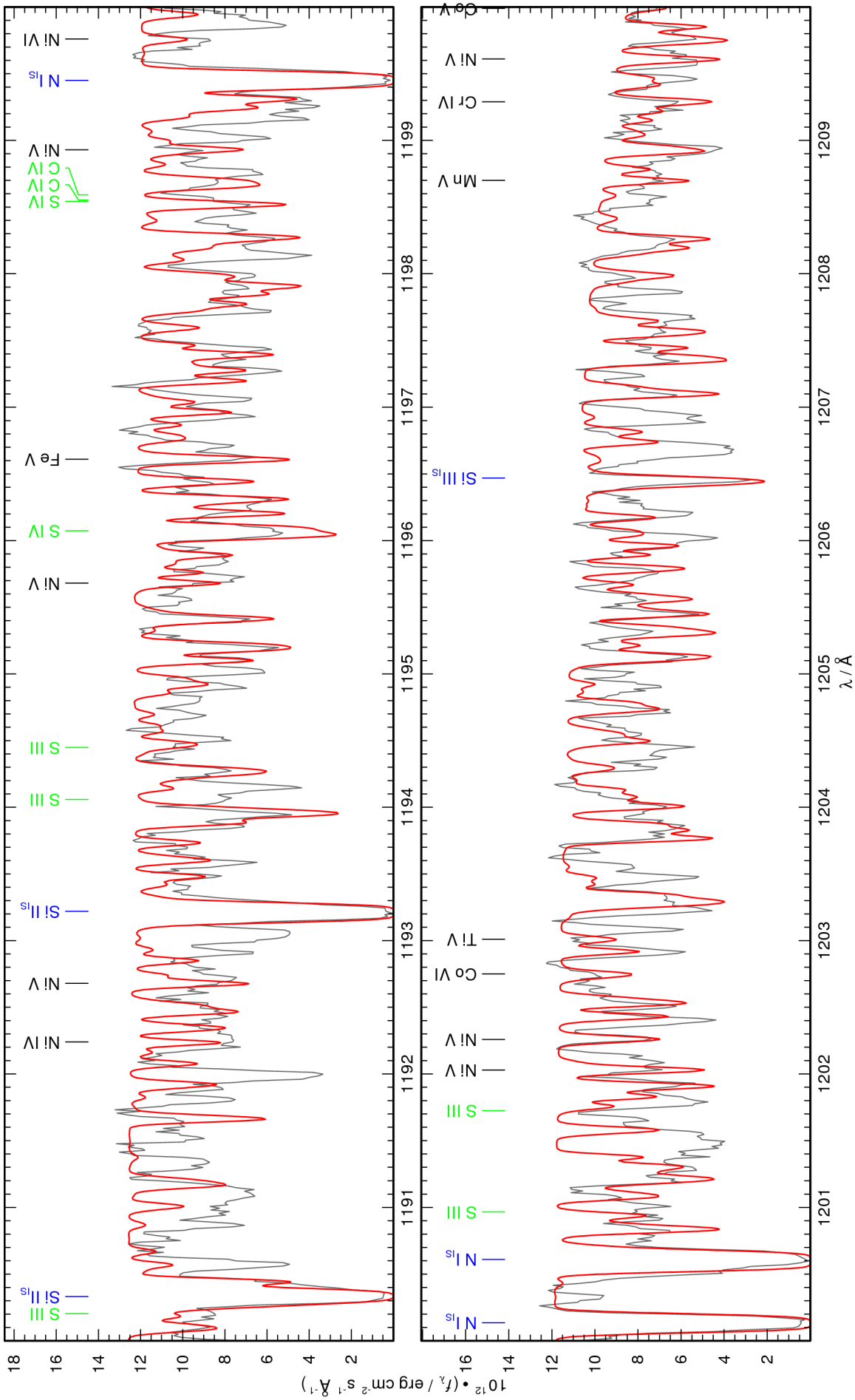

Figure 48: continued.

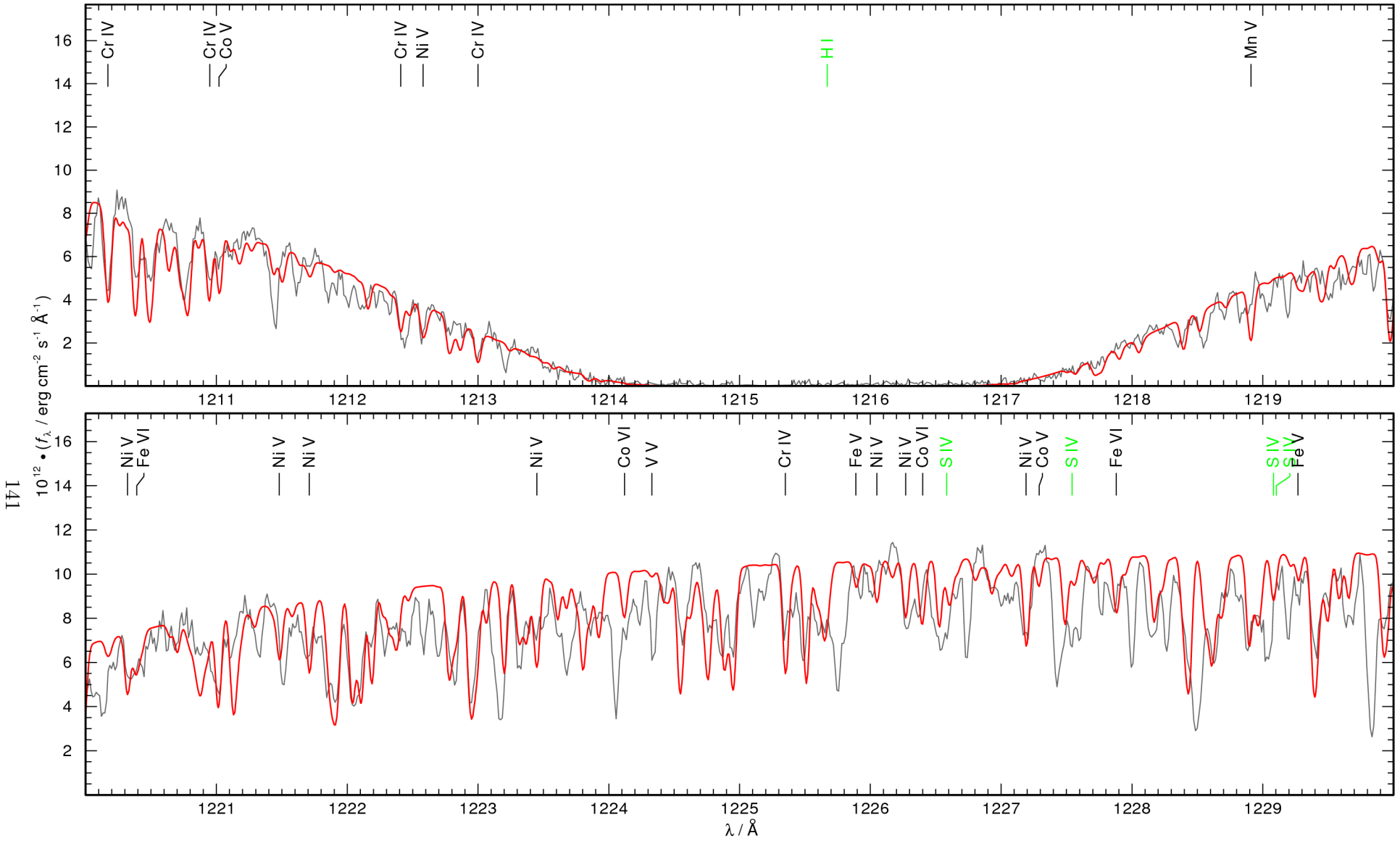

Figure 48: continued.

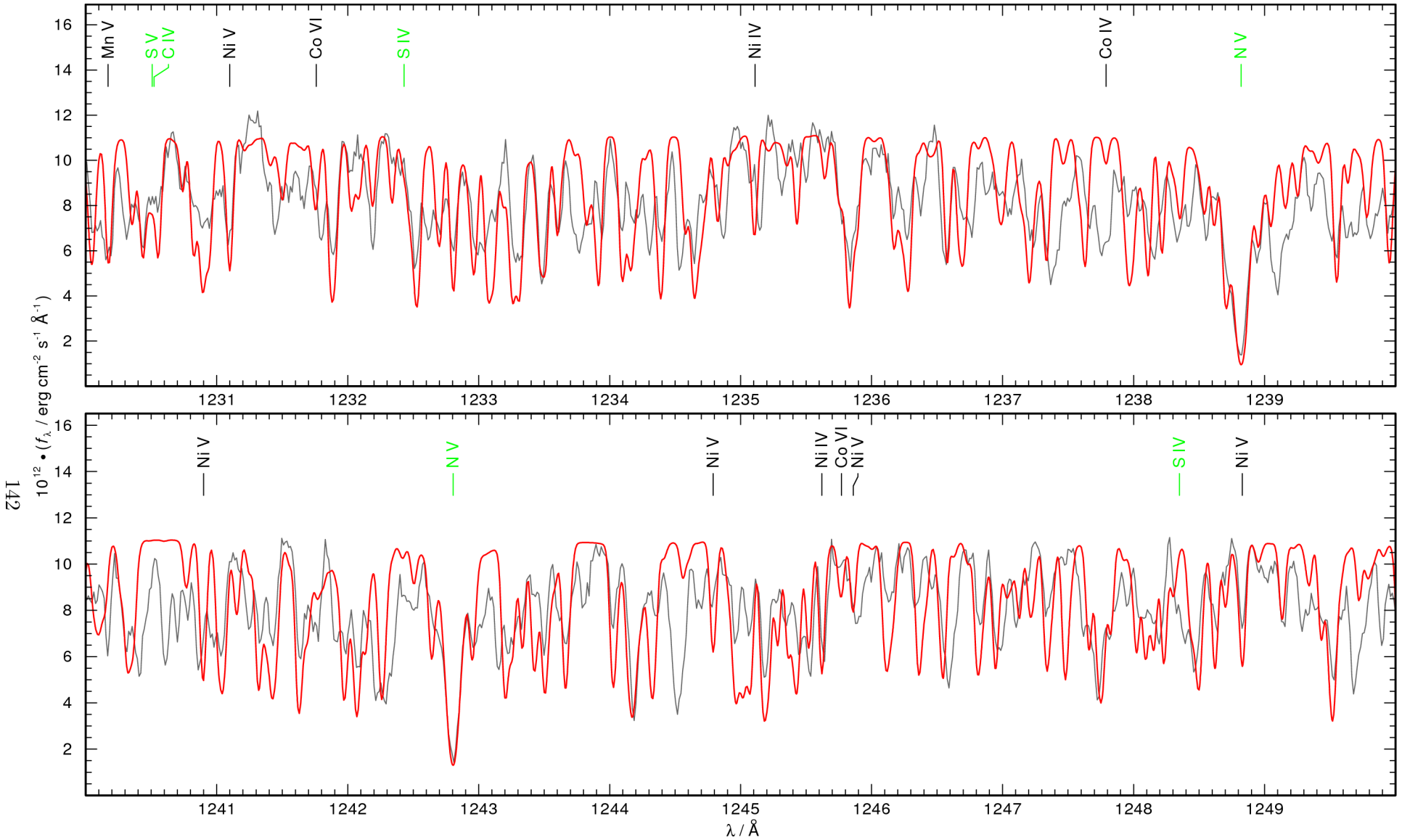

Figure 48: continued.

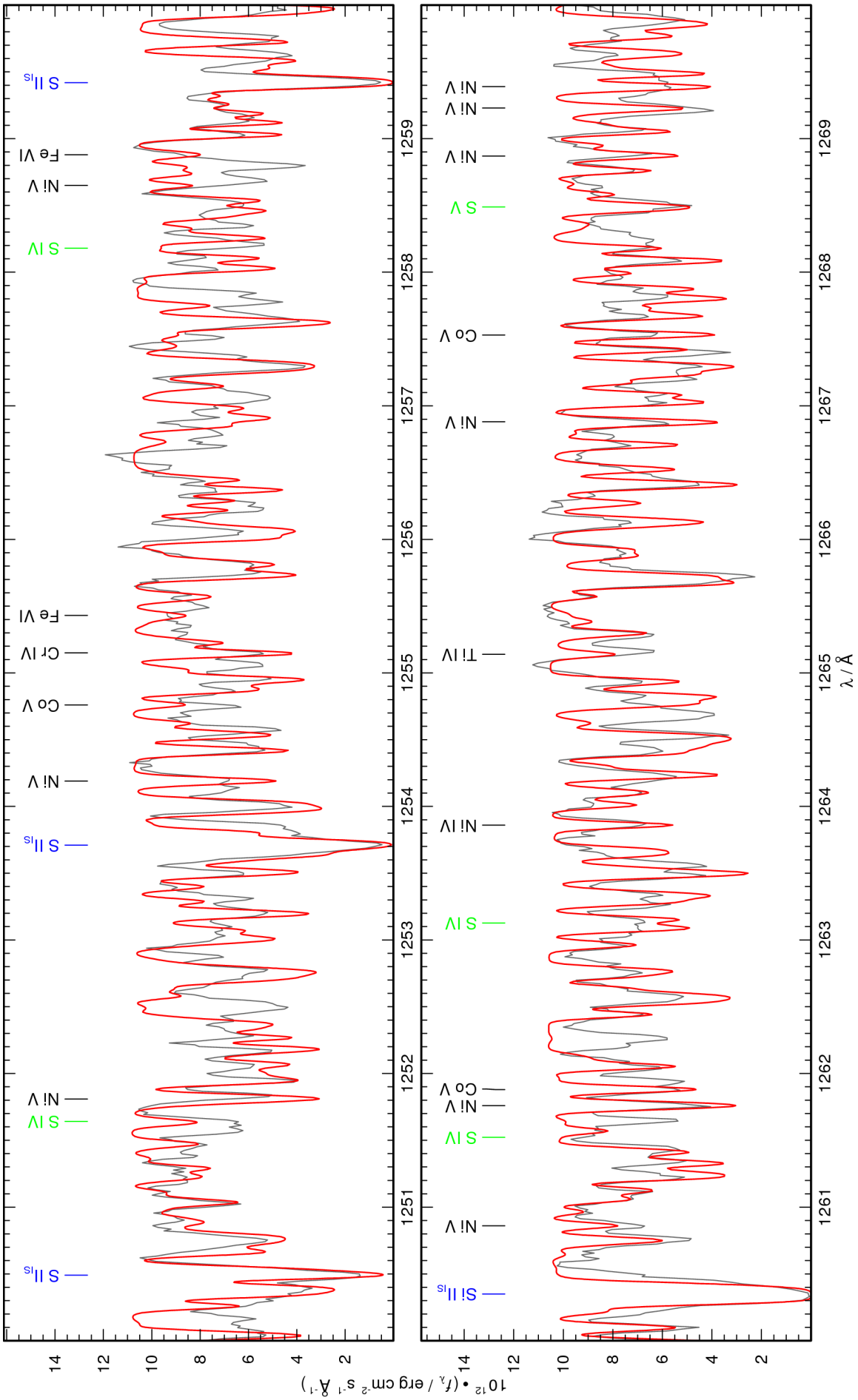

Figure 48: continued.

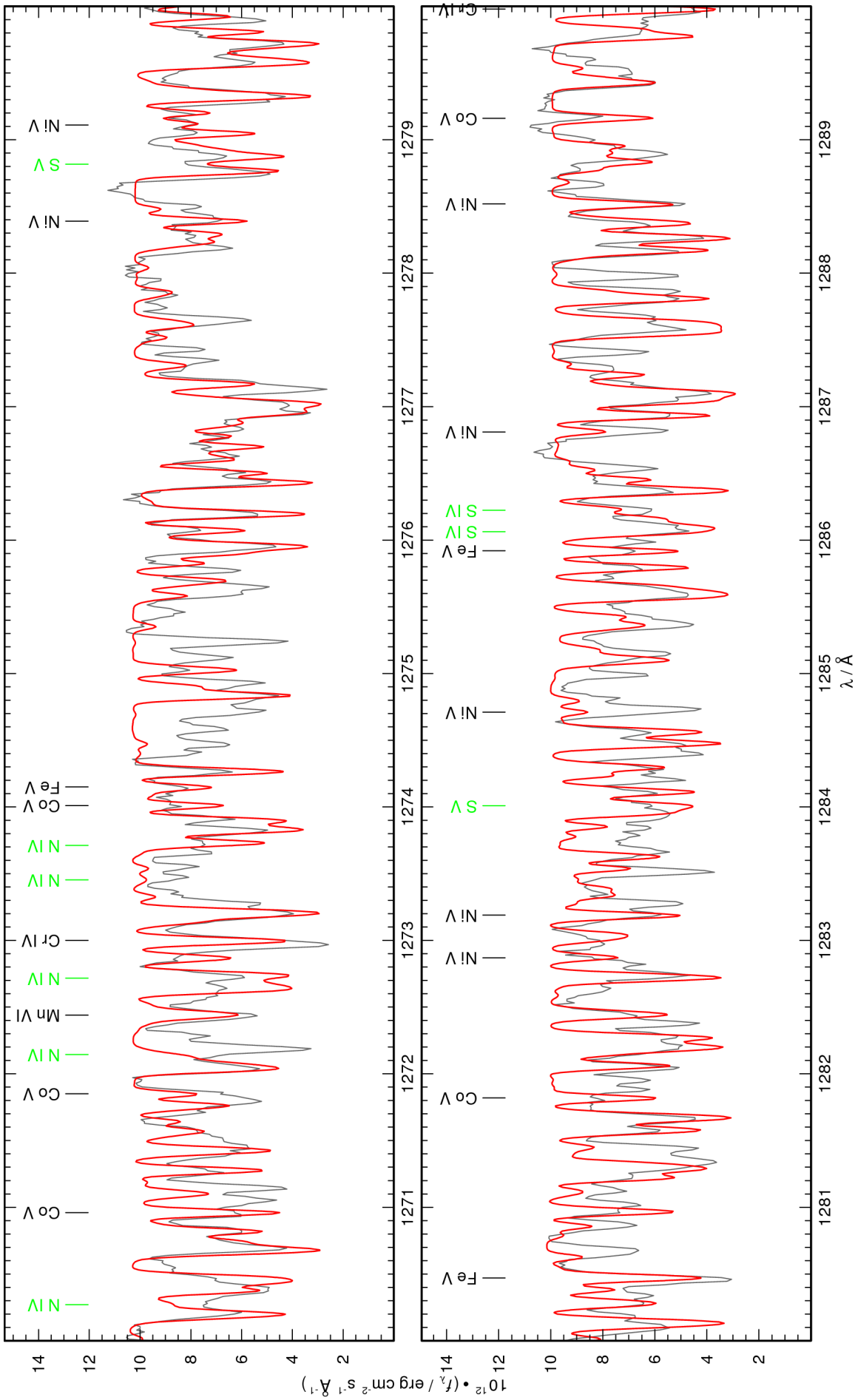

Figure 48: continued.

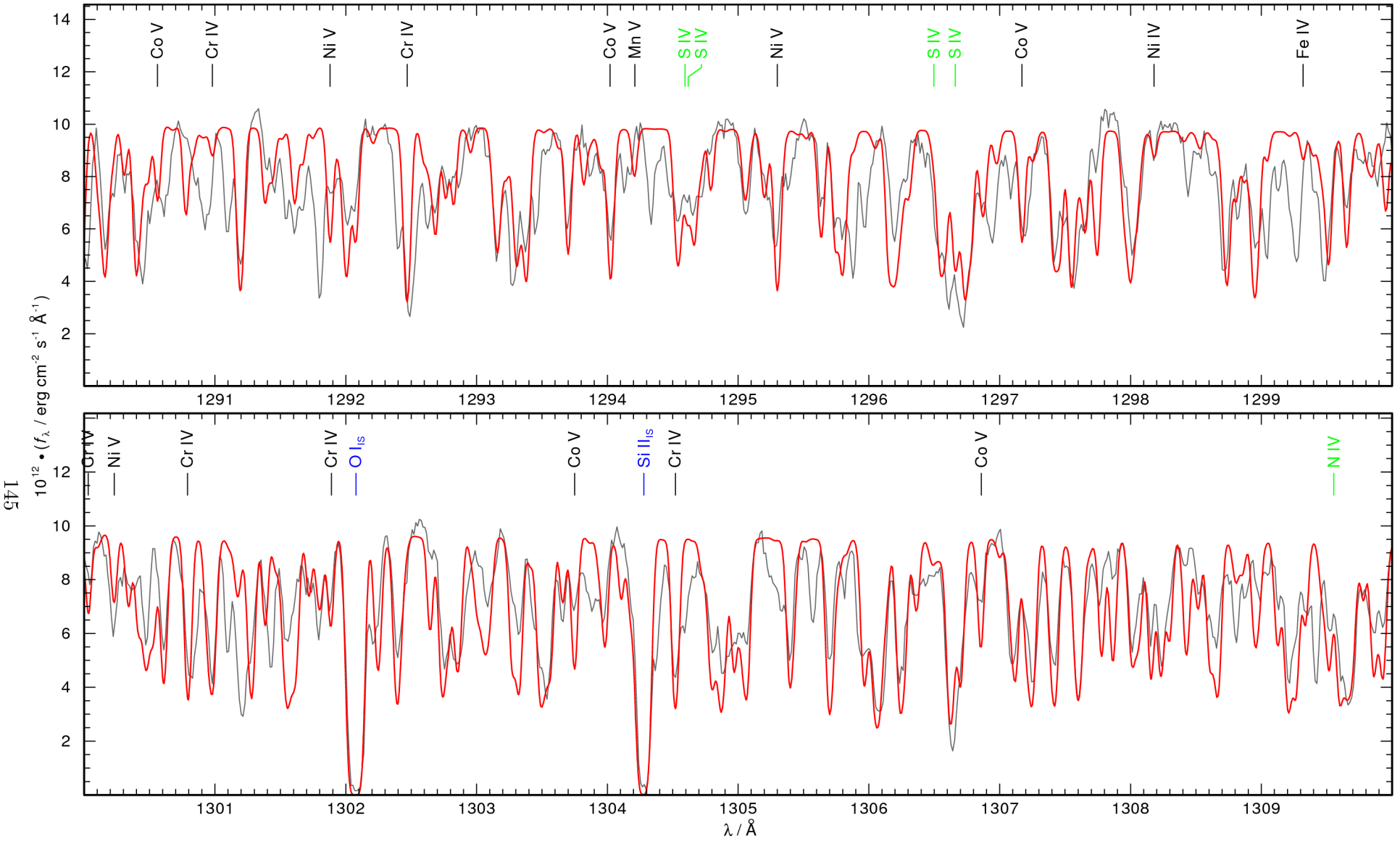

Figure 48: continued.

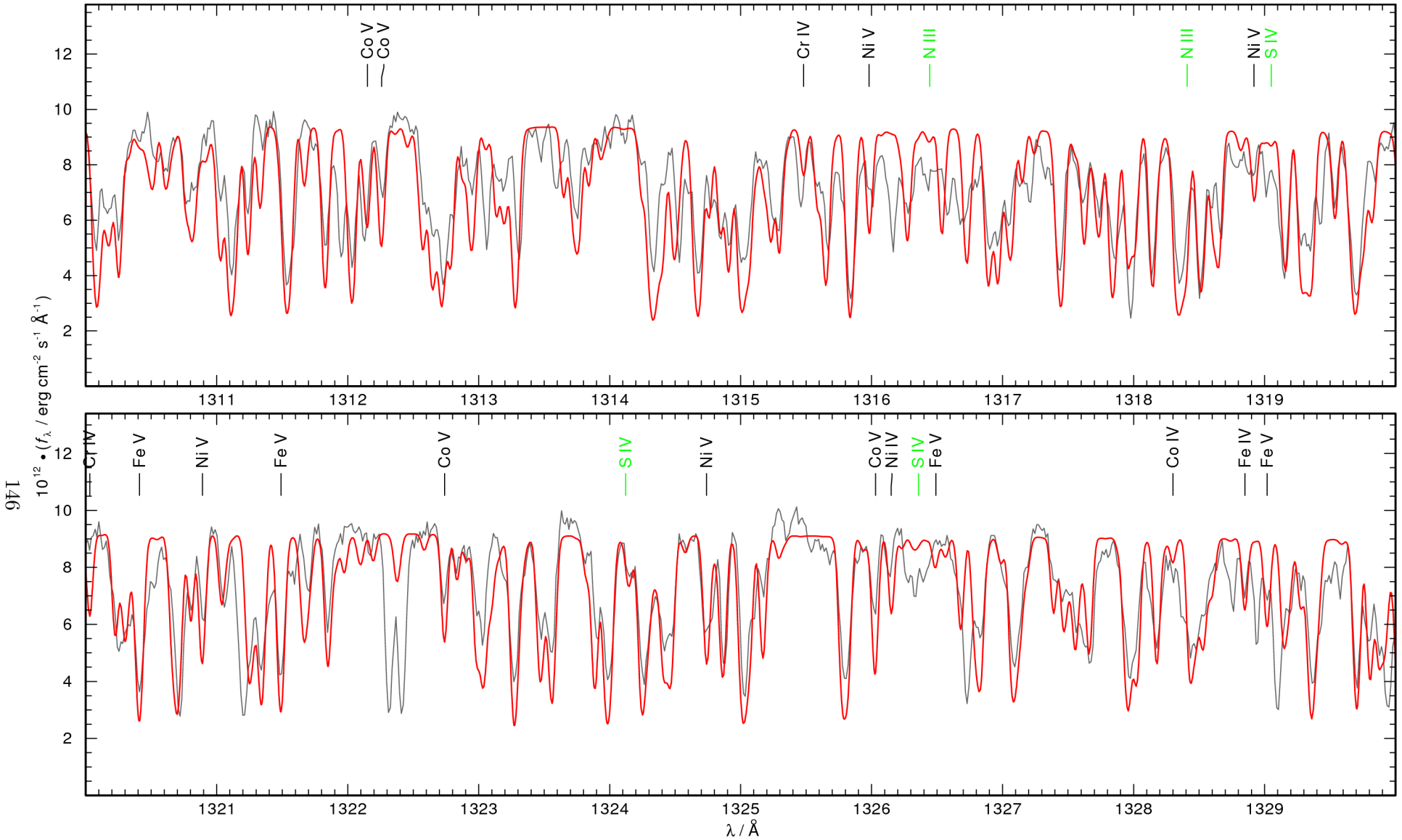

Figure 48: continued.

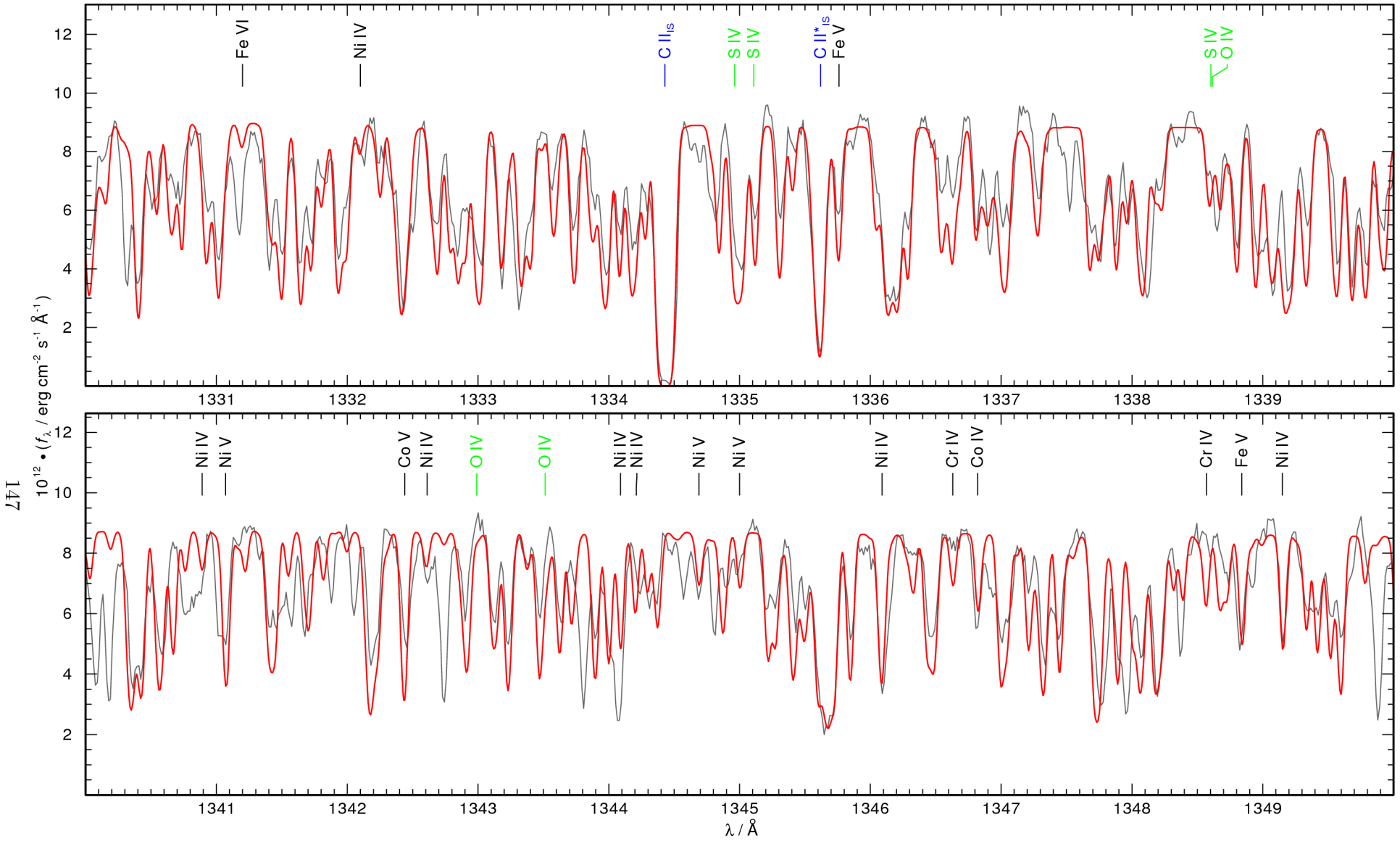

Figure 48: continued.

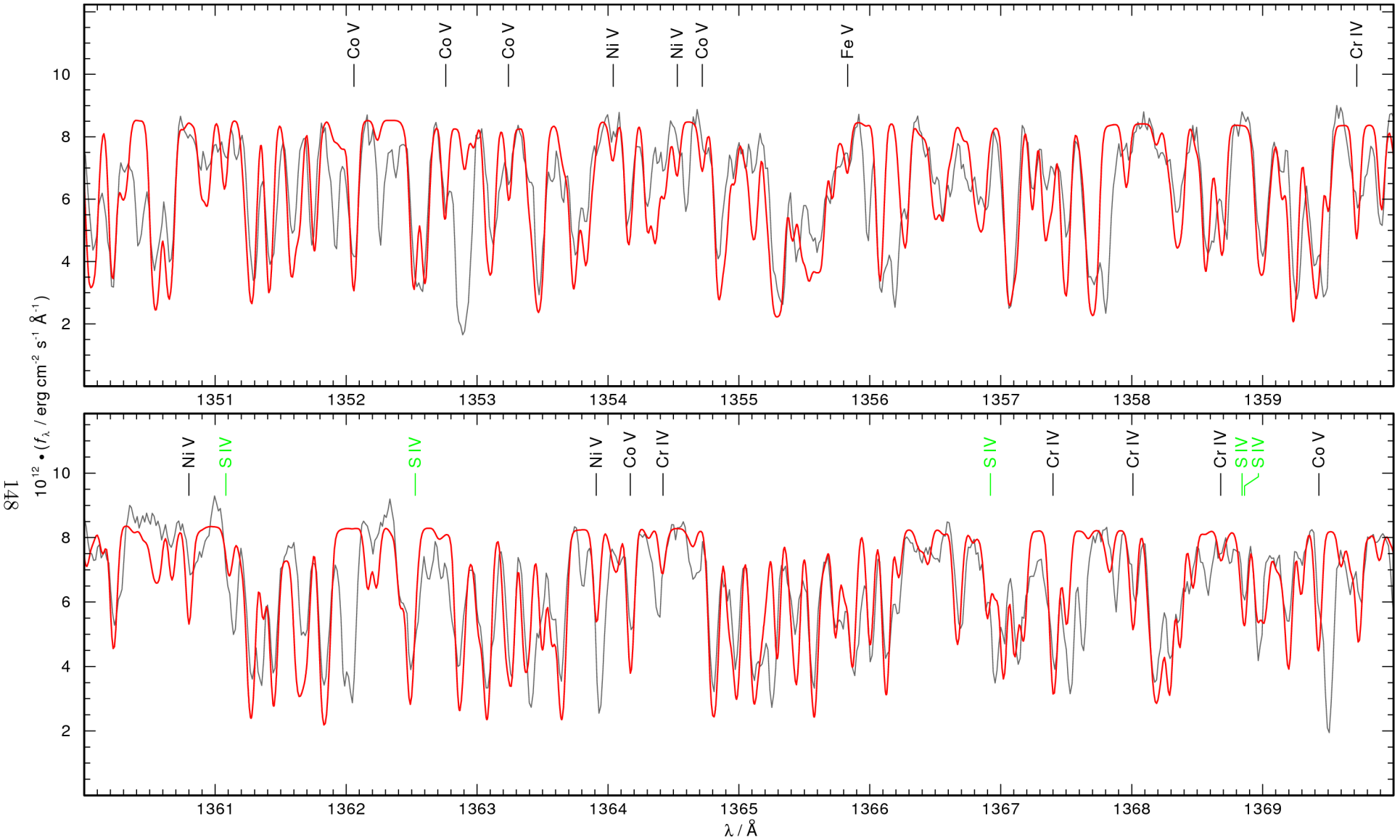

Figure 48: continued.

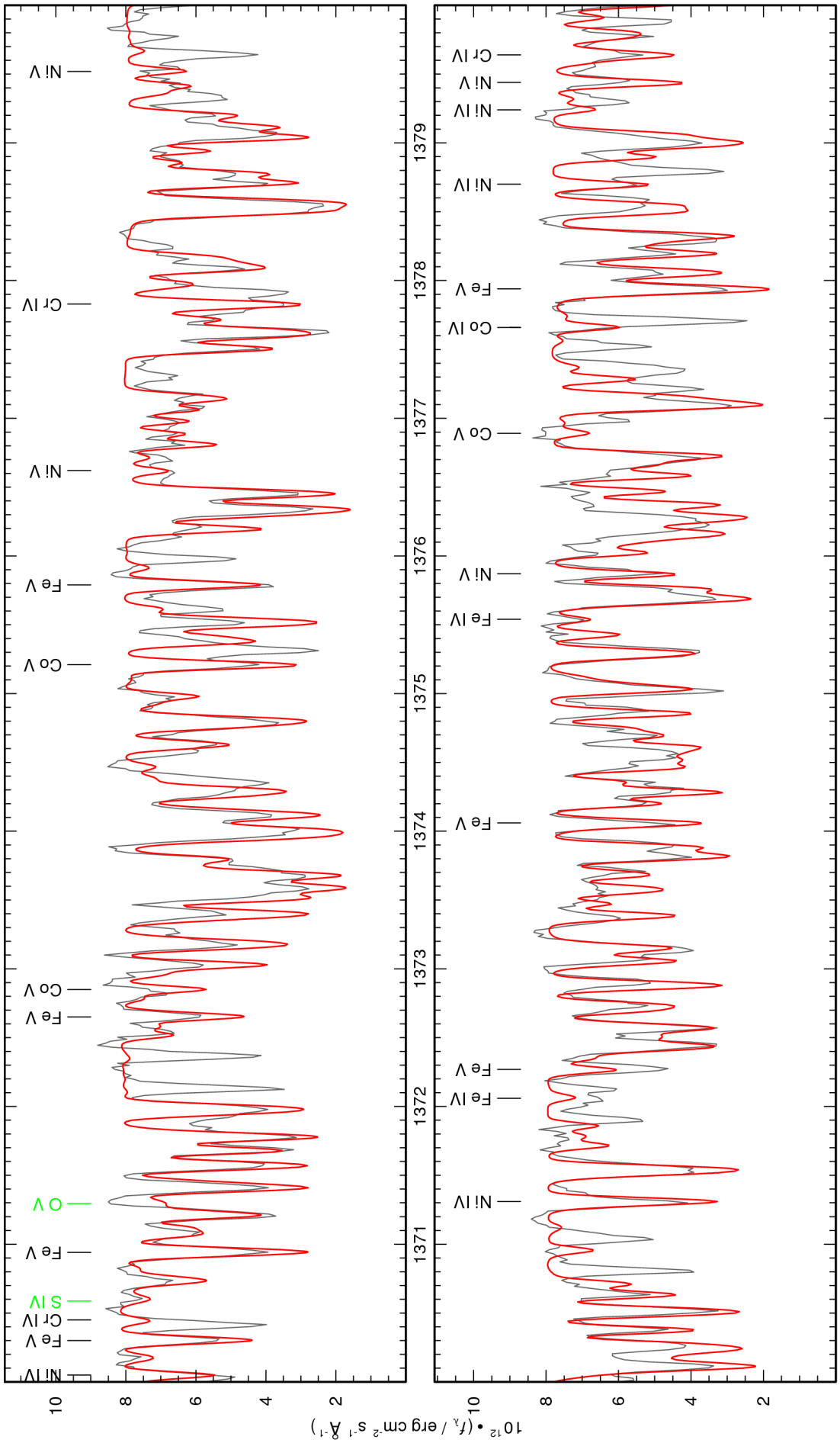

Figure 48: continued.

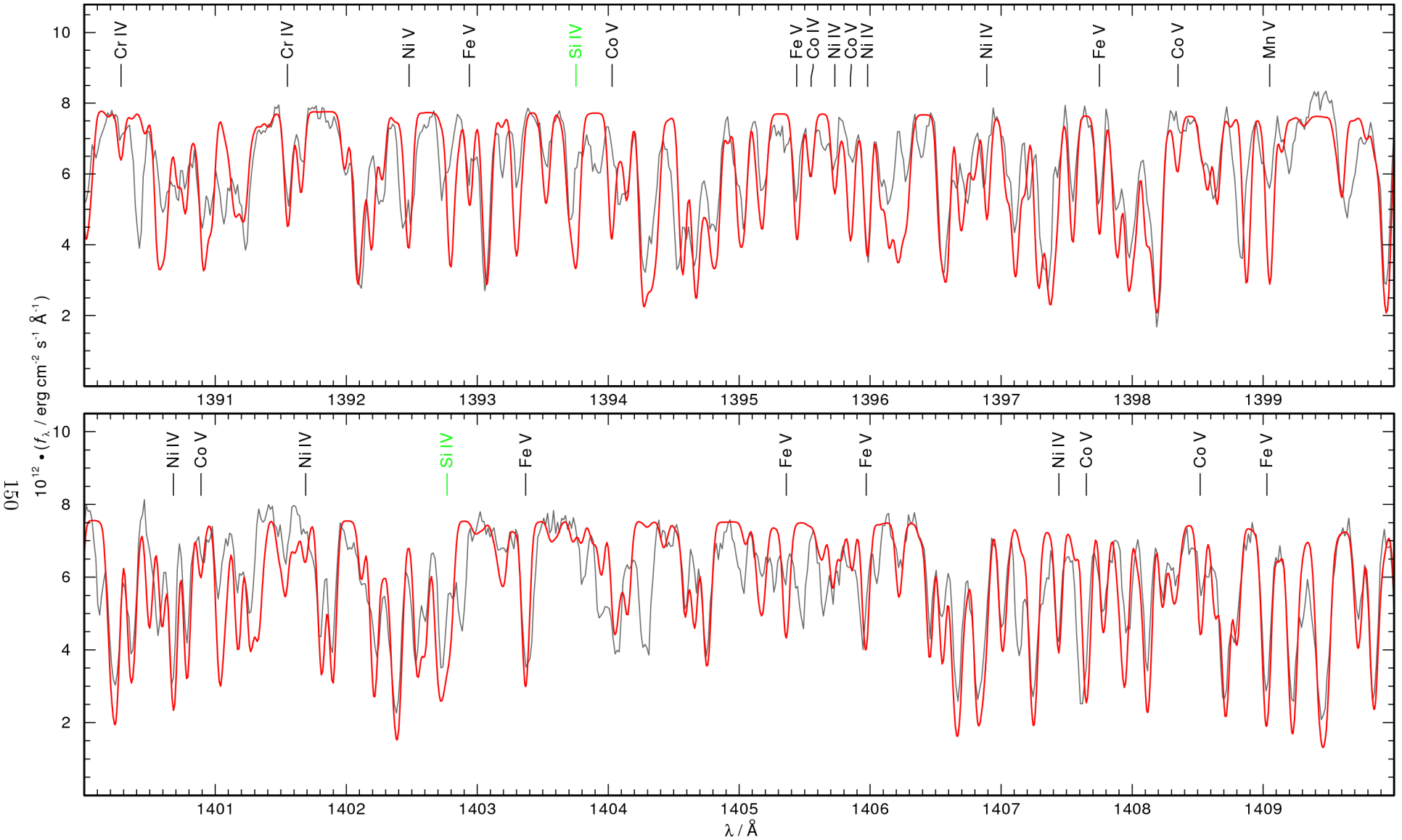

Figure 48: continued.

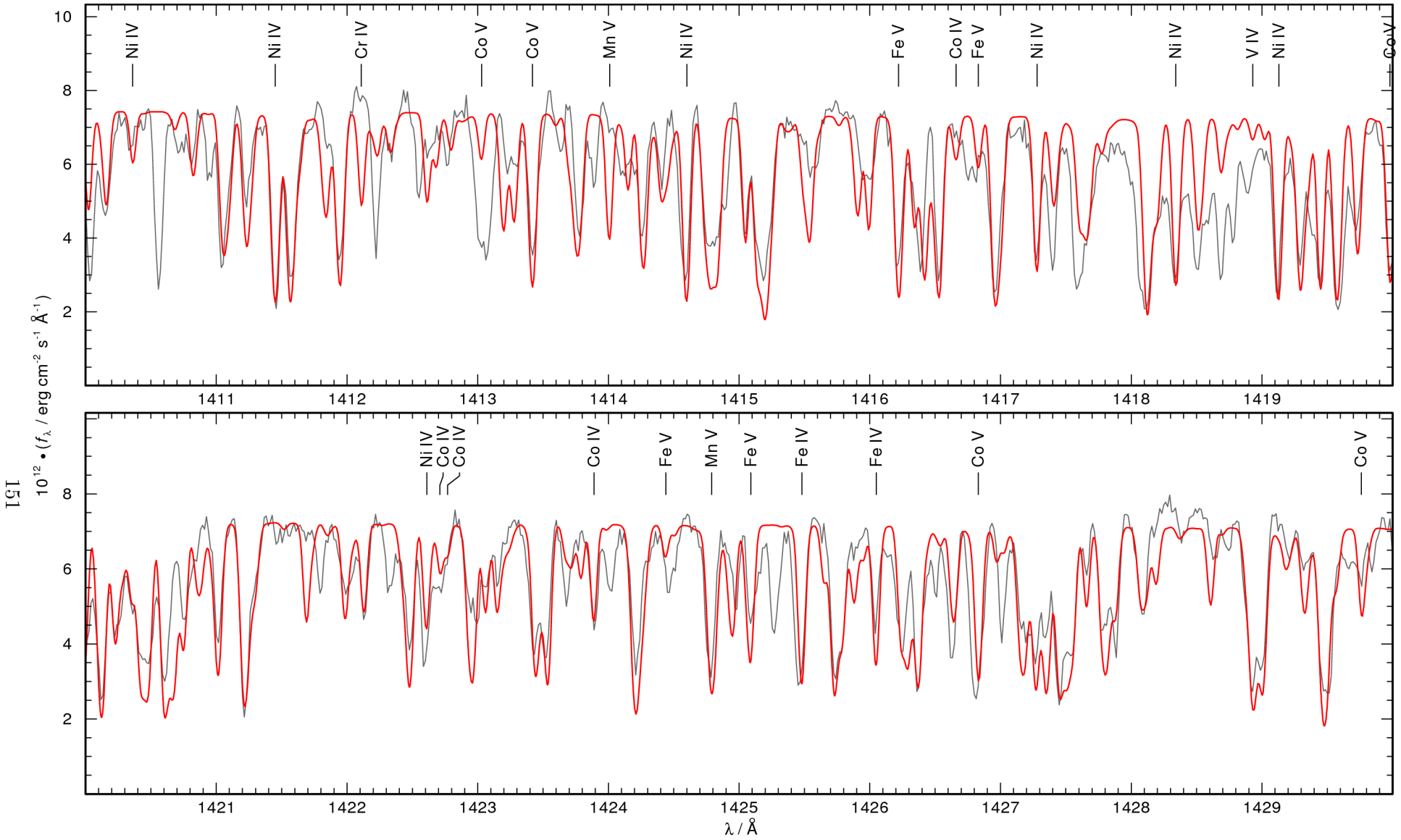

Figure 48: continued.

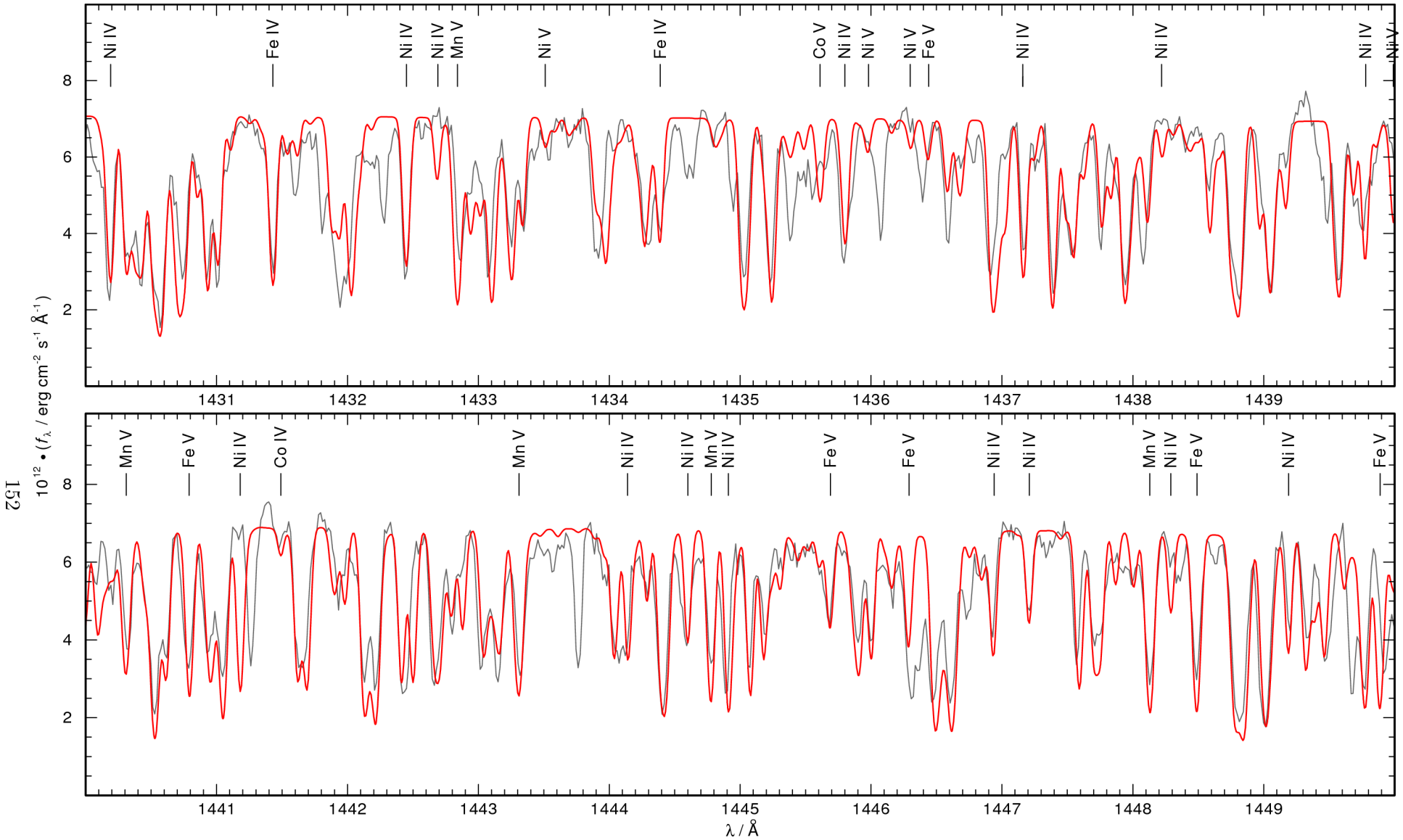

Figure 48: continued.

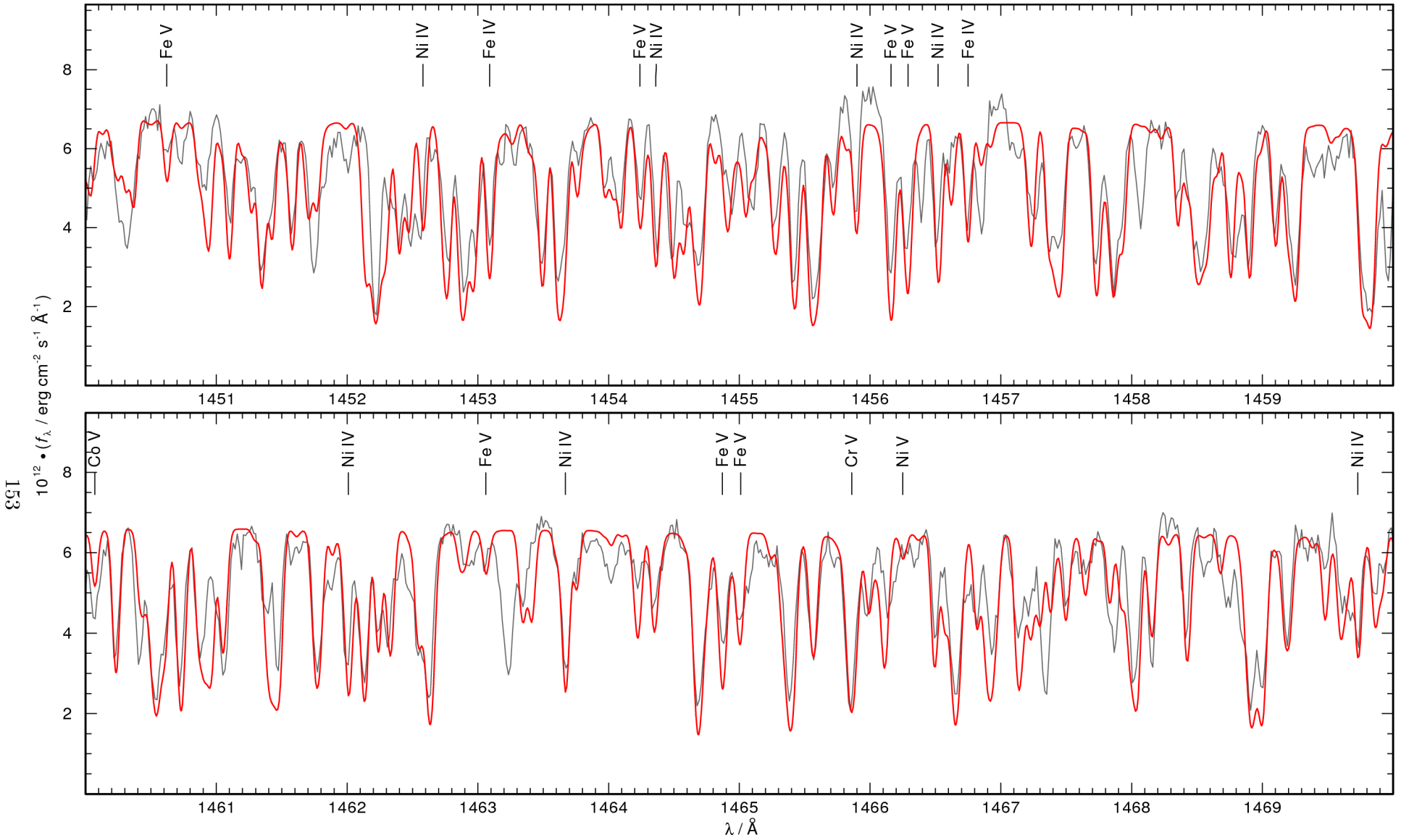

Figure 48: continued.

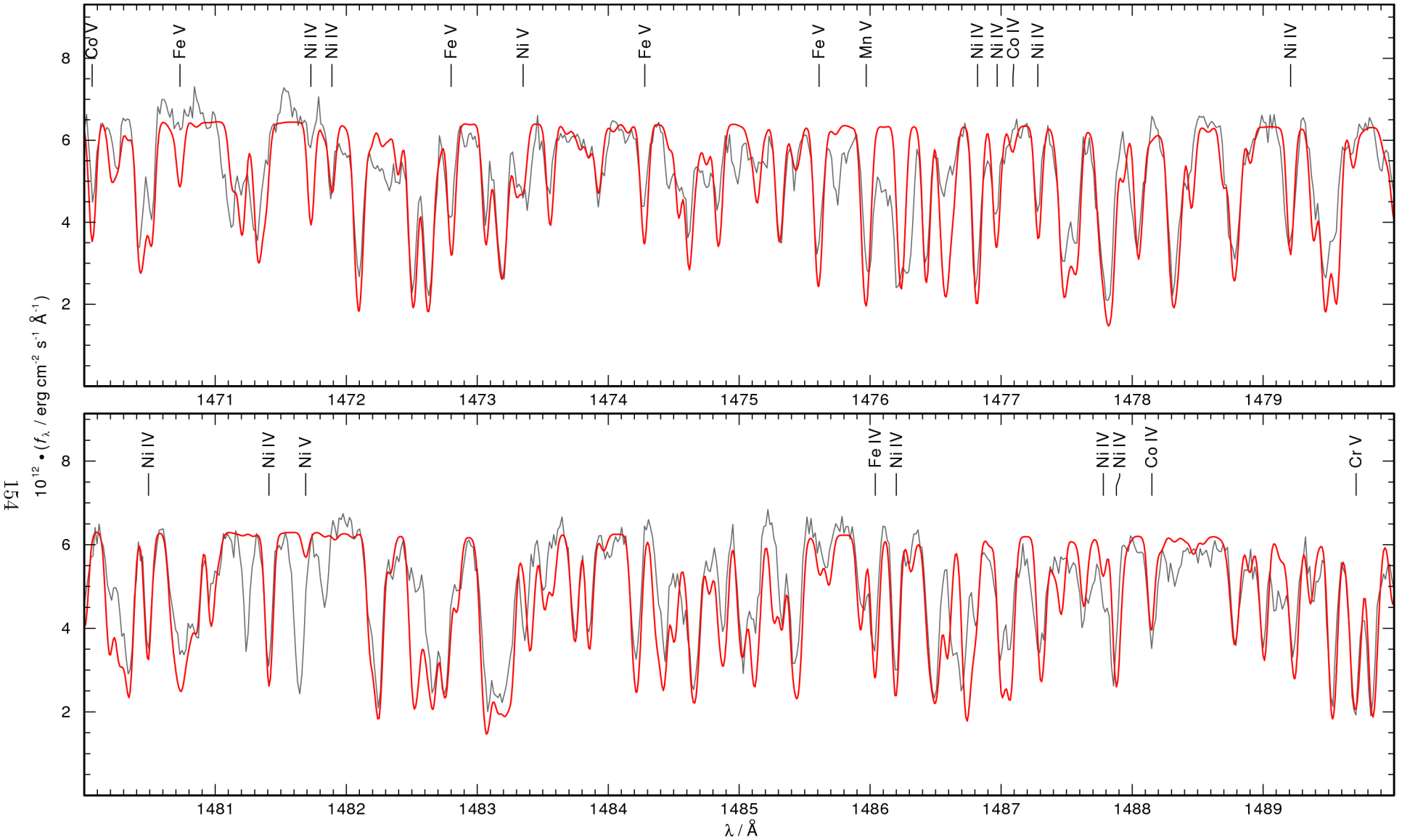

Figure 48: continued.

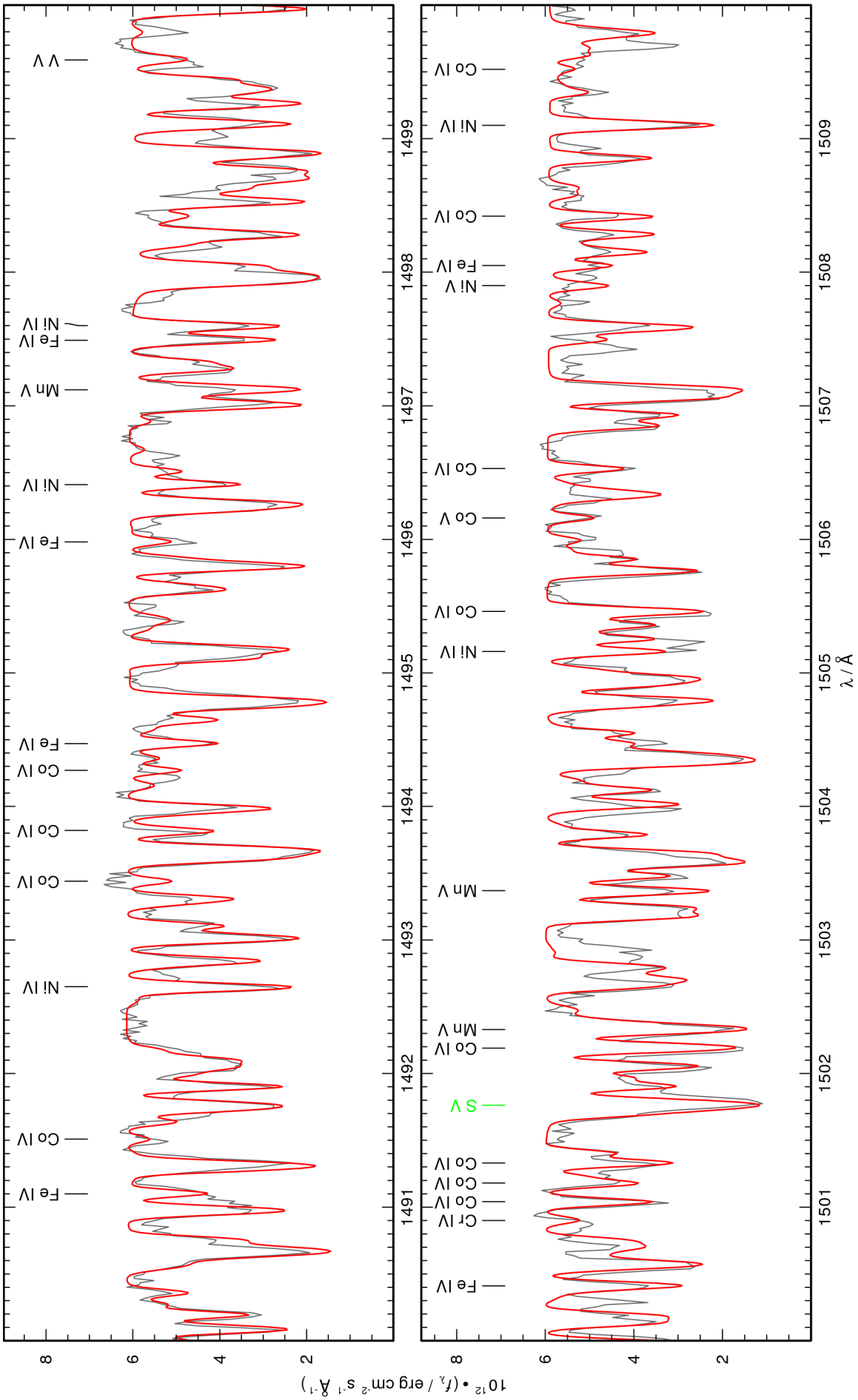

Figure 48: continued.

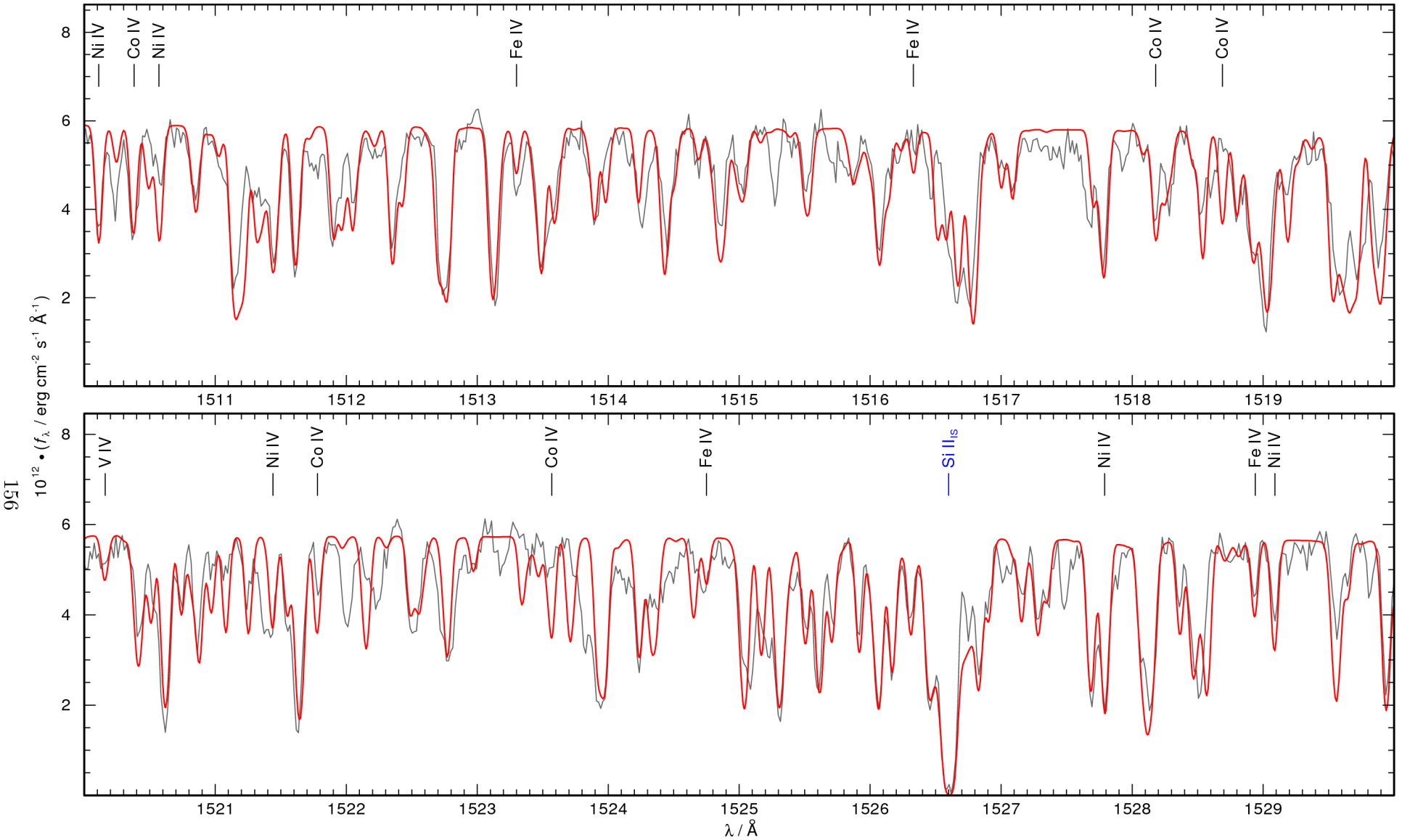

Figure 48: continued.

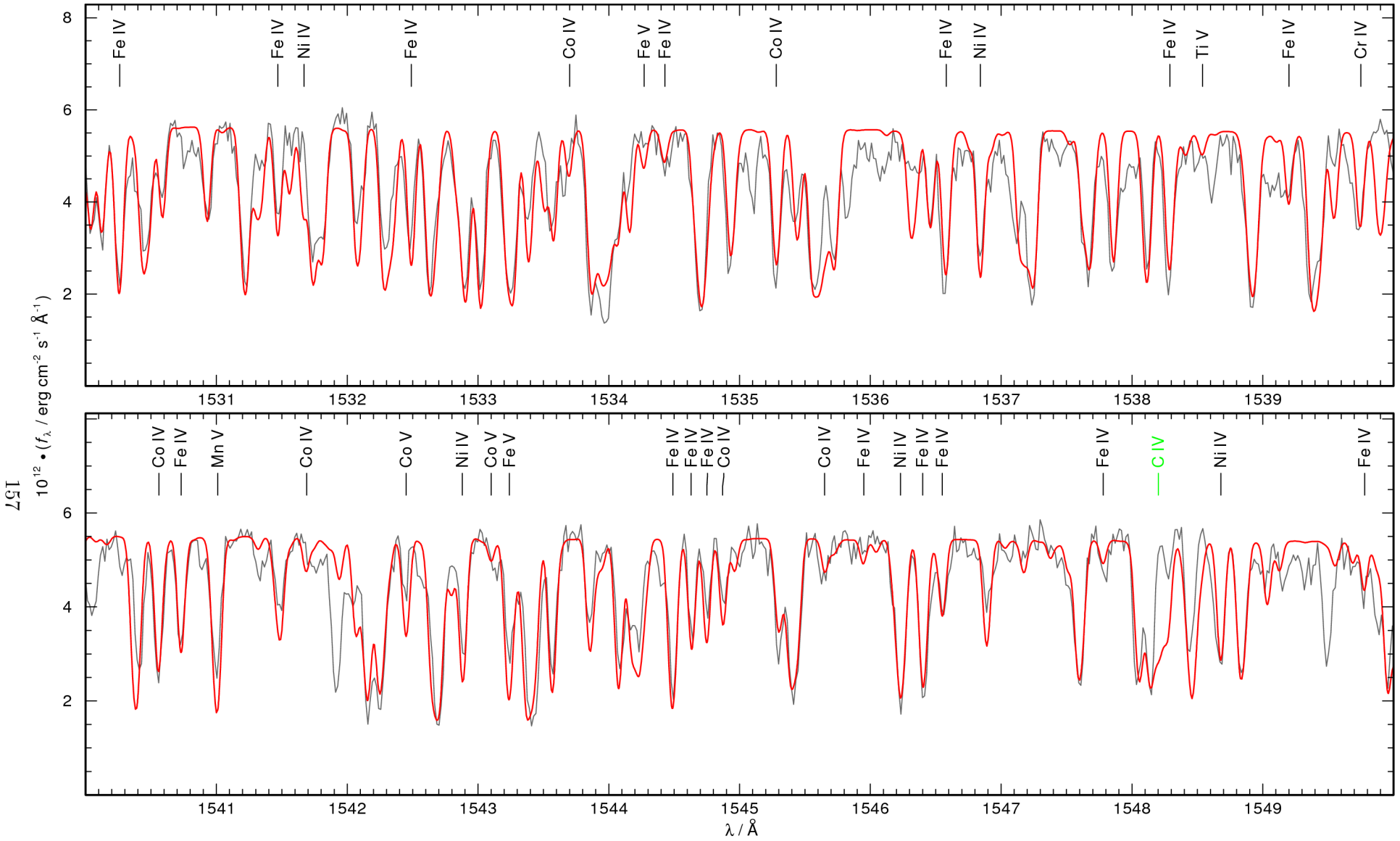

Figure 48: continued.

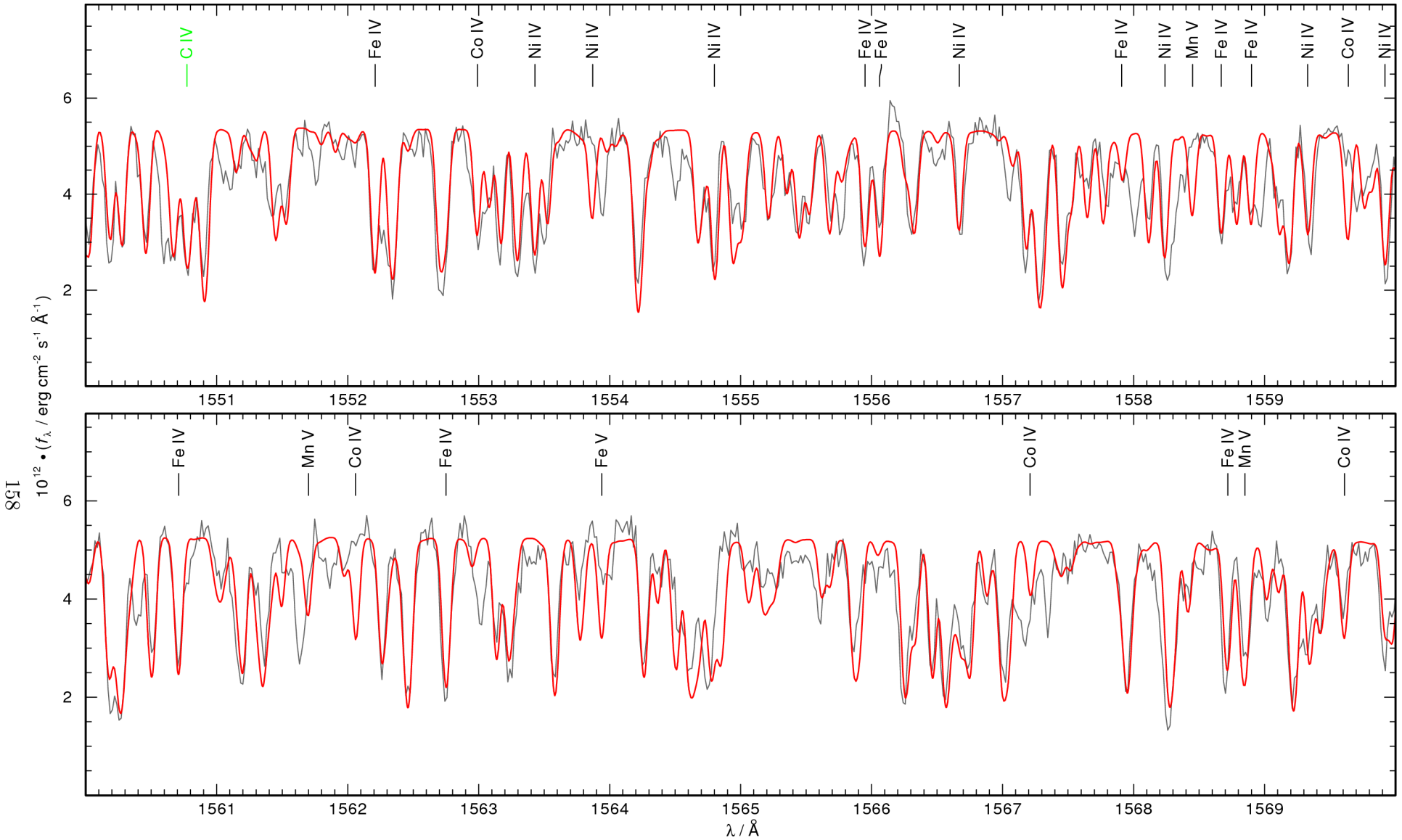

Figure 48: continued.

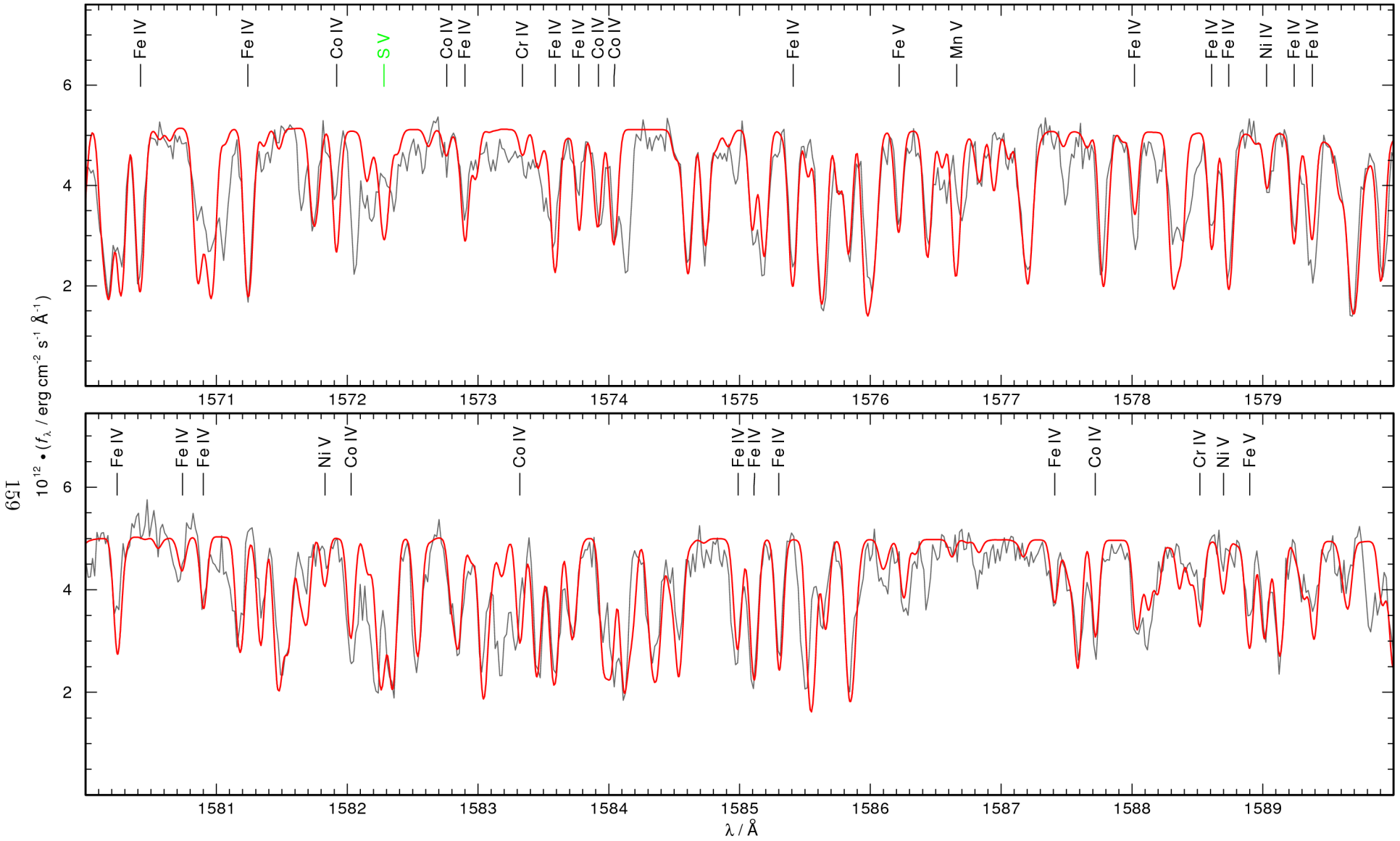

Figure 48: continued.

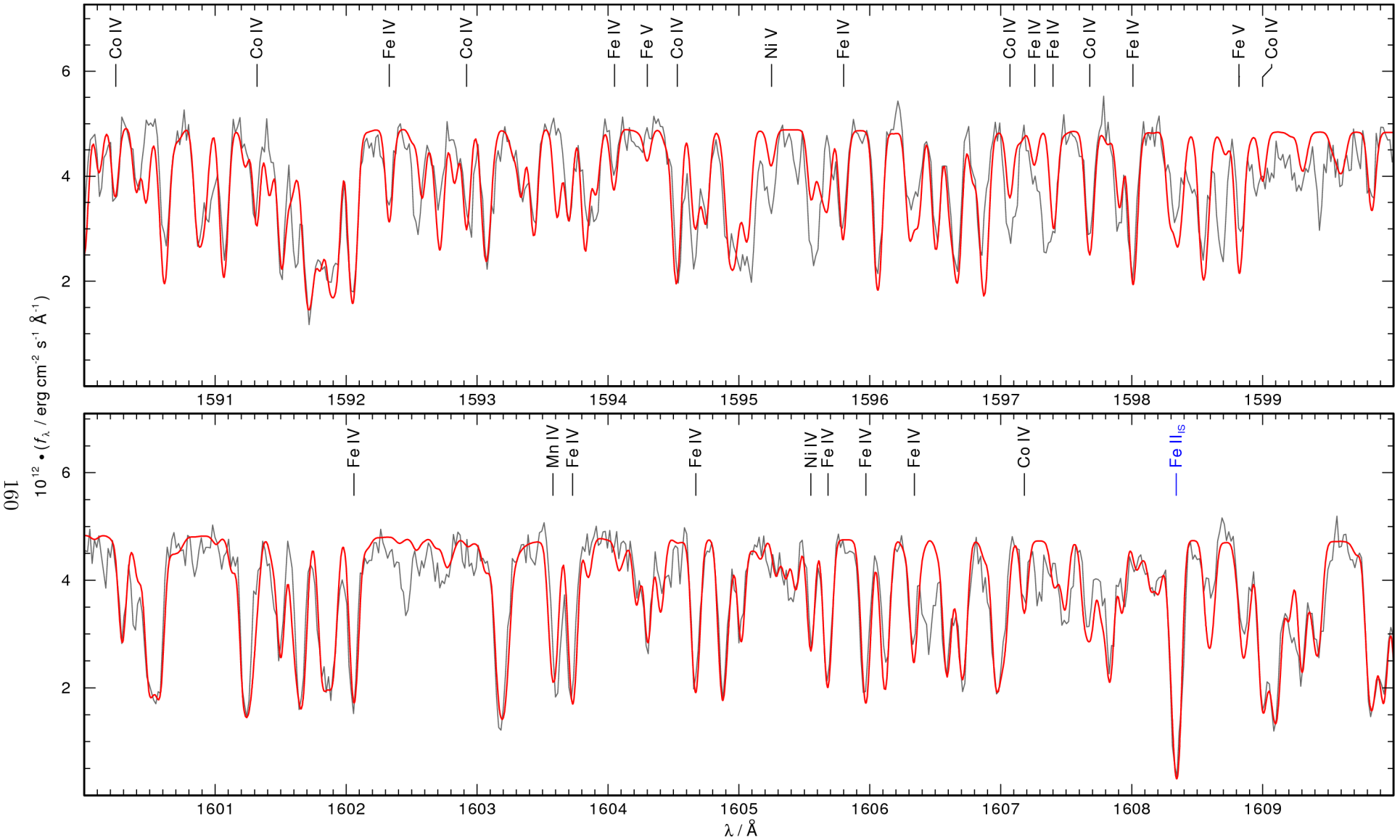

Figure 48: continued.

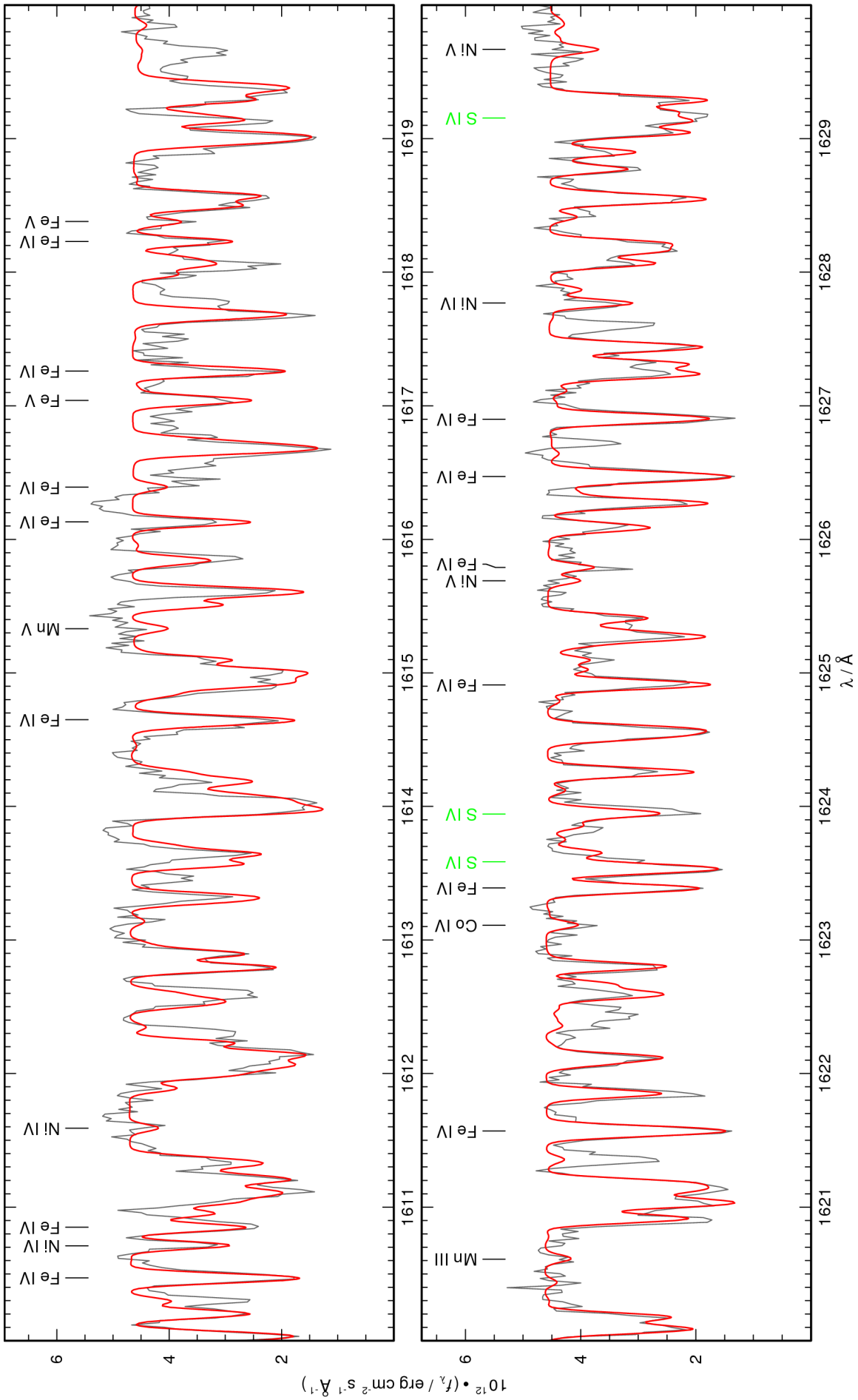

Figure 48: continued.

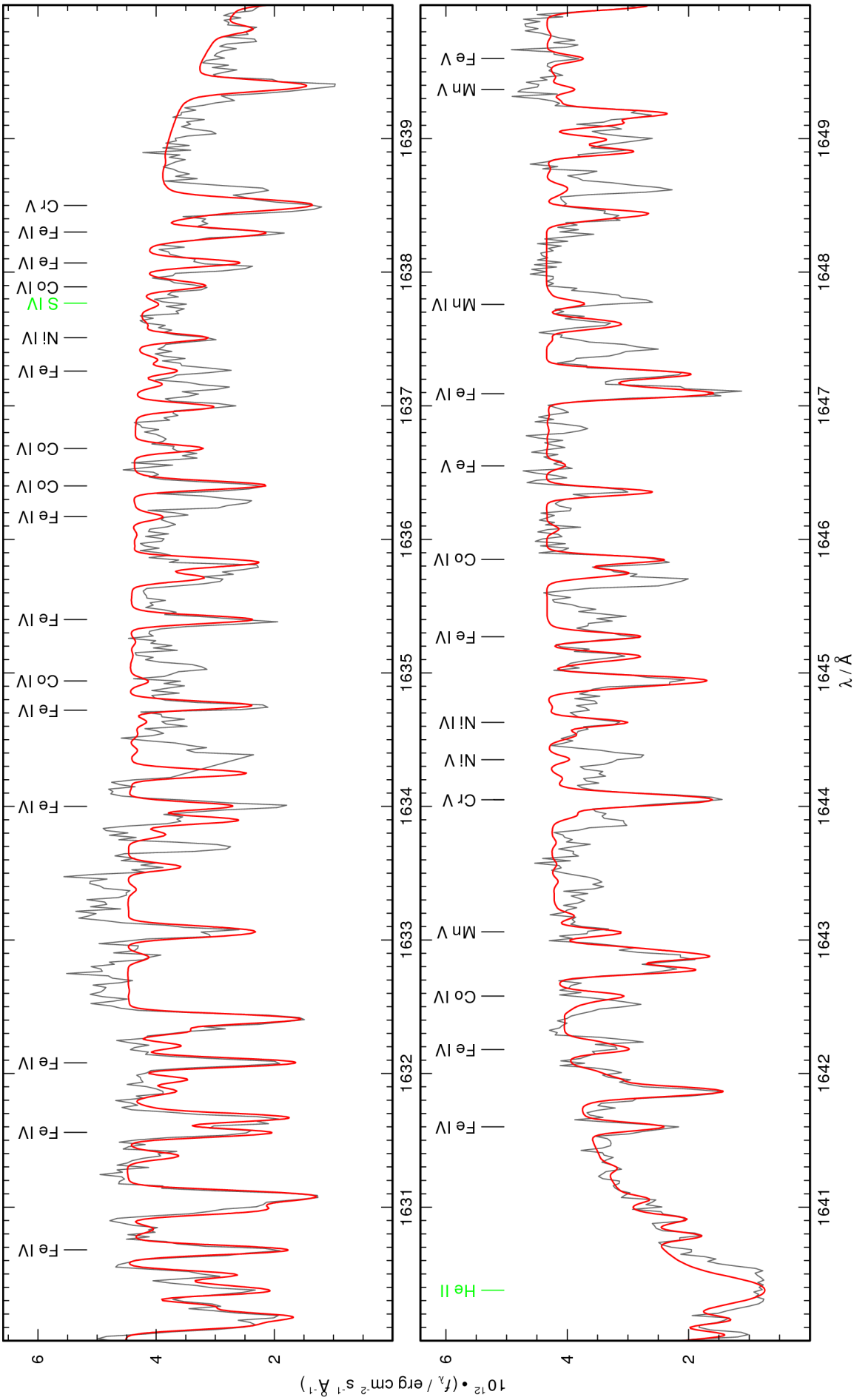

Figure 48: continued.

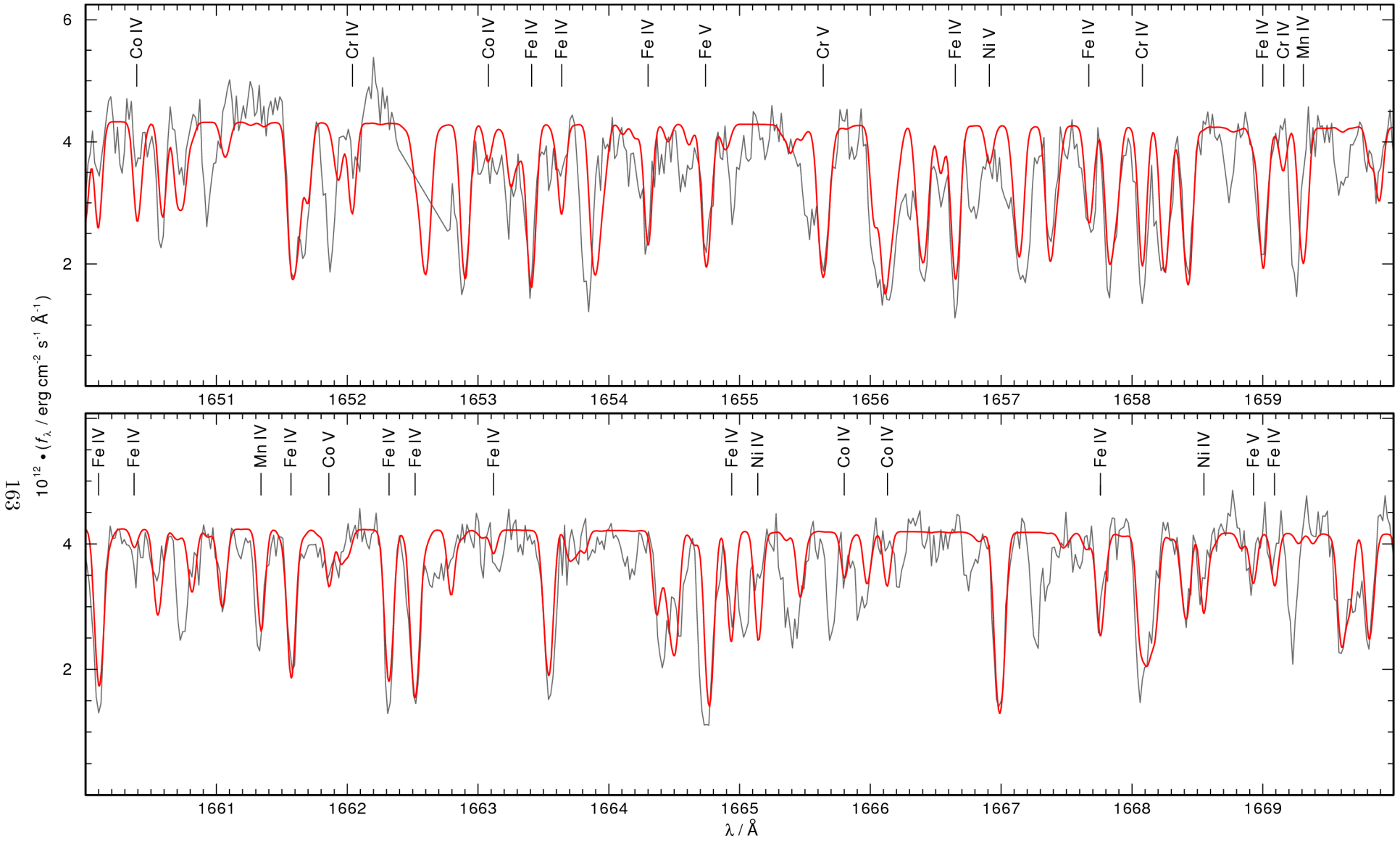

Figure 48: continued.

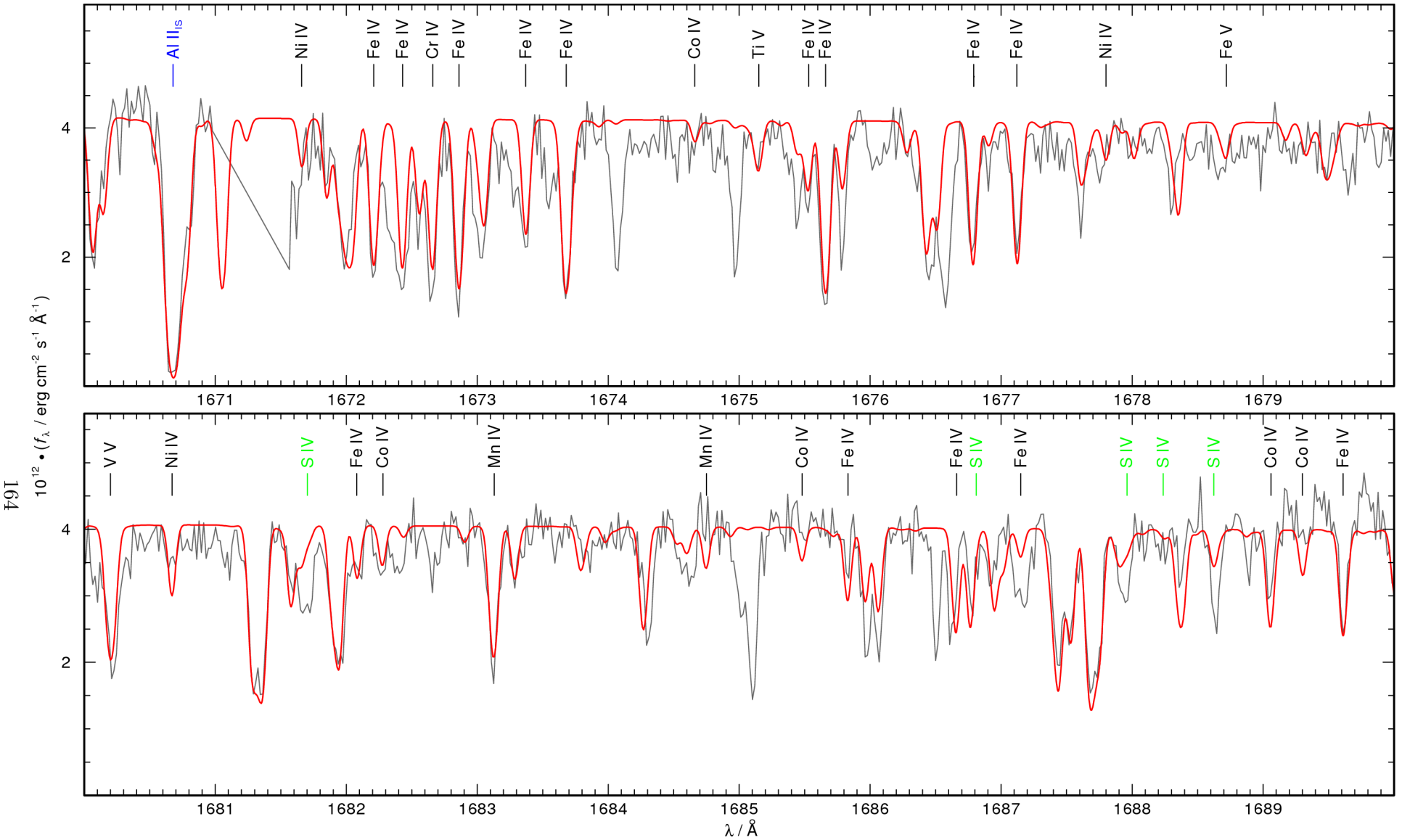

Figure 48: continued.

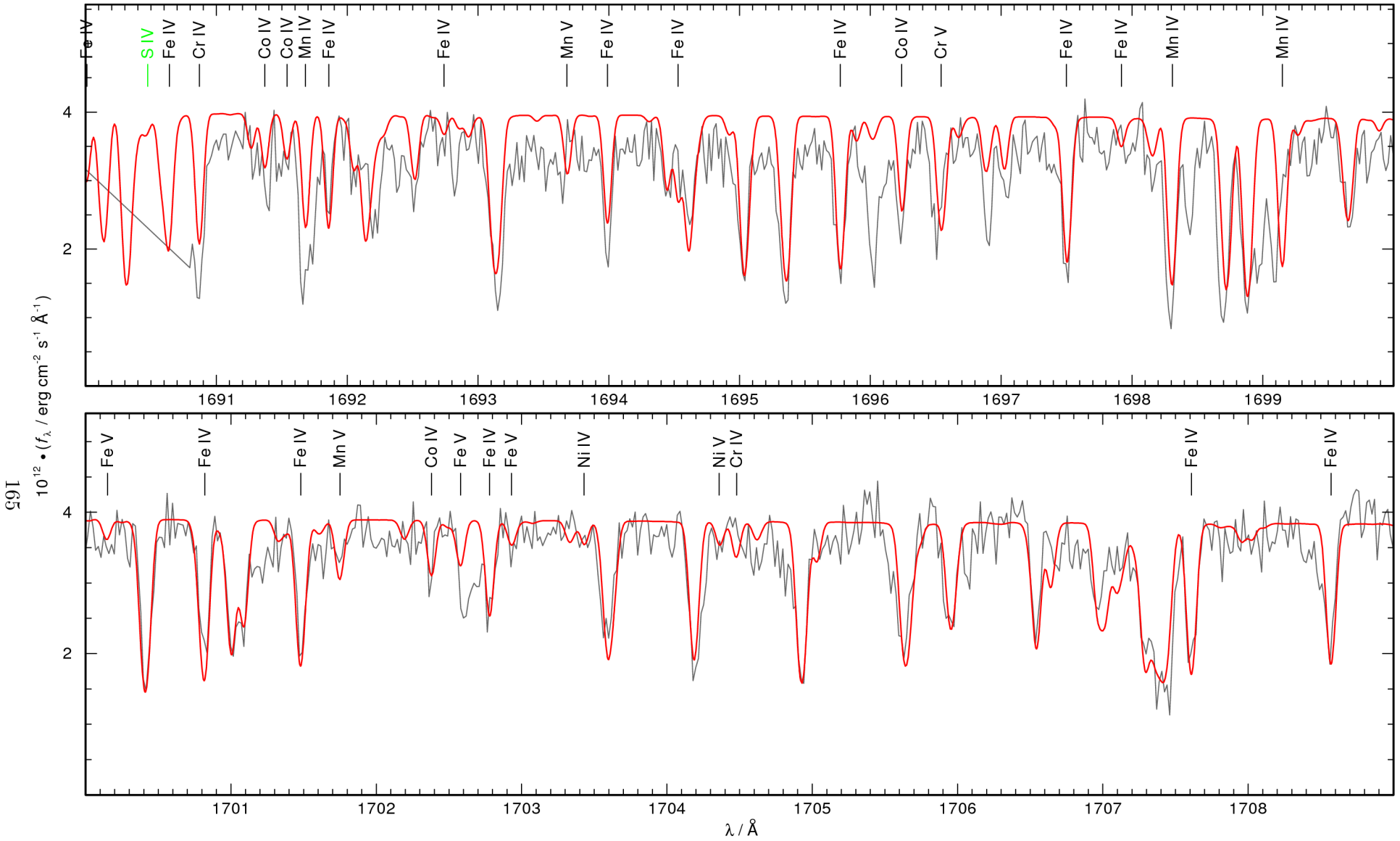

Figure 48: continued.

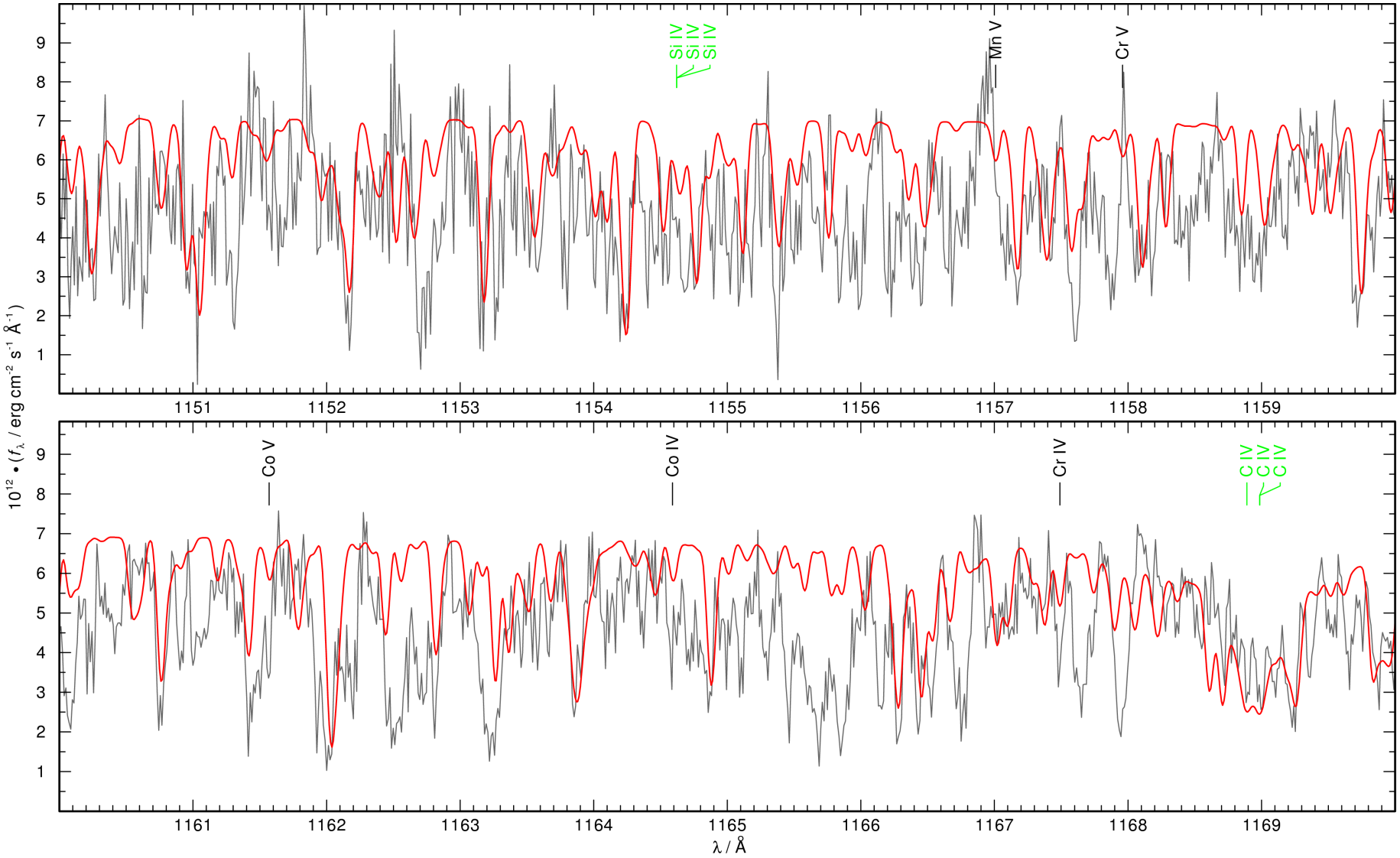

Figure 49: Like Fig. 48, for PG 0909+276.

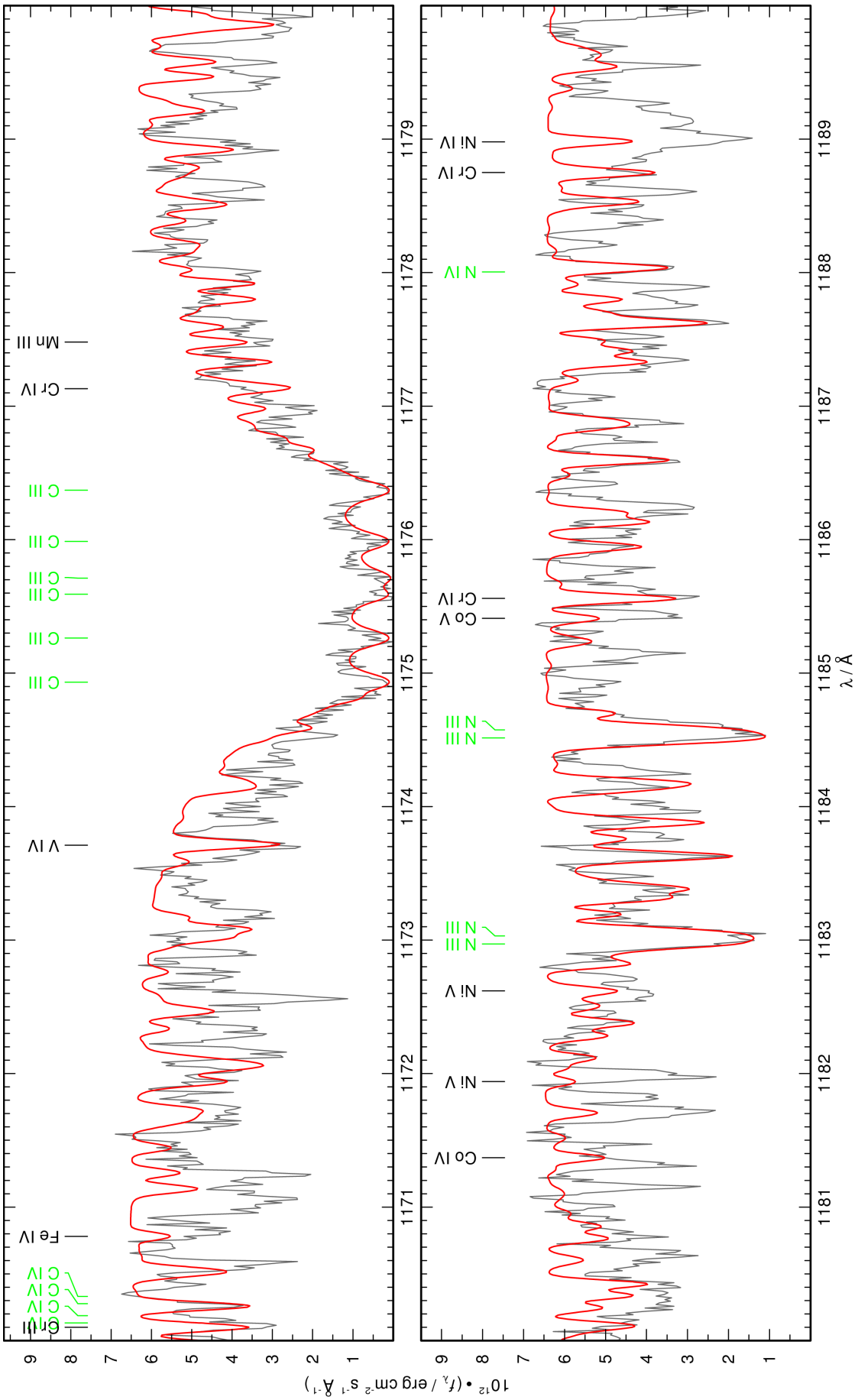

Figure 49: continued.

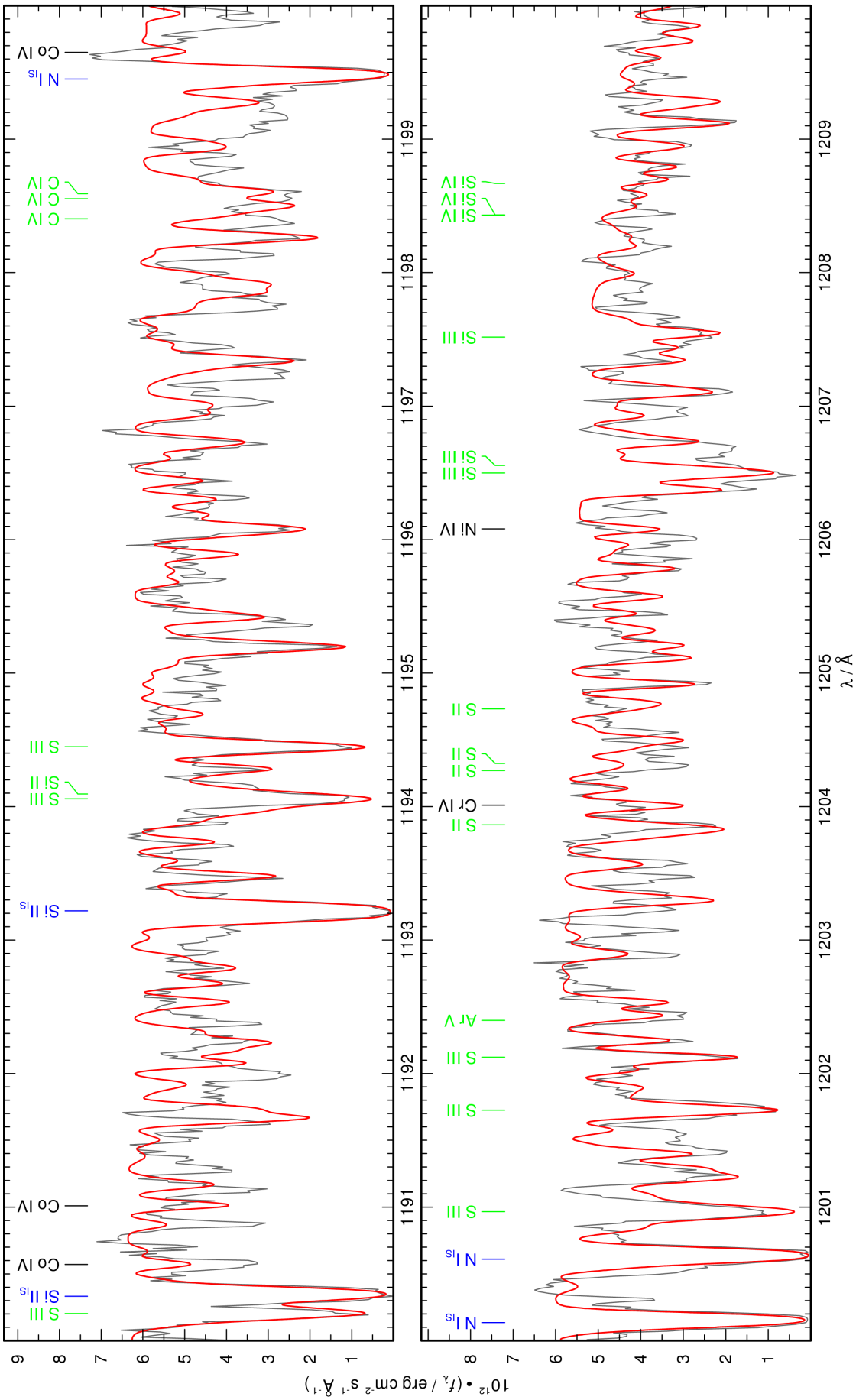

Figure 49: continued.

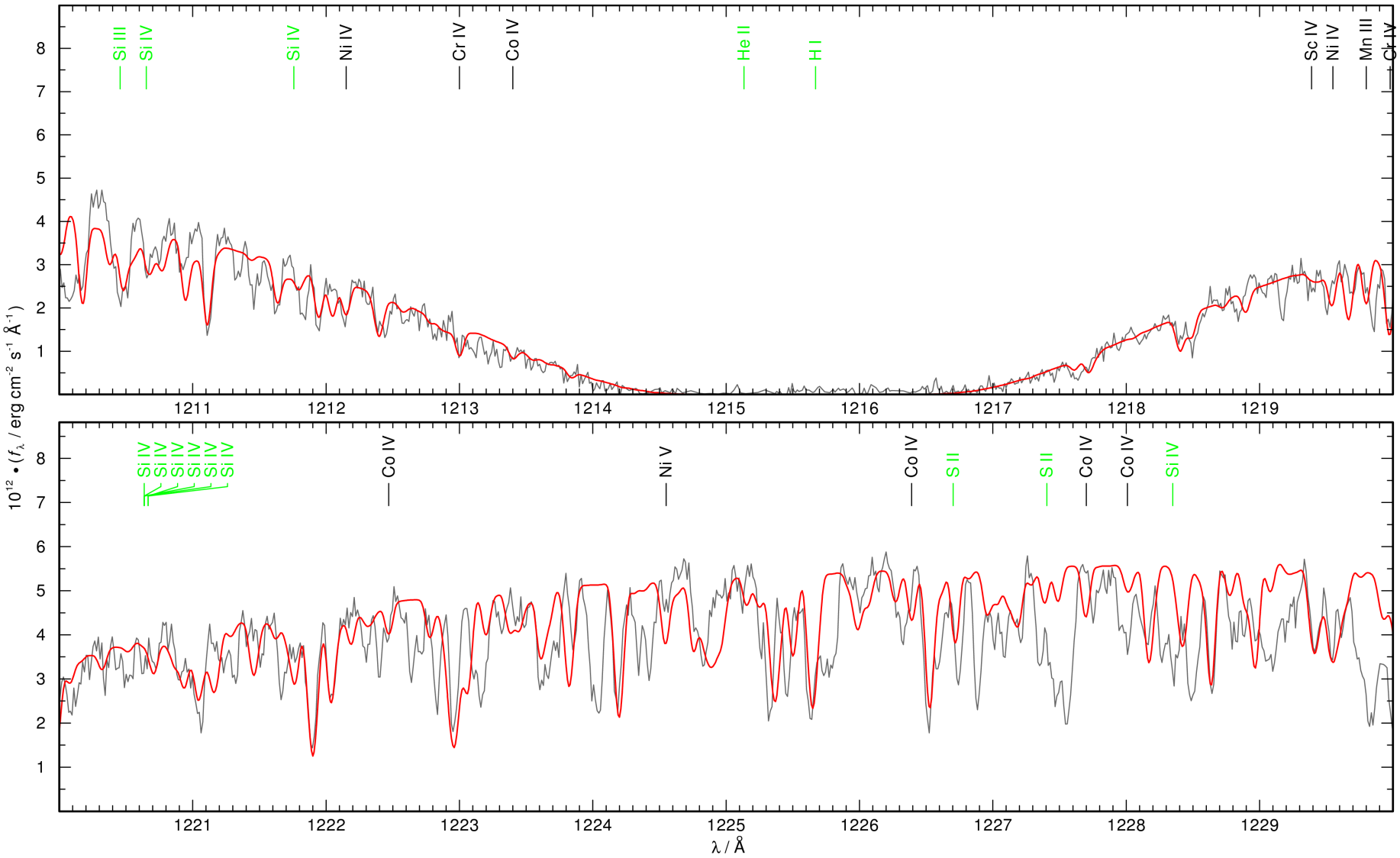

Figure 49: continued.

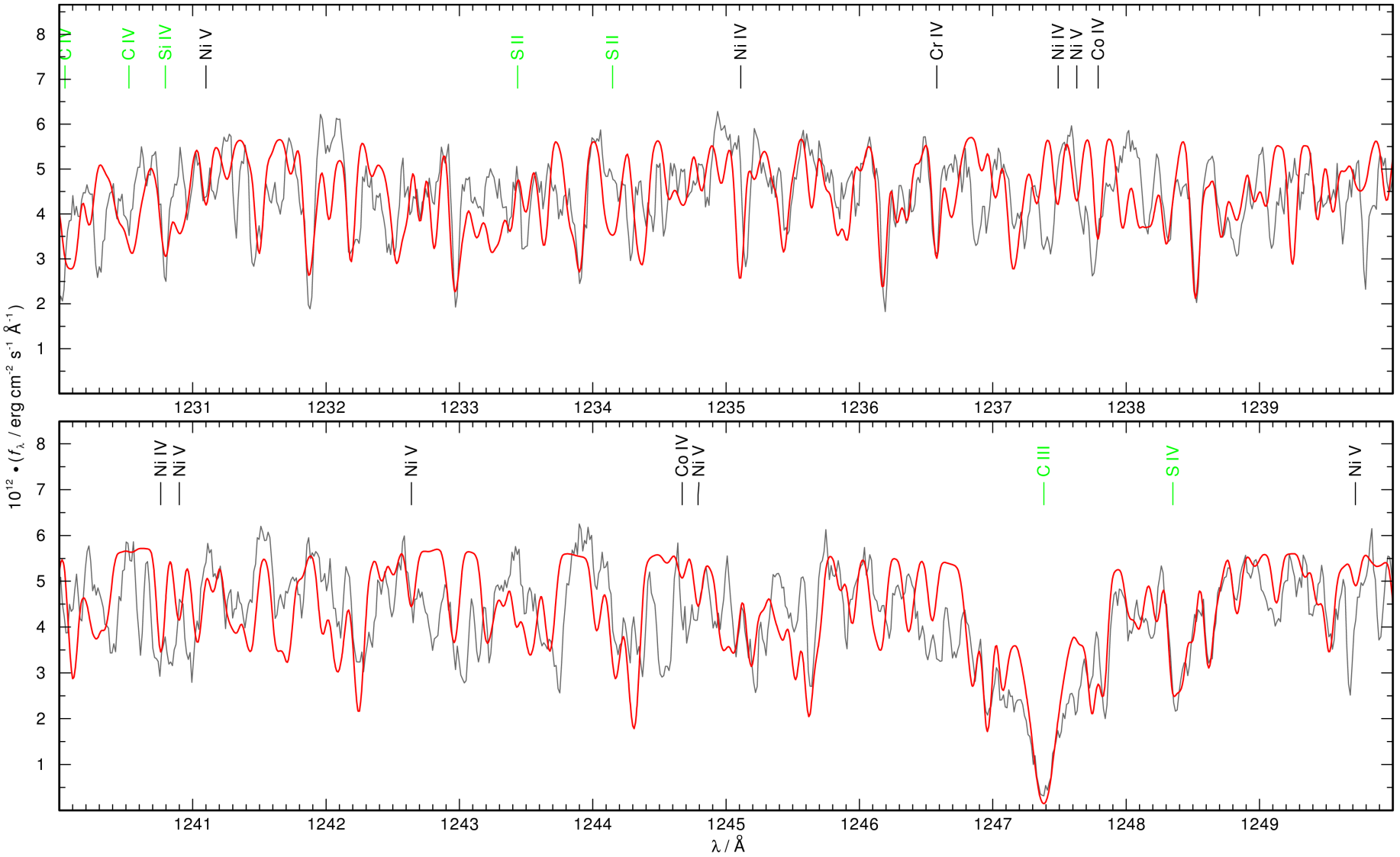

Figure 49: continued.

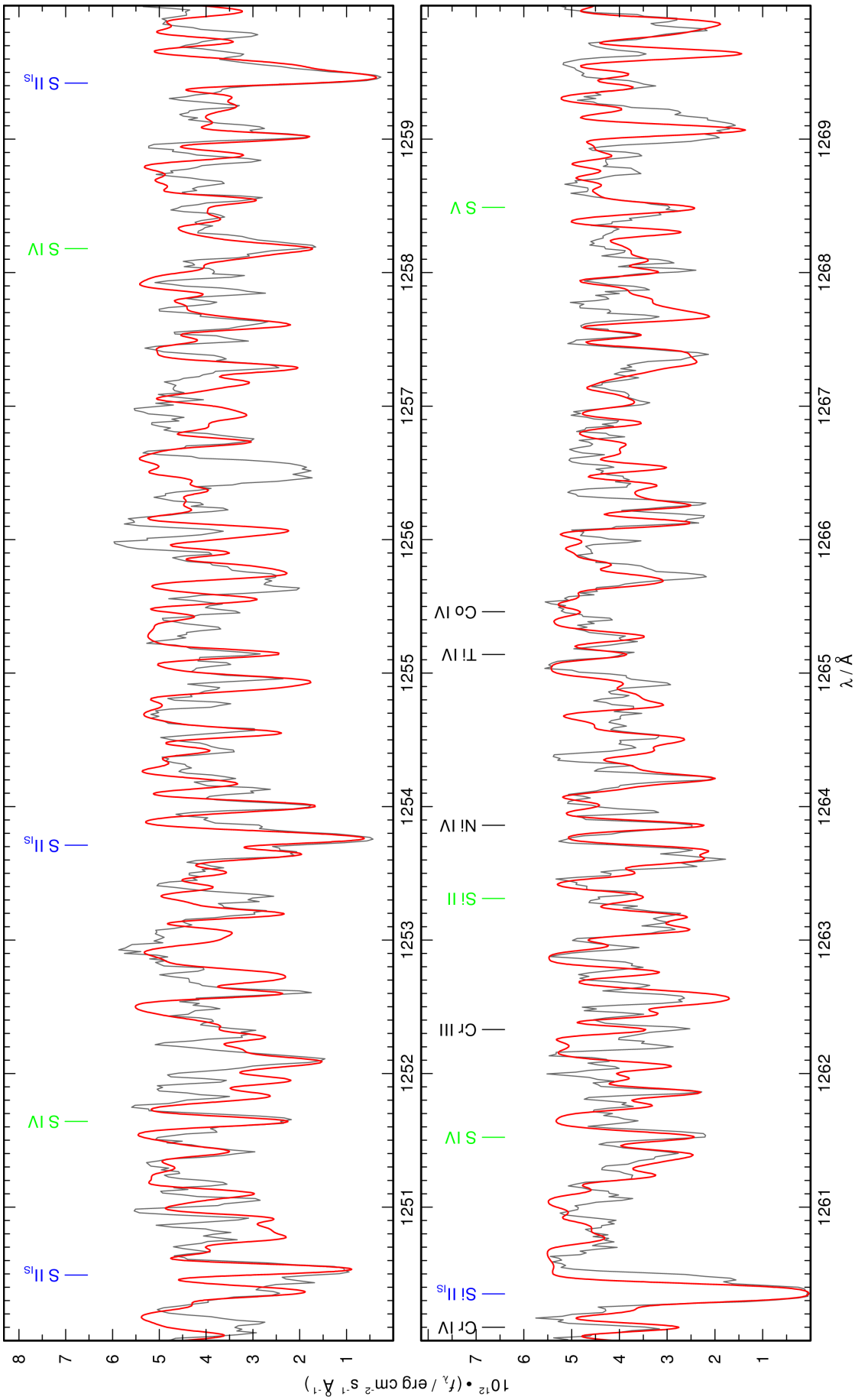

Figure 49: continued.

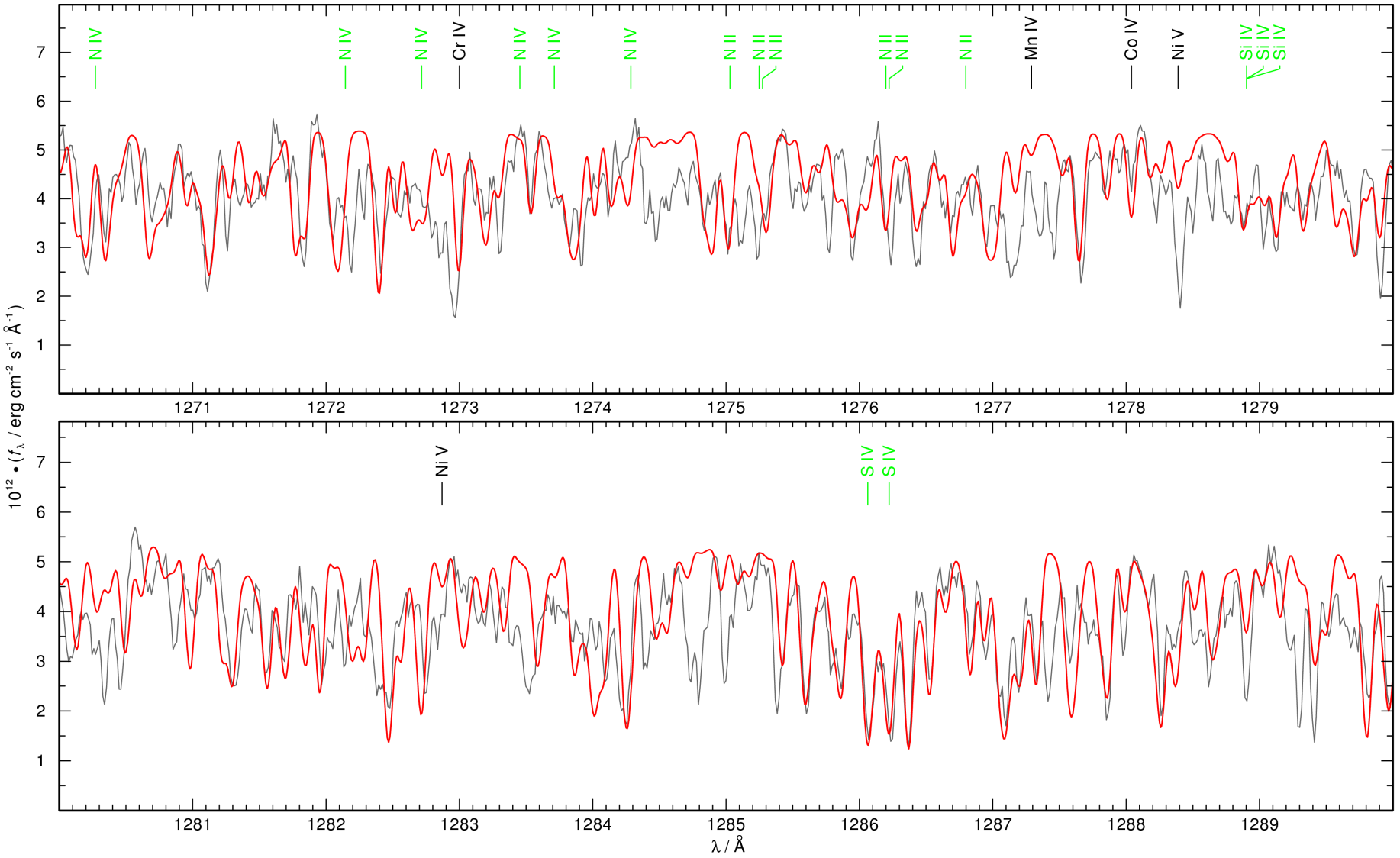

Figure 49: continued.

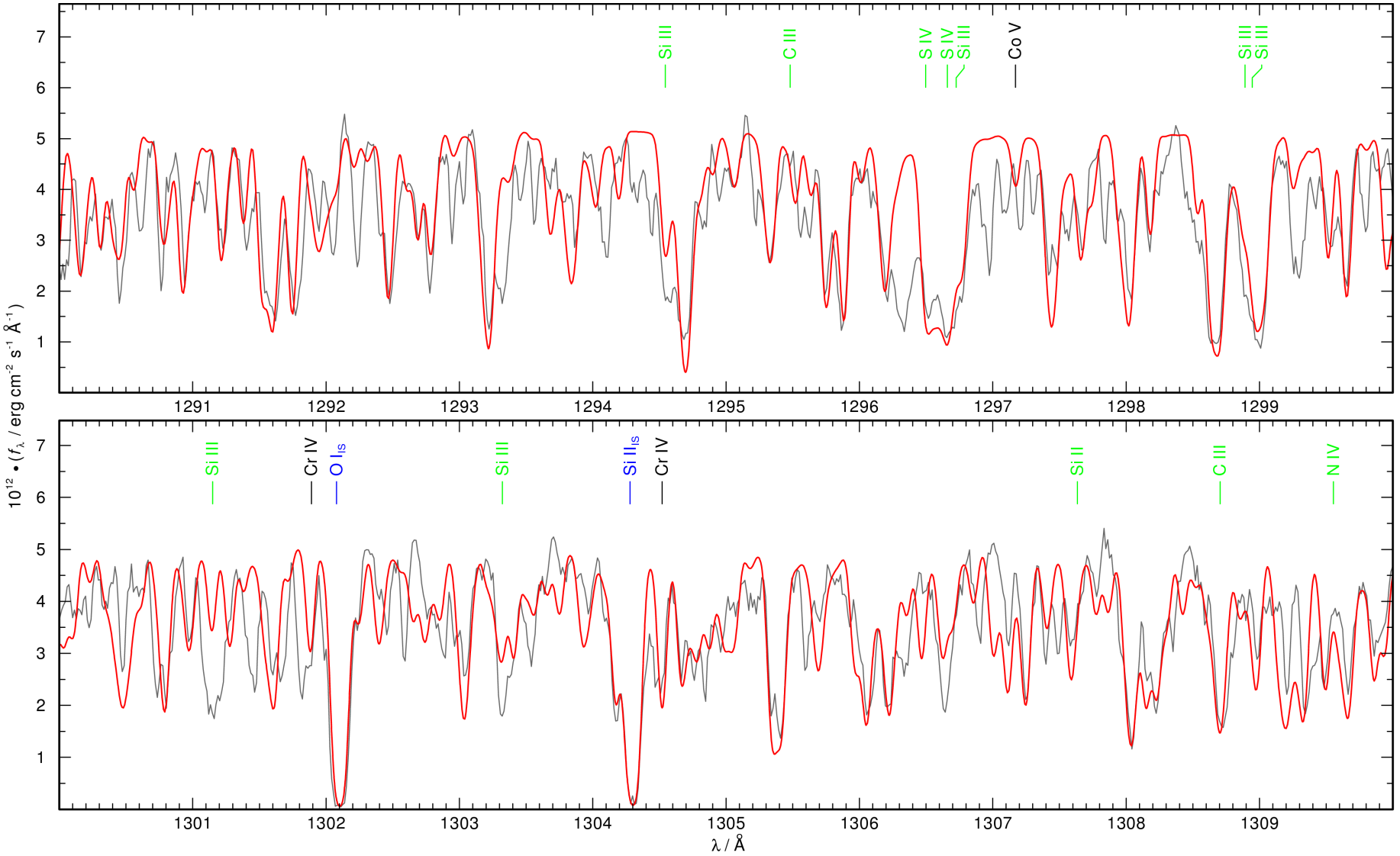

Figure 49: continued.

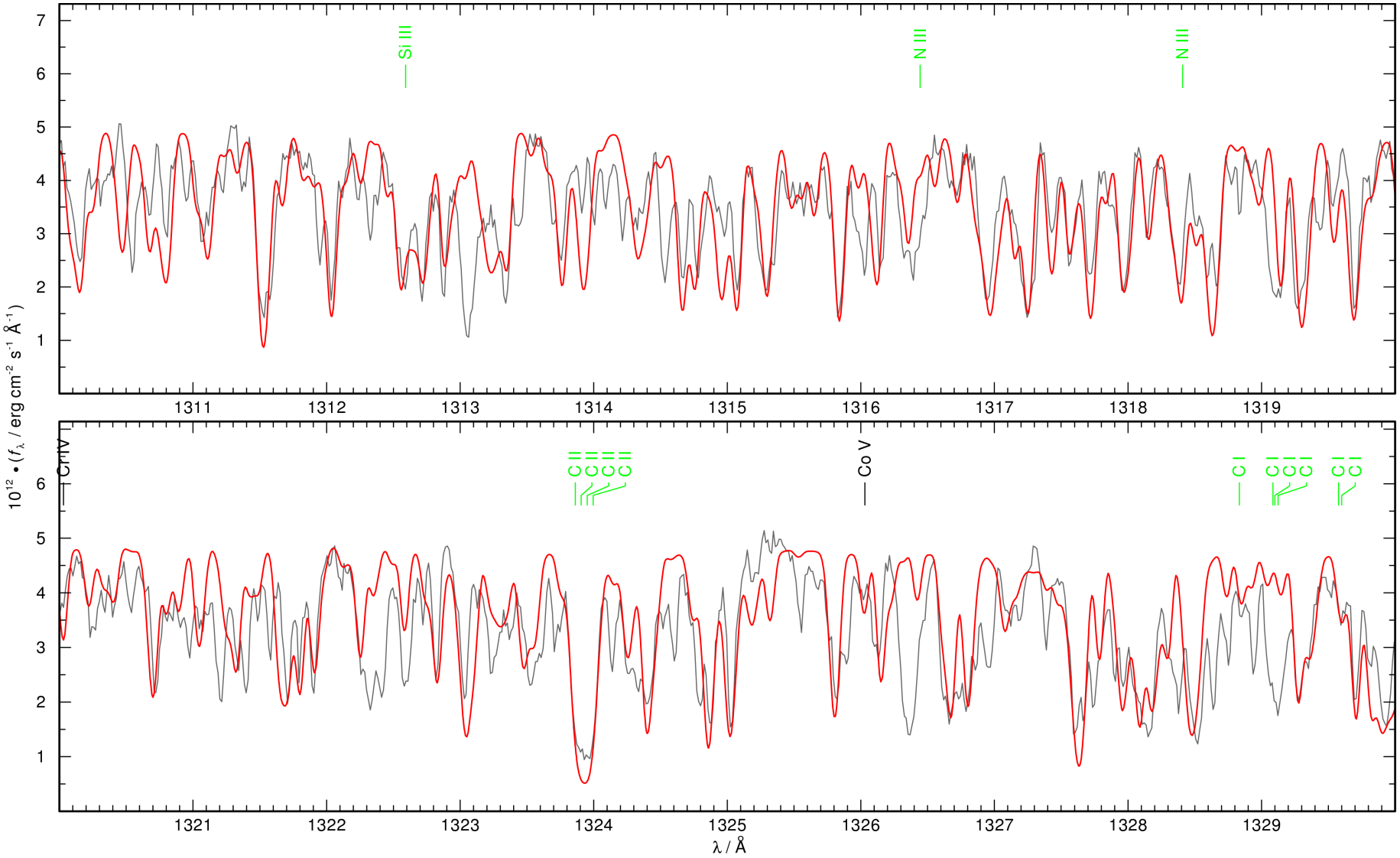

Figure 49: continued.

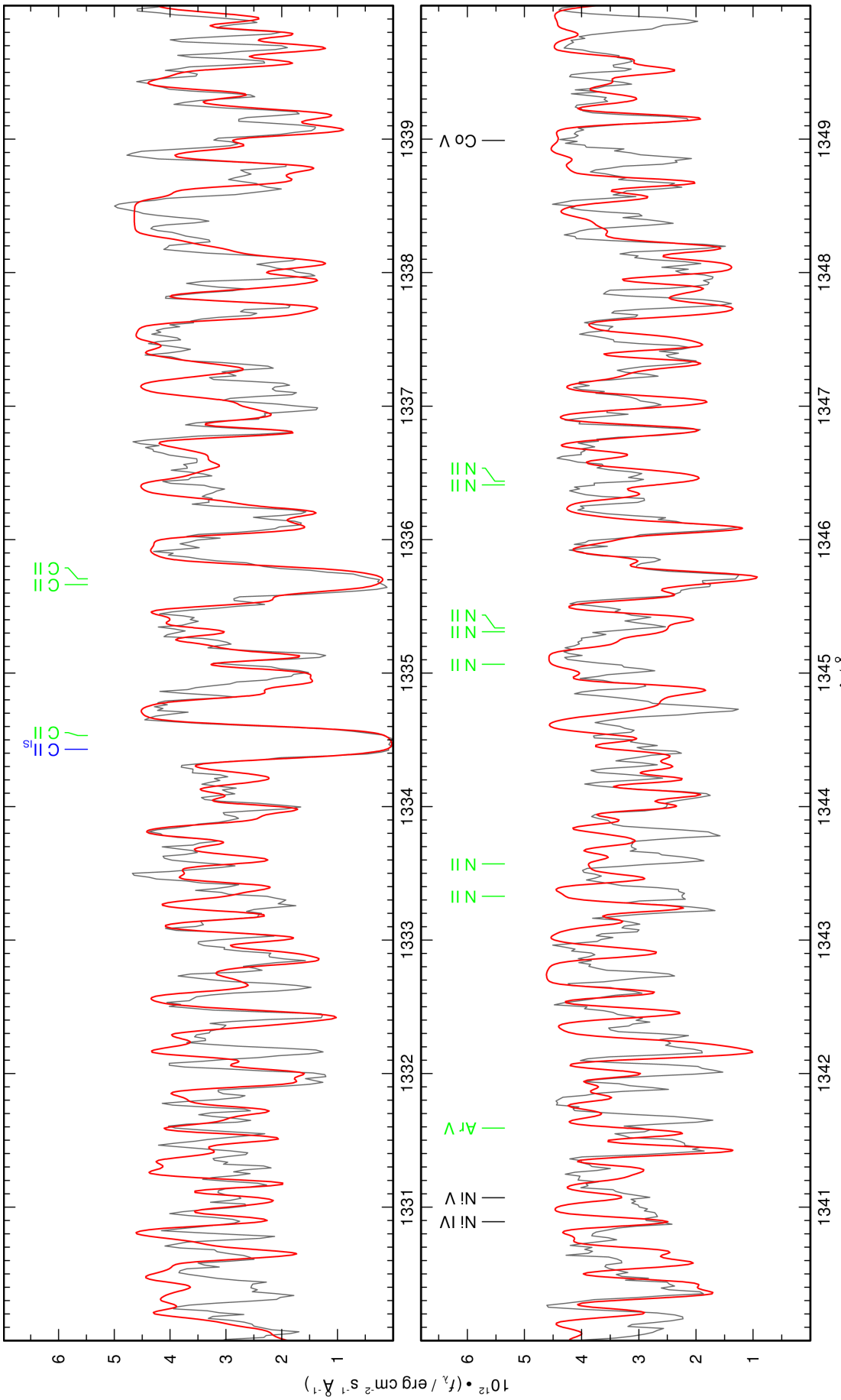

Figure 49: continued.

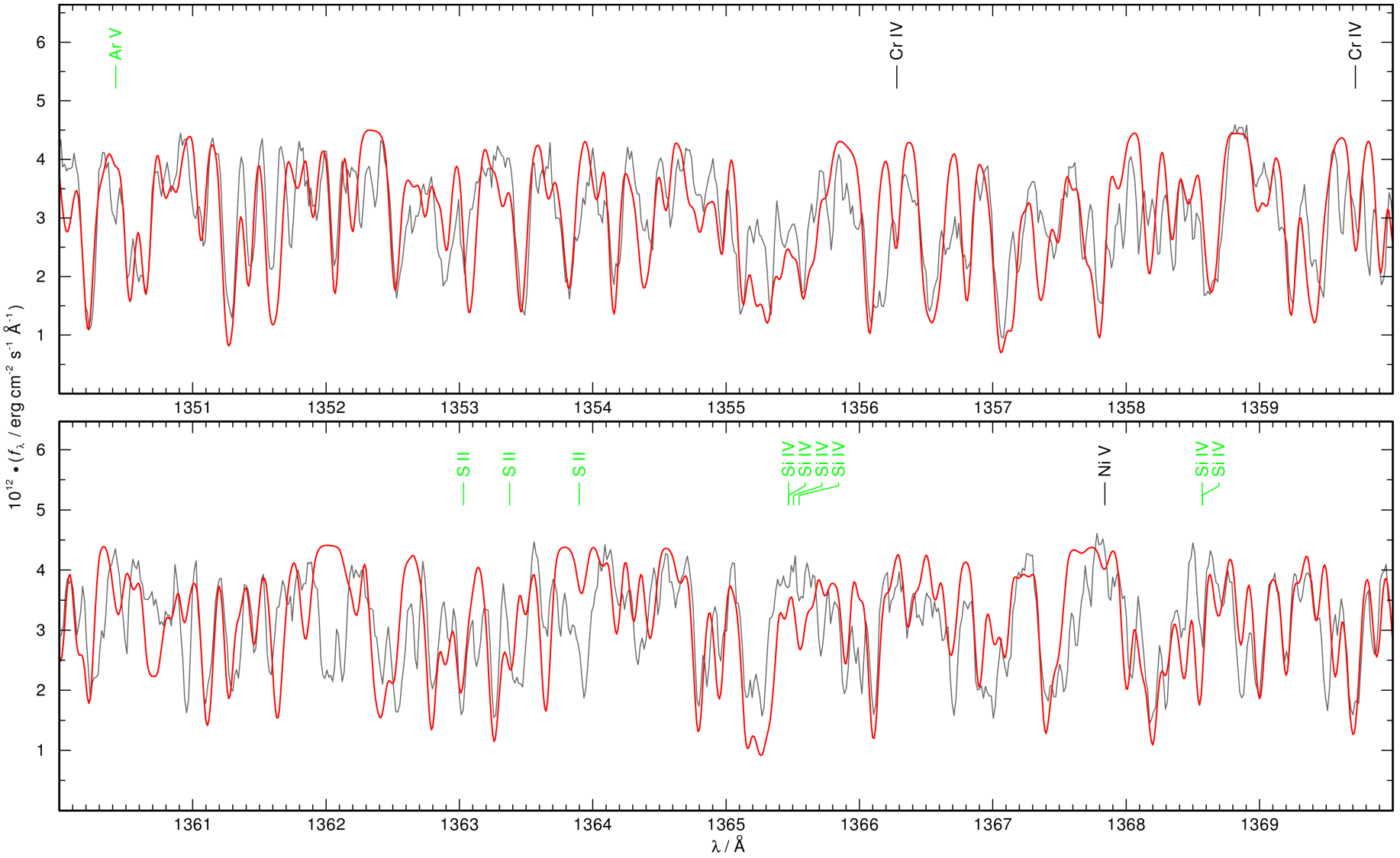

Figure 49: continued.

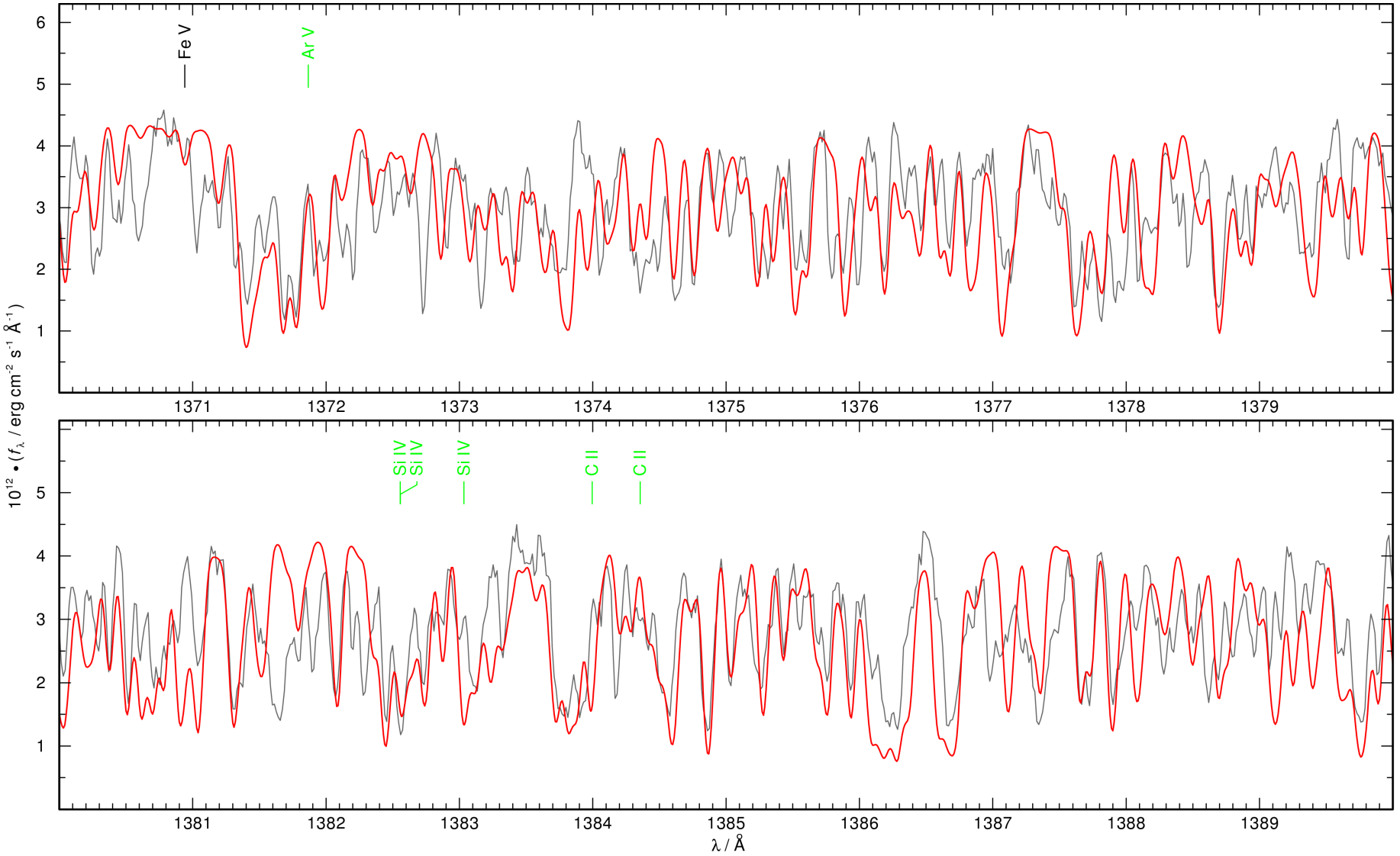

Figure 49: continued.

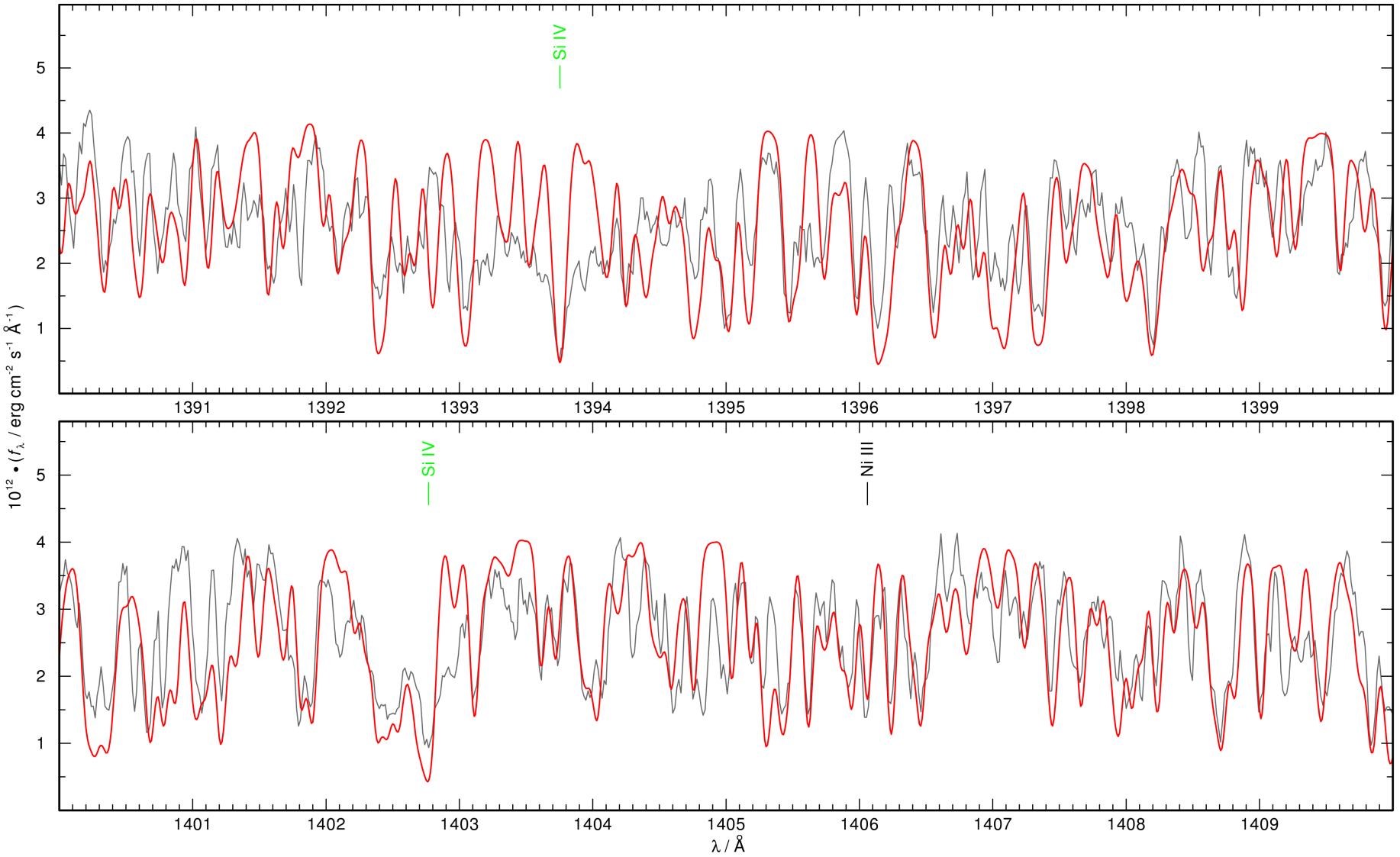

Figure 49: continued.

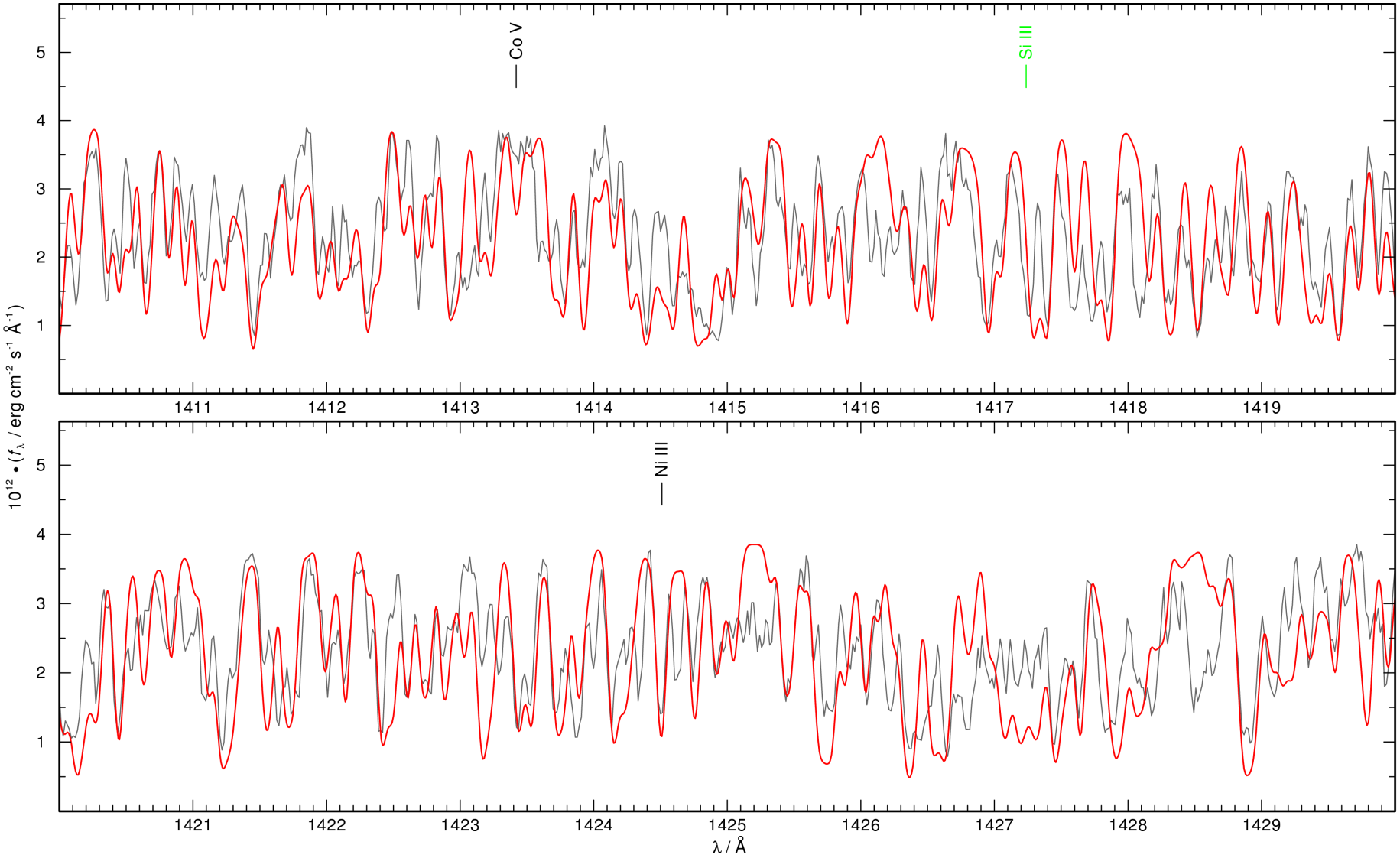

Figure 49: continued.

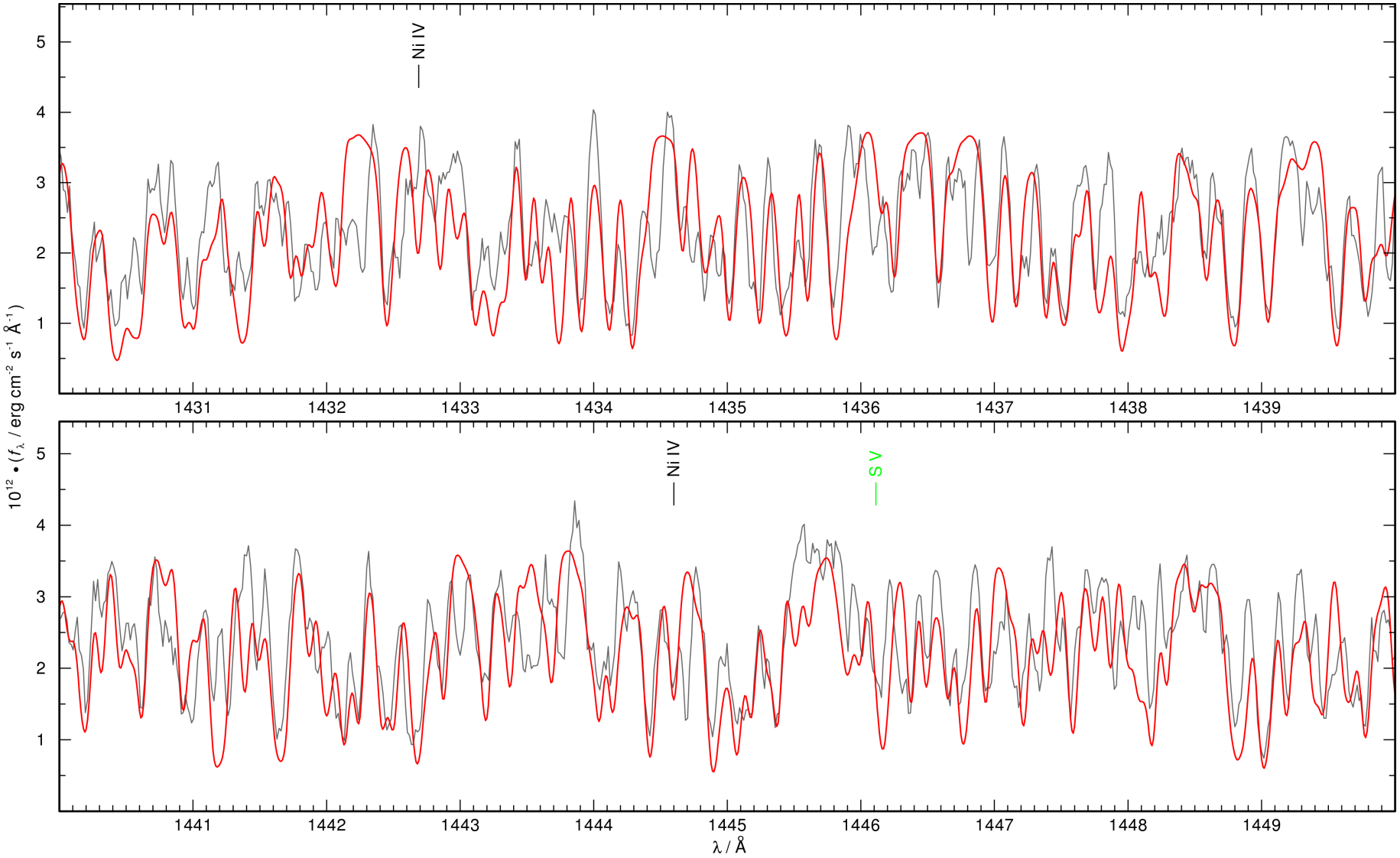

Figure 49: continued.

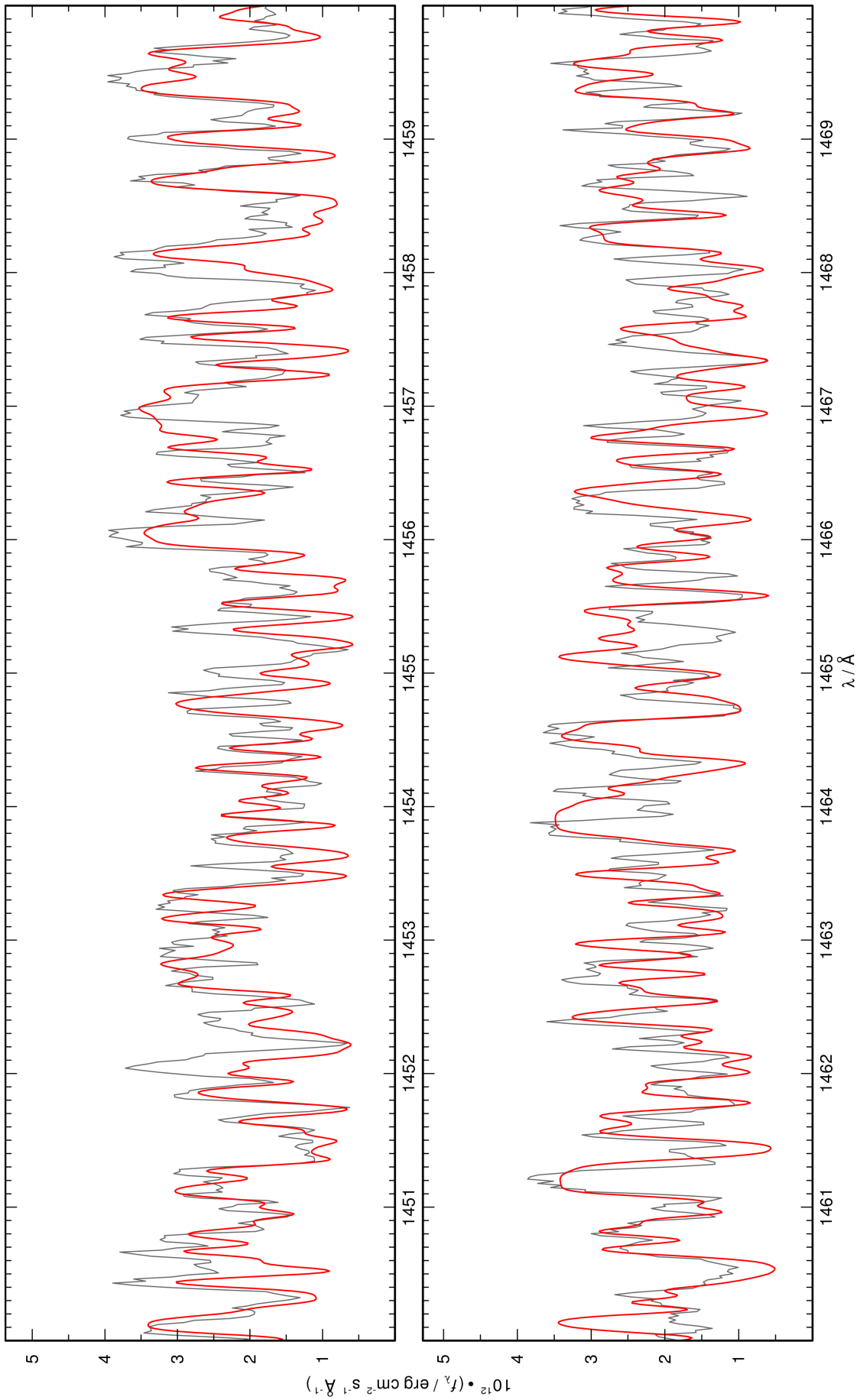

Figure 49: continued.

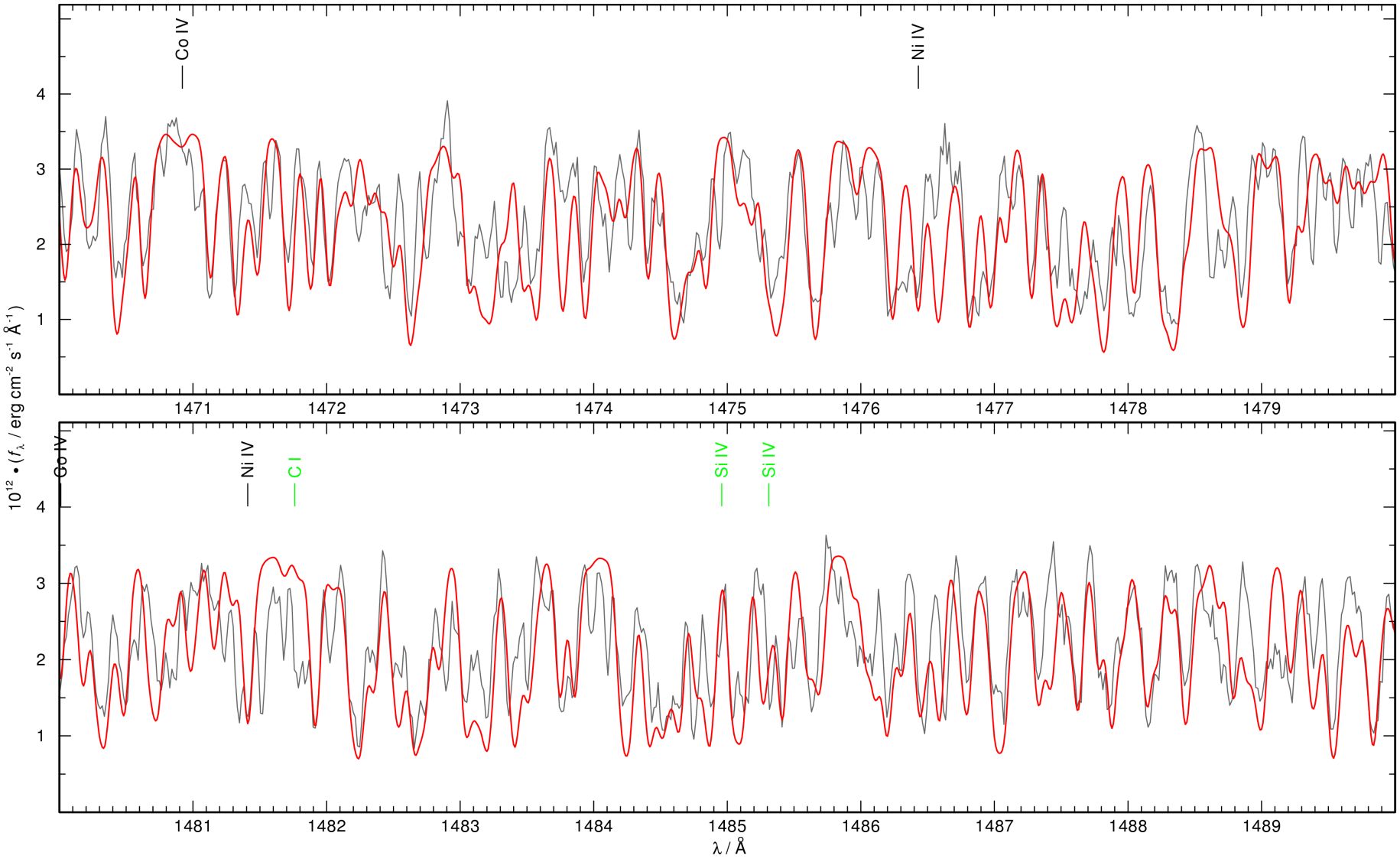

Figure 49: continued.

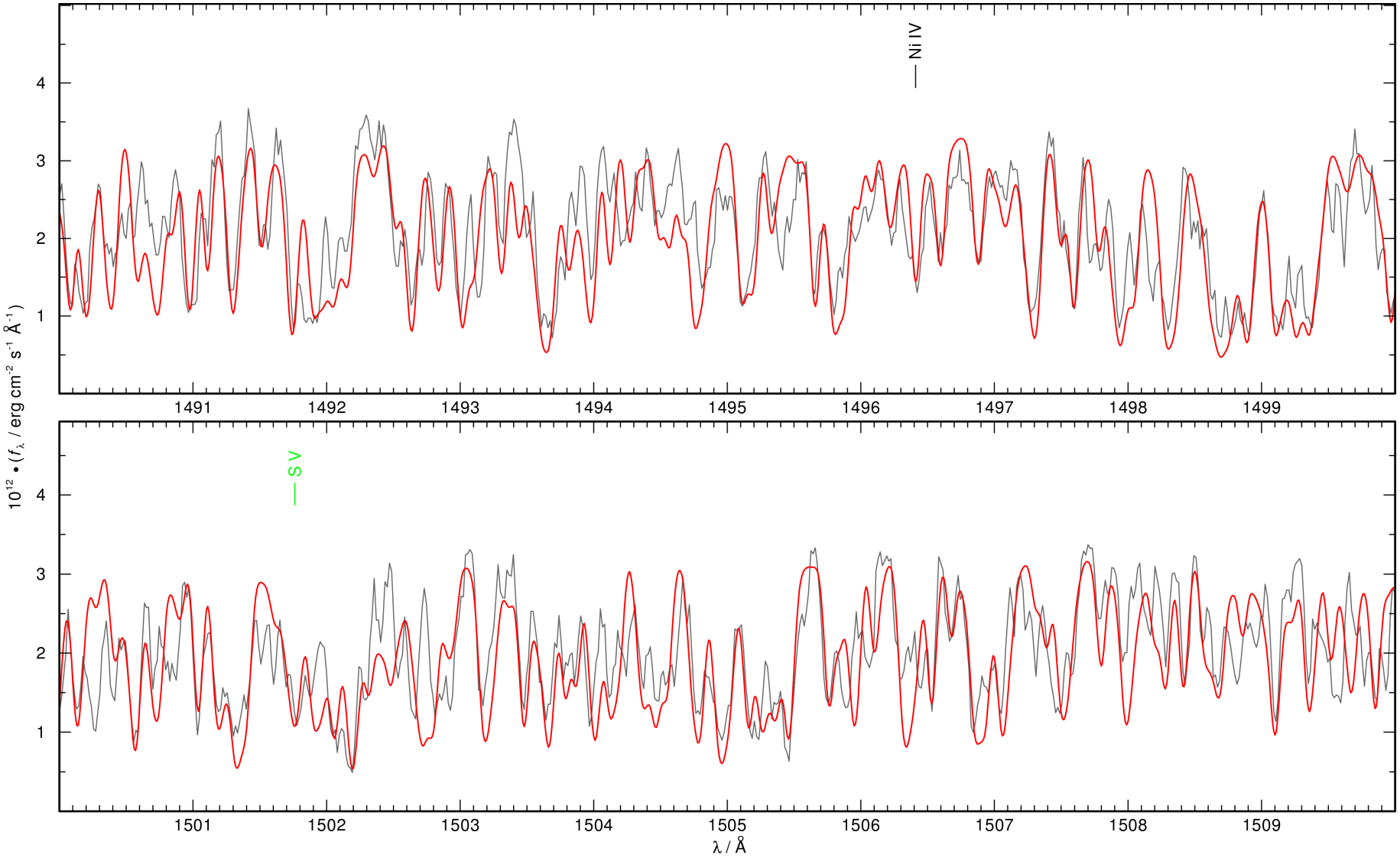

Figure 49: continued.

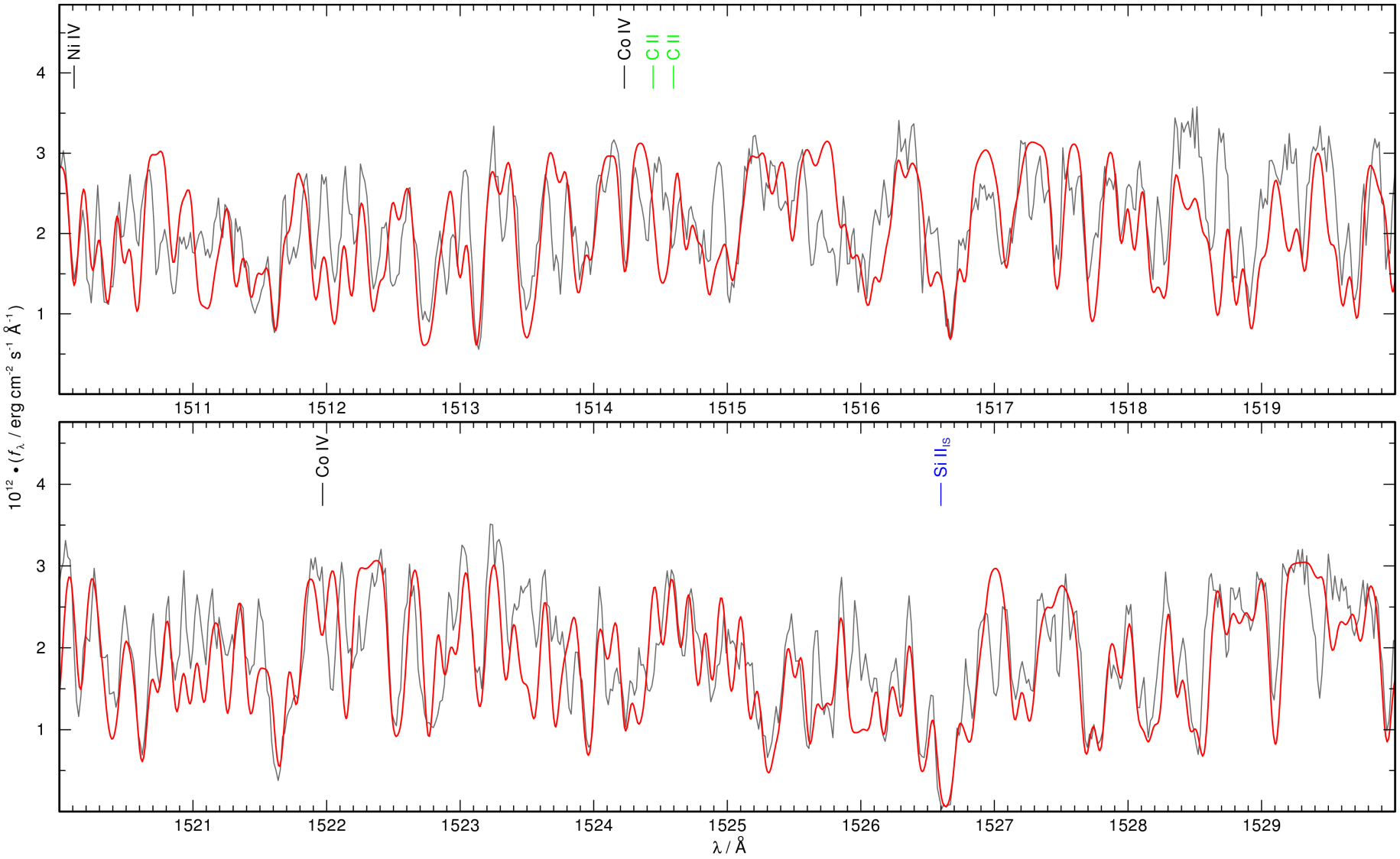

Figure 49: continued.

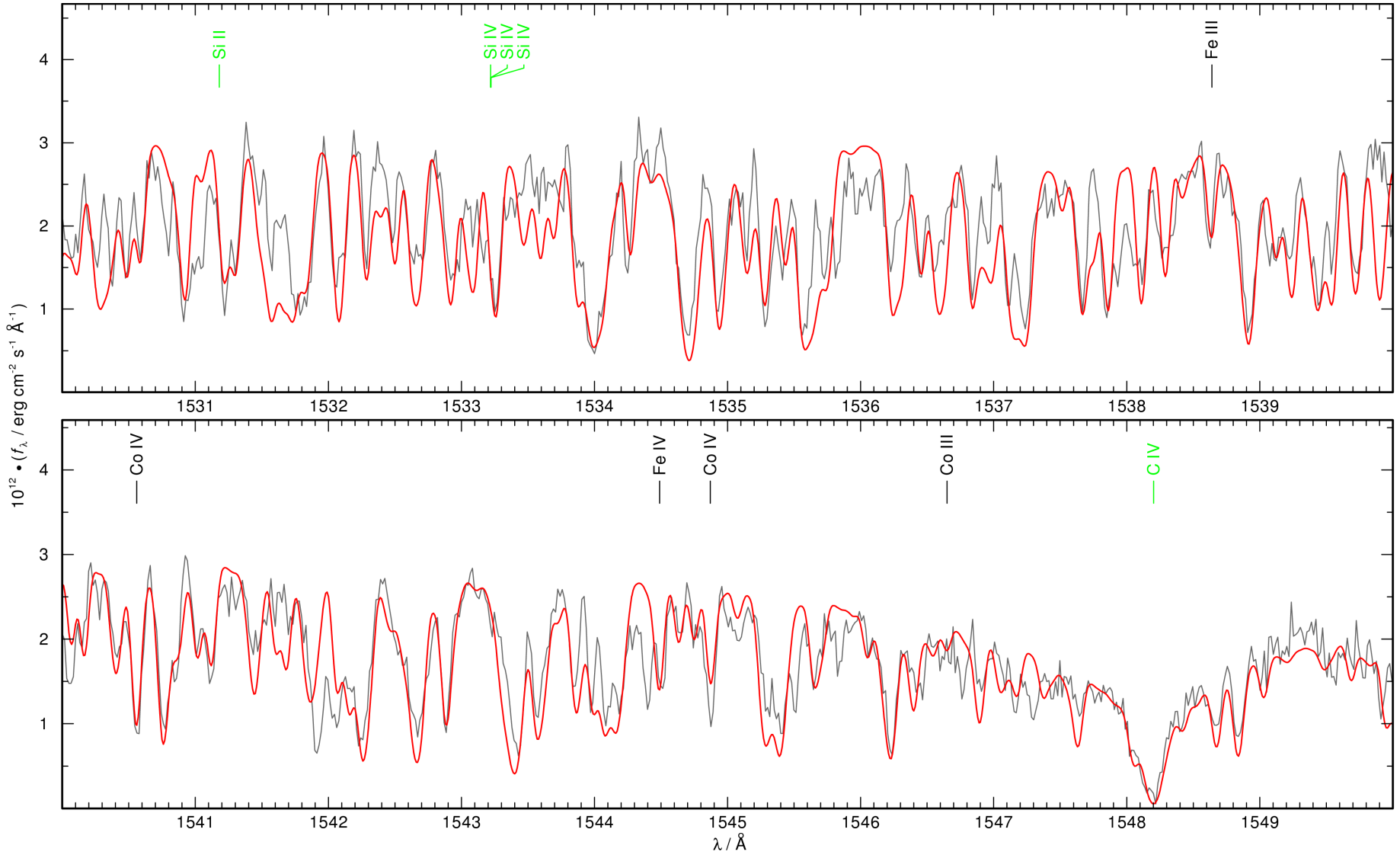

Figure 49: continued.

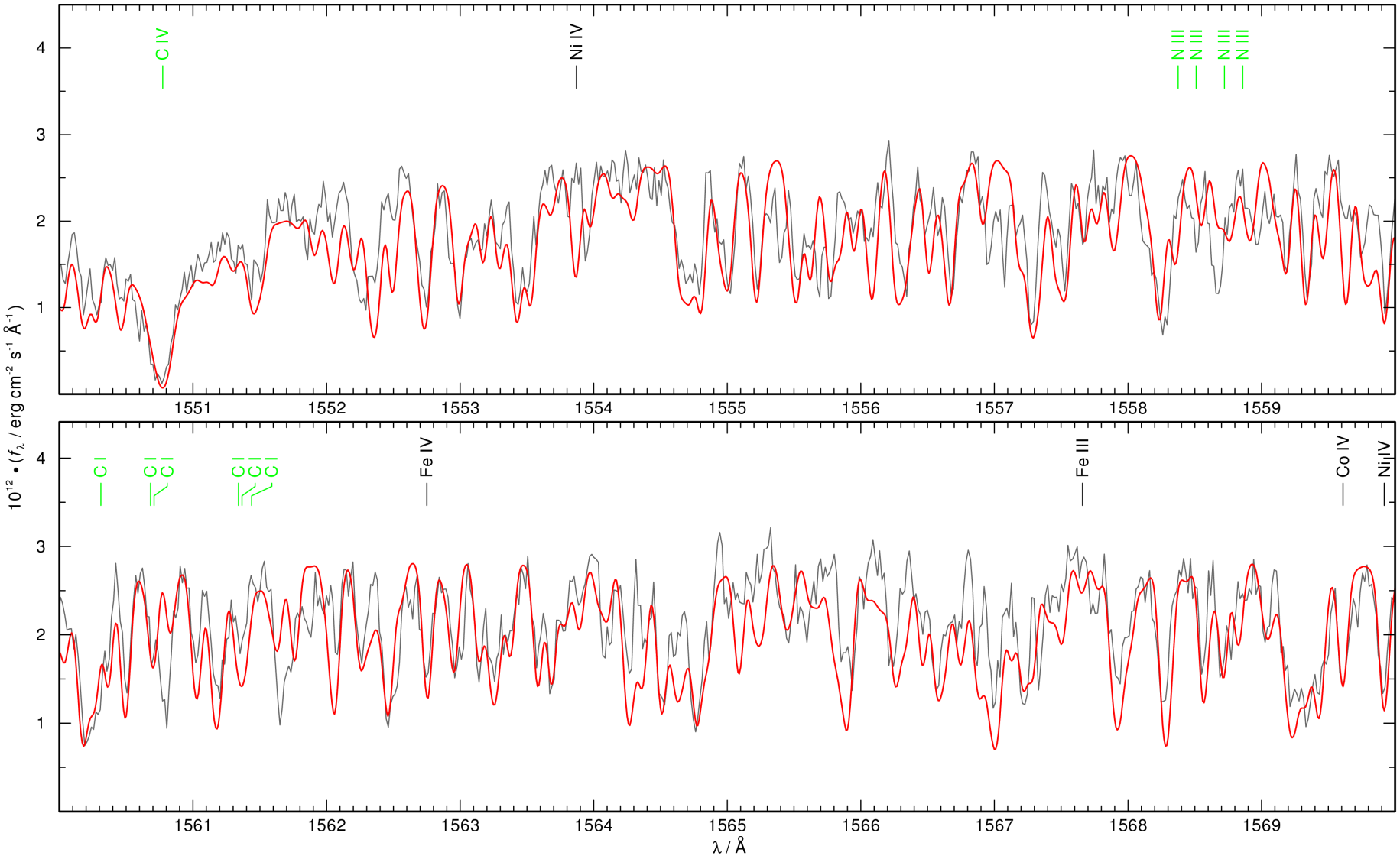

Figure 49: continued.

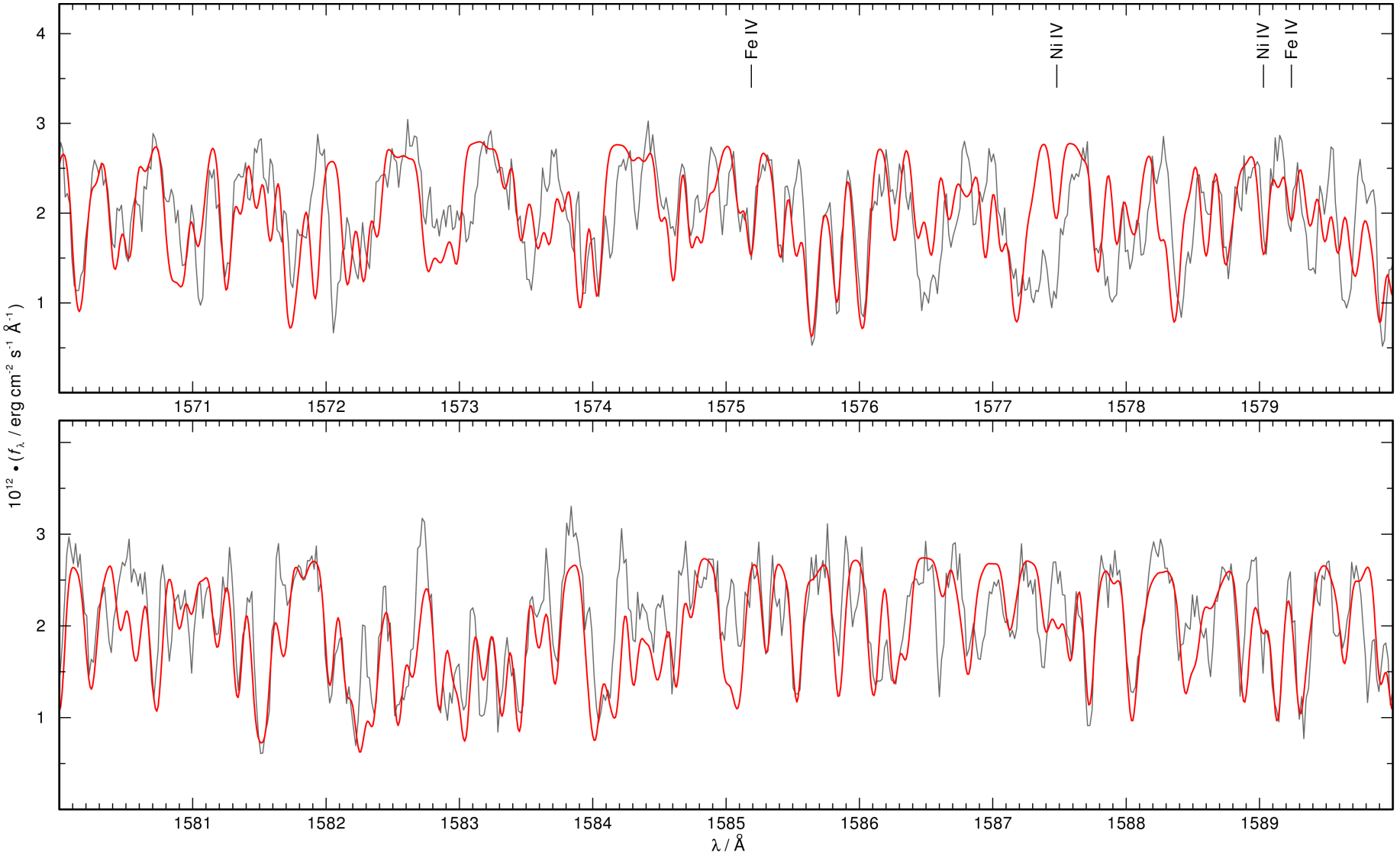

Figure 49: continued.

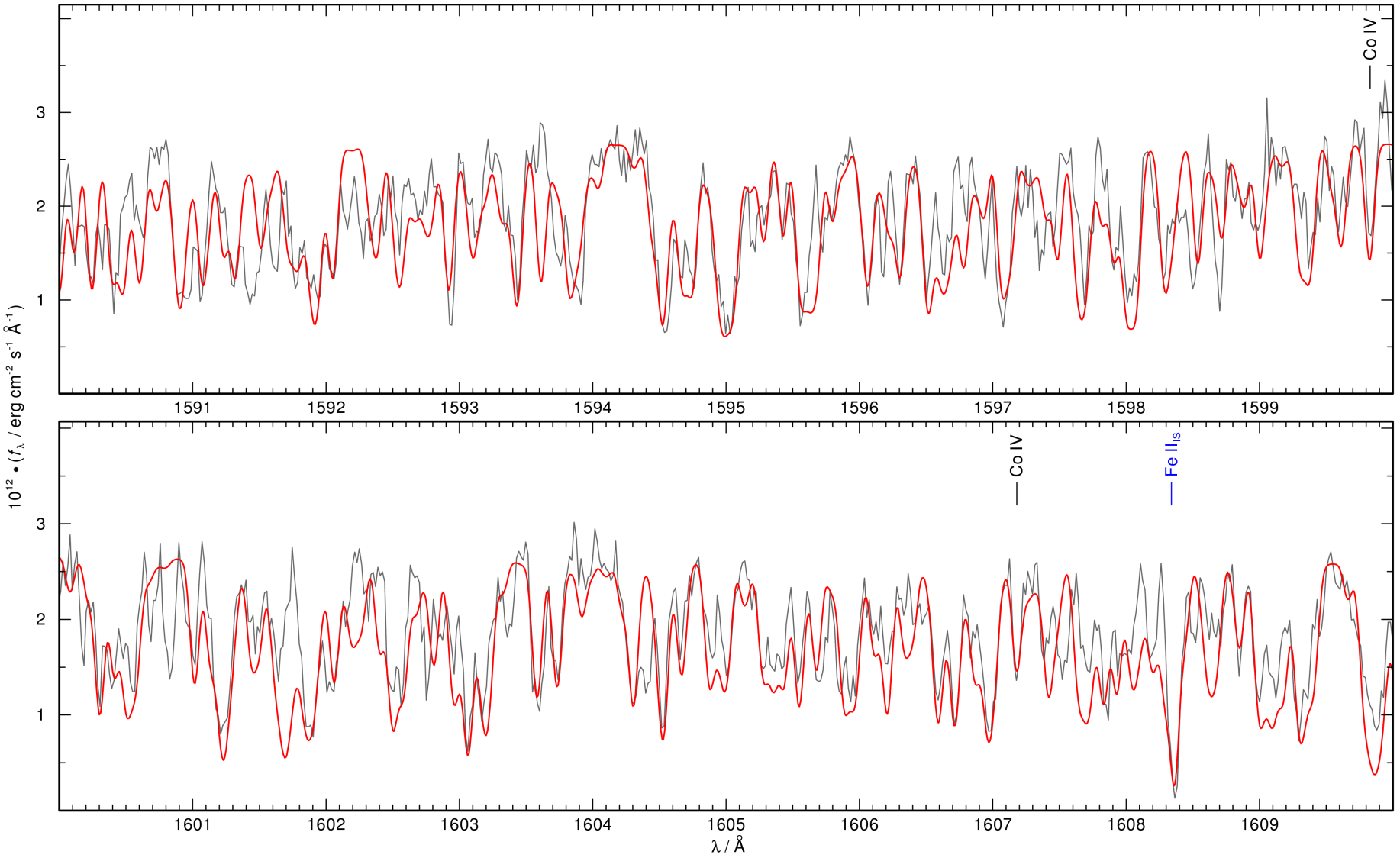

Figure 49: continued.

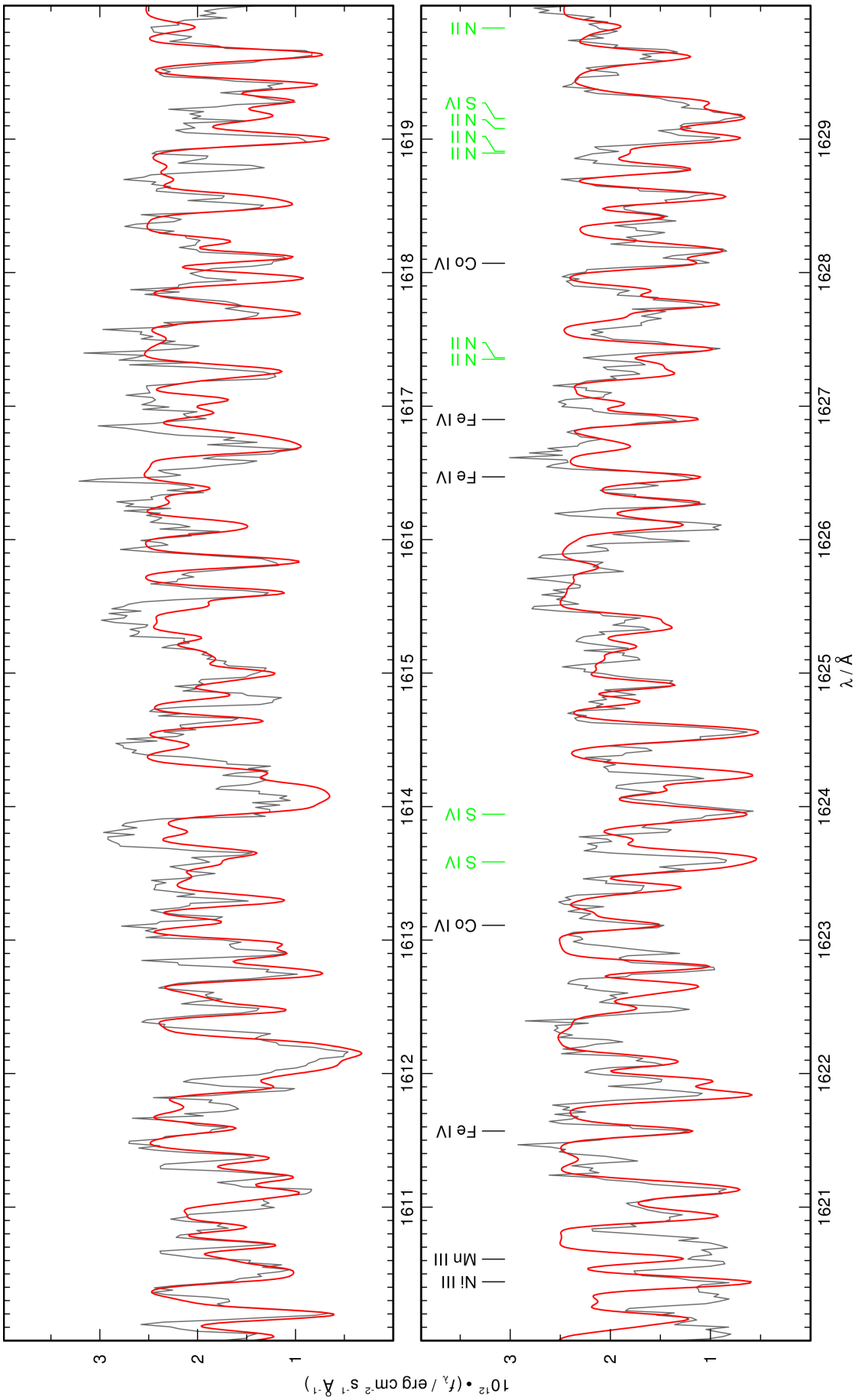

Figure 49: continued.

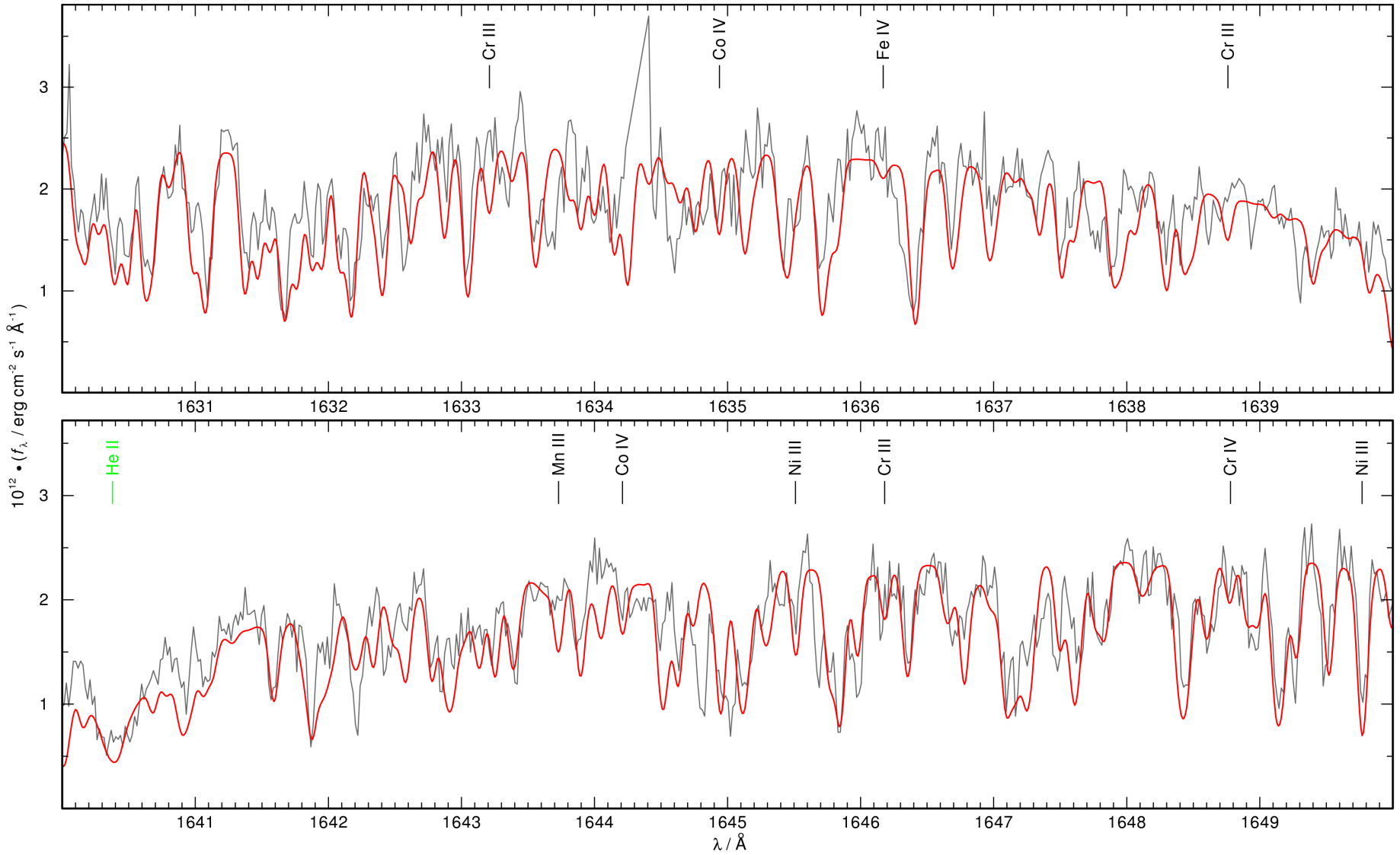

Figure 49: continued.

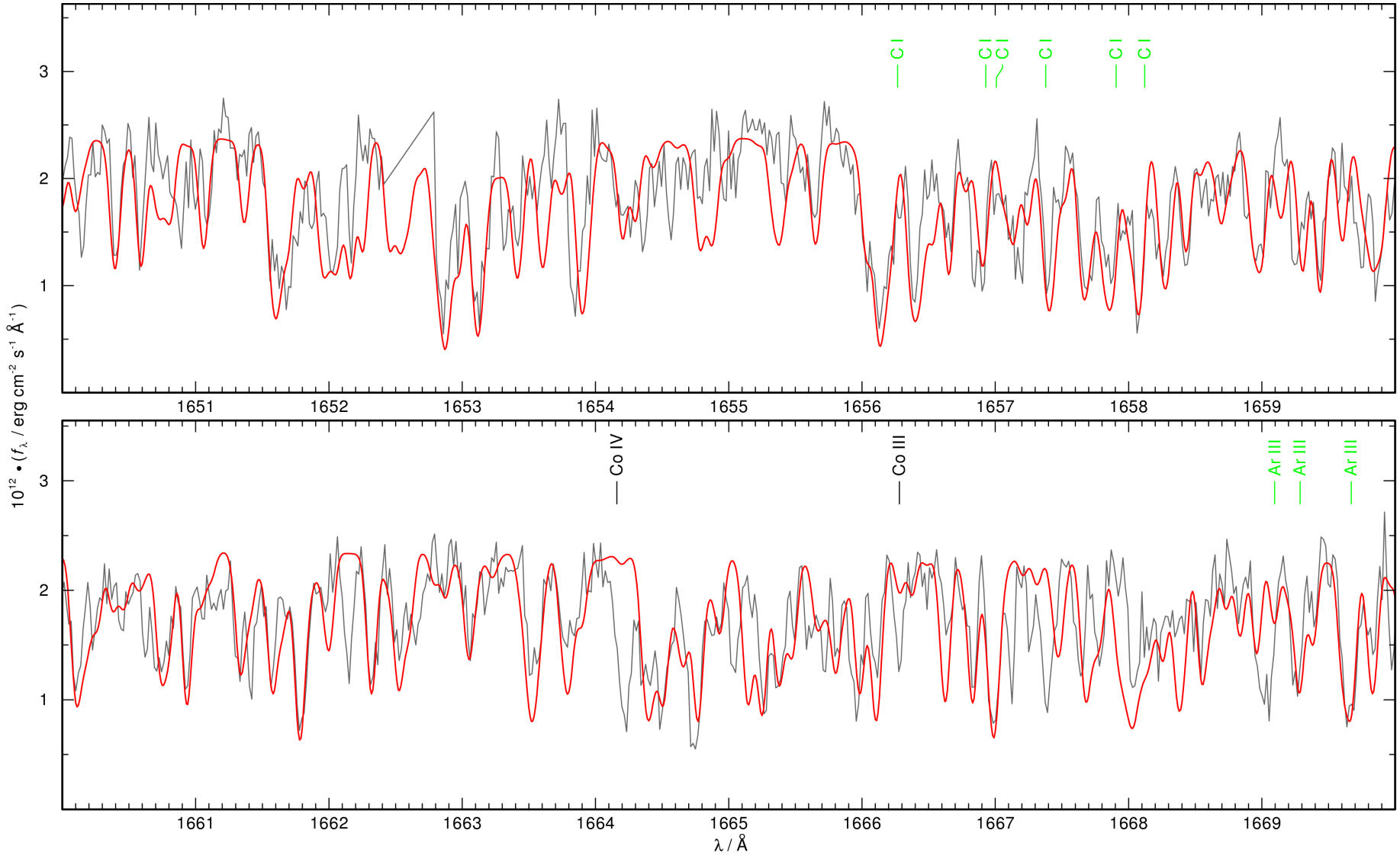

Figure 49: continued.

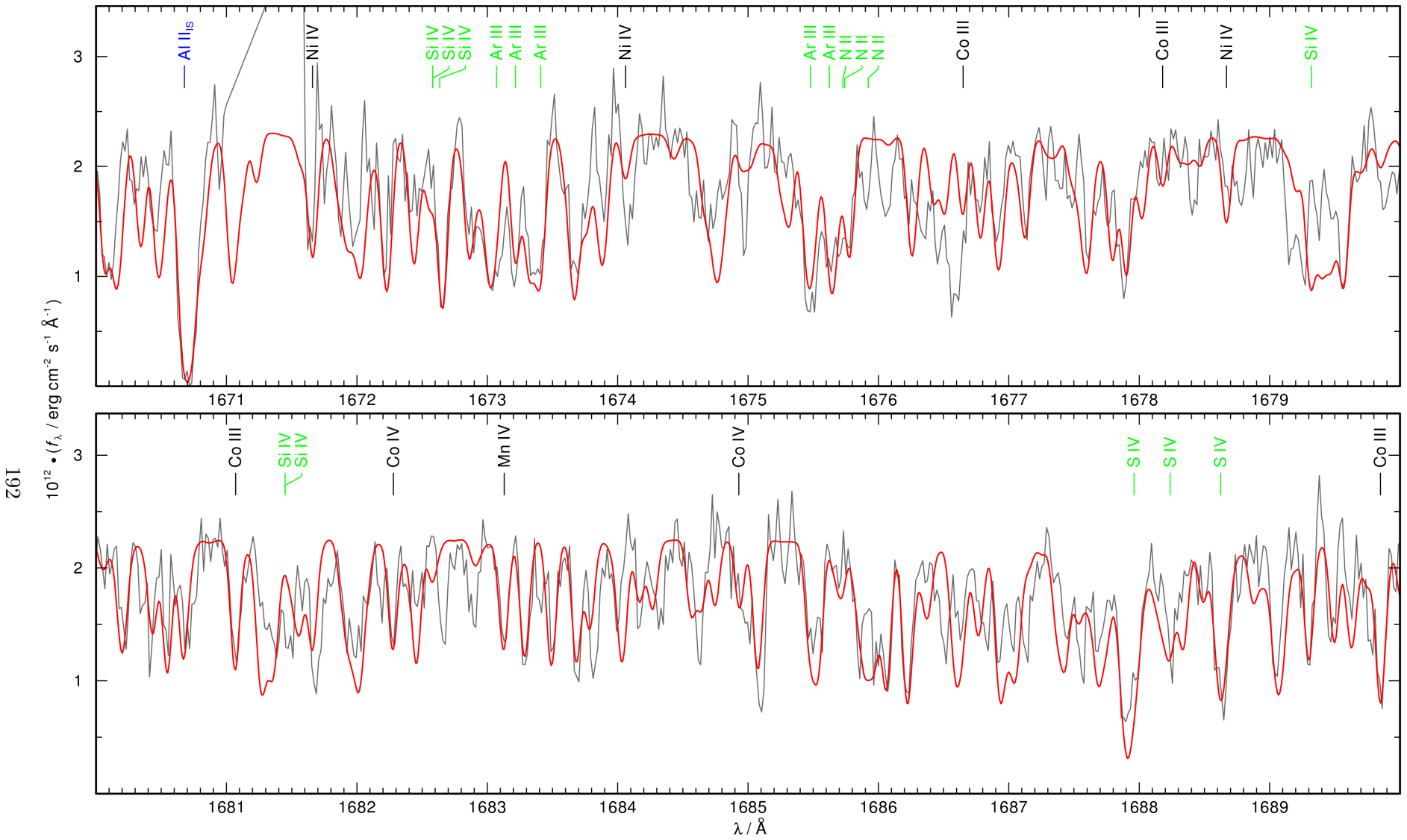

Figure 49: continued.

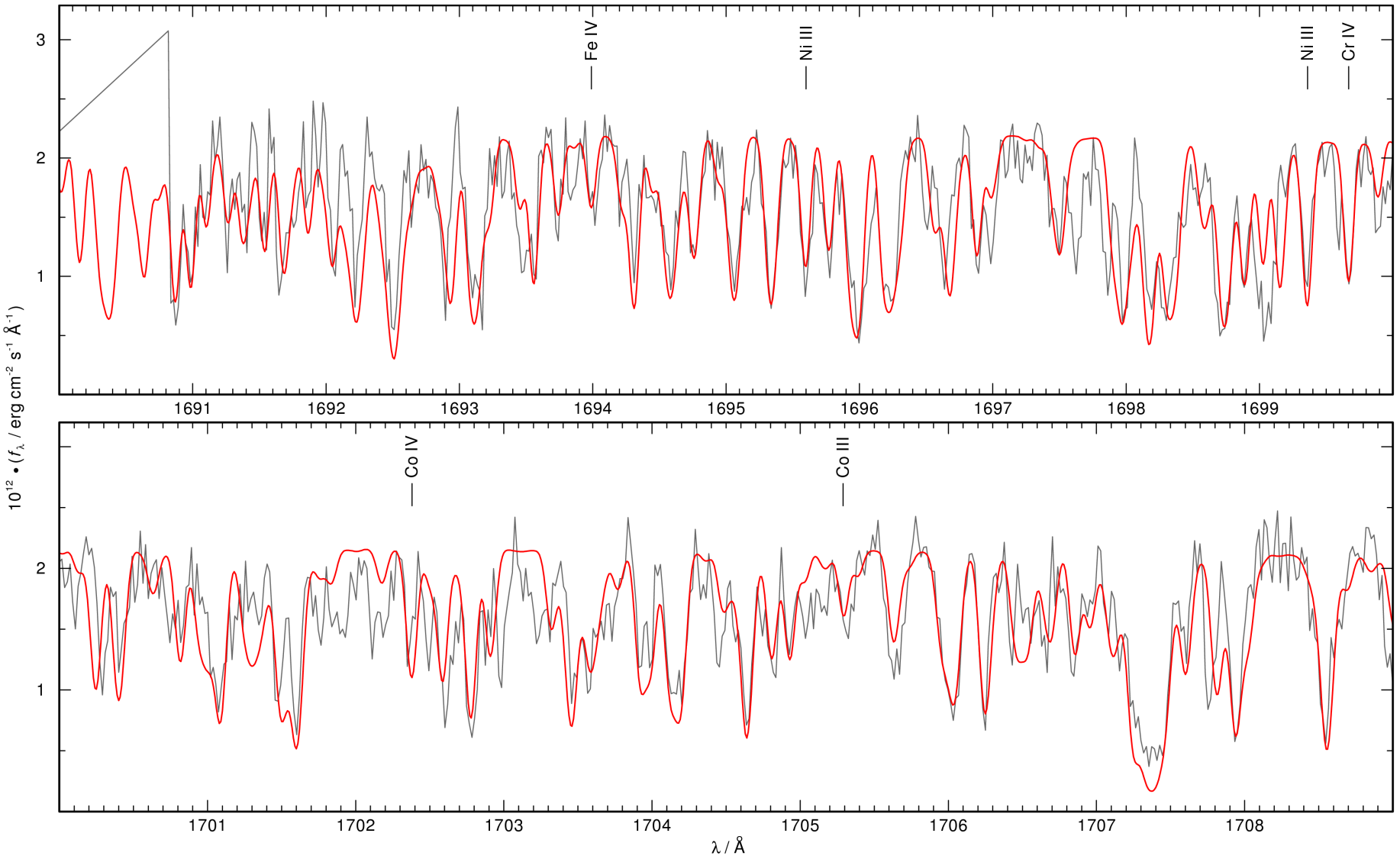

Figure 49: continued.

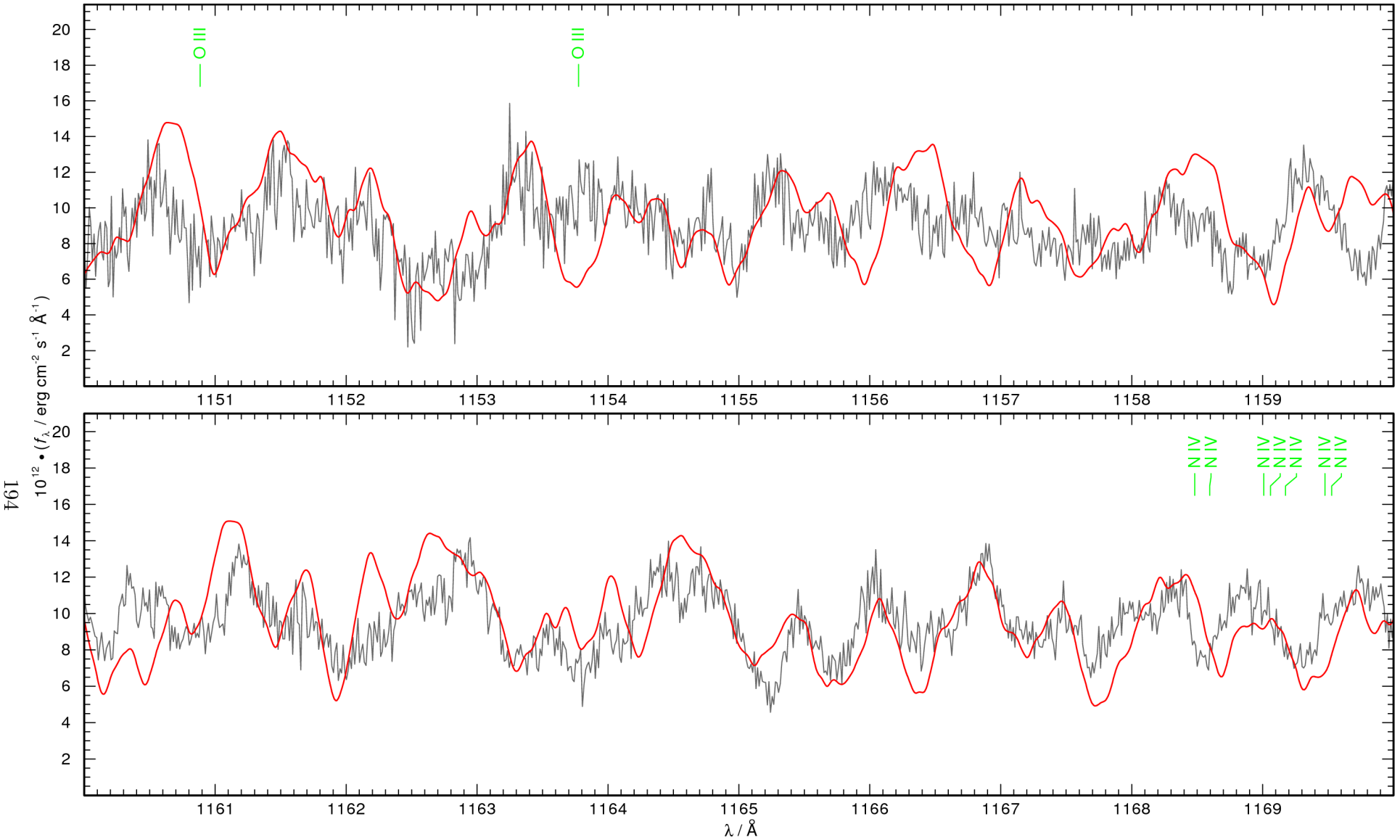

Figure 50: Like Fig. 48, for EC 11481–2303.

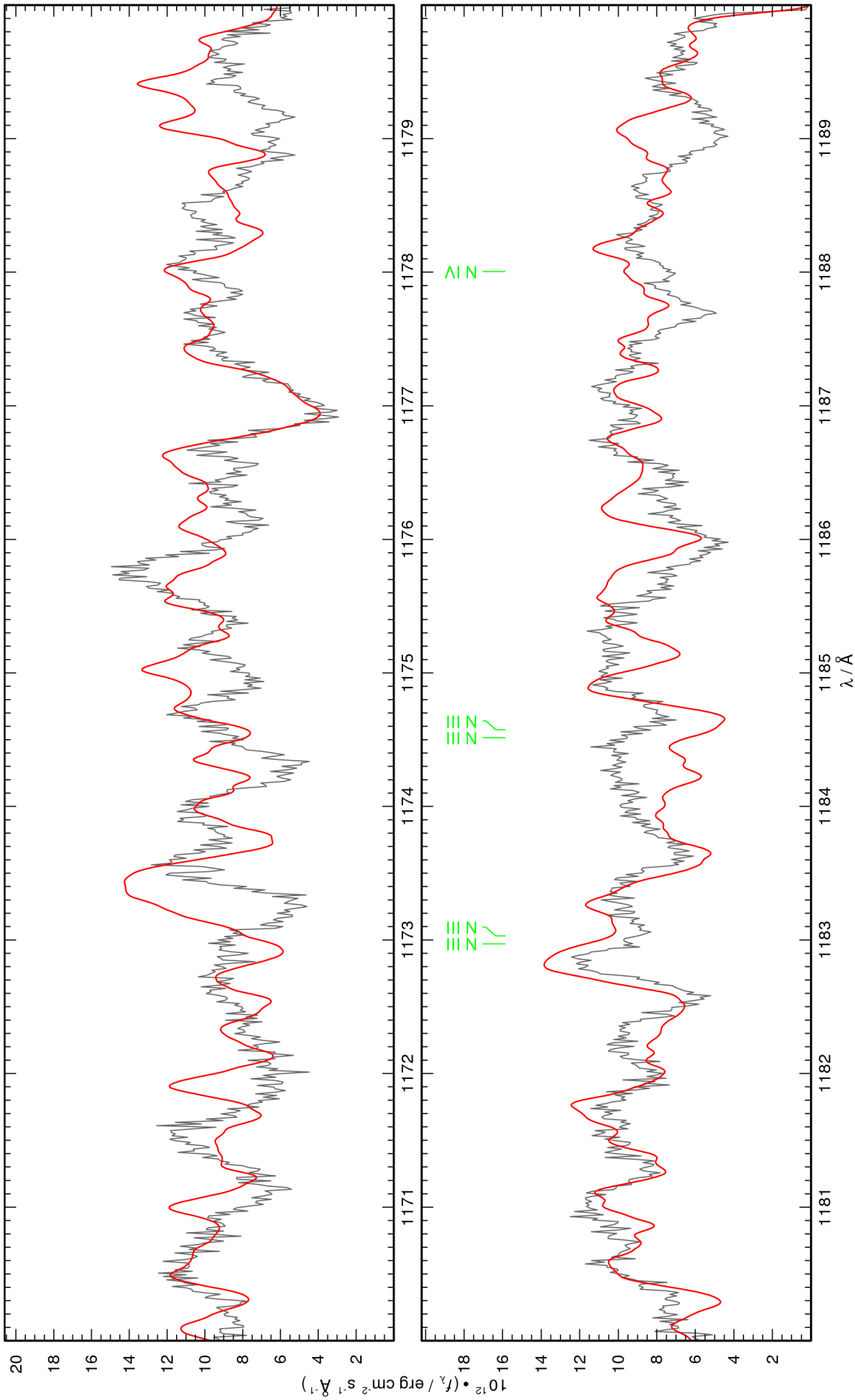

Figure 50: continued.

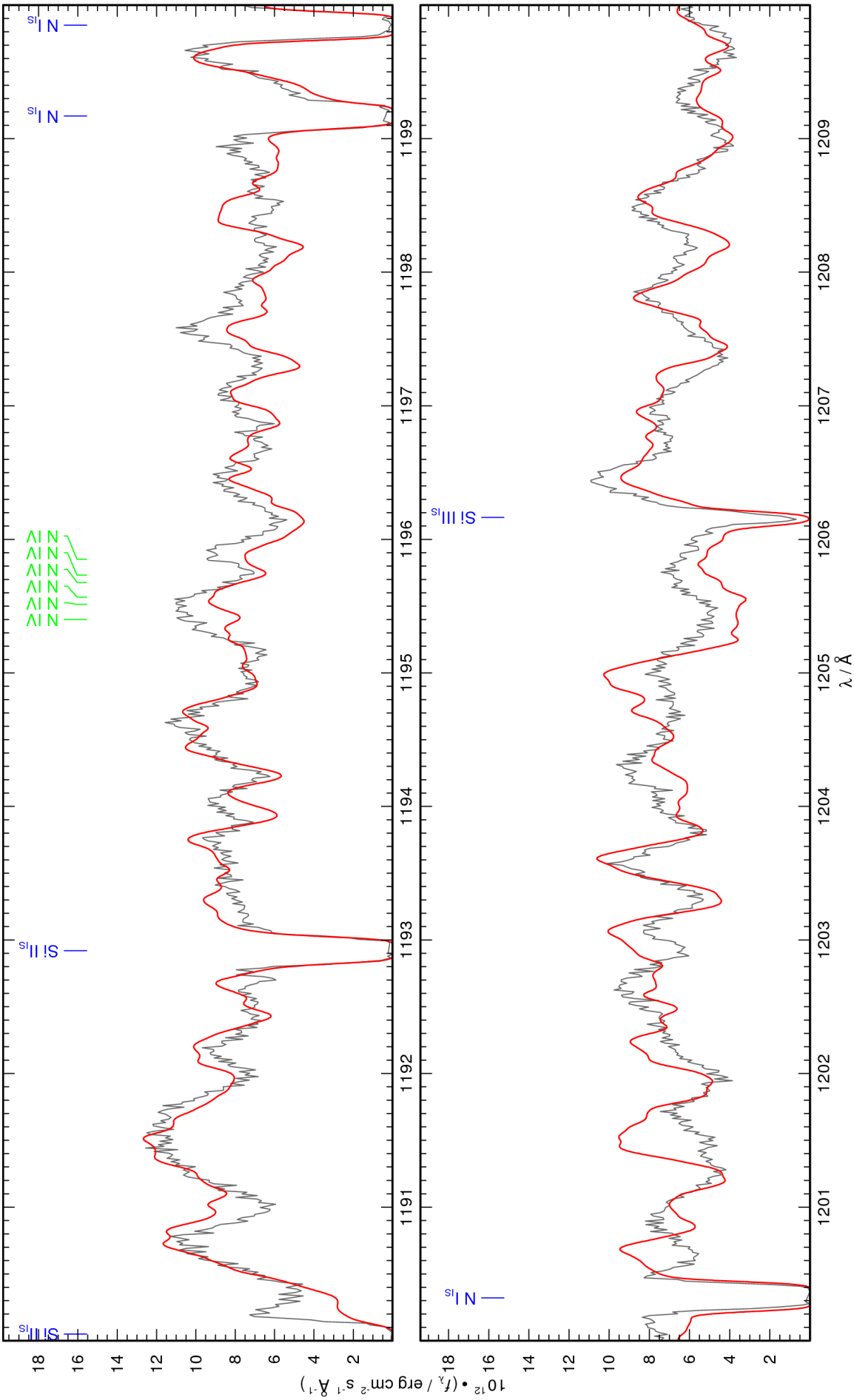

Figure 50: continued.

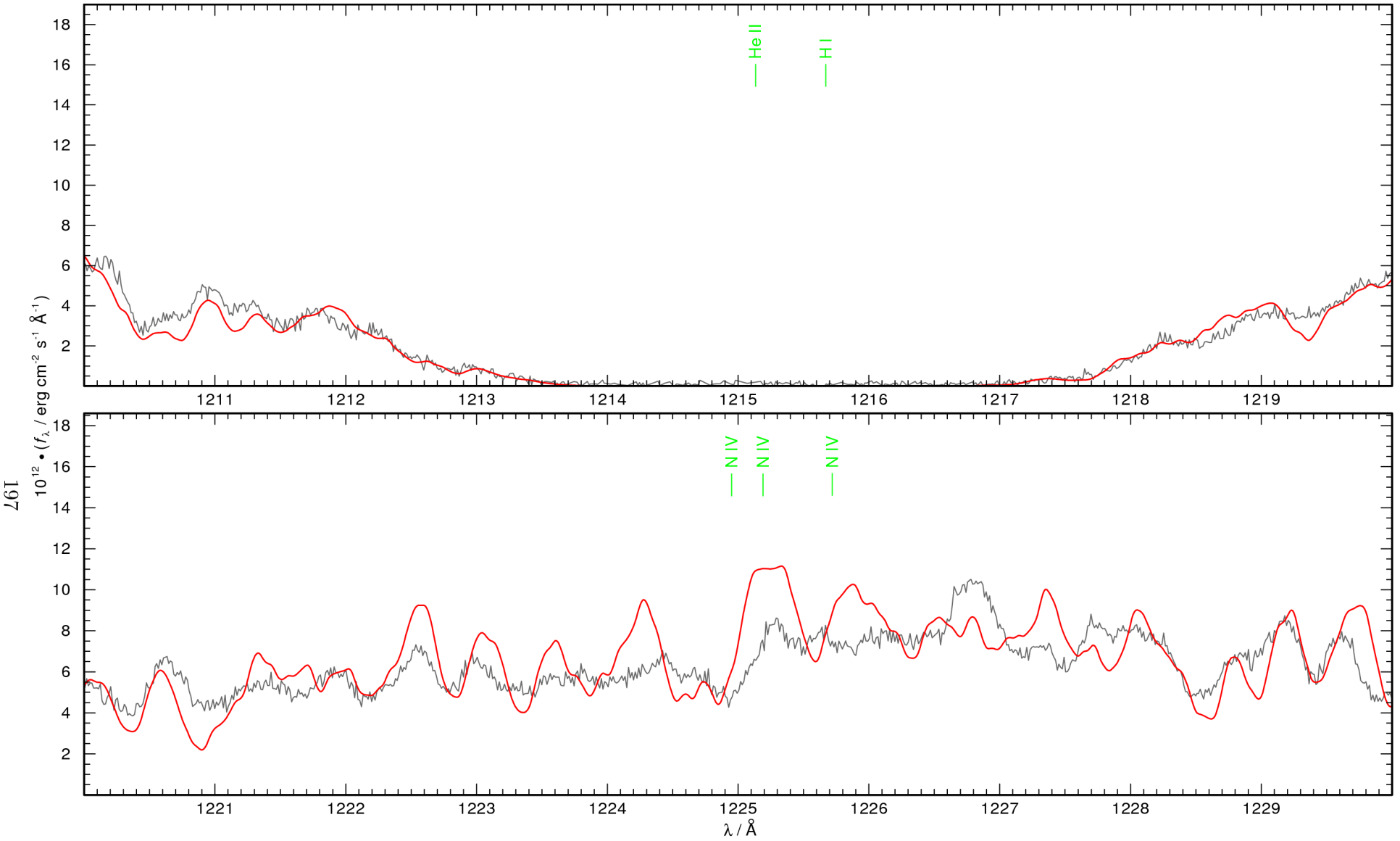

Figure 50: continued.

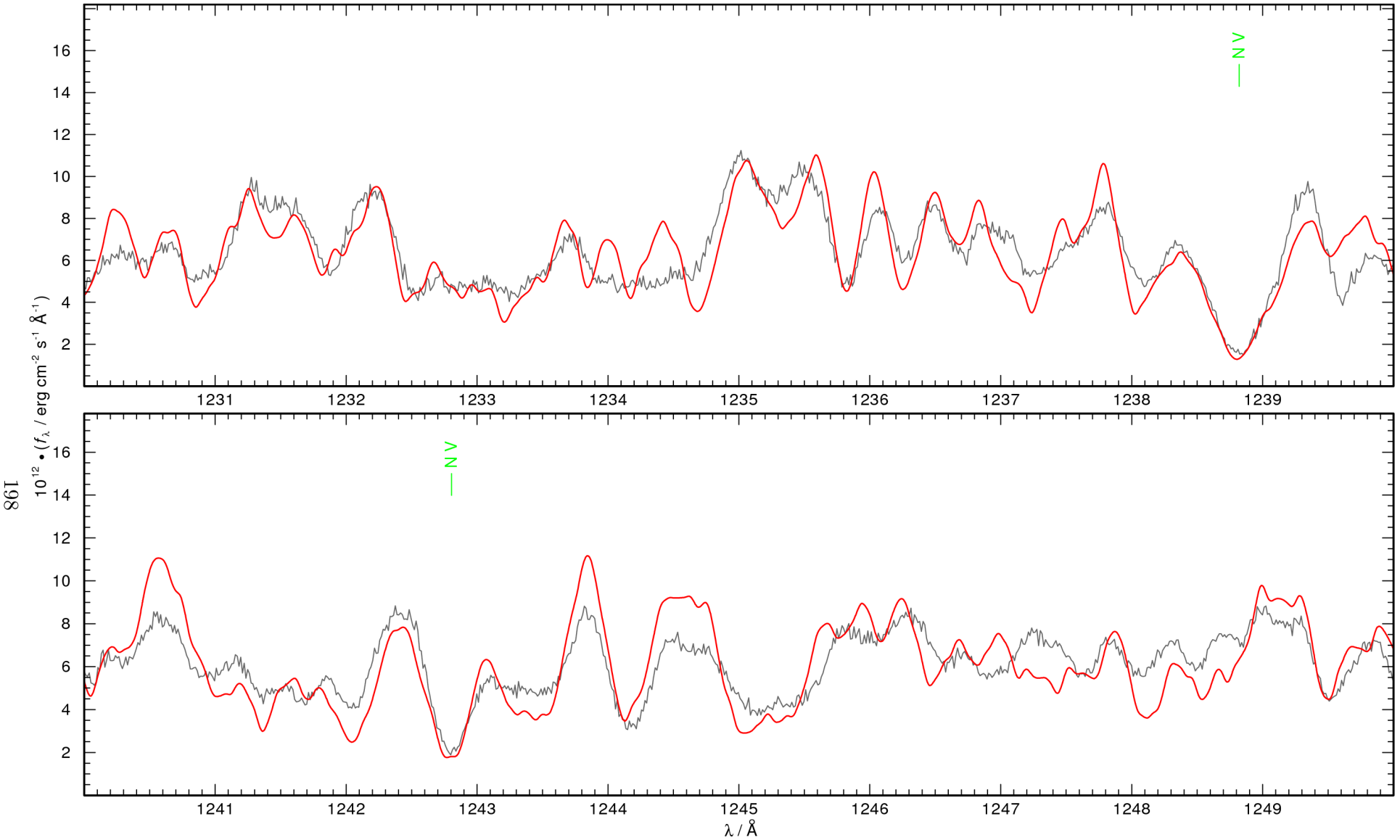

Figure 50: continued.

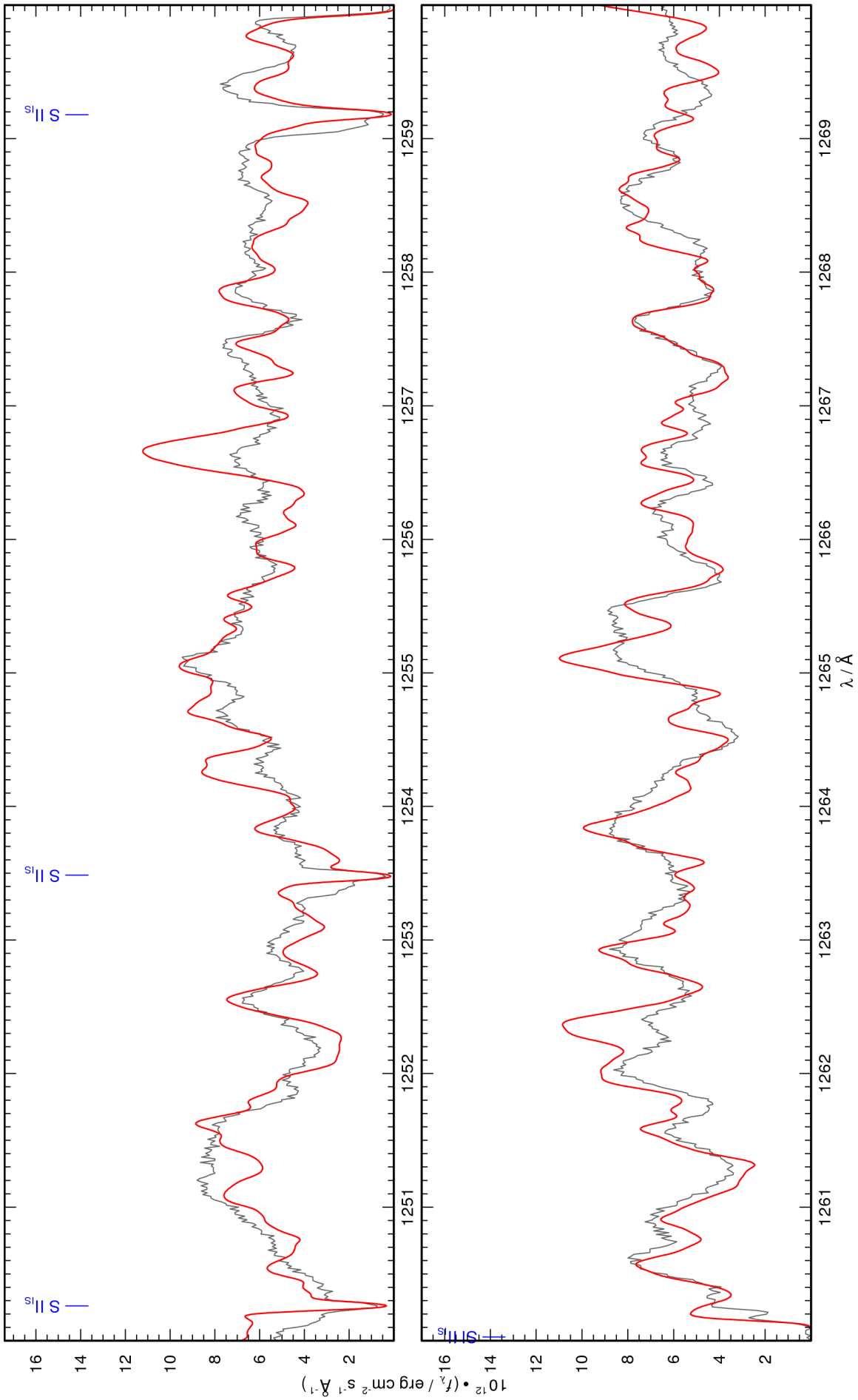

Figure 50: continued.

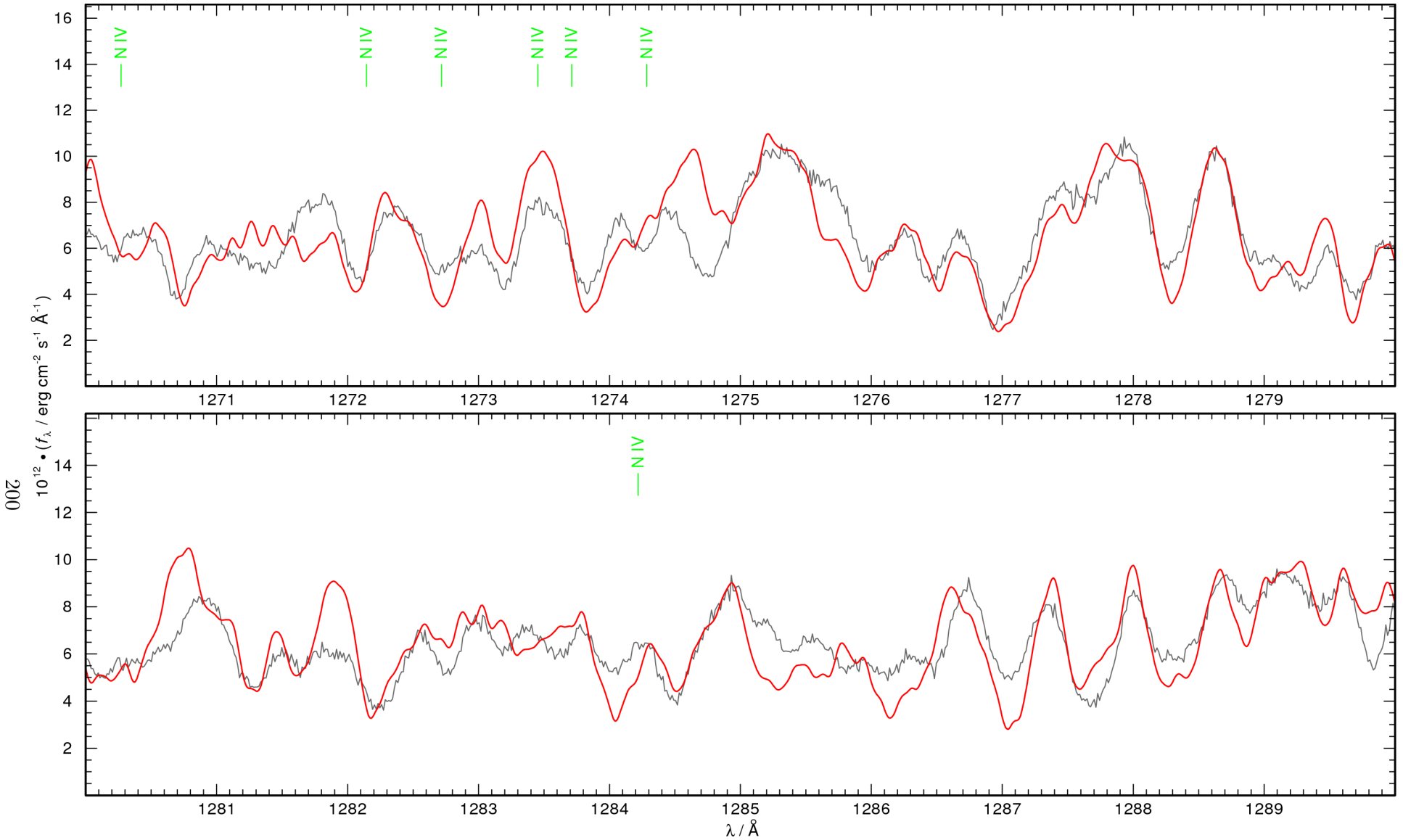

Figure 50: continued.

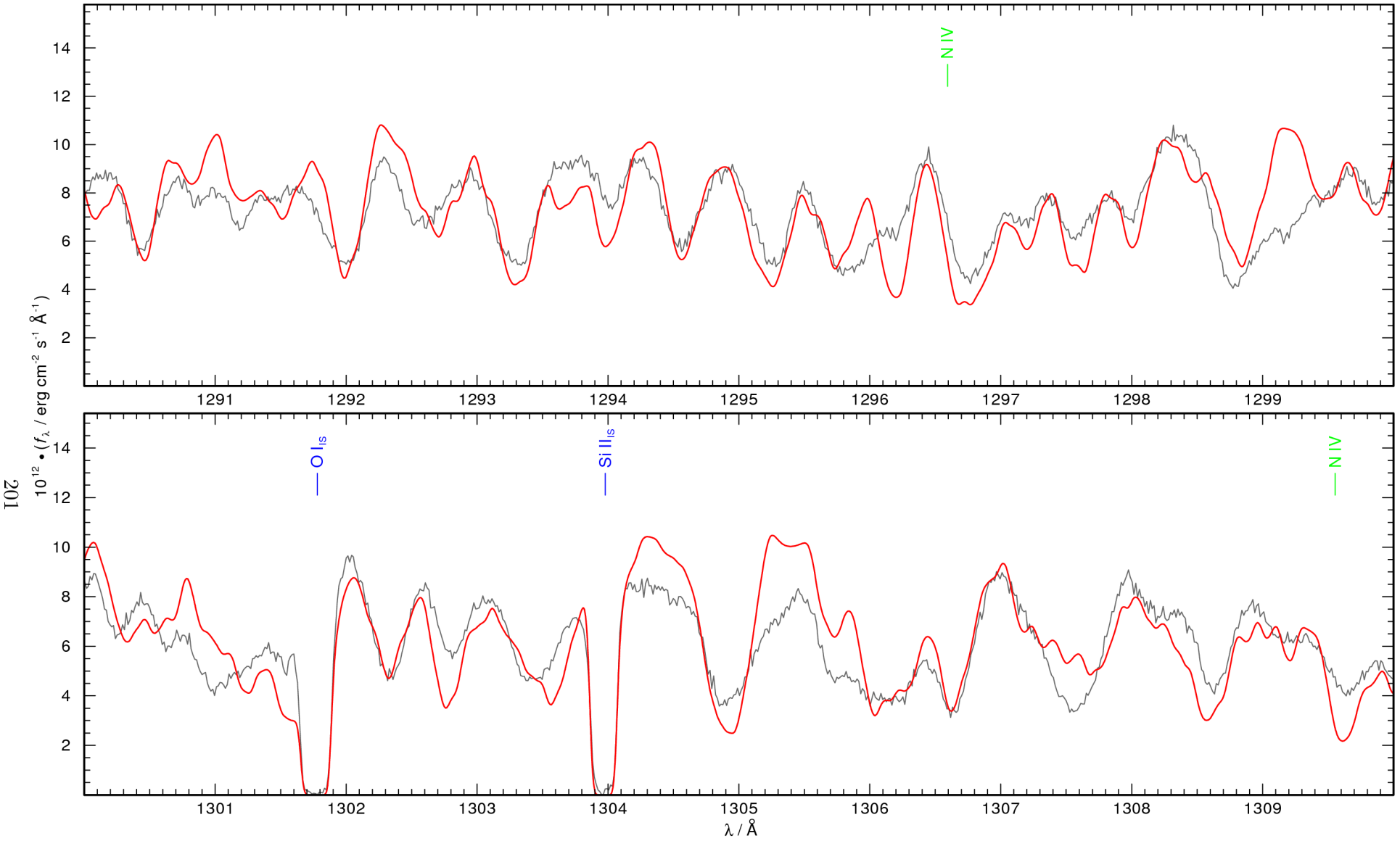

Figure 50: continued.

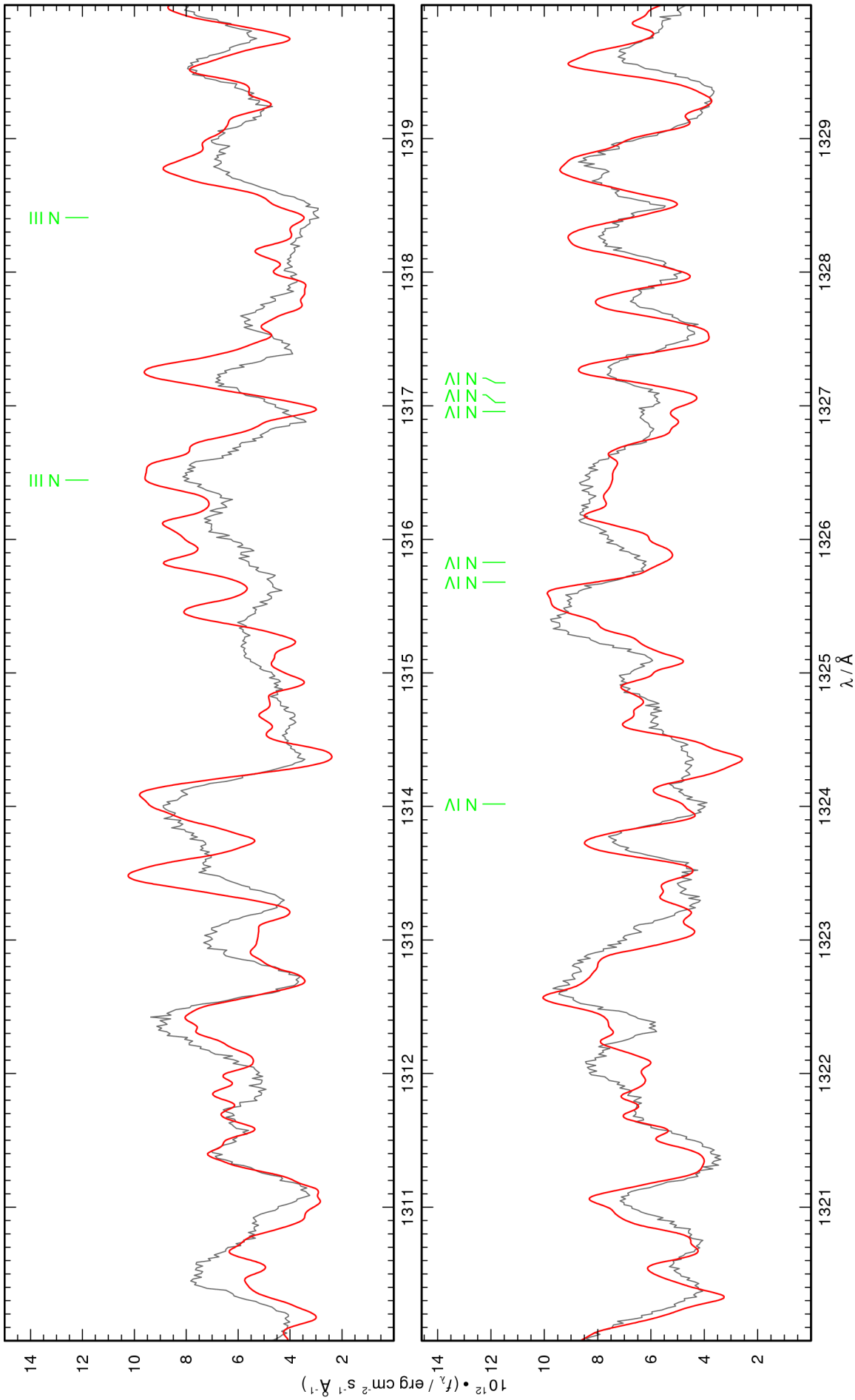

Figure 50: continued.

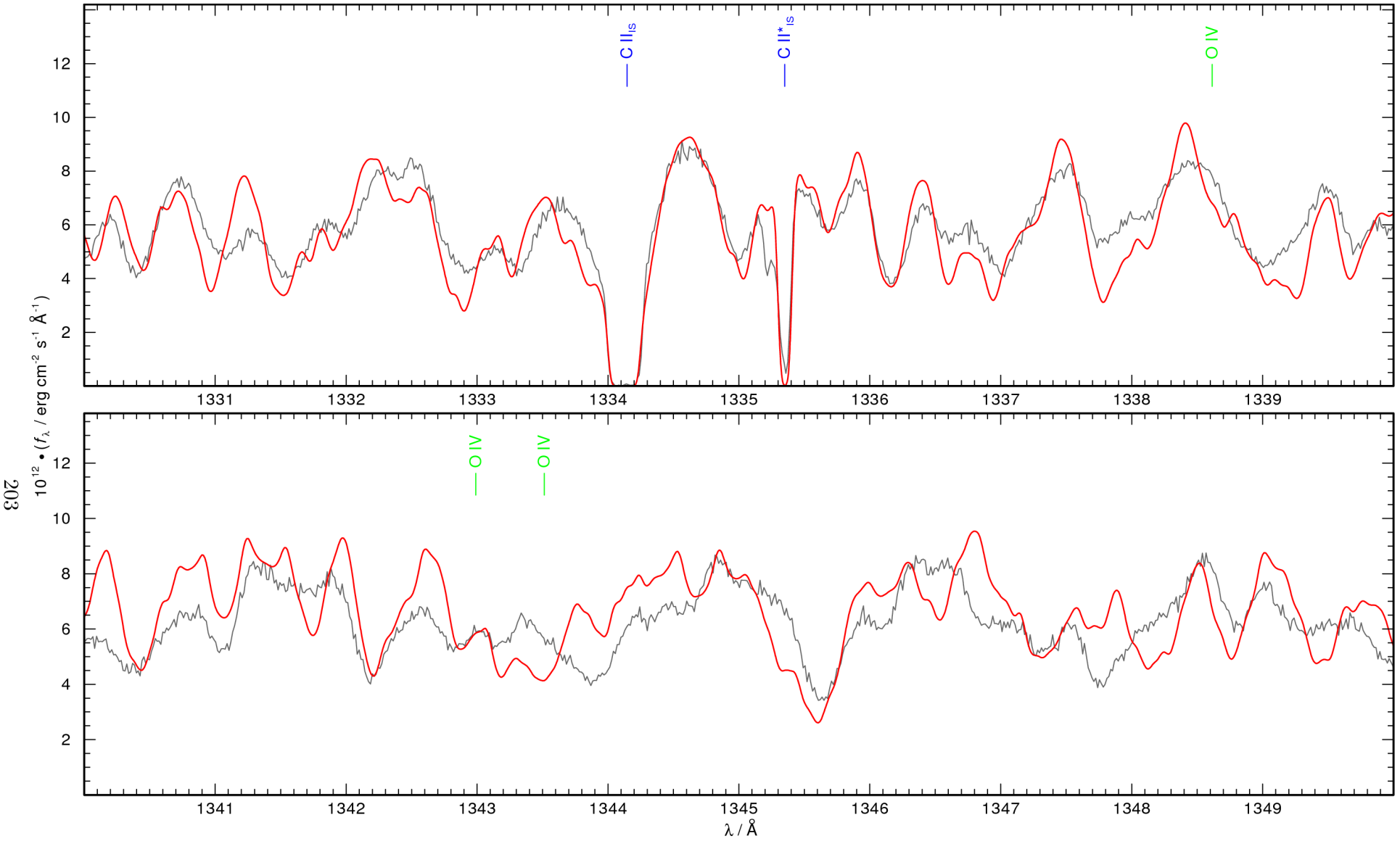

Figure 50: continued.

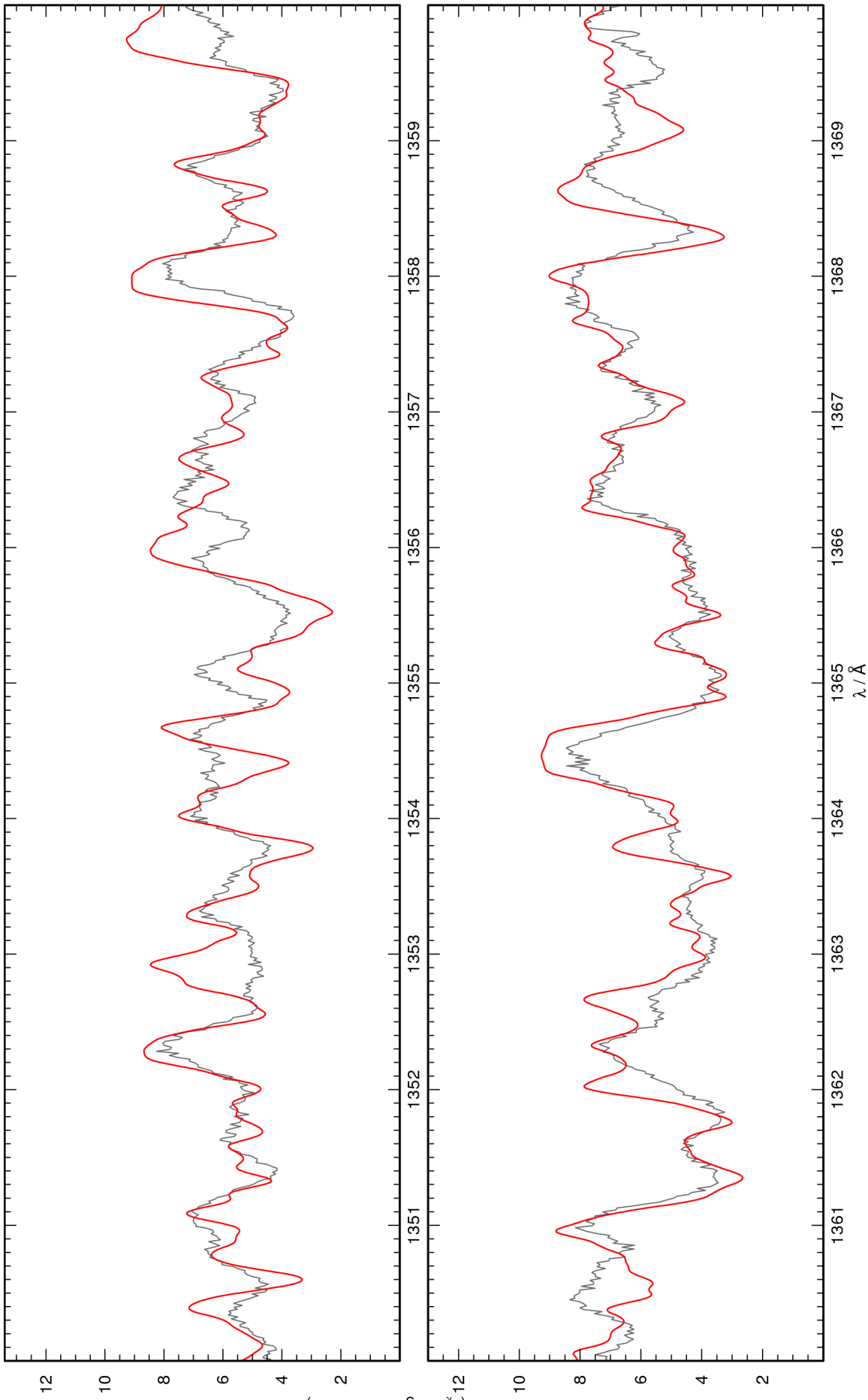

Figure 50: continued.

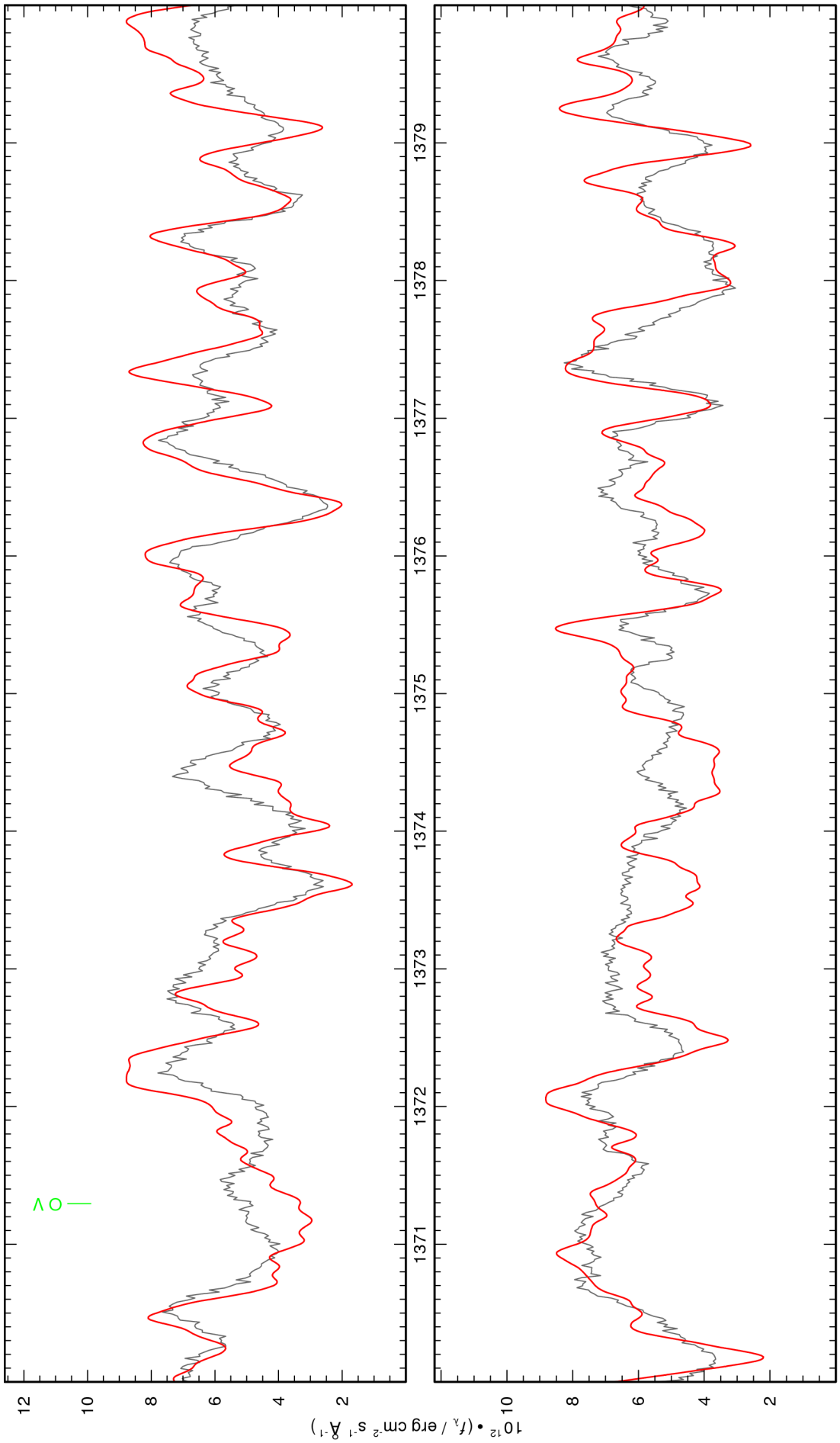

Figure 50: continued.

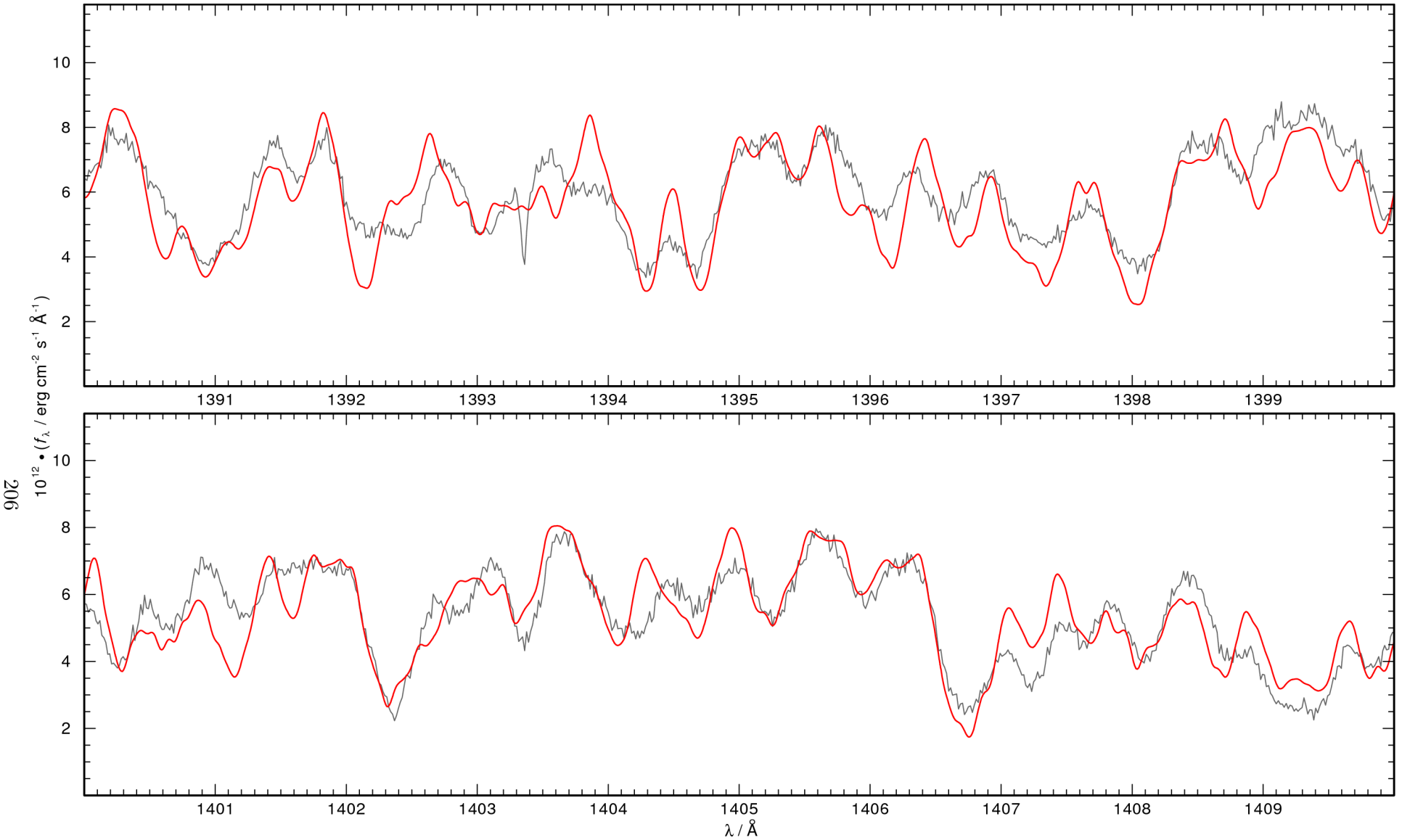

Figure 50: continued.

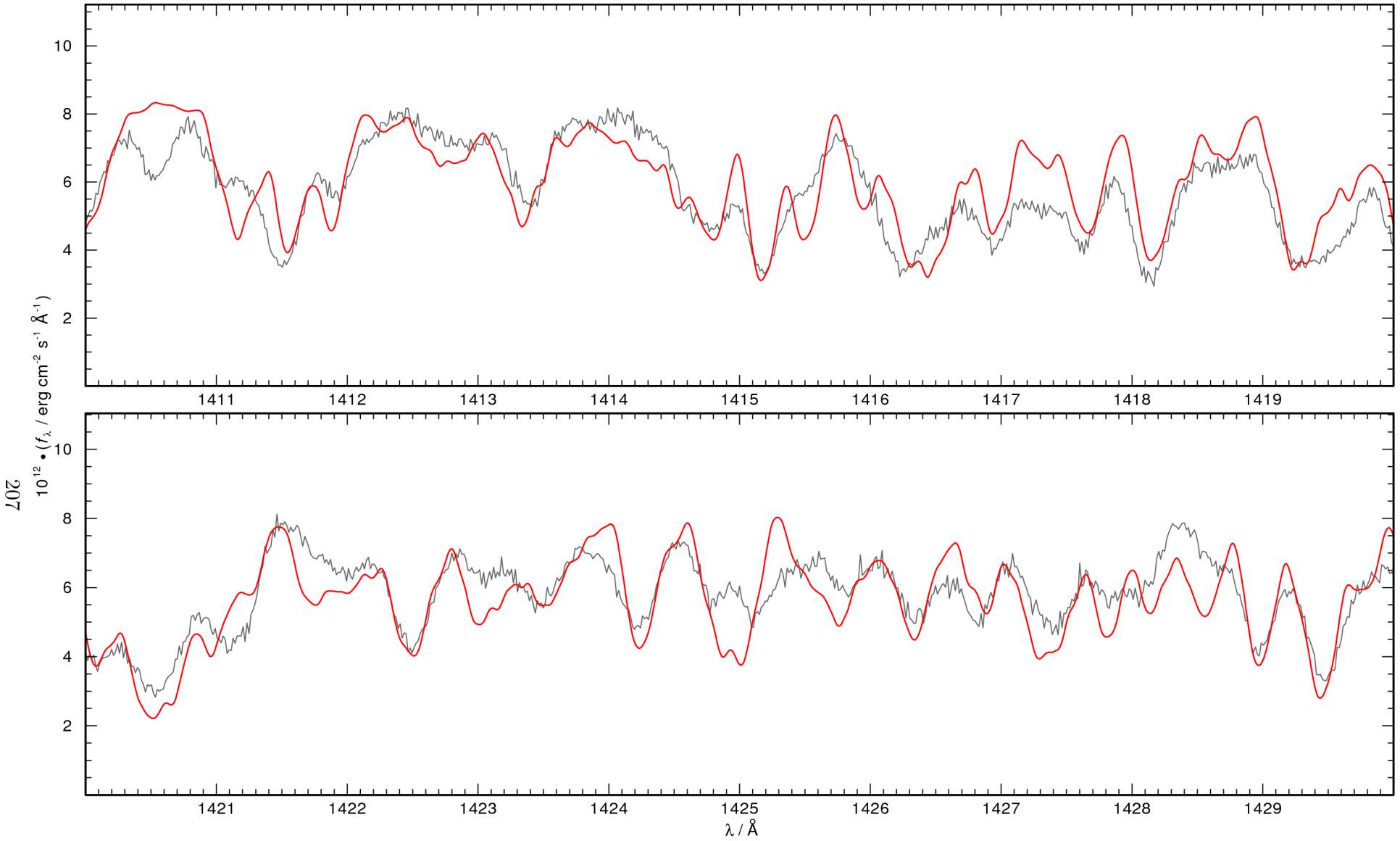

Figure 50: continued.

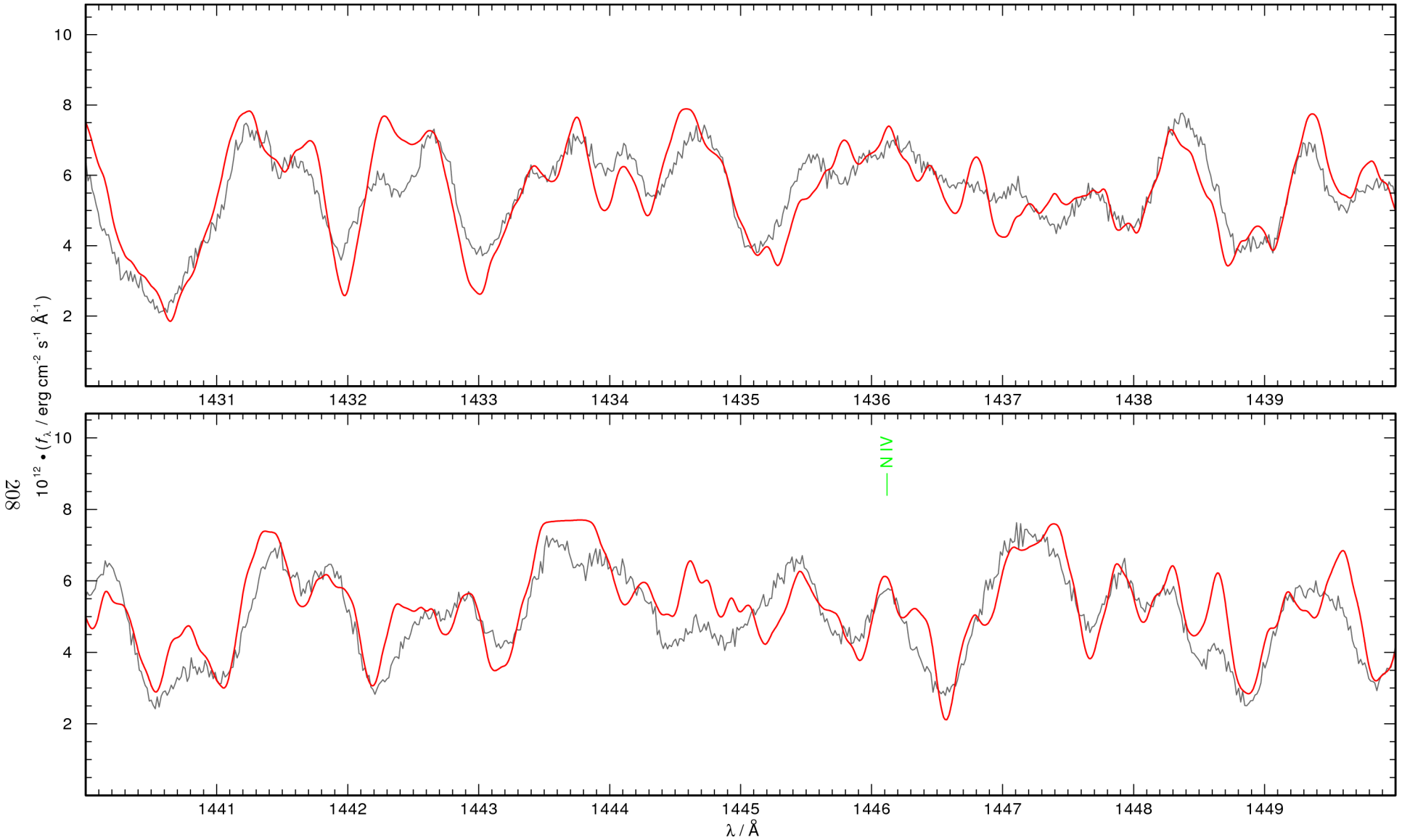

Figure 50: continued.

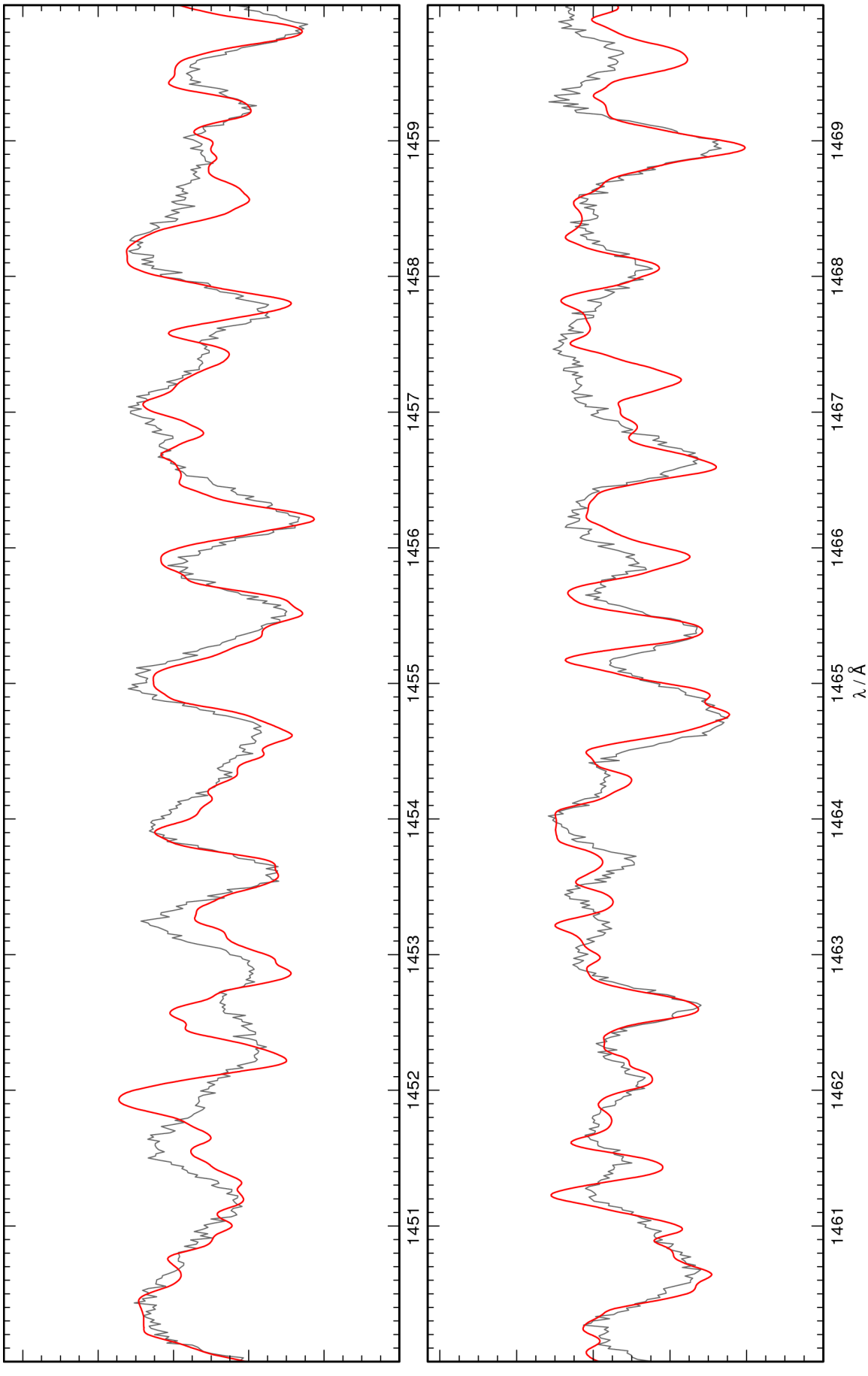

Figure 50: continued.

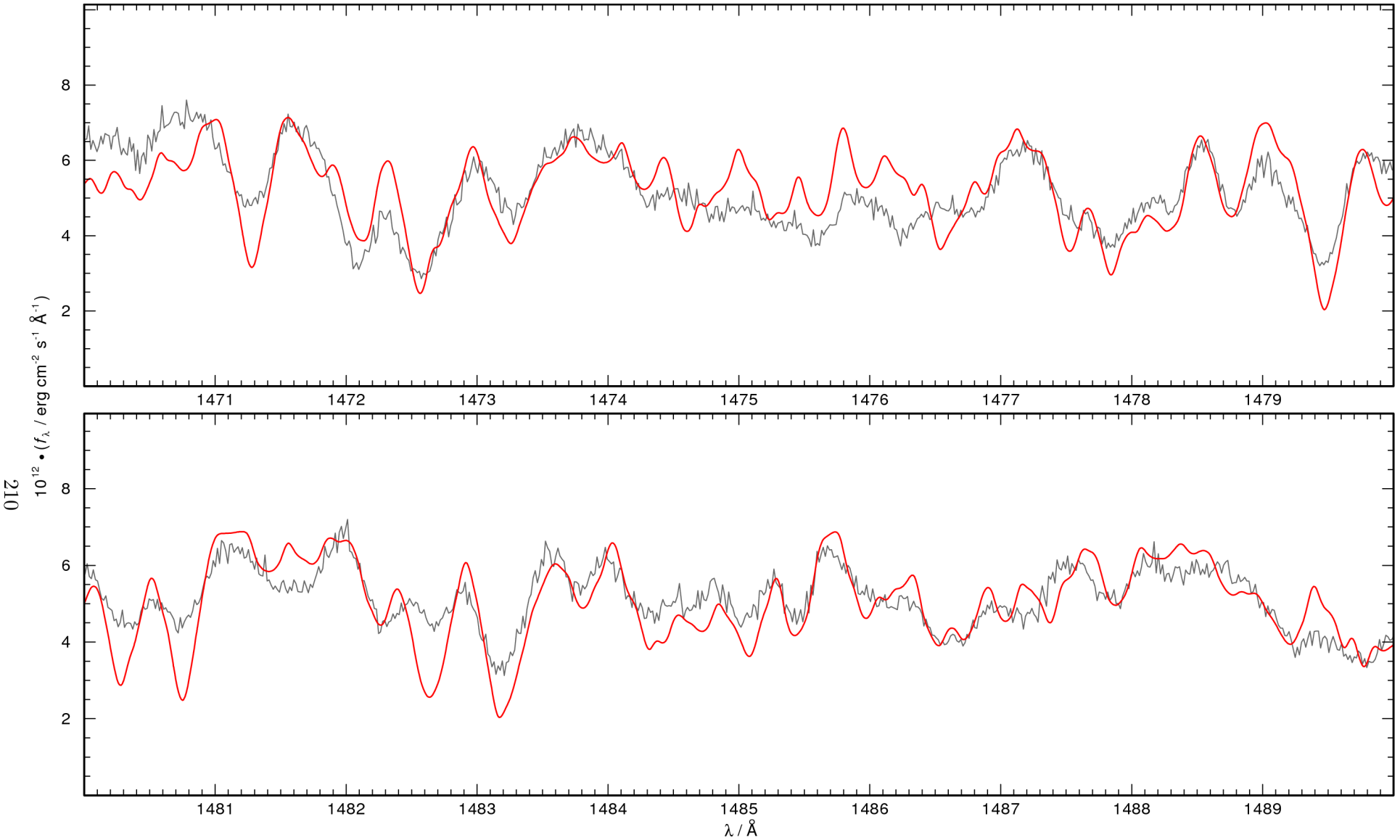

Figure 50: continued.

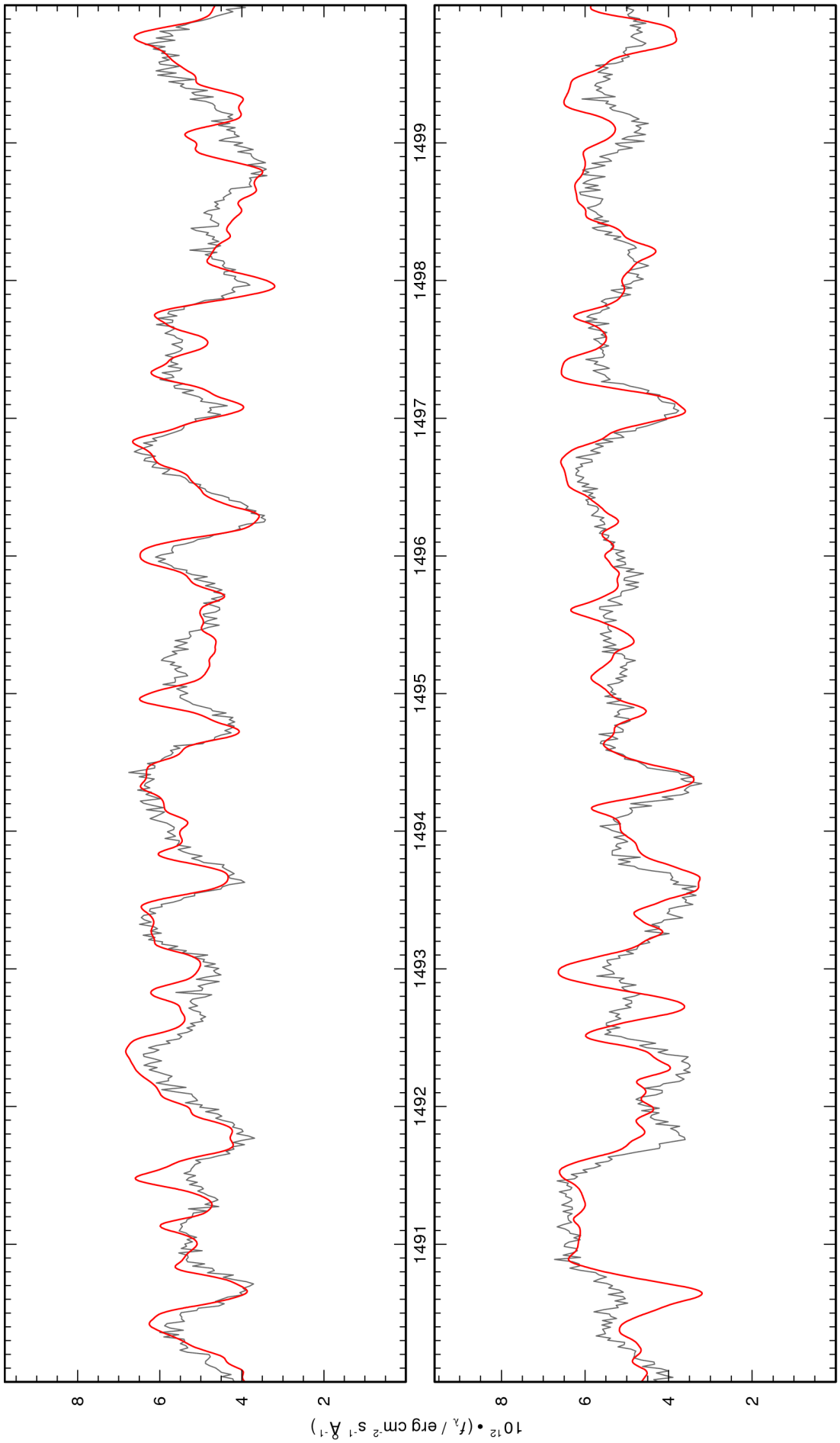

Figure 50: continued.

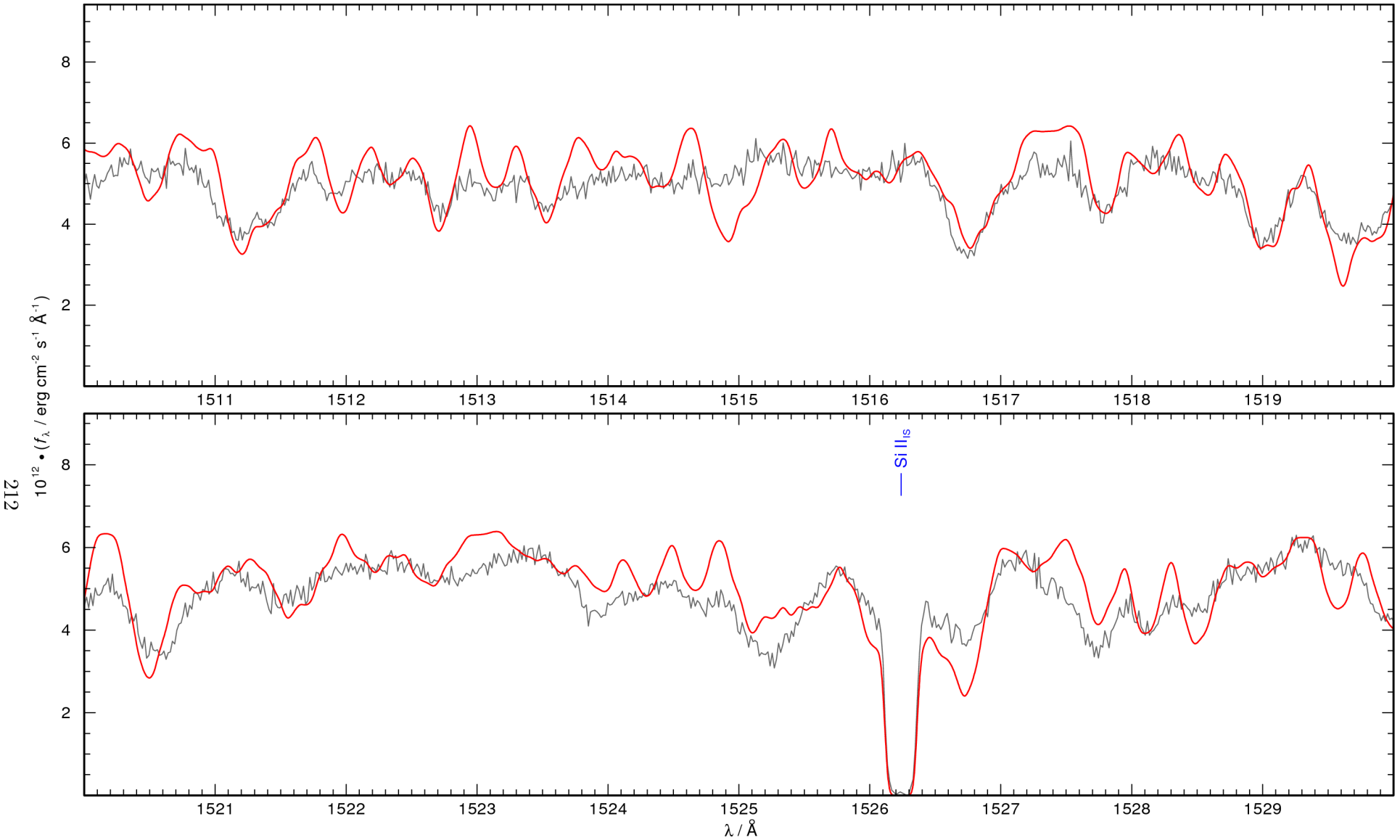

Figure 50: continued.

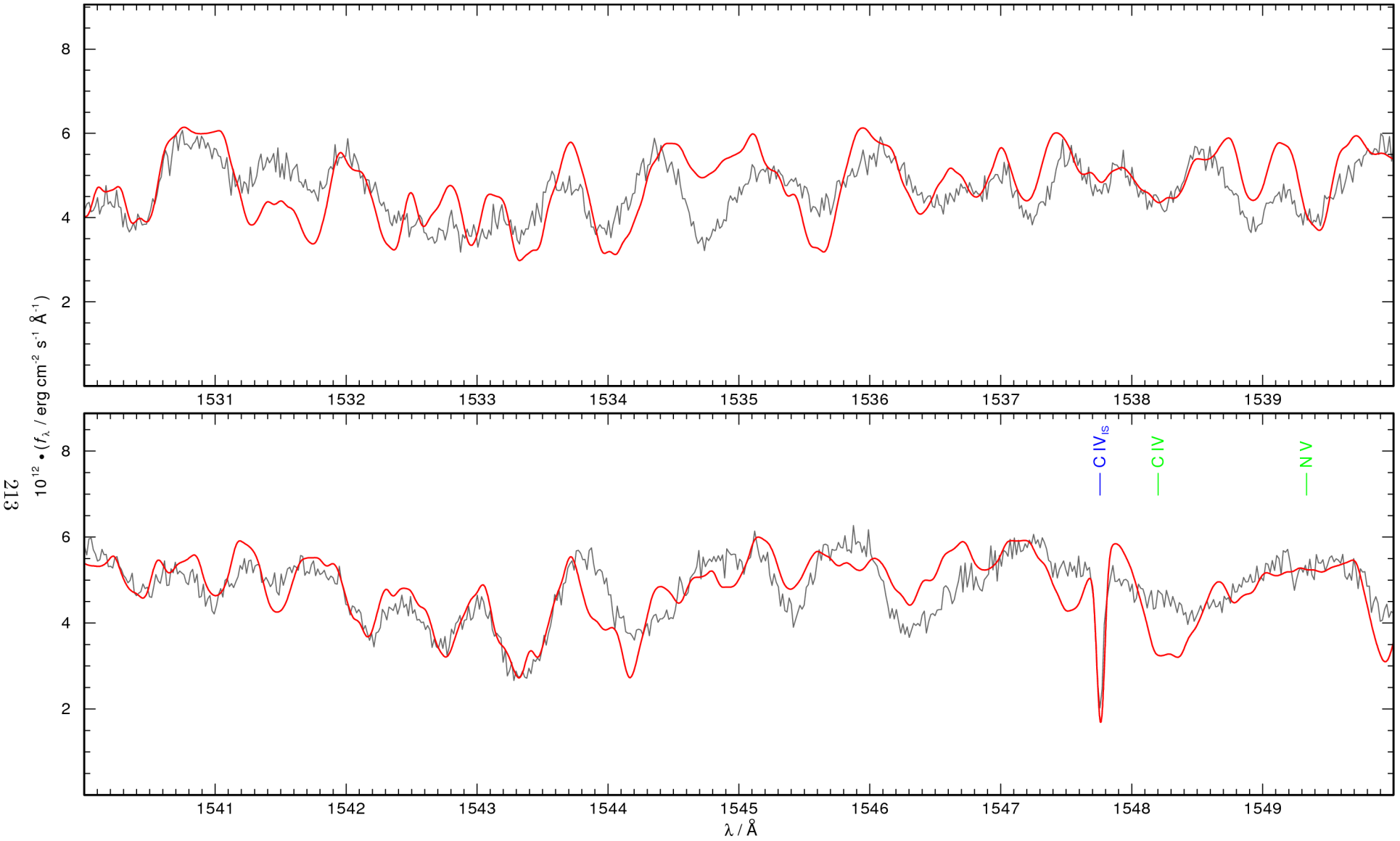

Figure 50: continued.

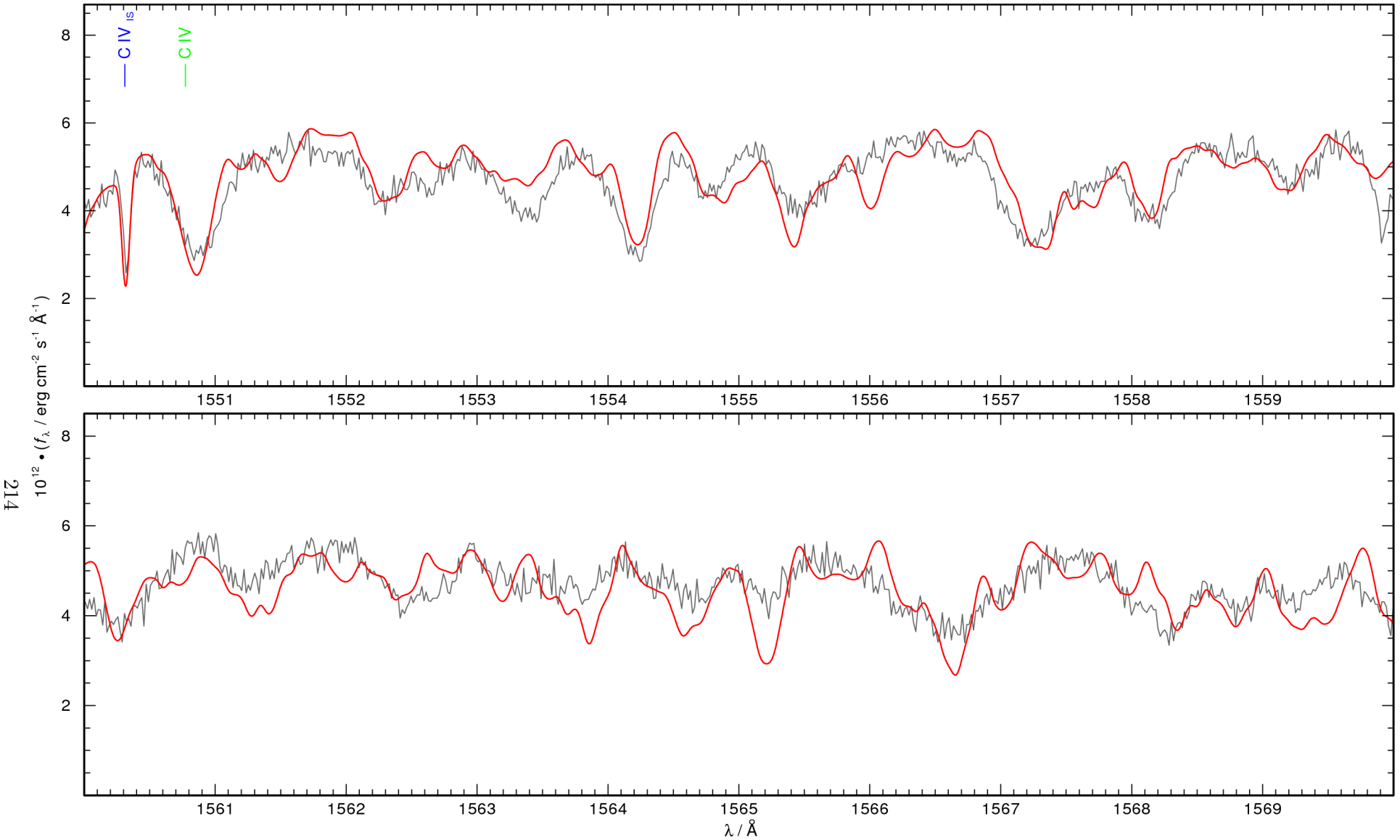

Figure 50: continued.

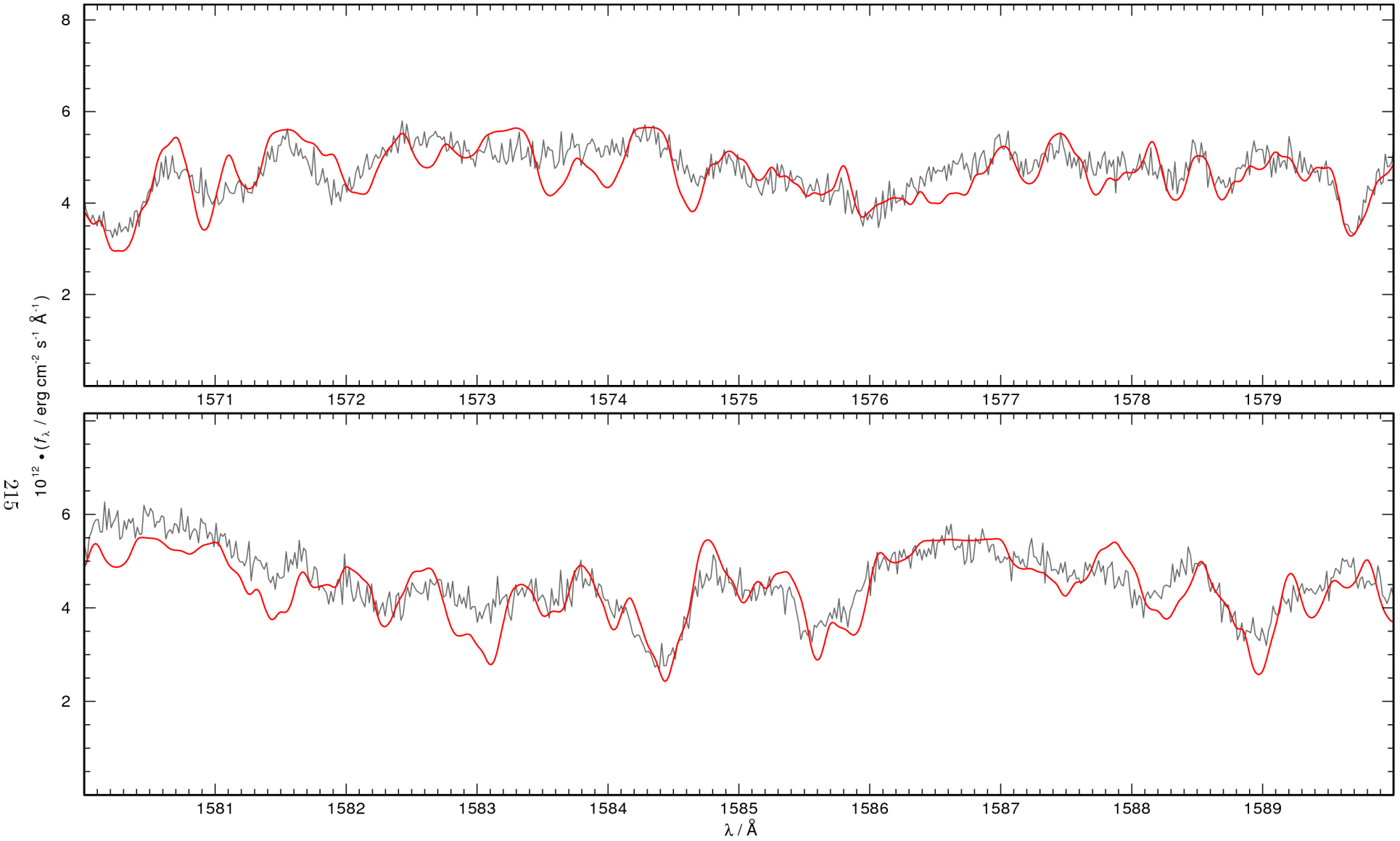

Figure 50: continued.

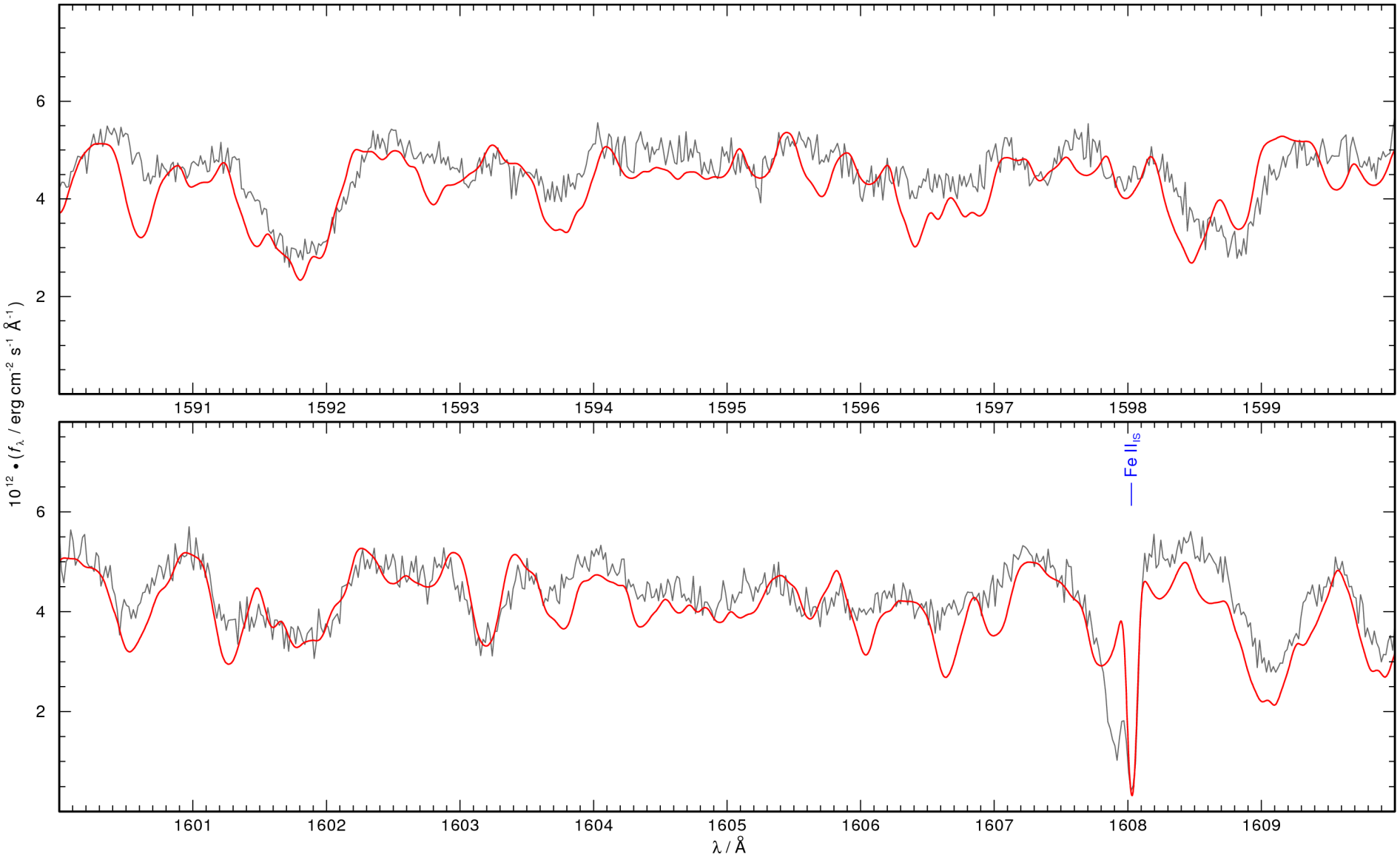

Figure 50: continued.

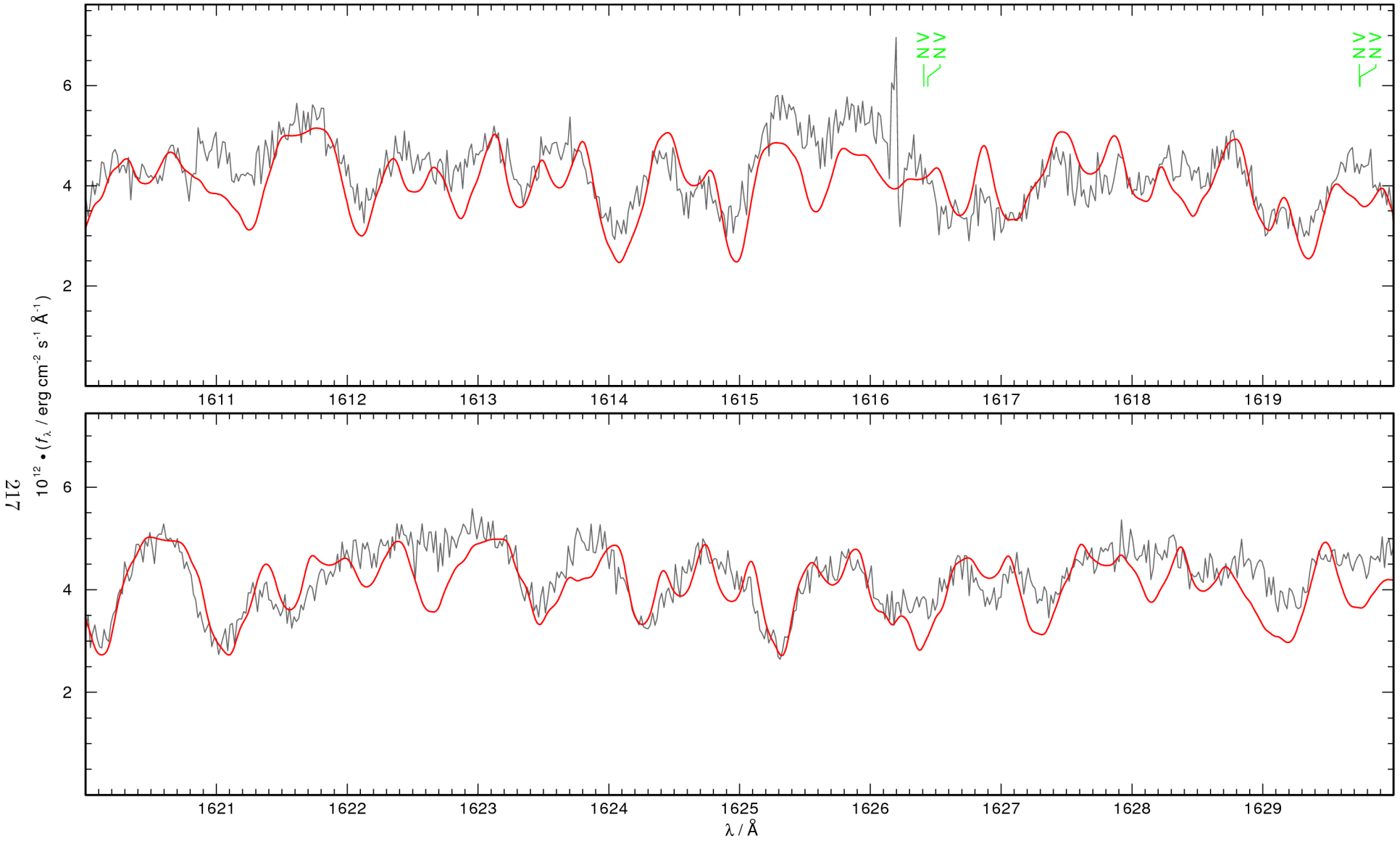

Figure 50: continued.

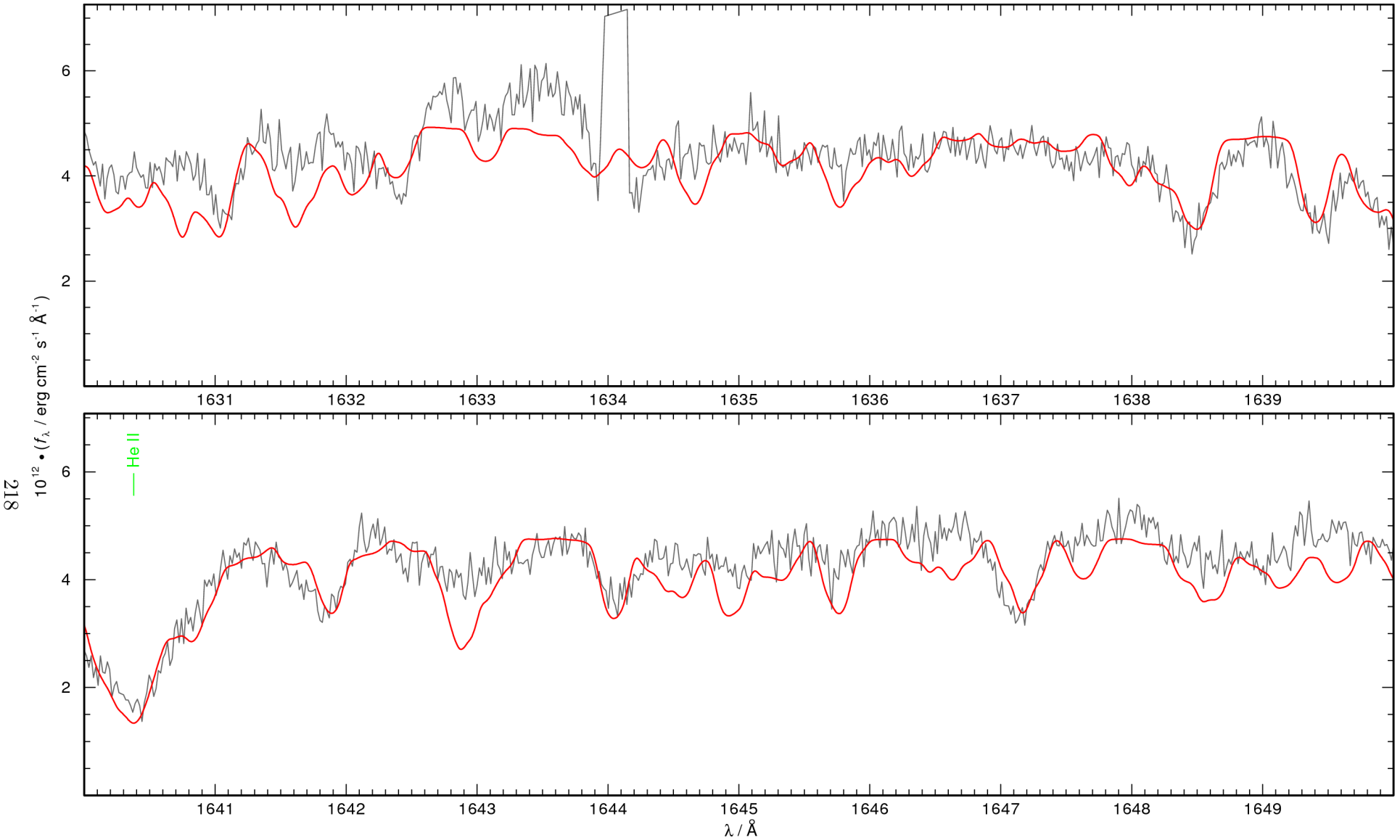

Figure 50: continued.

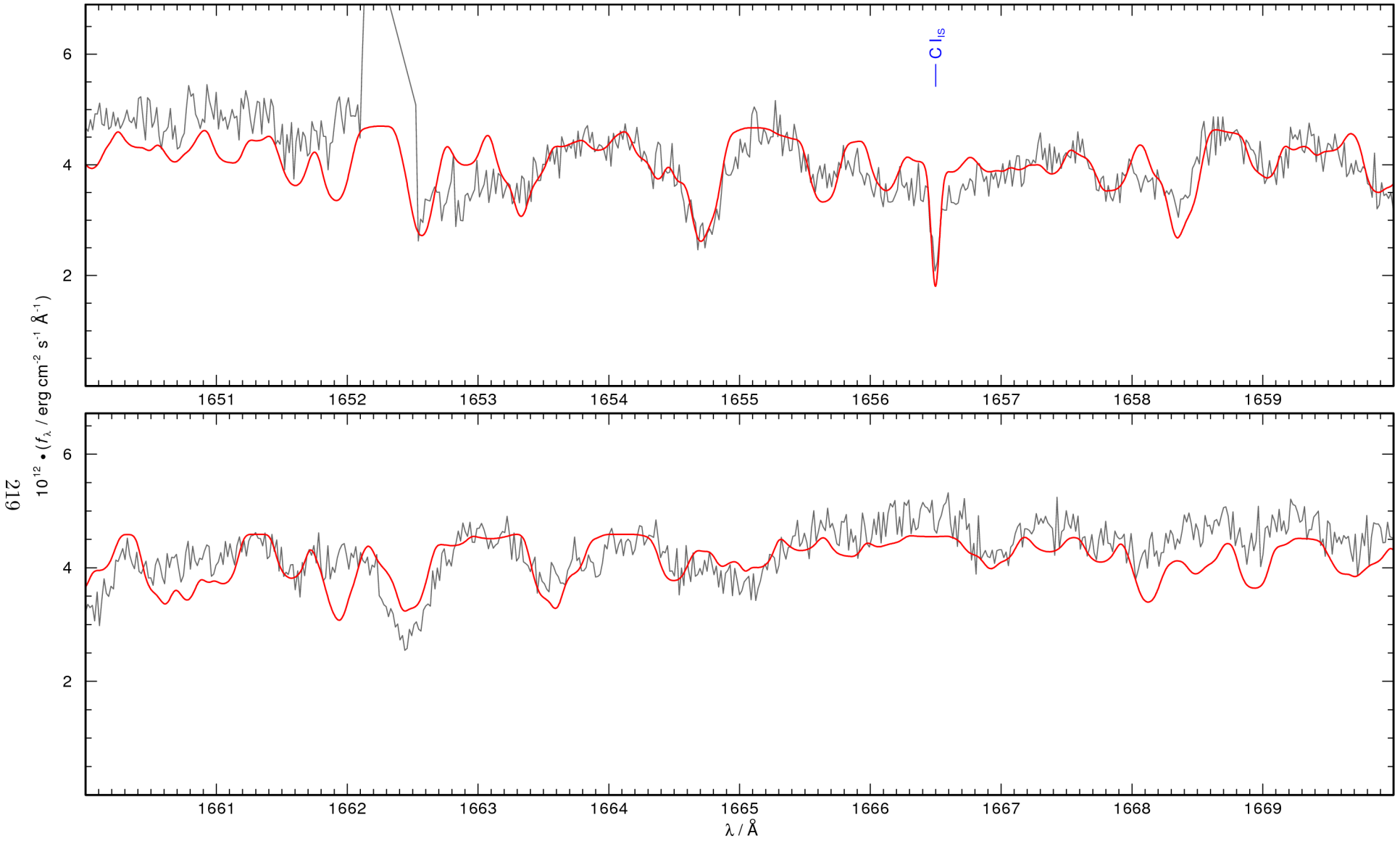

Figure 50: continued.

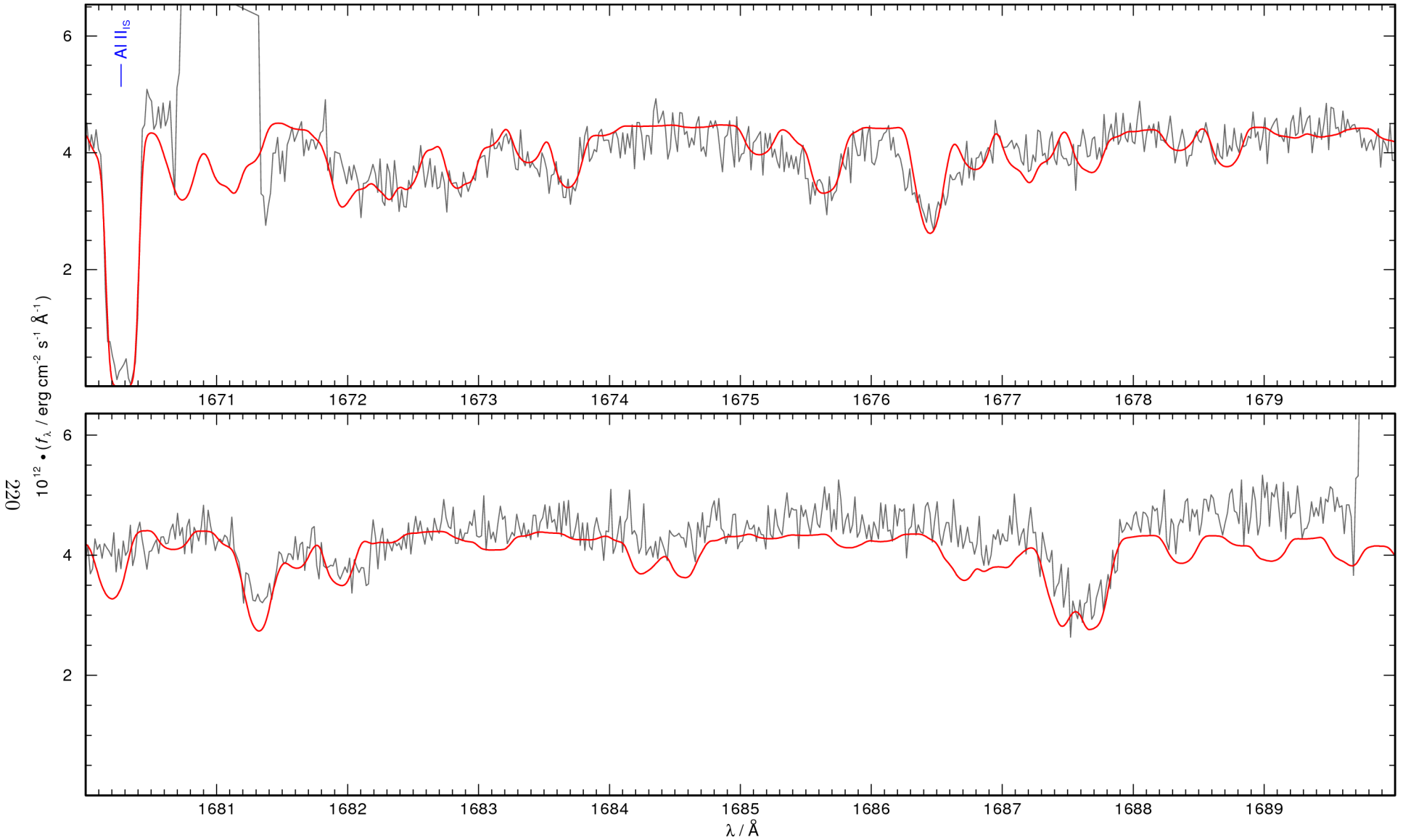

Figure 50: continued.

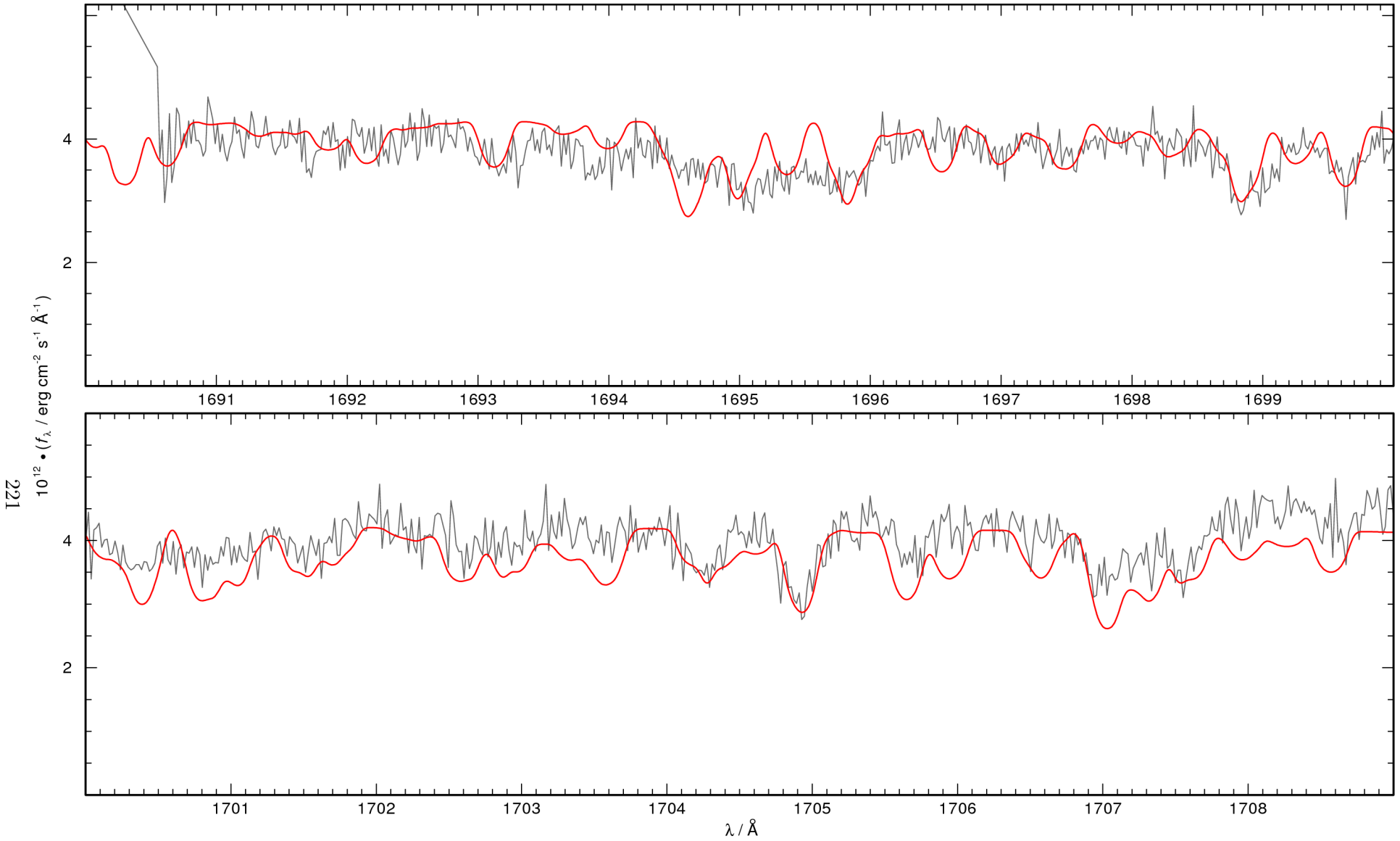

Figure 50: continued.

A.5 Line tables 2

Table 28: Manually identified isolated lines in Feige 110. The weighted oscillator strengths and the energy levels were taken from Kurucz's line lists.

λ/ Å	Ion	$\log(gf)$	E_{low}/ cm^{-1}	E_{up}/ cm^{-1}
1202.74	Co VI	0.49	307627.00	390770.10
1205.44	Ni V	−0.11	234275.20	317232.00
1209.60	Ni V	−0.03	247104.90	329776.30
1210.17	Cr IV	0.25	263875.90	181243.10
1210.38	Ni V	0.09	234125.40	316744.00
1210.94	Cr IV	−0.57	241472.80	158892.70
1211.02	Co V	0.14	277192.40	359767.20
1212.78	Ni V	−0.23	216590.50	299045.60
1213.00	Cr IV	0.09	240967.90	158527.70
1218.91	Mn V	−0.92	183538.80	265579.30
1219.97	Cr IV	0.55	241832.50	159863.60
1221.01	Co V	−0.60	207548.50	289447.50
1221.71	Ni V	−0.61	243370.50	325222.90
1222.18	Ni V	−0.67	221429.00	303249.50
1224.54	Ni V	−0.22	232545.90	314208.80
1225.35	Cr IV	−0.58	241472.80	159863.60
1225.51	Co V	−0.17	236746.00	318344.60
1226.27	Ni V	−1.49	216434.70	297982.80
1227.19	Ni V	0.27	311470.30	392957.10
1228.89	Ni V	−0.87	232545.90	313919.80
1230.43	Ni V	0.11	268273.90	349546.00
1231.10	Ni V	−0.50	216189.90	297418.10
1232.33	Ni V	−1.54	208151.50	289298.00
1235.64	Cr IV	−1.46	239822.20	158892.70
1236.57	Cr IV	−0.15	255836.90	174968.60
1239.55	Ni V	−0.01	234082.10	314756.40
1239.95	Ni V	−0.43	235420.60	316068.80
1242.64	Ni V	−0.55	234125.40	314599.20
1244.02	Ni V	−0.35	216189.90	296574.00
1244.32	Mn IV	0.71	248665.00	168300.30
1244.79	Ni V	−0.66	229408.80	309743.60
1245.52	Ni V	−0.72	234275.20	314562.80
1245.62	Ni IV	−0.53	144815.10	225096.40
1246.94	Cr IV	−0.55	241182.50	160986.50
1247.47	Ni V	−0.05	243370.50	323532.20
1248.83	Ni V	−0.24	247281.80	327356.60
1249.13	Co V	−0.93	235199.90	315255.40
1251.81	Ni V	0.47	217048.70	296932.90
1254.19	Ni V	−0.06	240193.80	319926.50
1255.14	Cr IV	0.35	257588.60	177916.50

Table 28 – continued.

λ/ Å	Ion	$\log(gf)$	$E_{\rm low}$/ cm^{-1}	$E_{\rm up}$/ cm^{-1}
1260.86	Ni V	−1.17	232655.60	311966.50
1261.76	Ni V	0.47	216189.90	295444.30
1261.88	Co V	0.04	241875.40	321122.20
1262.05	Cr IV	−0.55	239541.40	160305.40
1262.44	Cr IV	−0.78	240967.90	161756.30
1263.86	Ni IV	−0.65	145702.20	224824.90
1264.00	Ni V	−1.17	221087.60	300201.00
1264.10	Mn VI	−0.19	250527.00	329634.50
1266.87	Ni V	−0.04	212455.70	291390.00
1267.53	Co V	−0.11	206962.20	285855.70
1268.87	Ni V	0.30	274738.60	353548.70
1269.22	Ni V	−0.29	235420.60	314208.80
1269.38	Ni V	0.25	241082.20	319860.40
1270.95	Co V	−0.40	206962.20	285643.00
1271.27	Ni V	−0.66	212095.80	290757.00
1272.44	Mn VI	0.07	251403.00	329992.00
1272.99	Cr IV	−0.11	239541.40	160986.50
1273.20	Ni V	0.39	208164.60	286706.60
1280.47	Fe V	−0.55	209523.90	287620.20
1281.81	Co V	−0.47	238164.60	316178.90
1282.06	Fe V	−1.04	209110.10	287109.60
1282.72	Ni V	0.02	229440.60	307399.70
1282.87	Ni V	−1.12	235736.50	313686.60
1283.18	Ni V	−0.14	247049.10	324980.20
1284.11	Fe V	−0.78	204729.90	282604.80
1284.47	Ni V	0.13	216590.50	294443.30
1285.91	Fe V	−0.88	212818.10	290583.70
1286.93	Co V	0.39	248855.90	326560.00
1288.51	Ni V	−0.34	242290.40	319899.10
1289.16	Co V	−0.38	248698.20	326267.90
1291.88	Ni V	−0.55	232545.90	309952.50
1292.46	Cr IV	0.60	250007.70	172636.40
1292.68	Cr IV	−0.46	251017.30	173659.10
1293.70	Co V	−0.70	206962.20	284259.90
1294.02	Co V	0.28	249006.80	326285.10
1294.79	Ni V	−1.19	236454.10	313686.60
1300.79	Cr IV	0.41	250535.20	173659.10
1301.88	Cr IV	−0.88	237798.20	160986.50
1302.25	Ni V	−0.21	242862.60	319652.70
1302.64	Co V	−0.55	241174.10	317941.00
1304.52	Cr IV	0.57	250752.70	174096.20
1306.85	Co V	−0.87	206476.00	282995.60
1307.77	Ni V	−0.17	253905.20	330370.70

Table 28 – continued.

λ/ Å	Ion	$\log(gf)$	$E_{\rm low}$/ cm^{-1}	$E_{\rm up}$/ cm^{-1}
1307.86	Co V	−0.15	243455.20	319915.70
1311.23	Fe V	−0.82	213649.20	289913.00
1311.33	Ni V	−0.87	239107.70	315366.10
1312.14	Co V	0.15	289449.20	365660.10
1312.25	Co V	0.45	283592.10	359796.70
1315.48	Cr IV	−1.10	247099.10	171081.30
1315.98	Ni V	−0.86	221429.00	297417.90
1316.53	Mn V	−1.38	194011.40	269968.30
1317.62	Co V	−0.85	206108.50	282002.80
1318.92	Ni V	−0.88	247165.00	322984.50
1319.16	Ni V	−0.11	241082.20	316887.80
1320.02	Cr IV	−1.03	233117.30	157361.40
1320.40	Fe V	0.27	216779.10	292513.20
1320.80	Fe IV	−1.12	161571.59	237283.09
1320.88	Ni V	−0.66	212253.40	287960.00
1321.03	Cr IV	−1.12	237999.50	162301.40
1321.48	Fe V	−0.04	209523.90	285196.10
1322.73	Co V	−0.38	242340.30	317941.00
1322.83	Ni IV	−1.54	140140.90	215736.10
1324.74	Ni V	−0.53	221087.60	296574.00
1324.86	Ni IV	−0.56	110410.60	185890.00
1325.16	Co V	−0.26	238164.60	313626.70
1326.02	Co V	0.02	244821.20	320234.50
1326.15	Ni IV	−1.19	139886.70	215292.90
1328.84	Fe IV	−1.11	167712.50	242965.62
1329.02	Fe V	−1.31	217122.50	292365.90
1330.40	Fe V	0.43	217122.50	292287.60
1333.57	Ni V	−0.59	241082.20	316068.80
1335.75	Fe V	−0.67	214525.80	289389.70
1341.07	Ni V	−0.12	216189.90	290757.00
1341.22	Cr IV	−1.19	255836.90	181277.90
1342.43	Co V	0.52	236158.00	310649.40
1343.62	Ni V	−0.69	217129.10	291554.60
1344.69	Ni V	−1.22	240959.60	315326.20
1345.84	Co V	−0.34	206476.00	280778.70
1346.08	Ni IV	−0.34	112151.90	186441.40
1346.63	Cr IV	−1.33	233708.50	159449.20
1346.82	Co IV	−1.51	90554.40	164803.20
1348.56	Cr IV	−0.98	239582.80	165430.00
1348.84	Fe V	−0.76	234027.40	308165.00
1349.15	Ni IV	−0.85	139619.20	213739.70
1352.05	Co V	0.04	206962.20	280923.50
1352.75	Co V	0.00	276608.80	350532.00

Table 28 – continued.

λ/ Å	Ion	$\log(gf)$	$E_{\rm low}$/ cm^{-1}	$E_{\rm up}$/ cm^{-1}
1353.24	Co V	−0.62	249179.70	323076.20
1356.07	Ni IV	−0.23	111763.30	185505.30
1357.24	Fe IV	−1.03	165392.58	239071.40
1359.71	Cr IV	−0.66	232896.60	159352.00
1360.80	Ni V	−0.63	242504.30	315990.50
1364.17	Co V	0.12	241985.30	315289.80
1364.41	Cr IV	−0.90	254534.60	181243.10
1368.01	Cr IV	−0.83	234085.20	160986.50
1368.68	Cr IV	−1.25	251093.10	178030.00
1370.30	Fe V	−0.83	217122.50	290099.10
1370.94	Fe V	−0.47	186433.60	259376.10
1372.65	Fe V	−0.98	216538.10	289389.70
1373.03	Co V	0.45	277192.40	350024.00
1375.20	Co V	−0.06	206476.00	279192.40
1375.79	Fe V	−0.74	216860.40	289545.90
1376.80	Cr IV	−0.95	233618.40	160986.50
1381.30	Ni IV	−0.33	139886.70	212281.80
1382.88	Mn V	−0.67	200670.10	272982.90
1384.05	Fe V	−0.59	214611.40	286862.70
1384.85	Ni V	−0.25	233839.20	306049.00
1386.46	Fe V	−1.49	188395.30	260521.00
1387.93	Fe V	0.66	217122.50	289171.90
1388.69	Ni IV	−1.05	140140.90	212150.90
1389.43	Ni V	−0.65	216189.90	288161.60
1389.63	Cr IV	−0.23	255836.90	183875.60
1390.27	Cr IV	−1.03	255803.60	183875.60
1391.55	Cr IV	−0.65	233618.40	161756.30
1391.65	Ni V	−0.76	247281.80	319138.70
1392.47	Ni V	−0.15	240193.80	312008.30
1393.53	Co V	−0.87	244821.20	316581.00
1395.44	Fe V	−0.84	214525.80	286187.70
1395.54	Co IV	−0.74	132828.70	204485.30
1395.73	Ni IV	−0.86	153349.40	224996.50
1395.85	Co V	−0.27	238390.30	310031.10
1395.97	Ni IV	−0.57	110410.60	182044.90
1396.89	Ni IV	−0.65	153349.40	224936.90
1397.54	Ni V	−0.63	221429.00	292983.00
1397.75	Fe V	−0.93	214611.40	286154.90
1399.05	Mn V	−0.46	194011.40	265488.40
1401.89	Ni IV	0.01	153313.80	224645.70
1403.36	Fe V	−0.33	209110.10	280367.20
1405.35	Fe V	−0.99	213534.10	284690.30
1405.96	Fe V	−0.71	221305.20	292430.70

Table 28 – continued.

λ/ Å	Ion	log (gf)	$E_{\rm low}$/ cm^{-1}	$E_{\rm up}$/ cm^{-1}
1406.45	Ni IV	−0.64	139886.70	210987.50
1407.44	Ni IV	0.29	185967.00	257018.00
1407.65	Co V	0.42	218407.20	289447.50
1408.11	Fe V	−0.23	186725.50	257742.30
1408.52	Co V	−0.16	255292.50	326288.80
1409.02	Fe V	0.08	187157.50	258128.50
1410.36	Ni IV	−1.48	140343.00	211246.80
1411.45	Ni IV	0.44	111195.80	182044.90
1412.11	Cr IV	−0.83	233117.30	162301.40
1413.42	Co V	0.55	236746.00	307496.40
1414.00	Mn V	−1.06	194011.40	264732.40
1414.59	Ni IV	0.31	144815.10	215506.60
1415.05	Co IV	−0.06	132729.10	203398.00
1417.27	Ni IV	−0.33	139619.20	210177.00
1417.40	Cr IV	−0.70	110691.80	181243.10
1418.34	Ni IV	0.22	155253.70	225758.50
1419.12	Ni IV	0.15	138446.20	208912.10
1419.98	Co V	0.45	236431.20	306854.60
1421.68	Ni IV	−0.91	145192.10	215531.00
1421.99	Fe IV	−1.33	158738.69	229062.58
1422.13	Fe IV	−0.41	195864.15	266181.09
1423.88	Co IV	−0.39	132828.70	203059.00
1424.79	Mn V	0.01	195302.70	265488.40
1425.47	Fe IV	−0.27	159342.88	229494.74
1426.04	Fe IV	−0.57	158738.69	228862.61
1428.61	Ni V	−1.25	217129.10	287127.20
1430.19	Ni IV	0.15	120909.50	190830.30
1431.43	Fe IV	−0.23	154185.85	224045.96
1432.44	Ni IV	−0.12	121807.70	191618.20
1432.68	Ni IV	−0.92	159498.50	229297.50
1432.84	Mn V	−0.02	200176.90	269968.30
1435.80	Ni IV	−0.52	122386.10	192033.50
1440.30	Mn V	−0.52	195302.70	264732.40
1440.79	Fe V	−0.23	204729.90	274136.10
1441.18	Ni IV	−0.05	146153.80	215541.30
1443.30	Mn V	0.16	200670.10	269955.40
1444.60	Ni IV	−0.78	142023.50	211246.80
1444.77	Mn V	−0.52	176946.30	246161.20
1444.91	Ni IV	0.34	145702.20	214910.50
1445.68	Fe V	−0.42	258434.10	327605.40
1446.93	Ni IV	−0.66	141832.00	210943.60
1447.20	Ni IV	−0.88	146194.30	215292.90
1448.29	Ni IV	−1.13	139886.70	208933.60

Table 28 – continued.

λ/ Å	Ion	$\log(gf)$	$E_{\rm low}$/ cm^{-1}	$E_{\rm up}$/ cm^{-1}
1448.48	Fe V	0.16	213534.10	282571.60
1449.18	Ni IV	−0.66	142023.50	211027.60
1449.88	Fe V	0.41	233633.60	302604.50
1450.62	Fe V	−1.62	216538.10	285474.00
1451.10	Fe V	−0.69	204729.90	273643.10
1451.58	Co IV	0.23	158846.70	227737.10
1452.58	Ni IV	−0.48	156294.00	225136.90
1453.09	Fe IV	−0.35	154731.29	223550.14
1454.36	Ni IV	−0.33	141832.00	210590.60
1456.52	Ni IV	−0.01	146061.50	214718.10
1456.75	Fe IV	−0.83	156224.88	224870.85
1460.73	Fe V	−0.21	187719.00	256177.90
1462.01	Ni IV	0.00	145702.20	214101.00
1462.13	Ni IV	0.11	146194.30	214587.40
1465.57	Co IV	−0.18	136612.50	204845.10
1468.42	Ni IV	−0.47	147635.90	215736.10
1469.48	Ni IV	−1.50	159498.50	227549.40
1470.73	Fe V	−1.58	214611.40	282604.80
1471.73	Ni IV	−0.77	146153.80	214101.00
1472.80	Fe V	−0.60	214525.80	282423.50
1473.55	Co IV	−0.48	160351.40	228214.70
1474.27	Fe V	−0.74	216860.40	284690.30
1475.60	Fe V	−0.18	209523.90	277292.70
1475.96	Mn V	−0.24	178572.50	246324.70
1476.42	Ni IV	0.21	159818.40	227549.40
1476.81	Ni IV	0.30	141220.30	208933.60
1476.96	Ni IV	−0.62	145702.20	213408.60
1477.28	Ni IV	−0.73	141220.30	208912.10
1478.45	Cr IV	−0.64	239822.20	172184.00
1479.20	Ni IV	0.08	171406.00	239009.70
1480.48	Ni IV	−0.48	146194.30	213739.70
1481.41	Ni IV	−0.24	140343.00	207846.20
1486.03	Fe IV	−0.37	160311.64	227604.73
1486.19	Ni IV	0.17	151574.70	218860.60
1487.88	Ni IV	−0.02	152343.70	219553.40
1488.14	Co IV	−0.28	136362.90	203560.60
1489.24	Fe V	−0.44	216538.10	283686.30
1489.70	Cr V	−0.17	167491.00	234618.40
1489.83	Ni IV	0.27	139619.20	206740.70
1490.19	Co IV	0.33	152126.20	219231.60
1491.90	Ni IV	−0.20	141577.20	208605.70
1492.64	Ni IV	−0.07	140140.90	207136.00
1493.81	Co IV	0.16	182501.40	249444.10

Table 28 – continued.

λ/ Å	Ion	$\log(gf)$	$E_{\rm low}$/ cm^{-1}	$E_{\rm up}$/ cm^{-1}
1494.47	Fe IV	−1.19	154325.96	221239.21
1496.41	Ni IV	−0.77	141220.30	208046.80
1497.49	Fe IV	−0.48	154325.96	221104.17
1497.59	Ni IV	−0.25	141832.00	208605.70
1498.52	Mn V	−0.43	176946.30	243678.50
1500.41	Fe IV	−0.63	154512.67	221161.02
1500.90	Cr IV	−1.16	241472.80	174846.20
1501.03	Co IV	0.17	152113.30	218733.80
1502.19	Co IV	0.46	90554.40	157123.70
1502.33	Mn V	0.37	178572.50	245135.60
1503.36	Mn V	−0.36	194288.80	260806.20
1505.99	Ni V	−1.43	242862.60	309264.00
1506.16	Co V	−0.92	248698.20	315092.20
1506.52	Co IV	−0.61	129228.70	195606.50
1507.89	Ni V	−1.01	241082.20	307399.70
1508.41	Co IV	−0.06	160351.40	226646.10
1509.10	Ni IV	0.14	148358.20	214622.80
1510.11	Ni IV	−0.57	146061.50	212281.80
1510.37	Co IV	0.61	188138.40	254347.10
1513.30	Fe IV	−1.40	165392.58	231473.32
1521.43	Ni IV	−0.01	185967.00	251694.30
1522.77	Co IV	0.02	150970.90	216640.40
1524.23	Ni IV	−0.42	120909.50	186516.10
1524.75	Fe IV	−1.64	154474.85	220059.33
1528.93	Fe IV	−1.28	154185.85	219590.84
1529.08	Ni IV	−0.63	145192.10	210590.60
1530.25	Fe IV	0.11	159227.90	224576.43
1530.58	Co IV	0.38	188138.40	253472.80
1530.92	Co IV	−0.36	132729.10	198048.90
1532.49	Fe IV	−0.03	177005.97	242259.25
1533.02	Mn V	−0.15	178572.50	243803.10
1534.26	Fe V	−1.88	216860.40	282038.10
1534.42	Fe IV	−1.69	162087.81	227258.80
1535.28	Co IV	0.66	158846.70	223981.30
1536.57	Fe IV	−0.30	128191.54	193271.27
1538.28	Fe IV	−0.41	128541.85	193549.25
1539.19	Fe IV	−0.28	201212.22	266181.09
1539.74	Cr IV	−0.14	252464.80	187519.00
1540.55	Co IV	0.33	136612.50	201524.10
1540.72	Fe IV	−0.81	155744.87	220649.22
1541.00	Mn V	−0.18	177874.20	242766.90
1543.23	Fe V	−0.30	195196.30	259995.20
1543.56	Ni IV	−0.07	141220.30	206005.30

Table 28 – continued.

λ/ Å	Ion	$\log(gf)$	$E_{\rm low}$/ cm^{-1}	$E_{\rm up}$/ cm^{-1}
1544.48	Fe IV	0.47	168526.37	233272.84
1544.63	Fe IV	−0.79	158738.69	223478.96
1544.74	Fe IV	−0.86	159010.39	223745.82
1544.87	Co IV	−0.17	163717.90	228448.10
1546.40	Fe IV	−0.23	127929.12	192595.28
1546.55	Fe IV	−1.21	158738.69	223398.62
1547.77	Fe IV	−1.97	156049.32	220658.04
1548.68	Ni IV	−0.35	122386.10	186957.20
1549.77	Fe IV	−1.56	156123.77	220649.22
1550.45	Co IV	0.12	148105.50	212602.70
1550.90	Fe V	−0.07	195933.00	260411.40
1552.20	Fe IV	−0.36	156224.88	220649.22
1553.17	Fe IV	−0.59	137700.81	202085.22
1553.86	Ni IV	−0.55	159818.40	224174.00
1554.80	Ni IV	−0.12	144815.10	209131.90
1555.21	Co IV	−0.31	136611.20	200911.10
1555.94	Fe IV	−0.58	138338.83	202608.33
1556.06	Fe IV	−0.56	160311.64	224576.43
1556.66	Ni IV	−0.65	122717.40	186957.20
1557.64	Fe V	−1.08	219486.90	283686.30
1558.23	Ni IV	−0.44	112379.30	176554.40
1558.44	Mn V	−1.57	183538.80	247705.20
1558.67	Fe IV	0.05	201212.22	265369.48
1558.78	Fe IV	−1.10	154325.96	218478.36
1558.89	Fe IV	−1.05	156049.32	220197.25
1559.33	Ni IV	−0.59	122386.10	186516.10
1560.70	Fe IV	−0.48	156123.77	220197.25
1561.69	Mn V	−1.65	177874.20	241907.10
1562.75	Fe IV	0.03	138338.83	202328.53
1563.58	Fe IV	−0.14	155744.87	219700.53
1563.93	Fe V	−0.99	212818.10	276759.20
1568.71	Fe IV	−0.30	138338.83	202085.22
1568.84	Mn V	−0.14	195302.70	259043.80
1569.61	Co IV	−0.14	159482.30	223192.40
1571.24	Fe IV	0.15	154731.29	218375.12
1571.91	Co IV	0.35	148105.50	211722.00
1573.59	Fe IV	−0.40	154474.85	218023.81
1573.77	Fe IV	−0.95	156049.32	219590.84
1573.91	Co IV	0.15	153524.90	217060.70
1574.04	Co IV	0.16	159851.50	223382.30
1574.60	Fe IV	−0.08	171476.39	234984.35
1575.40	Fe IV	−0.08	156224.88	219700.53
1576.21	Fe V	−1.20	195933.00	259376.10

Table 28 – continued.

λ/ Å	Ion	$\log(gf)$	$E_{\rm low}$/ cm^{-1}	$E_{\rm up}$/ cm^{-1}
1576.43	Fe IV	−0.52	160311.64	223745.82
1578.02	Fe IV	−1.20	154474.85	217845.29
1578.61	Fe IV	−0.73	155744.87	219091.67
1578.74	Fe IV	0.14	165720.94	229062.58
1579.03	Ni IV	−1.20	146061.50	209391.40
1579.24	Fe IV	−0.81	156012.29	219333.90
1580.24	Fe IV	−0.72	158738.69	222020.09
1580.90	Fe IV	−1.36	127766.15	191021.18
1581.82	Ni V	−1.28	229413.00	292631.00
1583.32	Co IV	−0.27	129223.70	192382.00
1585.11	Fe IV	−0.32	160311.64	223398.62
1585.30	Fe IV	−0.54	156012.29	219091.67
1587.41	Fe IV	−1.12	171476.39	234472.00
1587.72	Co IV	−0.24	132729.10	195712.40
1588.69	Ni V	−1.21	229408.80	292353.40
1589.14	Co IV	−0.09	150970.90	213897.90
1590.11	Ni IV	−1.30	148358.20	211246.80
1590.23	Co IV	−0.59	132828.70	195712.40
1592.05	Fe IV	0.45	159342.88	222154.99
1592.32	Fe IV	−0.83	165392.58	228193.67
1594.04	Fe IV	−1.41	155744.87	218478.36
1594.52	Co IV	−0.02	102773.90	165488.50
1595.79	Fe IV	0.17	201212.22	263876.91
1597.67	Co IV	0.49	162889.00	225479.80
1597.90	Fe IV	−1.17	158738.69	221320.54
1598.82	Fe V	−0.57	195196.30	257742.30
1602.06	Fe IV	0.19	159227.90	221647.49
1603.58	Mn IV	0.35	137930.10	200290.40
1603.73	Fe IV	0.14	156123.77	218478.36
1604.67	Fe IV	0.08	165600.96	227919.05
1604.87	Fe IV	0.06	159010.39	221320.54
1605.54	Ni IV	0.14	179655.00	241939.00
1605.67	Fe IV	−0.24	155744.87	218023.81
1605.97	Fe IV	0.30	165392.58	227660.25
1606.33	Fe IV	−0.64	156224.88	218478.36
1611.59	Ni IV	−1.63	144815.10	206865.50
1614.64	Fe IV	0.04	159227.90	221161.02
1615.84	Co IV	−0.45	136612.50	198499.60
1616.12	Fe IV	−0.67	159227.90	221104.17
1617.04	Fe V	−0.94	196838.60	258680.00
1617.25	Fe IV	−0.21	156012.29	217845.29
1620.61	Mn III	0.97	173306.45	111601.45
1621.56	Fe IV	0.69	168526.37	230195.02

Table 28 – continued.

λ/ Å	Ion	$\log(gf)$	$E_{\rm low}$/ cm^{-1}	$E_{\rm up}$/ cm^{-1}
1623.38	Fe IV	0.37	183159.61	244759.25
1624.91	Fe IV	0.12	162087.81	223629.59
1625.69	Ni V	−1.46	235420.60	296932.90
1625.79	Fe IV	−0.83	190435.47	251944.03
1626.46	Fe IV	0.55	154325.96	215808.91
1626.90	Fe IV	0.05	128541.85	190008.28
1627.76	Ni IV	−0.91	145702.20	207136.00
1628.77	Ni IV	−0.83	152343.70	213739.70
1628.89	Fe IV	−1.00	162087.81	223478.96
1630.67	Fe IV	0.06	162074.42	223398.62
1632.08	Fe IV	0.08	154731.29	216002.72
1634.75	Fe IV	−0.47	165720.94	226892.10
1635.39	Fe IV	0.09	190811.79	251958.94
1636.68	Co IV	−0.43	159851.50	220950.80
1636.99	Fe IV	−1.00	165804.47	226892.10
1637.50	Ni IV	−0.86	152343.70	213412.10
1638.07	Fe IV	−0.67	165804.47	226851.93
1640.78	Fe IV	−0.06	168526.37	229472.83
1640.86	Ni IV	−1.27	145702.20	206645.70
1643.05	Mn V	−1.62	184635.60	245497.80
1644.05	Cr V	−0.17	167176.40	228001.80
1644.62	Ni IV	−0.93	146061.50	206865.50
1645.27	Fe IV	−0.75	168526.37	229306.61
1648.44	Co IV	−0.09	159482.30	220145.60
1650.39	Co IV	0.11	167856.50	228448.10
1654.30	Fe IV	−0.56	161571.59	222020.09
1655.64	Cr V	−0.50	168089.50	228489.10
1658.08	Cr IV	0.27	127208.30	187519.00
1658.43	Fe IV	−0.04	159342.88	219640.76
1659.15	Cr IV	−0.99	233637.60	173366.00
1659.31	Mn IV	0.51	152700.50	212966.50
1660.10	Fe IV	−0.04	128191.54	188428.78
1661.34	Mn IV	−0.47	111506.00	171698.30
1661.57	Fe IV	0.47	190318.34	250502.29
1662.31	Fe IV	−0.14	127929.12	188086.05
1662.51	Fe IV	0.21	160311.64	220461.33
1663.54	Fe IV	−0.32	127766.15	187878.81
1664.93	Fe IV	−0.82	156049.32	216111.69
1667.75	Fe IV	−0.18	190318.34	250279.06
1669.09	Fe IV	−1.02	177005.97	236918.79
1669.81	Fe IV	−0.91	128541.85	188428.78
1672.20	Fe IV	0.23	183164.49	242965.62
1672.86	Fe IV	0.15	156224.88	216002.72

Table 28 – continued.

λ/ Å	Ion	$\log(gf)$	E_{low}/ cm^{-1}	E_{up}/ cm^{-1}
1673.37	Fe IV	−0.01	190435.47	250195.07
1673.67	Fe IV	0.51	168566.43	228315.03
1675.66	Fe IV	0.53	168526.37	228204.33
1676.78	Fe IV	−0.08	168566.43	228204.33
1677.12	Fe IV	−0.18	164950.50	224576.43
1680.66	Ni IV	−1.02	147635.90	207136.00
1683.12	Mn IV	0.28	152986.00	212399.30
1683.28	Co IV	−0.74	136362.90	195770.50
1685.82	Fe IV	−1.18	160015.88	219333.90
1689.05	Co IV	−0.01	157513.10	216717.80
1689.61	Fe IV	−0.84	159010.39	218195.66
1690.86	Cr IV	0.06	124734.40	183875.60
1691.68	Mn IV	0.12	131170.10	190282.80
1691.85	Fe IV	−0.74	158738.69	217845.29
1693.68	Mn V	−1.82	184635.60	243678.50
1693.99	Fe IV	−0.81	159342.88	218375.12
1695.77	Fe IV	−0.28	154474.85	213445.05
1696.24	Co IV	−0.10	140863.50	199817.30
1697.02	Co V	−0.69	255292.50	314219.10
1697.50	Fe IV	−0.36	156123.77	215033.81
1698.15	Ni IV	−1.62	147635.90	206523.20
1698.30	Mn IV	0.44	112882.80	171765.00
1699.14	Mn IV	0.09	112013.30	170866.30
1700.81	Fe IV	0.04	164950.50	223745.82
1701.74	Mn V	−1.78	203811.80	262574.90
1702.38	Co IV	−0.56	141076.00	199817.30
1702.78	Fe IV	−0.98	158738.69	217466.19
1704.47	Cr IV	−1.08	233637.60	174968.60
1704.93	Fe IV	0.02	165392.58	224046.02

Table 29: Reduced Cu transitions according to the criteria and results obtained in Sect. 11.

λ/ Å	Ion	$\log(gf)_{\mathrm{TOSS}}$	$\log(gf)_{\mathrm{Kurucz}}$	E_{low}/ cm^{-1}	E_{up}/ cm^{-1}
900.05	Cu VI	−2.35	−2.26	309046	420151
900.85	Cu IV	−1.63	−1.52	200720	311727
901.44	Cu V	−2.29	−2.28	200648	311582
901.72	Cu IV	−2.47	−2.34	228480	339379
902.91	Cu VI	−1.93	−1.85	309111	419864
903.27	Cu V	−2.38	−2.30	229774	340483
905.02	Cu IV	−0.96	−1.03	228480	338975
905.59	Cu V	−2.32	−2.32	201413	311838
906.07	Cu VI	−1.63	−1.58	308998	419365
906.13	Cu V	−2.26	−2.23	199441	309801
906.38	Cu IV	−1.60	−1.49	229064	339393
906.46	Cu VI	−1.99	−1.97	309046	419365
906.67	Cu V	−2.41	−2.36	201413	311706
906.70	Cu IV	−2.35	−2.21	200720	311011
906.96	Cu V	−1.71	−1.69	227801	338059
907.00	Cu VI	−2.10	−2.03	309111	419365
907.87	Cu VI	−1.44	−1.39	322792	432939
908.22	Cu V	−2.47	−2.42	200648	310754
908.33	Cu IV	−1.01	−0.98	218628	328720
908.79	Cu VI	−1.44	−1.44	322805	432841
909.14	Cu IV	−1.43	−1.45	218726	328720
909.82	Cu IV	−1.14	−1.02	217445	327357
910.28	Cu V	−2.07	−2.05	201850	311706
910.88	Cu IV	−1.58	−1.52	214835	324619
910.95	Cu IV	−1.21	−1.23	218945	328720
911.28	Cu IV	−1.03	−1.08	217621	327357
912.09	Cu IV	−2.00	−1.96	222398	332036
912.37	Cu V	−2.39	−2.36	229774	339378
914.27	Cu V	−1.62	−1.59	199441	308818
914.44	Cu IV	−0.82	−0.91	218000	327357
914.57	Cu V	−2.13	−2.08	201413	310754
914.77	Cu IV	−2.12	−2.20	219403	328720
915.09	Cu V	−1.85	−1.82	243140	352419
915.59	Cu IV	−1.00	−0.91	218138	327357
916.14	Cu V	−1.90	−1.86	200648	309801
917.64	Cu VI	−2.45	−2.41	322792	431767
919.13	Cu V	−1.22	−1.18	256272	365071
919.13	Cu V	−2.20	−2.08	256273	365071
921.95	Cu VI	−1.57	−1.52	309046	417512
922.15	Cu IV	−2.35	−2.24	201211	309653
922.39	Cu VI	−2.17	−2.13	322805	431218
922.65	Cu V	−2.20	−2.22	199441	307825
923.07	Cu V	−1.36	−1.30	256272	364607

Table 29 – continued.

λ/ Å	Ion	$\log(gf)_{\mathrm{TOSS}}$	$\log(gf)_{\mathrm{Kurucz}}$	E_{low}/ cm^{-1}	E_{up}/ cm^{-1}
923.15	Cu V	−2.12	−2.06	278380	386705
923.54	Cu IV	−1.74	−1.68	201211	309490
924.77	Cu IV	−1.85	−1.90	203140	311274
924.98	Cu VI	−1.25	−1.26	309111	417221
925.05	Cu VI	−2.26	−2.18	308998	417100
925.07	Cu VI	−2.40	−2.37	299256	407356
926.02	Cu VI	−1.67	−1.80	309111	417100
926.89	Cu V	−1.54	−1.56	228048	335935
928.37	Cu IV	−2.43	−2.48	216703	324419
929.33	Cu V	−2.41	−2.40	239615	347219
929.96	Cu IV	−1.67	−1.68	221650	329182
930.98	Cu VI	−1.13	−1.15	308998	416411
931.30	Cu VI	−2.39	−2.32	299282	406659
931.60	Cu V	−2.46	−2.47	200648	307991
932.03	Cu IV	−1.81	−1.76	202361	309653
932.97	Cu IV	−2.09	−2.00	215133	322317
933.50	Cu V	−0.89	−0.83	256273	363397
934.34	Cu VI	−2.24	−2.35	308998	416025
934.74	Cu IV	−0.49	−0.55	221739	328720
935.69	Cu VI	−0.88	−0.89	322877	429750
936.42	Cu IV	−1.82	−1.72	215734	322524
936.46	Cu VI	−2.14	−2.10	322792	429578
936.99	Cu IV	−2.33	−2.36	203140	309865
937.15	Cu IV	−2.18	−2.28	214835	321542
937.43	Cu V	−1.99	−1.96	199441	306116
939.50	Cu IV	0.34	0.39	220917	327357
940.54	Cu IV	0.21	0.26	222398	328720
941.51	Cu VI	−2.08	−1.99	309046	415258
941.82	Cu IV	−1.48	−1.53	225859	332036
942.89	Cu V	−2.11	−1.98	226889	332946
943.13	Cu V	−1.90	−1.93	200648	306678
943.29	Cu V	−1.77	−1.79	199441	305453
943.91	Cu V	−1.20	−1.18	246477	352419
944.55	Cu V	−1.00	−0.93	256272	362143
944.56	Cu V	−1.34	−1.29	256273	362143
945.14	Cu IV	−2.07	−1.94	218815	324619
945.23	Cu V	−2.49	−2.49	246624	352419
945.90	Cu IV	−0.89	−0.78	223000	328720
945.98	Cu IV	−1.86	−1.79	217445	323155
946.29	Cu IV	−1.81	−1.83	233299	338975
946.74	Cu VI	−1.06	−1.08	322805	428431
947.18	Cu V	−2.01	−2.05	201413	306989
948.16	Cu V	−1.57	−1.54	200648	306116

Table 29 – continued.

λ/ Å	Ion	$\log(gf)_{\mathrm{TOSS}}$	$\log(gf)_{\mathrm{Kurucz}}$	E_{low}/ cm^{-1}	E_{up}/ cm^{-1}
949.16	Cu IV	−2.07	−2.05	190554	295910
949.98	Cu V	−1.82	−1.82	201413	306678
950.02	Cu VI	−1.74	−1.68	250877	356137
950.10	Cu VI	−2.29	−2.25	309046	414299
950.45	Cu V	−2.30	−2.40	199441	304655
950.66	Cu IV	−1.94	−1.95	192741	297931
951.12	Cu V	−1.99	−2.03	201850	306989
951.50	Cu IV	−1.55	−1.41	223623	328720
951.80	Cu IV	−2.15	−2.28	216071	321135
952.75	Cu IV	−1.35	−1.29	222398	327357
953.54	Cu IV	−1.13	−1.19	217445	322317
953.94	Cu V	−1.93	−1.99	201850	306678
954.14	Cu V	−1.64	−1.63	246624	351431
954.15	Cu V	−2.24	−2.27	200648	305453
954.56	Cu V	−2.34	−2.32	236059	340820
954.58	Cu V	−1.74	−1.85	199441	304199
954.94	Cu IV	−2.29	−2.29	242530	347249
955.08	Cu V	−1.73	−1.73	201413	306116
955.27	Cu V	−2.15	−2.13	236040	340723
955.44	Cu V	−1.95	−1.92	236059	340723
955.57	Cu IV	−0.27	−0.21	224071	328720
956.25	Cu VI	−1.81	−1.86	322792	427367
956.58	Cu VI	−0.94	−0.95	322792	427331
956.97	Cu IV	−2.02	−2.02	193434	297931
957.05	Cu V	−1.75	−1.73	236331	340820
957.26	Cu V	−2.32	−2.25	226889	331354
957.36	Cu IV	−2.13	−2.03	215133	319587
957.46	Cu V	−2.45	−2.45	236040	340483
957.93	Cu V	−2.34	−2.32	236331	340723
958.01	Cu VI	−1.30	−1.24	250877	355259
958.09	Cu V	−2.45	−2.46	236109	340483
958.61	Cu IV	−2.36	−2.48	218000	322317
959.51	Cu IV	−0.68	−0.70	243029	347249
959.60	Cu IV	−1.97	−1.97	218945	323155
959.96	Cu IV	−2.19	−2.23	192741	296912
960.17	Cu IV	−2.18	−2.23	191762	295910
960.43	Cu IV	−2.21	−2.26	193434	297554
960.84	Cu V	−2.47	−2.40	222401	326477
961.33	Cu V	−1.37	−1.35	234036	338059
961.63	Cu VI	−1.16	−1.09	299143	403133
962.68	Cu VI	−2.25	−2.16	299256	403133
963.02	Cu VI	−2.00	−1.97	299293	403133
963.09	Cu IV	−1.98	−2.05	192741	296573

Table 29 – continued.

λ/ Å	Ion	$\log(gf)_{\mathrm{TOSS}}$	$\log(gf)_{\mathrm{Kurucz}}$	E_{low}/ cm^{-1}	E_{up}/ cm^{-1}
963.11	Cu VI	−1.64	−1.58	299256	403087
963.34	Cu V	−2.20	−2.18	236040	339846
963.35	Cu VI	−1.72	−1.68	299282	403087
963.43	Cu V	−1.93	−1.93	239541	343337
963.45	Cu VI	−2.16	−2.10	299293	403087
963.69	Cu V	−1.41	−1.33	199441	303209
963.97	Cu VI	−1.62	−1.57	299251	402989
963.98	Cu V	−2.28	−2.26	236109	339846
964.26	Cu VI	−2.26	−2.21	299282	402989
964.30	Cu IV	−1.73	−1.81	220917	324619
964.36	Cu VI	−2.30	−2.23	299293	402989
964.45	Cu V	−1.96	−1.97	239615	343301
964.80	Cu IV	0.29	0.38	203869	307517
965.07	Cu IV	−1.40	−1.26	217445	321064
965.66	Cu IV	−1.69	−1.55	228480	332036
965.71	Cu V	−2.16	−2.26	200648	304199
965.97	Cu IV	−1.35	−1.37	243725	347249
966.16	Cu IV	−1.58	−1.63	218815	322317
966.90	Cu IV	−1.35	−1.27	218628	322051
966.98	Cu V	−2.22	−2.18	228020	331435
967.37	Cu IV	−1.50	−1.41	218945	322317
967.74	Cu IV	−1.53	−1.57	225387	328720
967.88	Cu V	−2.23	−2.19	236059	339378
968.07	Cu IV	0.21	0.29	203869	307167
968.85	Cu VI	−2.26	−2.14	309111	412326
969.39	Cu IV	−1.70	−1.74	192753	295910
969.80	Cu IV	0.03	0.10	203869	306983
969.87	Cu IV	−1.77	−1.70	218945	322051
970.71	Cu IV	−0.97	−0.95	221602	324619
972.19	Cu IV	−0.84	−0.85	225859	328720
972.33	Cu IV	−2.15	−2.08	190554	293399
972.37	Cu VI	−1.80	−1.83	299293	402134
972.47	Cu V	−2.40	−2.39	200648	303479
972.93	Cu IV	−2.02	−2.05	218000	320782
972.95	Cu IV	−1.87	−1.87	194132	296912
973.21	Cu VI	−1.83	−1.86	322792	425544
973.34	Cu VI	−1.43	−1.42	322805	425544
973.95	Cu IV	−1.57	−1.56	216071	318746
975.03	Cu V	−2.12	−2.00	200648	303209
975.65	Cu IV	−0.52	−0.54	244753	347249
975.91	Cu IV	−2.18	−2.14	195086	297554
976.06	Cu V	−1.75	−1.70	256272	358725
976.07	Cu IV	−1.53	−1.51	217445	319896

Table 29 – continued.

λ/ Å	Ion	$\log(gf)_{\mathrm{TOSS}}$	$\log(gf)_{\mathrm{Kurucz}}$	E_{low}/ cm^{-1}	E_{up}/ cm^{-1}
976.10	Cu IV	−1.50	−1.44	226271	328720
976.19	Cu IV	−2.17	−2.05	216071	318510
977.20	Cu IV	−1.50	−1.50	222398	324731
977.28	Cu IV	−0.74	−0.64	218628	320953
977.76	Cu IV	−1.50	−1.57	217621	319896
977.97	Cu V	−2.16	−2.14	220623	322876
978.27	Cu IV	−0.27	−0.36	222398	324619
978.44	Cu IV	−0.70	−0.64	222527	324731
978.58	Cu IV	−2.01	−1.95	217079	319268
978.65	Cu IV	−0.98	−1.01	227160	329341
979.00	Cu V	−2.47	−2.37	199441	301587
979.23	Cu VI	−0.76	−0.76	299143	401264
979.25	Cu IV	−1.73	−1.88	218945	321064
979.51	Cu IV	−2.04	−2.01	222527	324619
979.97	Cu IV	−0.04	0.04	245204	347249
980.31	Cu VI	−1.26	−1.26	299256	401264
980.67	Cu VI	−2.26	−2.21	299293	401264
980.68	Cu IV	−0.59	−0.57	225387	327357
981.39	Cu IV	−1.25	−1.38	218000	319896
981.77	Cu IV	−2.19	−2.16	195055	296912
981.86	Cu V	−1.90	−1.84	229588	331435
982.06	Cu IV	−2.08	−2.12	195086	296912
982.26	Cu V	−1.85	−1.75	220938	322744
982.32	Cu IV	0.29	0.33	230236	332036
982.53	Cu IV	−1.77	−1.85	194132	295910
982.94	Cu IV	−1.51	−1.37	220316	322051
983.02	Cu IV	−1.54	−1.54	195827	297554
983.24	Cu IV	−0.33	−0.37	230331	332036
983.43	Cu V	−2.45	−2.42	236331	338016
983.52	Cu V	−2.38	−2.32	256273	357948
984.32	Cu IV	−2.39	−2.47	225387	326980
984.38	Cu IV	−2.19	−2.30	218000	319587
984.45	Cu V	−1.72	−1.66	229774	331354
984.53	Cu IV	−1.41	−1.38	194339	295910
984.74	Cu IV	−0.50	−0.39	219403	320953
984.83	Cu VI	−1.13	−1.20	322792	424333
986.50	Cu IV	−1.39	−1.36	195544	296912
986.80	Cu IV	−1.37	−1.22	190528	291865
986.98	Cu V	−2.39	−2.37	228020	329340
987.10	Cu VI	−0.76	−0.77	299256	400563
987.15	Cu IV	−2.44	−2.47	217445	318746
987.36	Cu VI	−2.05	−2.03	299282	400563
987.36	Cu IV	−1.76	−1.84	214319	315599

Table 29 – continued.

λ/ Å	Ion	$\log(gf)_{\mathrm{TOSS}}$	$\log(gf)_{\mathrm{Kurucz}}$	E_{low}/ cm^{-1}	E_{up}/ cm^{-1}
987.46	Cu VI	−1.14	−1.15	299293	400563
987.81	Cu V	−2.39	−2.30	228105	329340
989.04	Cu IV	−0.32	−0.28	223623	324731
989.26	Cu IV	−2.11	−2.14	195827	296912
990.02	Cu IV	−2.07	−2.12	190554	291562
990.88	Cu V	−1.90	−1.96	221272	322192
991.25	Cu V	−1.21	−1.19	235053	335935
991.38	Cu IV	−2.35	−2.25	221739	322608
991.52	Cu IV	−1.24	−1.21	195055	295910
991.80	Cu VI	−1.58	−1.57	322792	423618
992.33	Cu IV	−1.42	−1.51	192741	293514
992.45	Cu IV	−1.54	−1.44	227960	328720
992.89	Cu IV	−1.16	−1.04	221602	322317
993.58	Cu IV	−1.82	−1.71	192753	293399
993.73	Cu VI	−2.10	−2.08	299251	399881
993.79	Cu IV	−1.14	−1.17	220917	321542
994.04	Cu VI	−1.09	−1.10	299282	399881
994.10	Cu IV	−1.15	−1.28	190554	291147
994.15	Cu VI	−0.75	−0.75	299293	399881
994.23	Cu IV	−1.94	−1.82	193434	294015
994.33	Cu IV	−2.42	−2.33	233299	333869
994.75	Cu V	−2.20	−2.27	221664	322192
995.09	Cu IV	−2.27	−2.21	219403	319896
995.12	Cu V	−2.08	−2.12	226889	327380
995.28	Cu V	−1.20	−1.12	222401	322876
995.37	Cu IV	−0.32	−0.44	215133	315599
995.70	Cu V	−2.20	−2.11	200648	301081
996.35	Cu IV	−2.04	−2.04	195544	295910
996.69	Cu VI	−2.08	−2.18	322792	423124
996.77	Cu IV	−1.46	−1.32	218945	319268
996.88	Cu IV	−1.29	−1.28	221739	322051
997.67	Cu V	−2.00	−1.97	230532	330765
998.00	Cu V	−2.31	−2.22	219203	319404
998.04	Cu V	−1.83	−1.84	243140	343337
998.08	Cu IV	−1.29	−1.28	191762	291954
998.16	Cu IV	−1.73	−1.58	219403	319587
998.16	Cu VI	−1.17	−1.18	299251	399435
998.39	Cu IV	−1.56	−1.64	217650	317811
998.48	Cu IV	−1.10	−1.09	214835	314988
998.48	Cu VI	−0.67	−0.68	299282	399435
998.53	Cu IV	−1.02	−1.13	220917	321064
998.74	Cu IV	−1.00	−0.86	222398	322524
999.33	Cu VI	−1.58	−1.57	322792	422859

Table 29 – continued.

λ/ Å	Ion	$\log(gf)_{\mathrm{TOSS}}$	$\log(gf)_{\mathrm{Kurucz}}$	E_{low}/ cm^{-1}	E_{up}/ cm^{-1}
999.51	Cu VI	−1.40	−1.55	322792	422841
999.58	Cu VI	−2.44	−2.43	322792	422834
1000.01	Cu IV	−0.86	−0.89	190554	290553
1000.03	Cu IV	0.19	0.11	222527	322524
1000.10	Cu V	−1.90	−1.85	222886	322876
1000.19	Cu VI	−1.05	−0.99	322877	422859
1000.24	Cu IV	−2.38	−2.49	226271	326248
1000.60	Cu IV	0.46	0.52	221602	321542
1000.66	Cu IV	−0.73	−0.65	213360	313295
1000.82	Cu IV	−0.75	−0.82	190528	290445
1001.35	Cu IV	−1.21	−1.06	219403	319268
1001.36	Cu IV	−0.38	−0.36	215734	315599
1001.36	Cu IV	−0.38	−0.36	215734	315599
1001.38	Cu VI	−0.70	−0.84	299251	399113
1001.42	Cu V	−2.44	−2.41	222886	322744
1001.45	Cu IV	−0.30	−0.25	215133	314988
1002.40	Cu IV	−0.92	−0.97	213535	313295
1002.49	Cu V	−1.49	−1.44	229588	329340
1002.55	Cu V	−2.46	−2.38	223477	323222
1002.81	Cu V	−1.59	−1.55	219203	318923
1003.17	Cu IV	0.02	0.11	220917	320601
1003.33	Cu V	−2.33	−2.28	201413	301081
1003.45	Cu IV	−2.34	−2.24	229064	328720
1003.48	Cu IV	−0.92	−0.82	222398	322051
1003.54	Cu IV	−1.50	−1.45	229694	329341
1003.72	Cu IV	−0.71	−0.73	213665	313295
1004.14	Cu IV	−2.30	−2.20	193434	293022
1005.38	Cu VI	−2.09	−2.00	322805	422270
1005.41	Cu IV	−0.27	−0.20	221602	321064
1005.74	Cu V	−2.03	−1.95	230532	329961
1005.76	Cu IV	−1.22	−1.24	214835	314262
1005.81	Cu IV	−0.79	−0.73	213535	312957
1006.37	Cu IV	−0.69	−0.55	217650	317017
1006.98	Cu V	−0.78	−0.72	222886	322192
1007.13	Cu IV	−0.26	−0.20	213665	312957
1007.34	Cu V	−2.28	−2.27	221664	320935
1007.50	Cu V	−1.11	−1.07	223214	322470
1007.56	Cu V	−1.84	−1.73	223214	322464
1007.90	Cu IV	−2.32	−2.22	231825	331042
1008.05	Cu IV	−0.91	−0.97	192753	291954
1008.76	Cu VI	−1.34	−1.41	309046	408178
1008.78	Cu IV	−1.41	−1.29	215133	314262
1008.85	Cu IV	−0.65	−0.77	191762	290885

Table 29 – continued.

λ/ Å	Ion	$\log(gf)_{\mathrm{TOSS}}$	$\log(gf)_{\mathrm{Kurucz}}$	E_{low}/ cm^{-1}	E_{up}/ cm^{-1}
1008.94	Cu IV	−0.36	−0.48	190528	289642
1009.12	Cu V	−2.18	−2.16	265975	365071
1009.14	Cu VI	−1.53	−1.47	299282	398377
1009.16	Cu V	−1.43	−1.38	223477	322569
1009.24	Cu IV	−2.03	−2.04	218726	317811
1009.25	Cu VI	−1.86	−1.79	299293	398377
1009.64	Cu IV	−0.51	−0.52	190528	289573
1009.75	Cu V	−1.31	−1.45	226889	325923
1009.90	Cu IV	0.16	0.24	190554	289573
1009.98	Cu IV	−0.17	−0.20	191762	290774
1010.11	Cu IV	−1.17	−1.09	221602	320601
1010.17	Cu V	−1.83	−1.80	223477	322470
1010.21	Cu IV	−0.66	−0.64	192741	291730
1010.31	Cu IV	−0.55	−0.40	220917	319896
1010.33	Cu V	−1.90	−1.88	223214	322192
1010.35	Cu IV	0.01	0.01	190554	289530
1011.02	Cu V	−1.81	−1.72	222886	321796
1011.23	Cu IV	−1.97	−1.90	194132	293022
1011.36	Cu IV	−2.33	−2.25	228480	327357
1011.37	Cu IV	−1.22	−1.19	222666	321542
1011.84	Cu IV	−0.34	−0.38	192741	291571
1012.06	Cu IV	−0.54	−0.49	192753	291562
1012.24	Cu IV	0.08	0.22	191762	290553
1012.79	Cu IV	0.11	0.13	233299	332036
1012.83	Cu IV	−0.99	−0.91	198179	296912
1012.86	Cu VI	−1.18	−1.12	299293	398023
1013.16	Cu IV	−1.84	−1.95	213360	312061
1013.52	Cu IV	−0.14	−0.07	222398	321064
1013.81	Cu IV	−0.89	−0.88	214319	312957
1013.86	Cu V	−1.94	−1.88	256272	354905
1013.87	Cu V	−2.08	−2.04	265975	364607
1013.89	Cu V	−1.73	−1.72	226889	325519
1014.25	Cu IV	−1.07	−1.14	218138	316732
1014.35	Cu IV	−0.54	−0.49	197325	295910
1014.69	Cu V	−2.40	−2.28	221664	320216
1014.73	Cu IV	−1.75	−1.62	213535	312083
1014.76	Cu IV	−1.22	−1.19	192753	291299
1014.85	Cu IV	−1.42	−1.41	222527	321064
1014.94	Cu IV	−0.72	−0.68	215734	314262
1015.03	Cu IV	−0.80	−0.89	217079	315599
1015.04	Cu V	−1.98	−1.94	239541	338059
1015.55	Cu IV	0.53	0.59	222666	321135
1015.56	Cu IV	−1.75	−1.72	217445	315912

Table 29 – continued.

λ/ Å	Ion	$\log(gf)_{\mathrm{TOSS}}$	$\log(gf)_{\mathrm{Kurucz}}$	E_{low}/ cm^{-1}	E_{up}/ cm^{-1}
1015.98	Cu IV	−1.14	−1.26	195086	293514
1016.07	Cu IV	−0.28	−0.21	214835	313253
1016.30	Cu IV	−1.78	−1.67	213665	312061
1016.32	Cu IV	−0.32	−0.41	192753	291147
1016.38	Cu IV	−1.69	−1.78	230331	328720
1016.38	Cu IV	−1.69	−1.78	230331	328720
1016.61	Cu IV	−0.83	−0.71	213360	311727
1016.69	Cu VI	−2.15	−2.10	308998	407356
1017.16	Cu V	−2.32	−2.33	226311	324624
1017.18	Cu IV	−0.10	0.02	214319	312630
1017.22	Cu IV	−0.43	−0.50	194132	292440
1017.34	Cu IV	0.17	0.22	193434	291730
1017.39	Cu IV	−1.88	−1.90	217621	315912
1017.39	Cu IV	−1.56	−1.64	218726	317017
1017.55	Cu V	−2.34	−2.31	256272	354548
1017.69	Cu VI	−0.95	−0.89	299143	397404
1017.85	Cu IV	−0.84	−0.87	221650	319896
1017.86	Cu VI	−2.09	−2.02	309111	407356
1018.03	Cu V	−1.28	−1.20	223214	321443
1018.45	Cu IV	−1.91	−1.93	195827	294015
1018.45	Cu IV	0.02	0.05	214413	312602
1018.64	Cu IV	0.64	0.69	190528	288698
1018.84	Cu V	−1.18	−1.11	223214	321365
1018.87	Cu VI	−1.06	−1.00	299256	397404
1018.98	Cu IV	0.23	0.28	215734	313872
1018.99	Cu IV	−0.52	−0.47	193434	291571
1019.12	Cu IV	−0.86	−0.72	215133	313257
1019.26	Cu VI	−1.26	−1.39	322805	420915
1019.35	Cu IV	−0.79	−0.71	221602	319704
1019.71	Cu V	−2.07	−2.09	223376	321443
1020.07	Cu IV	−0.21	−0.13	192741	290774
1020.28	Cu IV	0.32	0.38	190554	288566
1020.87	Cu IV	−0.90	−0.82	199599	297554
1020.90	Cu IV	−0.64	−0.67	223000	320953
1021.08	Cu IV	−0.26	−0.17	222666	320601
1021.27	Cu IV	−1.55	−1.62	193948	291865
1021.57	Cu V	−1.88	−1.83	223477	321365
1022.19	Cu IV	0.53	0.58	220917	318746
1022.55	Cu IV	−0.91	−1.00	214835	312630
1022.55	Cu IV	−0.91	−1.00	214835	312630
1022.83	Cu IV	−0.09	0.01	191762	289530
1022.85	Cu V	−2.13	−2.08	256273	354039
1023.12	Cu V	−2.43	−2.41	221664	319404

Table 29 – continued.

λ/ Å	Ion	$\log(gf)_{\mathrm{TOSS}}$	$\log(gf)_{\mathrm{Kurucz}}$	E_{low}/ cm^{-1}	E_{up}/ cm^{-1}
1023.22	Cu IV	0.33	0.39	198179	295910
1023.44	Cu IV	−0.72	−0.67	199202	296912
1023.76	Cu IV	−1.53	−1.61	214319	311998
1023.76	Cu IV	−1.53	−1.50	214319	311998
1023.82	Cu VI	−1.27	−1.22	299256	396929
1024.10	Cu VI	−2.05	−1.98	299282	396929
1024.13	Cu IV	−0.68	−0.79	216071	313715
1024.21	Cu VI	−2.41	−2.40	299293	396929
1024.26	Cu IV	−0.22	−0.10	214835	312467
1024.50	Cu IV	0.15	0.21	191762	289370
1024.53	Cu V	−1.65	−1.68	229774	327380
1024.62	Cu V	−1.24	−1.17	223477	321074
1024.80	Cu IV	−0.25	−0.14	214835	312416
1024.97	Cu IV	−0.32	−0.30	218628	316192
1025.00	Cu IV	−1.07	−1.01	218631	316192
1025.19	Cu IV	0.19	0.11	217445	314988
1025.24	Cu IV	0.04	0.16	241855	339393
1025.40	Cu IV	−0.34	−0.31	215734	313257
1025.44	Cu IV	0.49	0.52	215734	313253
1025.51	Cu IV	−1.02	−1.02	213665	311177
1025.53	Cu V	−1.85	−1.81	265886	363397
1025.88	Cu IV	−2.14	−2.01	195544	293022
1025.89	Cu IV	−1.88	−1.88	213535	311011
1025.90	Cu IV	−1.02	−0.93	222666	320142
1026.00	Cu IV	0.02	0.02	218726	316192
1026.08	Cu V	−1.61	−1.50	223477	320935
1026.71	Cu V	−0.68	−0.63	234036	331435
1026.80	Cu IV	−0.16	−0.20	222603	319993
1026.98	Cu V	−1.44	−1.45	256273	353646
1027.02	Cu IV	−0.72	−0.65	195544	292913
1027.05	Cu IV	−0.76	−0.64	217621	314988
1027.05	Cu VI	−1.97	−1.92	299251	396617
1027.13	Cu IV	−0.92	−0.95	224959	322317
1027.27	Cu IV	−1.85	−1.70	213665	311011
1027.30	Cu V	−2.42	−2.37	243140	340483
1027.38	Cu VI	−2.31	−2.25	299282	396617
1027.39	Cu IV	0.11	0.19	215133	312467
1027.44	Cu IV	−0.54	−0.54	223623	320953
1027.44	Cu IV	−0.54	−0.54	223623	320953
1027.49	Cu VI	−1.04	−0.99	299293	396617
1027.61	Cu IV	0.21	0.27	199599	296912
1027.61	Cu IV	−0.29	−0.30	214413	311727
1027.69	Cu V	−2.47	−2.47	226311	323617

Table 29 – continued.

λ/ Å	Ion	$\log(gf)_{\mathrm{TOSS}}$	$\log(gf)_{\mathrm{Kurucz}}$	E_{low}/ cm^{-1}	E_{up}/ cm^{-1}
1027.79	Cu IV	0.19	0.19	225859	323155
1028.18	Cu V	−1.94	−1.88	221664	318923
1028.45	Cu IV	−0.77	−0.78	242530	339764
1028.46	Cu IV	−0.16	−0.10	192741	289974
1028.57	Cu IV	−0.84	−0.81	194339	291562
1028.67	Cu V	−2.10	−2.03	256272	353486
1028.81	Cu IV	−2.13	−2.19	193948	291147
1028.85	Cu V	−1.60	−1.52	226311	323506
1028.92	Cu IV	0.20	0.06	222398	319587
1029.06	Cu IV	0.87	0.92	222527	319704
1029.20	Cu IV	0.26	0.28	214835	311998
1029.39	Cu IV	−1.20	−1.16	221602	318746
1029.52	Cu IV	−0.44	−0.49	243029	340162
1030.01	Cu IV	0.53	0.59	195827	292913
1030.17	Cu IV	−0.75	−0.69	200483	297554
1030.27	Cu IV	0.14	0.19	190528	287589
1030.55	Cu IV	0.48	0.52	190554	287589
1031.05	Cu IV	0.02	0.02	218000	314988
1031.24	Cu IV	−0.63	−0.54	218628	315599
1031.41	Cu IV	−0.15	−0.09	195684	292639
1031.87	Cu IV	−0.12	−0.12	195086	291997
1031.90	Cu IV	0.93	0.99	221602	318510
1031.91	Cu IV	0.84	0.89	214835	311743
1031.96	Cu V	−1.99	−1.97	222401	319304
1032.03	Cu IV	−1.39	−1.53	215734	312630
1032.03	Cu IV	−1.39	−1.53	215734	312630
1032.10	Cu V	−2.02	−2.13	229588	326477
1032.11	Cu IV	0.43	0.40	192753	289642
1032.34	Cu V	−2.28	−2.32	227801	324668
1032.36	Cu IV	0.25	0.31	215133	311998
1032.39	Cu IV	0.15	0.21	242530	339393
1032.41	Cu V	−1.27	−1.20	246477	343337
1032.41	Cu IV	−0.83	−0.70	214413	311274
1032.44	Cu IV	−1.08	−1.09	214319	311177
1032.69	Cu IV	0.19	0.25	200720	297554
1032.80	Cu V	−1.88	−1.83	246477	343301
1032.84	Cu IV	0.21	0.27	192753	289573
1032.87	Cu IV	−0.56	−0.44	217445	314262
1033.01	Cu IV	0.15	0.18	191762	288566
1033.14	Cu IV	−0.67	−0.66	217079	313872
1033.15	Cu IV	0.58	0.64	190528	287320
1033.18	Cu IV	−1.23	−1.22	219403	316192
1033.23	Cu IV	−0.37	−0.36	218815	315599

Table 29 – continued.

λ/ Å	Ion	$\log(gf)_{\mathrm{TOSS}}$	$\log(gf)_{\mathrm{Kurucz}}$	E_{low}/ cm^{-1}	E_{up}/ cm^{-1}
1033.28	Cu IV	0.29	0.29	243029	339809
1033.30	Cu IV	0.22	0.29	192753	289530
1033.42	Cu IV	−0.18	−0.17	190554	287320
1033.56	Cu IV	0.25	0.29	194132	290885
1033.56	Cu IV	0.25	0.29	194132	290885
1033.70	Cu IV	−1.36	−1.39	232442	329182
1033.74	Cu V	−1.93	−2.05	230532	327268
1033.75	Cu IV	0.07	0.17	243029	339764
1033.78	Cu IV	−1.26	−1.33	215734	312467
1034.04	Cu IV	−0.36	−0.35	199202	295910
1034.05	Cu IV	−0.22	−0.24	195932	292639
1034.16	Cu IV	−0.18	−0.14	213360	310057
1034.21	Cu IV	−1.54	−1.68	214319	311011
1034.32	Cu IV	0.35	0.41	215734	312416
1034.37	Cu V	−1.51	−1.45	246624	343301
1034.49	Cu IV	−0.23	−0.31	222603	319268
1034.62	Cu IV	0.15	0.19	218945	315599
1034.72	Cu IV	−0.25	−0.16	195086	291730
1034.76	Cu IV	0.07	0.08	194132	290774
1034.88	Cu IV	−0.02	0.02	192741	289370
1034.92	Cu IV	0.45	0.48	250623	347249
1035.38	Cu IV	−1.21	−1.11	224959	321542
1035.49	Cu VI	−0.57	−0.71	322792	419365
1035.57	Cu V	−0.54	−0.52	226311	322876
1035.84	Cu IV	−0.16	−0.11	193434	289974
1036.03	Cu IV	−0.85	−0.78	213535	310057
1036.20	Cu IV	0.77	0.82	195055	291562
1036.22	Cu IV	0.03	0.05	213360	309865
1036.30	Cu IV	−1.20	−1.17	193948	290445
1036.43	Cu IV	−0.22	−0.26	195086	291571
1036.47	Cu IV	−1.05	−0.96	214319	310800
1036.70	Cu VI	−2.07	−1.98	309046	405506
1036.77	Cu IV	−1.25	−1.22	195544	291997
1036.88	Cu IV	0.38	0.42	216071	312515
1037.03	Cu IV	−0.62	−0.61	200483	296912
1037.13	Cu IV	0.16	0.14	194132	290553
1037.15	Cu V	−2.35	−2.30	222886	319304
1037.41	Cu V	−2.38	−2.41	239541	335935
1037.53	Cu V	−1.92	−1.87	235053	331435
1037.67	Cu IV	−1.38	−1.26	223623	319993
1037.88	Cu VI	−2.26	−2.14	299251	395601
1037.90	Cu IV	−1.05	−1.03	222398	318746
1037.95	Cu IV	−1.00	−0.98	216071	312416

Table 29 – continued.

λ/ Å	Ion	$\log(gf)_{\mathrm{TOSS}}$	$\log(gf)_{\mathrm{Kurucz}}$	E_{low}/ cm^{-1}	E_{up}/ cm^{-1}
1038.10	Cu IV	0.05	0.11	213535	309865
1038.20	Cu V	−1.96	−1.91	239615	335935
1038.28	Cu IV	0.00	−0.01	195684	291997
1038.30	Cu IV	−0.72	−0.70	199599	295910
1038.32	Cu V	−1.19	−1.19	256272	352582
1038.58	Cu IV	−1.51	−1.54	198179	294464
1038.89	Cu V	−1.82	−1.78	265886	362143
1039.33	Cu IV	−0.87	−0.76	217079	313295
1039.36	Cu IV	0.08	0.01	195086	291299
1039.50	Cu IV	−0.85	−0.78	213665	309865
1039.55	Cu IV	−0.16	−0.09	219403	315599
1039.58	Cu IV	−1.79	−1.77	225859	322051
1039.58	Cu IV	−1.79	−1.77	225859	322051
1039.58	Cu IV	−0.65	−0.61	200720	296912
1039.58	Cu IV	−0.65	−0.61	200720	296912
1039.61	Cu V	−1.61	−1.58	223214	319404
1039.65	Cu IV	−0.94	−0.87	195544	291730
1039.74	Cu IV	−0.01	0.02	217079	313257
1039.82	Cu IV	−0.57	−0.48	195827	291997
1039.85	Cu V	−1.74	−1.68	265975	362143
1040.03	Cu VI	−0.48	−0.55	299256	395407
1040.04	Cu V	−1.32	−1.30	229774	325923
1040.08	Cu V	−1.22	−1.18	256272	352419
1040.31	Cu VI	−1.66	−1.74	299282	395407
1040.31	Cu IV	−0.20	−0.16	213932	310057
1040.38	Cu IV	0.37	0.43	213535	309653
1040.43	Cu VI	−0.94	−1.02	299293	395407
1040.52	Cu IV	0.85	0.92	194339	290445
1040.55	Cu VI	−1.57	−1.53	309111	405214
1040.68	Cu IV	−1.44	−1.41	200483	296573
1040.86	Cu V	−1.54	−1.44	227543	323617
1040.86	Cu IV	−1.42	−1.35	197325	293399
1041.17	Cu IV	−1.14	−1.15	195684	291730
1041.25	Cu IV	−0.03	0.12	243725	339764
1041.26	Cu V	−1.79	−1.75	222886	318923
1041.36	Cu V	−2.19	−2.10	223376	319404
1041.80	Cu IV	0.08	0.13	213665	309653
1042.01	Cu V	−2.49	−2.46	190100	286069
1042.06	Cu IV	−1.13	−1.17	223623	319587
1042.11	Cu V	−1.97	−1.93	189587	285546
1042.25	Cu IV	0.43	0.54	243029	338975
1042.30	Cu V	−1.75	−1.73	220208	316149
1042.36	Cu IV	−1.51	−1.43	193434	289370

Table 29 – continued.

λ/ Å	Ion	$\log(gf)_{\mathrm{TOSS}}$	$\log(gf)_{\mathrm{Kurucz}}$	E_{low}/ cm^{-1}	E_{up}/ cm^{-1}
1042.44	Cu V	−1.92	−1.90	221272	317201
1042.45	Cu V	−2.05	−2.03	223477	319404
1042.46	Cu IV	−0.23	−0.14	216071	311998
1042.51	Cu IV	−0.56	−0.58	224071	319993
1042.72	Cu IV	−0.32	−0.32	195827	291730
1043.06	Cu IV	−1.78	−1.78	218000	313872
1043.26	Cu IV	−1.03	−1.15	200720	296573
1043.36	Cu IV	−0.86	−0.75	222666	318510
1043.51	Cu IV	−0.53	−0.52	195055	290885
1043.54	Cu IV	−1.35	−1.45	191762	287589
1043.56	Cu IV	0.59	0.64	213665	309490
1043.68	Cu IV	0.14	0.14	220917	316732
1043.75	Cu IV	0.02	0.10	217445	313253
1044.06	Cu IV	0.25	0.27	226271	322051
1044.34	Cu IV	−0.02	0.07	195544	291299
1044.45	Cu IV	−2.18	−2.12	195827	291571
1044.49	Cu IV	0.95	1.00	193948	289688
1044.80	Cu V	−1.24	−1.24	235053	330765
1044.84	Cu V	−2.49	−2.46	223214	318923
1044.87	Cu V	−1.29	−1.31	227801	323506
1044.92	Cu IV	−1.07	−1.03	201211	296912
1045.06	Cu V	−1.74	−1.70	188833	284521
1045.15	Cu V	−2.33	−2.22	226889	322569
1045.22	Cu IV	−1.34	−1.33	217621	313295
1045.24	Cu IV	−0.29	−0.16	216071	311743
1045.29	Cu IV	0.10	0.05	229064	324731
1045.29	Cu IV	0.10	0.05	229064	324731
1045.29	Cu IV	0.10	0.05	229064	324731
1045.29	Cu IV	0.38	0.44	215133	310800
1045.29	Cu IV	0.38	0.44	215133	310800
1045.29	Cu IV	0.38	0.44	215133	310800
1045.61	Cu IV	−0.30	−0.43	228480	324118
1045.75	Cu IV	−1.36	−1.29	193948	289573
1046.35	Cu IV	−0.02	0.05	202361	297931
1046.36	Cu V	−1.15	−1.24	228048	323617
1046.50	Cu IV	0.94	0.99	216071	311628
1046.79	Cu IV	−1.87	−2.00	220316	315846
1046.88	Cu IV	−0.75	−0.87	217079	312602
1046.99	Cu IV	−1.97	−1.95	217445	312957
1047.14	Cu IV	0.21	0.25	195055	290553
1047.21	Cu IV	−0.86	−0.81	217109	312602
1047.23	Cu IV	0.33	0.39	244671	340162
1047.43	Cu IV	−0.51	−0.41	195827	291299

Table 29 – continued.

λ/ Å	Ion	$\log(gf)_{\mathrm{TOSS}}$	$\log(gf)_{\mathrm{Kurucz}}$	E_{low}/ cm^{-1}	E_{up}/ cm^{-1}
1047.69	Cu IV	0.37	0.42	218815	314262
1048.12	Cu IV	0.30	0.38	244753	340162
1048.25	Cu IV	−1.35	−1.41	194132	289530
1048.28	Cu IV	0.79	0.81	225387	320782
1048.36	Cu IV	−0.14	0.01	217079	312467
1048.44	Cu IV	−0.49	−0.46	216703	312083
1048.63	Cu IV	0.22	0.28	201211	296573
1048.80	Cu IV	0.34	0.36	244417	339764
1048.94	Cu IV	−1.16	−1.11	214319	309653
1048.94	Cu IV	−1.16	−1.11	214319	309653
1048.95	Cu V	−1.16	−1.15	227543	322876
1049.13	Cu IV	0.42	0.47	218945	314262
1049.29	Cu IV	−0.48	−0.50	194339	289642
1049.74	Cu IV	−0.97	−0.92	199202	294464
1049.83	Cu IV	−0.90	−0.77	218000	313253
1049.93	Cu V	−2.42	−2.42	236109	331354
1049.94	Cu IV	0.24	0.31	218628	313872
1050.05	Cu IV	0.36	0.41	194339	289573
1050.30	Cu V	−1.92	−1.90	220938	316149
1050.40	Cu V	−2.11	−2.00	227543	322744
1050.61	Cu IV	0.94	0.99	224959	320142
1050.73	Cu IV	−0.06	−0.01	214319	309490
1050.89	Cu V	−1.30	−1.26	256273	351431
1051.26	Cu IV	−0.11	−0.08	218171	313295
1051.34	Cu V	−1.34	−1.31	228105	323222
1051.58	Cu IV	0.76	0.82	214319	309414
1051.59	Cu IV	0.47	0.54	225859	320953
1051.61	Cu IV	−1.58	−1.44	244671	339764
1051.72	Cu IV	0.51	0.54	221650	316732
1052.00	Cu IV	−2.23	−2.16	218815	313872
1052.02	Cu IV	−0.08	0.01	244753	339809
1052.25	Cu V	−2.39	−2.38	219203	314238
1052.39	Cu IV	−0.39	−0.27	217445	312467
1052.51	Cu IV	−0.30	−0.32	244753	339764
1052.54	Cu IV	−0.42	−0.40	195544	290553
1052.54	Cu IV	−0.42	−0.40	195544	290553
1052.83	Cu IV	−0.08	−0.08	217079	312061
1052.95	Cu IV	0.15	0.19	217445	312416
1053.10	Cu IV	0.23	0.28	245204	340162
1053.16	Cu IV	−1.30	−1.43	217109	312061
1053.36	Cu V	−2.44	−2.39	189587	284521
1053.44	Cu IV	−0.63	−0.61	218945	313872
1053.50	Cu V	−0.74	−0.68	227543	322464

Table 29 – continued.

λ/ Å	Ion	$\log(gf)_{\mathrm{TOSS}}$	$\log(gf)_{\mathrm{Kurucz}}$	E_{low}/ cm^{-1}	E_{up}/ cm^{-1}
1053.73	Cu IV	0.87	0.92	218815	313715
1054.01	Cu V	−1.70	−1.62	243140	338016
1054.11	Cu VI	−1.43	−1.44	299251	394117
1054.24	Cu V	−2.14	−2.14	228020	322876
1054.46	Cu VI	−0.55	−0.57	299282	394117
1054.48	Cu V	−2.27	−2.15	227543	322376
1054.53	Cu IV	−1.50	−1.37	201211	296040
1054.58	Cu VI	−0.17	−0.20	299293	394117
1054.95	Cu IV	−0.26	−0.20	203140	297931
1055.25	Cu VI	−0.28	−0.23	299251	394015
1055.41	Cu IV	0.49	0.54	193948	288698
1055.47	Cu IV	−1.21	−1.12	224959	319704
1055.75	Cu VI	0.25	0.19	322792	417512
1055.88	Cu IV	0.85	0.89	244671	339379
1055.97	Cu IV	0.23	0.27	201211	295910
1056.34	Cu IV	−1.44	−1.38	218628	313295
1056.37	Cu IV	−1.05	−0.95	218631	313295
1056.66	Cu IV	0.06	0.06	217445	312083
1056.76	Cu IV	0.04	0.09	218628	313257
1057.04	Cu IV	0.55	0.62	245204	339809
1057.31	Cu IV	−1.90	−1.78	244813	339393
1057.36	Cu V	−0.72	−0.74	227801	322376
1057.46	Cu IV	0.04	0.08	192753	287320
1057.59	Cu V	−1.90	−1.82	226889	321443
1057.62	Cu IV	0.11	0.14	202361	296912
1057.75	Cu IV	0.85	0.92	197325	291865
1057.86	Cu IV	−0.11	−0.06	218726	313257
1057.86	Cu IV	−0.11	−0.06	218726	313257
1058.00	Cu IV	−0.57	−0.54	195055	289573
1058.03	Cu IV	0.70	0.76	218000	312515
1058.29	Cu IV	0.02	−0.05	218138	312630
1058.55	Cu IV	0.11	0.12	219403	313872
1058.57	Cu IV	−1.22	−1.15	218000	312467
1058.61	Cu IV	−0.73	−0.73	218138	312602
1058.62	Cu VI	−0.62	−0.59	322805	417267
1058.63	Cu IV	−2.00	−2.13	217621	312083
1058.83	Cu IV	−1.02	−0.93	195086	289530
1058.83	Cu V	−1.00	−0.89	228020	322464
1058.89	Cu IV	−1.10	−1.13	218815	313253
1058.94	Cu IV	−1.30	−1.22	194132	288566
1058.99	Cu VI	−0.75	−0.88	322792	417221
1059.14	Cu VI	0.30	0.33	322805	417221
1059.14	Cu IV	0.22	0.22	218000	312416

Table 29 – continued.

λ/ Å	Ion	$\log(gf)_{\mathrm{TOSS}}$	$\log(gf)_{\mathrm{Kurucz}}$	E_{low}/ cm^{-1}	E_{up}/ cm^{-1}
1059.16	Cu IV	−0.09	−0.07	203140	297554
1059.16	Cu IV	−0.76	−0.78	222603	317017
1059.43	Cu VI	−0.80	−0.68	322877	417267
1059.79	Cu V	−2.06	−2.03	228105	322464
1059.79	Cu IV	−0.70	−0.73	194339	288698
1059.80	Cu IV	−1.66	−1.70	215133	309490
1059.82	Cu V	−2.46	−2.37	228020	322376
1059.96	Cu V	−2.05	−2.04	246477	340820
1060.17	Cu IV	−2.26	−2.21	227993	322317
1060.31	Cu IV	−0.96	−0.96	218945	313257
1060.32	Cu IV	−0.85	−0.80	199202	293514
1060.35	Cu IV	0.17	0.21	218945	313253
1060.36	Cu IV	−0.19	−0.31	216703	311011
1060.41	Cu IV	−0.67	−0.60	244671	338975
1060.56	Cu IV	−0.95	−0.91	195684	289974
1060.59	Cu V	−0.95	−0.86	235053	329340
1060.62	Cu IV	−0.93	−0.88	195086	289370
1060.66	Cu IV	−0.76	−0.73	215133	309414
1060.89	Cu VI	0.38	0.43	250877	345137
1061.33	Cu IV	0.44	0.45	244753	338975
1061.43	Cu IV	−0.12	−0.07	202361	296573
1061.61	Cu IV	0.80	0.85	199202	293399
1061.63	Cu IV	−0.03	0.08	217079	311274
1061.71	Cu IV	−1.60	−1.51	223623	317811
1061.97	Cu IV	−1.19	−1.29	217109	311274
1062.17	Cu IV	−1.13	−1.12	195827	289974
1062.30	Cu VI	0.41	0.46	308998	403133
1062.32	Cu IV	−1.10	−1.12	225859	319993
1062.72	Cu V	−2.13	−2.05	246624	340723
1062.73	Cu IV	−1.14	−1.05	216703	310800
1062.80	Cu IV	−2.08	−1.94	229064	323155
1062.82	Cu VI	−0.71	−0.64	308998	403087
1063.03	Cu IV	−0.41	−0.40	220917	314988
1063.21	Cu IV	−0.84	−0.71	218028	312083
1063.30	Cu V	−2.23	−2.16	226889	320935
1063.36	Cu IV	−0.80	−0.79	195932	289974
1063.50	Cu V	−2.43	−2.31	229588	323617
1063.58	Cu VI	−1.12	−1.09	309111	403133
1063.76	Cu V	−2.12	−2.07	246477	340483
1063.84	Cu IV	0.28	0.34	218000	311998
1064.02	Cu IV	−1.44	−1.40	213535	307517
1064.04	Cu IV	0.70	0.76	200483	294464
1064.10	Cu VI	0.26	0.32	309111	403087

Table 29 – continued.

λ/ Å	Ion	$\log(gf)_{\mathrm{TOSS}}$	$\log(gf)_{\mathrm{Kurucz}}$	E_{low}/ cm^{-1}	E_{up}/ cm^{-1}
1064.13	Cu IV	−1.36	−1.44	218628	312602
1064.41	Cu IV	−0.91	−0.82	221650	315599
1064.43	Cu VI	0.59	0.64	299143	393090
1064.69	Cu IV	−1.87	−1.78	218138	312061
1064.80	Cu IV	−0.27	−0.21	199599	293514
1065.07	Cu IV	−0.72	−0.63	218171	312061
1065.21	Cu VI	−0.79	−0.71	309111	402989
1065.44	Cu V	−1.23	−1.17	246624	340483
1065.48	Cu IV	−0.38	−0.40	219403	313257
1065.66	Cu IV	−0.68	−0.67	218628	312467
1065.80	Cu IV	−1.11	−1.11	195544	289370
1065.85	Cu IV	0.39	0.43	197325	291147
1065.92	Cu IV	−2.38	−2.48	218815	312630
1066.02	Cu IV	−1.30	−1.23	213360	307167
1066.09	Cu V	−2.04	−2.00	265692	359492
1066.25	Cu IV	−2.43	−2.39	224959	318746
1066.39	Cu IV	0.05	0.12	198179	291954
1066.43	Cu IV	−0.58	−0.52	245204	338975
1066.87	Cu IV	−1.06	−0.92	217445	311177
1067.00	Cu IV	−0.90	−0.91	217079	310800
1067.25	Cu IV	−2.26	−2.26	218028	311727
1067.40	Cu IV	−0.57	−0.57	195684	289370
1067.91	Cu V	−1.58	−1.61	226311	319952
1067.98	Cu V	−1.72	−1.69	229588	323222
1068.12	Cu IV	−1.26	−1.11	213360	306983
1068.16	Cu VI	−0.66	−0.52	322792	416411
1068.31	Cu VI	0.02	0.13	322805	416411
1068.31	Cu V	−2.49	−2.48	265886	359492
1068.88	Cu IV	0.13	0.01	217621	311177
1068.96	Cu IV	−1.87	−1.99	227993	321542
1069.14	Cu VI	0.29	0.30	322877	416411
1069.27	Cu IV	0.03	0.14	218945	312467
1069.39	Cu IV	−1.06	−1.07	195055	288566
1069.50	Cu IV	−0.97	−0.85	213665	307167
1069.74	Cu IV	−0.50	−0.53	195086	288566
1069.85	Cu IV	−1.46	−1.35	218945	312416
1070.01	Cu IV	−0.25	−0.26	194132	287589
1070.02	Cu VI	−0.01	0.07	299256	392713
1070.04	Cu IV	−0.38	−0.40	218628	312083
1070.08	Cu VI	−0.96	−0.89	299143	392594
1070.11	Cu IV	−1.24	−1.14	213535	306983
1070.31	Cu VI	−0.70	−0.58	299282	392713
1070.32	Cu IV	0.02	0.07	218631	312061

Table 29 – continued.

λ/ Å	Ion	$\log(gf)_{\mathrm{TOSS}}$	$\log(gf)_{\mathrm{Kurucz}}$	E_{low}/ cm^{-1}	E_{up}/ cm^{-1}
1070.34	Cu V	−2.23	−2.24	223214	316643
1070.39	Cu VI	−1.51	−1.48	309111	402534
1070.40	Cu IV	0.08	0.13	199599	293022
1070.44	Cu VI	−0.41	−0.30	299293	392713
1070.91	Cu V	−0.83	−0.71	226311	319689
1070.97	Cu VI	0.15	0.16	299143	392517
1070.99	Cu IV	−0.16	−0.13	193948	287320
1071.11	Cu IV	−0.17	−0.10	217650	311011
1071.13	Cu IV	−0.77	−0.71	225387	318746
1071.17	Cu IV	−1.94	−1.90	218726	312083
1071.17	Cu IV	−0.42	−0.45	217445	310800
1071.30	Cu V	−0.55	−0.49	228020	321365
1071.38	Cu V	−1.70	−1.58	228105	321443
1071.38	Cu VI	0.51	0.56	299256	392594
1071.87	Cu IV	−0.16	−0.11	200720	294015
1072.26	Cu VI	−0.33	−0.26	299256	392517
1072.28	Cu V	−1.35	−1.32	228105	321365
1072.33	Cu V	−1.93	−1.91	265886	359141
1072.35	Cu IV	0.35	0.50	229064	322317
1072.35	Cu IV	0.35	0.50	229064	322317
1072.38	Cu IV	−0.91	−0.93	194339	287589
1072.41	Cu V	−2.39	−2.38	222886	316134
1072.58	Cu VI	0.00	0.09	322792	416025
1072.95	Cu IV	−2.38	−2.38	222398	315599
1073.15	Cu IV	−0.92	−0.78	218815	311998
1073.22	Cu IV	−0.85	−0.73	218000	311177
1073.46	Cu V	−1.16	−1.29	229588	322744
1073.63	Cu IV	0.72	0.77	227993	321135
1073.68	Cu IV	−0.79	−0.73	218945	312083
1074.02	Cu V	−1.49	−1.35	226311	319419
1074.08	Cu IV	−2.00	−1.94	218171	311274
1074.55	Cu IV	0.62	0.67	228480	321542
1074.81	Cu IV	0.41	0.49	218138	311177
1074.91	Cu IV	0.07	0.13	200483	293514
1075.00	Cu VI	−1.33	−1.41	309111	402134
1075.01	Cu IV	−1.78	−1.84	195544	288566
1075.30	Cu IV	−1.06	−1.01	226271	319268
1075.46	Cu IV	−0.14	−0.08	218028	311011
1075.50	Cu IV	−0.79	−0.79	194339	287320
1075.59	Cu V	−1.73	−1.69	265752	358725
1075.63	Cu V	−0.65	−0.60	228105	321074
1075.64	Cu IV	0.50	0.57	198179	291147
1075.95	Cu IV	−1.52	−1.42	220316	313257

Table 29 – continued.

λ/ Å	Ion	$\log(gf)_{\mathrm{TOSS}}$	$\log(gf)_{\mathrm{Kurucz}}$	E_{low}/ cm^{-1}	E_{up}/ cm^{-1}
1076.41	Cu V	−2.11	−2.10	246477	339378
1076.55	Cu VI	0.27	0.32	322805	415694
1076.74	Cu IV	−0.33	−0.21	218138	311011
1077.31	Cu IV	0.48	0.51	230331	323155
1077.39	Cu VI	0.30	0.35	322877	415694
1077.61	Cu IV	−2.24	−2.23	220917	313715
1077.64	Cu V	−1.96	−1.84	229774	322569
1077.66	Cu IV	0.23	0.32	200720	293514
1077.72	Cu IV	−1.14	−1.00	227993	320782
1077.72	Cu V	−1.13	−1.12	229588	322376
1078.13	Cu IV	−1.08	−1.14	214413	307167
1078.13	Cu V	−1.24	−1.24	246624	339378
1078.17	Cu V	−1.64	−1.62	265975	358725
1078.29	Cu IV	−1.42	−1.34	195827	288566
1078.68	Cu IV	−1.22	−1.15	198179	290885
1078.86	Cu V	−0.70	−0.66	230532	323222
1078.98	Cu IV	−0.03	0.02	219403	312083
1079.24	Cu V	−2.24	−2.24	223477	316134
1079.38	Cu IV	−0.53	−0.46	218628	311274
1079.41	Cu IV	−0.25	−0.34	218631	311274
1079.42	Cu VI	0.64	0.69	322877	415520
1079.82	Cu IV	0.51	0.52	227993	320601
1079.86	Cu V	−2.08	−1.97	229588	322192
1080.10	Cu IV	0.43	0.42	228480	321064
1080.52	Cu IV	−0.68	−0.64	218726	311274
1080.62	Cu IV	−1.82	−1.73	200483	293022
1080.68	Cu IV	−1.36	−1.39	195055	287589
1080.83	Cu V	−2.29	−2.28	190100	282622
1081.78	Cu V	−0.82	−0.75	234036	326477
1082.12	Cu IV	−2.07	−2.15	217079	309490
1082.15	Cu V	−2.15	−2.10	227543	319952
1082.25	Cu VI	0.25	0.30	250877	343277
1082.27	Cu VI	0.31	0.31	299293	391692
1082.45	Cu IV	−0.68	−0.65	218628	311011
1082.56	Cu IV	−1.10	−1.11	198179	290553
1082.75	Cu IV	−0.38	−0.51	229694	322051
1082.77	Cu V	−1.71	−1.69	189587	281942
1082.78	Cu IV	−0.89	−0.86	199599	291954
1083.23	Cu IV	−2.16	−2.07	197325	289642
1083.24	Cu V	−0.89	−0.87	272755	365071
1083.39	Cu IV	−1.42	−1.53	201211	293514
1083.56	Cu IV	−0.06	0.08	230236	322524
1083.59	Cu IV	−0.22	−0.34	220316	312602

Table 29 – continued.

λ/ Å	Ion	$\log(gf)_{\mathrm{TOSS}}$	$\log(gf)_{\mathrm{Kurucz}}$	E_{low}/ cm^{-1}	E_{up}/ cm^{-1}
1083.77	Cu V	−1.60	−1.55	272801	365071
1083.84	Cu IV	−1.37	−1.34	195055	287320
1083.93	Cu V	−2.45	−2.40	265692	357948
1084.22	Cu IV	−2.12	−2.11	218945	311177
1084.42	Cu V	−1.19	−1.08	235053	327268
1084.72	Cu V	−1.85	−1.83	265692	357881
1085.15	Cu VI	−1.12	−1.14	309111	401264
1085.18	Cu V	−1.43	−1.58	227801	319952
1085.52	Cu IV	−1.26	−1.39	228480	320601
1085.53	Cu IV	−1.33	−1.37	224071	316192
1085.82	Cu V	−1.34	−1.32	188833	280929
1086.18	Cu IV	−1.83	−1.79	218945	311011
1086.22	Cu V	−2.00	−1.94	265886	357948
1086.42	Cu IV	−1.34	−1.31	195544	287589
1087.27	Cu V	−2.40	−2.34	265975	357948
1087.32	Cu IV	−2.42	−2.43	217445	309414
1087.64	Cu VI	−0.70	−0.59	299256	391198
1087.95	Cu VI	0.30	0.35	299282	391198
1088.17	Cu V	−1.55	−1.46	220208	312106
1088.21	Cu V	−0.60	−0.59	239541	331435
1088.28	Cu V	−0.67	−0.61	227801	319689
1088.36	Cu IV	−1.28	−1.31	241855	333737
1088.50	Cu IV	−1.05	−1.01	217621	309490
1088.67	Cu IV	−1.24	−1.18	218945	310800
1088.71	Cu V	−0.92	−0.88	272755	364607
1088.83	Cu V	−1.94	−1.92	190100	281942
1089.08	Cu V	−1.33	−1.33	239615	331435
1089.20	Cu IV	−0.43	−0.38	201211	293022
1089.59	Cu V	−1.45	−1.44	229588	321365
1089.62	Cu IV	−2.04	−2.00	224071	315846
1089.64	Cu V	−1.68	−1.67	223214	314988
1090.27	Cu IV	−0.17	−0.09	230331	322051
1090.51	Cu IV	−1.26	−1.34	199599	291299
1090.74	Cu V	−0.27	−0.22	220208	311889
1091.05	Cu IV	−0.54	−0.49	202361	294015
1091.21	Cu V	−1.21	−1.19	187779	279421
1091.21	Cu V	−1.22	−1.17	228048	319689
1091.49	Cu V	−1.00	−0.95	227801	319419
1091.61	Cu IV	−0.75	−0.69	219403	311011
1092.12	Cu VI	−1.97	−1.90	308998	400563
1092.43	Cu V	−0.41	−0.39	246477	338016
1092.72	Cu V	−1.04	−0.95	220623	312138
1092.76	Cu V	−1.76	−1.75	223477	314988

Table 29 – continued.

λ/ Å	Ion	$\log(gf)_{\mathrm{TOSS}}$	$\log(gf)_{\mathrm{Kurucz}}$	E_{low}/ cm^{-1}	E_{up}/ cm^{-1}
1093.10	Cu V	−0.57	−0.52	220623	312106
1093.47	Cu VI	−1.82	−1.76	309111	400563
1093.78	Cu IV	−2.24	−2.37	218631	310057
1093.96	Cu IV	−0.70	−0.80	220316	311727
1094.17	Cu IV	−0.30	−0.37	198179	289573
1094.19	Cu V	−1.09	−1.07	246624	338016
1094.42	Cu IV	−1.66	−1.65	197325	288698
1094.48	Cu VI	0.22	0.27	299251	390618
1094.66	Cu V	−1.76	−1.72	222886	314238
1094.69	Cu IV	−1.05	−1.06	198179	289530
1094.71	Cu VI	0.10	0.16	250877	342225
1094.79	Cu V	−1.45	−1.44	189587	280929
1094.81	Cu V	−2.15	−2.01	236040	327380
1094.86	Cu VI	−2.31	−2.28	299282	390618
1094.93	Cu IV	−1.80	−1.92	221272	312602
1094.99	Cu VI	−1.20	−1.10	299293	390618
1095.48	Cu V	−1.74	−1.69	228020	319304
1095.70	Cu V	−1.12	−1.11	220623	311889
1095.81	Cu V	−0.58	−0.58	228048	319304
1095.92	Cu IV	−2.48	−2.43	200483	291730
1095.93	Cu V	−2.21	−2.15	219203	310450
1096.20	Cu IV	−1.73	−1.86	228480	319704
1096.27	Cu IV	−2.46	−2.44	221739	312957
1096.38	Cu V	−1.89	−1.84	236059	327268
1096.49	Cu V	−0.72	−0.68	220938	312138
1096.50	Cu V	−1.79	−1.82	228105	319304
1096.88	Cu V	−1.38	−1.37	220938	312106
1096.95	Cu V	−1.92	−1.83	229774	320935
1097.09	Cu V	−0.79	−0.84	239615	330765
1097.87	Cu IV	−1.40	−1.50	201211	292297
1097.92	Cu IV	−1.85	−1.79	220917	311998
1098.48	Cu VI	−0.12	−0.06	265639	356674
1098.60	Cu IV	−2.34	−2.19	218628	309653
1098.62	Cu V	−2.16	−2.17	223214	314238
1098.78	Cu IV	−1.92	−1.92	200720	291730
1099.26	Cu V	−0.98	−0.95	265692	356662
1099.40	Cu IV	−0.74	−0.73	220316	311274
1099.46	Cu IV	−0.77	−0.83	199599	290553
1099.55	Cu V	−1.92	−1.88	256273	347219
1099.97	Cu V	−1.87	−1.83	230532	321443
1100.23	Cu V	−1.67	−1.62	226311	317201
1100.31	Cu V	−0.52	−0.46	187779	278663
1100.40	Cu IV	−0.19	−0.14	203140	294015

Table 29 – continued.

λ/ Å	Ion	$\log(gf)_{\mathrm{TOSS}}$	$\log(gf)_{\mathrm{Kurucz}}$	E_{low}/ cm^{-1}	E_{up}/ cm^{-1}
1100.52	Cu V	−1.54	−1.56	221272	312138
1100.56	Cu IV	−1.10	−0.97	221739	312602
1100.92	Cu V	−1.30	−1.24	230532	321365
1100.98	Cu IV	−0.68	−0.63	230236	321064
1101.31	Cu V	−0.63	−0.63	221272	312073
1101.89	Cu IV	0.38	0.42	227993	318746
1102.01	Cu IV	0.28	0.36	201211	291954
1102.22	Cu IV	−1.53	−1.47	222527	313253
1102.97	Cu V	−0.90	−0.84	188833	279497
1103.01	Cu IV	−0.04	0.02	202361	293022
1103.21	Cu V	−1.23	−1.21	220938	311582
1103.25	Cu V	−1.72	−1.69	272755	363397
1103.36	Cu V	−1.33	−1.27	234036	324668
1103.49	Cu IV	−0.02	−0.11	230331	320953
1103.51	Cu V	−0.74	−0.67	265752	356372
1103.63	Cu V	−0.89	−0.82	220623	311233
1103.78	Cu V	−2.40	−2.40	219203	309801
1103.80	Cu V	−1.12	−1.07	272801	363397
1103.89	Cu V	−1.10	−1.09	188833	279421
1104.01	Cu IV	−1.58	−1.52	200720	291299
1104.17	Cu V	−1.19	−1.08	221272	311838
1104.33	Cu IV	−2.16	−2.17	202361	292913
1104.46	Cu V	−1.33	−1.31	230532	321074
1104.77	Cu IV	−0.87	−0.92	227993	318510
1105.00	Cu VI	0.10	0.15	265639	356137
1105.14	Cu V	−0.84	−0.80	265886	356372
1105.23	Cu V	−1.63	−1.53	189587	280066
1105.52	Cu IV	−0.74	−0.84	221272	311727
1105.67	Cu V	−2.08	−2.10	229774	320216
1106.06	Cu IV	−1.95	−1.95	221650	312061
1106.23	Cu V	−0.05	−0.01	265975	356372
1106.56	Cu IV	−1.95	−1.96	199202	289573
1106.75	Cu IV	−2.38	−2.46	222603	312957
1106.88	Cu IV	−0.86	−0.87	221739	312083
1107.02	Cu IV	−2.16	−2.30	225859	316192
1107.08	Cu IV	−2.02	−1.98	199202	289530
1107.14	Cu IV	−1.08	−1.08	221739	312061
1107.20	Cu V	−1.95	−1.95	221664	311982
1107.64	Cu V	−1.11	−1.05	220938	311220
1107.72	Cu V	−0.45	−0.39	220208	310483
1107.75	Cu V	−2.49	−2.47	190100	280373
1107.83	Cu IV	−0.88	−0.86	228480	318746
1107.86	Cu IV	−1.17	−1.19	197325	287589

Table 29 – continued.

λ/ Å	Ion	$\log(gf)_{\mathrm{TOSS}}$	$\log(gf)_{\mathrm{Kurucz}}$	E_{low}/ cm^{-1}	E_{up}/ cm^{-1}
1107.91	Cu IV	−0.75	−0.71	220917	311177
1108.01	Cu V	−1.38	−1.42	220623	310875
1108.77	Cu IV	−1.90	−1.86	219867	310057
1109.31	Cu V	−1.05	−1.00	236331	326477
1109.37	Cu IV	−1.64	−1.69	221602	311743
1109.60	Cu V	0.34	0.39	265752	355875
1111.08	Cu V	−0.67	−0.62	189587	279590
1111.18	Cu IV	−1.59	−1.56	197325	287320
1111.45	Cu V	−1.70	−1.68	190400	280373
1111.54	Cu V	−0.81	−0.75	190100	280066
1111.75	Cu V	−1.72	−1.69	221272	311220
1111.89	Cu V	−1.15	−1.02	220938	310875
1112.17	Cu V	−0.75	−0.71	265692	355606
1112.23	Cu V	−0.68	−0.62	189587	279497
1112.35	Cu V	−0.58	−0.53	265975	355875
1112.39	Cu IV	−0.05	0.04	217621	307517
1112.55	Cu V	−2.19	−2.09	236040	325923
1112.57	Cu IV	−0.95	−0.85	203140	293022
1112.79	Cu V	−1.85	−1.74	236059	325923
1112.88	Cu IV	−0.97	−0.93	233299	323155
1113.20	Cu V	−1.48	−1.42	229588	319419
1113.21	Cu V	−0.85	−0.79	188833	278663
1113.51	Cu V	−1.12	−1.08	243140	332946
1113.94	Cu IV	−2.31	−2.41	199599	289370
1114.34	Cu IV	−1.80	−1.92	225859	315599
1114.51	Cu IV	−1.39	−1.26	222336	312061
1114.52	Cu V	−0.70	−0.66	239615	329340
1114.58	Cu V	−0.02	0.03	265886	355606
1114.62	Cu V	−0.85	−0.80	229588	319304
1115.02	Cu IV	−1.01	−0.91	222398	312083
1115.15	Cu IV	−0.80	−0.84	201211	290885
1115.18	Cu V	−1.79	−1.80	222401	312073
1115.26	Cu V	−1.92	−1.77	190400	280066
1115.63	Cu VI	0.25	0.29	322805	412440
1115.65	Cu IV	−1.72	−1.63	223623	313257
1115.65	Cu IV	−2.31	−2.22	226558	316192
1115.69	Cu V	−1.35	−1.26	265975	355606
1115.70	Cu IV	−2.09	−2.16	223000	312630
1115.82	Cu VI	0.24	0.29	265639	355259
1116.03	Cu V	−1.25	−1.22	221272	310875
1116.05	Cu IV	−2.15	−2.21	223000	312602
1116.06	Cu IV	−1.06	−0.99	225387	314988
1116.16	Cu IV	−0.98	−0.85	202361	291954

Table 29 – continued.

λ/ Å	Ion	$\log(gf)_{\mathrm{TOSS}}$	$\log(gf)_{\mathrm{Kurucz}}$	E_{low}/ cm^{-1}	E_{up}/ cm^{-1}
1116.51	Cu VI	0.49	0.54	299143	388708
1116.54	Cu IV	−1.73	−1.78	201211	290774
1116.54	Cu VI	0.21	0.26	322877	412440
1116.75	Cu IV	−0.50	−0.43	217621	307167
1116.89	Cu VI	0.19	0.23	322792	412326
1117.05	Cu VI	−0.28	−0.19	322805	412326
1117.45	Cu V	−0.50	−0.45	190100	279590
1117.54	Cu V	−2.48	−2.37	221272	310754
1117.58	Cu V	−1.99	−1.92	236040	325519
1117.69	Cu V	−0.89	−0.75	234036	323506
1117.79	Cu V	−0.28	−0.23	188833	278295
1117.82	Cu V	−2.03	−1.99	236059	325519
1117.83	Cu V	−2.39	−2.32	246477	335935
1117.92	Cu VI	−1.13	−1.06	299256	388708
1118.44	Cu IV	−1.80	−1.75	198179	287589
1118.56	Cu V	−1.48	−1.52	227801	317201
1118.72	Cu V	−0.45	−0.39	272755	362143
1119.02	Cu IV	−1.81	−1.83	199202	288566
1119.29	Cu V	−1.36	−1.33	272801	362143
1119.35	Cu IV	−1.89	−2.02	220316	309653
1119.83	Cu VI	−0.34	−0.26	299143	388442
1120.17	Cu IV	−1.12	−1.08	221739	311011
1120.25	Cu VI	−1.08	−1.04	309111	398377
1120.38	Cu IV	−1.09	−1.15	230331	319587
1120.40	Cu IV	−2.33	−2.40	200720	289974
1120.51	Cu V	−2.01	−1.98	226889	316134
1120.76	Cu IV	0.29	0.43	233299	322524
1120.95	Cu IV	−2.10	−2.20	202361	291571
1121.21	Cu V	−0.39	−0.34	190400	279590
1121.24	Cu V	−1.33	−1.31	236331	325519
1121.25	Cu VI	0.34	0.39	299256	388442
1121.32	Cu V	−1.53	−1.54	228020	317201
1121.66	Cu V	−0.06	−0.06	228048	317201
1121.67	Cu V	−0.22	−0.17	265752	354905
1121.72	Cu VI	−1.33	−1.26	299293	388442
1121.72	Cu V	−0.86	−0.81	220623	309772
1121.83	Cu IV	−1.50	−1.54	198179	287320
1122.27	Cu V	−0.07	−0.02	265692	354797
1122.58	Cu VI	0.30	0.35	322792	411872
1122.75	Cu VI	0.05	0.10	322805	411872
1122.82	Cu V	−1.76	−1.79	220208	309269
1122.89	Cu VI	−0.29	−0.22	299256	388312
1123.21	Cu VI	−1.63	−1.54	299282	388312

Table 29 – continued.

λ/ Å	Ion	$\log(gf)_{\mathrm{TOSS}}$	$\log(gf)_{\mathrm{Kurucz}}$	E_{low}/ cm^{-1}	E_{up}/ cm^{-1}
1123.28	Cu VI	−1.08	−1.06	308998	398023
1123.35	Cu VI	0.23	0.27	299293	388312
1123.35	Cu V	−0.80	−0.72	265886	354905
1123.51	Cu IV	−1.17	−1.18	243029	332036
1123.64	Cu IV	−0.50	−0.47	218171	307167
1123.66	Cu VI	−0.98	−0.91	322877	411872
1124.07	Cu IV	−1.38	−1.40	222666	311628
1124.18	Cu VI	0.10	0.14	299282	388236
1124.31	Cu VI	−0.35	−0.29	299293	388236
1124.34	Cu VI	−0.04	0.01	299251	388192
1124.48	Cu V	−0.22	−0.14	265975	354905
1124.71	Cu VI	0.39	0.45	309111	398023
1124.72	Cu V	−2.28	−2.38	265886	354797
1124.74	Cu VI	−0.56	−0.49	299282	388192
1125.00	Cu IV	−1.78	−1.73	218628	307517
1125.02	Cu IV	−2.16	−2.15	200483	289370
1125.33	Cu V	−1.15	−1.15	220938	309801
1125.38	Cu V	−2.21	−2.22	223214	312073
1125.41	Cu V	−1.14	−1.08	265692	354548
1125.63	Cu V	−2.15	−2.23	234036	322876
1125.70	Cu V	−2.32	−2.30	220938	309772
1125.73	Cu V	−1.41	−1.35	222401	311233
1125.89	Cu V	−1.88	−1.94	222401	311220
1125.98	Cu IV	−1.00	−0.98	218171	306983
1126.13	Cu V	−1.67	−1.68	236109	324909
1126.21	Cu IV	−2.46	−2.39	244943	333737
1126.29	Cu V	−2.19	−2.17	219203	307991
1126.30	Cu V	−1.52	−1.51	221664	310450
1126.39	Cu IV	−2.35	−2.43	222398	311177
1126.68	Cu IV	−1.72	−1.62	224959	313715
1127.30	Cu V	−0.36	−0.31	189587	278295
1127.44	Cu V	−0.95	−0.93	222886	311582
1127.88	Cu V	−0.74	−0.66	265886	354548
1128.08	Cu V	−0.70	−0.65	220623	309269
1128.37	Cu V	−1.21	−1.23	223214	311838
1128.38	Cu V	−1.22	−1.21	228020	316643
1128.50	Cu IV	−1.40	−1.52	222398	311011
1128.58	Cu V	−1.03	−1.02	227543	316149
1128.59	Cu V	−1.88	−1.81	223376	311982
1128.73	Cu V	−1.28	−1.30	228048	316643
1128.76	Cu IV	−1.77	−1.83	221272	309865
1128.79	Cu IV	−1.74	−1.73	203140	291730
1128.81	Cu V	0.01	0.07	187779	276368

Table 29 – continued.

λ/ Å	Ion	$\log(gf)_{\mathrm{TOSS}}$	$\log(gf)_{\mathrm{Kurucz}}$	E_{low}/ cm^{-1}	E_{up}/ cm^{-1}
1129.01	Cu V	−0.45	−0.41	265975	354548
1129.12	Cu V	−0.60	−0.52	235053	323617
1129.45	Cu IV	−2.13	−2.08	218628	307167
1129.47	Cu V	−2.11	−2.09	228105	316643
1129.57	Cu V	−1.81	−1.79	221272	309801
1129.63	Cu IV	−1.59	−1.69	202361	290885
1130.28	Cu V	−0.82	−0.84	222401	310875
1130.73	Cu IV	−1.15	−1.08	223623	312061
1131.13	Cu VI	0.48	0.53	308998	397404
1131.72	Cu V	−1.96	−2.04	223477	311838
1131.79	Cu V	−0.92	−0.84	220938	309294
1131.88	Cu V	0.21	0.25	227801	316149
1132.06	Cu V	−1.33	−1.34	222886	311220
1132.11	Cu V	−1.18	−1.14	220938	309269
1132.26	Cu IV	−1.49	−1.54	201211	289530
1132.53	Cu V	−0.25	−0.21	221272	309570
1132.54	Cu IV	−1.27	−1.16	223764	312061
1132.57	Cu V	−1.88	−1.77	243140	331435
1132.84	Cu IV	−2.35	−2.46	223000	311274
1133.11	Cu IV	−1.61	−1.75	244753	333006
1133.11	Cu IV	−1.61	−1.75	244753	333006
1133.23	Cu IV	−0.72	−0.74	233299	321542
1133.37	Cu IV	−1.64	−1.71	227960	316192
1133.40	Cu V	−1.19	−1.19	223477	311706
1133.82	Cu IV	−1.39	−1.38	222603	310800
1133.85	Cu V	−1.60	−1.63	220623	308818
1133.86	Cu V	−0.42	−0.38	190100	278295
1134.17	Cu V	−0.62	−0.61	235053	323222
1134.31	Cu IV	−1.92	−1.91	201211	289370
1134.39	Cu V	−0.27	−0.22	265886	354039
1134.89	Cu IV	−2.19	−2.06	219403	307517
1135.08	Cu V	−1.47	−1.41	226889	314988
1135.31	Cu V	−1.94	−1.91	222401	310483
1135.86	Cu V	−2.02	−2.00	221664	309703
1135.99	Cu V	−1.23	−1.19	228105	316134
1136.08	Cu V	−1.14	−1.10	221272	309294
1136.23	Cu IV	−2.49	−2.42	223000	311011
1136.29	Cu V	−1.01	−0.97	223214	311220
1136.50	Cu V	−1.34	−1.29	222886	310875
1137.20	Cu V	−2.20	−2.26	219203	307139
1137.25	Cu VI	0.27	0.33	308998	396929
1137.68	Cu V	−0.51	−0.47	265692	353590
1137.74	Cu V	−1.42	−1.46	265752	353646

Table 29 – continued.

λ/ Å	Ion	$\log(gf)_{\mathrm{TOSS}}$	$\log(gf)_{\mathrm{Kurucz}}$	E_{low}/ cm^{-1}	E_{up}/ cm^{-1}
1137.92	Cu V	−1.90	−1.91	220938	308818
1138.07	Cu V	−2.40	−2.37	222886	310754
1138.21	Cu V	−0.47	−0.40	220208	308065
1138.72	Cu VI	−0.74	−0.67	309111	396929
1138.95	Cu IV	−1.67	−1.63	223000	310800
1139.03	Cu V	−1.64	−1.57	265692	353486
1139.40	Cu IV	−0.53	−0.57	233299	321064
1139.47	Cu V	−0.89	−0.87	265886	353646
1140.22	Cu V	−1.61	−1.67	219203	306906
1140.63	Cu V	−0.95	−0.98	265975	353646
1140.85	Cu IV	−1.02	−1.11	233299	320953
1140.86	Cu V	−0.68	−0.67	239615	327268
1141.23	Cu V	−1.46	−1.47	243140	330765
1141.31	Cu IV	−2.21	−2.10	244417	332036
1141.38	Cu IV	−2.11	−2.09	202361	289974
1141.56	Cu V	−1.33	−1.24	265886	353486
1142.34	Cu V	−1.13	−1.11	223214	310754
1142.35	Cu IV	−2.31	−2.43	219403	306942
1142.40	Cu V	−0.41	−0.35	188833	276368
1142.72	Cu V	−0.40	−0.35	265975	353486
1142.73	Cu IV	−1.25	−1.24	223764	311274
1142.78	Cu VI	0.12	0.18	309111	396617
1143.13	Cu IV	−0.79	−0.89	230331	317811
1143.19	Cu V	−2.30	−2.19	219203	306678
1143.61	Cu V	−0.67	−0.64	220623	308065
1144.01	Cu V	−1.59	−1.66	235053	322464
1144.55	Cu V	−1.49	−1.44	222401	309772
1144.75	Cu IV	−1.39	−1.40	201211	288566
1144.83	Cu V	−0.64	−0.58	226889	314238
1145.44	Cu V	−2.33	−2.30	272755	360058
1145.44	Cu IV	−2.11	−2.17	233299	320601
1145.70	Cu IV	−0.92	−0.89	244753	332036
1145.77	Cu V	−1.54	−1.55	223477	310754
1146.77	Cu IV	−1.78	−1.78	220316	307517
1146.77	Cu V	−0.42	−0.35	220623	307825
1147.75	Cu V	−0.78	−0.86	220938	308065
1148.13	Cu IV	−2.41	−2.39	225859	312957
1148.44	Cu V	−1.32	−1.28	223376	310450
1148.57	Cu V	0.22	0.27	256272	343337
1148.58	Cu V	−0.76	−0.71	256273	343337
1148.70	Cu V	−0.91	−0.89	229588	316643
1148.73	Cu V	−0.46	−0.39	220938	307991
1149.05	Cu V	0.14	0.19	256273	343301

Table 29 – continued.

λ/ Å	Ion	$\log(gf)_{\mathrm{TOSS}}$	$\log(gf)_{\mathrm{Kurucz}}$	E_{low}/ cm^{-1}	E_{up}/ cm^{-1}
1149.30	Cu IV	−1.55	−1.55	202361	289370
1150.22	Cu IV	−1.14	−1.02	224071	311011
1150.27	Cu V	−0.85	−0.84	239541	326477
1150.54	Cu V	−1.30	−1.28	222886	309801
1150.59	Cu V	−1.80	−1.74	219203	306116
1150.60	Cu IV	−2.33	−2.24	218945	305856
1150.84	Cu V	−0.70	−0.68	222401	309294
1150.93	Cu V	−0.44	−0.41	220938	307825
1150.93	Cu V	−0.44	−0.41	220938	307825
1150.93	Cu V	−0.49	−0.47	222886	309772
1150.93	Cu V	−0.49	−0.47	222886	309772
1150.98	Cu V	−1.79	−1.71	228105	314988
1151.24	Cu V	−2.11	−2.03	239615	326477
1151.39	Cu IV	−2.06	−2.10	220316	307167
1151.62	Cu IV	−1.82	−1.81	203140	289974
1151.65	Cu IV	−0.51	−0.40	245204	332036
1151.68	Cu V	−0.90	−0.88	265752	352582
1151.80	Cu V	−2.30	−2.26	243140	329961
1152.22	Cu V	−0.56	−0.54	278282	365071
1152.33	Cu V	−0.43	−0.41	189587	276368
1152.91	Cu V	−1.01	−0.95	272755	359492
1153.15	Cu V	−0.69	−0.64	221272	307991
1153.52	Cu V	0.14	0.19	272801	359492
1153.52	Cu V	0.14	0.19	272801	359492
1153.52	Cu V	0.22	0.27	278380	365071
1153.52	Cu V	0.22	0.27	278380	365071
1153.61	Cu V	−1.01	−0.95	220208	306892
1153.61	Cu V	−1.02	−1.04	222886	309570
1153.84	Cu IV	−1.45	−1.47	220316	306983
1154.23	Cu V	−0.56	−0.49	221272	307910
1154.64	Cu V	−0.65	−0.60	265975	352582
1154.77	Cu IV	−1.26	−1.15	233299	319896
1155.37	Cu V	−0.80	−0.83	221272	307825
1155.45	Cu V	−2.29	−2.27	229588	316134
1155.47	Cu V	0.32	0.38	236331	322876
1155.63	Cu V	−1.92	−1.87	265886	352419
1155.68	Cu V	−1.11	−1.07	236040	322569
1156.20	Cu VI	−2.34	−2.39	309111	395601
1156.47	Cu V	−0.49	−0.41	246477	332946
1156.60	Cu V	−0.89	−0.84	236109	322569
1156.82	Cu V	−1.41	−1.36	265975	352419
1156.94	Cu V	−0.85	−0.79	238234	324668
1157.00	Cu V	−0.77	−0.74	236040	322470

Table 29 – continued.

λ/ Å	Ion	$\log(gf)_{\mathrm{TOSS}}$	$\log(gf)_{\mathrm{Kurucz}}$	E_{low}/ cm^{-1}	E_{up}/ cm^{-1}
1157.19	Cu V	−1.18	−1.21	222401	308818
1157.23	Cu V	−0.18	−0.09	236331	322744
1157.26	Cu V	−0.89	−0.86	236059	322470
1157.30	Cu V	−1.30	−1.30	222886	309294
1157.34	Cu V	0.03	−0.00	236059	322464
1157.34	Cu IV	−1.32	−1.36	233299	319704
1157.39	Cu IV	−1.80	−1.91	230331	316732
1157.54	Cu V	0.55	0.60	238234	324624
1157.70	Cu IV	−2.34	−2.41	201211	287589
1157.90	Cu V	0.48	0.53	238305	324668
1157.93	Cu V	−0.66	−0.61	236109	322470
1158.00	Cu V	−1.92	−1.82	223214	309570
1158.21	Cu V	−1.23	−1.20	272801	359141
1158.38	Cu V	−1.63	−1.67	223376	309703
1158.42	Cu V	0.35	0.40	278282	364607
1158.45	Cu V	−0.41	−0.36	246624	332946
1158.50	Cu V	−0.58	−0.54	238305	324624
1158.58	Cu V	−1.22	−1.16	235053	321365
1158.80	Cu VI	−1.80	−1.85	309111	395407
1158.83	Cu V	−2.25	−2.38	187779	274073
1158.95	Cu V	−0.74	−0.68	187779	274065
1159.16	Cu V	−1.84	−1.81	220623	306892
1159.48	Cu IV	−2.20	−2.15	218000	304245
1159.48	Cu V	−2.16	−2.11	221664	307910
1159.74	Cu V	−0.51	−0.47	278380	364607
1159.74	Cu V	−2.31	−2.35	223477	309703
1159.76	Cu V	0.52	0.57	187779	274004
1159.78	Cu IV	−0.86	−0.88	225859	312083
1159.86	Cu V	−1.17	−1.12	228020	314238
1160.74	Cu V	−0.03	0.02	236040	322192
1160.99	Cu V	−0.39	−0.36	236059	322192
1161.19	Cu V	−1.28	−1.26	265886	352005
1161.29	Cu V	−1.25	−1.22	230532	316643
1161.53	Cu V	−0.33	−0.30	223477	309570
1161.71	Cu V	−0.47	−0.45	223214	309294
1163.20	Cu V	0.19	0.24	272755	358725
1163.41	Cu V	−0.43	−0.44	220938	306892
1163.71	Cu V	−1.57	−1.44	222886	308818
1163.82	Cu V	−1.36	−1.32	272801	358725
1163.94	Cu V	−0.56	−0.53	234036	319952
1164.21	Cu IV	−2.29	−2.34	221272	307167
1164.67	Cu V	−1.62	−1.56	236331	322192
1165.13	Cu V	−1.19	−1.11	226311	312138

Table 29 – continued.

λ/ Å	Ion	$\log(gf)_{\mathrm{TOSS}}$	$\log(gf)_{\mathrm{Kurucz}}$	E_{low}/ cm^{-1}	E_{up}/ cm^{-1}
1165.35	Cu IV	−1.76	−1.80	226271	312083
1165.57	Cu V	−0.73	−0.70	226311	312106
1165.64	Cu IV	−2.31	−2.29	226271	312061
1165.64	Cu IV	−2.31	−2.29	226271	312061
1165.64	Cu IV	−2.27	−2.26	225387	311177
1165.64	Cu IV	−2.27	−2.26	225387	311177
1166.33	Cu V	−1.76	−1.70	265692	351431
1166.36	Cu V	−1.24	−1.22	236059	321796
1166.56	Cu IV	−2.26	−2.22	227993	313715
1166.98	Cu IV	−0.92	−0.86	243029	328720
1167.36	Cu V	0.25	0.31	222401	308065
1167.51	Cu V	0.32	0.36	234036	319689
1167.76	Cu V	−2.15	−2.17	221272	306906
1168.19	Cu V	−0.95	−0.92	230532	316134
1168.53	Cu V	0.21	0.22	226311	311889
1168.98	Cu V	−1.26	−1.23	265886	351431
1169.94	Cu V	−1.28	−1.36	221664	307139
1170.31	Cu IV	−2.05	−2.12	233299	318746
1170.78	Cu IV	−1.88	−1.83	225387	310800
1170.92	Cu V	−0.90	−0.89	236040	321443
1171.18	Cu V	−1.70	−1.82	236059	321443
1171.20	Cu V	−1.78	−1.67	234036	319419
1171.86	Cu V	−0.43	−0.36	236109	321443
1171.99	Cu V	−0.54	−0.51	236040	321365
1172.15	Cu V	−1.71	−1.65	188833	274146
1172.17	Cu V	0.30	0.36	238305	323617
1172.25	Cu V	−0.16	−0.11	236059	321365
1172.71	Cu V	0.02	0.12	238234	323506
1172.78	Cu V	−1.04	−0.96	234036	319304
1172.78	Cu IV	−1.72	−1.70	230331	315599
1172.88	Cu V	−0.21	−0.22	220623	305883
1173.14	Cu V	−0.11	−0.11	221664	306906
1173.15	Cu V	−0.22	−0.18	188833	274073
1173.27	Cu V	0.39	0.44	188833	274065
1173.51	Cu V	−0.66	−0.60	229774	314988
1173.69	Cu V	−0.70	−0.63	238305	323506
1173.80	Cu V	−0.35	−0.30	272755	357948
1174.43	Cu V	−1.41	−1.35	272801	357948
1174.71	Cu V	−1.33	−1.30	239541	324668
1175.02	Cu V	−2.32	−2.19	222886	307991
1175.18	Cu V	−1.00	−1.03	226889	311982
1175.37	Cu V	0.09	0.15	199441	284521
1176.00	Cu V	−0.33	−0.27	236040	321074

Table 29 – continued.

λ/ Å	Ion	$\log(gf)_{\mathrm{TOSS}}$	$\log(gf)_{\mathrm{Kurucz}}$	E_{low}/ cm^{-1}	E_{up}/ cm^{-1}
1176.00	Cu V	−1.26	−1.20	236331	321365
1176.14	Cu V	−1.87	−1.80	222886	307910
1176.24	Cu V	0.11	0.17	278380	363397
1176.26	Cu V	−1.88	−1.74	236059	321074
1176.28	Cu V	−1.37	−1.31	221664	306678
1176.38	Cu VI	−1.68	−1.75	309111	394117
1176.53	Cu V	0.20	0.18	219203	304199
1176.95	Cu V	−0.71	−0.70	236109	321074
1177.05	Cu V	0.21	0.26	246477	331435
1177.18	Cu V	−2.46	−2.43	226889	311838
1177.32	Cu V	0.08	0.14	222886	307825
1177.55	Cu V	−1.82	−1.80	226311	311233
1177.88	Cu V	−0.19	−0.13	200648	285546
1178.88	Cu V	−0.48	−0.44	236109	320935
1179.57	Cu V	−0.15	−0.09	223214	307991
1179.61	Cu IV	−2.22	−2.18	228480	313253
1180.23	Cu V	−0.40	−0.35	246624	331354
1181.25	Cu V	−0.58	−0.53	201413	286069
1181.33	Cu V	0.07	0.12	229588	314238
1181.52	Cu V	−1.92	−1.84	235053	319689
1182.01	Cu V	−1.16	−1.11	189587	274189
1182.10	Cu V	−1.00	−1.00	227543	312138
1182.54	Cu V	−1.11	−1.17	226311	310875
1182.55	Cu V	0.14	0.11	227543	312106
1182.60	Cu V	−0.18	−0.13	189587	274146
1182.77	Cu V	−1.23	−1.23	256272	340820
1182.78	Cu V	−2.11	−2.10	256273	340820
1183.22	Cu V	−1.05	−1.05	220938	305453
1183.56	Cu V	−0.59	−0.50	222401	306892
1183.62	Cu V	0.15	0.21	189587	274073
1184.04	Cu V	−0.14	−0.09	230532	314988
1184.13	Cu V	−1.24	−1.13	256272	340723
1184.13	Cu V	−1.54	−1.53	256273	340723
1184.37	Cu V	−0.63	−0.56	223477	307910
1184.88	Cu IV	−2.43	−2.44	213535	297931
1185.31	Cu V	−0.43	−0.34	235053	319419
1185.71	Cu V	−1.62	−1.68	227801	312138
1186.17	Cu V	−0.66	−0.64	227801	312106
1186.20	Cu IV	−1.60	−1.50	244417	328720
1186.40	Cu V	−0.53	−0.41	246477	330765
1186.58	Cu V	−2.34	−2.41	219203	303479
1186.92	Cu V	0.04	0.08	235053	319304
1187.38	Cu V	−0.57	−0.52	201850	286069

Table 29 – continued.

λ/ Å	Ion	$\log(gf)_{\mathrm{TOSS}}$	$\log(gf)_{\mathrm{Kurucz}}$	E_{low}/ cm^{-1}	E_{up}/ cm^{-1}
1187.51	Cu V	−0.29	−0.22	256273	340483
1187.93	Cu V	−1.97	−1.92	221664	305844
1187.98	Cu V	−0.45	−0.39	236040	320216
1188.04	Cu V	0.27	0.34	226311	310483
1188.48	Cu V	−0.14	−0.11	246624	330765
1188.59	Cu V	−0.46	−0.41	201413	285546
1188.67	Cu V	−2.01	−1.96	243140	327268
1188.81	Cu V	0.20	0.26	228020	312138
1188.93	Cu V	−1.03	−0.98	190100	274210
1189.20	Cu V	−0.95	−0.89	228048	312138
1189.23	Cu V	0.21	0.28	227801	311889
1189.23	Cu V	−0.23	−0.18	190100	274189
1189.40	Cu V	−1.02	−1.11	239541	323617
1189.66	Cu V	−0.03	0.11	228048	312106
1189.83	Cu V	−0.07	−0.02	190100	274146
1189.93	Cu V	−0.53	−0.48	219203	303242
1189.98	Cu IV	−2.41	−2.38	228480	312515
1190.10	Cu IV	−0.11	−0.09	230236	314262
1190.44	Cu V	−0.59	−0.57	239615	323617
1190.93	Cu V	−0.01	0.04	228105	312073
1190.95	Cu IV	−1.53	−1.60	244753	328720
1190.97	Cu V	0.25	0.26	239541	323506
1191.39	Cu IV	−2.36	−2.35	228480	312416
1192.28	Cu V	−0.51	−0.46	200648	284521
1192.39	Cu V	−2.17	−2.10	226889	310754
1192.42	Cu V	0.50	0.54	278282	362145
1192.45	Cu V	−0.48	−0.43	272801	356662
1192.45	Cu V	−0.48	−0.43	272801	356662
1192.45	Cu V	0.03	0.09	278282	362143
1192.45	Cu V	0.03	0.09	278282	362143
1192.54	Cu V	0.14	0.20	220208	304062
1192.84	Cu V	−0.98	−0.91	220623	304456
1193.07	Cu V	−0.59	−0.58	228020	311838
1193.18	Cu V	−0.38	−0.33	190400	274210
1193.49	Cu V	−0.43	−0.38	190400	274189
1193.84	Cu V	−0.63	−0.66	223376	307139
1193.85	Cu V	−0.37	−0.35	278380	362143
1194.03	Cu IV	−1.94	−2.07	232442	316192
1194.28	Cu V	−0.23	−0.16	228105	311838
1194.40	Cu V	−1.03	−0.98	220208	303932
1194.50	Cu V	−0.57	−0.54	220938	304655
1194.53	Cu VI	−1.59	−1.56	308998	392713
1194.66	Cu V	−1.68	−1.59	230532	314238

Table 29 – continued.

λ/ Å	Ion	$\log(gf)_{\mathrm{TOSS}}$	$\log(gf)_{\mathrm{Kurucz}}$	E_{low}/ cm^{-1}	E_{up}/ cm^{-1}
1194.79	Cu V	−1.24	−1.20	201850	285546
1194.88	Cu V	0.24	0.29	227543	311233
1195.06	Cu V	−1.00	−1.12	227543	311220
1195.93	Cu V	−1.76	−1.73	272755	356372
1196.06	Cu V	−0.05	0.01	239615	323222
1196.16	Cu V	−0.21	−0.14	228105	311706
1196.23	Cu VI	−1.32	−1.27	308998	392594
1196.58	Cu V	−1.47	−1.49	272801	356372
1196.72	Cu V	0.00	0.06	228020	311582
1196.72	Cu V	−0.26	−0.20	226889	310450
1197.33	Cu VI	−1.59	−1.62	308998	392517
1197.35	Cu V	−0.65	−0.61	220938	304456
1197.35	Cu IV	−1.57	−1.59	214413	297931
1197.42	Cu V	−0.38	−0.32	223477	306989
1197.83	Cu V	−0.54	−0.49	246477	329961
1198.04	Cu V	−0.70	−0.70	220623	304092
1198.12	Cu V	−0.37	−0.39	223214	306678
1198.47	Cu V	0.22	0.27	220623	304062
1198.58	Cu V	−1.12	−1.04	227801	311233
1198.82	Cu V	0.50	0.55	265752	349168
1199.28	Cu V	−0.91	−0.86	221272	304655
1199.55	Cu V	−1.03	−0.95	236040	319404
1199.65	Cu V	−1.84	−1.83	236331	319689
1199.74	Cu IV	−2.01	−2.05	229064	312416
1199.83	Cu V	−0.12	−0.07	236059	319404
1199.95	Cu V	0.19	0.24	243140	326477
1199.95	Cu V	−0.29	−0.23	246624	329961
1200.35	Cu V	−0.10	−0.03	220623	303932
1200.44	Cu V	−1.78	−1.88	223376	306678
1201.22	Cu V	0.64	0.68	220208	303456
1201.49	Cu V	−0.30	−0.30	222886	306116
1201.74	Cu V	−1.51	−1.61	228020	311233
1201.90	Cu V	−0.51	−0.49	223477	306678
1201.92	Cu V	−1.57	−1.51	228020	311220
1202.15	Cu V	−0.64	−0.65	221272	304456
1202.32	Cu V	−1.39	−1.31	228048	311220
1202.73	Cu VI	−1.75	−1.65	309111	392255
1203.08	Cu V	−0.58	−0.55	272755	355875
1203.15	Cu V	−0.26	−0.21	228105	311220
1203.17	Cu IV	−1.35	−1.29	250623	333737
1203.25	Cu V	−1.40	−1.36	201413	284521
1203.30	Cu V	−0.51	−0.48	256273	339378
1203.74	Cu V	−1.41	−1.35	227801	310875

Table 29 – continued.

λ/ Å	Ion	$\log(gf)_{\mathrm{TOSS}}$	$\log(gf)_{\mathrm{Kurucz}}$	E_{low}/ cm^{-1}	E_{up}/ cm^{-1}
1204.07	Cu V	−0.28	−0.22	222401	305453
1204.57	Cu IV	−0.81	−0.83	230236	313253
1204.91	Cu V	0.13	0.19	220938	303932
1205.21	Cu V	−1.56	−1.54	236331	319304
1205.43	Cu V	−0.42	−0.51	226311	309269
1205.68	Cu V	−0.46	−0.48	227543	310483
1205.94	Cu V	−0.56	−0.52	239541	322464
1206.15	Cu IV	−2.35	−2.29	213665	296573
1206.25	Cu V	−0.24	−0.21	223214	306116
1206.79	Cu V	−0.92	−0.86	236059	318923
1206.81	Cu V	−0.13	−0.09	246477	329340
1206.99	Cu V	−1.92	−1.83	272755	355606
1207.01	Cu V	−0.70	−0.76	239615	322464
1207.22	Cu V	0.24	0.31	239541	322376
1207.33	Cu V	−0.04	0.02	228048	310875
1207.52	Cu V	−0.40	−0.33	226889	309703
1208.29	Cu V	−0.21	−0.20	239615	322376
1208.70	Cu V	−0.10	−0.04	228020	310754
1208.97	Cu V	−0.69	−0.56	246624	329340
1209.28	Cu VI	−1.63	−1.49	308998	391692
1209.41	Cu IV	−0.78	−0.76	244671	327357
1209.47	Cu V	−2.26	−2.22	226889	309570
1209.94	Cu V	−1.04	−1.06	228105	310754
1210.08	Cu V	−1.14	−1.10	223477	306116
1210.56	Cu V	−0.02	0.04	234036	316643
1210.60	Cu IV	−1.35	−1.20	244753	327357
1210.77	Cu V	0.12	0.17	236331	318923
1210.93	Cu VI	−1.20	−1.14	309111	391692
1211.08	Cu V	−0.44	−0.39	265752	348324
1211.13	Cu V	−0.29	−0.27	222886	305453
1211.38	Cu V	−0.38	−0.37	229588	312138
1212.02	Cu V	−0.04	−0.02	226311	308818
1212.11	Cu V	−2.14	−2.04	199441	281942
1212.58	Cu V	−0.13	−0.06	223376	305844
1213.92	Cu V	0.16	0.21	243140	325519
1214.22	Cu V	−0.86	−0.73	220623	302980
1214.35	Cu V	0.33	0.37	265975	348324
1214.40	Cu V	−1.03	−1.11	228105	310450
1214.62	Cu V	−1.59	−1.63	219203	301533
1215.07	Cu IV	−0.53	−0.47	233299	315599
1215.49	Cu V	−1.16	−1.31	220938	303209
1215.50	Cu IV	−2.00	−2.04	230331	312602
1215.68	Cu V	−0.04	−0.03	227543	309801

Table 29 – continued.

λ/ Å	Ion	$\log(gf)_{\mathrm{TOSS}}$	$\log(gf)_{\mathrm{Kurucz}}$	E_{low}/ cm^{-1}	E_{up}/ cm^{-1}
1215.75	Cu V	−1.10	−0.99	222401	304655
1215.97	Cu V	−0.88	−0.87	223214	305453
1216.42	Cu V	−0.41	−0.35	229774	311982
1216.44	Cu V	−0.63	−0.63	221272	303479
1216.54	Cu VI	−1.92	−1.84	308998	391198
1216.85	Cu IV	−0.69	−0.73	230236	312416
1217.14	Cu IV	−1.59	−1.60	214413	296573
1217.25	Cu IV	−2.00	−1.92	245204	327357
1217.31	Cu V	0.01	0.03	235053	317201
1217.50	Cu IV	−2.43	−2.49	230331	312467
1217.83	Cu V	0.08	0.12	234036	316149
1217.96	Cu V	−0.63	−0.64	272801	354905
1218.22	Cu VI	−1.63	−1.54	309111	391198
1218.31	Cu IV	−2.34	−2.34	214413	296494
1218.88	Cu V	−0.64	−0.52	220938	302980
1218.91	Cu V	−1.97	−1.93	265752	347793
1219.57	Cu V	−1.98	−1.93	272801	354797
1219.59	Cu V	−0.40	−0.34	229588	311582
1219.91	Cu V	−1.81	−1.74	200648	282622
1219.96	Cu V	−2.37	−2.41	221272	303242
1220.44	Cu V	−0.46	−0.43	221272	303209
1220.51	Cu V	−0.96	−0.98	229774	311706
1220.90	Cu V	0.21	0.26	265886	347793
1221.34	Cu V	0.08	0.13	219203	301081
1221.80	Cu IV	−1.57	−1.44	230236	312083
1222.22	Cu V	−0.43	−0.38	265975	347793
1222.60	Cu V	−0.89	−0.85	272755	354548
1222.69	Cu V	0.40	0.45	256272	338059
1222.78	Cu V	−0.65	−0.65	228020	309801
1222.80	Cu IV	−1.73	−1.69	215133	296912
1222.85	Cu V	−0.55	−0.50	278282	360058
1222.95	Cu V	−0.38	−0.33	222886	304655
1222.97	Cu V	−0.61	−0.50	243140	324909
1223.06	Cu IV	−1.68	−1.79	230236	311998
1223.18	Cu V	−0.62	−0.57	226311	308065
1223.22	Cu V	−0.37	−0.32	228020	309772
1223.22	Cu V	−1.85	−1.72	227543	309294
1223.22	Cu IV	−0.82	−0.82	230331	312083
1223.34	Cu V	−0.04	0.02	256272	338016
1223.59	Cu V	−0.97	−0.89	227543	309269
1223.62	Cu V	−0.36	−0.31	228048	309772
1223.72	Cu V	0.16	0.18	238234	319952
1223.86	Cu V	0.12	0.15	221272	302980

Table 29 – continued.

λ/ Å	Ion	$\log(gf)_{\mathrm{TOSS}}$	$\log(gf)_{\mathrm{Kurucz}}$	E_{low}/ cm^{-1}	E_{up}/ cm^{-1}
1224.05	Cu V	−1.00	−1.03	228105	309801
1224.13	Cu V	0.20	0.25	222401	304092
1224.32	Cu V	0.35	0.40	278380	360058
1224.80	Cu V	−1.52	−1.55	238305	319952
1224.81	Cu V	−0.70	−0.75	229588	311233
1225.00	Cu V	−1.88	−1.86	229588	311220
1225.64	Cu V	−1.43	−1.38	235053	316643
1225.79	Cu IV	−2.19	−2.29	229694	311274
1225.83	Cu V	−0.20	−0.14	221664	303242
1225.94	Cu V	−0.81	−0.89	222886	304456
1226.25	Cu V	−1.15	−1.07	228020	309570
1226.37	Cu V	−0.16	−0.11	230532	312073
1226.54	Cu V	−0.27	−0.29	222401	303932
1226.58	Cu V	0.09	0.14	265692	347219
1226.79	Cu V	−1.20	−1.19	226311	307825
1226.88	Cu VI	−2.01	−1.94	309111	390618
1227.18	Cu V	−0.73	−0.66	199441	280929
1227.47	Cu V	0.06	0.13	227801	309269
1227.53	Cu V	−0.89	−0.84	228105	309570
1227.89	Cu V	−1.17	−1.13	223214	304655
1228.30	Cu IV	−0.42	−0.30	250623	332036
1229.51	Cu V	−0.60	−0.55	265886	347219
1229.92	Cu V	−0.43	−0.37	230532	311838
1230.06	Cu V	−0.31	−0.26	221664	302961
1230.10	Cu V	−0.49	−0.43	200648	281942
1230.20	Cu V	−0.28	−0.20	229588	310875
1230.39	Cu V	−0.65	−0.67	227543	308818
1230.41	Cu V	−0.75	−0.69	228020	309294
1230.82	Cu V	−1.67	−1.52	228048	309294
1230.86	Cu V	−1.96	−1.91	265975	347219
1230.94	Cu V	−1.40	−1.38	272801	354039
1231.40	Cu V	−0.56	−0.51	201413	282622
1231.43	Cu V	−0.48	−0.40	222886	304092
1231.70	Cu V	−1.39	−1.36	228105	309294
1231.91	Cu V	−1.40	−1.35	230532	311706
1231.92	Cu V	0.63	0.68	238234	319408
1232.04	Cu V	−1.01	−0.95	229588	310754
1232.62	Cu V	0.27	0.31	220208	301336
1232.84	Cu V	−0.73	−0.77	238305	319419
1232.87	Cu V	−0.96	−0.91	278380	359492
1233.33	Cu V	−0.14	−0.08	235053	316134
1233.37	Cu V	−0.84	−0.82	220208	301286
1233.42	Cu IV	−1.90	−1.89	214835	295910

Table 29 – continued.

λ/ Å	Ion	$\log(gf)_{\mathrm{TOSS}}$	$\log(gf)_{\mathrm{Kurucz}}$	E_{low}/ cm^{-1}	E_{up}/ cm^{-1}
1234.30	Cu V	0.02	0.10	227801	308818
1234.48	Cu IV	−2.15	−2.02	243725	324731
1235.44	Cu IV	−2.19	−2.16	230331	311274
1236.24	Cu V	−1.21	−1.17	272755	353646
1236.93	Cu V	0.23	0.28	272801	353646
1237.50	Cu V	−0.20	−0.18	222401	303209
1237.66	Cu V	−1.37	−1.44	228020	308818
1237.75	Cu V	−1.12	−1.08	246477	327268
1238.06	Cu V	−0.13	−0.08	201850	282622
1238.19	Cu V	−0.07	−0.04	220623	301386
1238.31	Cu V	−1.06	−0.97	246624	327380
1238.69	Cu V	−2.09	−2.07	272755	353486
1238.95	Cu V	0.16	0.22	220623	301336
1239.33	Cu V	0.02	0.09	230532	311220
1239.39	Cu V	−2.40	−2.35	272801	353486
1239.47	Cu IV	−1.32	−1.24	230331	311011
1239.51	Cu V	−0.63	−0.55	229774	310450
1239.72	Cu V	0.22	0.26	220623	301286
1239.95	Cu V	−0.09	−0.07	220938	301587
1240.02	Cu V	−0.37	−0.33	246624	327268
1240.30	Cu IV	−1.99	−1.91	242530	323155
1240.80	Cu V	−0.32	−0.26	222886	303479
1240.95	Cu V	−1.50	−1.51	236059	316643
1241.02	Cu V	−0.78	−0.71	222401	302980
1241.25	Cu IV	−2.14	−2.21	230236	310800
1241.78	Cu V	0.08	0.13	201413	281942
1242.62	Cu IV	−1.86	−1.85	217079	297554
1243.04	Cu V	−1.29	−1.17	227543	307991
1243.05	Cu V	−0.19	−0.14	220938	301386
1243.12	Cu V	−0.32	−0.27	278282	358725
1243.52	Cu IV	−2.00	−2.13	233299	313715
1243.62	Cu V	0.14	0.23	239541	319952
1244.46	Cu V	−1.73	−1.67	222886	303242
1244.58	Cu V	0.05	0.12	220938	301286
1244.96	Cu V	−0.63	−0.73	222886	303209
1245.15	Cu V	−1.71	−1.69	236331	316643
1245.61	Cu V	−1.00	−0.93	227543	307825
1245.63	Cu V	0.26	0.31	200648	280929
1245.88	Cu V	−0.41	−0.36	223214	303479
1245.93	Cu V	−0.35	−0.29	221272	301533
1246.11	Cu V	−0.54	−0.54	226889	307139
1246.54	Cu V	−0.45	−0.43	230532	310754
1246.66	Cu V	−0.26	−0.19	220623	300837

Table 29 – continued.

λ/ Å	Ion	$\log(gf)_{\mathrm{TOSS}}$	$\log(gf)_{\mathrm{Kurucz}}$	E_{low}/ cm^{-1}	E_{up}/ cm^{-1}
1246.67	Cu V	−0.88	−0.85	229588	309801
1246.94	Cu IV	−1.69	−1.83	241855	322051
1246.99	Cu V	0.32	0.37	220208	300401
1247.12	Cu V	−0.04	0.03	229588	309772
1248.03	Cu IV	−2.27	−2.28	243029	323155
1248.23	Cu V	−0.26	−0.15	221272	301386
1248.52	Cu V	−1.31	−1.43	222886	302980
1248.53	Cu V	−1.51	−1.51	236040	316134
1248.83	Cu V	−1.82	−1.81	236059	316134
1249.13	Cu V	−0.49	−0.44	199441	279497
1249.57	Cu V	−1.92	−1.96	223214	303242
1249.73	Cu V	−0.47	−0.48	228048	308065
1249.73	Cu V	−0.29	−0.27	226889	306906
1249.96	Cu V	−0.62	−0.56	223477	303479
1249.99	Cu V	−0.81	−0.77	246477	326477
1250.08	Cu V	−0.86	−0.90	223214	303209
1250.26	Cu V	−0.15	−0.18	221272	301255
1250.32	Cu V	0.39	0.44	199441	279421
1250.46	Cu V	−0.50	−0.46	228020	307991
1250.89	Cu V	−1.14	−1.17	228048	307991
1251.11	Cu V	−1.29	−1.32	229774	309703
1251.27	Cu V	−1.95	−1.85	230532	310450
1251.58	Cu V	−0.03	−0.02	220938	300837
1251.73	Cu V	−1.46	−1.42	228020	307910
1251.91	Cu V	−0.47	−0.48	239541	319419
1252.71	Cu V	0.32	0.37	272755	352582
1253.00	Cu V	−1.98	−1.97	221272	301081
1253.07	Cu V	0.18	0.23	239615	319419
1253.07	Cu V	−1.20	−1.16	228020	307825
1253.07	Cu V	−1.20	−1.16	228020	307825
1253.07	Cu V	−0.26	−0.22	228105	307910
1253.07	Cu V	−0.26	−0.22	228105	307910
1253.47	Cu V	−1.02	−1.01	220623	300401
1253.71	Cu V	−0.56	−0.48	239541	319304
1253.76	Cu IV	−1.93	−2.02	218171	297931
1254.55	Cu VI	−0.93	−0.87	308998	388708
1254.60	Cu V	−0.22	−0.15	229588	309294
1254.87	Cu V	−1.39	−1.49	239615	319304
1255.27	Cu V	−0.11	−0.06	272755	352419
1255.29	Cu V	−0.76	−0.71	256272	335935
1255.30	Cu V	0.24	0.29	256273	335935
1255.99	Cu V	−1.16	−1.12	272801	352419
1256.51	Cu V	−1.94	−1.94	223376	302961

Table 29 – continued.

λ/ Å	Ion	$\log(gf)_{\mathrm{TOSS}}$	$\log(gf)_{\mathrm{Kurucz}}$	E_{low}/ cm^{-1}	E_{up}/ cm^{-1}
1256.73	Cu V	0.13	0.23	226311	305883
1256.83	Cu V	−0.53	−0.51	221272	300837
1257.52	Cu IV	−1.77	−1.81	242530	322051
1257.94	Cu IV	−2.36	−2.49	243029	322524
1257.95	Cu IV	−2.35	−2.36	217079	296573
1258.37	Cu IV	−1.72	−1.64	217445	296912
1258.45	Cu V	−1.01	−1.07	220938	300401
1258.70	Cu V	−0.51	−0.56	246477	325923
1258.71	Cu IV	−1.73	−1.81	244671	324118
1258.74	Cu VI	−2.48	−2.41	308998	388442
1259.17	Cu V	−0.46	−0.41	200648	280066
1259.19	Cu V	−1.23	−1.16	221664	301081
1260.54	Cu VI	−1.34	−1.29	309111	388442
1260.56	Cu V	−0.52	−0.48	243140	322470
1260.80	Cu VI	−1.71	−1.65	308998	388312
1261.04	Cu IV	−1.49	−1.50	218631	297931
1261.05	Cu V	−1.88	−1.83	246624	325923
1261.37	Cu IV	−1.18	−1.28	213360	292639
1261.52	Cu V	−1.43	−1.47	230532	309801
1262.14	Cu V	−1.49	−1.61	229588	308818
1262.28	Cu V	0.19	0.23	199441	278663
1263.14	Cu IV	−1.84	−1.80	233299	312467
1263.82	Cu VI	−1.41	−1.35	309111	388236
1264.36	Cu V	−1.05	−1.02	227801	306892
1265.00	Cu V	−2.31	−2.21	243140	322192
1265.21	Cu V	−0.94	−0.79	230532	309570
1265.29	Cu V	−1.58	−1.63	228105	307139
1265.46	Cu IV	−2.42	−2.40	243029	322051
1265.71	Cu V	−0.62	−0.58	238234	317240
1266.07	Cu V	−0.81	−0.83	222401	301386
1266.46	Cu V	−0.60	−0.55	201413	280373
1266.65	Cu V	−2.17	−2.18	236040	314988
1266.76	Cu V	−1.51	−1.43	200648	279590
1266.86	Cu V	0.53	0.58	238305	317240
1267.00	Cu IV	−1.36	−1.27	218628	297554
1267.49	Cu V	−0.79	−0.67	238305	317201
1267.52	Cu V	−2.49	−2.39	246624	325519
1267.66	Cu V	−2.20	−2.26	228020	306906
1267.67	Cu V	−1.43	−1.56	222401	301286
1267.76	Cu V	−2.30	−2.29	236109	314988
1268.17	Cu V	−0.47	−0.45	222401	301255
1268.18	Cu V	−1.64	−1.58	199441	278295
1268.25	Cu V	−0.15	−0.10	200648	279497

Table 29 – continued.

λ/ Å	Ion	$\log(gf)_{\mathrm{TOSS}}$	$\log(gf)_{\mathrm{Kurucz}}$	E_{low}/ cm^{-1}	E_{up}/ cm^{-1}
1268.32	Cu V	0.22	0.21	228048	306892
1268.52	Cu IV	−2.33	−2.28	232442	311274
1269.35	Cu V	−0.10	−0.05	187779	266560
1269.64	Cu V	−1.58	−1.64	230532	309294
1270.54	Cu IV	−1.14	−1.26	213932	292639
1271.41	Cu V	−0.48	−0.43	201413	280066
1271.49	Cu V	−0.79	−0.78	222886	301533
1271.78	Cu V	−0.26	−0.21	272801	351431
1273.50	Cu V	−0.62	−0.56	201850	280373
1273.89	Cu V	−0.80	−0.79	222886	301386
1274.44	Cu IV	−1.81	−1.72	217445	295910
1274.49	Cu IV	−0.92	−1.00	213535	291997
1274.74	Cu V	0.39	0.44	187779	266227
1274.93	Cu IV	−1.68	−1.72	218138	296573
1274.93	Cu V	−0.50	−0.39	222401	300837
1275.14	Cu IV	−2.47	−2.44	242530	320953
1275.20	Cu IV	−2.46	−2.40	217621	296040
1275.46	Cu V	−1.20	−1.18	229588	307991
1275.47	Cu IV	−1.65	−1.67	218171	296573
1275.96	Cu V	−0.73	−0.77	223214	301587
1276.00	Cu V	−0.39	−0.28	222886	301255
1276.72	Cu IV	−2.46	−2.48	243725	322051
1276.76	Cu IV	−1.69	−1.83	218171	296494
1276.83	Cu V	−0.43	−0.38	223214	301533
1277.10	Cu V	−0.62	−0.59	243140	321443
1277.40	Cu IV	−1.86	−1.76	218628	296912
1277.69	Cu IV	−1.88	−1.95	215133	293399
1278.17	Cu V	−0.49	−0.46	229588	307825
1278.18	Cu V	−0.04	0.01	188833	267069
1278.35	Cu IV	−1.56	−1.48	214413	292639
1278.37	Cu V	−2.07	−2.03	243140	321365
1278.51	Cu V	−0.77	−0.71	201850	280066
1278.85	Cu IV	−2.14	−2.10	213535	291730
1279.15	Cu V	−1.11	−1.04	201413	279590
1279.56	Cu IV	−2.42	−2.48	219403	297554
1279.67	Cu V	−0.22	−0.11	226311	304456
1280.49	Cu V	−1.66	−1.61	228020	306116
1280.57	Cu V	−1.58	−1.56	278282	356372
1280.67	Cu V	−0.71	−0.65	201413	279497
1280.70	Cu V	0.24	0.26	227801	305883
1280.92	Cu V	−0.94	−0.89	234036	312106
1281.01	Cu IV	−2.33	−2.37	219867	297931
1281.12	Cu V	−0.29	−0.25	223477	301533

Table 29 – continued.

λ/ Å	Ion	$\log(gf)_{\mathrm{TOSS}}$	$\log(gf)_{\mathrm{Kurucz}}$	E_{low}/ cm^{-1}	E_{up}/ cm^{-1}
1281.37	Cu V	−0.44	−0.36	223214	301255
1281.46	Cu IV	−1.02	−1.17	213535	291571
1281.48	Cu IV	−2.03	−1.97	243029	321064
1281.81	Cu V	−0.94	−0.85	200648	278663
1281.88	Cu V	−1.36	−1.41	228105	306116
1282.05	Cu V	−0.21	−0.15	222401	300401
1282.59	Cu IV	−1.33	−1.27	218945	296912
1282.85	Cu V	−0.41	−0.35	222886	300837
1282.86	Cu IV	−1.59	−1.72	245204	323155
1282.95	Cu IV	−2.13	−2.16	218628	296573
1283.14	Cu V	−1.28	−1.22	243140	321074
1283.31	Cu IV	−1.92	−1.87	243029	320953
1283.52	Cu IV	−0.99	−0.93	218000	295910
1283.52	Cu V	−0.67	−0.55	227543	305453
1283.59	Cu V	−2.25	−2.23	236331	314238
1283.67	Cu V	−0.12	−0.08	189587	267489
1285.65	Cu V	−1.28	−1.22	226311	304092
1285.83	Cu IV	−2.31	−2.36	244753	322524
1286.13	Cu IV	−1.83	−1.90	243029	320782
1286.15	Cu V	−0.11	−0.12	226311	304062
1286.34	Cu V	−1.45	−1.37	201850	279590
1286.35	Cu V	−1.58	−1.70	228105	305844
1286.55	Cu V	−0.01	0.04	188833	266560
1287.22	Cu IV	−1.66	−1.63	217621	295308
1287.66	Cu V	−0.77	−0.66	239541	317201
1287.69	Cu V	−0.36	−0.32	190100	267759
1287.89	Cu V	−0.71	−0.65	200648	278295
1288.04	Cu VI	−1.43	−1.37	265639	343277
1288.31	Cu V	−1.45	−1.43	226311	303932
1288.40	Cu IV	−2.17	−2.23	220316	297931
1288.50	Cu V	−1.77	−1.74	265692	343301
1288.59	Cu V	−2.02	−2.08	223477	301081
1288.77	Cu V	−2.27	−2.27	278282	355875
1288.88	Cu V	−0.73	−0.59	239615	317201
1288.91	Cu V	−1.53	−1.54	265752	343337
1288.93	Cu IV	−1.70	−1.64	214413	291997
1289.56	Cu V	−1.32	−1.36	234036	311582
1290.62	Cu V	−0.53	−0.49	189587	267069
1291.01	Cu V	−1.05	−1.00	230532	307991
1291.14	Cu V	−2.07	−2.04	265886	343337
1291.44	Cu V	−1.81	−1.84	228020	305453
1291.89	Cu V	−0.80	−0.79	228048	305453
1292.09	Cu V	−0.64	−0.59	188833	266227

Table 29 – continued.

λ/ Å	Ion	$\log(gf)_{\mathrm{TOSS}}$	$\log(gf)_{\mathrm{Kurucz}}$	E_{low}/ cm^{-1}	E_{up}/ cm^{-1}
1292.18	Cu V	−1.75	−1.70	190100	267489
1292.24	Cu IV	−1.93	−1.98	217079	294464
1292.36	Cu V	−0.60	−0.56	230532	307910
1292.55	Cu IV	−1.98	−1.86	242530	319896
1292.57	Cu V	−0.76	−0.72	229774	307139
1292.62	Cu V	−2.15	−2.11	265975	343337
1292.68	Cu V	−1.01	−0.97	190400	267759
1292.82	Cu IV	−1.53	−1.40	213535	290885
1292.86	Cu V	−1.24	−1.17	228105	305453
1293.22	Cu V	−1.93	−1.91	265975	343301
1293.33	Cu IV	−2.08	−2.19	245204	322524
1293.36	Cu V	−1.12	−1.11	229588	306906
1293.45	Cu IV	−2.21	−2.30	216703	294015
1294.69	Cu IV	−1.50	−1.61	244813	322051
1294.88	Cu IV	−2.00	−1.88	243725	320953
1294.90	Cu V	−2.05	−2.03	278380	355606
1295.00	Cu IV	−1.10	−1.02	213665	290885
1295.61	Cu V	−1.59	−1.51	234036	311220
1296.87	Cu IV	−0.76	−0.86	213665	290774
1296.99	Cu V	−0.77	−0.72	239541	316643
1297.09	Cu IV	−1.89	−1.76	218815	295910
1297.21	Cu V	−0.53	−0.48	190400	267489
1297.26	Cu V	−1.56	−1.44	235053	312138
1299.16	Cu V	−0.44	−0.40	189587	266560
1299.23	Cu V	−0.41	−0.36	190100	267069
1299.28	Cu IV	−2.25	−2.21	218945	295910
1299.94	Cu V	−0.51	−0.45	199441	276368
1300.16	Cu V	−1.46	−1.42	227543	304456
1300.29	Cu IV	−2.24	−2.29	217109	294015
1300.70	Cu V	−1.27	−1.19	201413	278295
1301.43	Cu V	−2.44	−2.34	234036	310875
1301.60	Cu IV	−2.29	−2.32	214319	291147
1301.73	Cu IV	−1.43	−1.42	215133	291954
1302.33	Cu V	−1.44	−1.45	235053	311838
1304.23	Cu V	−1.67	−1.66	256273	332946
1304.30	Cu V	−0.53	−0.49	226311	302980
1304.54	Cu V	−0.32	−0.26	227801	304456
1304.89	Cu V	−0.97	−0.93	228020	304655
1305.08	Cu V	−2.25	−2.17	278282	354905
1305.34	Cu V	−2.43	−2.44	239541	316149
1305.36	Cu V	−0.44	−0.44	228048	304655
1305.36	Cu V	−0.99	−0.98	230532	307139
1305.52	Cu V	−1.91	−1.84	246624	323222

Table 29 – continued.

λ/ Å	Ion	$\log(gf)_{\mathrm{TOSS}}$	$\log(gf)_{\mathrm{Kurucz}}$	E_{low}/ cm^{-1}	E_{up}/ cm^{-1}
1305.65	Cu V	−1.62	−1.54	226889	303479
1305.72	Cu VI	−1.87	−1.82	265639	342225
1306.20	Cu IV	−1.22	−1.36	243029	319587
1306.34	Cu V	−0.72	−0.67	228105	304655
1306.34	Cu V	−1.19	−1.19	227543	304092
1306.66	Cu IV	−1.23	−1.37	217621	294152
1306.68	Cu V	−2.37	−2.47	235053	311582
1306.86	Cu V	−1.05	−1.02	239615	316134
1308.10	Cu V	−0.39	−0.38	234036	310483
1308.22	Cu IV	−2.44	−2.40	213535	289974
1308.29	Cu V	−0.51	−0.48	228020	304456
1308.31	Cu IV	−2.49	−2.43	217079	293514
1308.41	Cu IV	−2.14	−2.13	215133	291562
1308.75	Cu V	−2.23	−2.25	228048	304456
1309.09	Cu V	−0.43	−0.42	227543	303932
1309.49	Cu IV	−2.40	−2.38	217650	294015
1309.71	Cu V	−0.34	−0.29	226889	303242
1310.29	Cu IV	−1.72	−1.79	216703	293022
1310.76	Cu V	−0.82	−0.90	227801	304092
1311.17	Cu V	−1.55	−1.60	246477	322744
1311.24	Cu V	−1.11	−1.12	243140	319404
1311.34	Cu IV	−1.99	−1.95	220316	296573
1312.67	Cu V	−0.60	−0.59	235053	311233
1312.96	Cu V	−1.53	−1.52	243140	319304
1313.52	Cu V	−1.40	−1.31	227801	303932
1313.88	Cu IV	−1.62	−1.61	244671	320782
1314.17	Cu V	−1.39	−1.40	228105	304199
1314.54	Cu V	−1.94	−1.92	226889	302961
1314.57	Cu V	−0.76	−0.80	229774	305844
1315.02	Cu V	−1.40	−1.27	228048	304092
1315.30	Cu IV	−1.95	−1.82	244753	320782
1315.54	Cu IV	−1.03	−1.05	215133	291147
1316.00	Cu IV	−2.41	−2.40	218028	294015
1316.00	Cu V	−1.38	−1.32	246477	322464
1316.20	Cu IV	−1.45	−1.47	213665	289642
1316.75	Cu V	−1.77	−1.83	246624	322569
1316.79	Cu IV	−1.53	−1.51	217079	293022
1318.12	Cu V	−1.95	−1.86	229588	305453
1318.19	Cu IV	−1.20	−1.25	243725	319587
1318.22	Cu IV	−2.40	−2.36	245204	321064
1318.47	Cu V	−2.36	−2.34	246624	322470
1318.49	Cu IV	−2.37	−2.34	218171	294015
1318.64	Cu IV	−2.44	−2.35	213535	289370

Table 29 – continued.

λ/ Å	Ion	$\log(gf)_{\mathrm{TOSS}}$	$\log(gf)_{\mathrm{Kurucz}}$	E_{low}/ cm^{-1}	E_{up}/ cm^{-1}
1318.87	Cu V	−0.33	−0.26	235053	310875
1319.30	Cu V	−0.98	−0.95	236040	311838
1319.56	Cu V	−1.31	−1.29	243140	318923
1319.63	Cu V	−1.12	−1.09	236059	311838
1319.87	Cu V	−1.64	−1.67	234036	309801
1320.16	Cu IV	−2.18	−2.20	245204	320953
1320.38	Cu V	−1.38	−1.28	234036	309772
1320.57	Cu IV	−2.30	−2.36	220316	296040
1320.66	Cu V	−1.53	−1.43	200648	276368
1320.70	Cu IV	−1.56	−1.58	243029	318746
1320.91	Cu IV	−1.88	−1.86	213665	289370
1320.98	Cu V	−1.74	−1.75	235053	310754
1321.59	Cu V	−1.15	−1.09	236040	311706
1321.92	Cu V	−2.07	−2.00	236059	311706
1322.80	Cu V	−0.89	−0.83	236109	311706
1323.02	Cu VI	−1.29	−1.27	322792	398377
1323.03	Cu V	−1.74	−1.74	230532	306116
1323.15	Cu IV	−1.96	−2.05	245204	320782
1323.30	Cu V	−1.02	−0.96	272755	348324
1324.09	Cu V	−0.88	−0.87	236059	311582
1324.39	Cu V	−2.13	−2.10	236331	311838
1324.87	Cu IV	−1.12	−1.20	244417	319896
1326.02	Cu IV	−1.90	−1.77	215734	291147
1326.54	Cu IV	−1.76	−1.67	218631	294015
1326.75	Cu IV	−1.86	−1.79	217650	293022
1327.62	Cu IV	−0.91	−1.02	214319	289642
1327.80	Cu V	−1.25	−1.31	230532	305844
1328.12	Cu IV	−2.35	−2.33	216703	291997
1328.21	Cu IV	−1.43	−1.44	218726	294015
1328.62	Cu V	−1.38	−1.33	278380	353646
1328.77	Cu V	−0.53	−0.48	234036	309294
1328.83	Cu IV	−2.30	−2.32	214319	289573
1328.88	Cu V	−1.17	−1.16	236331	311582
1329.09	Cu IV	−1.75	−1.82	244753	319993
1329.21	Cu V	−0.01	0.04	234036	309269
1329.41	Cu V	−1.54	−1.52	228020	303242
1329.47	Cu VI	−1.23	−1.20	322805	398023
1329.59	Cu IV	−0.61	−0.70	214319	289530
1329.98	Cu V	−2.22	−2.14	228020	303209
1330.14	Cu IV	−1.85	−1.71	244813	319993
1330.14	Cu V	−0.79	−0.80	227801	302980
1330.45	Cu V	−1.70	−1.60	256272	331435
1330.46	Cu V	−1.65	−1.62	228048	303209

Table 29 – continued.

λ/ Å	Ion	$\log(gf)_{\mathrm{TOSS}}$	$\log(gf)_{\mathrm{Kurucz}}$	E_{low}/ cm^{-1}	E_{up}/ cm^{-1}
1330.47	Cu V	−1.90	−1.97	236059	311220
1330.80	Cu IV	−1.31	−1.36	244753	319896
1331.49	Cu V	−1.25	−1.27	228105	303209
1332.01	Cu V	−1.60	−1.54	226311	301386
1332.13	Cu V	−0.77	−0.69	229588	304655
1332.14	Cu V	0.09	0.14	265752	340820
1332.78	Cu V	−2.47	−2.44	265692	340723
1333.45	Cu IV	−0.75	−0.69	220917	295910
1333.47	Cu V	−1.48	−1.42	272801	347793
1333.77	Cu V	−2.30	−2.22	226311	301286
1333.93	Cu V	−2.32	−2.20	246477	321443
1334.04	Cu V	−1.24	−1.10	228020	302980
1334.52	Cu V	−2.28	−2.28	265886	340820
1334.53	Cu V	−1.13	−1.13	228048	302980
1334.70	Cu IV	−1.60	−1.71	221650	296573
1334.84	Cu IV	−1.55	−1.59	244671	319587
1335.08	Cu V	−1.02	−0.97	236331	311233
1335.09	Cu IV	−2.24	−2.12	213665	288566
1335.40	Cu IV	−1.70	−1.64	218138	293022
1335.57	Cu IV	−2.16	−2.20	217079	291954
1336.10	Cu V	−1.08	−1.03	265975	340820
1336.24	Cu V	−0.99	−0.94	265886	340723
1336.28	Cu IV	−2.21	−2.10	221739	296573
1336.56	Cu V	−2.46	−2.43	246624	321443
1337.06	Cu V	−1.45	−1.44	265692	340483
1337.13	Cu IV	−1.00	−1.00	218726	293514
1337.23	Cu V	−1.86	−1.88	234036	308818
1337.83	Cu V	−0.15	−0.11	265975	340723
1337.96	Cu V	−2.10	−2.11	246624	321365
1338.34	Cu V	−0.72	−0.69	235053	309772
1338.44	Cu V	−1.13	−1.05	236040	310754
1338.60	Cu V	−2.23	−2.23	199441	274146
1338.78	Cu V	−1.46	−1.38	236059	310754
1339.91	Cu V	−1.61	−1.62	199441	274073
1340.07	Cu V	−1.01	−1.00	199441	274065
1340.28	Cu V	−1.14	−1.10	229588	304199
1340.54	Cu V	−0.77	−0.75	265886	340483
1341.50	Cu V	−1.41	−1.44	236331	310875
1341.79	Cu VI	−1.14	−1.11	322877	397404
1341.81	Cu V	−1.32	−1.37	226311	300837
1341.97	Cu V	−0.97	−0.90	235053	309570
1342.02	Cu IV	−0.84	−0.78	222398	296912
1342.11	Cu IV	−1.75	−1.72	217445	291954

Table 29 – continued.

λ/ Å	Ion	$\log(gf)_{\mathrm{TOSS}}$	$\log(gf)_{\mathrm{Kurucz}}$	E_{low}/ cm^{-1}	E_{up}/ cm^{-1}
1342.20	Cu V	−1.27	−1.26	229588	304092
1342.42	Cu V	−0.50	−0.45	256272	330765
1343.76	Cu V	−2.24	−2.20	272801	347219
1343.90	Cu V	−2.28	−2.42	236040	310450
1344.20	Cu IV	−2.24	−2.33	218628	293022
1344.26	Cu IV	−2.08	−2.05	218631	293022
1345.14	Cu V	−2.12	−2.22	236109	310450
1345.80	Cu IV	−1.02	−0.96	272944	347249
1345.89	Cu V	−1.02	−0.98	278282	352582
1345.98	Cu IV	−2.46	−2.47	218726	293022
1346.84	Cu IV	−1.47	−1.49	214319	288566
1346.95	Cu V	−1.38	−1.34	235053	309294
1347.67	Cu V	−2.49	−2.47	278380	352582
1347.86	Cu V	−0.64	−0.61	226889	301081
1348.31	Cu IV	−2.11	−2.17	223764	297931
1348.55	Cu V	−0.65	−0.60	265692	339846
1349.70	Cu V	−0.61	−0.58	226311	300401
1349.83	Cu IV	−2.31	−2.20	223847	297931
1349.99	Cu IV	−1.16	−1.11	244671	318746
1350.18	Cu IV	−1.90	−1.93	245204	319268
1350.64	Cu V	−2.31	−2.29	278380	352419
1351.48	Cu IV	−1.82	−1.77	244753	318746
1352.19	Cu V	−0.83	−0.83	234036	307991
1352.61	Cu IV	−0.98	−0.92	223623	297554
1353.33	Cu V	−1.48	−1.46	229588	303479
1353.70	Cu V	−1.06	−1.04	238234	312106
1353.91	Cu IV	−2.10	−2.20	224071	297931
1354.30	Cu IV	−2.47	−2.48	215734	289573
1354.41	Cu V	−1.49	−1.44	238305	312138
1355.23	Cu V	−1.75	−1.70	234036	307825
1355.65	Cu V	−1.91	−1.84	235053	308818
1356.07	Cu V	−1.09	−1.00	236059	309801
1356.62	Cu V	−1.04	−1.08	227543	301255
1356.80	Cu IV	−1.62	−1.62	217445	291147
1357.08	Cu V	−0.90	−0.87	256273	329961
1357.10	Cu V	−1.28	−1.21	265692	339378
1357.70	Cu V	−1.09	−1.04	229588	303242
1358.29	Cu V	−1.30	−1.38	229588	303209
1358.35	Cu IV	−2.43	−2.43	219403	293022
1358.84	Cu V	−2.17	−2.18	246624	320216
1358.97	Cu V	−1.06	−1.08	227801	301386
1359.32	Cu V	−2.00	−1.85	228020	301587
1359.77	Cu IV	−1.67	−1.75	245204	318746

Table 29 – continued.

λ/ Å	Ion	$\log(gf)_{\mathrm{TOSS}}$	$\log(gf)_{\mathrm{Kurucz}}$	E_{low}/ cm^{-1}	E_{up}/ cm^{-1}
1359.80	Cu V	−2.02	−2.00	200648	274189
1359.82	Cu V	−0.50	−0.51	228048	301587
1359.89	Cu V	−0.43	−0.40	227801	301336
1360.30	Cu V	−1.65	−1.66	228020	301533
1360.34	Cu V	−2.32	−2.20	236059	309570
1360.50	Cu V	−0.42	−0.38	243140	316643
1360.58	Cu V	−1.91	−1.90	200648	274146
1360.70	Cu V	−0.61	−0.54	265886	339378
1360.84	Cu IV	−2.24	−2.19	224071	297554
1360.89	Cu V	−1.11	−1.05	228105	301587
1361.03	Cu IV	−2.08	−2.18	217079	290553
1361.10	Cu V	−1.50	−1.42	236331	309801
1361.88	Cu V	−1.59	−1.52	228105	301533
1361.93	Cu V	−1.03	−1.01	200648	274073
1362.53	Cu V	−2.15	−2.13	229588	302980
1363.04	Cu V	−0.99	−0.97	228020	301386
1364.36	Cu V	−1.22	−1.18	227543	300837
1364.80	Cu IV	−1.69	−1.63	214319	287589
1365.40	Cu V	−0.76	−0.71	228048	301286
1365.46	Cu V	−2.01	−2.01	236059	309294
1365.46	Cu V	−2.01	−2.01	236059	309294
1365.47	Cu V	−1.25	−1.22	228020	301255
1365.47	Cu V	−1.25	−1.22	228020	301255
1366.35	Cu V	−2.26	−2.24	229774	302961
1368.61	Cu V	−0.79	−0.82	256272	329340
1368.61	Cu V	−2.03	−1.92	256273	329340
1368.73	Cu V	−2.08	−2.06	228020	301081
1369.18	Cu V	−1.68	−1.59	227801	300837
1369.69	Cu IV	−2.48	−2.48	218945	291954
1370.56	Cu V	−1.92	−1.84	236331	309294
1370.85	Cu V	−1.33	−1.29	230532	303479
1371.02	Cu V	−1.20	−1.19	235053	307991
1371.22	Cu V	−1.10	−1.08	238305	311233
1371.22	Cu V	−2.48	−2.42	246477	319404
1372.52	Cu V	−1.33	−1.33	227543	300401
1372.55	Cu V	−0.78	−0.76	235053	307910
1373.10	Cu V	−2.09	−2.02	246477	319304
1373.69	Cu V	−2.04	−2.02	201413	274210
1374.09	Cu V	−2.10	−2.08	201413	274189
1374.88	Cu V	−1.25	−1.22	201413	274146
1375.33	Cu V	−2.33	−2.28	230532	303242
1377.99	Cu V	−1.00	−0.94	238305	310875
1379.26	Cu IV	−1.84	−1.85	224071	296573

Table 29 – continued.

λ/ Å	Ion	$\log(gf)_{\mathrm{TOSS}}$	$\log(gf)_{\mathrm{Kurucz}}$	E_{low}/ cm^{-1}	E_{up}/ cm^{-1}
1379.57	Cu V	−0.76	−0.69	236331	308818
1380.33	Cu V	−2.28	−2.28	246477	318923
1381.98	Cu V	−1.99	−1.97	201850	274210
1382.38	Cu V	−1.59	−1.57	201850	274189
1382.99	Cu V	−2.23	−2.22	265752	338059
1384.09	Cu V	−0.81	−0.80	238234	310483
1384.60	Cu V	−2.07	−2.02	239615	311838
1386.39	Cu V	−2.23	−2.12	265886	338016
1386.42	Cu IV	−2.18	−2.30	217445	289573
1387.72	Cu IV	−1.02	−1.06	244671	316732
1388.09	Cu V	−2.26	−2.19	239541	311582
1388.10	Cu V	−1.52	−1.42	265975	338016
1388.90	Cu V	−0.93	−0.90	229588	301587
1389.51	Cu V	−1.96	−2.03	239615	311582
1389.93	Cu V	−2.09	−2.05	229588	301533
1390.21	Cu V	−1.89	−1.86	236059	307991
1391.41	Cu V	−1.89	−1.89	236040	307910
1391.73	Cu V	−2.04	−1.94	235053	306906
1392.80	Cu V	−1.62	−1.63	229588	301386
1394.86	Cu V	−1.81	−1.82	239541	311233
1395.10	Cu IV	−2.30	−2.28	222336	294015
1395.90	Cu IV	−2.43	−2.40	220316	291954
1396.54	Cu V	−1.32	−1.28	239615	311220
1398.73	Cu V	−2.09	−2.03	236331	307825
1398.74	Cu V	−1.62	−1.58	229588	301081
1399.25	Cu V	−0.93	−0.90	238305	309772
1400.00	Cu IV	−1.92	−1.97	250623	322051
1400.23	Cu V	−1.98	−1.96	234036	305453
1401.71	Cu IV	−2.41	−2.37	242530	313872
1401.86	Cu V	−1.92	−1.87	239541	310875
1403.52	Cu V	−1.67	−1.62	229588	300837
1405.69	Cu V	−1.92	−1.89	239615	310754
1407.36	Cu V	−1.61	−1.61	230532	301587
1407.75	Cu V	−0.62	−0.56	238234	309269
1408.42	Cu V	−1.72	−1.68	230532	301533
1408.42	Cu IV	−1.73	−1.74	222398	293399
1408.55	Cu V	−1.59	−1.59	256273	327268
1409.46	Cu V	−1.37	−1.31	236040	306989
1409.48	Cu IV	−1.73	−1.70	220917	291865
1410.83	Cu V	−1.45	−1.36	236109	306989
1411.11	Cu V	−2.22	−2.08	236040	306906
1411.52	Cu IV	−2.34	−2.19	244753	315599
1411.60	Cu IV	−1.82	−1.83	223623	294464

Table 29 – continued.

λ/ Å	Ion	$\log(gf)_{\mathrm{TOSS}}$	$\log(gf)_{\mathrm{Kurucz}}$	E_{low}/ cm^{-1}	E_{up}/ cm^{-1}
1413.00	Cu IV	−1.70	−1.82	227160	297931
1413.88	Cu IV	−1.79	−1.73	242530	313257
1415.66	Cu V	−1.18	−1.17	236040	306678
1416.05	Cu V	−1.23	−1.25	236059	306678
1416.79	Cu V	−2.03	−1.96	272755	343337
1417.02	Cu IV	−2.45	−2.39	244417	314988
1417.05	Cu V	−1.89	−1.94	236109	306678
1417.97	Cu IV	−2.25	−2.21	225387	295910
1418.43	Cu V	−1.97	−1.92	272801	343301
1420.06	Cu V	−0.52	−0.45	234036	304456
1420.44	Cu V	−1.06	−0.99	235053	305453
1422.40	Cu IV	−1.31	−1.42	221650	291954
1423.46	Cu IV	−1.85	−1.95	223764	294015
1423.87	Cu V	−1.38	−1.35	239541	309772
1423.89	Cu IV	−1.71	−1.74	220917	291147
1424.19	Cu IV	−2.42	−2.31	221739	291954
1424.41	Cu V	−1.50	−1.51	256272	326477
1424.77	Cu V	−2.16	−2.20	239615	309801
1425.19	Cu V	−0.65	−0.62	246477	316643
1425.26	Cu V	−2.42	−2.30	234036	304199
1427.42	Cu V	−0.91	−0.92	236059	306116
1427.43	Cu V	−1.46	−1.53	234036	304092
1429.15	Cu IV	−2.30	−2.28	227960	297931
1429.48	Cu V	−1.79	−1.66	239615	309570
1429.70	Cu IV	−1.92	−1.92	224071	294015
1430.71	Cu V	−2.01	−1.99	234036	303932
1430.81	Cu IV	−1.74	−1.75	223623	293514
1432.02	Cu V	−1.98	−1.98	238234	308065
1432.99	Cu V	−1.28	−1.26	236331	306116
1433.63	Cu V	−1.17	−1.11	239541	309294
1435.14	Cu V	−1.75	−1.65	239615	309294
1435.60	Cu V	−1.98	−1.93	246477	316134
1436.73	Cu V	−0.98	−0.93	235053	304655
1437.41	Cu IV	−2.32	−2.32	243725	313295
1438.19	Cu IV	−2.41	−2.42	243725	313257
1438.26	Cu IV	−1.99	−2.14	220917	290445
1438.45	Cu V	−2.04	−2.02	238305	307825
1438.65	Cu V	−1.06	−1.03	246624	316134
1440.85	Cu V	−1.49	−1.45	235053	304456
1443.48	Cu V	−1.53	−1.54	239541	308818
1443.89	Cu IV	−2.21	−2.20	223764	293022
1444.13	Cu V	−1.26	−1.25	256272	325519
1445.39	Cu IV	−2.08	−2.18	244072	313257

Table 29 – continued.

λ/ Å	Ion	$\log(gf)_{\mathrm{TOSS}}$	$\log(gf)_{\mathrm{Kurucz}}$	E_{low}/ cm^{-1}	E_{up}/ cm^{-1}
1445.65	Cu V	−2.11	−2.18	234036	303209
1446.72	Cu V	−0.73	−0.71	236331	305453
1450.30	Cu IV	−1.82	−1.82	224071	293022
1450.45	Cu V	−1.05	−1.04	234036	302980
1451.28	Cu IV	−2.42	−2.43	243725	312630
1451.85	Cu IV	−2.01	−1.88	244417	313295
1452.67	Cu V	−2.23	−2.20	278380	347219
1456.48	Cu V	−2.17	−2.19	238234	306892
1456.96	Cu V	−1.28	−1.35	256273	324909
1457.43	Cu IV	−1.98	−2.02	227960	296573
1457.81	Cu V	−1.48	−1.53	236059	304655
1459.34	Cu V	−2.23	−2.20	239541	308065
1460.93	Cu V	−1.80	−1.81	239541	307991
1462.50	Cu V	−1.43	−1.43	239615	307991
1463.62	Cu V	−1.44	−1.34	236331	304655
1464.24	Cu V	−1.59	−1.55	239615	307910
1464.48	Cu V	−1.92	−1.93	239541	307825
1465.49	Cu IV	−2.03	−2.01	229694	297931
1466.61	Cu IV	−1.80	−1.86	244417	312602
1467.89	Cu V	−1.79	−1.83	236331	304456
1469.20	Cu V	−2.38	−2.34	272755	340820
1469.52	Cu IV	−2.37	−2.44	244417	312467
1473.12	Cu IV	−2.29	−2.27	224071	291954
1475.77	Cu V	−1.94	−1.90	246477	314238
1475.78	Cu V	−0.91	−0.89	236331	304092
1476.14	Cu IV	−2.07	−2.08	244671	312416
1476.81	Cu IV	−2.17	−2.15	244753	312467
1477.50	Cu V	−1.61	−1.59	272801	340483
1478.99	Cu V	−1.98	−1.98	246624	314238
1482.54	Cu IV	−2.05	−2.18	243725	311177
1482.82	Cu V	−0.91	−0.88	236040	303479
1483.24	Cu V	−2.04	−2.05	236059	303479
1484.80	Cu V	−1.83	−1.86	234036	301386
1485.29	Cu IV	−1.83	−1.78	244671	311998
1486.55	Cu IV	−2.16	−2.19	244813	312083
1488.48	Cu V	−2.11	−2.12	236059	303242
1489.19	Cu V	−1.09	−1.13	236059	303209
1489.90	Cu V	−2.05	−2.03	199441	266560
1489.90	Cu IV	−1.93	−1.94	244943	312061
1493.65	Cu V	−2.39	−2.36	256272	323222
1493.66	Cu V	−2.35	−2.27	256273	323222
1494.29	Cu V	−2.29	−2.25	236040	302961
1494.46	Cu IV	−2.06	−2.19	244813	311727

Table 29 – continued.

λ/ Å	Ion	$\log(gf)_{\mathrm{TOSS}}$	$\log(gf)_{\mathrm{Kurucz}}$	E_{low}/ cm^{-1}	E_{up}/ cm^{-1}
1494.53	Cu V	−2.04	−1.96	236331	303242
1495.23	Cu IV	−1.79	−1.74	229694	296573
1497.33	Cu V	−1.74	−1.71	199441	266227
1497.91	Cu IV	−2.42	−2.45	244417	311177
1498.12	Cu IV	−2.40	−2.43	226271	293022
1498.92	Cu IV	−2.23	−2.20	231216	297931
1500.39	Cu V	−1.43	−1.40	236331	302980
1502.02	Cu V	−1.81	−1.82	272801	339378
1502.99	Cu V	−1.35	−1.28	235053	301587
1504.40	Cu V	−2.15	−2.22	256272	322744
1505.56	Cu V	−2.22	−2.19	200648	267069
1510.51	Cu V	−2.08	−2.18	235053	301255
1510.62	Cu IV	−2.32	−2.41	244813	311011
1510.77	Cu V	−2.47	−2.43	256272	322464
1511.63	Cu V	−2.21	−2.24	243140	309294
1512.73	Cu IV	−2.13	−2.13	231825	297931
1513.41	Cu V	−2.47	−2.44	201413	267489
1514.07	Cu IV	−2.33	−2.45	244753	310800
1518.86	Cu V	−1.65	−1.59	239615	305453
1522.47	Cu V	−2.43	−2.45	265752	331435
1526.07	Cu V	−1.83	−1.74	236059	301587
1530.04	Cu V	−2.02	−1.94	246624	311982
1530.06	Cu IV	−2.47	−2.42	231216	296573
1530.98	Cu V	−2.26	−2.18	219203	284521
1531.30	Cu V	−1.75	−1.79	272755	338059
1532.32	Cu V	−1.26	−1.25	272755	338016
1533.04	Cu V	−2.31	−2.43	246477	311706
1533.83	Cu V	−1.82	−1.83	236059	301255
1535.77	Cu V	−2.22	−2.12	239541	304655
1537.15	Cu V	−0.79	−0.75	278282	343337
1537.50	Cu V	−1.66	−1.62	239615	304655
1540.33	Cu V	−1.01	−0.97	278380	343301
1540.47	Cu V	−1.19	−1.11	239541	304456
1542.01	Cu V	−2.23	−2.26	243140	307991
1544.42	Cu V	−1.80	−1.79	236331	301081
1549.16	Cu V	−1.98	−2.03	239541	304092
1550.25	Cu V	−2.20	−2.18	236331	300837
1563.14	Cu V	−1.30	−1.25	246477	310450
1566.76	Cu V	−2.34	−2.31	246624	310450
1568.25	Cu V	−2.44	−2.43	243140	306906
1576.31	Cu V	−1.59	−1.57	239541	302980
1576.88	Cu V	−1.34	−1.34	256272	319689
1583.92	Cu V	−2.20	−2.25	272801	335935

Table 29 – continued.

λ/ Å	Ion	$\log(gf)_{\mathrm{TOSS}}$	$\log(gf)_{\mathrm{Kurucz}}$	E_{low}/ cm^{-1}	E_{up}/ cm^{-1}
1585.32	Cu V	−1.81	−1.79	246624	309703
1586.51	Cu V	−1.25	−1.25	256273	319304
1613.63	Cu V	−1.84	−1.79	239615	301587
1616.95	Cu V	−2.20	−2.22	239541	301386
1625.63	Cu V	−2.36	−2.38	243140	304655
1641.27	Cu V	−2.26	−2.24	256272	317201
1648.47	Cu V	−2.19	−2.20	246477	307139
1656.45	Cu V	−2.02	−2.01	256272	316643
1658.56	Cu V	−2.36	−2.35	219203	279497
1663.86	Cu V	−2.10	−2.09	243140	303242
1670.53	Cu V	−2.46	−2.44	256273	316134
1672.87	Cu V	−1.22	−1.18	278282	338059
1681.81	Cu V	−1.57	−1.57	219203	278663
1692.27	Cu IV	−1.34	−1.37	272944	332036

Table 30: Like Table 29, for Zn.

λ/ Å	Ion	$\log(gf)_{\mathrm{TOSS}}$	$\log(gf)_{\mathrm{Kurucz}}$	E_{low}/ cm^{-1}	E_{up}/ cm^{-1}
901.35	Zn V	−0.70	−0.69	234846	345791
902.50	Zn V	−2.22	−2.24	210973	321776
902.64	Zn V	−2.01	−1.97	231831	342616
903.15	Zn V	−2.10	−2.08	241829	352553
903.22	Zn V	−1.58	−1.57	200644	311359
904.14	Zn V	−1.73	−1.78	235599	346201
908.06	Zn V	−1.83	−1.76	235599	345723
908.59	Zn V	−1.63	−1.63	235730	345791
908.88	Zn V	−2.38	−2.38	235599	345624
909.14	Zn V	−1.26	−1.29	235730	345723
910.03	Zn V	−2.30	−2.35	235903	345790
910.13	Zn V	−0.82	−0.83	200644	310519
911.40	Zn V	−1.64	−1.74	235903	345624
912.84	Zn V	−1.42	−1.36	235599	345146
914.42	Zn V	−1.89	−1.98	212471	321830
914.88	Zn V	−2.15	−2.17	212471	321776
915.22	Zn V	−1.76	−1.77	208715	317978
916.84	Zn V	−1.93	−1.95	210973	320043
919.47	Zn V	−2.28	−2.24	237032	345790
919.50	Zn V	−2.22	−2.26	236969	345723
920.88	Zn V	−1.61	−1.57	237032	345624
921.27	Zn V	−1.27	−1.29	201973	310519
921.90	Zn V	−1.40	−1.43	235599	344070
922.79	Zn V	−1.42	−1.36	202929	311296
923.36	Zn V	−2.04	−2.06	212471	320772
923.43	Zn V	−0.94	−0.97	201973	310265
924.41	Zn V	−1.69	−1.74	236969	345146
924.97	Zn V	−2.45	−2.44	208715	316827
928.10	Zn V	−1.70	−1.65	203548	311296
928.17	Zn V	−2.22	−2.12	237032	344771
929.16	Zn V	−1.69	−1.56	208715	316339
929.17	Zn V	−1.78	−1.79	235599	343221
929.46	Zn V	−2.24	−2.25	202929	310519
930.30	Zn V	−0.83	−0.82	235730	343221
931.66	Zn V	−1.26	−1.29	202929	310265
933.49	Zn V	−1.50	−1.46	208715	315840
933.61	Zn V	−1.38	−1.43	203548	310659
933.69	Zn V	−2.05	−2.05	236969	344070
934.24	Zn V	−1.19	−1.22	237032	344070
936.95	Zn V	−1.39	−1.49	202929	309658
937.06	Zn V	−2.23	−2.27	203548	310265
941.15	Zn V	−1.69	−1.68	236969	343221
941.20	Zn V	−1.99	−2.02	210973	317220

Table 30 – continued.

λ/ Å	Ion	$\log(gf)_{\mathrm{TOSS}}$	$\log(gf)_{\mathrm{Kurucz}}$	E_{low}/ cm^{-1}	E_{up}/ cm^{-1}
942.31	Zn V	−1.58	−1.58	208715	314838
942.42	Zn V	−1.64	−1.74	203548	309658
943.87	Zn V	−1.79	−1.70	239843	345790
945.34	Zn V	−1.93	−1.86	239843	345624
945.58	Zn V	−1.52	−1.47	240446	346201
945.86	Zn V	−1.46	−1.49	235903	341627
946.54	Zn V	−0.75	−0.76	236969	342616
946.85	Zn V	−1.91	−1.99	210973	316586
947.11	Zn V	−2.09	−2.09	237032	342616
948.03	Zn V	−2.44	−2.49	208715	314197
949.07	Zn V	−1.87	−1.84	210973	316339
949.87	Zn V	−1.69	−1.75	240446	345723
953.03	Zn V	−1.84	−1.87	239843	344771
959.96	Zn V	−1.34	−1.40	212471	316643
960.48	Zn V	−1.20	−1.22	212471	316586
962.79	Zn V	−2.40	−2.41	210973	314838
963.22	Zn V	−1.93	−1.88	208715	312534
967.41	Zn V	−2.41	−2.47	212471	315840
968.76	Zn V	−1.18	−1.21	210973	314197
969.00	Zn V	−2.40	−2.38	226334	329533
970.11	Zn V	−1.33	−1.35	208715	311796
971.42	Zn V	−2.29	−2.26	241829	344771
972.07	Zn V	−1.74	−1.76	227195	330069
974.24	Zn V	−1.34	−1.44	208715	311359
977.16	Zn V	−1.72	−1.73	227195	329533
978.08	Zn V	−1.54	−1.57	241829	344070
982.28	Zn V	−1.84	−1.87	208715	310519
982.96	Zn V	−2.38	−2.42	228335	330069
983.03	Zn V	−1.91	−1.92	212471	314197
984.02	Zn V	−1.68	−1.68	231831	333455
986.91	Zn IV	−2.11	−2.16	130366	231693
987.61	Zn V	−1.87	−1.94	230614	331869
988.17	Zn V	−2.30	−2.29	228335	329533
988.40	Zn V	−2.04	−1.93	227195	328369
988.65	Zn IV	−1.12	−1.10	128730	229878
991.83	Zn V	−2.15	−2.13	210973	311796
992.19	Zn V	−2.17	−2.19	241829	342616
993.51	Zn V	−1.36	−1.36	226334	326987
996.15	Zn V	−2.24	−2.33	210973	311359
996.15	Zn V	−1.55	−1.54	227195	327581
998.42	Zn IV	−2.36	−2.38	135951	236109
999.66	Zn V	−1.82	−1.83	228335	328369
1000.35	Zn V	−1.57	−1.50	231122	331087

Table 30 – continued.

λ/ Å	Ion	$\log(gf)_{\mathrm{TOSS}}$	$\log(gf)_{\mathrm{Kurucz}}$	E_{low}/ cm^{-1}	E_{up}/ cm^{-1}
1002.03	Zn V	−2.05	−2.06	241829	341627
1004.56	Zn V	−2.29	−2.32	210973	310519
1004.91	Zn IV	−1.81	−1.81	130366	229878
1007.13	Zn V	−1.96	−1.97	210973	310265
1007.66	Zn V	−2.48	−2.43	221631	320871
1011.62	Zn IV	−1.39	−1.41	135951	234802
1011.90	Zn V	−2.27	−2.23	212471	311296
1012.18	Zn IV	−1.24	−1.22	130366	229163
1014.11	Zn V	−1.67	−1.69	234846	333455
1015.53	Zn V	−1.61	−1.54	230614	329085
1017.94	Zn V	−0.52	−0.54	231831	330069
1018.94	Zn V	−2.17	−2.30	232946	331087
1019.66	Zn V	−2.38	−2.23	231997	330069
1021.01	Zn V	−1.94	−1.94	222042	319984
1022.16	Zn V	−2.01	−1.90	222940	320772
1022.57	Zn V	−2.45	−2.47	212471	310265
1023.28	Zn V	−2.42	−2.32	235730	333455
1023.52	Zn V	−0.11	−0.13	231831	329533
1024.28	Zn IV	−1.44	−1.46	138479	236109
1025.09	Zn V	−2.26	−2.23	226334	323886
1026.38	Zn V	−2.09	−2.05	222042	319472
1026.42	Zn IV	−1.28	−1.27	131805	229231
1027.13	Zn IV	−1.75	−1.74	131805	229163
1027.43	Zn V	−1.73	−1.73	227195	324526
1027.77	Zn V	−2.39	−2.49	226334	323632
1029.99	Zn V	−0.66	−0.70	231997	329085
1030.17	Zn V	−1.76	−1.80	255482	352553
1033.01	Zn V	−1.17	−1.16	221631	318436
1035.86	Zn V	−0.95	−0.86	231831	328369
1035.89	Zn V	−0.60	−0.62	285885	382420
1036.42	Zn V	−1.13	−1.15	236969	333455
1036.53	Zn IV	−1.38	−1.38	132777	229253
1036.77	Zn IV	−1.78	−1.77	132777	229231
1036.89	Zn V	−1.98	−2.01	202929	299372
1037.32	Zn V	−1.84	−1.81	201973	298375
1037.46	Zn V	−1.68	−1.72	200644	297033
1038.23	Zn V	−1.38	−1.41	256235	352553
1038.39	Zn IV	−1.83	−1.81	128730	225033
1040.02	Zn V	−2.24	−2.20	200644	296796
1040.07	Zn V	−2.32	−2.47	285523	381670
1041.12	Zn V	−1.31	−1.21	230614	326664
1042.04	Zn V	−0.86	−0.94	235903	331869
1043.35	Zn V	0.25	0.24	286575	382420

Table 30 – continued.

λ/ Å	Ion	$\log(gf)_{\mathrm{TOSS}}$	$\log(gf)_{\mathrm{Kurucz}}$	E_{low}/ cm^{-1}	E_{up}/ cm^{-1}
1043.58	Zn V	−1.85	−1.89	203548	299372
1044.00	Zn V	−0.87	−0.96	285885	381670
1044.38	Zn V	−2.45	−2.39	231831	327581
1044.48	Zn IV	−1.71	−1.67	135951	231693
1047.16	Zn V	−1.10	−1.18	222940	318436
1047.72	Zn V	−2.23	−2.22	202929	298375
1048.45	Zn V	−0.51	−0.53	285523	380902
1050.66	Zn V	−2.02	−1.92	222042	317220
1051.58	Zn V	−2.29	−2.37	286575	381670
1052.44	Zn V	−0.03	−0.03	285885	380902
1053.28	Zn V	−0.17	−0.18	285523	380464
1054.56	Zn V	−1.86	−1.86	203548	298375
1054.60	Zn V	−1.77	−1.82	201973	296796
1055.88	Zn V	−0.43	−0.52	221631	316339
1056.33	Zn V	−0.62	−0.74	231997	326664
1056.53	Zn V	−2.35	−2.41	200644	295293
1057.30	Zn V	−2.19	−2.17	227195	321776
1057.31	Zn V	−0.84	−0.84	285885	380464
1057.91	Zn V	−2.23	−2.27	222940	317466
1057.93	Zn V	−1.33	−1.38	200644	295168
1058.19	Zn V	−1.18	−1.21	198962	293463
1058.53	Zn V	−1.49	−1.50	235599	330069
1058.66	Zn IV	−2.13	−2.06	138479	232938
1060.15	Zn V	−0.89	−0.90	286575	380902
1062.65	Zn V	−1.43	−1.45	202929	297033
1063.21	Zn V	−0.35	−0.33	237032	331087
1063.98	Zn V	−0.39	−0.43	222042	316029
1064.70	Zn V	−2.45	−2.37	226334	320257
1065.34	Zn V	−1.66	−1.78	202929	296796
1065.78	Zn V	−1.86	−1.89	202929	296757
1066.06	Zn V	−1.05	−1.06	235730	329533
1066.55	Zn V	−1.02	−1.05	198962	292722
1067.14	Zn V	−1.97	−1.99	226334	320043
1068.28	Zn V	−0.44	−0.29	221631	315239
1069.67	Zn V	−0.26	−0.23	235599	329085
1070.20	Zn V	−1.32	−1.28	228335	321776
1071.50	Zn V	−0.64	−0.72	221631	314958
1071.58	Zn V	−1.76	−1.79	201973	295293
1072.46	Zn IV	−2.45	−2.43	130366	223609
1072.86	Zn V	−1.33	−1.38	203548	296757
1072.89	Zn V	−2.35	−2.38	221631	314838
1072.99	Zn V	0.03	0.03	222042	315239
1073.01	Zn V	−0.83	−0.89	201973	295168

Table 30 – continued.

λ/ Å	Ion	$\log(gf)_{\mathrm{TOSS}}$	$\log(gf)_{\mathrm{Kurucz}}$	E_{low}/ cm^{-1}	E_{up}/ cm^{-1}
1073.17	Zn V	−1.13	−1.22	235903	329085
1074.11	Zn V	−1.17	−1.18	236969	330069
1074.24	Zn V	−0.72	−0.82	222940	316029
1074.55	Zn V	−2.38	−2.46	227195	320257
1075.17	Zn V	0.52	0.51	240446	333455
1076.24	Zn V	−1.01	−0.94	222042	314958
1076.88	Zn V	−0.33	−0.21	222940	315801
1077.04	Zn V	−1.58	−1.53	227195	320043
1077.36	Zn V	−2.15	−2.13	200644	293463
1078.34	Zn V	−2.16	−2.14	234846	327581
1078.81	Zn V	−0.85	−0.91	231831	324526
1079.45	Zn V	−1.41	−1.39	235730	328369
1080.00	Zn V	−2.05	−2.05	226334	318927
1080.31	Zn V	−1.75	−1.67	221631	314197
1080.33	Zn V	−0.81	−0.73	236969	329533
1080.74	Zn V	−0.70	−0.82	232946	325476
1082.67	Zn V	−1.28	−1.34	202929	295293
1082.98	Zn V	−2.22	−2.13	239843	332181
1084.75	Zn V	−1.11	−1.11	222042	314229
1085.29	Zn V	0.56	0.55	234846	326987
1086.03	Zn V	−0.39	−0.47	200644	292722
1086.33	Zn V	−0.75	−0.68	237032	329085
1086.64	Zn V	−0.80	−0.75	239843	331869
1088.71	Zn V	0.50	0.49	235730	327581
1090.83	Zn V	0.32	0.31	260880	352553
1091.18	Zn V	−1.95	−1.83	226334	317978
1093.01	Zn V	−1.24	−1.30	201973	293463
1094.09	Zn V	0.41	0.39	236969	328369
1094.44	Zn IV	−1.96	−1.97	130366	221737
1095.13	Zn V	−0.97	−0.97	291107	382420
1095.42	Zn V	−1.54	−1.66	222940	314229
1095.77	Zn V	−0.63	−0.67	285885	377144
1095.80	Zn V	−0.49	−0.51	235730	326987
1095.96	Zn V	−0.41	−0.46	239843	331087
1096.30	Zn V	−1.83	−1.83	230614	321830
1098.11	Zn V	−0.61	−0.67	235599	326664
1099.97	Zn V	−1.08	−1.11	285523	376434
1100.08	Zn V	−1.80	−1.72	221631	312534
1100.53	Zn V	−1.55	−1.55	198962	289827
1101.53	Zn V	−1.67	−1.74	227195	317978
1102.43	Zn V	−1.67	−1.73	231122	321830
1102.49	Zn V	−0.66	−0.81	222940	313644
1103.60	Zn V	−0.62	−0.65	236969	327581

Table 30 – continued.

λ/ Å	Ion	$\log(gf)_{\mathrm{TOSS}}$	$\log(gf)_{\mathrm{Kurucz}}$	E_{low}/ cm^{-1}	E_{up}/ cm^{-1}
1104.13	Zn V	−1.69	−1.63	286575	377144
1104.20	Zn V	0.13	0.13	291107	381670
1105.06	Zn V	−2.10	−2.14	226334	316827
1105.55	Zn V	−1.16	−1.09	226334	316786
1106.79	Zn V	−0.06	−0.06	241829	332181
1106.96	Zn V	−1.05	−1.03	230435	320772
1107.32	Zn V	−0.07	−0.08	255482	345790
1107.59	Zn V	−0.80	−0.81	235903	326189
1107.95	Zn V	−1.10	−0.98	230614	320871
1109.08	Zn V	0.03	−0.05	221631	311796
1109.17	Zn V	−0.81	−0.77	230614	320772
1109.35	Zn V	−1.14	−1.20	255482	345624
1109.89	Zn IV	−1.08	−1.12	135951	226050
1110.82	Zn V	−1.21	−1.15	232946	322969
1111.53	Zn V	0.01	−0.05	256235	346201
1111.60	Zn V	0.22	0.20	255763	345723
1111.79	Zn V	−1.72	−1.83	231831	321776
1111.84	Zn V	−1.77	−1.89	198962	288903
1112.83	Zn V	0.01	−0.01	255763	345624
1113.65	Zn V	−0.89	−0.98	291107	380902
1113.84	Zn V	−1.27	−1.24	200644	290424
1114.48	Zn V	0.18	0.21	221631	311359
1115.27	Zn V	−0.19	−0.24	255482	345146
1115.45	Zn V	−1.33	−1.40	231122	320772
1115.68	Zn V	0.08	0.07	227195	316827
1115.80	Zn IV	−2.41	−2.42	131805	221426
1116.18	Zn V	−0.29	−0.32	227195	316786
1116.63	Zn V	0.50	0.49	256235	345791
1116.70	Zn V	−1.21	−1.20	230435	319984
1116.84	Zn V	0.61	0.60	198962	288500
1117.47	Zn V	−0.39	−0.29	256235	345723
1118.78	Zn V	0.06	0.04	255763	345146
1119.10	Zn V	−1.05	−1.08	291107	380464
1119.95	Zn V	0.01	−0.01	255482	344771
1120.33	Zn V	0.39	0.38	226334	315594
1120.55	Zn V	−0.84	−0.98	239843	329085
1121.29	Zn V	−2.20	−2.26	200644	289827
1121.61	Zn V	−0.74	−0.61	237032	326189
1121.78	Zn V	−1.11	−1.21	227195	316339
1122.50	Zn V	0.25	0.24	240446	329533
1122.57	Zn IV	−2.09	−2.10	135951	225033
1124.52	Zn V	−1.85	−1.94	235599	324526
1124.72	Zn V	−0.59	−0.52	256235	345146

Table 30 – continued.

λ/ Å	Ion	$\log(gf)_{\mathrm{TOSS}}$	$\log(gf)_{\mathrm{Kurucz}}$	E_{low}/ cm^{-1}	E_{up}/ cm^{-1}
1125.02	Zn V	−0.02	−0.04	221631	310519
1125.05	Zn V	0.08	0.02	228335	317220
1125.18	Zn V	−1.51	−1.56	231997	320871
1126.66	Zn V	−1.00	−0.92	201973	290731
1128.10	Zn V	−0.62	−0.64	227195	315840
1128.24	Zn V	−0.73	−0.76	221631	310265
1128.81	Zn V	−0.57	−0.55	255482	344070
1129.90	Zn V	−0.34	−0.35	226334	314838
1130.05	Zn V	−0.17	−0.19	228335	316827
1130.24	Zn V	−0.11	−0.10	222042	310519
1130.57	Zn V	−2.35	−2.24	201973	290424
1130.88	Zn V	−2.23	−2.21	231831	320257
1131.24	Zn V	−0.22	−0.25	227195	315594
1131.79	Zn V	−0.40	−0.38	222940	311296
1132.27	Zn V	0.10	0.08	208715	297033
1132.41	Zn V	−1.21	−1.06	255763	344070
1132.66	Zn V	0.44	0.43	235599	323886
1133.03	Zn V	0.48	0.48	200644	288903
1133.13	Zn V	0.17	0.16	228335	316586
1133.28	Zn V	0.23	0.22	241829	330069
1133.50	Zn V	−0.08	−0.10	222042	310265
1133.72	Zn IV	−1.37	−1.43	138479	226685
1135.32	Zn V	−0.87	−0.78	208715	296796
1135.59	Zn V	−0.41	−0.40	200644	288704
1136.31	Zn V	−0.26	−0.23	228335	316339
1136.42	Zn IV	−0.77	−0.77	148180	236175
1136.60	Zn V	−0.35	−0.33	198962	286943
1136.99	Zn V	−0.55	−0.57	201973	289925
1137.36	Zn V	−1.30	−1.22	240446	328369
1137.63	Zn V	−0.20	−0.24	235730	323632
1138.25	Zn V	0.41	0.40	201973	289827
1138.50	Zn V	0.19	0.16	256235	344070
1138.67	Zn V	−1.11	−1.17	230614	318436
1138.94	Zn V	−1.53	−1.56	231831	319632
1139.28	Zn V	−0.48	−0.48	202929	290704
1140.00	Zn V	−0.60	−0.63	222940	310659
1140.70	Zn V	0.43	0.41	286575	374241
1140.80	Zn IV	−2.01	−1.99	135951	223609
1141.00	Zn V	−0.06	−0.07	227195	314838
1141.10	Zn V	−0.33	−0.27	231997	319632
1141.34	Zn V	−0.42	−0.45	222042	309658
1141.93	Zn IV	−1.91	−1.94	138479	226050
1142.11	Zn V	−0.93	−1.02	236969	324526

Table 30 – continued.

λ/ Å	Ion	$\log(gf)_{\mathrm{TOSS}}$	$\log(gf)_{\mathrm{Kurucz}}$	E_{low}/ cm^{-1}	E_{up}/ cm^{-1}
1142.79	Zn V	−0.64	−0.58	228335	315840
1142.93	Zn V	0.30	0.29	202929	290424
1142.94	Zn V	0.23	0.24	237032	324526
1143.20	Zn V	−0.57	−0.58	203548	291022
1143.40	Zn V	−0.09	−0.08	255763	343221
1144.14	Zn V	−0.05	−0.01	210973	298375
1145.15	Zn V	−0.64	−0.65	222940	310265
1146.06	Zn V	−0.49	−0.52	241829	329085
1146.15	Zn V	−0.45	−0.51	234582	321830
1147.02	Zn V	0.13	0.10	203548	290731
1147.37	Zn V	−0.31	−0.33	203548	290704
1147.65	Zn V	0.00	−0.01	255482	342616
1148.55	Zn V	−1.04	−0.97	235903	322969
1148.92	Zn V	0.00	0.05	232946	319984
1149.40	Zn V	0.23	0.22	227195	314197
1149.49	Zn V	0.01	−0.01	202929	289925
1149.61	Zn V	0.08	0.06	256235	343221
1149.63	Zn IV	−1.33	−1.33	149191	236175
1149.87	Zn V	0.60	0.59	226334	313300
1150.50	Zn IV	−1.09	−1.10	149191	236109
1150.74	Zn V	−0.08	−0.09	212471	299372
1151.37	Zn V	−0.09	−0.11	255763	342616
1151.39	Zn V	−0.87	−1.00	230614	317466
1152.27	Zn V	−1.17	−1.10	230435	317220
1152.99	Zn V	0.20	0.18	201973	288704
1153.16	Zn V	−0.84	−0.95	222940	309658
1154.43	Zn IV	−1.20	−1.20	148180	234802
1155.03	Zn V	−0.19	−0.19	208715	295293
1155.36	Zn IV	−2.37	−2.38	138479	225033
1155.52	Zn V	−1.37	−1.40	240446	326987
1155.73	Zn V	−0.42	−0.39	232946	319472
1155.83	Zn IV	−1.05	−1.07	138479	224998
1156.04	Zn V	−1.85	−1.83	228335	314838
1156.39	Zn V	0.20	0.19	285885	372360
1156.69	Zn V	−1.26	−1.27	208715	295168
1157.66	Zn V	−1.20	−1.24	256235	342616
1157.73	Zn V	−1.06	−0.91	203548	289925
1158.76	Zn V	0.33	0.31	200644	286943
1159.98	Zn V	−1.46	−1.54	230435	316643
1160.09	Zn V	−0.94	−0.82	226334	312534
1160.22	Zn V	−0.54	−0.54	234582	320772
1160.40	Zn V	−1.82	−1.80	235599	321776
1160.80	Zn V	−1.71	−1.71	231831	317978

Table 30 – continued.

λ/ Å	Ion	$\log(gf)_{\mathrm{TOSS}}$	$\log(gf)_{\mathrm{Kurucz}}$	E_{low}/ cm^{-1}	E_{up}/ cm^{-1}
1160.83	Zn V	−0.44	−0.43	255482	341627
1161.97	Zn V	−0.41	−0.45	210973	297033
1162.28	Zn V	0.27	0.26	291107	377144
1162.40	Zn V	−0.56	−0.67	230614	316643
1163.78	Zn V	−0.34	−0.33	235903	321830
1164.10	Zn V	−0.48	−0.44	212471	298375
1164.63	Zn V	−0.45	−0.46	255763	341627
1164.66	Zn V	−0.92	−0.95	228335	314197
1165.19	Zn V	−0.50	−0.48	210973	296796
1165.69	Zn IV	−1.37	−1.40	135951	221737
1165.71	Zn V	−0.51	−0.53	286575	372360
1165.72	Zn V	−0.41	−0.42	210973	296757
1165.84	Zn V	−1.67	−1.59	202929	288704
1165.88	Zn V	0.67	0.65	234846	320618
1168.30	Zn V	−0.75	−0.87	230435	316029
1169.20	Zn V	0.06	0.05	285523	371051
1169.30	Zn V	−0.40	−0.44	231122	316643
1170.11	Zn V	0.05	0.07	226334	311796
1170.76	Zn V	−1.23	−1.09	230614	316029
1171.11	Zn V	−0.20	−0.18	231831	317220
1171.42	Zn V	−0.75	−0.82	230435	315801
1171.80	Zn V	−0.46	−0.51	227195	312534
1171.95	Zn V	−0.09	−0.10	291107	376434
1172.04	Zn V	0.21	0.23	260880	346201
1172.29	Zn IV	−1.02	−1.03	149191	234494
1173.37	Zn V	−0.03	0.06	239843	325068
1174.17	Zn V	−0.57	−0.59	285885	371051
1174.35	Zn V	0.52	0.50	198962	284116
1176.12	Zn V	−0.05	−0.12	226334	311359
1176.53	Zn V	−0.18	−0.19	231831	316827
1176.87	Zn V	0.31	0.29	198962	283933
1176.88	Zn V	−2.23	−2.22	201973	286943
1176.98	Zn V	0.01	−0.01	201973	286936
1177.02	Zn V	−0.08	−0.10	226334	311295
1177.04	Zn V	−0.30	−0.32	202929	287888
1177.04	Zn V	0.18	0.16	200644	285603
1177.09	Zn V	0.44	0.42	231831	316786
1177.50	Zn IV	−0.40	−0.40	151250	236175
1178.29	Zn V	−0.87	−0.97	235903	320772
1178.41	Zn IV	−1.54	−1.55	151250	236109
1178.64	Zn V	−0.24	−0.33	260880	345723
1178.76	Zn V	−0.25	−0.11	241829	326664
1179.15	Zn V	0.24	0.24	236969	321776

Table 30 – continued.

λ/ Å	Ion	$\log(gf)_{\mathrm{TOSS}}$	$\log(gf)_{\mathrm{Kurucz}}$	E_{low}/ cm^{-1}	E_{up}/ cm^{-1}
1179.49	Zn IV	−0.56	−0.57	151392	236175
1179.82	Zn IV	−2.01	−2.04	148180	232938
1179.97	Zn V	0.40	0.39	208715	293463
1180.02	Zn V	−0.48	−0.47	260880	345624
1180.03	Zn V	−0.94	−1.03	237032	321776
1180.28	Zn IV	−2.16	−2.23	151250	235976
1181.39	Zn V	−1.42	−1.32	231997	316643
1182.02	Zn V	−0.70	−0.65	227195	311796
1182.02	Zn IV	−0.47	−0.47	151574	236175
1182.57	Zn V	−0.44	−0.39	212471	297033
1183.04	Zn V	−0.67	−0.70	235730	320257
1183.10	Zn V	−0.80	−0.87	230435	314958
1183.16	Zn V	−1.16	−1.01	232946	317466
1183.31	Zn V	−0.57	−0.70	231831	316339
1183.77	Zn V	−1.84	−1.86	286575	371051
1185.68	Zn V	−0.41	−0.42	203548	287888
1185.90	Zn V	0.21	0.18	212471	296796
1185.95	Zn V	0.11	0.10	210973	295293
1185.96	Zn V	−0.51	−0.52	285523	369843
1186.06	Zn V	0.38	0.36	235730	320043
1186.45	Zn V	0.01	−0.00	212471	296757
1187.66	Zn V	0.28	0.26	228335	312534
1187.71	Zn V	0.39	0.38	210973	295168
1188.16	Zn V	−1.18	−1.24	227195	311359
1189.07	Zn V	0.34	0.33	227195	311295
1189.33	Zn V	−0.48	−0.51	234846	318927
1189.54	Zn IV	−0.91	−0.92	148180	232246
1190.34	Zn V	−0.24	−0.22	231831	315840
1190.38	Zn V	0.45	0.45	208715	292722
1190.38	Zn V	−0.38	−0.38	202929	286936
1192.01	Zn V	−0.36	−0.37	260880	344771
1193.26	Zn V	−1.08	−1.13	231997	315801
1193.30	Zn IV	−1.59	−1.63	130366	214167
1193.62	Zn V	−0.80	−0.81	285523	369302
1193.85	Zn V	−0.49	−0.49	231831	315594
1194.07	Zn IV	−1.51	−1.54	149191	232938
1194.17	Zn V	−1.02	−1.02	237032	320772
1195.75	Zn V	−0.30	−0.29	201973	285603
1196.62	Zn V	−1.41	−1.35	235903	319472
1197.41	Zn IV	−1.36	−1.38	148180	231693
1198.16	Zn V	−1.00	−0.87	228335	311796
1198.80	Zn V	−0.12	−0.13	285885	369302
1199.22	Zn V	−1.31	−1.32	203548	286936

Table 30 – continued.

λ/ Å	Ion	$\log(gf)_{\mathrm{TOSS}}$	$\log(gf)_{\mathrm{Kurucz}}$	E_{low}/ cm^{-1}	E_{up}/ cm^{-1}
1200.14	Zn V	−2.21	−2.24	227195	310519
1200.33	Zn V	−2.39	−2.41	285523	368833
1200.64	Zn V	−0.25	−0.24	200644	283933
1200.64	Zn V	0.48	0.46	236969	320257
1201.28	Zn IV	−1.52	−1.52	151250	234494
1201.31	Zn V	−1.12	−0.99	231997	315239
1201.52	Zn IV	−0.51	−0.54	151574	234802
1201.96	Zn V	0.48	0.47	235730	318927
1202.06	Zn V	−1.29	−1.33	260880	344070
1202.13	Zn V	0.52	0.51	240446	323632
1202.91	Zn V	0.49	0.48	234846	317978
1202.98	Zn V	−0.90	−1.00	239843	322969
1203.26	Zn V	−1.50	−1.45	231122	314229
1203.35	Zn IV	−1.76	−1.79	151392	234494
1203.46	Zn IV	−1.59	−1.60	128730	211824
1203.62	Zn V	−1.49	−1.51	232946	316029
1203.75	Zn V	−1.86	−1.86	236969	320043
1204.02	Zn IV	−1.39	−1.39	149191	232246
1204.47	Zn V	−1.72	−1.72	228335	311359
1204.72	Zn V	−0.08	−0.10	231831	314838
1205.57	Zn V	−0.81	−0.82	285885	368833
1205.59	Zn IV	−1.73	−1.76	138479	221426
1207.19	Zn V	−0.82	−0.91	235599	318436
1207.41	Zn V	−1.29	−1.29	212471	295293
1209.24	Zn V	−1.45	−1.52	241829	324526
1209.58	Zn V	−1.43	−1.43	202929	285603
1209.73	Zn V	−2.17	−2.28	236969	319632
1212.09	Zn IV	−2.05	−2.17	149191	231693
1212.26	Zn V	−1.59	−1.57	210973	293463
1212.71	Zn IV	−1.81	−1.85	128730	211190
1214.08	Zn V	−0.74	−0.80	231831	314197
1214.14	Zn IV	−2.00	−2.06	131805	214167
1214.29	Zn V	−0.87	−0.78	230614	312967
1214.45	Zn V	−0.31	−0.37	260880	343221
1215.70	Zn V	0.13	0.12	286575	368833
1215.83	Zn V	−2.22	−2.23	235730	317978
1216.07	Zn V	−0.38	−0.45	231997	314229
1216.54	Zn V	−1.99	−2.05	231997	314197
1220.10	Zn V	−1.76	−1.75	201973	283933
1220.40	Zn V	−1.44	−1.47	234846	316786
1223.18	Zn IV	0.46	0.46	160886	242640
1223.44	Zn V	−2.32	−2.37	260880	342616
1223.68	Zn IV	−0.69	−0.70	160919	242640

Table 30 – continued.

λ/ Å	Ion	$\log(gf)_{\mathrm{TOSS}}$	$\log(gf)_{\mathrm{Kurucz}}$	E_{low}/ cm^{-1}	E_{up}/ cm^{-1}
1224.02	Zn IV	−0.28	−0.30	148180	229878
1224.16	Zn IV	−1.54	−1.59	151250	232938
1224.36	Zn IV	−1.36	−1.37	131805	213480
1224.79	Zn V	−0.43	−0.54	231997	313644
1226.06	Zn V	−1.11	−1.11	235903	317466
1226.31	Zn IV	−1.55	−1.61	151392	232938
1227.63	Zn IV	−1.83	−1.85	130366	211824
1227.79	Zn V	−1.82	−1.97	234582	316029
1227.99	Zn IV	−2.44	−2.41	160886	242320
1228.49	Zn IV	0.39	0.39	160919	242320
1228.65	Zn IV	−1.14	−1.17	132777	214167
1229.05	Zn IV	−1.59	−1.63	151574	232938
1230.27	Zn V	−0.68	−0.61	232946	314229
1230.71	Zn V	−0.85	−0.90	291107	372360
1231.47	Zn IV	−1.36	−1.36	130366	211570
1232.87	Zn V	−1.68	−1.75	208715	289827
1233.09	Zn V	−1.47	−1.39	235730	316827
1233.79	Zn IV	−1.68	−1.69	148180	229231
1234.83	Zn IV	−1.25	−1.25	148180	229163
1235.65	Zn V	−1.44	−1.56	239843	320772
1236.69	Zn V	−0.64	−0.67	230435	311296
1237.27	Zn IV	−1.38	−1.42	130366	211190
1238.43	Zn V	−0.15	−0.18	260880	341627
1238.55	Zn V	−1.32	−1.37	235903	316643
1239.11	Zn V	−0.62	−0.62	231831	312534
1239.12	Zn IV	−0.84	−0.85	132777	213480
1239.60	Zn IV	−1.08	−1.09	151574	232246
1243.11	Zn IV	−0.69	−0.74	151250	231693
1246.08	Zn V	−1.68	−1.68	236969	317220
1246.24	Zn V	−1.62	−1.47	235599	315840
1247.02	Zn IV	−1.84	−1.82	128730	208921
1247.07	Zn V	−1.20	−1.24	237032	317220
1247.07	Zn V	−0.46	−0.53	208715	288903
1247.29	Zn V	−1.05	−1.10	231122	311296
1248.15	Zn IV	−1.16	−1.23	151574	231693
1249.03	Zn IV	−1.82	−1.85	149191	229253
1249.37	Zn IV	−1.78	−1.77	149191	229231
1249.70	Zn IV	−0.64	−0.68	131805	211824
1249.99	Zn V	−1.90	−1.97	241829	321830
1250.44	Zn IV	−1.07	−1.06	149191	229163
1250.54	Zn V	−1.07	−1.09	231831	311796
1250.84	Zn V	−1.26	−1.26	241829	321776
1250.87	Zn V	−2.04	−2.11	291107	371051

Table 30 – continued.

λ/ Å	Ion	$\log(gf)_{\mathrm{TOSS}}$	$\log(gf)_{\mathrm{Kurucz}}$	E_{low}/ cm^{-1}	E_{up}/ cm^{-1}
1252.13	Zn V	−1.77	−1.72	235730	315594
1252.86	Zn V	−2.31	−2.27	236969	316786
1252.96	Zn V	−1.19	−1.20	240446	320257
1253.68	Zn IV	−1.09	−1.09	131805	211570
1255.49	Zn V	−1.22	−1.31	230614	310265
1255.53	Zn V	−1.24	−1.27	234582	314229
1255.82	Zn V	−1.56	−1.48	239843	319472
1256.34	Zn V	−0.81	−0.80	240446	320043
1257.34	Zn IV	−1.30	−1.30	130366	209899
1257.41	Zn V	−1.20	−1.29	231831	311359
1258.44	Zn V	−0.64	−0.68	231831	311295
1258.63	Zn V	−1.57	−1.63	210973	290424
1259.68	Zn IV	−2.12	−2.09	131805	211190
1260.92	Zn V	−1.46	−1.54	237032	316339
1262.25	Zn V	−0.70	−0.59	230435	309658
1264.10	Zn V	−1.45	−1.44	235730	314838
1264.94	Zn V	−1.37	−1.36	235903	314958
1265.12	Zn V	−1.15	−1.17	230614	309658
1265.27	Zn IV	−1.46	−1.47	157075	236109
1265.71	Zn IV	0.31	0.30	128730	207737
1265.87	Zn V	−1.93	−2.02	237032	316029
1266.74	Zn V	−1.73	−1.79	241829	320772
1267.42	Zn IV	−0.29	−0.30	157075	235976
1268.16	Zn V	−0.86	−0.92	210973	289827
1268.90	Zn V	−1.15	−1.23	237032	315840
1269.16	Zn IV	−2.47	−2.36	132777	211570
1272.20	Zn IV	−0.18	−0.21	130366	208970
1272.38	Zn V	−2.14	−2.05	239843	318436
1272.99	Zn IV	0.12	0.11	130366	208921
1273.80	Zn IV	−0.96	−0.93	148180	226685
1274.20	Zn V	−0.27	−0.31	240446	318927
1274.63	Zn V	−1.35	−1.35	234846	313300
1275.79	Zn IV	−1.09	−1.09	131805	210187
1276.33	Zn V	−1.73	−1.67	232946	311296
1277.08	Zn IV	0.25	0.24	151574	229878
1277.67	Zn V	−1.78	−1.67	231997	310265
1277.81	Zn V	−1.46	−1.54	212471	290731
1278.31	Zn V	−1.52	−1.51	208715	286943
1278.51	Zn IV	−1.45	−1.55	135951	214167
1280.50	Zn IV	0.01	0.01	131805	209899
1281.30	Zn IV	−0.98	−0.95	157930	235976
1281.31	Zn V	−0.50	−0.55	235599	313644
1282.00	Zn IV	−1.28	−1.29	151250	229253

Table 30 – continued.

λ/ Å	Ion	$\log(gf)_{\mathrm{TOSS}}$	$\log(gf)_{\mathrm{Kurucz}}$	E_{low}/ cm^{-1}	E_{up}/ cm^{-1}
1282.36	Zn IV	−0.31	−0.31	151250	229231
1282.83	Zn V	−1.31	−1.37	212471	290424
1283.26	Zn V	−1.64	−1.63	237032	314958
1283.48	Zn IV	0.07	0.06	151250	229163
1284.18	Zn IV	−0.61	−0.63	148180	226050
1284.21	Zn V	−1.78	−1.68	236969	314838
1284.35	Zn IV	−0.31	−0.32	151392	229253
1284.71	Zn IV	−0.25	−0.26	151392	229231
1286.33	Zn V	−1.59	−1.46	235903	313644
1286.48	Zn V	−1.69	−1.69	210973	288704
1288.28	Zn V	−1.75	−1.80	239843	317466
1288.85	Zn IV	−0.80	−0.79	151574	229163
1289.79	Zn V	−1.71	−1.73	240446	317978
1290.06	Zn IV	0.09	0.08	199369	276885
1290.42	Zn IV	−0.20	−0.23	149191	226685
1291.10	Zn V	−1.71	−1.69	212471	289925
1291.67	Zn IV	−1.10	−1.07	157075	234494
1291.83	Zn IV	−0.01	−0.02	132777	210187
1292.48	Zn IV	−0.05	−0.05	130366	207737
1294.31	Zn IV	−2.05	−2.07	128730	205991
1294.86	Zn V	−1.76	−1.75	236969	314197
1295.38	Zn V	−1.30	−1.32	237032	314229
1295.85	Zn V	−0.14	−0.11	221631	298801
1296.65	Zn IV	−0.20	−0.21	132777	209899
1296.73	Zn IV	0.00	−0.01	131805	208921
1300.60	Zn V	−1.80	−1.82	208715	285603
1301.08	Zn IV	−0.67	−0.68	149191	226050
1301.19	Zn IV	0.27	0.26	148180	225033
1301.78	Zn IV	−1.14	−1.17	148180	224998
1301.93	Zn IV	−1.77	−1.79	130366	207175
1302.01	Zn V	−1.87	−1.87	235730	312534
1302.79	Zn V	−0.38	−0.36	222042	298801
1305.37	Zn V	−1.45	−1.46	241829	318436
1306.09	Zn IV	−0.38	−0.40	157930	234494
1306.66	Zn IV	0.58	0.57	128730	205261
1308.07	Zn V	−1.90	−1.88	234846	311295
1309.23	Zn V	−0.79	−0.81	240446	316827
1309.93	Zn V	−1.58	−1.58	240446	316786
1311.77	Zn V	−1.69	−1.72	212471	288704
1311.94	Zn IV	−0.52	−0.53	149191	225414
1316.30	Zn V	−1.34	−1.38	210973	286943
1316.42	Zn V	−1.68	−1.70	210973	286936
1318.00	Zn IV	0.14	0.14	135951	211824

Table 30 – continued.

λ/ Å	Ion	$\log(gf)_{\mathrm{TOSS}}$	$\log(gf)_{\mathrm{Kurucz}}$	E_{low}/ cm^{-1}	E_{up}/ cm^{-1}
1318.16	Zn IV	−1.88	−1.79	157075	232938
1318.20	Zn V	−0.76	−0.70	222940	298801
1319.14	Zn IV	−0.52	−0.49	149191	224998
1320.70	Zn IV	0.04	0.03	128730	204447
1321.22	Zn IV	0.22	0.22	138479	214167
1322.32	Zn IV	0.04	0.02	130366	205991
1322.43	Zn IV	0.20	0.19	135951	211570
1323.36	Zn V	−1.76	−1.73	236969	312534
1323.36	Zn V	−1.87	−1.88	235730	311295
1325.64	Zn IV	−1.72	−1.78	151250	226685
1325.74	Zn IV	−2.08	−1.98	148180	223609
1325.96	Zn V	−1.72	−1.75	212471	287888
1326.25	Zn V	−1.05	−1.09	208715	284116
1326.42	Zn V	−0.95	−0.96	241829	317220
1326.66	Zn IV	−0.22	−0.23	199369	274746
1326.77	Zn IV	−0.19	−0.21	131805	207175
1328.15	Zn IV	−2.15	−2.10	151392	226685
1329.11	Zn IV	−0.05	−0.08	135951	211190
1329.47	Zn V	−1.40	−1.44	208715	283933
1329.96	Zn IV	0.24	0.23	160919	236109
1330.30	Zn IV	0.01	−0.01	157075	232246
1331.28	Zn V	−1.92	−2.00	239843	314958
1331.37	Zn IV	−0.66	−0.64	151574	226685
1333.18	Zn IV	0.04	0.03	157930	232938
1333.33	Zn IV	−0.02	−0.03	138479	213480
1333.49	Zn V	−2.24	−2.21	222042	297033
1334.76	Zn V	−2.36	−2.44	235599	310519
1336.89	Zn IV	−0.74	−0.74	151250	226050
1337.67	Zn V	−2.24	−2.31	241829	316586
1339.94	Zn V	−1.85	−1.89	210973	285603
1340.16	Zn IV	0.17	0.17	157075	231693
1342.10	Zn V	−1.26	−1.40	241829	316339
1342.72	Zn IV	0.06	0.05	151574	226050
1342.92	Zn V	−2.36	−2.40	212471	286936
1343.75	Zn IV	0.16	0.15	149191	223609
1344.12	Zn IV	0.07	0.06	132777	207175
1344.24	Zn V	−0.31	−0.32	240446	314838
1344.33	Zn V	−2.04	−1.92	239843	314229
1345.79	Zn V	−2.08	−2.06	255763	330069
1347.95	Zn IV	0.11	0.10	131805	205991
1348.35	Zn IV	−0.71	−0.73	151250	225414
1349.88	Zn IV	0.20	0.20	130366	204447
1350.96	Zn IV	−1.88	−1.90	151392	225414

Table 30 – continued.

λ/ Å	Ion	$\log(gf)_{\mathrm{TOSS}}$	$\log(gf)_{\mathrm{Kurucz}}$	E_{low}/ cm^{-1}	E_{up}/ cm^{-1}
1351.15	Zn V	−0.96	−0.97	241829	315840
1351.87	Zn V	−2.08	−2.22	241829	315801
1352.31	Zn IV	−1.00	−1.00	135951	209899
1352.88	Zn IV	0.32	0.31	160886	234802
1353.49	Zn IV	−2.43	−2.43	160919	234802
1354.40	Zn V	−1.67	−1.75	256235	330069
1355.97	Zn IV	−0.80	−0.80	151250	224998
1356.17	Zn IV	0.57	0.56	160886	234623
1356.20	Zn IV	−0.23	−0.24	132777	206513
1357.80	Zn IV	0.03	0.01	131805	205453
1358.60	Zn IV	−1.00	−1.03	151392	224998
1359.48	Zn IV	0.15	0.14	148180	221737
1361.32	Zn IV	−0.39	−0.41	151574	225033
1361.97	Zn IV	−0.32	−0.35	151574	224998
1363.43	Zn IV	−0.08	−0.11	138479	211824
1363.91	Zn IV	0.22	0.21	130366	203685
1365.25	Zn IV	−0.15	−0.17	148180	221426
1367.54	Zn V	−2.08	−2.08	239843	312967
1368.17	Zn IV	−1.17	−1.25	138479	211570
1369.51	Zn IV	0.39	0.38	135951	208970
1370.42	Zn IV	−0.84	−0.87	135951	208921
1371.19	Zn IV	−0.68	−0.69	149191	222120
1375.33	Zn IV	0.17	0.17	138479	211190
1375.98	Zn IV	−0.97	−0.98	132777	205453
1377.30	Zn V	−1.95	−1.98	255763	328369
1377.62	Zn IV	0.36	0.35	128730	201319
1381.98	Zn IV	−1.93	−1.90	151250	223609
1384.36	Zn IV	−1.14	−1.14	149191	221426
1385.46	Zn IV	−2.36	−2.37	157075	229253
1387.06	Zn IV	−0.73	−0.75	160886	232981
1387.19	Zn IV	−0.54	−0.59	157075	229163
1387.20	Zn V	−1.44	−1.42	240446	312534
1387.69	Zn IV	0.46	0.44	160919	232981
1388.21	Zn IV	−0.55	−0.57	151574	223609
1391.21	Zn IV	−1.06	−1.07	131805	203685
1392.14	Zn V	−2.20	−2.26	221631	293463
1392.48	Zn V	−2.07	−2.22	241829	313644
1393.03	Zn IV	−0.64	−0.68	135951	207737
1394.55	Zn IV	−0.81	−0.82	138479	210187
1400.18	Zn IV	−1.42	−1.44	138479	209899
1401.54	Zn V	−1.31	−1.30	240446	311796
1401.62	Zn V	−1.83	−1.86	256235	327581
1402.07	Zn IV	−1.88	−1.90	157930	229253

Table 30 – continued.

λ/ Å	Ion	$\log(gf)_{\mathrm{TOSS}}$	$\log(gf)_{\mathrm{Kurucz}}$	E_{low}/ cm^{-1}	E_{up}/ cm^{-1}
1402.50	Zn IV	−1.17	−1.22	157930	229231
1404.02	Zn IV	−1.92	−1.94	135951	207175
1409.39	Zn IV	−1.53	−1.55	130366	201319
1410.18	Zn V	−1.56	−1.64	240446	311359
1410.29	Zn IV	−2.38	−2.39	132777	203685
1411.02	Zn IV	−0.48	−0.49	151250	222120
1411.46	Zn V	−2.29	−2.29	240446	311295
1412.95	Zn IV	−1.72	−1.72	160919	231693
1413.88	Zn IV	−1.18	−1.19	151392	222120
1418.68	Zn IV	−0.62	−0.63	151250	221737
1419.61	Zn IV	−1.53	−1.58	138479	208921
1424.97	Zn IV	−1.05	−1.07	151250	221426
1425.25	Zn IV	−0.81	−0.82	151574	221737
1427.76	Zn IV	−2.28	−2.29	135951	205991
1427.88	Zn IV	−0.60	−0.61	151392	221426
1431.60	Zn IV	−1.18	−1.19	151574	221426
1431.89	Zn V	−2.04	−2.03	227195	297033
1436.57	Zn IV	−0.77	−0.78	157075	226685
1437.07	Zn V	−2.07	−1.95	255482	325068
1442.91	Zn V	−1.42	−1.48	255763	325068
1447.19	Zn V	−2.48	−2.45	221631	290731
1448.35	Zn V	−2.08	−2.16	255482	324526
1449.45	Zn IV	−0.85	−0.88	160886	229878
1449.79	Zn IV	−2.12	−2.24	157075	226050
1452.76	Zn V	−2.28	−2.30	226334	295168
1453.65	Zn V	−2.02	−2.04	221631	290424
1454.39	Zn V	−2.07	−2.14	230614	299372
1454.43	Zn IV	−1.34	−1.34	157930	226685
1455.69	Zn IV	−1.68	−1.70	138479	207175
1455.85	Zn V	−1.60	−1.56	222042	290731
1456.41	Zn V	−1.50	−1.53	222042	290704
1456.60	Zn V	−1.25	−1.28	260880	329533
1459.94	Zn IV	−0.44	−0.47	135951	204447
1461.53	Zn V	−1.23	−1.27	228335	296757
1462.38	Zn V	−1.79	−1.81	222042	290424
1463.29	Zn IV	−1.50	−1.52	157075	225414
1464.28	Zn V	−2.03	−2.09	221631	289925
1464.33	Zn V	−1.15	−1.21	256235	324526
1465.20	Zn V	−1.49	−1.51	231122	299372
1465.34	Zn IV	−1.60	−1.65	160919	229163
1466.16	Zn V	−1.99	−2.08	260880	329085
1466.37	Zn V	−1.93	−1.97	221631	289827
1468.47	Zn V	−1.16	−1.20	227195	295293

Table 30 – continued.

λ/ Å	Ion	$\log(gf)_{\mathrm{TOSS}}$	$\log(gf)_{\mathrm{Kurucz}}$	E_{low}/ cm^{-1}	E_{up}/ cm^{-1}
1468.81	Zn V	−1.39	−1.42	222940	291022
1472.26	Zn IV	−1.52	−1.60	157075	224998
1473.14	Zn V	−1.14	−1.21	222042	289925
1475.13	Zn V	−1.88	−1.85	222940	290731
1475.71	Zn V	−1.09	−1.13	222940	290704
1475.79	Zn V	−1.33	−1.24	230614	298375
1476.38	Zn IV	−1.61	−1.63	135951	203685
1478.17	Zn V	−1.36	−1.37	256235	323886
1481.23	Zn IV	−1.05	−1.08	138479	205991
1481.82	Zn IV	−1.11	−1.12	157930	225414
1489.67	Zn V	−0.99	−1.02	226334	293463
1490.92	Zn V	−1.28	−1.32	221631	288704
1491.02	Zn IV	−1.89	−1.97	157930	224998
1492.88	Zn V	−1.44	−1.50	222940	289925
1493.13	Zn IV	−2.11	−2.14	138479	205453
1493.47	Zn V	−2.28	−2.29	228335	295293
1500.11	Zn V	−1.06	−1.09	222042	288704
1508.43	Zn V	−0.87	−0.90	255482	321776
1509.03	Zn V	−2.35	−2.33	227195	293463
1514.86	Zn V	−1.69	−1.72	255763	321776
1515.44	Zn IV	−1.89	−1.97	148180	214167
1515.67	Zn V	−2.48	−2.49	286575	352553
1520.12	Zn V	−1.89	−1.95	260880	326664
1525.77	Zn V	−2.22	−2.30	256235	321776
1529.81	Zn IV	−1.62	−1.64	135951	201319
1531.12	Zn V	−0.93	−0.95	221631	286943
1531.39	Zn IV	−1.99	−2.05	148180	213480
1533.62	Zn IV	−2.07	−2.09	138479	203685
1535.36	Zn IV	−1.69	−1.71	160919	226050
1535.91	Zn V	−1.26	−1.25	255763	320871
1537.60	Zn V	−1.19	−1.18	231997	297033
1539.75	Zn V	−1.54	−1.61	255763	320709
1540.98	Zn V	−1.91	−1.97	222042	286936
1543.24	Zn V	−2.13	−2.02	231997	296796
1546.49	Zn IV	−2.22	−2.24	157075	221737
1551.02	Zn V	−1.19	−1.12	256235	320709
1553.97	Zn IV	−1.60	−1.64	157075	221426
1555.48	Zn IV	−1.05	−1.08	149191	213480
1555.71	Zn V	−0.79	−0.82	255763	320043
1557.86	Zn IV	−1.88	−1.92	157930	222120
1558.93	Zn IV	−0.67	−0.70	160886	225033
1562.60	Zn V	−2.23	−2.30	222940	286936
1563.20	Zn V	−1.78	−1.83	221631	285603

Table 30 – continued.

λ/ Å	Ion	$\log(gf)_{\mathrm{TOSS}}$	$\log(gf)_{\mathrm{Kurucz}}$	E_{low}/ cm^{-1}	E_{up}/ cm^{-1}
1567.22	Zn V	−1.68	−1.70	256235	320043
1573.30	Zn V	−1.56	−1.62	222042	285603
1575.58	Zn V	−1.74	−1.78	235903	299372
1575.74	Zn V	−2.46	−2.45	231831	295293
1577.54	Zn IV	−1.23	−1.27	148180	211570
1579.87	Zn V	−2.28	−2.20	231997	295293
1592.96	Zn V	−2.19	−2.20	235599	298375
1595.14	Zn IV	−1.11	−1.13	160919	223609
1597.62	Zn IV	−2.15	−2.22	151574	214167
1604.11	Zn V	−2.22	−2.26	237032	299372
1605.09	Zn V	−1.09	−1.14	221631	283933
1606.93	Zn IV	−1.84	−1.87	151250	213480
1615.37	Zn IV	−2.32	−2.36	151574	213480
1619.62	Zn V	−0.72	−0.74	256235	317978
1619.74	Zn V	−1.51	−1.53	255482	317220
1620.24	Zn IV	−1.88	−1.90	148180	209899
1627.15	Zn V	−2.00	−2.01	255763	317220
1627.44	Zn V	−2.01	−2.08	291107	352553
1627.75	Zn V	−1.52	−1.58	235599	297033
1630.18	Zn V	−1.71	−1.72	237032	298375
1634.06	Zn V	−2.39	−2.33	235599	296796
1635.02	Zn V	−1.80	−1.83	255482	316643
1636.54	Zn V	−2.26	−2.28	255482	316586
1637.64	Zn V	−1.61	−1.60	255763	316827
1639.44	Zn IV	−1.82	−1.85	149191	210187
1650.40	Zn V	−2.38	−2.40	256235	316827
1659.28	Zn V	−1.70	−1.72	285523	345790
1663.85	Zn V	−2.21	−2.21	285523	345624
1666.79	Zn IV	−1.39	−1.41	151574	211570
1669.30	Zn V	−2.20	−2.22	285885	345790
1671.49	Zn V	−2.01	−2.04	236969	296796
1673.93	Zn V	−1.69	−1.74	285885	345624
1675.19	Zn V	−2.31	−2.37	235599	295293
1677.12	Zn V	−1.49	−1.57	286575	346201
1677.71	Zn V	−2.14	−2.17	256235	315840
1679.85	Zn V	−2.48	−2.38	239843	299372
1681.33	Zn V	−2.47	−2.48	255482	314958
1682.40	Zn V	−1.91	−1.93	235730	295168
1684.68	Zn V	−1.69	−1.68	256235	315594
1687.43	Zn V	−1.76	−1.81	285885	345146
1687.80	Zn V	−1.76	−1.81	285523	344771
1689.33	Zn V	−1.97	−2.04	255763	314958
1690.67	Zn V	−1.67	−1.60	286575	345723

Table 30 – continued.

λ/ Å	Ion	$\log(gf)_{\mathrm{TOSS}}$	$\log(gf)_{\mathrm{Kurucz}}$	E_{low}/ cm^{-1}	E_{up}/ cm^{-1}
1693.51	Zn V	−2.35	−2.37	286575	345624
1698.17	Zn V	−1.76	−1.77	285885	344771
1703.12	Zn V	−1.68	−1.68	255482	314197
1706.42	Zn V	−2.26	−2.28	256235	314838
1707.33	Zn V	−1.48	−1.48	286575	345146